UNIVERSITY OF STRATHCLYDE

DEPARTMENT OF MECHANICS OF MATERIALS

THE INFLUENCE OF END CONSTRAINTS ON PIPE BENDS

A Study of Smooth Pipe Bends with Flange and Tangent Pipe End Constraints Under In-Plane Bending

Thesis presented for the
Degree of Doctor of Philosophy

by

Gordon Thomson, B.Sc.

December
1980

PAGE NUMBERS ARE CLOSE TO THE EDGE OF THE PAGE.

SOME ARE CUT OFF

THE INFLUENCE OF END CONSTRAINTS ON PIPE BENDS

A Study of Smooth Pipe Bends with Flange and Tangent Pipe End Constraints Under In-Plane Bending

ABSTRACT

The importance of smooth pipe bends in design of piping systems is well established. Recent publications have been increasingly concerned with the effect of end constraints on the behaviour of smooth bends but there have been relatively few attempts at a solution to the problem. The divergence between the results of those which do exist tend to confuse the picture for pipework designers. The present thesis is aimed at clarifying the situation.

After an historical review of the literature on smooth bends, a theoretical analysis is formulated for the in-plane bending of linear elastic curved pipes with rigid flange terminations. The method employs the theorem of minimum total potential energy with suitable kinematically admissible displacements in the form of fourier series. Integration and minimisation is performed numerically, thereby permitting the removal of several of the assumptions made by previous authors. Results are given for a wide range of practical bend geometries. These are compared with the previous theoretical predictions, highlighting the problems in some earlier works and substantiating more recent results using different solution procedures. During the

development of the theory several possible simplifications to the method are examined. The theoretical predictions are shown to be in favourable agreement with published experimental data and with results from tests performed by the author.

The approach is extended to examine the behaviour of smooth bends with connected tangent pipes under in-pane bending. The tangent pipes can be of any length and are assumed to be terminated by rigid flanges. Comprehensive results are given for bends with tangent pipes of length greater than one pipe circumference.

Finally, possible extensions of the solution procedure to other configurations and loadings are discussed.

G. Thomson

Gordon Thomson

To MARGARET and GORDON,

my wife, and son.

THE INFLUENCE OF END CONSTRAINTS ON PIPE BENDS

A Study of Smooth Pipe Bends with Flange and Tangent Pipe End Constraints Under In-Plane Bending

Contents

Figures are located at the end of each chapter.

NOTATION

$A, (\bar{A})$	with subscripts, displacement coefficient (non-dimensionalised)
$B, (\bar{B})$	with subscripts, displacement coefficient (non-dimensionalised)
$C, (\bar{C})$	with subscripts, displacement coefficient (non-dimensionalised)
C	$Et/(1-\nu^2)$
$D, (\bar{D})$	with subscript, displacement coefficient (non-dimensionalised)
D	$Et^3/12(1-\nu^2)$
$\mathcal{D}$	distortion displacement subscript
E	Young's Modulus
$F, (\bar{F})$	with subscript, displacement coefficient (non-dimensionalised)
$G, (\bar{G})$	with subscript, displacement coefficient (non-dimensionalised)
$H, (\bar{H})$	with subscript, displacement coefficient (non-dimensionalised)
H	shear moment stress resultant
I	second moment of area, $I = \pi r^3 t$
$J\ T$	total number of terms in rigid displacement series

K	with subscripts, curvature
K	flexibility factor
L	bend tangent assembly centreline length $(2\ell + R\alpha)$
M	applied in-plane bending moment
M	with subscript, moment stress resultant
MT	total number of circumferential terms in distortion displacement series.
N	with subscript, force stress resultant
NT	total number of meridional terms in distortion displacement series
P	with subscript, number of integration points
R	radius of pipe bend centreline
R'	$R + r \sin\phi$
R	with subscript, principal radius of shell curvature
R	rigid section displacements subscript
S	shear force resultant
T	$t^2/12r^2$
U	strain energy
U	circumferential rigid section displacement.
$V, (\bar{V})$	total potential energy (non-dimensionalised)

W	shear strain (curvilinear co-ordinate system)
Z	$(1 + \frac{r}{R} \sin \phi)$
j	rigid section displacement coefficient subscript
k	rigid section displacement coefficient subscript
ℓ	tangent pipe length
m	distortion displacement coefficient subscript
n	distortion displacement coefficient subscript
p	internal pressure
p	distortion displacement coefficient subscript
q	with subscript, shell surface loading
q	distortion displacement coefficient subscript
r	mid-surface radius of pipe cross-section
t	pipe wall thickness
u	circumferential displacement
v	tangential displacement
w	radial displacement
z	through thickness co-ordinate

α subtended bend angle

β with subscript, shell surface rotation

$\gamma_{\theta\phi}$ shear strain

γ rotation between ends of bend

γ_o $MR\alpha/EI$

γ_T $M\ell/EI$

δ_{jk} kronecker delta $\begin{cases} = 1 & j = k \\ = 0 & j \neq k \end{cases}$

ϵ with subscript, strain

θ angle along bend measured from centre, circumferential co-ordinate

θ subscript, circumferential direction

λ pipe factor, Rt/r^2

ν poissons ratio

ρ $\frac{R}{r}\left(1 + \frac{r}{R}\sin\phi\right)$

η $R\pi/L$

σ with subscript, stress

$\bar{\sigma}$ with subscript, stress factor

$\hat{\bar{\sigma}}$ with subscript, peak stress factor

ϕ meridional angle measured around cross-section from midway between intrados and extrados

ψ_{ej} $\begin{cases} = 1, \; j \text{ - even} \\ = 0, \; j \text{ - odd} \end{cases}$

ψ_{oj} $\begin{cases} = 0, \; j \text{ - even} \\ = 1, \; j \text{ - odd} \end{cases}$

$\$$ PR^2/Ert

GENERAL INTRODUCTION: STATEMENT OF THE PROBLEM

With present trends in the power and petro-chemical industries towards higher operating temperatures and pressures, problems associated with the design and safety assessment of pipework systems have become increasingly complex. The importance of pipework in the overall design of plant can rarely be over emphasised. It can account for nearly a quarter of the total cost of an installation. Although many industrial pipelines are essentially fluid carrying components where flexibility and stressing are of little consequence there is nevertheless a substantial minority which operate under such conditions as to warrant detailed design analyses. Within such analyses the smooth curved pipe bend merits special attention.

The fundamental problem in piping analyses is to design a system with sufficient flexibility to contend with thermal expansion loading on the pipeline itself and on the vessels to which it is connected. The deformations and stresses within the system are analysed for protection against failure in service. Failure is usually associated with fracture but this is not always true for some systems. Excessive deformation causing interference with other components, leakage of bolted flanged joints, intolerable noise and vibration, etc. can all contribute to system failure.

Perhaps the most important pipeline component in a structural sense is the smooth pipe bend. It's behaviour has attracted the interest of many authors over the last seventy years. It is now well established that the flexibility of smooth bends can be orders

of/

of magnitude higher than an equivalent length of straight pipe with the same cross-section geometry when both are subjected to the same external bending moment. Thus conventional simple beam theory can seriously over-estimate the stiffness of pipe bends, except of course when the wall thickness or the bend radius of curvature is large, when the geometry approaches that of a solid curved beam and a straight pipe, respectively. The additional flexibility is associated with the ability of the bend cross-section to "ovalise" or flatten when a bending moment is applied to it.

Theoretical analyses usually consider the smooth bend as a sector of a toriodal shell under a pure bending moment. The majority of the work on bends has been based on "strain" or "complementary" energy concepts although several solutions exist which make use of the more traditional approach of solving the governing thin shell equations. Until recently, most of the analytical work was concerned with what, in a shell theory sense, might be termed "axi-symmetric" solutions where cross-sectional deformations and stresses were assumed to be uniform along the length and independant of the subtended angle of the bend. This type of solution treats the problem as an isolated smooth bend with no terminal connections. When the bend is part of a piping system the natural cross-sectional deformations are constrained by the connections between it and the other components, violating the axi-symmetric assumption.

There exists a considerable variance in the results of experiments conducted on smooth bends with end constraints. Tests performed on bends, of similar geometries, with flanged constraints produced flexibilities that differed by as much as 100%. However, the/

the evidence seemed to suggest, perhaps fortuitously, that bends with connected tangent pipes supported the theoretical predictions of the axi-symmetric analyses provided the bend angle was greater than about 90°. Bends with shorter angles did show some reduction. Long tangents provide the least mode of constraint whereas flanges constitute the most extreme mode. For the latter case, experimental evidence conclusively indicated a substantial reduction in the flexibility indicated by the axi-symmetric analyses, particularly for short radius bends with small angles. This is hardly surprising since flanges prevent any distortion of the cross-section at the ends of the bend.

In the last fifteen years, several attempts have been made to provide an analytical method which solves the problem of smooth bends with various forms of end terminations. The additional complications introduced by involving end constraints has meant that either simplifying assumptions have had to be made or complex and time consuming numerical procedures were employed. Often the techniques were so complicated that only results for geometries of special interest were published. Further, a substantial divergence existed between the results of these analyses, especially for flanged bends. The primary objectives of the present thesis are to formulate suitable theoretical solutions for the flexibility and stress characteristics of smooth circular pipe bends with rigid flange and tangent pipe end constraints, to compare the predictions with published analytical work and to compare the results with experiments. Primarily, in-plane bending will be considered but extensions of the methods to other forms of loading/

loading and end constraints will be discussed.

An historical review of relevant publications is presented in chapter (1). Only work which was considered important or of some interest has been included. The majority of previous investigators confined their activities to a linear-elastic examination of circular, smooth bends and neglected end effects. All the available publications known to the author dealing with end constraints have been included. Work on some other important features, such as non-circular cross-sections, creep, etc., are included for comparative purposes.

Chapter (2) deals with some preliminary theoretical formulations. Thin shell theory is discussed and equations for a straight pipe and a smooth bend derived. The theorem of minimum total potential energy and its application are discussed.

Chapter (3) presents theoretical solutions to the problem of a smooth bend with flanged ends under in-plane bending. General displacements in the form of fourier series are derived which satisfy internal and external compatibility for problem. Two solutions methods are then presented which use a simplified form of these displacements with hand integration of the total potential energy. These solutions differ by their inherent assumptions. The results are discussed and compared to other published analytical solutions. A numerical solution procedure is then presented which uses the complete displacements. These latter results are discussed and compared to the other solutions. A comprehensive set of results for flexibilities and stresses for a wide range of bend geometries are then given.

Chapter (4) compares the theory of chapter (3) with published/

published experimental data and results from experiments detailed herein.

Chapter (5) examines the problem of a smooth bend with connected tangent pipes under in-plane bending using a similar treatment to that of chapter (3).

Chapter (6) compares the theory of chapter (5) with past and present experiments.

Chapter (7) considers possible extensions of the theory presented in chapters (3) and (5) to some other loading, constraint and geometric configurations.

CHAPTER .1

SMOOTH PIPE BENDS: AN HISTORICAL REVIEW

Abstract

The present chapter is concerned with the historical development of the theoretical and experimental investigations associated with smooth pipe bends subjected to various forms of loading. Publications dealing with and without end constraints are reviewed separately. Finally, the existing design procedures are examined.

CHAPTER (1)

SMOOTH PIPE BENDS: AN HISTORICAL REVIEW

(1.1) Introduction

(1.2) Smooth Pipe Bends Without End Effects

(a) Linear Elastic Analyses

(b) Considerations Other than Linear Elasticity

(i) Elastic Plastic Behaviour

(ii) Fracture and Fatigue

(iii) Inelastic and Creep Behaviour

(1.3) Smooth Pipe Bends With End Constraints

(1.4) Current Design Codes

(1.1) Introduction

Piping components can be made from a variety of materials and are expected to operate in a diversity of environments. The material behaviour is usually linear and elastic but non-linear materials are occasionally used. Pipework is often subjected to temperatures where the effect of creep becomes significant or to load levels where plasticity occurs.

Smooth bends undergo various forms of applied loading. The most important of these are in-plane bending, out-of-plane bending and pressure (see fig. (1.1)). Each produces different behavioural characteristics. The stresses and displacements from independent analyses of each type of loading cannot be indiscriminately superimposed on the others to obtain the response of combined loading.

Piping system design normally assumes that bend cross-sections are circular and that the wall thickness is the same throughout. Manufacturing processes usually are such that the attainment of this ideal is rarely achieved. The most common method of manufacture involves forcing a section of straight pipe around a specially shaped die or former. This process often results in some ovalisation of the bend cross-sections and non-uniform thinning of the pipe walls. The quality of bends can be improved by using welding fabrication or forging but these tend to be more expensive. In most situations a certain amount of imperfection is acceptable occasionally even helpful.

An extensive volume of work has been written associated with the aforementioned considerations. In the following sections of this chapter the more important, and relevant available publications/

publications are reviewed. In section (1.2) articles concerned with smooth pipe bends without end effects, are examined. Section (1.3) deals with the previous work on end effects and section (1.4) examines some of the current design codes on the structural behaviour of smooth bends.

Throughout the present work reference will be made to bend "flexibility factors". It is worth defining these, even at this early stage as follows,

$$K = \frac{\text{The end rotation of the bend under a given load}}{\text{The end rotation of a similar length of straight pipe under the same load}}$$

The "end rotation of the bend" is the change in the subtended angle of the bend when the load is applied. This is the normal flexibility referred to in connection with a smooth bend when it is considered alone. Later, a further definition will be required when the bend is connected to two straight pipes. In this case any change in the flexibility of the straights will be referred to the bend. Thus only one flexibility factor will be necessary for the determination of the behaviour of a system of a bend with straight pipes. The "flexibility factor" for this situation will be defined as,

$$K = \frac{\text{The overall end rotation of the assembly under a given load} - 2 \times \text{the end rotation of one of the straight sections loaded alone}}{\text{The end rotation of a straight pipe of the same length as the bend, under the same load}}$$

where the overall rotation of the assembly is the relative rotation between the loaded ends of the straight pipes. The bend length referred to is the length of the arc of the mean radius of the bend equal to ($R\alpha$) where R is the mean radius and α is the subtended/

subtended angle of the bend. The straight pipe in a bend-straight combination will be referred to in the present work as a "tangent pipe".

Reference will also be made to a "stress concentration factor" (S.C.F.) which unless otherwise stated, will be defined as,

$$\text{S.C.F.} = \frac{\text{The elastic stress in a bend under a given load}}{\text{The maximum elastic stress in a similar straight pipe under the same load}}$$

When quoting and discussing the work of other people the notation used will be that of the present thesis and not of the original publications. Similar comments apply to the graphical presentation of results. An attempt has been made herein to use similar notation to that of many previous authors on the subject of pipe bends.

(1.2) Smooth Pipe Bends Without End Effects

(1.2a) Linear Elastic Analyses

The earliest reported work on circular pipe bends was by BANTLIN [1]* in 1910. He compared the behaviour of curved bars and thin walled curved tubes under in-plane bending. From his experiments he concluded that the tubes were about five times more flexible than simple beam theory predicted. He attributed the discrepancy to the wrinkles and creases on the inside (intrados) of the bend which were formed during the manufacturing process. Bantlin suggested that the wrinkles behaved in a "spring like" manner.

In 1911, KÁRMÁN [2] developed the first theoretical solution for smooth curved pipes under in-plane bending. He demonstrated conclusively that curved tubes were inherently more flexible than a solid curved bar or an equivalent length of straight pipe. However, he postulated that the increase in flexibility was due to the initially circular cross-section tending to ovalise when the bending moment was applied (see fig. (1.2)). Kármán assumed that the tangential displacement of the cross-section could be expressed by the following series,

$$v = \sum_n C_n \sin 2n\phi \qquad , \quad n = 1, 2, 3, \text{----} \qquad \ldots (1.1)$$

He formulated the strain energy expression using equation (1.1) and the bend geometry. By minimising the strain energy he was able to/

*references are given in the bibliography

to determine values for the coefficients in the displacement series. By taking one term in the displacement series, i.e. $v = C_1 \sin 2\phi$, he was able to obtain what is usually referred to as the "Kármán first approximation" for the flexibility factor, i.e.

$$K_1 = \frac{10 + 12\lambda^2}{1 + 12\lambda^2} \qquad \ldots (1.2)$$

By taking two terms in the series, he obtained a second approximation,

$$K_2 = \frac{105 + 4136\lambda^2 + 4800\lambda^4}{3 + 536\lambda^2 + 4800\lambda^4} \qquad \ldots (1.3)$$

Kármán also gave numerical results for a third approximation, for values of λ he thought were necessary. The term λ is herein referred to as the pipe factor and is given by,

$$\lambda = \frac{t\,R}{r^2} \qquad \ldots (1.4)$$

This is sometimes referred to as the "pipe bend parameter" or "bend characteristic". However, it will be shown later, that when end effects are introduced then more than one parameter is required to define the solution. Kármán's analysis gives results which depend uniquely on λ. Figure (1.3) gives a plot of the numerical values of K given by Kármán. It confirms his assertion that the first approximation is valid for $\lambda > 0.5$, the second for $\lambda > 0.1$ and below $\lambda = 0.1$ a third approximation is necessary.

Kármán's analysis forms the basis of much of the work of his successors. Many of these publications give the impression that/

that Kármán only developed the first approximation and that the second and third were given by those following him. Even today, the solutions developed by contemporary authors for the axi-symmetric problem, rarely differ from that of Kármán by more than a single figure percentage. It is therefore worth examining the assumptions he made in some detail. His major assumptions, stated or implied, were as follows,

1. All cross-sections of the bend were assumed to deform by the same amount.
2. The mid-surface meridional strain (ϵ_ϕ) (sometimes referred to as the transverse strain) was assumed to be zero.
3. The circumferential strain (ϵ_θ) was assumed to be constant through the thickness, thereby neglecting the circumferential curvature (K_θ).
4. $R \gg r$. This permitted the 'pipe bore term' $(R + r)$ to be approximated to R.
5. $r \gg t$. This implies that the solution is only applicable to thin shells.
6. Stresses normal to the shell mid-surface were neglected.
7. Shear strains were neglected.

Assumptions 1. and 7. were because of axisymmetry and pure bending. Assumption 2., sometimes referred to as the "Kármán assumption", allows the deformation of the cross-section to be expressed in terms of only one displacement component. Assumption 4. limits the solution to long radius bends, however later work will show this assumption to be useful even for shorter radius bends. Assumptions 5. and 6. are simply two of the basic assumptions of thin shell theory./

theory. However, it should be noted that Kármán did not use equations derived from thin shell theory but obtained his own strain-displacement relationships from bend geometry.

In the same year, 1911, MARBEC [3] attempted to solve the identical problem by assuming that the initially circular cross-section deformed into an ellipse. He used the same strain-displacement and strain energy relationships as Kármán. The formula he obtained for the flexibility factor was,

$$K_1 = \frac{1 + 4}{3\lambda^2} \qquad \ldots (1.5)$$

Although he used similar assumptions to Kármán there are serious discrepancies between values obtained from (1.2) and (1.5). Curiously, although this formula has been quoted by many authors over the years, it was not until nearly 60 years later that Spence [4] corrected Marbec's work. Marbec failed to distinguish between the meridional angle of the initially circular cross-section and the angle used to denote the equation of his ellipse. The corrected flexibility factor is given by,

$$K_1 = \frac{2 + 3\lambda^2}{1 + 3\lambda^2} \qquad \ldots (1.6)$$

which is considerably lower than Kármán's. It is, however, consistent with a lower bound strain energy analysis but even the corrected results are of little practical value. Both Marbec's and Kármán's results are shown in figure (1.4).

LORENZ [5] in 1912 published a solution based on a complementary energy approach in which he specified stresses instead of/

of displacements. His first approximation for the flexibility factor was,

$$K_i = \frac{1 + 3}{4\lambda^2} \qquad \ldots (1.7)$$

Lorenz compared his and Karman's work with the experiments of Bantlin and concluded that his result was more accurate. However, later work disproved this. Lorenz's main inaccuracy, arose from his choice of stress distribution. He assumed that the circumferential stress across the section was linear whereas Kármán's analysis demonstrated that it was not.

In 1923, TIMOSHENKO [6] examined the case of a pipe bend with a rectangular cross-section. Using similar assumptions to those of Karman he was able to determine a flexibility factor in terms of the bend geometry. . The formulation for a rectangular section is rather complicated but for a square section of side b and thickness t and radius of curvature R, his flexibility factor can be expressed as,

$$K_i = \frac{3.232 + 49.18\,\lambda^2}{1.232 + 49.18\,\lambda^2} \qquad \ldots (1.8)$$

where $\lambda = \frac{Rt}{b}$

The result has received little attention in subsequent literature.

HOVGAARD [7] published the first of his contributions in 1926. He attempted to produce an independent solution for in-plane bending of circular smooth bends by specifying a series for the "vertical"/

"vertical" displacement component. His resulting expression was identical to that of Karman. He was the first to point out the existence of a direct meridional stress factor ($\bar{\sigma}_{\phi_2}$) and gave its peak value as,

$$\bar{\sigma}_{\phi_2} = \frac{2r}{R}\left(\frac{6\lambda^2 + 1}{12\lambda^2 + 1}\right) \qquad \ldots (1.9)$$

In 1928, HOVGAARD [8] published a modification to his earlier paper. He explained that both Karman's and his own results should be multiplied by a factor of $(1 - \nu^2)$. Although this factor is close to unity, (0.91 for $\nu = 0.3$) it should be included for consistency with a lower bound analysis.

WAHL [9] investigated piping systems and derived expressions for end moments and reactions. He was probably the first to investigate the effect of internal pressure. He erroneously concluded that it had little effect on the flexibility. At around this time a number of references appeared on the analysis of piping systems, too many to be examined here. However MARKL [10] gives references to over one hundred such works.

JENKS [11], in 1929, extended the results of Karman to the N^{th} approximation, i.e. using N terms in the displacement series. His generalised flexibility factor was given by,

$$K_N = \frac{10 + 12\lambda^2 - j}{1 + 12\lambda^2 - j} \qquad \ldots (1.9)$$

where j is a function of λ given as follows,

λ	0	0.05	0.1	0.2	0.3	0.4	0.5	0.75	1.0
j	1.0	0.7625	0.5684	0.3074	0.1764	0.1107	0.0749	0.03526	0.02026

Jenks, like Karman, omitted the $(1 - \nu^2)$ term from his analysis. He also provided data for the determination of stresses for λ values down to 0·05.

At about the same time THULOUP [12 to 14] published the first successful investigation of the combined loading effects of in-plane bending and internal pressure. His method was similar to that of Kármán, except that he specified the radial rather than the tangential displacement. Using one term in his solution, he obtained the following flexibility factor,

$$K_i = \frac{10 + 12\,\lambda^2 + 48\,\$}{1 + 12\,\lambda^2 + 48\,\$} \qquad \ldots (1.10)$$

where $\$ = \frac{Pr}{Et}\left(\frac{R}{r}\right)^2$

which reduces to that of Kármán's first approximation for zero internal pressure.

In [15], TEUDA attempted to present a general solution to the pipe bend problem. His analysis could accomodate arbitrary initial pipe profiles and removed the assumption of $R \gg r$. The method was mathematically complex involving the use of power series. However, he restricted his presentation to circular cross-sections.

In 1943, KARL [16] published two analyses, using strain energy and complementary energy methods, similar to those of Kármán and Lorenz. For the strain energy analysis, he provided the following/

following expression for a "third approximation" flexibility factor,

$$K_3 = \frac{252 + 73912\,\lambda^2 + 2446176\,\lambda^4 + 2822400\,\lambda^6}{3 + 3280\,\lambda^2 + 329376\,\lambda^4 + 2822400\,\lambda^6} \qquad \ldots (1.11)$$

In the complementary analysis, Karl used up to four terms in his stress resultant series. With one term, the solution was identical to that of Lorenz. The flexibility factor with four terms was

$$K_4 = 1 + \frac{3}{4\lambda^2} - \frac{(261 + 152304\,\lambda^4 + 11289600\,\lambda^6)}{(360\,\lambda^2 + 229792\,\lambda^4 + 2125863\,\lambda^6 + 180633600\,\lambda^8)} \qquad \ldots (1.12)$$

Although Karl appreciated that the strain energy and complementary energy methods should have given lower and upper bounds on the flexibility factor, for certain values of λ, the lower bound (1.11) gives higher results than the upper bound (1.12). He seemed to be aware that it had something to do with the $(1 - \nu^2)$ term but for some reason included it in the upper bound analysis in such a way that some results still exceeded those of the lower bound. The correct bound is obtained if the term is included in the strain energy solution. Karl also demonstrated that the inclusion of (r/R) in the complementary solution only marginally affected the results. His converged flexibility factors are included in figure (1.4).

In 1943, VIGNESS [17] was the first to publish an investigation/

investigation of smooth bends under out-of-plane bending. He assumed a tangential displacement of the cross-section with the form,

$$v = \sum_n C_n \cos n\phi \qquad , \qquad n = 1, 2, 3, \text{---}$$

... (1.13)

His method, for a small bend segment, was similar to Kármán's. Vigness obtained a first approximation flexibility factor identical to Kármán's. The maximum meridional bending stress was also identical but its position was moved by 45°. However, out-of-plane bending introduces a new problem since the applied and reaction loads are different to maintain external equilibrium for finite bend angles. For example, an out-of-plane moment becomes a pure torsion at a position 90° further along the bend. Thus the overall rotation for a bend must be found by integrating the effect of variable loading along the bend.

BESKIN [18], apparently unaware of the work of Lorenz [5] and Karl [16], performed an analysis for in-plane bending starting from equilibrium considerations and an assumed series for the circumferential stress. He considered more terms in the series than Lorenz or Karl and was able to show how many terms were necessary for a converged solution for a specified accuracy. He also repeated the analysis for out-of-plane bending and showed that identical formulae are obtained for flexibility factors.

BARTHELEMY generalised Kármán's theory for in-plane bending in [19] and Thuloup's method for combined bending and pressure in reference/

reference [20]. The effects of initial ovality are also considered in [20]. Barthelemy and DE LEIRIS presented experimental evidence is support of [19] and [20] in [21]. In [22] they presented further work and included the influence of thickness variations in the analysis.

HUBER [23] presented a solution to the problem of a smooth bend having an initially elliptical cross-section under in-plane bending. He derived a first approximation flexibility factor in terms of pipe parameters and elliptic functions which were evaluated in [24]. For a circular cross-section, it reduces to,

$$K = \frac{5.404 + 12\lambda^2}{0.5798 + 12\lambda^2} \qquad \ldots (1.14)$$

which, when compared to Karman's result, casts some doubt on Huber's result.

In 1949, REISSNER [25] generalised the equations of rotationally symmetric thin shells and reduced these to the governing differential equations of a toroidal shell under in-plane bending. These formed the basis of CLARK and REISSNER's [26] solution for smooth curved tubes, under in-plane bending, using shell theory as distinct from energy methods. Trigonometric and asymptotic solutions were obtained from the equations. From the latter, the following expression was obtained for the flexibility factor,

$$K = \frac{1.65}{\lambda} \qquad \ldots (1.15)$$

The maximum meridional stress was given as

$$\hat{\sigma}_{\phi} = \pm \frac{1.892}{\lambda^{2/3}} \qquad \ldots (1.16)$$

Clark and Reissner suggested a limit of applicability as $\lambda < 0.3$ although it can be used with reasonable accuracy up to $\lambda = 1.0$. They also obtained the following formula for eliptical cross-section tubes of major axis 2a and minor axis 2b,

$$K = B(\phi) \times \frac{1.65}{\lambda} \qquad \ldots (1.17)$$

and

$$\hat{\sigma}_{\phi} = \pm \frac{B(\phi)}{(b/a)^{1/3}} \times \frac{1.892}{\lambda^{2/3}} \qquad \ldots (1.18)$$

where

$$B(\phi) = \frac{1}{\pi} \left(\frac{b}{a}\right)^{4} \int \sin^2\phi / \left(1-\left(1-(b/a)^2\right)^2 \sin^2\phi\right)^{5/2} d\phi$$

Equations (1.17) and (1.18) reduce to (1.15) and (1.16) for circular (b/a = 1) cross-sections. These equations should only be used for b/a less than and close to unity.

In 1952, GROSS [27] and FORD [28] published the results of an extensive theoretical and experimental investigation of pipe bends under various conditions. Their experiments were principally aimed at confirming the applicability of the existing theories for short radius bends, with λ values as low as 0.048. They confirmed the need for the use of sufficient terms in the series solution at low λ. The radius ratio R/r was shown to have little effect on the flexibilities. By using strain gauges on the inside and outside of the bend, they showed the existence of a small/

small but significant meridional direct stress ($\sigma_{\phi D}$) and derived its value from equilibrium as,

$$\sigma_{\phi D} = -\frac{r}{R}\cos\phi\int_{\phi}^{\frac{\pi}{2}}\sigma_{\theta D}\,d\phi \qquad \ldots (1.19)$$

where $\sigma_{\theta D}$ is the circumferential direct stress. This was added to the meridional bending stress obtained from Karman's analysis and gave the maximum stress for a bend on the inside surface. The above modification has become known as the "Gross correction factor". In [27] convenient formulae were given for the flexibility and stresses obtained from a Karman's analysis. Gross and Ford also conducted experiments on bends with combined bending and internal pressure and demonstrated that this gives reduced flexibility factors. Their work attracted a considerable amount of useful discussion. Among the contributers were PARDUE & VIGNESS and ZENO who pointed to the influence of end effects on the results. These will be discussed further in section (1.3).

During the years 1956 and 1957, three important papers appeared dealing with combined bending and pressure. KAFKA and DUNN [29] included the effect of pressure in a strain energy analysis by adding the work done by the pressure on the cross-section. The extra term was of a second order but proved nevertheless to be significant. The results of some experiments were also given showing reasonable agreement with their theory. CRANDALL and DAHL [30] modified the shell theory approach of Clark and Reissner [26] to include the effect of pressure. As before, they obtained asymptotic and series solutions. The series solution gave similar results to those of Thuloup and to Kafka and/

and Dunn. The asymptotic solution predicted even lower flexibilities than the series solution, especially for higher pressures, but appeared to compare better with experimental results.

RODABAUGH and GEORGE [31] generalized the method given in [29] using a general displacement series for in and out-of-plane bending. They gave graphical results and presented experimental work to justify their analysis. The flexibility factors for in-plane and out-of-plane bending were shown to be the same.

TURNER and FORD [32], in 1957, attempted an analysis with as few assumptions as possible. They examined the effect of each assumption by including and removing the relevant terms. They concluded that although stress distributions could be seriously in error, the flexibility factors and maximum stresses were unlikely to be in error by more than 5 - 10%.

FINDLAY and SPENCE [33] reported an experimental investigation conducted on a 6ft. 6in. diameter 90° smooth bend ($R/r = 2.94$, $\lambda = 0.107$). The stress distribution at the centre of the bend showed good agreement with the theories of Turner & Ford, Karman and Clark & Reissner. They also extracted an expression for the peak meridional stress (including direct stress correction) from the asymptotic solution of Clark and Reissner. This was given as,

$$\hat{\sigma}_\phi = -\frac{1.862}{\lambda^{2/3}(1-\nu^2)^{1/6}} - \frac{0.644}{\lambda^{1/3}}\frac{r}{R}\left[12(1-\nu^2)\right]^{1/6}$$

For $\nu = 0.3$ this becomes,

$$\hat{\alpha}_{\phi} = -\frac{1.892}{\lambda^{2/3}} - \frac{0.96}{\lambda^{1/3}}\frac{r}{R}$$

... (1.20)

JONES [34] reviewed the literature on smooth and mitred bends. In [35], he presented a generalization of Karman's original work. The assumption R >> r was removed and the radial displacement series was taken as,

$$\omega = \sum_{n=2} C_n \cos n\xi \qquad , \qquad n = 2, 3, 4, 5, \text{----}$$

where $\xi = \phi - 90^{\circ}$ ... (1.21)

Up to nine terms in the series were used and the earlier conclusions regarding the unimportance of the R >> r assumption confirmed. Further discussion was also given on convergence and the relative insignificance of the odd displacement series terms, particularly for larger R/r.

CHENG and THAILER [36] investigated in-plane bending using Clark & Reissner's method of analysis but included the r/R terms in their solution. They further refined their analysis in a subsequent paper [37]. Both papers concluded that the inclusion of r/R had little consequence.

In 1970, SPENCE [4] examined the bounding characteristics of flexibility factors obtained from minimum total potential or strain energy methods and complementary potential energy methods. Spence, to some extent, resolved the dilemma concerning the $(1 - \nu^2)$ term, stating that a true lower bound is only achieved from a strain energy type analysis if this term is retained in the flexibility factors. This paper also included the correction to/

to Marbec's work mentioned earlier. In 1971 FINDLAY and SPENCE [38] published theoretical solutions for elliptical pipe bends under in-plane and out-of-plane bending. The results from their strain energy based method, demonstrate that ellipticity has a greater influence on out-of-plane bending. In [39], they extended their solution to bends of elliptic cross-section with thickness variations and concluded that normally accepted values of thinning have virtually no effect on flexibility.

In 1972, DODGE and MOORE [40] presented a generalization of Rodbaugh and George's method for in-plane and out-of-plane bending with internal pressure. They also included the Gross correction factor in the meridional peak stresses. A computer program for detailed analysis of pipe bends, based on the work in [40] was given in [41]. The program, "ELBOW", was used to obtain the comprehensive set of results given in [40]. In the same year, BLOMFIELD and TURNER [42] published a further contribution on the same topic and KITCHING and BOND [43] examined the out-of-circularity effects in a pipe bend, also with pressure and bending loads.

J. J. THOMPSON [44] attempted an "exact" solution to the problem of a smooth curved pipe with in-plane bending. His method involved a matrix solution of the thin shell equations with prescribed displacement series. The work was intended as a prelude to an investigation of the influence of end constraints.

(1.2b) Considerations Other than Linear Elasticity

In recent years an increasing number of publications have been appearing on aspects of pipe bend behaviour other than linear elasticity. These will be examined in three separate sub-sections. Occasionally, some of these publications will include a reference to the effect of end constraints and will be considered again in section (1.3).

(i) Elastic Plastic Behaviour

In 1967, MARCAL [45] applied a computer program for the elastic plastic behaviour of general shells of revolution, to pipe bends under in-plane bending. He gave the relationship between the applied bending moment and elastic-plastic strains up to values of 6%. Collapse moments were also given which when non-dimensionalized compared favourably with the experimental results given by GROSS and FORD [28].

BOLT and GREENSTREET [46] presented an experimental investigation on the plastic collapse loads for pipe bends under both in-plane and out-of-plane bending, with and without internal pressure. They made no attempt to compare their results with theoretical computations.

In 1973, SPENCE and FINDLAY [47] calculated theoretical limit moments for smooth circular pipe bends using two different methods. The first method involved using a suitable elastic solution for the stresses with equations derived from the interaction of yield surfaces for the limit moments. These were compared with an approximate limit moment derived from a creep analysis using a Norton power law. The ratio of limit moment to

first/

first yield moment can be found from the ratio of the maximum stresses where the creep index is equal to unity with the maximum stress where the creep index approaches infinity. A year later, CALLADINE [48] obtained limit moments by working directly from a Mises yield surface with the asymptotic elastic solution developed by Clark and Reissner [26]. Calladine's results are surprisingly high for a lower bound when compared with the bounds given in [47]. MELLOW and GRIFFIN presented further results for collapse loads using finite element analysis in [49]. SPENCE and FINDLAY extended their work to bends with non-circular cross-sections in [50]. Their results show that ovality introduced by modern manufacturing processes should have little influence on the value of the limit moments.

Several 'elements' for the plastic analysis of pipe bends have been developed and included in finite element computer programs (see for instance [51] to [55]). The major problem with these is the cost and time involved in obtaining a solution for a particular bend. The cost has generally restricted published data to a few examples.

(ii) Fracture and Fatigue

Fatigue tests on pipe bends were performed as early as 1935 by DENNISON [56]. Further experimental studies were carried out by ROSSHEIM and MARKL [57], MARKL [58], [59] and LANE [60]. Reference [58] is particularly noteworthy since it contains the results from over 400 fatigue tests on piping components,/

components, including smooth bends. The results of these tests have been incorporated into various design procedures.

BLOMFIELD and JACKSON [61] used an elastic-plastic computer program with the relevant material property data to predict the low-cycle fatigue lives of cupro-nickel pipe bends. They compared the experimental fatigue lives of the bends with results from elastic and elastic-plastic computer solutions and published fatigue data. In conclusion, they stated that the latter method was more conservative. BLOMFIELD presented further results in [62].

In 1977, DOYEN and MARINI [63] published the results of fatigue tests conducted on bends made with ICL 167 CN steel. Their investigation was principally concerned with defects in seam welds at the intrados and extrados of bends made in halves.

JAMES [64] employed fracture mechanics techniques to estimate crack extension in piping elbows.

(iii) Inelastic and Creep Behaviour

In 1957, KACHANOV [65] investigated the effect of creep on pipe bends under in-plane bending. Using a complementary energy method with a creep power law he derived upper bound, second approximation, flexibility factors.

SPENCE and MACKENZIE [66] considered the same problem using strain energy and developed lower bound, first approximation, flexibility factors. The secondary creep law used in their analysis was that postulated by NORTON [67] given by,

$$\dot{\epsilon} = B\sigma^n$$

where $\dot{\epsilon}$ is the strain rate and where B and n are material constants.

'n'/

'n' is often referred to as the creep index. The flexibility factors obtained from both methods were shown to be dependent on the creep index and the pipe factor.

In 1969, SPENCE [68] extended the earlier work to include up to five terms in his displacement series. A subsequent paper [69] presented an upper bound analysis. Figure (1.5) shows flexibility factors from the upper and lower bounds and clearly demonstrates that creep flexibilities can be considerably higher than those of an elastic analysis. [70] details the previous work of Spence together with 'improvements' to the upper and lower bound analyses. Stress distributions, maximum stress factors and reference stresses are all presented in some detail. Some of the work developed in [70] was subsequently presented in [71] and [72]. [70] contained some work on the creep of pipe bends with elliptical cross-section which was expanded in [73a], [73b] and [74]. Further work by Spence on creep in short radius bends was presented in [75]. These publications gave factors for stresses and flexibilities for a range of geometries suitable for design.

In 1973, WORKMAN and RODABAUGH [76] examined the effect of creep relaxation on a piping system operating at high temperature with particular interest focused on pipe bends. They reviewed the earlier work of Kachanov and Spence but failed to notice Kachanov's typographical error in stating the pipe factor as $\sqrt{tR}/r$ and failed to appreciate the reason for the inclusion of the $(1 - \nu^2)$ type term in Spence's lower bound analysis. In the discussion to [76], Spence pointed these out and further errors/

errors in their work. Workman and Rodabaugh published another paper [77] a year later.

Several attempts at a solution to the creep problem were published between 1973 and 1975, [51], [52], [78] and [79] using finite elements. However, results are only available for a few typical geometries which were of particular interest to the respective authors.

In 1975, BOYLE [80] presented a dissertation on rational creep mechanics with further work on creep in pipe bends. He approached the problem using a numerical solution to the non-linear thin shell equations developed in [80]. Boyle compared the non-linear solution of pressurized curved tubes with the earlier work, which included only non-linear terms involving the pressure. His results suggest that the linear analysis could be in error for high ratios of bending moment to pressure (see [81]). He also performed a redistribution analysis to examine transient creep in pipe bends. An important conclusion from his work was that the steady state results of Spence were verified.

SPENCE and BOYLE [82] developed an analysis for out-of-plane bending of a curved pipe in creep. As indicated earlier, out-of-plane bending of bends with finite bend angles involves a combination of bending and torsion which has to be included in a creep analysis. A solution was achieved by minimising the total potential energy rate. Their results were presented in terms of an "energy factor" because of the combined loading. Spence and Boyle published two further papers in 1977, the first [83] on the redistribution analysis in [80], and the second [84] on the creep analysis/

analysis of piping systems.

GRIFFITH and RODABAUGH [85] published results of creep tests conducted on 4 inch, schedule 10, pipe assemblies. IMAZU et al. [86] reported the results of tests conducted on 12 inch, schedule 20, type 304 stainless steel pipe assemblies. In the latter work, the comparison between the experiment and the finite element program [52] was disappointing. The authors attributed the difference to the choice of material constitutive equation and the influence of the tangent pipe end constraints.

In 1979, IMAZU and NAKUMURA [87] developed two simplified creep buckling analyses of pipe bends under in-plane bending. The two methods gave comparable results and showed some correlation with experiments. The simpler of them was based on Spence's results for elliptical bends by updating the flattening of the cross-section as creep proceeded.

In recent years, an attempt has been made to establish an international benchmark solution to the creep problem to provide a standard against which computer programs could be verified. Spence and Boyle in [88], compared the results of inelastic computer programs against the available benchmark data, concluding that sufficient information is available for the assessment of simple piping configurations.

(1.3) Smooth Pipe Bends with End Constraints

This section will be concerned with publications which contribute information to the study of smooth curved pipes with end constraints (figure (1.6)). Several authors speculated on the influence of end constraints but only those presenting factual data will/

will be considered. Only a brief examination will be given here since detailed discussion and comparison will be made later.

In 1945, SYMONDS and VIGNESS, in the discussion to Beskin's paper [18], presented some experimental results which demonstrated the importance of end effects. For a bend with a pipe factor $\lambda = 0.043$ and $r/R = 3$ they gave the following flexibility factors,

Bend	Constraint	Flexibility Factor
180°	tangent pipes	37
90°	tangent pipes	32
90°	one flange and one tangent	18
90°	two flanges	8

The flexibility factor from a theory without end effects, like that given in equation (1.15), would be in the region of 38.4. Although there is some doubt about the quality of the results, there is no doubting the obvious conclusions which can be drawn. The most severe form of constraint was clearly flanges which substantially reduced the flexibility of smooth bends. Tangent pipes had some influence particularly at the shorter bend angle.

In 1951, PARDUE and VIGNESS [89a] published the results of an extensive investigation into the effect of end constraints on short radius bends confirming earlier conclusions. A more comprehensive report was published two years later [89b]. Pardue and Vigness investigated bends with subtended angles of 180°, 90° and 45° with two tangent pipes, one tangent plus one flange and two flanges. In-plane bending, out-of-plane bending, torque and shear loads were all examined. Several of their conclusions are worth stating at this stage. They concluded that flexibility factors/

factors and stresses, for bends where end constraints are important, depend on the pipe factor (λ), bend angle (α), radius ratio (R/r) and the type of loading. Typical results from Pardue and Vigness are given in figure (1.7) for 90° bends with flanges.

GROSS and FORD [28] in their experimental study determined the variation of the ovalisation along the bends with flanged tangents. The flattening was shown to progressively decrease away from the centre section of the bend and along the tangent pipe. In the discussion following [38], PARDUE and VIGNESS published further stress and flexibility factors for flanged bends. They also pointed out that the maximum meridional stress factor ($\hat{\sigma}_\phi$) shifted from midway between the intrados and extrados (pipe centreline), towards the intrados, as the bend length decreased and end constraints became more rigid. Thus further discrepancies were shown to exist between the axisymmetric theories and experiment.

VISSAT and DEL BUONO [90] reported tests on twelve 180° short radius bends with both flange and tangent pipe terminations. Only a small difference was noticed between the results of the different end effects. However some scepticism must be expressed about the manner in which the tests were conducted and about their definition of flexibility factor. Additional discussion on their results will be made later.

In 1966, FINDLAY and SPENCE [33], pointed out that since the change in diameter showed a significant variation along the bend then the flexibility would probably vary in the same manner. This has implications for experimental flexibility factors since they will be an average of the flexibility along the bend/

bend and possibly along the tangent pipes. SMITH and FORD [91] suggested an empirical formula for the variation of the flexibility factor for 90° bends.

KALNINS, [92], [93] and [94], developed a numerical method for analysis of thin shells. The technique involved multisegment integration and finite difference solution of the thin shell equations. The advantage of this method is that it allows end effects to be included in the analysis. However, the cost of running the computer program has prevented it from being run for a comprehensive set of parameters.

In 1970, THAILER and CHENG [95] published a theoretical solution for 180° bends with flanged ends under in-plane bending. They selected results from the experiments of Pardue and Vigness which gave rough agreement with their theory. Considerable discussion on this work and the inherent unquoted assumptions will be made later during the development of the present theoretical analysis for flanged bends.

NATARAJAN and BLOMFIELD, [96] to [98], reported a significant contribution to the subject of pipe bends with end constraints. This was perhaps the earliest publication on the use of the finite element method for bends with end constraints. They provided flexibility factors and stresses for a variety of end constraints and a relatively wide set of geometrical parameters. An unfortunate limitation of this work and of other finite element solutions is their inability to contend with a bend with two flanges. The problem is specifying the necessary boundary conditions for the loaded flange.

In 1973, FINDLAY [99] published a dissertation on the effect/

effect of end constraints on pipe bends. Most of his work was concerned with flanged bends under in-plane loading. He developed a total potential energy based theory with specified displacements satisfying the boundary conditions of a rigid flange. Findlay compared his results with experiments conducted by himself and others. The stresses provided a better comparison than the flexibility factors. Findlay concluded from these that his solution was satisfactory. He also pointed to what he thought were erroneous assumptions in Thailer and Cheng's solution and felt that their comparison with experiment was fortuitous. This work was also published by FINDLAY and SPENCE in [100], [101] and [102].

In 1974, AKSEL'RAD and KVASNIKOV [103] developed a "semi-moment" theory for curvilinear bar-shells and as an example dealt with the problem of flanged bends. They give a first approximation formula for the flexibility factor but no stress results. The results are different from those of Findlay and Thailer-Cheng. More will be said about the comparison and assumptions in this work later. The first author, Aksel'rad, later published a similar contribution [104] but this time his name was translated as AXELRAD [105]. In the present work comparisons will generally be made with the latter work and the author referred to as Axelrad.

IMAMASA and URAGAMI [106] published an experimental study of bends with end effects. They compared the results with those from a finite element program [107] and obtained a relatively good comparison. In the experiments on bends with one tangent and one flange the highest stresses occurred adjacent to the flange and not at the position of maximum ovalisation nearer the/

the centre of the bend.

WRIGHT, RODABAUGH and THAILER [108] performed a finite element analysis on a tapered bend with one flange and one tangent pipe using the "MARC" program [52]. The authors also used the program of Kalnin's [94] but found that the total moment acting on each cross-section varied significantly along the bend and that the stress at the centre of the bend continued to increase with increasing tangent pipe length to values well above that predicted by theories without end effects. This casts some doubt on the earlier work of Kalnins.

SOBEL [109] suggested guidelines for the use of the "MARC" finite element program on bends with end effects. Detailed results are given for a single elbow with two short tangent pipes. RODABAUGH, MOORE and ISKANDER [110] obtained some results for bends with connected tangent pipes using the EPACA [111] finite element program. KANO et al [112] compared the results from the ANSYS [113], ASKA [114] and MARC [52] finite element programs for pipe bends with tangent pipes under in-plane and out-of-plane bending. The stress comparisons were surprisingly poor. They concluded that it is necessary to use higher order elements for an accurate analysis.

In [115], and [116], OHTSUBO and WATANABE presented a finite element in the form of a ring. The ring element used trigonometric series in the meridional direction and Hermitian polynomials in the circumferential direction. Smooth bends with tangent pipes were modelled by connecting several elements together. Ohtsubo and Watanabe presented some results for 90° bends with tangents. They also presented results for bends with varying thickness,/

thickness, but without end effects.

In 1978, WHATHAM [117] published a theoretical analysis of flanged pipe bends under in-plane bending. He used NOVOZHILOV's [118] four parameter method where the governing differential equations of a thin shell are solved using four functions, with the same forms as the displacements, which satisfy the equilibrium and compatibility equations simultaneously. Considerable discussion of the results in this paper will be given later. Figure (1.8) shows a brief comparison of the theoretical analyses for flanged bends by Thailer-Cheng [95], Findlay 99], Axelrad [104] and Whatham. In 1979, WHATHAM and THOMPSON [119] extended the earlier work to bends with flanged tangents of any length.

KANO et al [120] examined three elbow-pipe assemblies under various loadings using the FINAS [121] finite element system. TAKEDA et al [122] and BATHE and ALMEIDA [123] proposed two further finite elements for pipe bends with end effects. KWEE [124] analysed a bend with varying pipe radii using the ASKA program [114].

BROUARD et al [125] performed experimental tests on bends with tangent pipes and flanges. The bends were loaded into the plastic regime with large displacements. Under these conditions flexibility factors for opening and closing bending moments were found to be different.

Although numerous papers have been written on the influence of end constraints on smooth pipe bends, there exists no conclusive general solutions; indeed many of the available publications are contradictory. The comparison of the existing theories on flanged bends in figure (1.8) highlights this dilemma. Comparing/

Comparing these with the available experiments produces further confusion. The position with regard to tangent pipes is somewhat different. Experimental work appears to agree with the axisymmetric theory, for flexibility factors and maximum stresses, over a range of practical geometries. However, for short radius, small angle bends some deviation clearly exists. Available theoretical work would seem to roughly agree with this but a detailed and truly comprehensive set of results is not available. No useful attempt has been made to try to bring together all of the available evidence with definite conclusions.

(1.4) Current Design Codes

The two most commonly employed British design codes are BS 806 [126] and BS 3351 [127] for land boilers and petrochemical plant respectively. BS 806 was rewritten in 1975 and includes a relatively extensive section on the flexibility and stressing of smooth pipe bends. A graphical presentation was used for the various stress and flexibility factors, the latter including a small variation with radius ratio. The stress factors were also slightly different for in-plane and out-of-plane bending. Correction factors were given for bends with one or two flanges within 4r of the bend-tangent junctions. Although these were given on a graph, they can be found from the following formulae,

$$\text{One flange, correction factor} = \lambda^{1/6}$$
$$\text{Two flanges, correction factor} = \lambda^{1/3} \qquad \ldots (1.22)$$

No/

No other form of end constraint was considered. BS 3351 suggests the following flexibility and stress factors for bends without end effects,

$$K = \frac{1.65}{\lambda} \qquad \ldots (1.23)$$

and,

$$\hat{\sigma} = \frac{0.9}{\lambda^{2/3}} \qquad \ldots (1.24)$$

The flexibility factor is the same as that given by Clark and Reissner [26] in equation (1.15). The stress factor is similar to the Clark and Reissner asymptotic formula for the peak circumferential stress factor, which is virtually half the peak meridional stress factor given in equation (1.16). The reason for the use of the circumferential rather than the meridional stress factor is due to a peculiar continuing argument as to which is most likely to cause failure. BS 806 gives graphs of both stress factors and requires that the maximum stress range for combined loading must satisfy certain limits. Pardue and Vigness [89] suggested that the circumferential stress factors, being constant through the wall thickness, were the most important design stresses but in the discussion which followed [89], Gross and Ford suggested that an equivalent (combination of meridional and circumferential factors) stress factor should be used as indicated by Hovgaard [128], and Markl further suggested that failure was due to either meridional or circumferential factor, whichever was the greater. Markl's suggestion was based on the results of fatigue tests presented in [58]. BS 3351 also uses/

uses the correction factors given by equation (1.22) for bends with flanges.

Perhaps the most detailed British design data for smooth bends is that of the "Engineering Sciences Data Unit" (E.S.D.U.) [129]. This provides graphs for flexibility, meridional stress and equivalent stress factors, for bends with connected tangent pipes. The results are based on the work of Natarajan and Blomfield [97] using finite element analysis. Unfortunately the results are limited to the range $r/t \geqslant 10$ and $R/r = 2$. This is the only current code which considers the tangent pipe as an end constraint and it demonstrates the necessity for information, particularly at low bend angles. E.S.D.U. also suggest sources for data on other forms of end constraints. One further interesting statement, which will be examined later, is that the circumferential stress at flanges on flanged bends can exceed the maximum meridional stress.

Numerous American standards are available [130 - 133] which give the same stress and flexibility factors as BS 3351 i.e. equations (1.23) and (1.24). They also incorporate the flange corrections given in (1.22). It is believed that these flange corrections are largely based on the work of Pardue and Vigness [89].

To summarise the current design codes, in the context of end constraints, it is noted that all of the codes, excepting E.S.D.U., suggest the correction factors given by (1.22). For comparison purposes, the following results from the A.S.M.E. code will be used herein, for bends with two flanges:

$$K = \frac{1.65}{\lambda^{2/3}} \qquad \ldots (1.25)$$

and/

and

$$\hat{\sigma} = \frac{0.9}{\lambda^{1/3}} \qquad \ldots (1.26)$$

These are illustrated in figure (1.9). Only the E.S.D.U. data sheet acknowledges the influence of tangent pipes as end constraints. Some of the flexibility factors are shown in figure (1.10).

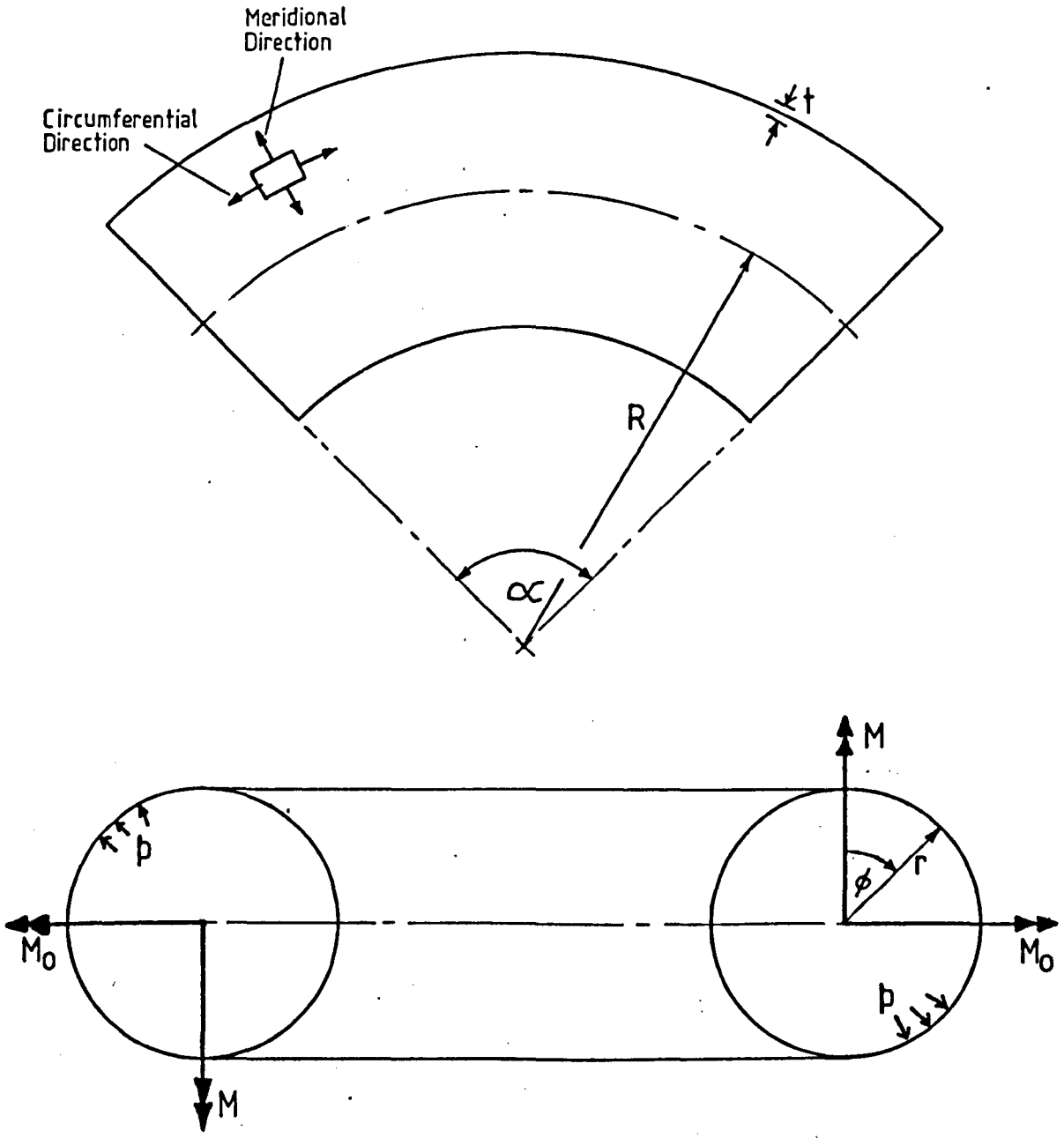

M in-plane bending moment
M_o out-of-plane bending moment
p internal pressure

Smooth Pipe Bend with Various Loads

Figure (1.1)

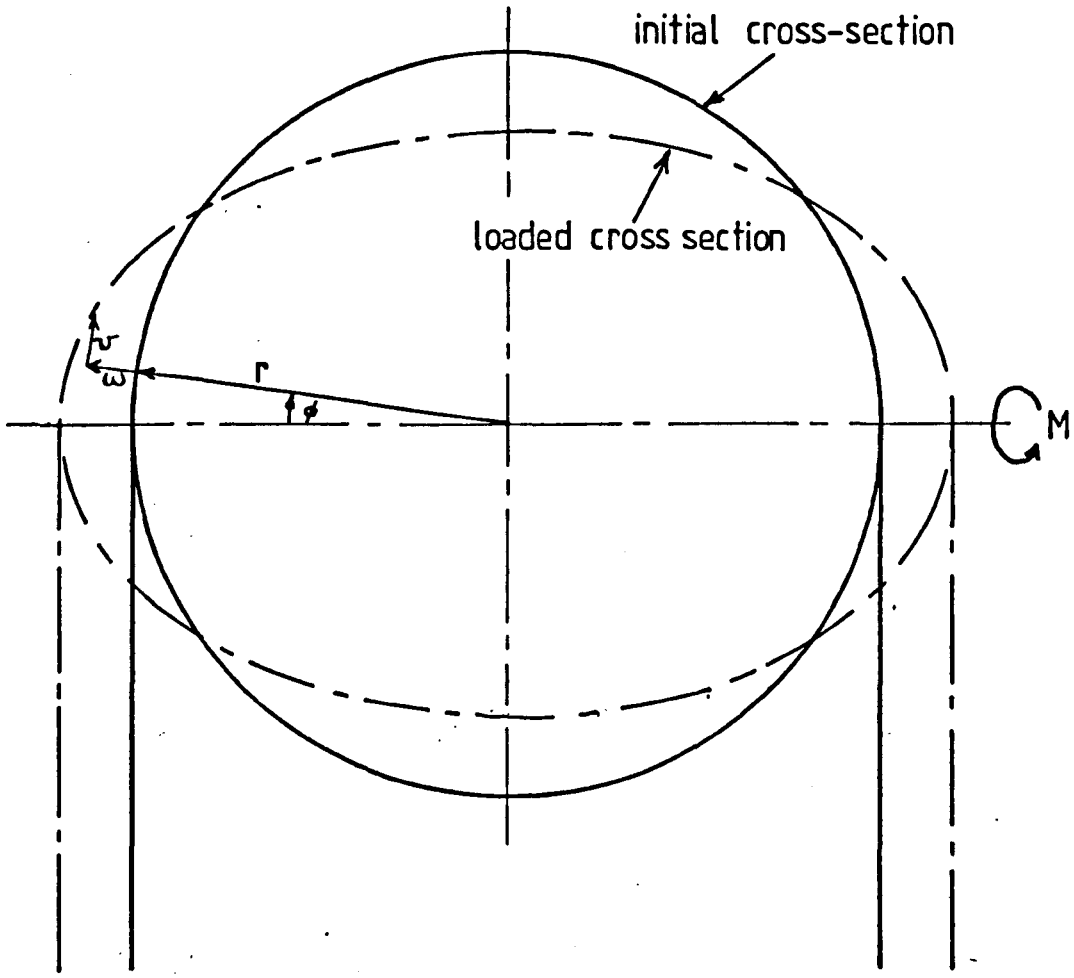

Deformation of Pipe Bend Cross-section

Figure (1.2)

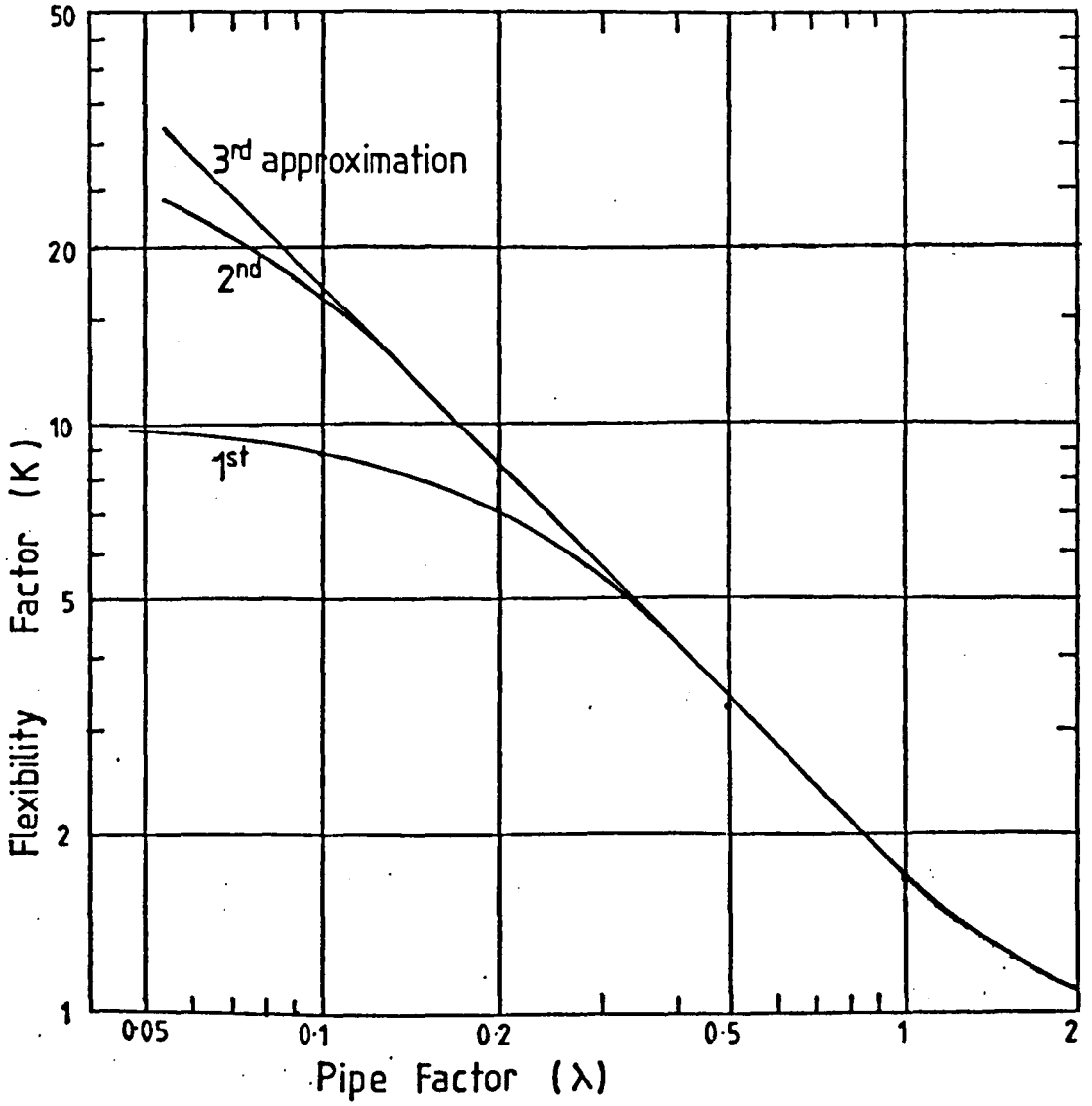

Convergence of Karman's Flexibility Factors

Figure (1.3)

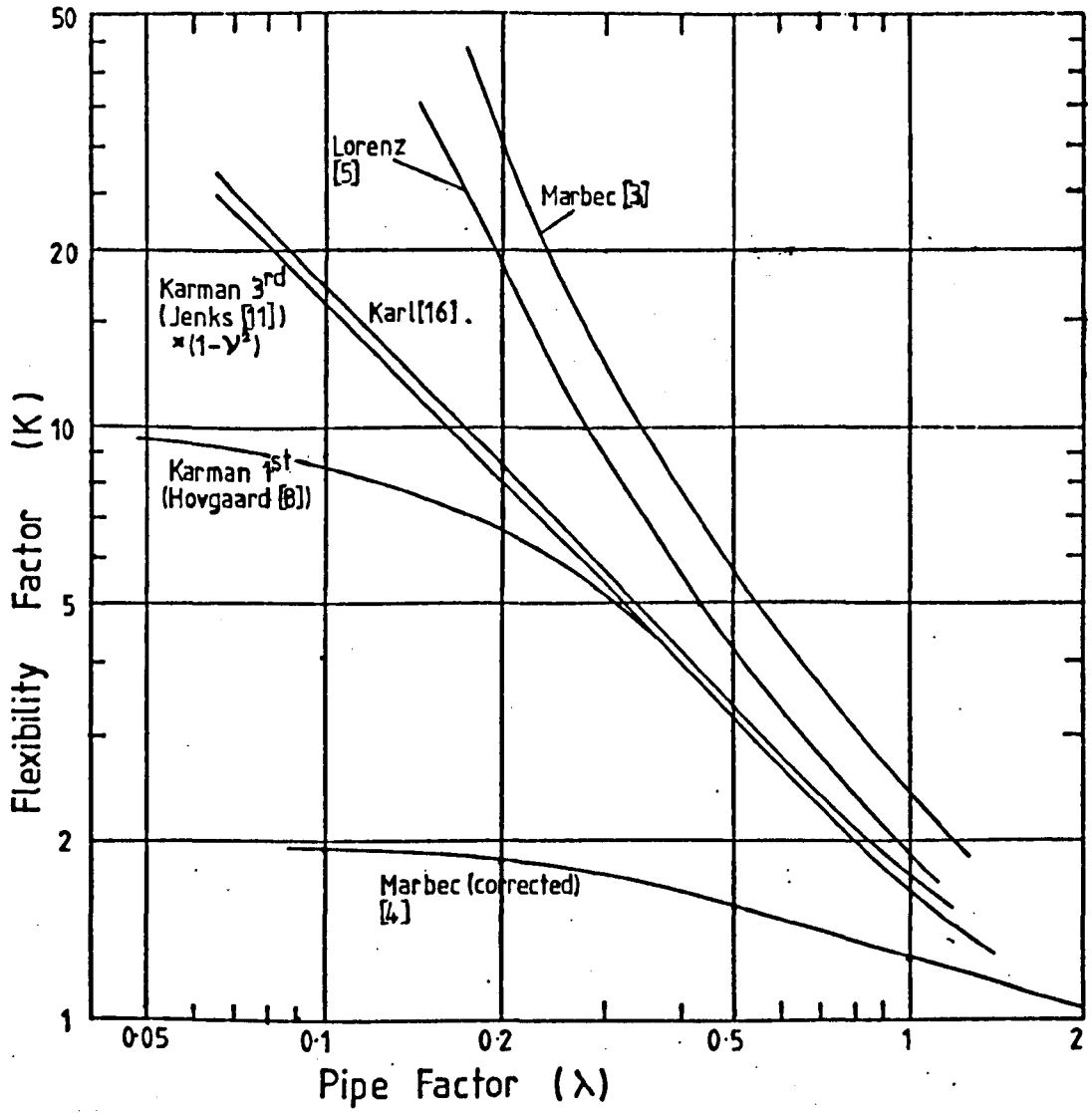

Comparison of Flexibility Factors from Early Research

Figure (1.4)

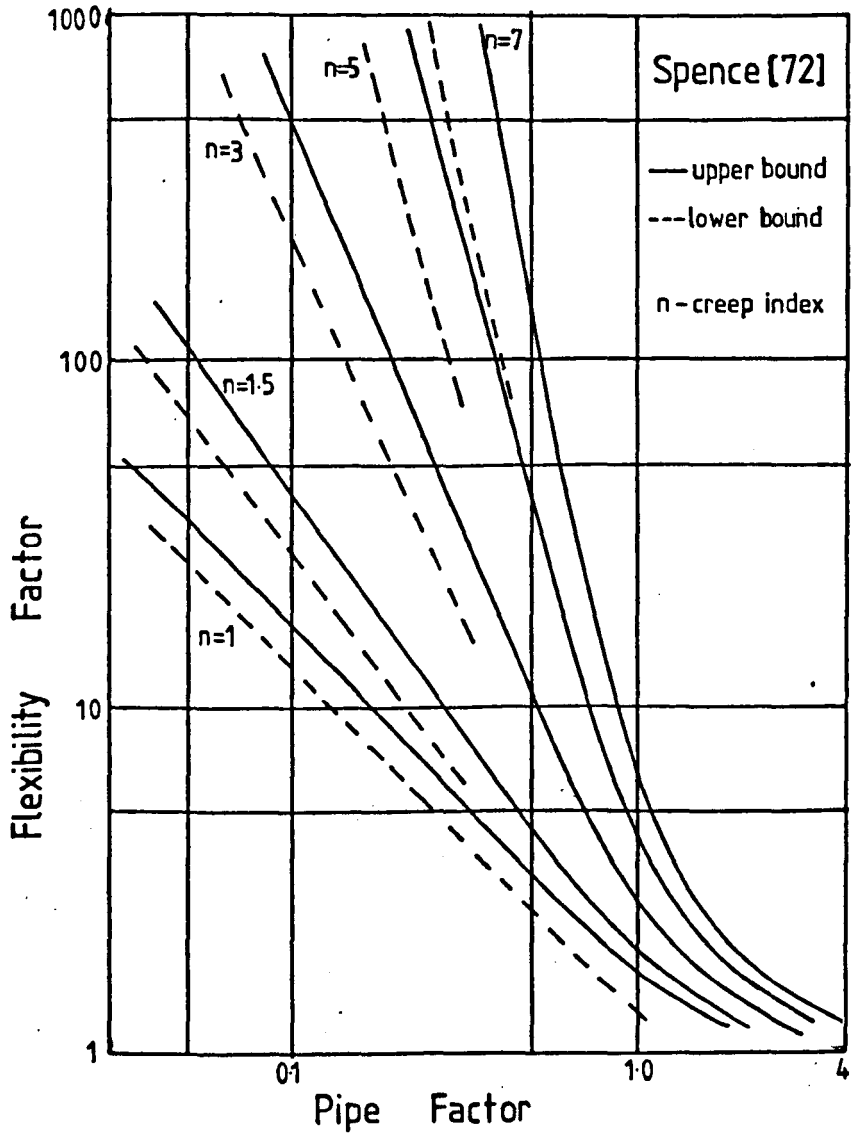

Pipe Bend Flexibility Factors in Creep

Figure (1.5)

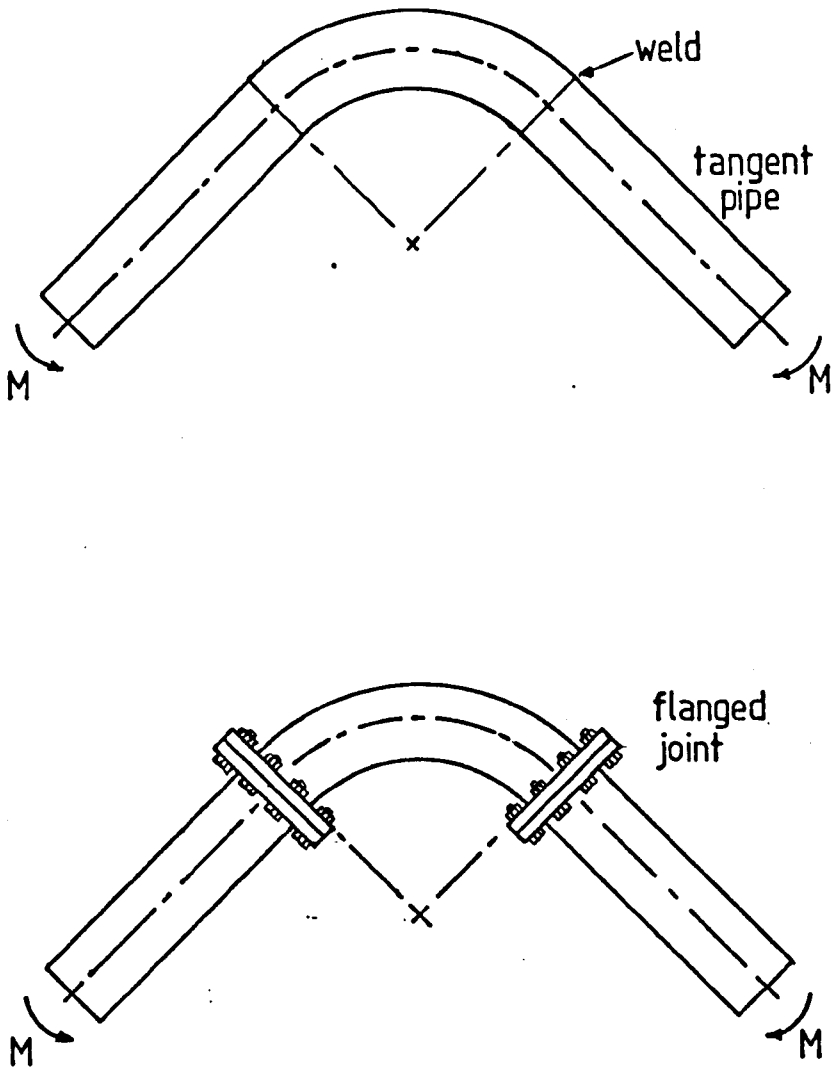

Typical end Constraints

Figure (1.6)

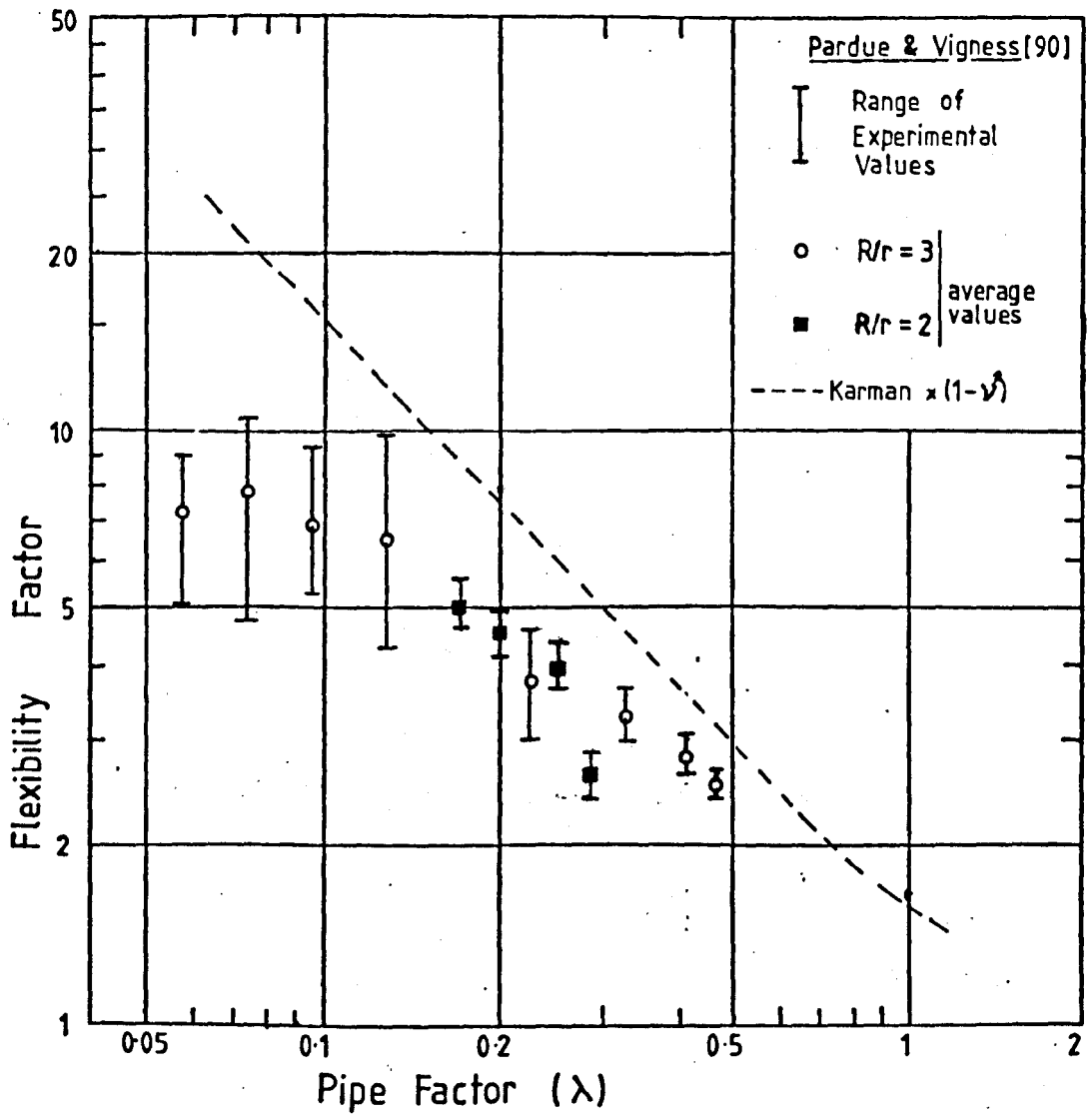

Typical Experimental Flexibility Factors From Pardue and Vigness For 90° Bends

Figure (1.7)

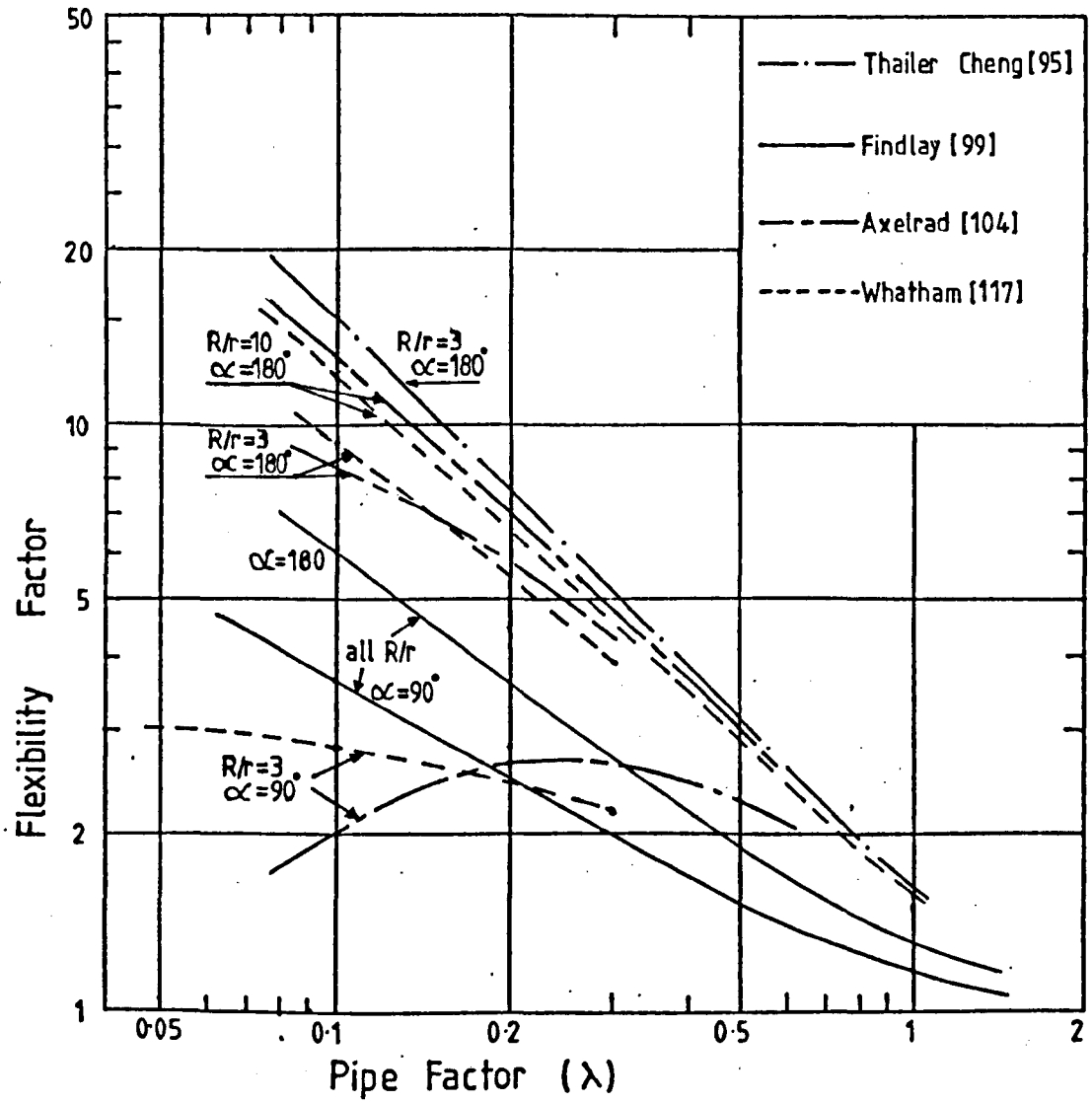

Comparison of Some Flexibility Factors From Flanged Bend Theories

Figure (1.8)

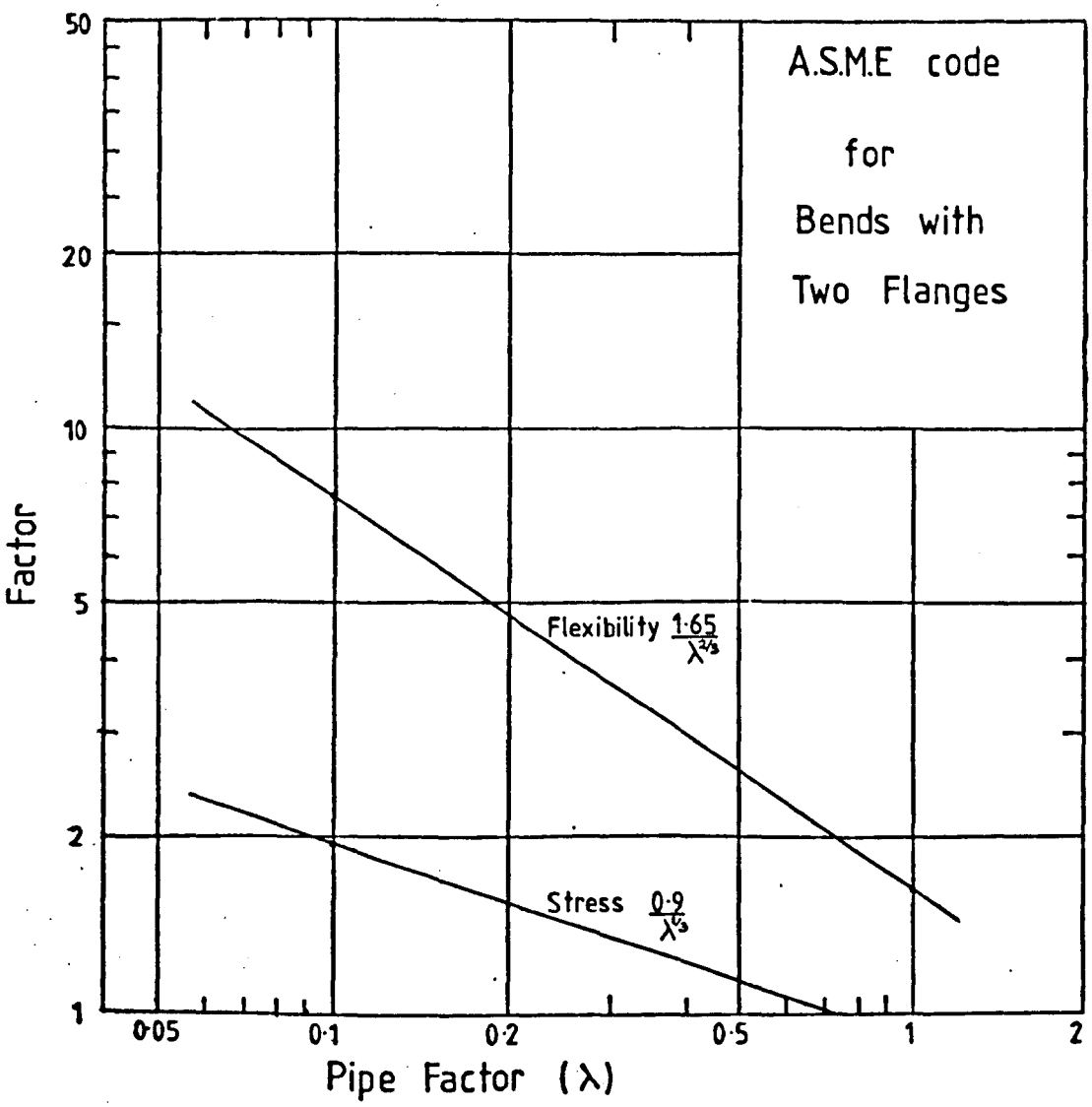

A.S.M.E Code for Bends with Two Flanges

Figure (1.9)

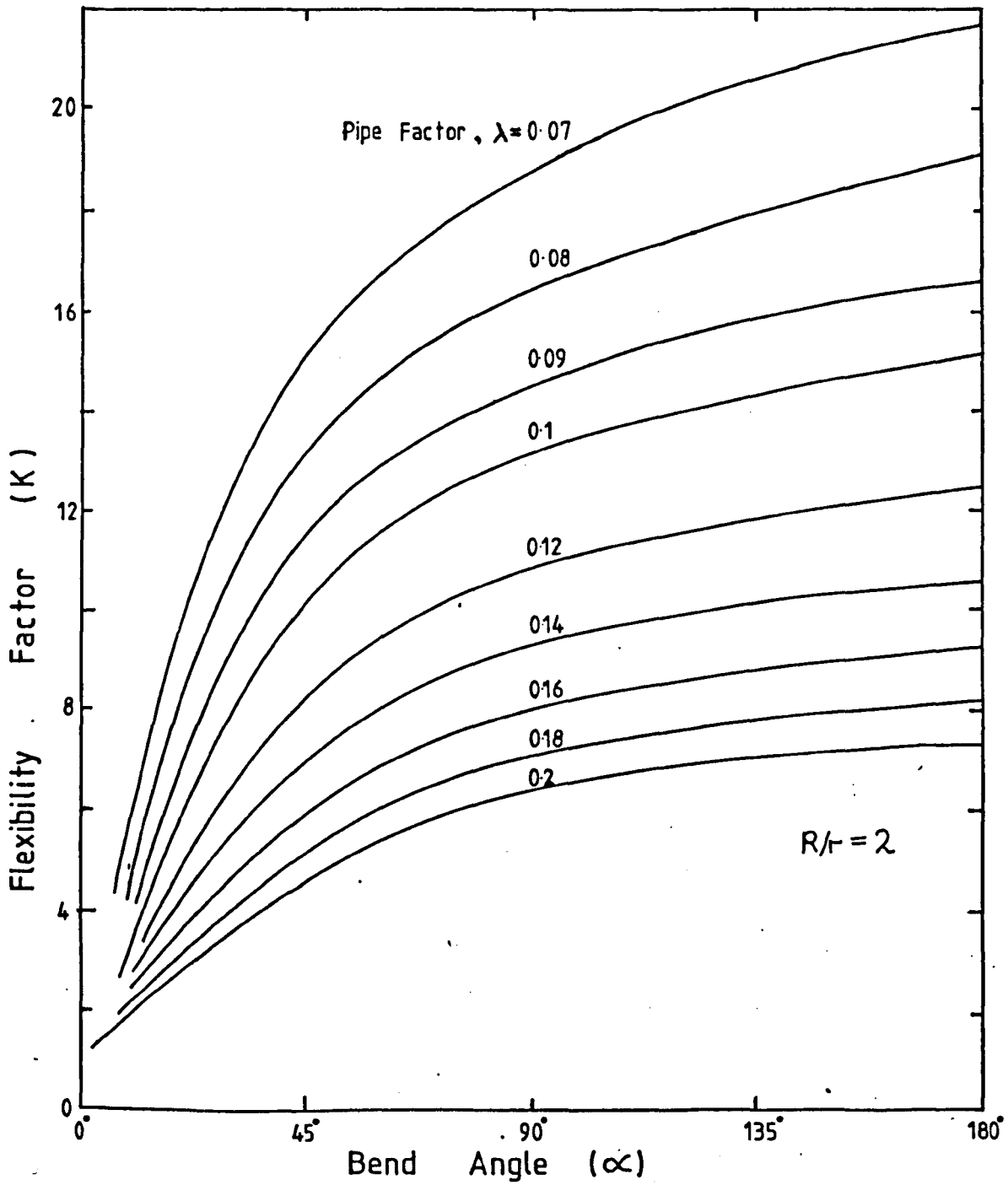

E.S.D.U. Recommendation for the Flexibility of Bends with Connected Tangent Pipes

Figure (1.10)

CHAPTER .2

BASIC THEORETICAL RELATIONSHIPS

Abstract

The present chapter is aimed at establishing the basic theoretical relationships which are required in the subsequent analyses.

Equations for a general shell in curvilinear orthogonal co-ordinates are described and an explanation is given of the choice of equations to be used herein. These are then converted to equations for a smooth pipe bend and a straight pipe.

The theorem of minimum total potential energy is outlined and its application using the Rayleigh-Ritz method discussed.

CHAPTER (2)

BASIC THEORETICAL RELATIONSHIPS

Abstract

(2.1) Pipes as Thin Shells

- (a) Introduction
- (b) Thin Shell Theory Assumptions
- (c) General Thin Shell Theory

(2.2) The Toroidal Shell or Smooth Pipe Bend

(2.3) The Cylindrical Shell or Straight Pipe

(2.4) Total Potential Energy

- (a) Principle of Minimum Total Potential Energy
- (b) Lower Bound on Flexibility

(2.1) Pipes as Thin Shells

(2.1a) Introduction

To quote Flügge [134] a shell is the "... materialization of a curved surface". Thus, the definition of a shell is strictly a matter of geometry and not of material. Typical examples of shells in everyday use are concrete roofs, water tanks, balloons and even parachutes.

Shell theory attempts to model a three-dimensional structure as a two-dimensional surface, mainly for simplicity since three-dimensional general solutions to elasticity problems are not easy.

The smooth pipe bend seems an ideal candidate for analysis using shell theory as it can be modelled as part of a toroid. Straight pipes can be examined as a cylindrical shell.

The principle of minimum total potential energy will be used later to solve the pipe bend problems. Although this technique only requires the strain-displacement and constitutive equations with the strain energy equation, the full set of shell equations will be given for completeness.

(2.1b) Thin Shell Theory Assumptions

The first set of basic equations governing the behaviour of thin shells were derived by Love [135]. These were later modified by Reissner [136] to form what is often referred to as the "classical" first approximation of shell theory. Love and those after him use several simplifying assumptions concerning the geometry and behaviour of the shell. These can be summarised as follows:

(1)/

(1) The thickness of the shell surface is small relative to its mean radius of curvature. Typically, the thickness should be less than a tenth of the mean radius although this is known to vary according to the problem being examined.

(2) Deflections of the shell surface are small. This limits the change in the shape of the shell between the unloaded and loaded shapes allowing the complete analysis to be performed on the original geometry of the shell.

(3) Stresses normal to the shell surface are negligible. This states that the normal (radial) stress is small relative to the stresses in the plane of the shell and also allows the use of the two-dimensional constitutive relations.

(4) Lines originally normal to the shell reference surface, remain normal to the deformed reference surface and unstrained. The reference surface is usually the mid-surface. This is analogous to the Euler hypothesis of "plane sections remain plane" in beam theory. It is sometimes referred to as the "hairbrush hypothesis". It should be emphasised that the 'plane sections' referred to are through the thickness of the shell surface and not through the cross-section as in beam theory. This assumption also implies that all the strain components, including shears, normal to the shell surface are negligible.

The theoretical work discussed herein is based on the equations correspondong to the first order linear theory of shells. Other higher order theories have been derived which remove some of the above assumptions ([137], [138]), but it has been established by many previous authors that the first order approximations give results which are suitable for most engineering applications.

(2.1c) General Thin Shell Theory

Love's original publication contained a number of inconsistencies. He omitted some small terms and retained others with the same order of magnitude. Several authors attempted to improve these equations but many of them retained a further deficiency in the relations between the forces and displacements. Eventually most of these problems were removed and a set of equations, derived independently by several authors, became "established". These equations can be found in the texts of Novozhilov [139], Kraus [140] and Dym [141] The author found the latter book to be an excellent introduction to the theory of thin shells.

Sanders [142] pointed out a further inconsistency in the "established" equations. He showed that they do not give zero strains for all rigid body displacements, except for spherical shells, flat plates or symmetrically loaded shells of revolution. The inconsistency occurred in the shear curvature term which makes its significance for most problems relatively small. Sanders removed this inconsistency using a method based on the principle of virtual work. His only change for the compatibility equations was in the shear curvature term.

Koiter [143] derived similar equations to those of Sanders which also gave zero strain for rigid body displacements. He concluded that the shear curvature inconsistency would only produce errors of the same order as those of the basic assumptions of shell theory.

Flügge [134] derived equations for particular classes of shells using a more physically intuitative approach which is more readable to non-mathematicians. However, his equations are different

to/

to most other works. The difference between Flügge and the others is also dependant on the class of shell (e.g. cylinder) which is being considered. Flügge also does not separate the bending and direct strains making comparison with other theories difficult. Dym [141] compares Flügge's equations for a cylinder with Donnell and Sanders [142] and concludes that Flügge's equations will differ in regions of rapid deformation change.

Goldenveizer [144] derived similar equations to Novozhilov but with a different shear curvature expression. He also substituted his strain-displacement equations into the equilibrium equations, using the constitutive relations, which gave the three differential equations, in terms of the shell displacements, that govern shell behaviour. This is the only text that the author has read in which these equations are given. A mention will be made later of the application of similar equations with the finite difference method.

Donnell [145], Mushtari [146] and Vlasov [147] derived an approximate set of equations which have become internationally known as the Donnell-Mushtari-Vlasov equations. These equations use only the radial displacement in the curvature strain terms. The benefit of this is that it produces relatively simple governing differential equations. These equations will be more justified the smaller the stresses due to the moments are in comparison with the stresses due to the forces. The present author has tried these equations with the 'classical' pipe bend problem. The flexibility of a typical bend with a pipe factor of 0.5. is underestimated by 25.5%.

Axelrad [104] derived equations for a class of shells which sustain membrane or slowly varying deformation in one direction and an/

an intensive variation in the orthogonal direction. These equations are particularly applicable to the pipe bend problem.

Some decision on the choice of equations to be used for the present project had to be made. The equations are the tools with which the problems will be solved and may affect the quality of the results. A version of the theory given by Novozhilov was chosen for its simplicity and consistency. It differs from the "established" version in the shear curvature and equilibrium equations. The equations give zero strain for all rigid body displacements and are simpler than the equations of Sanders.

In orthogonal curvilinear co-ordinates the strain-displacement relations for a general shell are:

$$\epsilon_1 = \frac{1}{A_1}\frac{\partial u_1}{\partial \alpha_1} + \frac{u_2}{A_1 A_2}\frac{\partial A_1}{\partial \alpha_2} + \frac{\omega}{R_1}$$

$$\epsilon_2 = \frac{1}{A_2}\frac{\partial u_2}{\partial \alpha_2} + \frac{u_1}{A_1 A_2}\frac{\partial A_2}{\partial \alpha_1} + \frac{\omega}{R_2}$$

$$K_1 = \frac{1}{A_1}\frac{\partial \beta_1}{\partial \alpha_1} + \frac{\beta_2}{A_1 A_2}\frac{\partial A_1}{\partial \alpha_2}$$

$$K_2 = \frac{1}{A_2}\frac{\partial \beta_2}{\partial \alpha_2} + \frac{\beta_1}{A_1 A_2}\frac{\partial A_2}{\partial \alpha_1}$$

$$W_1 = \frac{1}{A_1}\frac{\partial u_{\#2}}{\partial \alpha_1} - \frac{u_1}{A_1 A_2}\frac{\partial A_1}{\partial \alpha_2}$$

$$W_2 = \frac{1}{A_2}\frac{\partial u_{\#1}}{\partial \alpha_2} - \frac{u_2}{A_1 A_2}\frac{\partial A_2}{\partial \alpha_1}$$

$$\tau_1 = \frac{1}{A_1}\frac{\partial \beta_2}{\partial \alpha_1} - \frac{\beta_1}{A_1 A_2}\frac{\partial A_{\#1}}{\partial \alpha_{\#2}}$$

$$\tau_2 = \frac{1}{A_2}\frac{\partial \beta_1}{\partial \alpha_2} - \frac{\beta_2}{A_1 A_2}\frac{\partial A_2}{\partial \alpha_1}$$

where

$$\beta_1 = \frac{u_1}{R_1} - \frac{1}{A_1}\frac{\partial \omega}{\partial \alpha_1}$$

$$\beta_2 = \frac{u_2}{R_2} - \frac{1}{A_2}\frac{\partial \omega}{\partial \alpha_2} \qquad \ldots (2.1)$$

β_1 and β_2 are the rotations of the mid-surface normal in directions 1 and 2 respectively.

ϵ_1 and ϵ_2 are the mid-surface strains in directions '1' and '2' respectively. K1 and K_2 are the curvatures in directions '1' and '2'. The problem of consistency, mentioned earlier, arises from the combination of W1, W2, γ_1 and γ_2 to give the mid surface shear strain, W, and the shear curvature, γ . W is usually found from,

$$W = W_1 + W_2 \qquad \ldots (2.2)$$

Novozhilov gives two definitions of the shear curvature, i.e.

$$\gamma = \gamma_1 + \gamma_2 \qquad \ldots (2.3)$$

$$\gamma^* = \gamma_1 + \frac{W_2}{R_1} = \gamma_2 + \frac{W_1}{R_2} \qquad \ldots (2.4)$$

In deriving the equilibrium equations, using the principle of minimum total potential energy (e.g. see Dym [141 pp. 28-33]), γ^* is normally used together with the stress variables,

$$S = N_{12} - \frac{M_{21}}{R_2} = N_{21} - \frac{M_{12}}{R_1}$$

$$H = \tfrac{1}{2}(M_{12} + M_{21}) \qquad \ldots (2.5)$$

This gives a variationally consistent set of equations which also satisfy the conditions of zero strain for all rigid body displacements. Unfortunately, the shear stress resultants N12 , N21, M12 and M21 cannot be obtained from simply knowing W and γ^*. This will only be

a/

a problem if N_{12}, N_{21}, M_{12} and M_{21} are required explicitly, in many situations, including the one to be considered herein, they are not, and S and H are sufficient. Novozhilov, Dym and Kraus go on to show that taking the alternative definition for the shear curvature, $\tau = \tau_1 + \tau_2$, allows N_{12}, N_{21}, M_{12} and M_{21} to be found from

$$N_{12} = N_{21} = \frac{Et}{2(1+\nu)} W$$

$$M_{12} = M_{21} = \frac{Et^3}{24(1+\nu)} \tau \qquad \ldots (2.6)$$

This is the definition used in the "established" equations, which is variationally consistent but does not produce zero strains for a rigid body rotation (Dym [141] p. 42) .

The (2.4) τ^* definition will be used from here on since N_{12}, N_{21}, M_{12} and M_{21} will not be required explicitly. It should be noted that these can be found approximately using the following equations,

$$N_{12} = \frac{Et}{2(1+\nu)}\left(W + \frac{t^2}{6R_2}\tau^*\right)$$

$$N_{21} = \frac{Et}{2(1+\nu)}\left(W + \frac{t^2}{6R_1}\tau^*\right)$$

$$M_{12} = M_{21} = \frac{Et^3}{12(1+\nu)} \tau^* \qquad \ldots (2.7)$$

The error in these equations is of the same order as the original assumptions of thin shell theory.

The constitutive relations corresponding to the above definition, with a constant shell thickness, for a linear isotropic material, are

$$N_1 = C(\epsilon_1 + \nu\epsilon_2) \quad , \quad M_1 = D(K_1 + \nu K_2)$$

$$N_2 = C(\epsilon_2 + \nu\epsilon_1) \quad , \quad M_2 = D(K_2 + \nu K_1)$$

$$S = (1-\nu)\tfrac{1}{2} C W \quad , \quad H_2 = (1-\nu) H \tau^*$$

where

$$C = \frac{Et}{(1-\nu^2)} \qquad D = \frac{Et^3}{12(1-\nu^2)}$$

... (2.8)

The corresponding equations of equilibrium are,

$$\frac{\partial(A_2 N_1)}{\partial \alpha_1} + \frac{\partial(A_1 S)}{\partial \alpha_2} + \left(\frac{\partial A_1}{\partial \alpha_2}\right) S - \left(\frac{\partial A_2}{\partial \alpha_1}\right) N_2 +$$

$$+ \frac{1}{R_1}\left[\frac{\partial(A_2 M_1)}{\partial \alpha_1} - \left(\frac{\partial A_2}{\partial \alpha_1}\right) M_2 + 2\frac{\partial(A_1 H)}{\partial \alpha_2} + 2\frac{R_1}{R_2}\left(\frac{\partial A_1}{\partial \alpha_2}\right) H\right] = -A_1 A_2 q_1$$

$$\frac{\partial(A S)}{\partial \alpha_1} + \frac{\partial(A_1 N_2)}{\partial \alpha_2} + \left(\frac{\partial A_2}{\partial \alpha_1}\right) S - \left(\frac{\partial A_1}{\partial \alpha_2}\right) N_1 +$$

$$+ \frac{1}{R_2}\left[\frac{\partial(A_1 M_2)}{\partial \alpha_2} - \left(\frac{\partial A_1}{\partial \alpha_2}\right) M_1 + 2\frac{\partial(A_2 H)}{\partial \alpha_1} + 2\frac{R_2}{R_1}\left(\frac{\partial A_2}{\partial \alpha_1}\right) H\right] = -A_1 A_2 q_2$$

$$\left(\frac{N_1}{R_1} + \frac{N_2}{R_2}\right) - \frac{1}{A_1 A_2}\left\{\frac{\partial}{\partial \alpha_1}\frac{1}{A_1}\left[\frac{\partial(A_2 M_1)}{\partial \alpha_1} + \frac{\partial(A_1 H)}{\partial \alpha_2} + \left(\frac{\partial A_1}{\partial \alpha_2}\right) H - \left(\frac{\partial A_2}{\partial \alpha_1}\right) M_2\right] +\right.$$

$$\left. + \frac{\partial}{\partial \alpha_2}\frac{1}{A_2}\left[\frac{\partial(A_2 H)}{\partial \alpha_1} + \frac{\partial(A_1 M_2)}{\partial \alpha_2} + \left(\frac{\partial A_2}{\partial \alpha_1}\right) H - \left(\frac{\partial A_1}{\partial \alpha_2}\right) M_1\right]\right\} = q_n$$

... (2.9)

The established shell theory has six equations of equilibrium. However, these can be reduced to three equations similar to the above by substitution for the normal shear force resultants.

The necessary boundary conditions for the solution of these equations are, at constant α_1 specify,

N_1	or	u_1
$S + \frac{2H}{R_2}$	or	u_2
$\frac{1}{A_1 A_2}\left(2\frac{\partial(A_1 H)}{\partial \alpha_2} + \frac{\partial(A_2 M_1)}{\partial \alpha_1} - \left(\frac{\partial A_2}{\partial \alpha_1}\right) M_2\right)$	or	w
M_1	or	β_1

at constant α_2 specify,

N_2	or	u_2
$S + \frac{2H}{R_1}$	or	u_1
$\frac{1}{A_1 A_2}\left(2\frac{\partial(A_2 H)}{\partial \alpha_1} + \frac{\partial(A_1 M_2)}{\partial \alpha_2} - \left(\frac{\partial A_1}{\partial \alpha_2}\right) M_1\right)$	or	w
M_2	or	β_2

... (2.10)

The strain energy equation consistent with the above equations, for a constant thickness, linear isotropic material is,

$$U = \frac{C}{2}\int\int\left[(\epsilon_1+\epsilon_2)^2 - 2(1-\nu)\left(\epsilon_1\epsilon_2 - \frac{w^2}{4}\right)\right] A_1 A_2 \, d\alpha_1 \, d\alpha_2$$

$$+ \frac{D}{2}\int\int\left[(K_1+K_2)^2 - 2(1-\nu)(K_1K_2 - \tau^{*2})\right] A_1 A_2 \, d\alpha_1 \, d\alpha_2 \qquad \ldots (2.11)$$

The assumption that t/R_i can be neglected with respect to one, was used in the derivation of the above equation. This limits its use to thin shells.

(2.2) The Toroidal Shell or Smooth Pipe Bend

The general equations need to be converted to the specific case of a toroidal shell for the analysis of the smooth pipe bend. The geometry of the smooth pipe bend is given in Fig. 2.1.

The first fundamental form of the mid-surface of a shell element in curvilinear co-ordinate is,

$$(dS)^2 = A_1^2 (d\alpha_1)^2 + A_2^2 (d\alpha_2)^2$$

The corresponding equation for an element in the new (ϕ,θ) co-ordinate system is

$$(dS)^2 = r^2 (d\phi)^2 + R'^2 (d\theta)^2 \qquad , \; R' = R + r\sin\phi$$

Principal radii of curvature in the curvilinear system are R_1 and R_2; these become r and $R'/\sin\phi$ in the (ϕ,θ) co-ordinate system.

Curvilinear displacements U_1, U_2 and ω become v, u and ω in the (ϕ,θ) system.

Conversion of the curvilinear system to the (ϕ,θ) system therefore requires,

$$\begin{array}{lll} \alpha_1 = \phi & A_1 = r & R_1 = r \\ \alpha_2 = \theta & A_2 = R' & R_2 = R'/\sin\phi \\ u_1 = v & u_2 = u & \omega = \omega \end{array} \qquad \ldots (2.12)$$

Thus, the governing equations for part of a toroidal shell or pipe bend having a constant radius of cross-section r , are obtained by substituting equations (2.12) into (2.1-11). This gives:-

Strain Displacement Equations,/

Strain Displacement Equations,

$$\epsilon_\phi = \frac{1}{r}\left(\frac{\partial v}{\partial \phi} + w\right)$$

$$\epsilon_\theta = \frac{1}{R'}\left(\frac{\partial u}{\partial \theta} + v \sin\phi + w \cos\phi\right)$$

$$\gamma_{\theta\phi} = \frac{1}{R'}\left(\frac{\partial v}{\partial \theta} - u\cos\phi + \frac{R'}{r}\frac{\partial u}{\partial \phi}\right)$$

$$K_\phi = \frac{1}{r^2}\left(\frac{\partial v}{\partial \phi} - \frac{\partial^2 w}{\partial \phi^2}\right)$$

$$K_\theta = \frac{1}{R'^2}\left(\frac{\partial u}{\partial \theta}\sin\phi - \frac{\partial^2 w}{\partial \theta^2} + \frac{R'\cos\phi}{r}\left(v - \frac{\partial w}{\partial \phi}\right)\right)$$

$$K_{\theta\phi} = \frac{1}{rR'}\left(\frac{\partial u}{\partial \phi}\sin\phi + \frac{\partial v}{\partial \theta} - \frac{\partial^2 w}{\partial \theta \partial \phi} + \frac{r\cos\phi}{R'}\left(\frac{\partial w}{\partial \theta} - u\sin\phi\right)\right)$$

where

$$R' = R + r\sin\phi \qquad \text{... (2.13)}$$

(Note:- $\gamma_{\theta\phi} \equiv W_{,}$, $K_{\theta\phi} \equiv \tau^*$)

Constitutive Relations,

$$N_\phi = C(\epsilon_\phi + \nu\epsilon_\theta) \qquad N_\theta = C(\epsilon_\theta + \nu\epsilon_\phi)$$

$$M_\phi = D(K_\phi + \nu K_\theta) \qquad M_\theta = D(K_\theta + \nu K_\phi)$$

$$S = \tfrac{1}{2}(1-\nu)C\gamma_{\theta\phi} \qquad H = (1-\nu)D K_{\theta\phi}$$

where ... (2.14)

$$C = \frac{Et}{(1-\nu^2)} \qquad D = \frac{Et^3}{12(1-\nu^2)}$$

Equilibrium Equations,

$$\frac{\partial(R'N_\phi)}{\partial\phi} + r\frac{\partial S}{\partial\theta} - N_\theta r\cos\phi + \frac{1}{r}\frac{\partial(R'M_\phi)}{\partial\phi} - M_\theta\cos\phi + 2\frac{\partial H}{\partial\theta} = -rR'q_\phi$$

$$\frac{\partial(R'S)}{\partial\phi} + r\frac{\partial N_\theta}{\partial\theta} + Sr\cos\phi + \frac{r\sin\phi}{R'}\frac{\partial M_\theta}{\partial\theta} + \frac{2\sin\phi}{R'}\frac{\partial(R'H)}{\partial\phi} + 2H\cos\phi = -rR'q_\theta$$

$$(-R'N_\phi - r\sin\phi N_\theta) + \frac{1}{r}\frac{\partial^2(R'M_\phi)}{\partial\phi^2} + 2\frac{\partial H}{\partial\theta\partial\phi} - \frac{\partial(M_\theta\cos\phi)}{\partial\phi} +$$

$$+ \frac{r}{R'}\frac{\partial^2 M_\theta}{\partial\theta^2} + 2\frac{r\cos\phi}{R'}\frac{\partial H}{\partial\theta} = -rR'q_n \qquad \text{... (2.15)}$$

Strain Energy (constant thickness),

$$U = \frac{C}{2}\int\int\left[(\epsilon_\phi+\epsilon_\theta)^2-2(1-\nu)\left(\epsilon_\phi\epsilon_\theta-\frac{\gamma_{\theta\phi}^2}{4}\right)\right] r R' d\theta d\phi$$

$$+\frac{D}{2}\int\int\left[(K_\phi+K_\theta)^2-2(1-\nu)\left(K_\phi K_\theta-K_{\theta\phi}^2\right)\right] r R' d\theta d\phi \qquad \ldots(2.16)$$

Boundary Conditions necessary for a solution are;

at constant ϕ, specify,

N_ϕ	or	v
$S+\frac{2H}{R'}\sin\phi$	or	u
$\frac{2}{r}\frac{\partial H}{\partial\theta}+\frac{1}{r}\frac{\partial M_\phi}{\partial\phi}-M_\theta r\cos\phi$	or	ω
M_ϕ	or	β_ϕ

at constant θ, specify,

N_θ	or	u
$S+\frac{2H}{r}$	or	v
$\frac{2}{rR'}\frac{\partial(R'H)}{\partial\phi}+\frac{1}{R'}\frac{\partial M_\theta}{\partial\theta}$	or	ω
M_θ	or	β_θ

where

$$\beta_\phi = \frac{1}{r}\left(v-\frac{\partial\omega}{\partial\phi}\right) \qquad \ldots(2.17)$$

and

$$\beta_\theta = \frac{1}{R'}\left(u\sin\phi-\frac{\partial\omega}{\partial\theta}\right) \qquad \ldots(2.18)$$

The θ and ϕ directions will be termed the circumferential and meridional directions respectively.

(2.3) The Cylindrical Shell or Straight Pipe

The straight pipe may be considered as a cylindrical shell. The geometry of straight pipe is shown in Fig. 2.

The first fundamental form of the mid-surface of a cylindrical shell in the (ϕ, x) system is,

$$(ds)^2 = r^2(d\phi)^2 + (dx)^2$$

The meridional radius of curvature r will be taken as a constant along the length of the pipe.

Conversion of the curvilinear system to the (ϕ, x) system requires the following:

$$\alpha_1 = \phi \qquad A_1 = r \qquad R_1 = r$$

$$\alpha_2 = x \qquad A_2 = 1 \qquad R_2 d\phi \to dx \text{ as } R_2 \to \infty ; \phi \to \frac{\pi}{2}$$

$$u_1 = v \qquad u_2 = u \qquad \omega = \omega$$

... (2.19)

Therefore, the governing equations for a straight pipe of constant cross-section radius, r :

Strain Displacement Equations,

$$\epsilon_\phi = \frac{1}{r}\left(\omega + \frac{\partial v}{\partial \phi}\right) \qquad K_\phi = \frac{1}{r^2}\left(\frac{\partial v}{\partial \phi} - \frac{\partial^2 \omega}{\partial \phi^2}\right)$$

$$\epsilon_x = \frac{\partial u}{\partial x} \qquad K_x = -\frac{\partial^2 \omega}{\partial x^2}$$

$$\gamma_{x\phi} = \frac{\partial v}{\partial x} + \frac{1}{r}\frac{\partial u}{\partial \phi} \qquad K_{x\phi} = \frac{1}{r}\left(\frac{\partial v}{\partial x} - \frac{\partial^2 \omega}{\partial x \partial \phi}\right)$$

(Note: $\gamma_{x\phi} \equiv W_{12}$, $K_{x\phi} \equiv \tau^*$)

... (2.20)

Constitutive Relations,/

Constitutive Relations,

$$N_\phi = C(\epsilon_\phi + \nu \epsilon_x) \qquad M_\phi = D(K_\phi + \nu K_x)$$

$$N_x = D(\epsilon_x + \nu \epsilon_\phi) \qquad M_x = D(K_x + \nu K_\phi)$$

$$S = \frac{(1-\nu)}{2} C \gamma_{x\phi} \qquad H = (1-\nu) D K_{x\phi}$$

where ... (2.21)

$$C = \frac{Et}{(1-\nu^2)} \qquad D = \frac{Et^3}{12(1-\nu^2)}$$

Equilibrium Equations,

$$\frac{1}{r}\frac{\partial N_\phi}{\partial \phi} + \frac{\partial S}{\partial x} + \frac{1}{r^2}\frac{\partial M_\phi}{\partial \phi} + 2\frac{\partial H}{\partial x} = -q_\phi$$

$$\frac{1}{r}\frac{\partial S}{\partial \phi} + \frac{\partial N_x}{\partial x} = -q_x$$

$$-\frac{N_\phi}{r} + \frac{1}{r^2}\frac{\partial^2 M_\phi}{\partial \phi^2} + \frac{2}{r}\frac{\partial H}{\partial \phi \partial x} + \frac{\partial^2 M_x}{\partial x^2} = -q_n \qquad \text{... (2.22)}$$

Strain Energy, (constant thickness),

$$U = \frac{C}{2}\iint \left[(\epsilon_\phi + \epsilon_x)^2 - 2(1-\nu)\left(\epsilon_\phi \epsilon_x - \frac{\gamma_{x\phi}^2}{4}\right)\right] r\, dx\, d\phi$$
$$+ \frac{D}{2}\iint \left[(K_\phi + K_x)^2 - 2(1-\nu)(K_\phi K_x - K_{x\phi}^2)\right] r\, dx\, d\phi$$

... (2.23)

Boundary Conditions necessary for a solution,

at constant ϕ, specify

N_ϕ	or	v
S	or	u
$\frac{2}{r}\frac{\partial H}{\partial x} + \frac{\partial M_\phi}{\partial \phi}$	or	ω
M_ϕ	or	β_ϕ

at constant X, specify

$$N_x \quad \text{or} \quad u$$
$$S + \frac{2H}{r} \quad \text{or} \quad v$$
$$\frac{2}{r}\frac{\partial H}{\partial \phi} + \frac{\partial M_x}{\partial x} \quad \text{or} \quad \omega$$
$$M_x \quad \text{or} \quad \beta_x$$

... (2.24)

where

$$\beta_\phi = \frac{1}{r}\left(v - \frac{\partial \omega}{\partial \phi}\right) \qquad \beta_x = -\frac{\partial \omega}{\partial x}$$

(2.4a) Principle of Minimum Total Potential Energy

The principle of minimum total potential energy can be expressed as,

$$\int_V U(\epsilon^*)dV - \int_{S(P)} P\delta^* dS \geq \int_V U(\epsilon)dV - \int_{S(P)} P\delta\, dS \quad \ldots (2.25)$$

where

$\int_V U(\epsilon^*)\,dV$	is the total strain energy of a compatible strain field ϵ^*.
$\int_{S(P)} P\delta^* dS$	is the potential energy of the applied forces where δ^* is the associated compatible displacement of the load. S(P) denotes integration over the surface where the loads are applied.
$\int_V U(\epsilon)dV$	is the exact strain energy of the true strain field, ϵ.
$\int_{S(P)} P\delta\, dS$	is the potential energy of the applied forces where δ is the associated true displacement.

In the form presented above, the theorem states that the total energy associated with an arbitrarily assumed compatible strain and displacement field is always greater than or equal to the energy associated with the corresponding true strain and displacement field. This is true only if the assumed strains and displacements satisfy compatibility. Thus the total energy is only a minimum at the true state.

Use of this theorem is made by prescribing displacements as a series of terms each of which is made up of a function multiplied by a coefficient. Each function must satisfy internal compatibility and/

and the kinematic boundary conditions i.e. external compatibility. The values of the coefficients, and hence the true displacements, are obtained by finding the combination of the coefficients which give the minimum of the total potential energy function.

This is the basis of the Rayleigh-Ritz technique. The displacements are expressed as a series of trigonometric functions e.g.

$$\delta = C_1 \sin\frac{\pi x}{\ell} + C_2 \sin\frac{2\pi x}{\ell} + C_3 \sin\frac{3\pi x}{\ell} + \ldots \text{etc.}$$

If each of these terms satisfies compatibility for some problem, then

$$\delta = \sum_{n=1}^{\infty} C_n \sin\left(\frac{n\pi x}{\ell}\right) \quad , \quad n = 1,2,3,4,\ldots,\infty$$

must be the actual displacement state (providing all possible trigonometric functions satisfying the boundary conditions are included in the summation). To determine the C_n coefficients the total potential energy (T.P.E.), V, is expressed as a function of δ and hence of the coefficients. The solution to the problem is found by minimising the T.P.E., hence

$$\frac{\partial V}{\partial \delta} = 0$$

therefore,

$$\frac{\partial V}{\partial C_1} = \frac{\partial V}{\partial C_2} = \frac{\partial V}{\partial C_3} = \ldots\ldots = \frac{\partial V}{\partial C_n} = 0$$

since a variation with respect to δ will be equivalent to the variation with respect to each of the individual coefficients. Usually, each of the variations with respect to each coefficient produces an equation involving the other coefficients and the equations need to be solved simultaneously.

In practice, a finite number of terms in the displacement series/

series is usually sufficient as higher order terms rapidly become negligible.

Only the exact displacements give the true minimum of the T.P.E. and therefore corresponds to true equilibrium. Each displacement component contributes to the final equilibrium state and hence truncating the series after a finite number of terms gives partial equilibrium.

(2.4b) Lower Bound on Flexibility

Frequently for the application of the total potential energy theorem, recourse is made to a "displacement prescribed" type of solution i.e. one where the selected compatibility component (δ^*) is identical to the exact displacement (δ). For this particular case, it follows from(2.25) that,

$$\int_v U(\epsilon^*)\,dV \geqslant \int_v U(\epsilon)\,dV \qquad \ldots (2.26)$$

The equality only holds when the strain and displacement choices are exact.

If a structure is subjected to a single load then, from the principle of energy conservation, the strain energy will be equal to the work done by the external load increasing uniformly from zero. If the load is increased to the value P , where the displacement is equal to the prescribed displacement , then this can be written as,

$$\int_v U(\epsilon^*)\,dV = \tfrac{1}{2} P^* \delta \qquad \ldots (2.27)$$

The true state is,

$$\int_v U(\epsilon)\,dV = \tfrac{1}{2} P \delta \qquad \ldots (2.28)$$

Equations (2.27) and (2.28) can be combined using (2.26) to give,

$$P^* \geqslant P \tag{2.29}$$

i.e. the calculated load from an approximate solution is always greater than the exact load. The flexibility of a structure is inversely proportional to the applied load (since $P = \delta/F$, where F is the flexibility). Therefore, from (2.29), the flexibility of a structure must be underestimated. Thus a "lower bound" is obtained on the value of the flexibility from a minimum total potential energy analysis. This is not always true for more complex loading. Deflections and stresses away from the load point are not bounded.

The lower bound on flexibility will be useful in the study of pipe bends. Convergence of series solution can be examined since the addition of further terms to the series will increase the bend flexibility. Terms can be added until the change in the flexibility is less than some arbitrary quantity, say 1%.

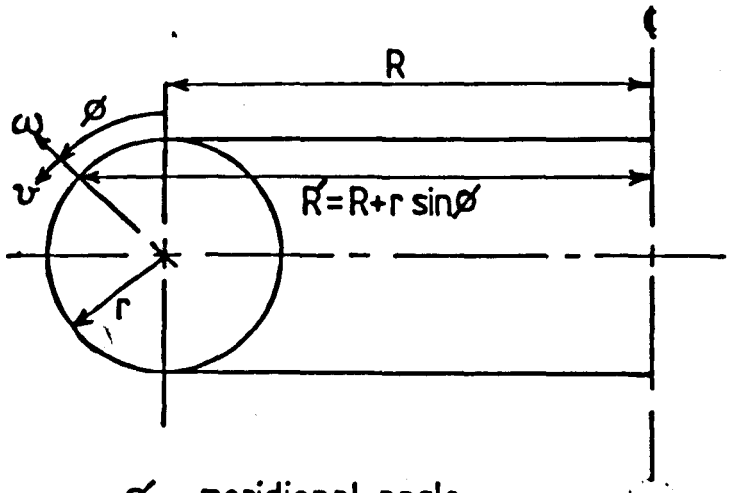

ø meridional angle

θ circumferential angle

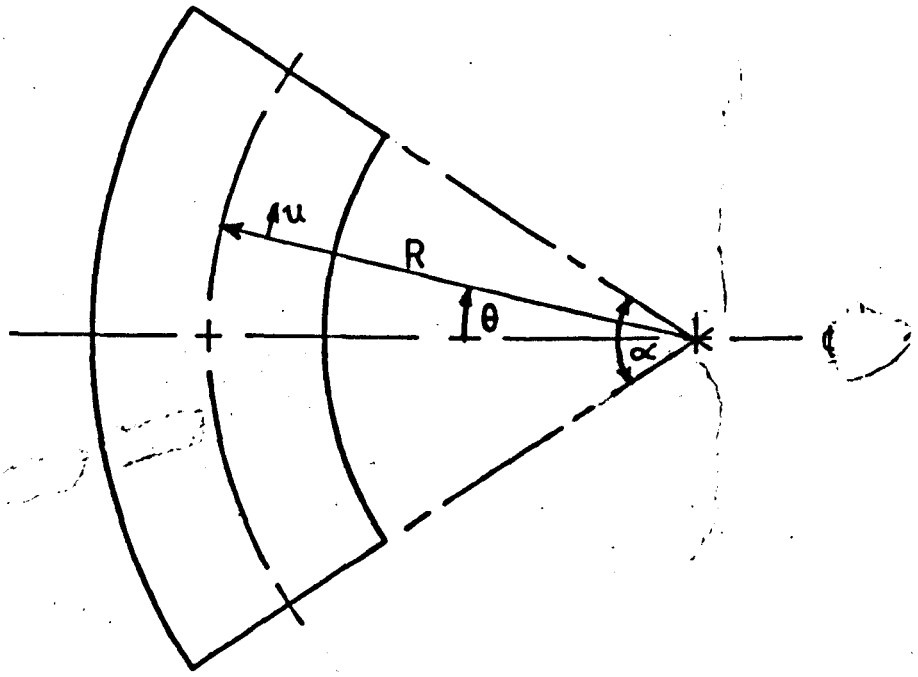

Geometry of the Smooth Pipe Bend

Fig. 2.1

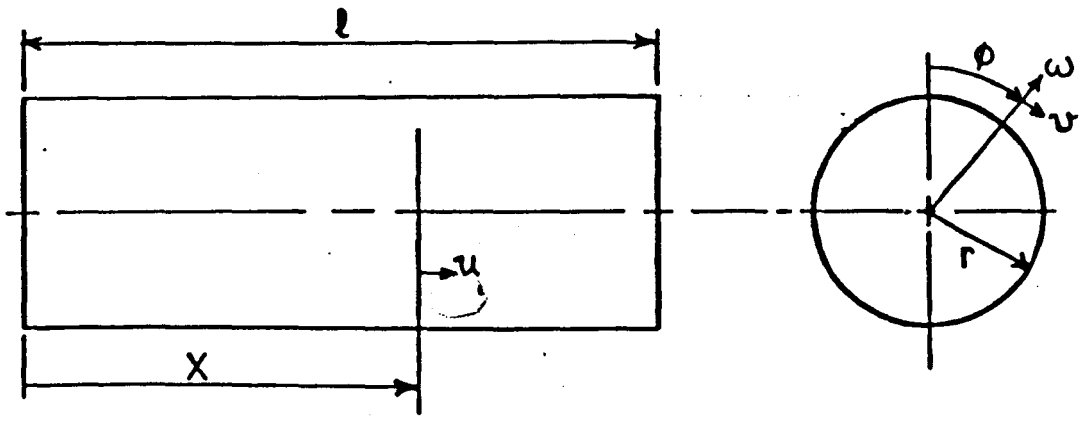

Geometry of the Straight Pipe

Fig 2.2

CHAPTER .3

THEORETICAL ANALYSIS OF A SMOOTH PIPE BEND WITH FLANGED END CONSTRAINTS UNDER IN-PLANE BENDING

Abstract

Theoretical solutions to the problem of a smooth pipe bend with flanged end constraints under in-plane bending are presented.

General displacements in the form of fourier series are suggested which satisfy internal and external compatibility. Strains are then derived using the strain-displacement equations.

Two solutions methods are first presented which use a simplified form of the displacements and strains together with hand integration of the total potential energy expression. The two methods differ in their inherent assumptions. The results of both methods are discussed and a comparison with other theoretical methods presented.

A numerical solution is then presented which uses the complete strains and displacements with few assumptions, excepting those of the thin shell theory. The results are then discussed and compared to other solutions. Finally flexibility and stress concentration factors are given for a wide range of practical bend geometries.

CHAPTER (3)

THEORETICAL ANALYSIS OF A SMOOTH PIPE BEND WITH FLANGED END CONSTRAINTS UNDER IN-PLANE BENDING

Abstract

(3.1) Introduction

(3.2) Displacements

- (a) Displacement Formulation
- (b) Rigid Section Displacements
- (c) Distortion Displacements
- (d) Radial Distortion Displacement
- (e) Meridional Tangential Distortion Displacement
- (f) Circumferential Tangential Distortion Displacement
- (g) Distortion Displacement Summary
- (h) Total Displacements

(3.3) Strains

(3.4) Solutions Using Hand Integration

- (a) Method no. 1
- (b) Method no. 2
- (c) Flexibility Factors from Methods 1 and 2.

(3.5)/

(3.5) Method No. 3 - Numerical Solution

(a) Introduction

(b) Numerical Solution Methods

(c) Minimisation Procedure

(d) Numerical Integration

(e) Solution of Matrix Equation

(f) Total Potential Energy

(g) Deformations

(h) Flexibility Factors

(i) Stress Concentration Factors

(3.6) Theoretical Results from Method No. 3

(a) Presentation of Results

(b) Integration Convergence

(c) Series Convergence

(d) Displacement Coefficients

(e) Flexibility Factors from Method No. 3

(f) Stress Concentration Factors from Method No. 3

(3.7) General Comments on the Results of Method No. 3

(3.1) Introduction

As mentioned in chapter 1, the study of the smooth pipe bend with flanged ends under in-plane bending has attracted the attention of a number of authors, but each has produced results which differ widely from the others.

The aim of the present work is to resolve this dilemma by highlighting the limitations and errors in some of these works and to develop a method which removes some of the problems by making as few assumptions as possible. The development of this method will be explained in some detail and at appropriate points it will be compared to the other works to illustrate the problems therein.

The first task undertaken was that of repeating the work of Findlay [99]. This proved to be both time consuming and difficult for various reasons, even with the help of G. Findlay himself (for which the author is grateful). His equation for the total potential energy unfortunately contains an error. The term,

$$\sum_{J}^{m} C_{J1}\left(1 + 3/8 \sum_{k}^{} D_k\right)$$

at the bottom of page 156 of [99] should be

$$\sum_{J}^{m} \bar{C}_{J1}\left(1 + 3/8\ D_J\right)$$

The equation was programmed on a computer and the results were compared with Findlay's. With the correction, the results were exactly the same as those of Findlay when up to three terms were used in each displacement series. With more than three terms in each series the results radically differed. The present author's results/

results demonstrated convergence within 1% with three terms in each series but Findlay's results converged, in some cases, by at least a further 100% and required up to six terms in each series. Several different solution procedures were used at this stage in an attempt to obtain Findlay's results but these proved unsuccessful. Eventually, it was concluded that the cause of the difference was probably due to Findlay having used two different solution procedures, one for three or less terms in each series and a second for use with more terms. The second procedure must have contained an error, but this could not be absolutely confirmed as Findlay's computer program could not be found. The "correct" set of Findlay's flexibility factors are given in fig. (3.1). These results are virtually the same as those given by Findlay with three terms in each series.

The corrected results still did not compare with the results of Thailer and Cheng [95], in fact the difference was now larger. At this point, several of the assumptions of Findlay were removed. The assumption of $\frac{r}{R}\sin\phi \ll 1$ was reduced to $(\frac{r}{R}\sin\phi)^2 << 1$ using a binomial expansion and the circumferential and shear curvatures were included in the analysis. This only changed Findlay's corrected flexibilities by about 5%. Various changes were made to Findlay's "primary displacements" but the flexibility factors never changed by more than 5%.

Thailer and Cheng's analysis was similar to Findlay's but, they ignored the contribution of the shear strain in their expression for the total potential energy. Their results were almost the same as Karman's [2], which did not include end effects. Thailer/

Thailer and Cheng's analysis was repeated with the shear strain included, but with the assumption $(\frac{r}{R}\sin\phi)^2 \ll 1$. This gave flexibilities which were about 30% higher than Findlay's (Fig. 3.2). Thailer and Cheng's assumed displacements do not contain the boundary condition of zero slope at the flange (this will be more fully explained later) whereas Findlay's displacements do. Physically, this can be interpreted as meaning that Thailer and Cheng's displacements are for a thin flange whereas Findlay's displacements are for a thick or rigid flange. This helps explain the difference between these results.

During this work, the author came across the work of E. Axelrad [103], [104] which to date has not been referred to by any other worker in this field. Axelrad develops a semi-membrane theory for curvilinear bar-shells, primarily with the intention of examining the stability of pipe bends but he also attempts the problem of a pipe bend with flanges. Care should be used when comparing the results of both papers as the same symbol is used to represent a 'stiffness factor' in the 1974 paper and a 'flexibility factor' in the later paper.

Axelrad's method involves reducing the semi-membrane equations to two fourth order differential equations in two unknowns. Fourier series are substituted for the unknowns and the resulting equations are solved simultaneously. The resulting flexibility factors are approximate involving only one term in the series. The expression for the flexibility factor was given as,

$$K = 1 + (K_k - 1)\left(1 - \frac{1}{8\ell^*}\frac{\sinh 8\ell^* + \sin 8\ell^*}{\cosh 8\ell^* \quad \cos 8\ell^*}\right) \qquad \ldots (3.1)$$

where (in the present notation)

$$\ell^* = \frac{\alpha}{\pi}\sqrt{\lambda \frac{R}{r}}\,(12(1-\nu^2))^{-\frac{1}{4}}$$

and

K is the flexibility factor for a flanged bend,

K_R is the flexibility factor given by Karman for a bend without flanges.

No graphs of the results are given in either of the papers but the flexibility factors calculated from the above equation are given in Fig. (3.3). The works of Findlay and Thailer-Cheng show no variation with radius ratio (R/r) but this can be seen to be important in Axelrad's results.

In his derivation, Axelrad assumed that the direct meridional and shear strains were zero and that $\frac{r}{R}\sin\phi \ll 1$. Although $\frac{r}{R}\sin\phi$ was neglected with respect to unity, this does not mean that it is not an important parameter. These were the same assumptions as Thailer and Cheng, but Axelrad enforced the assumption of zero strain on the displacements whereas Thailer and Cheng only neglected it. The importance of enforcing this was noticed by the author before discovering this work and more will be said about it later. Axelrad also assumed that the flanges were thin.

Each of the above authors has obtained different results according to his assumptions regarding the shear strain term. It would be easy at this point to imagine that Findlay's results are correct since he uses the shear strain term obtained by the substitution of his displacements but his displacement assumptions may not be correct.

In/

In early 1979 the author received the first paper by J. F. Whatham [117]. The method involves the use of Novozhilov's [118] technique using three arbitrary functions which have the same form as the mid-surface displacements. Fourier series are used to solve the equations for the simple case of a bend without end effects. The functions take the form, (in present notation)

$$a = -\frac{M}{2\pi}\xi\cos\xi + r^2 E t \sum_{n=1}^{N} a_n \sin n\xi$$

$$b = rEt\, b_1 (R + r\cos\xi)\theta$$

$$c = -\frac{M}{2\pi}\xi\sin\xi + r^2 E t \sum_{n=1}^{N} c_n \cos n\xi$$

where $\xi = \phi + 90^\circ$ ... (3.2a)

The functions a, b and C correspond to the displacements v, u and w respectively. The flanged bend problem is then solved by superposing on the results obtained without end effects a set of displacements which return the ends of the bend back from their ovalised state to the initial round condition. The second set of functions take the form,

$$\bar{a} = r^2 E t \sum_{j=1}^{J} e^{-\lambda_j \theta} C_j \sum_{n=1}^{N} \bar{a}_{nj} \sin n\xi$$

$$\bar{b} = r^2 E t \sum_{j=1}^{J} e^{-\lambda_j \theta} C_j \sum_{n=1}^{N} \bar{b}_{nj} \cos n\xi$$

$$\bar{c} = r^2 E t \sum_{j=1}^{J} e^{-\lambda_j \theta} C_j \sum_{n=1}^{N} \bar{c}_{nj} \cos n\xi$$

... (3.2b)

The work involved in performing the above task is numerically complicated and difficult to understand from the few details given in the paper. The flange boundary conditions as given in the paper are/

are those of a thin flange but communication with Whatham [117] revealed that the conditions actually used were those of a rigid flange.

Some of Whatham's results are given in fig. (3.4). Figure (3.5) shows that there is good correlation between the results of Whatham and Axelrad. Whatham gives reference to only two papers on the subject of pipe bends, neither including end effects, and he seems unaware of the results of Axelrad.

Early in 1980 Whatham published a second paper [119] but this gives fewer details than the previous paper but includes results for pipe bends with connected tangent pipes. Whatham appears to make no assumptions other than those of thin shell theory but this is not stated explicitly.

Results for maximum stress factors are given by Findlay and Thailer-Cheng but not by either Axelrad or Whatham. Ideally the correct set of results could be ascertained by experiment but each author (except Axelrad) has given a set of experimental results which "confirm" his theory. This is possible due to the nature of the pipe bend problem where certain effects can influence the results quite radically. It is also caused by the limited range of parameters examined by experiment.

A number of papers have been written [96], [107], [111-116], [121-123] on finite element models which can be used to examine end effects. None of these papers give results for a pipe bend with flanges at both ends. Some give results for a flange at one end. For most models the problem is specifying correct boundary conditions for a flange at the free or loaded end of the bend. More will be said about these papers in conjunction with the tangent/

tangent pipe problem later.

The author spent some time developing a finite difference model of the pipe bend based on the shell equations of Novozhilov [118]. To obtain the equations for the finite difference model, the strain-displacement relations were substituted into the constitutive relations and then these were substituted into the equilibrium equations. This gave three equations in the three unknown displacements u, v and w. The only text in which the author could find similar equations for a shell other than a cylinder was by Goldenveizer [144], but these were developed from equations different from those of Novozhilov. The three equations, which form a set of eighth order partial differential equations, are given in appendix (1). Finite difference approximations were substituted for the differentials (see references [148] and [149]) to give a set of linear equations involving the values of the displacements at a mesh of points, representing the bend middle surface. Boundary conditions were set by substitution of the boundary values of the displacements into the appropriate equations. The resulting set of equations were solved simultaneously for the unknown values of the displacements. The number of equations was about 600 for a reasonable bend mesh, which created storage and time problems on the computer. This is a problem in common with the finite element methods.

Eventually this method was abandoned. The major problem was a numerical one. The variation of the displacements in the meridional direction is very much greater than the variation in the circumferential direction which makes the equations poorly conditioned/

conditioned and the results subject to numerical instability. The problem was highlighted by examining the simple case of a straight pipe subjected to a pure bending moment. When the bend length to bore radius ratio was greater than about four or less than about a half the results were simply nonsense. There were also problems with specifying the boundary conditions although most of these were resolved. The problems meant that only a restricted set of parameters could be examined and even then the quality of the results would have been questionable. The work was not entirely wasted as the experience gained from it was valuable.

Three methods will be described in the current chapter for the solution of the problem of a smooth pipe bend with flanged ends subjected to an in-plane bending moment. These draw on the experience gained from the earlier attempts. All methods will use the theorem of minimum total potential energy. Method No. 1 employs all possible simplifications, some of which were used by the earlier authors. This was the first relatively successful solution using an energy method. The second method removes some of the assumptions of the first method. Both of these methods use hand integration, making it virtually impossible to remove all of the assumptions. Method No. 2 represented such a significant improvement over method No. 1 that a third method was developed to remove as many of the assumptions as possible. Although method No. 3 represents the best solution the other two methods help to explain the behaviour of the problem and assist in the examination of the work of earlier authors.

The

The displacement series for all methods will be derived at the same time but with emphasis put on the method No. 3 displacements. Methods Nos. 1 and 2 will then be described using simpler forms of the complete displacement series. A discussion of these methods will be given along with the reasons for the necessity of method No. 3. The latter method will then be described in some detail.

(3.2) Displacements

(3.2a) Displacement Formulation

The theorem of minimum total potential energy requires suitable kinematically admissable displacements. Here the displacement field will be decomposed into two parts. The first are termed "rigid section displacements" which are associated with the displacements of the circular tube cross-sections with no change in their configuration i.e. each point on a circular section, at some angle θ , has the same displacement. These displacements automatically satisfy the boundary requirements of a flanged bend. The second displacements are termed "distortion displacements" which are associated with the distortion of the circular sections.

The total displacements will be found by adding the two sets of displacements. This method of formulating the displacements is used because it allows the boundary conditions to be applied more easily.

Strains are obtained by substituting the total displacements into the strain-displacement equations (2.13).

(3.2b) Rigid Section Displacements

Rigid section displacements are the displacements of the circular tube cross-section with the cross-section remaining circular. These displacements must allow a general variation in the circumferential direction but also satisfy the boundary conditions.

A bend without end effects has the same displacements at any circumferential segment but flanges will cause the ovalisation at any circumferential/

circumferential segment to depend on its circumferential position. Thus, the rigid section displacements must be variable functions of the circumferential co-ordinate.

Consider a smooth circular pipe bend under the action of an applied bending moment, M, with a circumferential mean radius of curvature, R, meridional radius of curvature, r, and overall bend angle, α. The deformation of the bend will be symmetric about the circumferential centre of the bend. One half of such a bend is shown in figure (3.6).

The rigid section displacements of the bend can be found from the displacements of the centreline. Figure (3.7) gives an exaggerated illustration of the displacements. U_c is the circumferential tangential displacement of the centreline and V_c is the displacement of the centreline in the direction perpendicular to it. Note that V_c has the same value at all points on the cross-section at any particular circumferential angle.

From figure (3.7), the rotation of cross-section can be seen to be made up of two parts. The first is due to the variation of V_c in the circumferential direction and the second is due to the circumferential displacement U_c causing a rotation about the centre of the bend radius arc. Therefore the rotation γ_c of a point on the centreline is,

$$\gamma_c = \frac{1}{R}\left(U_c - \frac{\partial V_c}{\partial \theta}\right) \qquad \ldots (3.3)$$

The corresponding shell displacements, u_R, v_R and ω_R at some point 'ϕ' on the circular section are then given by,

$$u_R = U_c + \gamma_{\sigma r} \sin\phi$$
$$= U_c + \frac{r}{R}\sin\phi\left(U_c - \frac{\partial V_c}{\partial\theta}\right)$$

$$v_R = V_c \cos\phi$$
$$\omega_R = V_c \sin\phi$$

... (3.4)

In the derivation of the above equations the assumption that the deformed circular cross-section remains normal to the centreline, was used. This assumption was found to be correct even in the exact analysis of a thick curved beam by Timoshenko and Goodier (pp. 71-75 of [150]), although the stresses across the section varied logarthmically, and is necessary for the correct boundary conditions at the flange.

If equations (3.4) are substituted into the strain-displacement equations of Novozhilov as given earlier (eqn. 2.13) the mid-surface shear strain $\gamma_{\theta\phi}$ and shear curvature $K_{\theta\phi}$ are zero. If equations (3.4) are substituted in the classical shell equations the shear curvature $K_{\theta\phi}$ is not zero.

One useful simplification of equations (3.4), which will be used in a simpler analysis later, is to assume that the circumferential strain ϵ_θ is zero at the centreline, $\phi = 0$, for the rigid displacements, i.e. assuming that this centreline does not extend. The circumferential strain at the centreline is given by,

$$(\epsilon_\theta)_{\phi=0} = \frac{1}{R}\left[\frac{\partial U_c}{\partial\theta} + V_c\right]$$

equating this to zero gives,

$$V_c = -\frac{\partial U_c}{\partial \theta}$$

or $$U_c = -\int V_c \, d\theta \quad + \text{Constant}$$

... (3.5)

The constant of integration disappears because U_c has to be zero at the bend centre, $\theta = 0$. The above simplification is roughly equivalent to ignoring the thick curved beam effect and will be more correct for long radius bends. The displacement equations (3.4) with this simplification become

$$u_R = -\int V_c \, d\theta \left(1 + \frac{r}{R}\sin\phi\right) - \frac{\partial V_c}{\partial \theta}\frac{r}{R}\sin\phi$$
$$v_R = V_c \cos\phi$$
$$\omega_R = V_c \sin\phi$$

... (3.6)

The Rayleigh-Ritz method requires the displacements U_c and V_c to be specified as trigonometric series in the circumferential co-ordinate, .

To satisfy the necessary boundary conditions, of symmetry at $\theta = 0$ and free ends at $\theta = \pm \frac{\alpha}{2}$. the displacement V_c must be an even function of the variable, θ . Therefore this can be generally expressed as an even fourier series of the form,

$$V_c = d_0 + \sum_{j=1}^{\infty} d_j \cos\left(\frac{j\pi\theta}{\alpha}\right)$$

... (3.7)

The boundary conditions require

$$(V_c)_{\theta=0} = 0$$

therefore

$$d_0 = -\sum_{j} d_j$$

... (3.8)

Re-arranging (3.7) using (3.8) and the identity ($\cos 2a\alpha = 1 - 2 \times \sin^2(a\alpha)$) gives

$$V_c = -\sum_{J=1}^{\infty} 2 d_J \sin^2\left(\frac{J\pi\theta}{2\alpha}\right)$$

$$= -\sum_{J=1}^{\infty} D_J \sin^2\left(\frac{J\pi\theta}{2\alpha}\right) \qquad \ldots (3.9)$$

where the coefficient $D_J = 2 d_J$

Equation (3.9) also satisfies the condition of zero slope at $\theta = 0$.

The displacement U_c must satisfy the boundary conditions of antisymmetry at $\theta = 0$ and free end at $\pm \frac{\alpha}{2}$. These conditions can be met by a function of the following form,

$$U_c = \sum_{J=1}^{\infty} F_J \frac{1}{2}\left(\theta - \left(\frac{\alpha}{J\pi}\right)\sin\left(\frac{J\pi\theta}{\alpha}\right)\right) \qquad \ldots (3.10)$$

The above form is found by substituting equation (3.9) into equation (3.5) and then coefficients Dj are replaced by Fj. A fourier series was tried for U_c but it gives the same result as the above function and complicates the strain equations. Note that the above function does not mean that $\epsilon_\theta = 0$ at $\theta = 0$ since the coefficients of U_c and V_c are different. However, Dj and Fj will be of a similar numerical order which, as will be explained later, assists in the numerical stability of the solution procedure.

Substituting equations (3.9) and (3.10) into equations (3.4) gives the rigid section shell displacements,

$$u_R = \sum_{J=1}^{\infty} F_J \tfrac{1}{2}\left(\theta - \frac{\alpha}{J\pi}\sin\left(\frac{J\pi\theta}{\alpha}\right)\right)\left(1+\frac{r}{R}\sin\phi\right)$$

$$+ \tfrac{1}{2}\sum_{J=1}^{\infty} D_J\left(\frac{J\pi}{\alpha}\right)\sin\left(\frac{J\pi\theta}{\alpha}\right)\frac{r}{R}\sin\phi$$

$$v_R = -\sum_{J=1}^{\infty} D_J \sin^2\left(\frac{J\pi\theta}{2\alpha}\right)\cos\phi$$

$$w_R = -\sum_{J=1}^{\infty} D_J \sin^2\left(\frac{J\pi\theta}{2\alpha}\right)\sin\phi$$

where j = 1, 2, 3, ---

... (3.11)

As far as is known, the above method of deriving the rigid section displacements has not been published by any other author.

(3.2c) Distortion Displacements

Distortion displacements are associated with the distortion of the circular tube cross-sections. These displacements are similar to the "ovalisation" displacements referred to by other authors. The term, "distortion", is preferred because the deformation shapes for certain flanged bends are not strictly oval although occasionally the word "ovalisation" will be used.

Since the flanges are assumed to be rigid, deformation of the cross-section and rotation of the normal to the shell mid-surface at the flange are assumed to be zero relative to the flange. Cross-sectional planes away from the constraints will experience a degree of distortion which will vary according to the distance from the flange.

The variation of the distortion displacements can be considered/

considered in two parts. One describing deformation of the meridian and the other describing the variation along the circumferential direction. The three displacements u, v and ω will be formulated separately.

(3.2d) Radial Distortion Displacement

The radial distortion displacement, ω_b, will be considered first since it "characterises" the distortion shape of the cross-section.

The part describing the deformation of the meridian, $\omega(\phi)$, has been specified by most authors , from Karman onwards, with something like the following form,

$$\omega(\phi) = \sum_{n=2,4.}^{\infty}{}' C_n \cos n\phi$$

$n = 2, 4, 6, \text{---} \infty$

... (3.12a)

This followed from an intuitive view of the expected displacement shape and for a bend without end effects it works effectively. The first term of the above is the dominant term and describes an oval deformation pattern.

Symonds [151] , Jones [35] and several of those after them used $\omega(\phi)$ with the form,

$$\omega(\phi) = \sum_{n=2,4}' C_n \cos n\phi + \sum_{n=3,5}' C_n \sin n\phi$$

or $$\omega(\phi) = \sum_{n=2,3,4}^{\infty}{}' C_n \cos n\xi$$

where $\xi = \phi + 90^\circ$

... (3.12b)

The additional terms were found to have little significance on the results for a bend without end effects, except that the stress distributions changed slightly, particularly away from the maximum. This was more notable for short radius bends.

For in-plane loading, $\omega(\phi)$ must be symmetrical about the plane of the bend passing through $\phi = -90^\circ$ and $\phi = 90^\circ$. The complete fourier series describing the deformation and satisfying the above symmetry conditions, is

$$\omega(\phi) = \sum_{n=0,2}^{\infty} C_n \cos n\phi + \sum_{n=1,3}^{\infty} C_n \sin n\phi$$

where $\sum_{n=0,2}^{\infty}$ is 0, 2, 4, ——,∞

and $\sum_{n=1,3}^{\infty}$ is 1, 3, 5, ——,∞

... (3.13)

This contains two terms which the previous form did not have i.e., Co and $C_1 \sin \phi$. The $\sin \phi$ variation was used in the rigid section displacements and will be subsequently ignored here.

The Co term describes a constant radial expansion at all values of ϕ. It is normally ignored as it is usually found to have the value zero. In the following analysis it will be included as it was found to influence the stress distributions when end effects are involved. To simplify the analysis and eventually/

eventually the computer program, $\omega(\phi)$ will be used with the following form,

$$\omega(\phi) = \sum_{n=2,4,}^{\infty} C_n \cos n\phi + \sum_{n=1,3}^{\infty} C_n \sin n\phi + H$$

where $H = C_o$

... (3.14)

Whatham [117] and Axelrad [104] considered $\omega(\phi)$ as

$$\omega(\phi) = \sum_{n=0}^{\infty} C_n \cos n\xi \qquad \text{where } \xi = \phi + 90^\circ$$

in their analysis of the flanged bend which is the same as equation (3.13). Thailer and Cheng [95] used equation (3.13) without the zeroth term, Co. Findlay [99] used the simpler form given in equation (3.12a).

The second part of the radial displacement, $\omega(\theta)$, has to satisfy the condition of symmetry at $\theta = 0$ and the rigid flange conditions at $\theta = \pm \frac{\alpha}{2}$. The flange boundary conditions can be stated as,

$$\text{at } \theta = \pm \frac{\alpha}{2} \quad , \quad \omega(\theta) = \frac{\partial \omega(\theta)}{\partial \theta} = 0$$

Note that the slope condition, $\frac{\partial \omega}{\partial \theta} = 0$, is actually $\beta_\theta^{\circ} = 0$ but this reduces to the above because the distortion part of the u displacement is zero at the flange. β_θ° is the rotation of the shell mid-surface relative to the flange i.e., it only includes the distortion displacements.

Since the deformation is symmetric about $\theta = 0$ then an even fourier series will be used, i.e.

$$\omega(\theta) = C_0 + \sum_{m=1}^{\infty} C_m \cos(m\eta\theta) \qquad m = 1, 2, 3, \text{---}, \text{as}$$

... (3.15)

The flange boundary conditions are now applied to equation (3.15),

at $\theta = \frac{\alpha}{2}$

$$\omega(\theta) = 0 = C_0 + \sum_{m=1}^{\infty} C_m \cos\left(m\eta\tfrac{\alpha}{2}\right)$$

or

$$C_0 = -\sum_{m=1}^{\infty} C_m \cos\left(m\eta\tfrac{\alpha}{2}\right)$$

... (3.16)

also at $\theta = \frac{\alpha}{2}$,

$$\frac{\partial\omega(\theta)}{\partial\theta} = 0 = \sum_{m=1}^{\infty} C_m(m\eta)\sin\left(m\eta\tfrac{\alpha}{2}\right)$$

This is satisfied if,

$$\sin\left(m\eta\tfrac{\alpha}{2}\right) = 0 \qquad m = 1, 2, 3, \text{---}$$

or

$$m\eta\tfrac{\alpha}{2} = m\pi$$

therefore,

$$\eta = \frac{2\pi}{\alpha}$$

... (3.17)

Substituting (3.17) into (3.16) gives

$$C_0 = -\sum_{m=1}^{\infty} C_m \cos m\pi$$

$$\cos m\pi = \begin{cases} -1 & , m = 1, 3, 5, \text{---} \\ +1 & , m = 2, 4, 6, \text{---} \end{cases}$$

i.e. $$C_0 = \sum_{m=1,3,5}^{\infty} C_m - \sum_{m=2,4,6}^{\infty} C_m$$

... (3.18)

Substituting (3.17) and (3.18) into (3.15) gives,

$$\omega(\theta) = \sum_{m=1,3}^{\infty} C_m - \sum_{m=2,4}^{\infty} C_m + \sum_{m=1,2}^{\infty} C_m \cos\left(\frac{2m\pi\theta}{\alpha}\right)$$

using this with the identities

$$2\cos^2(\theta/2) = 1 + \cos\theta$$

$$2\sin^2(\theta/2) = 1 - \cos\theta$$

$\omega(\theta)$ finally becomes,

$$\omega(\theta) = \sum_{m=1,3}^{\infty} C_m \cos^2\left(\frac{m\pi\theta}{\alpha}\right) - \sum_{m=2,4}^{\infty} C_m \sin^2\left(\frac{m\pi\theta}{\alpha}\right)$$

... (3.19)

where $C_m = 2C_m$

Findlay, [99], used $\omega(\theta)$ with the following form,

$$\omega(\theta) = \sum_{m=1,3}^{\infty} C_m \cos^2\left(\frac{m\pi\theta}{\alpha}\right)$$

... (3.20)

He derived this on a purely intuitive basis by examining the expected deformation pattern. It should be noted however, that equation (3.20) is not the complete fourier series fitting the boundary conditions, whereas (3.19) is.

Thailer and Cheng [95] used $\omega(\theta)$ with the following form,

$$\omega(\theta) = \sum_{m=1,3}^{\infty} C_m \cos\left(\frac{m\pi\theta}{\alpha}\right)$$

... (3.21)

Note that this does not satisfy the requirement of $\left(\frac{\partial\omega}{\partial\theta}\right)_{\theta=\frac{\alpha}{2}} = 0$ and therefore does not satisfy the conditions of a rigid flange but does satisfy the conditions of a 'thin' flange. It is also not a complete fourier series satisfying the boundary conditions of a thin flange.

Whatham [117] and Axelrad [104] used a method of solving the differential equations which did not require the specification of $\omega(\theta)$ in a series form.

The radial distortion displacement ω_D is found from the product of $\omega(\phi)$ and $\omega(\theta)$. To write this in a concise and meaningful way the following function will be defined,

$$\psi_{ek} = \begin{cases} 1 \text{ if } k \text{ is even} \\ 0 \text{ if } k \text{ is odd} \end{cases}$$

$$\psi_{ok} = \begin{cases} 0 \text{ if } k \text{ is even} \\ 1 \text{ if } k \text{ is odd} \end{cases}$$

... (3.22)

Using this ω_D can be written as,

$$\omega_D = \sum_{m=1}^{\infty}\sum_{n=2}^{\infty} C_{mn}\left(\psi_{en}\cos n\phi + \psi_{on}\sin n\phi\right)\left(\psi_{om}\cos^2\left(\frac{m\pi\theta}{\alpha}\right) - \psi_{em}\sin^2\left(\frac{m\pi\theta}{\alpha}\right)\right)$$

$$+ \sum_{j=1}^{\infty} H_j\left(\psi_{oj}\cos^2\left(\frac{j\pi\theta}{\alpha}\right) - \psi_{ej}\sin^2\left(\frac{j\pi\theta}{\alpha}\right)\right)$$

where m = 1, 2, 3 ---

n = 2, 3, 4 ---

j = 1, 2, 3, ---

... (3.23)

The zeroth term in the $\omega(\theta)$ series H has become Hj, using the same subscript, j, as the rigid section displacements. This is for computational convenience and does not affect the final result.

The coefficients Cmn are not simply the product of Cm and Cn. Each Cmn coefficient corresponds to a particular pair of m and n. i.e. $\sum_m \sum_n C_{mn} \neq \sum_m C_m \times \sum_n C_n$. The use of Cm and Cn earlier was to make the derivation simple.

(3.2e) Meridional Tangential Distortion Displacements, v_b

The meridional tangential distortion displacement is often either derived from, or used to derive, the radial distortion displacement using the assumption of an inextensible meridian. In shell theory, this is equivalent to saying that the meridional direct strain, ϵ_ϕ, is zero. i.e.

$$\epsilon_\phi = \frac{1}{r}\left[\omega + \frac{\partial v}{\partial \phi}\right] = 0$$

which gives,

$$w = -\frac{\partial v}{\partial \phi} \qquad \ldots (3.24)$$

or,

$$v = -\int \omega \, d\phi + C \qquad \ldots (3.25)$$

(C = o from symmetry conditions)

As an example, substituting equation (3.12a) into equation (3.25) gives,

$$v(\phi) = -\sum_{n\neq 2,4}^{\infty} C_n \frac{1}{n} \sin n\phi$$

... (3.26)

or from equation (3.13),

$$v(\phi) = -\sum_{n=2,4}^{\infty} C_n \frac{1}{n} \sin n\phi + \sum_{n=3,5}^{\infty} C_n \frac{1}{n} \cos n\phi$$

... (3.27)

For the main analysis to be presented, this assumption of $\epsilon_\phi = 0$ will not be used and the effect of including ϵ_ϕ will be examined later.

In plane loading and the symmetric plane through $\phi = +90^\circ$ and $\phi = -90^\circ$ means that $v(\phi)$ must be antisymmetric about the same plane. A complete set of fourier terms satisfying this condition is,

$$v(\phi) = -\sum_{n=2,4}^{\infty} B_n \frac{1}{n} \sin n\phi + \sum_{n=1,3}^{\infty} B_n \frac{1}{n} \cos n\phi$$

... (3.28)

Note that the form of the function chosen would satisfy $\epsilon_\phi = 0$ if all Bn = Cn. This should mean that Bn and Cn will have approximately the same value which will assist the numerical stability as explained later. It also permits an easy examination of how good the assumption $\epsilon_\phi = 0$ would be for a particular geometry.

Equation (3.28) differs from the more usual form, equation (3.27), because it includes the term $B_1 \cos \phi$. This is one of the functions used in the rigid section displacements and therefore will not/

not be included in the final $U(\phi)$.

Therefore, $U(\phi)$ will be used with the following form,

$$U(\phi) = -\sum_{n=2,4}^{\infty} B_n \frac{1}{n} \sin n\phi + \sum_{n=3,5}^{\infty} B_n \frac{1}{n} \cos n\phi \qquad \ldots (3.29)$$

Axelrad [104], Findlay [99] and Thailer-Cheng [95] all used the Karman assumption of $\epsilon_\phi = 0$ to derive $U(\phi)$. Whatham used a form similar to equation (3.28).

The variation of the meridional tangential distortion displacement in the circumferential direction, $U(\theta)$, has to satisfy the boundary conditions of symmetry at $\theta = 0$ and of a rigid flange at $\theta = \pm \frac{\alpha}{2}$. The boundary condition for $U(\theta)$ at the flange is,

at $\theta = \pm \frac{\alpha}{2}$, $\qquad U(\theta) = 0 \ (= U_D)$

Note that $\frac{\partial U_D}{\partial \theta}$ is not required to be zero at the flange since is in the plane of the shell mid-surface. This can also be seen from the necessary boundary conditions for a pipe bend given in equations (2.17).

To satisfy the symmetry conditions $U(\theta)$ is specified as an even fourier series, i.e.

$$U(\theta) = b_0 + \sum_{m=1,2}^{\infty} b_m \cos(m\eta\theta) \qquad \ldots (3.30)$$

at $\theta = \frac{\alpha}{2}$, $\quad U_D = 0 = b_0 + \sum_{m=1,2}^{\infty} b_m \cos(m\eta \frac{\alpha}{2})$

therefore,

$$b_0 = -\sum_{m=1}^{\infty} b_m \cos\left(m\eta\frac{\alpha}{2}\right) \qquad \ldots (3.31)$$

Since $U(\theta)$ is not a periodic function, i.e. the range of θ is finite, then η is selected so that $U(\theta)$ is a half range expansion on the interval $0 \leq \theta \leq \alpha/2$ (See Kreyszig [152] p. 393). Therefore,

$$\eta = \frac{2\pi}{\alpha} \qquad \ldots (3.32)$$

Substituting in (3.31) gives,

$$b_0 = -\sum_{1}^{\infty} b_m \cos m\pi$$

$$-\cos m\pi = \begin{cases} +1, & m = 1, 3, 5, \text{---} \\ -1, & m = 2, 4, 6, \text{---} \end{cases}$$

therefore, $b_0 = \sum_{m=1,3}^{\infty} b_m - \sum_{m=2,4}^{\infty} b_m$

Substituting this and equation (3.32) in equation (3.30) gives,

$$U(\theta) = \sum_{m=1,3}^{\infty} B_m \cos^2\left(\frac{m\pi\theta}{\alpha}\right) - \sum_{m=2,4}^{\infty} B_m \sin^2\left(\frac{m\pi\theta}{\alpha}\right)$$

where $B_m = 2b_m$. $\qquad \ldots (3.33)$

Note that although the condition $\frac{\partial U}{\partial \theta} = 0$ at $\theta = \frac{\alpha}{2}$ was not used or required, it is satisfied by the above function. However, the function given in equation (3.33) has been derived in the/

the normally accepted way and will be used henceforth. The method of minimum total potential energy only requires that the displacements satisfy at least the necessary boundary conditions. If the condition of inextensibility had been used then the above form would have been obtained.

The same comments apply to $v(\theta)$ as applied to $\omega(\theta)$, regarding its specification by other authors.

The meridional tangential distortion displacement, v_D, is given by,

$$v_D = \sum_{m=1}^{\infty}\sum_{m=2}^{\infty} B_{mn}\left(-\psi_{en}\frac{1}{n}\sin n\phi + \psi_{on}\frac{1}{n}\cos n\phi\right)\left(\psi_{om}\cos^2\left(\frac{m\pi\theta}{\alpha}\right) - \psi_{em}\sin^2\left(\frac{m\pi\theta}{\alpha}\right)\right)$$

where m = 1, 2, 3, ---

n = 2, 3, 4, ---

... (3.34)

and the definitions of the function ψ is given in equation (3.22).

(3.2f) Circumferential Tangential Distortion Displacement u_D

The circumferential tangential distortion displacement is not used in the analysis of pipe bends without end effects. It is only important in the study of pipe bends with end effects and even then it is difficult to imagine what effect it has on a purely intuitive basis.

For in-plane bending, $v(\phi)$ must satisfy the conditions of symmetry at $\phi = +90^\circ$ and $\phi = -90^\circ$. A complete fourier series satisfying this condition is,

$$u(\phi) = \sum_{n=0,2}^{\infty} a_n \cos n\phi + \sum_{n=1,3}^{\infty} a_n \sin n\phi$$

... (3.35)

The first terms in each of these series, a_0 and $a_1 \sin \phi$, are involved in the rigid section displacements and will not be included in the final distortion displacements.

The variation of the circumferential tangential distortion displacement, $u(\theta)$ must be antisymmetric about $\theta = 0$ and equal zero at $\pm \frac{\alpha}{2}$. $u(\theta)$ equals zero at the flange because the flange is assumed not to distort. To satisfy antisymmetry, $u(\theta)$ is taken as an odd fourier expansion about $\theta = 0$, i.e.

$$u(\theta) = \sum_{m=1}^{\infty} a_m \sin(m\eta\theta)$$

at $\theta = \frac{\alpha}{2}$, $u_b = 0 = \sum_{m=1}^{\infty} a_m \sin(m\eta \frac{\alpha}{2})$

For this to be true, $\sin(m\eta\frac{\alpha}{2}) = 0$

or $\eta \frac{\alpha}{2} = \pi$

which gives $\eta = \frac{2\pi}{\alpha}$

which is the same as would be obtained by a half range expansion on the range $0 \leq \theta \leq \frac{\alpha}{2}$. $u(\theta)$ now becomes,

$$u(\theta) = \sum_{m=1,2}^{\infty} a_m \sin\left(\frac{2m\pi\theta}{\alpha}\right)$$

... (3.36)

Before giving the final form of the u_b displacement it is worth examining a simplification possible for long radius bends.

If/

If it is assumed that the shear strain is zero for long radius bends then it becomes possible to derive u from v. i.e. From equation (2.13)

$$\gamma_{\theta\phi} = \frac{1}{R'}\left[\frac{\partial v}{\partial \theta} - u\cos\phi + \frac{R'}{r}\frac{\partial u}{\partial \phi}\right]$$

$$= \frac{1}{R}\left[\frac{\partial v}{\partial \theta}\left(1 - \frac{r}{R'}\sin\phi\right) + \frac{R}{r}\left(\frac{\partial u}{\partial \phi} - u\frac{r}{R'}\cos\phi\right)\right]$$

where $R' = R + r\sin\phi$

If the bend radius R is much larger than the pipe radius r, i.e. for long radius bends, then $\frac{r}{R'}\sin\phi$ can be neglected with respect to one. If u and $\frac{\partial u}{\partial \phi}$ are of approximately the same order, then

$$\frac{\partial u}{\partial \phi} \gg u\frac{r}{R'}\cos\phi$$

This can be further justified when u is obtained, when it can be proved that $\frac{\partial u}{\partial \phi} > u$. From this then

$$\gamma_{\theta\phi} = \frac{1}{R}\left[\frac{\partial v}{\partial \theta} + \frac{R}{r}\frac{\partial u}{\partial \phi}\right] \qquad \ldots (3.37)$$

If this is equated to zero, then

$$u = -\frac{r}{R}\int \frac{\partial v}{\partial \theta}\, d\phi + c \qquad \ldots (3.38)$$

Note that this gives $u = 0$ for a bend with no end effects.

If v is derived using Karman's assumption of inextensibility, i.e./

i.e. $\epsilon_\phi = 0$, then

$$v = -\int \omega \, d\phi$$

substituting in equation (3.38) gives,

$$u = \frac{r}{R} \int\int \frac{\partial \omega}{\partial \theta} \, d\phi \, d\phi$$

... (3.39)

The constant of integration will be zero since u must be zero at $\theta = 0$. If ω_D is taken from equation (3.23), ignoring the Hj series which for u is included in the rigid section displacements, then

$$u_D = \frac{r}{R} \sum_{m=1}^{\infty} \sum_{n=2}^{\infty} C_{mn} \left(\psi_{en} \frac{1}{n^2} \cos n\phi + \psi_{on} \frac{1}{n^2} \sin n\phi \right) \left(\frac{m\pi}{\alpha} \right) \sin \left(\frac{2m\pi\theta}{\alpha} \right)$$

... (3.40)

The variation in the θ and ϕ directions is similar to that already determined for $u(\theta)$ and $u(\phi)$. The above form is useful as it gives an estimation of the possible magnitude of u_D relative to ω_D.

To keep the coefficients of the u_D displacement approximately the same as those of v_D and ω_D, and taking cognizance of the forms derived for $u(\phi)$ and $u(\theta)$, equations (3.35) and (3.36) respectively, u_D will be taken as,

$$u_D = \frac{r}{R} \sum_{m=1}^{\infty} \sum_{n=2}^{\infty} A_{mn} \left(\psi_{en} \frac{1}{n^2} \cos n\phi + \psi_{on} \frac{1}{n^2} \sin n\phi \right) \left(\frac{m\pi}{\alpha} \right) \sin \left(\frac{2m\pi\theta}{\alpha} \right)$$

where

$m = 1.\ 2.\ 3.\ ---$

$n = 2,\ 3,\ 4,\ ---$

and $$a_{mn} = \frac{r}{R} A_{mn} \left(\frac{m\pi}{n^2 \alpha}\right) \qquad \ldots (3.41)$$

The definition of ψ was given in equation (3.22). Note that the choice of the coefficients is arbitrary, their values will be decided by the minimisation procedure.

Findlay [99] and Thailer-Cheng [95] did not specify u_D at all. Neither thought that it was significant enough to merit inclusion in their analyses. Findlay argued that since u_D must be zero at $\theta = 0$ and $\theta = \pm\frac{\alpha}{2}$, then it must be small. Thailer and Cheng do not acknowledge the possibility of u_D existing. This seems curious since they assume that $\gamma_{\theta\phi} = 0$ but they do not enforce this condition on their displacements. Had they examined the shear strain equation (2.13) and applied $\gamma_{\theta\phi} = 0$ they would have obtained u_D from equation (3.38).

Axelrad makes the assumption that $\gamma_{\theta\phi} = 0$ in his governing differential equations and enforces this condition to obtain his displacements. u_D is derived using (3.39) but $u(\theta)$ is not used in his analysis.

Whatham specifies u_D in the form given in equation (3.2). $u(\theta)$ is not used in his analysis.

(3.2g) Distortion Displacement Summary

$$u_D = \frac{r}{R} \sum_{m=1}^{\infty} \sum_{n=2}^{4} A_{mn} \left(\psi_{en} \frac{1}{n^2} \cos n\phi + \psi_{on} \frac{1}{n^2} \sin n\phi\right)\left(\frac{m\pi}{\alpha}\right) \sin\left(\frac{2m\pi\theta}{\alpha}\right)$$

$$v_D = \sum_{m=1}^{\infty} \sum_{n=2}^{4} B_{mn} \left(-\psi_{en} \frac{1}{n} \sin n\phi + \psi_{on} \frac{1}{n} \cos n\phi\right)\left(\psi_{em} \cos^2\left(\frac{m\pi\theta}{\alpha}\right) - \psi_{en} \sin^2\left(\frac{m\pi\theta}{\alpha}\right)\right)$$

$$\omega_D = \sum_{m=1}^{\infty}\sum_{n=2}^{\infty} C_{mn}\left(\psi_{en}\cos n\phi + \psi_{on}\sin n\phi\right)\left(\psi_{om}\cos^2\left(\frac{m\pi\theta}{\alpha}\right) - \psi_{em}\sin\left(\frac{m\pi\theta}{\alpha}\right)\right)$$

$$+ \sum_{J=1}^{\infty} H_J\left(\psi_{oJ}\cos^2\left(\frac{J\pi\theta}{\alpha}\right) - \psi_{eJ}\sin^2\left(\frac{J\pi\theta}{\alpha}\right)\right)$$

... (3.42)

(3.2h) Total Displacements

The total displacements are found by adding the distortion and rigid section displacements. i.e.,

$$u = u_R + u_D$$
$$v = v_R + v_D$$
$$\omega = \omega_R + \omega_D$$

Using equations (3.11) and (3.42) gives

$$u = \sum_{J=1}^{J\pi} F_J \tfrac{1}{2}\left(\theta - \frac{\alpha}{J\pi}\sin\left(\frac{J\pi\theta}{\alpha}\right)\right)\left(1 + \frac{r}{R}\sin\phi\right)$$

$$+ \tfrac{1}{2}\sum_{J=1}^{J\pi} D_J\left(\frac{J\pi}{\alpha}\right)\sin\left(\frac{J\pi\theta}{\alpha}\right)\frac{r}{R}\sin\phi$$

$$+ \frac{r}{R}\sum_{m=1}^{M\pi}\sum_{n=2}^{N\pi+1} A_{mn}\left(\psi_{en}\tfrac{1}{n^2}\cos n\phi + \psi_{on}\tfrac{1}{n^2}\sin n\phi\right)\left(\frac{m\pi}{\alpha}\right)\sin\left(\frac{2m\pi\theta}{\alpha}\right)$$

$$v = -\sum_{J=1}^{J\pi} D_J \sin^2\left(\frac{J\pi\theta}{2\alpha}\right)\cos\phi$$

$$+ \sum_{m=1}^{M\pi}\sum_{n=2}^{N\pi+1} B_{mn}\left(-\psi_{en}\tfrac{1}{n}\sin n\phi + \psi_{on}\tfrac{1}{n}\cos n\phi\right)\left(\psi_{om}\cos^2\left(\frac{m\pi\theta}{\alpha}\right) - \psi_{em}\sin^2\left(\frac{m\pi\theta}{\alpha}\right)\right)$$

$$\omega = -\sum_{J=1}^{J\pi} D_J \sin^2\left(\frac{J\pi\theta}{2\alpha}\right)\sin\phi$$

$$+ \sum_{m=1}^{M\pi}\sum_{n=2}^{N\pi+1} C_{mn}\left(\psi_{en}\cos n\phi + \psi_{on}\sin n\phi\right)\left(\psi_{om}\cos^2\left(\frac{m\pi\theta}{\alpha}\right) - \psi_{em}\sin^2\left(\frac{m\pi\theta}{\alpha}\right)\right)$$

$$+ \sum_{J=1}^{J\pi} H_J\left(\psi_{oJ}\cos^2\left(\frac{J\pi\theta}{\alpha}\right) - \psi_{eJ}\sin^2\left(\frac{J\pi\theta}{\alpha}\right)\right)$$

where $j = 1, 2, 3, ---, JT$

$m = 1, 2, 3, ---, MT$

$n = 2, 3, 4, ---, NT + 1$

... (3.43)

The previously infinite summations have been replaced here by finite sums. JT, MT and NT are the total number of terms in the j, m and n series respectively.

The displacements given in (3.43) will be used later in method No. 3. Some of the assumptions described earlier will be used to derive simpler displacement series for methods Nos. 1 and 2.

(3.3) Strains

The strains are obtained by substituting the total displacements (3.43) into the strain-displacement equations (2.13). This gives,

$$\epsilon_\phi = \frac{1}{r}\Big[\sum_m{}'\sum_n{}' (C_{mn} - B_{mn})\Big(\psi_{en}\cos n\phi + \psi_{on}\sin n\phi\Big)\times$$

$$\times\Big(\psi_{om}\cos^2\Big(\frac{m\pi\theta}{\alpha}\Big) - \psi_{em}\sin^2\Big(\frac{m\pi\theta}{\alpha}\Big)\Big)$$

$$+\sum_j{}' H_j\Big(\psi_{oj}\cos^2\Big(\frac{j\pi\theta}{\alpha}\Big) - \psi_{ej}\sin^2\Big(\frac{j\pi\theta}{\alpha}\Big)\Big)\Big]$$

$$\epsilon_\theta = \frac{1}{R'}\Big[\sum_j{}'\Big(\Big(F_j\Big(1+\frac{r}{R}\sin\phi\Big) - D_j\Big)\sin^2\Big(\frac{j\pi\theta}{2\alpha}\Big) + D_j\frac{1}{2}\Big(\frac{j\pi}{\alpha}\Big)^2\cos\Big(\frac{j\pi\theta}{\alpha}\Big)\frac{r}{R}\sin\phi\Big)$$

$$+\frac{2r}{R}\sum_m{}'\sum_n{}'\Big\{A_{mn}\Big(\psi_{en}'\cos n\phi + \psi_{on}'\sin n\phi\Big)\Big(\frac{m\pi}{\alpha}\Big)^2\cos\Big(\frac{2m\pi\theta}{\alpha}\Big)$$

$$+\Big(B_{mn}\Big(-\psi_{en}\frac{1}{n}\sin n\phi + \psi_{on}\frac{1}{n}\cos n\phi\Big)\cos\phi$$

$$+C_{mn}\Big(\psi_{en}\cos n\phi + \psi_{on}\sin n\phi\Big)\sin\phi\Big)\Big(\psi_{om}\cos^2\Big(\frac{m\pi\theta}{\alpha}\Big) - \psi_{em}\sin^2\Big(\frac{m\pi\theta}{\alpha}\Big)\Big)\Big\}$$

$$+\sum_j{}' H_j\Big(\psi_{oj}\cos^2\Big(\frac{j\pi\theta}{\alpha}\Big) - \psi_{ej}\sin^2\Big(\frac{j\pi\theta}{\alpha}\Big)\Big)\sin\phi\Big]$$

$$\gamma_{\theta\phi} = \frac{1}{R'}\Big[\sum_m{}'\sum_n{}'\Big\{\Big(B_{mn} - A_{mn}\frac{R'}{R}\Big)\Big(\psi_{en}\frac{1}{n}\sin n\phi - \psi_{on}\frac{1}{n}\cos n\phi\Big)$$

$$+\frac{r}{R}A_{mn}\Big(\psi_{en}\frac{1}{n^2}\cos n\phi + \psi_{on}\frac{1}{n^2}\sin n\phi\Big)\cos\phi\Big\}\Big(\frac{m\pi}{\alpha}\Big)\sin\Big(\frac{2m\pi\theta}{\alpha}\Big)\Big]$$

$$K_\phi = \frac{1}{r^2}\Big[\sum_m{}'\sum_n{}'\Big(C_{mn} - B_{mn}\Big)\Big(\psi_{en}\cos n\phi + \psi_{on}\sin n\phi\Big)\times$$

$$\times\Big(\psi_{om}\cos^2\Big(\frac{m\pi\theta}{\alpha}\Big) - \psi_{em}\sin^2\Big(\frac{m\pi\theta}{\alpha}\Big)\Big)\Big]$$

$$K_\theta = \frac{1}{R'^2}\Bigg[\sum_j{}' \left(F_j \sin^2\left(\frac{j\pi\theta}{2\alpha}\right) + D_j \frac{1}{2}\left(\frac{j\pi}{\alpha}\right)^2 \cos\left(\frac{j\pi\theta}{\alpha}\right)\right)\left(1+\frac{r}{R}\sin\phi\right)\sin\phi$$

$$+\sum_m{}'\sum_n{}' \Bigg\{\frac{2r}{R} A_{mn}\left(\psi_{en}\frac{1}{n^2}\cos n\phi + \psi_{on}\frac{1}{n^2}\sin n\phi\right)\sin\phi$$

$$+2C_{mn}\left(\psi_{en}\cos n\phi + \psi_{on}\sin n\phi\right)\Bigg\}\left(\frac{m\pi}{\alpha}\right)^2\cos\left(\frac{2m\pi\theta}{\alpha}\right)$$

$$+\frac{R'}{r}\sum_m{}'\sum_n{}'\Bigg\{B_{mn}\left(-\psi_{en}\frac{1}{n}\sin n\phi + \psi_{on}\frac{1}{n}\cos n\phi\right)\cos\phi$$

$$+C_{mn}\left(\psi_{en} n \sin n\phi - \psi_{on} n \sin n\phi\right)\cos\phi\Bigg\}\times$$

$$\times\left(\psi_{om}\cos^2\left(\frac{m\pi\theta}{\alpha}\right) - \psi_{em}\sin^2\left(\frac{m\pi\theta}{\alpha}\right)\right)$$

$$+\sum_j{}' H_j 2\left(\frac{j\pi}{\alpha}\right)^2\cos\left(\frac{2j\pi\theta}{\alpha}\right)\Bigg]$$

$$K_{\theta\phi} = \frac{1}{rR'}\Bigg[\sum_m{}'\sum_n{}'\Bigg\{A_{mn}\frac{r}{R}\left(-\psi_{en}\frac{1}{n}\sin n\phi + \psi_{on}\cos n\phi\right)\sin\phi$$

$$-A_{mn}\frac{r^2}{RR'}\left(\psi_{en}\frac{1}{n^2}\cos n\phi + \psi_{on}\frac{1}{n^2}\sin n\phi\right)\cos\phi\sin\phi$$

$$+B_{mn}\left(\psi_{en}\frac{1}{n}\sin n\phi - \psi_{on}\frac{1}{n}\cos n\phi\right)$$

$$+C_{mn}\left(-\psi_{en} n \sin n\phi + \psi_{on} n \cos n\phi\right)$$

$$-C_{mn}\frac{r}{R'}\left(\psi_{en}\cos n\phi + \psi_{on}\sin n\phi\right)\cos\phi\Bigg\}\times$$

$$\times\left(\frac{m\pi}{\alpha}\right)\sin\left(\frac{2m\pi\theta}{\alpha}\right)$$

$$-\frac{r}{R'}\sum_j{}' H_j\cos\phi\left(\frac{j\pi}{\alpha}\right)\sin\left(\frac{2j\pi\theta}{\alpha}\right)\Bigg] \qquad \ldots (3.44)$$

where $R' = R + r \sin\phi$

and

$$\begin{aligned} W_J &= \text{[illegible]} \quad , \quad J = 1, 2, 3, \text{---}, JT \\ W_n &= \text{[illegible]} \quad , \quad n = 2, 3, 4, \text{---}, NT + 1 \\ W_m &= \text{[illegible]} \quad , \quad m = 1, 2, 3, \text{---}, MT \end{aligned}$$

The complete strains as given above will only be used in method No. 3. Simpler forms, described later, will be used for methods Nos. 1 and 2.

(3.4) Solutions Using Hand Integration

Before performing the more complex procedure using the complete strains as given in (3.44), it is worth examining some 'simpler' solutions. Although the displacements and strains in these simpler methods are not as complicated as the complete strains, the work involved in obtaining a solution is possibly more time consuming than method No. 3.

Method No. 3 was developed to overcome the limitations involved when using hand integration and to allow the removal of as many assumptions as possible. Nevertheless, the simple solutions are valuable as they give a useful insight to the problem.

(3.4a) Method No. 1

This method involves the use of most of the simplifications discussed earlier. These can be summarised as follows,

1. $\epsilon_\phi = 0$, giving $v_b = -\int \omega_b \, d\phi$ from (3.25)
2. $\gamma_{\theta\phi} = 0$, giving $u_b = \frac{r}{R} \iint \frac{\partial \omega_b}{\partial \theta} \, d\phi \, d\phi$ from (3.39)
3. $\frac{r}{R} \ll 1$
4. K_θ and $K_{\theta\phi}$ assumed to be small and neglected from strain energy.
5. $\epsilon_\theta^n = 0$ at $\phi = 0$, giving $u_c = \int V_c \, d\theta$, permitting use of equations (3.5) for rigid displacements.

Further, thin shell theory will be used and its inherent assumptions applied.

All the displacements can be derived from the specification of V_c and ω_b. These are taken from (3.9) and (3.12a) with (3.20) respectively. i.e.

$$V_c = -\sum_{J=1,2}^{1} D_J \sin^2\left(\frac{J\pi\theta}{2\alpha}\right)$$

$$\omega_D = \sum_{m=1,3}' \sum_{n=2,4}' C_{mn} \cos n\phi \cos^2\left(\frac{m\pi\theta}{\alpha}\right)$$

... (3.45)

These are the simplest possible displacements giving a recognizable solution. ω_D is the same as that used by Findlay [99].

The total displacements are now given by,

$$u = \sum_j' D_j \tfrac{1}{2}\left(\left(\theta - \left(\frac{\alpha}{j\pi}\right)\sin\left(\frac{j\pi\theta}{\alpha}\right)\right)\left(1 + \frac{r}{R}\sin\phi\right) + \left(\frac{j\pi}{\alpha}\right)\sin\left(\frac{j\pi\theta}{\alpha}\right)\frac{r}{R}\sin\phi\right.$$

$$\left. + \frac{r}{R}\sum_m' \sum_n' C_{mn}\left(\frac{m\pi}{n^2\alpha}\right)\cos n\phi \sin\left(\frac{2m\pi\theta}{\alpha}\right)\right)$$

$$v = -\sum_j' D_j \sin^2\left(\frac{j\pi\theta}{2\alpha}\right)\cos\phi - \sum_m' \sum_n' C_{mn}\frac{1}{n}\sin n\phi \cos^2\left(\frac{m\pi\theta}{\alpha}\right)$$

$$w = -\sum_j' D_j \sin^2\left(\frac{j\pi\theta}{2\alpha}\right)\sin\phi + \sum_m' \sum_n' C_{mn}\cos n\phi \cos^2\left(\frac{m\pi\theta}{\alpha}\right)$$

... (3.46)

where

m = 1, 3, 5 ---, MTx2-1

n = 2, 4, 6 ---, NTx2

j = 1, 2, 3 ---, JT

The displacements together with the previously stated assumptions give the strains as,

$$\epsilon_\theta = \frac{1}{R}\left[\frac{r}{R}\sum_j' D_j \tfrac{1}{2}\left(1 + \cos\left(\frac{j\pi\theta}{\alpha}\right)\left(\left(\frac{j\pi}{\alpha}\right)^2 - 1\right)\right)\sin\phi\right.$$

$$\left. + \sum_m' \sum_n' C_{mn}\cos^2\left(\frac{m\pi\theta}{\alpha}\right)\left(\cos n\phi \sin\phi - \frac{1}{n}\sin n\phi \cos\phi\right)\right.$$

$$+$$

$$+\frac{2r}{R}\sum_m'\sum_n' C_{mn}\left(\frac{m\pi}{n\alpha}\right)^2\cos n\phi\cos\left(\frac{2m\pi\theta}{\alpha}\right)\Bigg]$$

$$K_\phi = \frac{1}{r^2}\left[\sum_m'\sum_n' C_{mn}(n^2-1)\cos n\phi\cos^2\left(\frac{m\pi\theta}{\alpha}\right)\right]$$

... (3.47)

Comparison of these with (3.44) reveals the considerable simplification involved.

The total potential energy is found by substituting (3.47) into

$$V = \frac{C}{2}\int_0^{2\pi}\int_{-\frac{\alpha}{2}}^{\frac{\alpha}{2}}\left[\epsilon_\theta^2 + \frac{t^2}{12}K_\phi^2\right] r R\, d\theta\, d\phi - M\gamma$$

where $$C = \frac{Et}{(1-\nu^2)}$$ ... (3.48)

The rotation between the ends of the pipe bend, γ, is found from $2\gamma_c$ (equation (3.3)) at $\theta = \frac{\alpha}{2}$, as

$$\gamma = \frac{1}{R}\sum_j' D_j\left(\frac{\alpha}{2} + \sin\left(\frac{j\pi}{2}\right)\left(\frac{j\pi}{\alpha} - \frac{\alpha}{j\pi}\right)\right)$$

... (3.49)

Substituting (3.47) and (3.49) into (3.48), and integrating gives,

$$\bar{V} = \sum_j'\sum_k' D_j D_k \Phi_1 + \sum_m'\sum_j' \bar{C}_{m2}\bar{D}_j\Phi_2$$

$$+\sum_m'\sum_p'\sum_n'\left(\bar{C}_{mn}\bar{C}_{pn}\Phi_3 + \bar{C}_{mn}\bar{C}_{p,n+2}\Phi_4\right) - \sum_j' D_j\Phi_5$$

... (3.50)

where $\bar{V} = V \Big/ \left(\frac{M\gamma_0}{2(1-\nu^2)}\right)$, $\gamma_0 = \frac{MR\alpha}{EI}$, $I = \pi r^3 t$

$$\bar{D}_j = D_j / R\gamma_0 \quad , \quad \bar{C}_{mn} = C_{mn} \Big/ \left(\frac{\alpha}{r\gamma_0}\right) \quad , \quad \lambda = \frac{tR}{r^2}$$

$$\Phi_1 = \frac{\alpha}{2}\left\{\frac{\alpha}{2} + \left(\frac{j\pi}{\alpha} - \frac{\alpha}{j\pi}\right)\sin\frac{j\pi}{2} + \left(\frac{k\pi}{\alpha} - \frac{\alpha}{k\pi}\right)\sin\frac{k\pi}{2}\right.$$

$$\left. + \frac{1}{2}\left(\left(\frac{j\pi}{\alpha}\right)^2 - 1\right)\left(\left(\frac{k\pi}{\alpha}\right)^2 - 1\right)\left(\frac{\sin\left(\frac{\pi}{2}(j+k)\right)}{\frac{\pi}{2}(j+k)} + \frac{\sin\left(\frac{\pi}{2}(j-k)\right)}{\frac{\pi}{2}(j-k)}(1-\delta_{jk}) + \frac{\alpha}{2}\delta_{jk}\right)\right\}$$

$$\Phi_2 = -\frac{3}{2}\left\{\frac{\alpha}{4} + \frac{1}{2}\left(\frac{j\pi}{\alpha} - \frac{\alpha}{j\pi}\right)\sin\left(\frac{j\pi}{2}\right) + \frac{\left(\left(\frac{j\pi}{\alpha}\right)^2 - 1\right)}{4}\left(\frac{\sin\left(\frac{\pi}{2}(2m+j)\right)}{\frac{\pi}{2}(2m+j)} + \frac{\sin\left(\frac{\pi}{2}(2m-j)\right)}{\frac{\pi}{2}(2m-j)}(1-\delta_{(2m)j}) + \frac{\alpha}{2}\delta_{(2m)j}\right)\right\}$$

$$\Phi_3 = 2\left(\frac{r}{R}\right)^2\left(\frac{m\pi}{\alpha}\right)^4\delta_{mp} + (1+\delta_{mp})\left(\frac{(n^2+1)}{8n^2} + \frac{\lambda^2(n^2-1)^2}{48}\right)$$

$$\Phi_4 = -(1+\delta_{mp})\left(\frac{n^2+2n-3}{8n(n+2)}\right)$$

$$\Phi_5 = \left(\frac{\alpha}{2} + \sin\left(\frac{j\pi}{2}\right)\left(\frac{j\pi}{\alpha} - \frac{\alpha}{j\pi}\right)\right) 2(1-\nu^2) \qquad \ldots (3.51)$$

$\delta_{mp} = \begin{cases} 1 \text{ if } m = P \\ 0 \text{ if } m \neq P \end{cases}$ - kronecker delta symbol.

also $j,k = 1, 2, 3, \text{——}, JT$

$m,P = 1, 3, 5, \text{——}, MTx2 - 1$

$n = 2, 4, 6, \text{——}, NTx2$

Details of the integrations are given in appendix (2).

The values of the coefficients, D_j and Cmn are found by minimising the total potential energy function $\bar{V}$ using, for all j,

$$\frac{\partial \bar{V}}{\partial D_j} = 0 = 2\sum_k \bar{D}_k \Phi_1 + \sum_m \bar{C}_{m2}\Phi_2 - \Phi_5$$

for all "m" and "n"

$$\frac{\partial \bar{V}}{\partial C_{mn}} = 0 = \sum_j' D_j \Phi_2 + 2 \sum_p' \bar{C}_{pn} \Phi_3 + \sum_p' \bar{C}_{pn+2} \Phi_4 + \sum_p' \bar{C}_{pn-2} \Phi_6$$

... (3.52)

where

$$\Phi_6 = -\left(1 + \frac{\delta_{mp}}{2}\right)\left(\frac{n^2 - 2n - 3}{8n(n-2)}\right)$$

This gives a set of linear simultaneous equations which can be rewritten as a matrix equation of the form,

$$[A]\{x\} = \{b\}$$

... (3.53)

where [A] is a square matrix containing the constants in equations (3.52) corresponding to the required coefficients in the vector $\{x\}$. The vector $\{b\}$ contains the constants occuring in equations (3.52) which are not multiplied by one of the unknown coefficients. The above matrix equation can be solved using a standard method such as the Gauss algorithm. This will be discussed in more detail later with regard to the more complex solution procedure. The total number of equations to be solved is (MT x NT + JT).

The solution of the above matrix equation was performed on a "Compukit UK101" micro-computer constructed by the author. The solution program, written in "BASIC" [153], and the data necessary for finding up to thirty five coefficients, can be contained in 8 kilobytes of random access memory. The time taken for a solution

was/

less than three minutes even for the largest matrices. The program can be written in less than sixty lines of BASIC.

Once the coefficients have been obtained, the required flexibility factors can be found. From the definition of flexibility factor given in the introduction to chapter 1, and the end rotation given in equation (3.49), i.e.

$$K = \sum_{J}' \bar{D}_J \left(\frac{\alpha}{2} + \sin\left(\frac{J\pi}{2}\right)\left(\frac{J\pi}{\alpha} - \frac{\alpha}{J\pi}\right)\right)$$

where $\bar{D}_J = D_J / R\gamma_0$, $\gamma_0 = \frac{MR\alpha}{EI}$

... (3.54)

In the present work, K represents the overall flexibility factor of the bend.

Presentation and discussion of the results will be left until the second method has been explained.

(3.4b) Method No. 2

This method removes the assumption of zero shear strain used in the last analysis, and involves rather more complex displacements. All the other assumptions used in the last analysis will be used.

For this method three displacements have to be specified, V_c, u_D and ω_D. These are taken from (3.9), (3.41), (3.12b) and (3.20), i.e.

$$V_c = -\sum_{J=1,2}' D_J \sin^2\left(\frac{J\pi\theta}{2\alpha}\right)$$

$$u_D = \frac{r}{R} \sum_{m=1,3}' \sum_{n=2,3}' A_{mn} \left(\psi_{en}\frac{1}{n^2}\cos n\phi + \psi_{on}\frac{1}{n^2}\sin n\phi\right)\left(\frac{m\pi}{\alpha}\right)\sin\left(\frac{2m\pi\theta}{\alpha}\right)$$

$$\omega_D = \sum_{m=1,3}^{\prime} \sum_{n=2,3}^{\prime} C_{mn} \left(\psi_{en} \cos n\phi + \psi_{on} \sin n\phi \right) \cos^2\left(\frac{m\pi\theta}{\alpha}\right)$$

... (3.55)

From these the total displacements can be found, using equations (3.6) and (3.25), as

$$u = \sum_{j}^{\prime} D_j \tfrac{1}{2} \left(\left(\theta - \frac{\alpha}{j\pi} \sin\left(\frac{j\pi\theta}{\alpha}\right) \right) \left(1 + \frac{r}{R} \sin\phi \right) + \left(\frac{j\pi}{\alpha}\right) \sin\left(\frac{j\pi\theta}{\alpha}\right) \frac{r}{R} \sin\phi \right.$$

$$\left. + \frac{r}{R} \sum_{m}^{\prime} \sum_{n}^{\prime} A_{mn} \left(\psi_{en} \frac{1}{n^2} \cos n\phi + \psi_{on} \frac{1}{n^2} \sin n\phi \right) \left(\frac{m\pi}{\alpha}\right) \sin\left(\frac{2m\pi\theta}{\alpha}\right) \right.$$

$$v = -\sum_{j}^{\prime} D_j \sin\left(\frac{j\pi\theta}{2\alpha}\right) \cos\phi$$

$$+ \sum_{m}^{\prime} \sum_{n}^{\prime} C_{mn} \left(-\psi_{en} \frac{1}{n} \sin n\phi + \psi_{on} \frac{1}{n} \cos n\phi \right) \cos^2\left(\frac{m\pi\theta}{\alpha}\right)$$

$$\omega = -\sum_{j}^{\prime} D_j \cos\left(\frac{j\pi\theta}{\alpha}\right) \sin\phi$$

$$+ \sum_{m}^{\prime} \sum_{n}^{\prime} C_{mn} \left(\psi_{en} \cos n\phi + \psi_{on} \sin n\phi \right) \cos^2\left(\frac{m\pi\theta}{\alpha}\right)$$

... (3.56)

where $\sum_{m}^{\prime}$ is m = 1, 3, 5---, MT x 2-1

$\sum_{n}^{\prime}$ is n = 2, 3, 4——, NT + 1

$\sum_{j}^{\prime}$ is j = 1, 2, 3---, JT

Substituting these into the relevant strain displacement equations (2.13) but taking the shear strain $\gamma_{\theta\phi}$ from (3.37) gives,

$$\epsilon_\theta = \frac{1}{R}\left[\frac{r}{R}\sum_j{}' D_j \frac{1}{2}\left(1+\cos\left(\frac{j\pi\theta}{\alpha}\right)\left(\left(\frac{j\pi}{\alpha}\right)^2-1\right)\right)\sin\phi\right.$$

$$+\frac{2r}{R}\sum_m{}'\sum_n{}' A_{mn}\left(\psi_{en}\cos n\phi+\psi_{on}\sin n\phi\right)\left(\frac{m\pi}{\alpha}\right)^2\cos\left(\frac{2m\pi\theta}{\alpha}\right)$$

$$+\sum_m{}'\sum_n{}' C_{mn}\left(\left(-\psi_{en}\frac{1}{n}\sin n\phi+\psi_{on}\frac{1}{n}\cos n\phi\right)\cos\phi\right.$$

$$\left.\left.+\left(\psi_{en}\cos n\phi+\psi_{on}\sin n\phi\right)\sin\phi\right)\cos^2\left(\frac{m\pi\theta}{\alpha}\right)\right]$$

$$\gamma_{\theta\phi} = \frac{1}{R}\left[\sum_m{}'\sum_n{}' \left(C_{mn}-A_{mn}\right)\left(\psi_{en}\sin n\phi-\psi_{on}\cos n\phi\right)\left(\frac{m\pi}{\alpha}\right)\sin\left(\frac{2m\pi\theta}{\alpha}\right)\right]$$

$$K_\phi = \frac{1}{r^2}\left[\sum_m{}'\sum_n{}' C_{mn}\left(n^2-1\right)\left(\psi_{en}\cos n\phi+\psi_{on}\sin n\phi\right)\cos^2\left(\frac{m\pi\theta}{\alpha}\right)\right]$$

... (3.57)

The total potential energy is found by substituting (3.57) into,

$$V = \frac{C}{2}\int_0^{2\pi}\int_{-\frac{\alpha}{2}}^{\frac{\alpha}{2}}\left[\epsilon_\theta^2+\frac{(1-\nu)}{2}\gamma_{\theta\phi}^2+\frac{t^2}{12}K_\phi^2\right] rR\,d\theta\,d\phi - M\gamma$$

... (3.58)

When (3.58) is integrated, the following expression is derived for the non-dimensionalised total potential energy, $\bar{V}$,

$$\bar{V} = \sum_j{}'\sum_k{}' \bar{D}_j\bar{D}_k\bar{I}_1+\sum_m{}'\sum_j{}' \bar{C}_{m2}\bar{D}_j\bar{I}_2+\sum_m{}'\sum_n{}'\sum_p{}'\left(\bar{C}_{mn}\bar{C}_{pn}\bar{I}_7+\bar{C}_{mn}\bar{C}_{pm2}\bar{I}_4\right.$$

$$\left.+\bar{A}_{mn}\bar{A}_{pn}\bar{I}_8+\bar{A}_{mn}\bar{C}_{pn}\bar{I}_9+\bar{A}_{mn+1}\bar{C}_{pn}\bar{I}_{10}+\bar{A}_{mn-1}\bar{C}_{pn}\bar{I}_{11}\right)-\sum_j{}'\bar{D}_j\bar{I}_5$$

where $\bar{V} = V\Big/\left(\frac{M\gamma_0}{2(1-\nu^2)}\right)$, $\bar{D}_j = \frac{D_j}{R\gamma_0}$, $\bar{A}_{mn} = A_{mn}\left(\frac{\alpha}{r\gamma_0}\right)$, $\bar{C}_{mn} = C_{mn}\left(\frac{\alpha}{r\gamma_0}\right)$

... (3.59)

also $j,k = 1, 2, 3, \text{----}, JT$

$m,P = 1, 3, 5, \text{----}, MT \times 2-1$

$n = 2, 3, 4, \text{----}, NT + 1$

$\bar{\Phi}_1, \bar{\Phi}_2, \bar{\Phi}_4$ and $\bar{\Phi}_8$ were given in equations (3.51).

The others are,

$$\bar{\Phi}_7 = \frac{(1-\nu)}{4}\left(\frac{m\pi}{n\alpha}\right)^2\delta_{mp} + \left(1+\frac{\delta_{mp}}{2}\right)\left(\frac{n^2+1}{8n^2} + \frac{\lambda^2(n^2-1)^2}{48}\right)$$

$$\bar{\Phi}_8 = \frac{(1-\nu)}{4}\left(\frac{m\pi}{n\alpha}\right)^2\delta_{mp} + 2\left(\frac{\Gamma}{R}\right)^2\left(\frac{m\pi}{n\alpha}\right)^4\delta_{mp}$$

$$\bar{\Phi}_9 = -\frac{(1-\nu)}{2}\left(\frac{m\pi}{n\alpha}\right)^2\delta_{mp}$$

$$\bar{\Phi}_{10} = \frac{\Gamma}{2R}\left(\frac{m\pi}{n\alpha}\right)^2\frac{n(n-1)}{(n+1)^2}(-1)^n\delta_{mp}$$

$$\bar{\Phi}_{11} = \frac{-\Gamma}{2R}\left(\frac{m\pi}{n\alpha}\right)^2\frac{n(n+1)}{(n-1)^2}(-1)^n\delta_{mp}$$

... (3.60)

Details of the integrations can be found in appendix (2).

The values of the coefficients, D_j, Amn and Cmn are obtained by minimising the total potential energy function using,

for all j,

$$\frac{\partial\bar{V}}{\partial D_j} = 0 = 2\sum_1 \bar{D}_k\bar{\Phi}_1 + \sum_m \bar{C}_{m2}\bar{\Phi}_2 - \bar{\Phi}_5$$

for all m and n,

$$\frac{\partial\bar{V}}{\partial A_{mn}} = 0 = \sum_p\left(2\bar{A}_{pn}\bar{\Phi}_8 + \bar{C}_{pn}\bar{\Phi}_9 + \bar{C}_{p,n+1}\bar{\Phi}_{12} + \bar{C}_{p,n-1}\bar{\Phi}_{13}\right)$$

$$\frac{\partial\bar{V}}{\partial C_{mn}} = 0 = \sum_p\left(2\bar{C}_{pn}\bar{\Phi}_7 + \bar{A}_{pn}\bar{\Phi}_9 + \bar{C}_{p,n+2}\bar{\Phi}_4 + \bar{C}_{p,n-2}\bar{\Phi}_6 + \bar{A}_{m,n+1}\bar{\Phi}_{10} +\right.$$

$$+ \bar{A}_{mn-1} \mathcal{F}_{11}) + \sum_j D_j \mathcal{F}_2$$

... (3.61)

where

$$\mathcal{F}_{12} = \frac{\Gamma}{2R} \left(\frac{m\pi}{n\alpha}\right)^2 \frac{(n+2)}{(n+1)} (-1)^n \delta_{mp}$$

$$\mathcal{F}_{12} = -\frac{\Gamma}{2R} \left(\frac{m\pi}{n\alpha}\right)^2 \frac{(n-2)}{(n-1)} (-1)^n \delta_{mp}$$

... (3.62)

These give a system of (JT + 2×MT x NT) linear simultaneous equations which can be solved using the method previously outlined.

The flexibility factors can be found from equation (3.54).

(3.4c) Flexibility Factors from Methods 1 and 2

Previous investigators, working on a Karman type single series solution for a bend with no end effects, had a relatively simple task of ensuring that the flexibility factors had converged. Convergence was accepted when the difference between NT and (NT + 1) was below a certain arbitrary limit. Most people found, using a series of the type given in (3.12) that the following number of terms was adequate, for particular limits of the pipe parameter, λ,

$$\lambda > .5 \quad , \quad NT = 1$$
$$.5 > \lambda > .12 \quad , \quad NT = 2$$
$$.12 > \lambda > .06 \quad , \quad NT = 3$$
$$.06 > \lambda > .04 \quad , \quad NT = 4$$

where/

where NT is the total number of terms required. These results being taken from Rodabaugh and George [31].

In the current problem, convergence has to be considered with respect to j, m and n. Further, as will be shown later, the results are found to vary not only with the pipe parameter, λ, but also with the bend angle, α, and the radius ratio, R/r. Results also vary by a small amount with Poissons ratio, ν, but throughout this work this will be taken as 0.3. The simplest way to resolve this dilemma is to examine the flexibility factors for some low λ value, as j, m and n are increased. More terms will be necessary when the distortion of the cross-sections is greatest i.e. when the flexibility is highest. Therefore, the convergence will be examined for large R/r and α as these should have the highest flexibility. Once a set of j, m, and n is found for this set of parameters, it should be suitable for any bend with a higher λ and lower R/r and α values. The parameters chosen for convergence checking are $\alpha = 180^{\circ}$, $\lambda = 0.1$, R/r = 10, $\nu = 0.3$. The convergence results for both methods are given in the following table of flexibility factors (K):

Table (3.1) - Flexibility Convergence							
$\lambda = .1$, $R/r = 10$, $\alpha = 180^\circ$							
Method 1				Method 2			
JT	MT	NT	K	JT	MT	NT	K
1	1	1	2.22	1	1	1	2.22
1	1	2	2.42	1	1	2	2.23
1	2	1	2.66	1	2	1	2.71
2	1	1	5.56	2	1	1	5.57
2	2	2	9.69	2	2	2	5.76
2	2	3	10.04	2	2	3	10.00
2	3	2	9.71	2	2	5	10.41
3	2	2	9.69	3	2	5	10.41
3	3	3	10.06	2	3	5	10.48
5	5	5	10.14	3	3	5	10.48

For discussion purposes the number of terms required for convergence is conveniently expressed by (JT, MT, NT); for example, JT = 2, MT = 2 and NT = 3 are represented by (2, 2, 3).

From table (3.1), the flexibility factor for (2, 2, 3) has converged to within 1% of the result for (5, 5, 5) for method 1. Thus, method 1 can be considered as being sufficiently converged when using (2, 2, 3) with $\lambda \geq .1$, $R/r \leq 10$ and $\alpha \leq 180^\circ$. This has been confirmed by checking convergence for other values of the three main characterising parameters. Similarly, for method 2, (2, 2, 5) can be considered as sufficiently converged.

Some results for method 1 with (2, 2, 3) and method 2 with (2, 2, 5) are given in the following table:

Table (3.2)					
Flanged Bend - Flexibility Factors					
		METHOD 1 (2, 2, 3)		METHOD 2 (2, 2, 5)	
R/r	λ	$\alpha = 180^\circ$	$\alpha = 90^\circ$	$\alpha = 180^\circ$	$\alpha = 90^\circ$
10	.1	10.04	4.72	10.41	6.06
	.2	5.45	3.57	5.52	4.07
	.5	2.35	2.05	2.36	2.11
	1	1.37	1.31	1.37	1.32
3	.1	5.72	1.45	7.72	2.31
	.2	4.03	1.42	4.70	2.11
	.5	2.14	1.31	2.23	1.64
	1	1.32	1.15	1.34	1.24

These results show a significant variation not only with the pipe factor, λ, as in the Karman case, but also with the bend angle, α, and radius ratio R/r. The flexibility increases as λ reduces and as R/r and α increases. Methods 1 and 2 are compared in figure (3.8). Method 1 can be seen to give lower results, especially at low R/r and α. For R/r = 3 and $\alpha = 90^\circ$, method No. 2 can be more than 50% higher. The difference is probably worse for low R/r because the $\gamma_{\theta\phi} = 0$ assumption, which method No. 1 included and method No. 2 did not, is more valid for larger R/r. Examination of the Amn and Cmn coefficients from method no. 2 confirmed this. Examination of these coefficients also revealed that the odd fourier terms (i.e. sin $n\phi$, n = 3, 5, 7 ——) in the radial distortion displacement series were important. This is in contrast to the analysis of a bend without end effects where the odd fourier terms are zero if $\frac{r}{R}$ is neglected with respect to unity. Jones [35] stated/

stated that the odd fourier terms become more significant for low R/r if this parameter is included in the theory. Examples and further discussion of the coefficients will be given later.

The variation of the flexibility factors involves the pipe factor, λ, which can be written as,

$$\lambda = \frac{R}{r} \cdot \frac{t}{r}$$

Since this is the product of the thickness ratio, t/r, and radius ratio, R/r, the results could be presented in terms of these, but the pipe factor, λ, has become established as a major parameter in the analysis of pipe bends, and will be used herein. However it should not be forgotten that λ includes the thickness ratio since thin shell theory commonly limits this to,

$$t/r \leq 1/10$$

but this is an arbitrarily chosen value. For practical purposes, it should be set by whether or not the results from the theory agree with experiments.

Whatham, in presenting his results, does not give any flexibility factors for $t/r < 1/10$, However, the present author feels that this may be unnecessarily restrictive since some of the bends used in industry are just inside this limit. In the present work results will generally be given for $t/r \leq 1/5$. In figures (3.8) and (3.9) they are given outside this range demonstrating that there is no rapid or sudden transition of the results beyond this limit.

A comparison of the results of method No. 2 with those of Axelrad/

Axelrad and Whatham are given in figure (3.9). The present results show a generally similar variation to those of Axelrad and Whatham with respect to λ, R/r and α. The flexibility factors from method No. 2 are lower by as much as 25%, particularly at lower R/r and α. The results for R/r = 3 and $\alpha = 90^{\circ}$ are somewhat different from the rest. For these parameters, Axelrad's flexibility factors are higher than either of the other results for larger λ values but this changes when λ is low. This is in contrast to the comparison between Whatham and method No. 2 where the lines on the graph are almost parallel, method No. 2 always being lower. The behaviour of Axelrad's results is probably due to them being an approximation developed from one term of a series solution. Experience has shown that this usually gives poorer results for low λ values.

Flexibility factors obtained from the analyses of Findlay and of Thailer and Cheng, presented earlier (figures (3.1) and (3.2)), do not show any variation with R/r. Method No. 2 is an improvement over both of these methods in both displacement series and assumptions. The major difference between the analyses is in the assumption regarding the shear strain, $\gamma_{\theta\phi}$. Findlay appreciated the significance of the shear strain but not of the circumferential tangential displacement u_θ . Thailer and Cheng assumed the shear strain was zero but did not enforce it on their displacements.

Although the results of method No. 2 and Whatham show reasonable agreement, they are not close enough to confirm each other conclusively. To resolve this problem, as many as possible of the assumptions used in method No. 2 would have to be removed. This forms the basis of method No. 3 to be presented in section (3.5).

(3.5) Method No. 3 - Numerical Solution

(3.5a) Introduction

Displacement series (3.43) and strain equations (3.44) developed earlier will be used for the numerical solution of the flanged bend problem. The displacements (3.43) involved the use of few assumptions and included all possible fourier terms in their series. They also satisfy all of the necessary boundary conditions for a smooth pipe bend with flanges. The strains (3.44) were derived from the displacements and satisfy the requirements of internal and external compatibility.

If the strains given in (3.44) are substituted into the expression for the strain energy, given in equation (2.16) from which the total potential energy can be found, then integration of the expression by hand is virtually impossible. The solution therefore requires the use of numerical techniques.

(3.5b) Numerical Solution Methods

The numerical minimum of the total potential energy (T.P.E.) function is usually obtained in one of two basic ways.

The simplest way is to numerically integrate the whole T.P.E. function and then use a standard method of direct numerical minimisation. There are many different ways of performing direct minimisation (e.g. [154] and [155]). Most of them use some method of searching which is based on evaluation of the complete T.P.E. function. The simplicity of this method is that it only requires the values of the T.P.E. function, for coefficient values

that/

that the minimisation routine provides, which is straightforward to program on a computer. This was the procedure used by Spence [70] in his analyses of creep in pipe bends without end effects. Unfortunately, the procedure of having to numerically integrate the T.P.E. in two dimensions and then minimise with respect to a large number of variables (105 will eventually be used) is time consuming. The time required is also indeterminate as the minimisation uses as many function evaluations as it needs to find the minimum and not a fixed number. Spence only required a one dimensional integration and rarely needed to use more than five variables in his problem. An attempt was made to use this method but the number of variables was found to be limited to about fifty before the computer time and reliability limit of two hours was reached. The computer was an ICL 2980, which was the fastest available to the author.

Another method of finding the minimum numerically was used by Symonds [151], Jones [35] and Thailer-Cheng in their analyses of the pipe bend problem. This method involves differentiating with respect to each of the required displacement coefficients before performing the integrations. This then produces a set of simultaneous equations which can be solved. The difficulty in this method is that all of the terms in the solution matrix have to be numerically integrated separately. Although general expressions can be derived for many of the terms in the matrix there is still a large amount of hand manipulation involved in obtaining a solution. This method has advantages over the previous method. The time required for a solution would be much smaller and determinate. This method was attempted and abandoned because the size of the current/

current problem made it extremely difficult.

The ideal solution procedure would use only the values of the complete T.P.E. expression and minimisation would be performed using the matrix technique. It was from this, and the experience of the earlier hand integration methods that the author developed the following solution procedure which is designed to make full use of the facilities available from a computer.

(3.5c) Minimisation Procedure

The total potential energy expression for linear elasticity is a quadratic function of the displacement coefficients. This means that when the T.P.E. is differentiated with respect to the coefficients, the resulting equations are linear functions of the displacement coefficients. Since displacement coefficients are not functions of the bend co-ordinates, integration can be performed without numerical values for the coefficients.

The above principles are the basis of the minimisation procedure about to be described. The author has not found other reference to this method in any of the literature to date.

The simplest way to explain the method is with an example. Consider the following quadratic expression,

$$V = \int \left(a_1 x_1^2 + a_2 x_2^2 + a_3 x_1 x_2 + a_4 x_1 + a_5 x_2 + a_6 \right) d\xi \qquad \ldots (3.63)$$

where a_1, a_2, a_3, a_4, a_5 and a_6 are functions of ξ .

If V is an expression for the total potential energy then the minimum/

minimum of V can be found by differentiating with respect to the coefficients x_1 and x_2 i.e.

$$\frac{\partial V}{\partial x_1} = 0 = \int (2a_1 x_1 + a_3 x_2 + a_4)\, d\xi$$

$$\frac{\partial V}{\partial x_2} = 0 = \int (2a_2 x_2 + a_3 x_1 + a_5)\, d\xi \qquad \ldots (3.64)$$

These are two simultaneous equations in two unknowns, x_1 and x_2. This can be set up as a matrix equation,

$$\begin{bmatrix} 2\int a_1 d\xi & \int a_3 d\xi \\ \int a_3 d\xi & 2\int a_2 d\xi \end{bmatrix} \begin{Bmatrix} x_1 \\ x_2 \end{Bmatrix} = \begin{Bmatrix} -\int a_4 d\xi \\ -\int a_5 d\xi \end{Bmatrix}$$

or $$[A]\{x\} = \{B\} \qquad \ldots (3.65)$$

where $[A]$ is a matrix of constants, $\{x\}$ is a vector of the unknowns and $\{B\}$ is a vector of constants.

The terms in the matrix $[A]$ and vector $\{B\}$ can be numerically integrated and the matrix equation solved for the required coefficients x_1 and x_2. This is the basis of the second numerical method described in section (3.5b). The difficulties arise in the setting up of equation (3.64) and the separation and programming of equation (3.65).

The new method derives the terms of the matrix $[A]$ and vector $\{B\}$ directly from the complete T.P.E. function (3.63). To explain the method the following definitions will be used. A coefficient will be termed "active" if it is given the value of +1, "passive"/

"passive" if it is given the value of 0 and "negative active" if it is given the value of -1. i.e.

$\chi = 1$ is active

$\chi = 0$ is passive

$\chi = -1$ is negative active

If all the coefficients are made passive and V is evaluated then the following is obtained,

$$\chi_1 \text{ and } \chi_2 \text{ passive} \longrightarrow \int a_6 \, d\xi \qquad \ldots (3.66)$$

If each of the coefficients is made active in turn with the rest passive, then V gives,

$$\chi_1 \text{ active} \longrightarrow \int (a_1 + a_4 + a_6) \, d\xi$$
$$\chi_2 \text{ active} \longrightarrow \int (a_2 + a_5 + a_6) \, d\xi \qquad \ldots (3.67)$$

Similarly, if each coefficient is made negative active, with the rest passive, then

$$\chi_1 \text{ negative active} \longrightarrow \int (a_1 - a_4 + a_6) \, d\xi$$
$$\chi_2 \text{ negative active} \longrightarrow \int (a_2 - a_5 + a_6) \, d\xi \qquad \ldots (3.68)$$

Adding (3.67) and (3.68), and subtracting twice (3.66) gives

$$2 \int a_1 \, d\xi$$

$$2 \int a_2 \, d\xi \qquad \ldots (3.69)$$

which are the diagonal terms in the solution matrix [A].

Subtracting (3.67) from (3.68) and dividing the results by two gives/

gives $-\int a_4 d\xi$

$-\int a_5 d\xi$

... (3.70)

which are the terms of the vector $\{B\}$.

The off diagonal terms of the matrix [A] are obtained by making a term active and then the value of V is found with one of the remaining terms made active with the rest passive i.e. two different terms are made active for each evaluation. For the example this is,

x_1 and x_2 active, $\int(a_1+a_2+a_3+a_4+a_5+a_6)\,d\xi$ ... (3.71)

The off diagonal term is then found by sub tracting (3.66) and half of (3.69) from (3.71) and adding (3.70), giving,

$\int a_3 d\xi$

... (3.72)

Thus, the complete matrix equation can be formulated from the total potential energy function.

Generalising this to obtain a matrix of "N" equations is reasonably straightforward. The only additional comment necessary is with regard to the position of the off diagonal terms in the matrix. If the first active coefficient is x_r and the second is x_c then the obtained coefficient should be positioned on row "r" and column "c".

The total number of function evaluations required for a solution involving "N" coefficients is $(N^2 + N + 1)$. This can be reduced by nearly half if use is made of the symmetry of the matrix obtained/

obtained from the differentiation of the T.P.E. function.

The time involved in calculating the values of the T.P.E. can be reduced by just calculating the parts of the function which involve the active constants, where possible. This can represent a considerable saving in the running time of the computer program since most of the time is spent calculating the values of the function.

(3.5d) Numerical Integration

The strain energy part of the T.P.E. function has to be integrated in two dimensions, θ and ϕ. There are many different ways of numerically integrating a function of this type (e.g. see [148], [149] and [156]. These were examined to find the best one for use with the present method. The chosen method is an extension of the well known Simpson's $\frac{1}{3}$ rule to two dimensions.

Consider a double integral of the form,

$$\Phi = \int_c^d \int_a^b f(\theta, \phi)\, d\theta\, d\phi \qquad \ldots(3.73)$$

In the calculus, a double integral is evaluated as an iterated integral i.e. the inner integral is calculated first; then the outer integral. Similarly, a double numerical integral can be found by first applying Simpson's rule to the inner integral and then outer integral. This gives the integral as,

$$\Phi = \sum_{k=1}^{K} \sum_{j=1}^{J} W_j W_k^* f_{jk} \qquad \ldots(3.74)$$

where/

where f_{jk} are the values of the function $f(\theta,\phi)$ at θ_j and ϕ_k. The intervals $\theta = a$ to $\theta = b$ and $\phi = c$ to $\phi = d$ are subdivided into (J-1) and (K-1) intervals, respectively. θ_j and ϕ_k therefore correspond to,

$$\theta_j = a + j\Delta\theta \quad \text{and} \quad \phi = c + k\Delta\phi$$

where $\Delta\theta = (b-a)/(J-1)$ and $\Delta\phi = (d-c)/(K-1)$

... (3.75)

W_j and W_k^* in equation (3.74) are the weightings applied to each value of the function, f_{jk}. For Simpson's rule in two-dimensions, these are given by,

$$W_1 = W_J = \frac{\Delta\theta}{3} \quad \text{and} \quad W_1^* = W_K^* = \frac{\Delta\phi}{3}$$

$$W_j = \frac{\Delta\theta}{3}(3+(-1)^j) \qquad W_k^* = \frac{\Delta\phi}{3}(3+(-1)^k)$$

where

$$j = 2, 3, \text{----}, J-1 \qquad k = 2, 3, \text{----} K-1$$

... (3.76)

The above equation allows a different number of integration points in each direction which is useful in the pipe bend problem which has widely differing behaviour in the θ and ϕ directions.

One other property of Simpson's rule is that it converges to the correct answer when more points are taken between the integration limits.

(3.5e) Solution of Matrix Equation

In/

In [157], Meyer examined all of the major matrix solution routines in the context of structural analysis. In the present problem careful consideration has to be given to the choice of the solution routine because of the size of the matrix. A typical matrix for the present problem has 105 rows which requires at least ten thousand storage locations in a computer for the [A] matrix.

Meyer states that no method exists which requires less arithmetic operations than Gaussian elimination. Also most systems of linear equations arising from structural problems are positive definite and well-posed in a mathematical sense and the accuracy of the solution from the Gauss algorithm is usually sufficient. Gaussian elimination will be used herein.

The standard Gauss algorithm, which dates as far back as 1826, is given in Appendix (3). This method can be adapted to use the symmetry of the matrix and thus reduce the solution time. On the computer, the matrix can be solved in its own storage, reducing storage requirements to a minimum.

(3.5f) Total Potential Energy

The total potential energy expression is,

$$V = \frac{C}{2}\int_0^{\pi}\int_{-\frac{\pi}{2}}^{\frac{\pi}{2}}\left[(\epsilon_\phi+\epsilon_\theta)^2-2(1-\nu)(\epsilon_\theta\epsilon_\phi-\tfrac{1}{4}\gamma_{\theta\phi}^2)\right] r R' d\theta d\phi$$

$$+\frac{D}{2}\int_0^{\pi}\int_{-\frac{\pi}{2}}^{\frac{\pi}{2}}\left[(K_\phi+K_\theta)^2-2(1-\nu)(K_\theta K_\phi-K_{\theta\phi}^2)\right] r R' d\theta d\phi - M\gamma \qquad \ldots (3.77)$$

where

$$C=\frac{Et}{(1-\nu^2)}\quad,\quad D=\frac{Et^3}{12(1-\nu^2)}\quad,\quad R'=R+r\sin\phi$$

γ is the rotation between the ends of the bend which is found by substituting displacement equations (3.9) and (3.10) into (3.3), i.e.

$$\gamma = \frac{1}{R}\sum_{J=1}^{JT}\left(F_J\left(\frac{\alpha}{2} - \frac{\alpha}{J\pi}\sin\left(\frac{J\pi}{2}\right)\right) + D_J\left(\frac{J\pi}{\alpha}\right)\sin\left(\frac{J\pi}{2}\right)\right)$$

... (3.78)

Strain and curvatures from equations (3.44) can be substituted into (3.77) to give the complete T.P.E. function. This needs to be non-dimensionalised so that the solution can be in terms of as few characterising parameters as possible. It can also be used to simplify the function and improve the numerical condition of the matrix. The T.P.E. will be non-dimensionalised using,

$$\bar{V} = V \Big/ \left(\frac{2M\gamma_0}{(1-\nu^2)\pi\alpha}\right)$$

... (3.79)

The reasons for this choice will become apparent later. γ_0, as mentioned earlier, is the rotation of an equivalent length (i.e. $\ell = R\alpha$) of straight pipe under the same load M, as found from simple bending theory. i.e.

$$\gamma_0 = \frac{MR\alpha}{EI} \quad , \quad I = \pi r^3 t$$

... (3.80)

Note that the $(1 - \nu^2)$, omitted by many of the earlier authors using a lower bound approach, has been included in the present/

present work. This will mean that the end rotation will tend towards the value of $(1-\nu^2)\,\gamma_0$ and not γ_0 at high λ values ($\lambda > 2$). A full discussion of the implications of this was given by Spence [4]. A true lower bound is only achieved if it is included.

The non-dimensionalised T.P.E. becomes

$$\bar{V} = \frac{Et}{2(1-\nu^2)} \cdot \frac{(1-\nu^2)\pi\alpha}{2M\gamma_0} \cdot \frac{\Gamma}{R} \cdot 4\,\Phi - (1-\nu^2)\frac{\pi\alpha}{2}\frac{\gamma}{\gamma_0}$$

where in this case

$$\Phi = \int_{-\frac{\pi}{2}}^{\frac{\pi}{2}}\int_{0}^{\frac{\alpha}{2}} \Big[(\epsilon_\phi+\epsilon_\theta)^2 - 2(1-\nu)(\epsilon_\phi\epsilon_\theta - \tfrac{1}{4}\gamma_{\theta\phi}^2) + \frac{t^2}{12}\{(K_\phi+K_\theta)^2 - 2(1-\nu)(K_\phi K_\theta - K_{\theta\phi}^2)\}\Big] RR' d\theta d\phi \qquad \ldots (3.81)$$

re-arranging gives,

$$\bar{V} = \bar{\Phi} - (1-\nu^2)\frac{\pi\alpha}{2}\frac{\gamma}{\gamma_0}$$

where

$$\bar{\Phi} = \left(\frac{\alpha}{\Gamma\gamma_0}\right)^2 \Phi$$

$$= \int_{-\frac{\pi}{2}}^{\frac{\pi}{2}}\int_{0}^{\frac{\alpha}{2}} \Big[(\bar{\epsilon}_\phi+\bar{\epsilon}_\theta)^2 - 2(1-\nu)(\bar{\epsilon}_\phi\bar{\epsilon}_\theta - \tfrac{1}{4}\bar{\gamma}_{\theta\phi}^2) + \frac{\lambda^2}{12}\{(\bar{K}_\phi+\bar{K}_\theta)^2 - 2(1-\nu)(\bar{K}_\phi\bar{K}_\theta - \bar{K}_{\theta\phi}^2)\}\Big] Z\, d\theta\, d\phi$$

and/

and

$$\bar{\epsilon}_\phi = \epsilon_\phi \times \frac{R\alpha}{r\gamma_0} \quad , \quad \bar{\epsilon}_\theta = \epsilon_\theta \times \frac{R\alpha}{r\gamma_0} \quad , \quad \bar{\gamma}_{\theta\phi} = \gamma_{\theta\phi} \frac{R\alpha}{r\gamma_0}$$

$$\bar{K}_\phi = K_\phi \times \left(\frac{r\alpha}{R\gamma_0}\right) \quad , \quad \bar{K}_\theta = K_\theta \times \left(\frac{r\alpha}{R\gamma_0}\right) \quad , \quad \bar{K}_{\theta\phi} = K_{\theta\phi} \left(\frac{r\alpha}{R\gamma_0}\right)$$

$$Z = \left(1 + \frac{r}{R}\sin\phi\right) \quad , \quad \lambda = \frac{\pm R}{r^2}$$

... (3.82)

Integration limits in (3.82) have been reduced to make use of the problem symmetry.

Displacement coefficients will be non-dimensionalised using,

$$\bar{A}_{mn} = A_{mn} \cdot \left(\frac{\alpha}{r\gamma_0}\right) \quad , \quad \bar{B}_{mn} = B_{mn} \cdot \left(\frac{\alpha}{r\gamma_0}\right) \quad , \quad \bar{C}_{mn} = C_{mn} \left(\frac{\alpha}{r\gamma_0}\right)$$

$$\bar{D}_j = D_j \times \frac{1}{R\gamma_0} \quad , \quad \bar{F}_j = F_j \times \frac{1}{R\gamma_0} \quad , \quad \bar{H}_j = H_j \times \frac{1}{R\gamma_0}$$

... (3.83)

These were selected by experimentation to improve the conditioning of the solution matrix. When single precision was used for the variables on the computer, the matrix condition was found to be poor at $\lambda < 0.1$. The problem was aided by the above non-dimensionalisation. It was eventually removed by using double precision variables, but this meant doubling the necessary storage.

The strains as given in (3.44) can be arranged using (3.82) and/

and (3.83) into a form suitable for use on a computer. These are given in appendix (4).

A computer program was written which made use of all of the techniques just explained. This is given in appendix (5). The program also solves the problem of a pipe bend with connected tangent pipes, which will be presented later.

The program is written in FORTRAN [158] and uses double precision throughout. Values of the characterising parameters, α, R/r, λ and ν are required for each run. A typical, fully converged, run, takes less than three minutes on the ICL 2980 computer of the E.R.C.C. system. This is in contrast to the other solution systems considered which would have taken several hours.

(3.5g) Deformations

Minimising the total potential energy function in (3.82) using the procedure just outlined, numerical values are obtained for the Amn, Bmn, Cmn, Dj, Fj and Hj coefficients for any particular values of α, R/r, λ and ν.

It is then a relatively simple task to determine the mid-surface displacements, u, v and w at any circumferential (θ) and meridional (ϕ) position on the bend from equations (3.43).

(3.5h) Flexibility Factors

From the definition of the flexibility factor given in the introduction to chapter 1, it follows from (3.78) and (3.80) that the flexibility factor K is given by

$$K = \sum_{j=1}^{\infty} \left(\bar{F}_j \left(\frac{\alpha}{2} - \sin\left(\frac{j\pi}{2}\right)\left(\frac{j\pi}{\alpha} - \frac{\alpha}{j\pi}\right)\right) + \bar{D}_j \left(\frac{j\pi}{\alpha}\right) \sin\left(\frac{j\pi}{2}\right)\right)$$

... (3.84)

K corresponds to the overall rotation between the flanged ends of the bend since this is the parameter which is normally required in the analysis of complete piping systems.

(3.5i) Stress Concentration Factors (S.C.Fs.)

Once the displacement coefficients have been determined, it is then a relatively simple matter to calculate the strains using (3.44). Using the stress/strain relationships given in equation (2.14) for a linear elastic isotropic material the stresses at any point on the bend can be found.

The simplest way to examine the stresses is to use stress concentration factors (S.C.Fs.). These are defined as follows,

$$\text{S.C.F.} = \text{Stress}/\left(\frac{Mr}{I}\right)$$

... (3.85)

where $\left(\frac{Mr}{I}\right)$ is the maximum stress in an equivalent straight pipe under a bending moment, M, from simple bending theory. If the strains are found in their non-dimensional form given in (3.82), then the S.C.Fs. can be written as follows,

note that

$$\frac{Mr}{EI} = \frac{r\gamma_o}{R\alpha}$$

$$\bar{\sigma}_{\phi} = \left[(\bar{\epsilon}_{\phi} + \nu \bar{\epsilon}_{\theta}) \pm \frac{\lambda}{2}(\bar{K}_{\phi} + \nu \bar{K}_{\theta})\right] \frac{1}{(1-\nu^2)}$$

$$\bar{\sigma}_{\theta} = \left[(\bar{\epsilon}_{\theta} + \nu \bar{\epsilon}_{\phi}) \pm \frac{\lambda}{2}(\bar{K}_{\theta} + \nu \bar{K}_{\phi})\right] \frac{1}{(1-\nu^2)}$$

... (3.86)

where $\bar{\sigma}_{\phi}$ is the meridional S.C.F. and $\bar{\sigma}_{\theta}$ is the circumferential S.C.F. Also, the "+" and "-" signs in these equations, correspond to the stresses at the outside and inside surfaces of the shell respectively.

Similarly the shear stress concentration factor $\bar{\tau}_{\theta\phi}$ can be found as,

$$\bar{\tau}_{\theta\phi} = \left(\bar{\gamma}_{\theta\phi} \pm \lambda K_{\theta\phi}\right) \cdot \frac{1}{(1+\nu)}$$

... (3.87)

The above expression for shear stress is approximate, as explained in the shell theory, chapter (2). The degree of approximation is of the same order as the basic assumptions of shell theory and can be ignored.

(3.6) Theoretical Results from Method No. 3

(3.6a) Presentation of Results

The results from method No. 3 will be examined in two ways. In the present chapter, a comprehensive set of results covering a wide range of the characterising parameters will be presented along with a comparison with theoretical results given by other authors. In chapter (5), the theory will be compared with experimental results.

From here on, all results will be from method No. 3 unless otherwise specified.

(3.6b) Integration Convergence

The accuracy obtained using a large number of integration points has to be balanced against program running time. To determine the number of points necessary the program was run with $\lambda = 0.05$, $R/r = 10$, $\alpha = 180°$ and $\nu = 0.3$ and integration convergence checked.

Flexibility factors and meridional peak stresses ($\hat{\sigma}_\phi$) are compared for different numbers of integration points in the following table. The number of circumferential integration points is termed "P_θ". The number of meridional integration points is termed "P_ϕ".

Table (3.3) Integration Convergence				
P_θ	P_ϕ	K	$\hat{\sigma}_\phi$	running time (s)
7	13	21.65	13.14	106
9	17	21.62	12.46	171
13	21	21.41	12.76	303
15	25	21.41	12.76	412

To obtain these results a system of (5, 5, 6) was used. The convention defined earlier of (JT, MT, NT) is still used here.

From the table, it can be seen that $P_\theta = 9$ and $P_\phi = 17$ is sufficient to give a difference of less than 1% for flexibility factors and less than 3% for peak meridional stresses when compared against $P_\theta = 15$ and $P_\phi = 25$, with less than half the program running time. $P_\theta = 9$ and $P_\phi = 17$ was used for results given herein unless otherwise stated.

(3.6c) Series Convergence

The problem of series convergence for a pipe bend with end effect was discussed earlier in section (3.4c). The same principals will be applied in the examination of convergence in the present method.

Parameters chosen for checking convergence were,

$\lambda = 0.05$ $\quad R/r = 10$

$\alpha = 180°$ $\quad \nu = 0.3$

Some results obtained from running the program with these parameters are given in the following table:

Table (3.4) Series Convergence

JT	MT	NT	K	$\hat{\sigma}_\phi$
1	1	1	2.25	0.46
2	2	2	6.67	1.38
3	3	3	16.14	6.98
4	4	5	21.21	12.63
5	5	6	21.62	12.46

The difference between the systems (4, 4, 5) and (5, 5, 6) is better than 3% for K and 2% for $\hat{\sigma}_\phi$. The system of (5, 5, 6) was deemed to give satisfactory convergence. This requires the use of 105 displacement series coefficients in the analysis.

Convergence was found to be faster for higher λ and lower R/r and α. This confirmed earlier ideas and allows the system of (5, 5, 6) to be used for parameters inside the above ranges. For values outside these ranges more terms may be needed for convergence.

(3.6d) Displacement Coefficients

Displacement coefficients for $\lambda = 0.05$, $R/r = 10$, $\alpha = 180^\circ$ and $\nu = 0.3$ are given in Table (3.5). These illustrate several interesting features of the flanged pipe bend problem.

As explained during the derivation of the displacement series, the similarity of the Amn, Bmn and Cmn coefficients indicates/

indicates that ϵ_ϕ and $\gamma_{\theta\phi}$ are small (from equations (3.25), (3.39) and (3.42)). This is found to be less true for lower R/r and α.

The similarity of the D_j and F_j series also confirms the usefulness of equation (3.5) for the rigid section displacements with R/r large.

The zeroth meridional function coefficients, H_j, of the displacement are small when compared to C_{12}. These terms are more significant at low R/r and considerably affect the stress distributions.

The Karman solution for a pipe bend without end effects uses only the even fourier terms in the ω_b series. Table (3.5) shows that these are the most significant terms in the analysis but the odd terms are certainly not negligible. The latter are even more important for lower R/r and α, particularly influencing the stresses.

Convergence of the series is easily seen from the table of coefficients. First and last terms in the Amn, Bmn and Cmn series (e.g. C_{12} and C_{57}) differs by about 3 orders. A similar convergence is also shown by the D_j and F_j series. Convergence of the coefficients is more rapid for larger λ and lower R/r and α.

Table (3.5)

Displacement Coefficients for $\lambda = 0.05$, $R/r = 10$, $\alpha = 180°$, $\nu = 0.3$

$P_\theta = 15$, $P_\phi = 25$

J	D_j	F_j	H_j
1	10.39	11.45	0.0013
2	3.47	2.73	-0.0032
3	- 0.02	0.37	0.0012
4	- 0.17	- 0.31	-0.0037
5	- 0.02	0.01	0.0019

Amn

m \ n	2	3	4	5	6	7
1	-43.42	5.38	-11.86	2.23	- 3.11	0.78
2	11.95	- 5.01	1.52	- 1.47	0.24	- 0.31
3	1.36	- 3.31	- 0.86	- 1.13	- 0.43	- 0.19
4	- 0.74	2.56	1.49	0.36	0.47	0.00
5	0.16	- 0.86	- 0.34	- 0.32	- 0.19	- 0.04

Bmn

m \ n	2	3	4	5	6	7
1	-43.76	3.53	-12.22	1.15	- 3.29	0.28
2	12.25	- 4.40	1.91	- 1.31	0.39	- 0.26
3	0.92	- 3.37	- 0.73	- 1.21	- 0.31	- 0.26
4	- 0.45	2.69	1.41	0.50	0.43	0.07
5	0.23	- 1.03	- 0.36	- 0.37	- 0.17	- 0.07

Cmn

m \ n	2	3	4	5	6	7
1	-43.73	3.60	-12.20	1.23	- 3.28	0.32
2	12.22	- 4.41	1.89	- 1.32	0.39	- 0.27
3	0.92	- 3.37	- 0.74	- 1.21	- 0.32	- 0.25
4	- 0.43	2.68	1.42	0.49	0.44	0.06
5	- 0.00	- 1.03	- 0.37	- 0.37	- 0.17	- 0.06

(3.6e) Flexibility Factors from Method No. 3

Flexibility factors for flanged bends under in-plane bending using method no. 3 are given in figures (3.10), (3.11), (3.12) and (3.13) for 180°, 135°, 90° and 45° bends respectively. Each figure has curves for radius ratios (R/r) of 2, 3, 5 and 10. All results were obtained using JT = 5, MT = 5 and NT = 6 with P_θ = 9 and P_ϕ = 17.

The results show that flanged bends of smaller subtended angles and shorter radius have lowest flexibility. Generally, this indicates that shorter length bends have lower flexibility.

As the pipe factor reduces the flexibility increases. Unlike the Karman converged solution, the present results are not straight lines on a log-log graph. This means that simple formulas cannot be derived easily covering wide ranges of parameters.

Figure (3.14) illustrates a typical variation with bend angle for $\lambda = 0.1$. It demonstrates how the flexibility reduces with bend angle. The diagram also shows that flanged bends with a subtended angle of less than about 45° behave almost like an equivalent straight pipe.

Variation with bend radius ratio (R/r) is given in figure (3.15). It demonstrates how the flexibility reduces with R/r and shows how it falls rapidly for R/r less than about five. Note that the curves for the various bend angles all tend to a flexibility factor of $0.91, (1-\nu^2)$, as the radius ratio tends to zero. Similar behaviour was shown in figure (3.14) as the bend angle tended to zero.

In figure (3.16), the present method no. 3 is compared with/

with the simpler method no. 2. It shows that method no. 3 gives higher flexibilities, the difference being greatest at lower values. Method no. 2 gives factors within 12% of method no. 3 for $\lambda \geq .1$. The difference is greatest for larger R/r. This is probably due to the simpler displacement series used in the circumferential direction in method 2 not being fully capable of representing the more rapidly varying deformation at higher R/r. Table (3.5) shows that the additional circumferential terms (m = 2, 4, 6 ...) are significant for R/r = 10. Examination of the coefficients for other geometries reveals these terms to be relatively less significant for lower R/r.

A comparison of method no. 3 with Thailer-Cheng and Findlay (corrected results, see section (3.1)) is given in figure (3.17). Neither of the latter methods shows a variation with the radius ratio unlike the present results.

The present method is compared with Axelrad's results in figure (3.18). Axelrad's results are only an approximation and are therefore more valid at larger λ. For $\alpha = 180^{\circ}$ and $R/r \geq 3$ Axelrad's results are within 20% of method no. 3. For lower bend angles and radius ratios the comparison is generally poorer. The degree of approximation of Axelrad's results can be seen when R/r = 3 and $\alpha = 90^{\circ}$ where the flexibility falls when $\lambda < 0.2$.

Also given in figure (3.18) is the A.S.M.E. code for flanged and unflanged bends [133] . A comparison of the present results with the unflanged flexibilities demonstrates the substantial reduction caused by rigid flanges at low R/r and α. The A.S.M.E. code for flanged bends deviates significantly from the current results.

Figure (3.19) is a comparison with Whatham's flexibility factors/

factors. These results are taken from a graph making accurate comparisons difficult. It appears that the two sets of results give parallel curves on the log-log plot. Whatham's results are about 10% higher than those of method no. 3 for all R/r, α and λ.

The present flexibility factors are lower bounds, as explained in section (2.4b). In [117] Whatham gives results from his method for an unflanged bend. These agree with solutions obtained from an upper bound analysis for the same problem. It is therefore to be expected that if Whatham's results for a flanged bend are valid then they will be greater than the present lower bound. If the $(1-\nu^2)$ term in the total potential energy of the present method is neglected, in the way it was by many previous authors (see ref. [4]), then the flexibility factors from method no. 3 agree with the results of Whatham, within the limits of plotting.

(3.6f) Stress Concentration Factors from Method No. 3

For a pipe bend with end effects, the stress concentration factors (S.C.Fs.) vary in the meridional and circumferential directions and through the thickness. This makes it difficult to present a comprehensive stress distribution for all points on a bend. The problem is further aggravated by the maximum stresses not being at the same position for all bend geometries, making it necessary to examine more than a single pipe section. Therefore some typical distributions will be examined and then the maximum S.C.Fs. for a range of geometries presented.

Meridional Stress Distributions/

Meridional Stress Distributions

Figure (3.20) illustrates the effect of the radius ratio on the distribution of the meridional S.C.Fs. at the centre of the bend ($\theta = 0$) for $\alpha = 90^{\circ}$, $\lambda = 0.2$ and $\nu = 0.3$. For R/r = 10, the maximum meridional S.C.F. occurs on the inside surface at approximately $\phi = -7^{\circ}$, i.e. towards the intrados. The Karman analysis predicted the maximum meridional S.C.F. at $\phi = 0$ for a bend without end constraints. The small difference is introduced by the present significance of the odd terms in the distortion displacement series. At R/r = 5, the stress on the outside surface at the intrados is slightly greater than the stress on the inside surface close to the pipe centreline at $\phi = 0$. As R/r decreases further, the stress at the intrados becomes relatively larger than the pipe centreline stress. A similar variation can be shown as the bend angle reduces.

Figure (3.21) shows typical distributions of the meridional S.C.Fs. along the length of the bend at the intrados ($\phi = -90^{\circ}$), pipe centre ($\phi = 0$) and extrados ($\phi = +90^{\circ}$) for R/r = 10 and 3. It demonstrates that the maximum meridional S.C.F. ($\hat{\bar{\sigma}}_{\phi}$) occurs at the bend centre ($\theta = 0$), regardless of whether it is close to the pipe centre ($\phi = 0$) or at the intrados ($\phi = -90^{\circ}$). This was found to be true for all practical bend geometries.

Circumferential Stress Distributions

In figure (3.22) typical distributions of the circumferential S.C.Fs. at the bend centre ($\theta = 0$) are given for $\lambda = 0.2$, R/r = 10 and R/r = 3. The diagram shows that for the bends considered, with R/r = 3 the maximum circumferential S.C.F. ($\hat{\bar{\sigma}}_{\theta}$) occurs at the intrados/

intrados ($\phi = -90^\circ$) whereas for R/r = 10, the maximum occurs nearer the pipe centreline ($\phi = 0$). As with the meridional peak stress, the circumferential peak stress at the bend centre ($\theta = 0$) has a position which is dependant on both the bend angle, α , and the radius ratio, R/r, i.e. it is dependant on the length of the pipe centreline arc ($\phi = 0$).

Typical circumferential S.C.Fs. at the flanged ends of the bend ($\theta = \frac{\alpha}{2}$) are shown in figure (3.23) for R/r = 10 and R/r = 3, again with $\alpha = 90^\circ$ and $\lambda = 0.2$. For both radius ratios, the maximum S.C.F. occurs on the outside surface at the extrados. For shorter length bends, $R/r \leq 2$ and $\alpha \leq 45^\circ$, the maximum can occur on the inside surface at the intrados. Equations (3.44) show that the meridional strain and curvature, $\epsilon\phi$ and $K\phi$ are zero at the flange. Thus the meridional stresses at the flange are equal to the circumferential stresses multiplied by poissons ratio, ν, (from equation (3.86)). This also means that the difference between the curves for the S.C.Fs. at the inside and outside surfaces in figure (3.23) is due to the contribution of the circumferential curvature K_θ. The figure shows that K_θ becomes more significant at lower R/r.

Figure (3.24) illustrates the distribution of the circumferential S.C.Fs. along the bend at the intrados, pipe centre, and extrados. It shows that $\overline{\sigma}_\theta$ has high values at the bend centre ($\theta = 0$) and flange positions. The maximum circumferential stress can occur at either position, depending on the bend geometry.

Shear Stress Distributions

Distributions of Shear S.C.Fs. at $\theta = 35^\circ$, for the same bend geometries/

geometries as before, are given in figure (3.25). This is approximately the position with the maximum shear stress (see figure (3.26)). Note that the vertical scales on shear S.C.F. diagrams are double those of the previous figures. The maximum shear S.C.F. is much smaller than the meridional or circumferential S.C.Fs. For R/r = 3, the peak shear S.C.F. ($\hat{\tau}_{\theta\phi}$) is 1.32 and for R/r = 10, $\hat{\tau}_{\theta\phi}$ = 0.72 i.e. the shear stress reduces as the radius ratio increases. Similarly, it can be shown that $\tau_{\theta\phi}$ is smaller for larger bend angles. The peak shear stress occurs between the pipe centre ($\phi = 0$) and the intrados ($\phi = -90^{\circ}$). The shear stress is zero at the intrados and extrados because of the bend symmetry through these points.

Figure (3.26) shows the distribution of the shear S.C.Fs. along the bend circumference. It shows that the shear stress increases slowly from the bend centre to a peak at approximately $\theta = 35^{\circ}$ and it falls rapidly at the flange. The shear stress is zero at the bend centre ($\theta = 0$) because of symmetry and at the flange because the bend is maintained circular.

Comparisons of Theoretical Distributions

A comparison of meridional and circumferential S.C.Fs. from the present work with those of Whatham [117] are given in figures (3.27) and (3.28) for $\alpha = 180^{\circ}$, $\lambda = 0.362$, R/r = 2.83 and $\nu = 0.3$. The results of Whatham were taken from a private communication [159] which contained numerical values intended for comparison with some experimental data given by Spence and Findlay in [102]. The results for the meridional S.C.Fs. in figure (3.27) show good general agreement. The peak meridional S.C.Fs., $\hat{\sigma}_{\phi}$, differ by about 6%. Circumferential S.C.Fs. in figure (3.28) show a similarly good comparison./

comparison. Generally the results of the present method No. 3 are numerically higher. At the peak circumferential S.C.F. ($\hat{\sigma}_\theta$) the difference is about 9%. The communication [159] contained results for two other bend geometries. These showed a similar comparison. One of these will be shown in chapter (4) for comparison with experimental data.

Maximum Meridional S.C.Fs.

Maximum meridional S.C.Fs. ($\hat{\sigma}_\phi$) for bend angles of 180°, 135°, 90° and 45° are given in figures (3.29), (3.30), (3.31) and (3.32) respectively. Each figure contains curves for R/r = 10, 5, 3 and 2. All results were obtained at the bend centre ($\theta = 0$). Note that the curves for the different R/r cross each other, unlike the flexibility curves. At lower values of the pipe factor (λ) $\hat{\sigma}_\phi$ is greater for larger R/r. This changes over at higher λ, which coincides with the change in the meridional position of $\hat{\sigma}_\phi$. At lower λ, $\hat{\sigma}_\phi$ tends to occur close to the pipe centreline, $\phi = 0$, but moves to the intrados at higher λ and lower R/r as explained earlier.

Maximum Circumferential S.C.Fs. at Bend Centre

The maximum circumferential S.C.Fs. at the bend centre ($\theta = 0$) are given in figures (3.33), (3.34), (3.35) and (3.36) for bend angles of 180°, 135°, 90° and 45° respectively. Again the crossing over of some of the curves is associated with a change in the meridional position of the peak S.C.F. Note that for bend angles less than 180°, the peak stress for R/r = 2 is greater than the peak stress for R/r = 3, i.e. when the peak stress occurs at the intrados it increases as the radius ratio decreases.

Maximum Circumferential S.C.Fs. at Flanges/

Maximum Circumferential S.C.Fs at Flanges

Figures (3.37), (3.38), (3.39) and (3.40) show the peak circumferential S.C.Fs. ($\hat{\sigma}_\theta$) at the flanged ends of the bend ($\theta = \pm \frac{\alpha}{2}$), for bend angles of 180°, 135°, 90° and 45° respectively. For bend angles greater than 90° and radius ratios greater than 2, the curves are close together, showing little variation with anything other than the pipe factor, λ . These S.C.Fs. tend to occur at the extrados on the outside surface. For parameters outside the above range, the S.C.Fs. move to the intrados and the values are sensitive to R/r and α.

Results from the present work are for completely rigid flanges. In practice, real flanges will have a certain amount of flexibility, depending on their dimensions. The radial stiffness of standard flanges should be sufficient to maintain the pipe cross-section circular but the usually thinner flange thickness may allow some distortion out of the plane of the flange. Examination of the predominant flange strain, ϵ_θ, in equations (2.13) and (3.44) indicates that the ($\frac{\partial u}{\partial \theta}$) term is principally the cause of the high stresses. This term is related to the change in the u displacement along the bend. This change will be less severe if the flange distorts, thereby reducing the flange stresses. The stresses nearer the centre of the bend should be less affected by the out of plane distortion but would be affected by any loss of circularity of the flange. Figures (3.21) and (3.24) show that the stresses due to the cross-section distortion persist over a longer length than those due to the flanges. It is therefore likely that flange distortion will have a small effect on the overall/

overall behaviour.

The high stresses at the flange were noted by several previous authors. Natarajan and Blomfield [97] obtained high stresses at the flanged end of a bend with one tangent and one flange using finite element analysis. However, they considered that the stress was a singularity and that the results had no meaning. In [106], Imamasa and Uragami presented experimental and finite element results for two bends each with one flanged end and one tangent pipe. The flange distributions show a similar behaviour to the present work but direct comparison would not be valid because of the different boundary conditions. Whatham [117] mentions the existence of high flange stresses but does not present a comprehensive set of results. The two-dimensional stress distributions he presents are difficult to take comparisons from but his flange distributions appear to be similar to the present work.

Comparison of Theoretical Peak S.C.Fs.

Figure (3.41) shows comparisons of the peak meridional S.C.Fs. from method no. 3 with available theoretical results. The only published sets of peak stresses for flanged bends are those of Thailer-Cheng and Findlay. The errors in both of these methods were highlighted earlier. Peak meridional stresses ($\hat{\sigma}_\phi$) from the Karman analysis without end effects are also given. Present results for R/r = 10 and $\alpha = 180^\circ$ are about 5% higher than Karman's results. $\hat{\sigma}_\phi$ for flanged bends with $R/r < 10$ and $\alpha < 180^\circ$ are generally lower than Karman's results when $\lambda < 0.5$. The current A.S.M.E. code shown in the figure is lower than the present/

present results for most bend geometries. Figure (3.42) shows similar comparisons for peak circumferential stresses.

When using the present results for the design of a flanged bend each of the different peak stresses must be considered since any one of them can be the true maximum, depending on the bend geometry.

(3.7) General Comments on the Results of Method No. 3

Method No. 3 used virtually only the assumptions of thin shell theory to solve the problem of a smooth pipe bend with rigid flanges under an in-plane bending moment. The resulting flexibility factors are a lower bound on the stated problem. "Real" flanges are not completely rigid, particularly out of the plane of the flange, making the bend flexibility slightly higher. Thus the present results should also be a lower bound on the "real" problem. In chapter (5) the flexibility factors will be compared with some experimental results and further comments will be made then about the effect of "real" flanges.

The correlation between Whatham [117] and the present work, using two completely different methods, suggests that both methods give a close approximation to the correct result. Axelrad's[104] results are close to the present work when his assumption of zero shear strain is valid. Thailer-Cheng [95] and Findlay [99] used invalid assumptions in their theories making their results incorrect. The flexibilities and stresses from the present work suggests that the design code values need to be amended. Unfortunately the present results cannot be given in a simple formula covering the variation of all parameters.

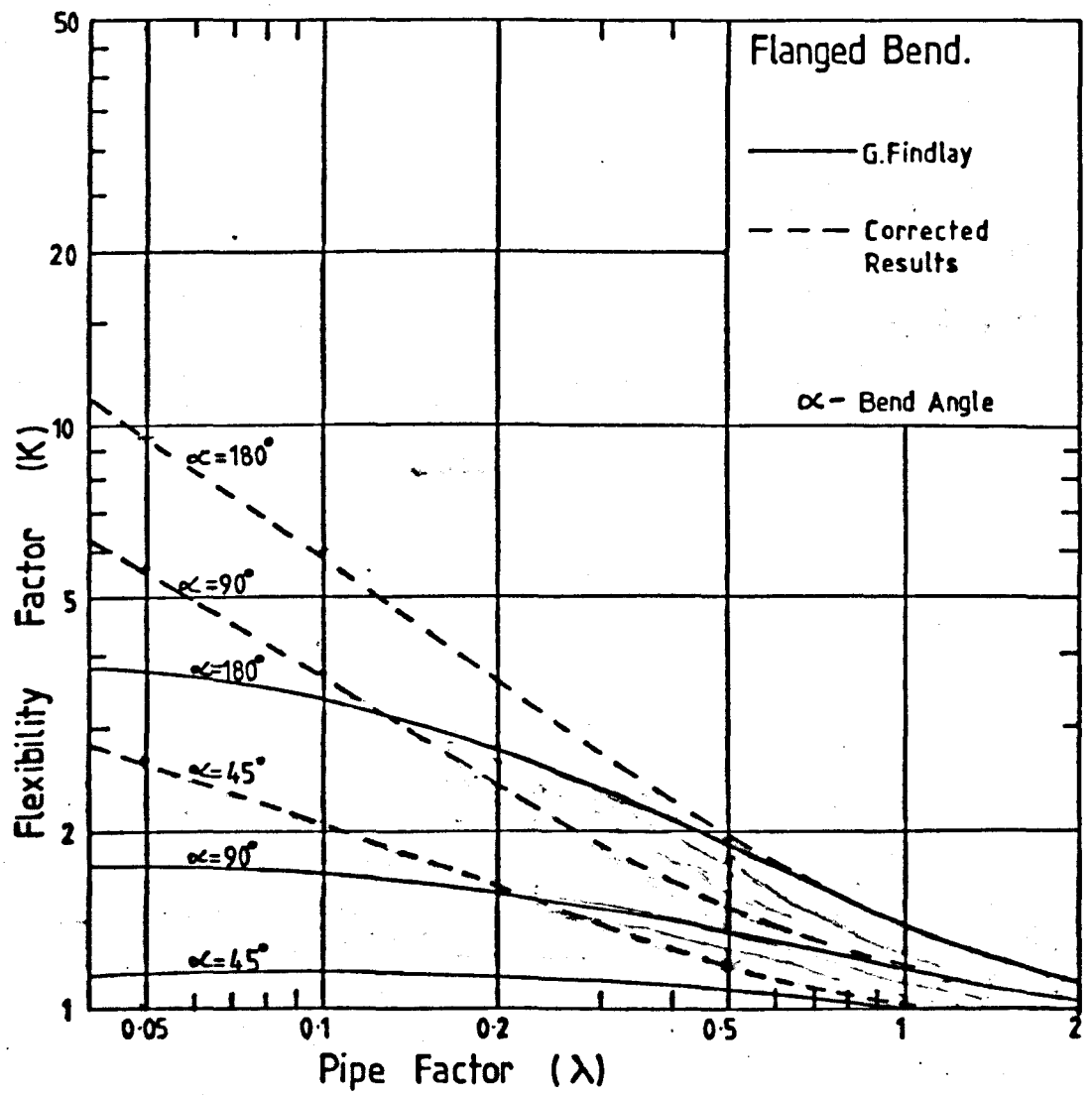

Corrected Results From G.Findlay's Analysis.

Figure (3.1)

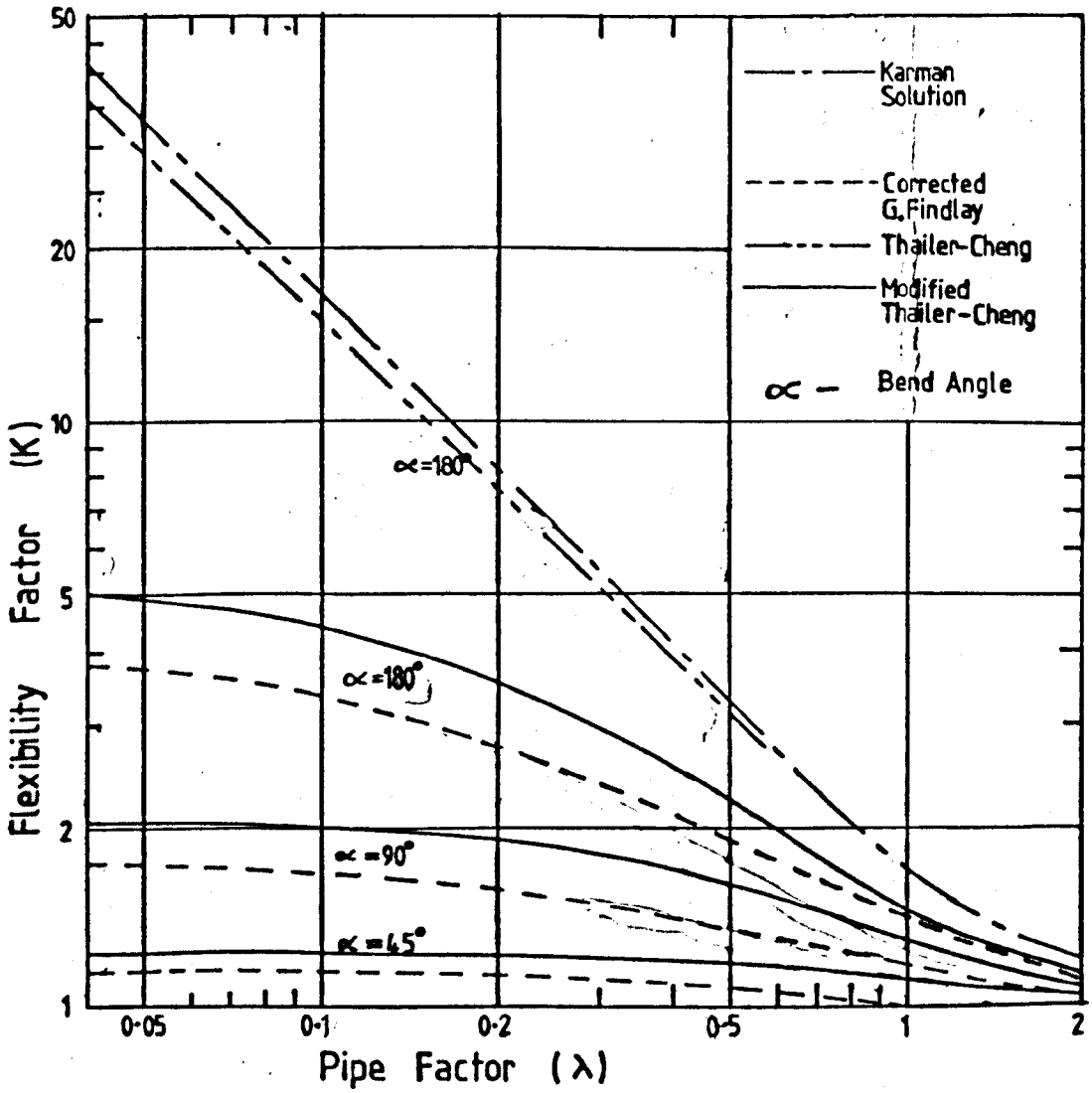

Comparison of Flexibility Factors.

Figure (3·2).

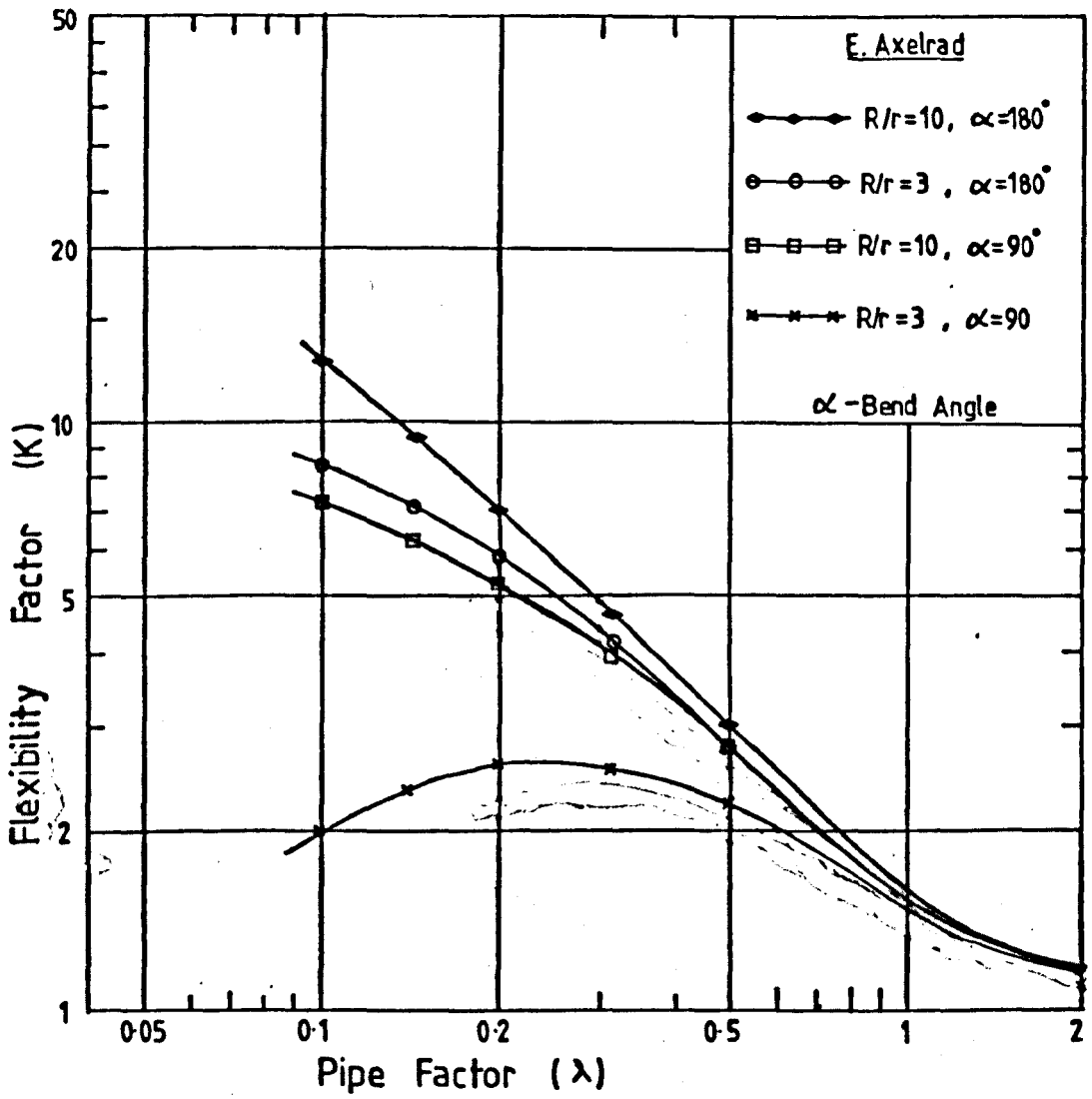

Results of E.Axelrad for Flanged Bends

Figure (3.3)

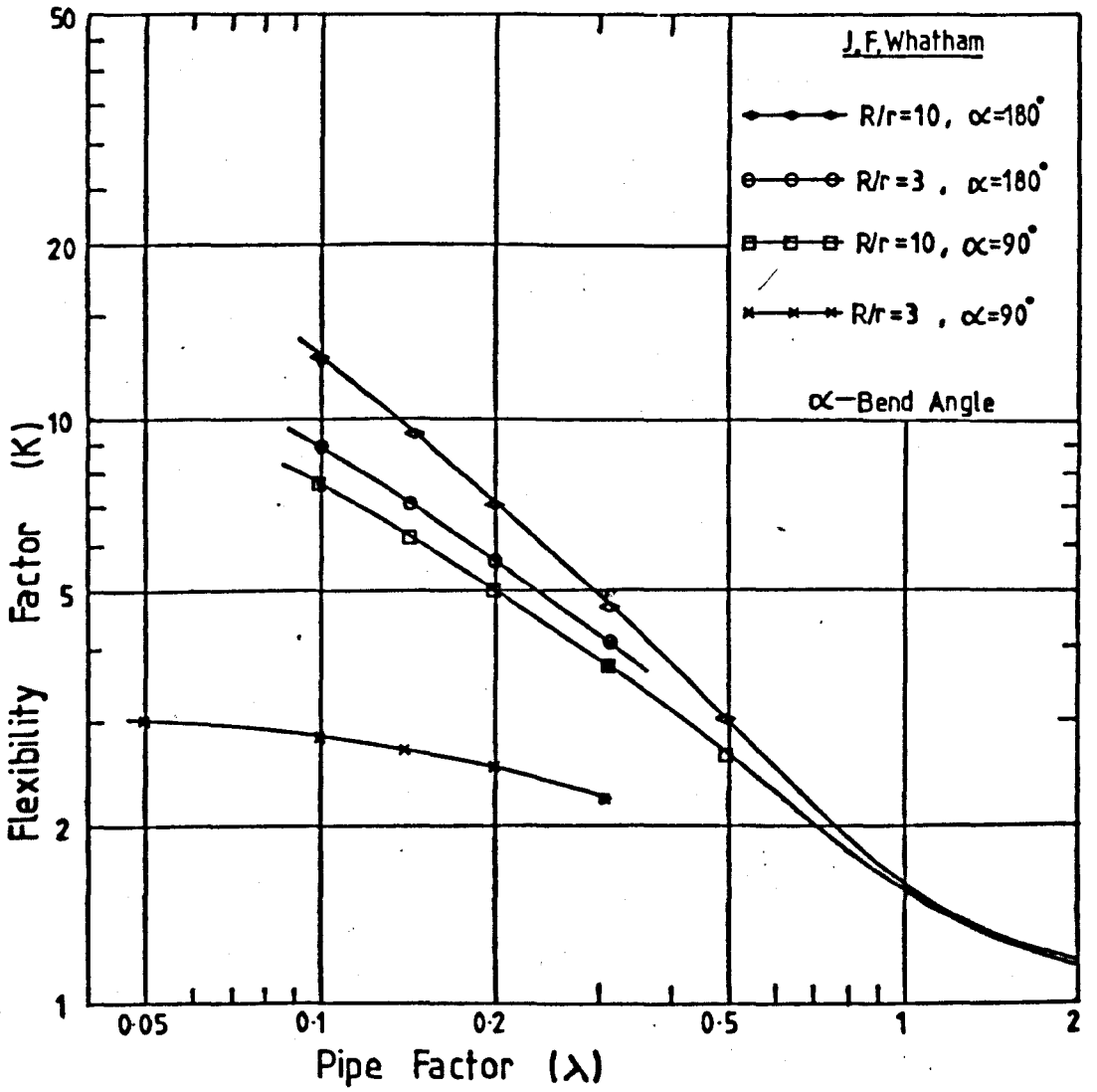

J.F.Whatham's Flexibility Factors for Flanged Bends.

Figure B.4)

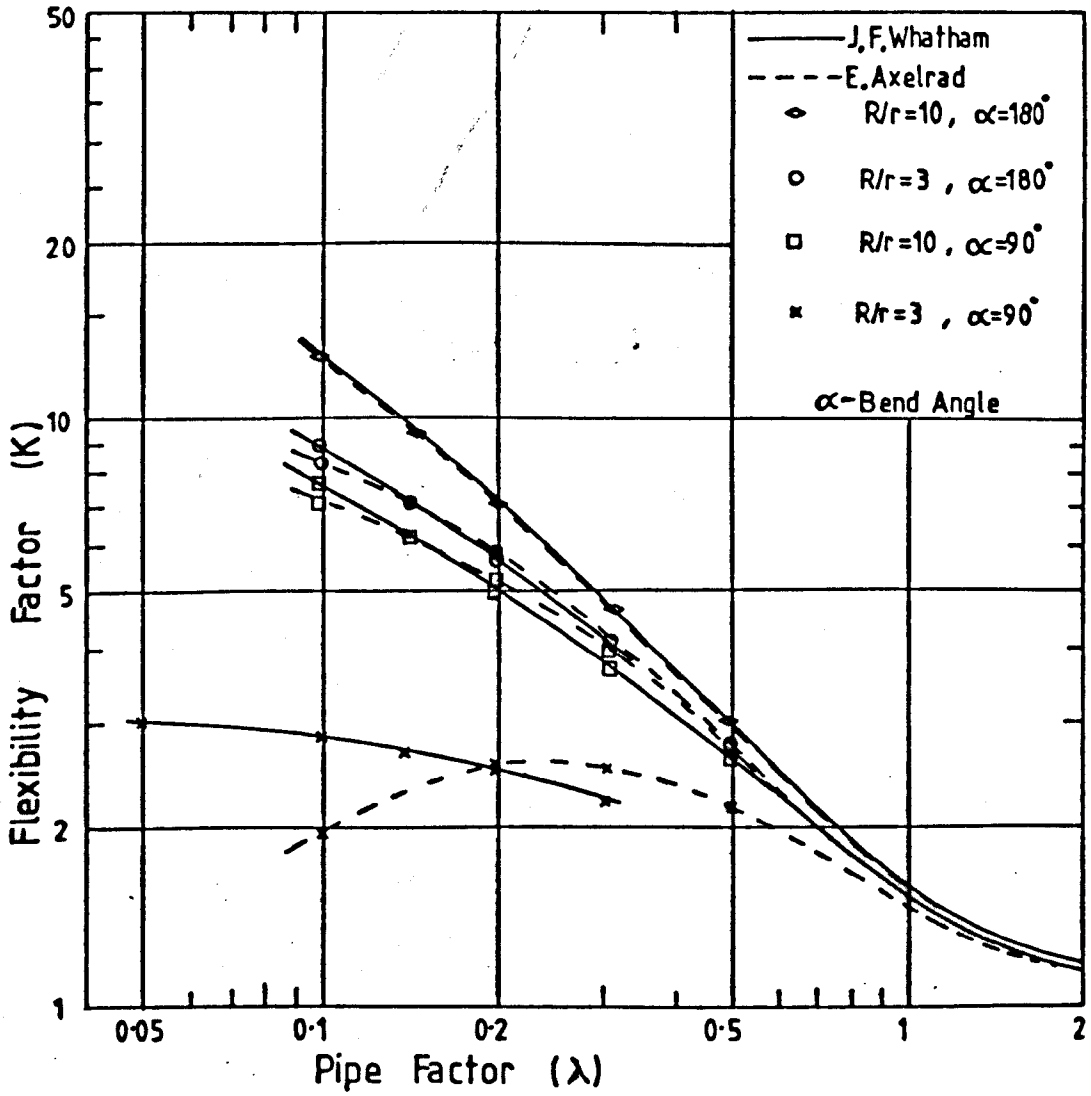

Comparison of Results from

J.F.Whatham and E.Axelrad

Figure (3.5)

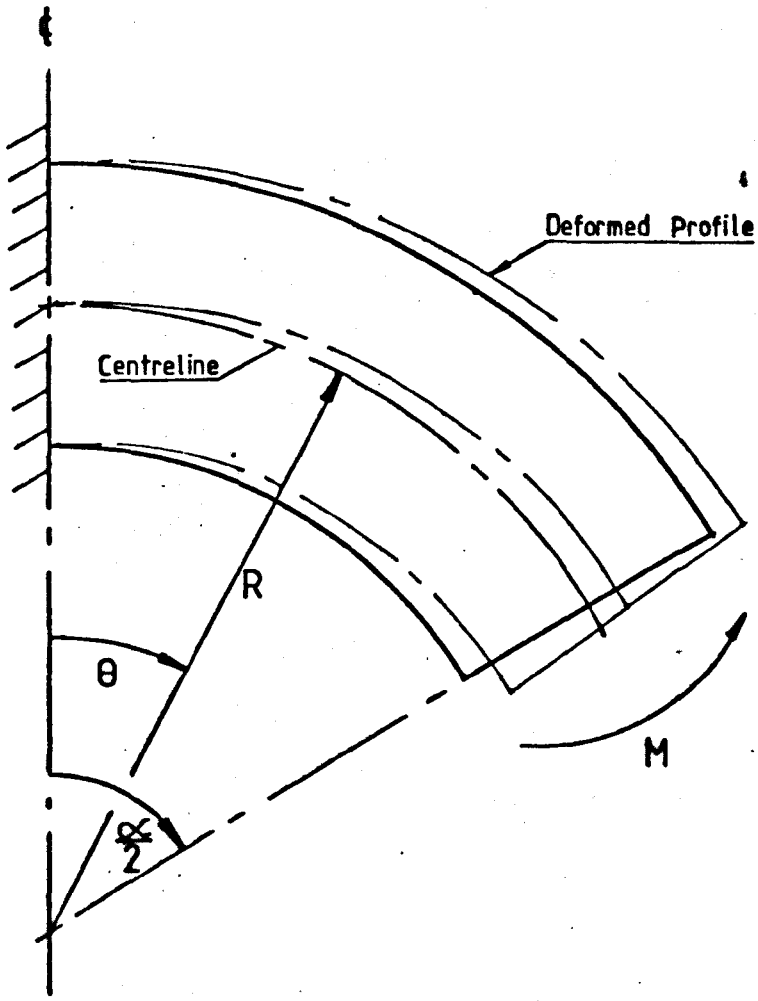

General Deformation of a Smooth Pipe Bend

Figure (3.6)

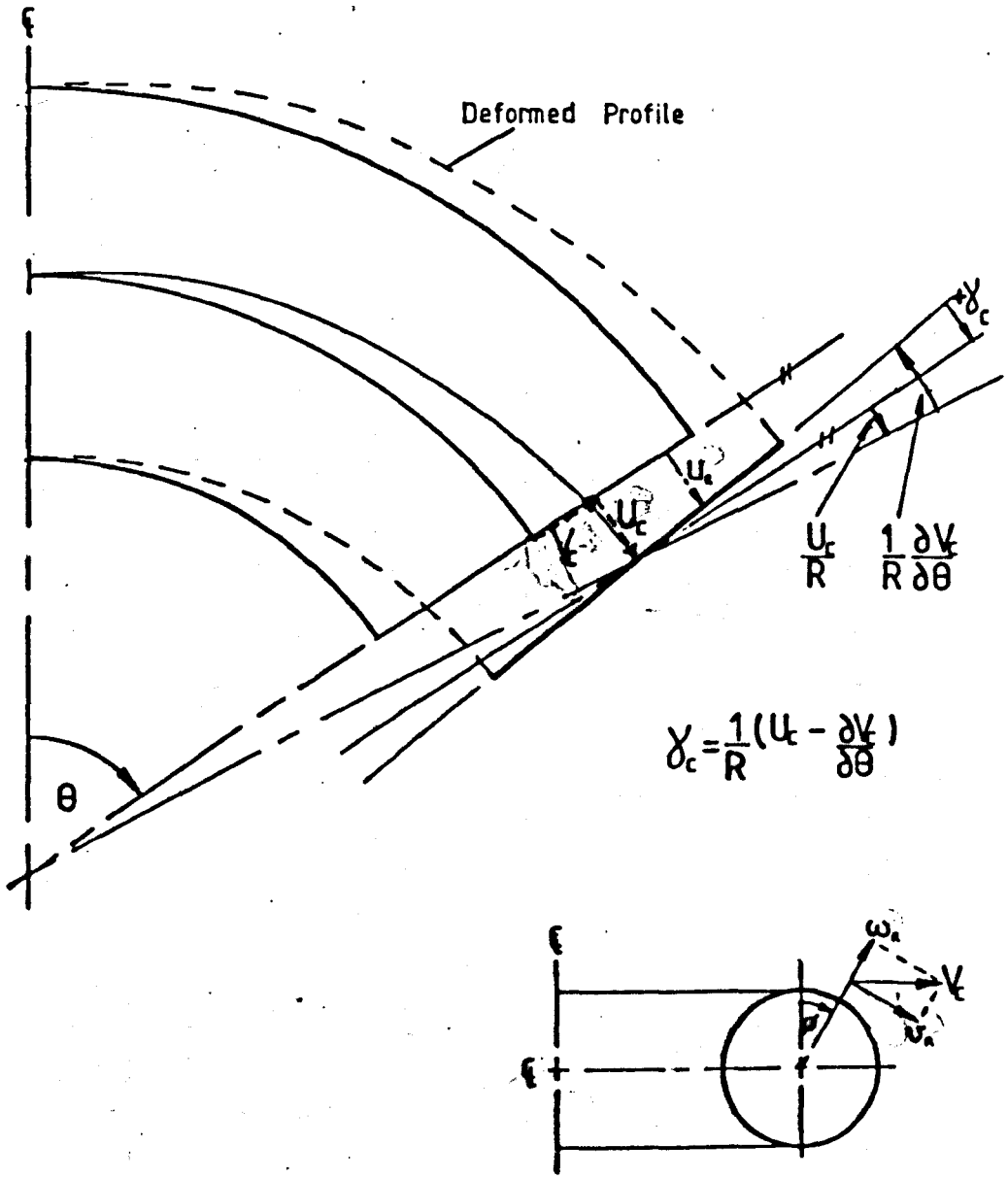

Displacements are exaggerated for clarity

Rigid Section Displacements

Figure (3.7)

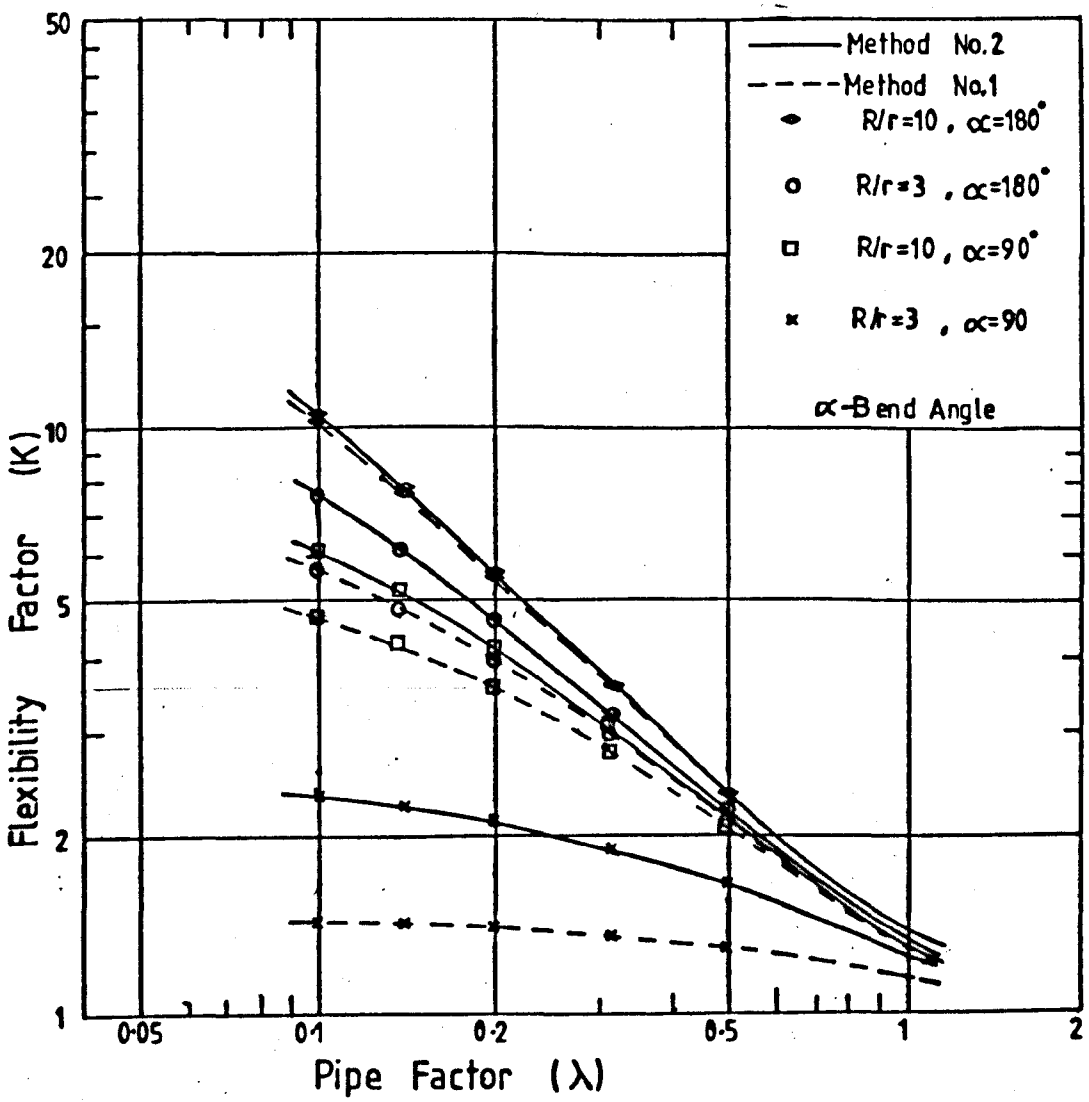

Comparison of Flexibilities from Methods 1 and 2.

Figure (3.8)

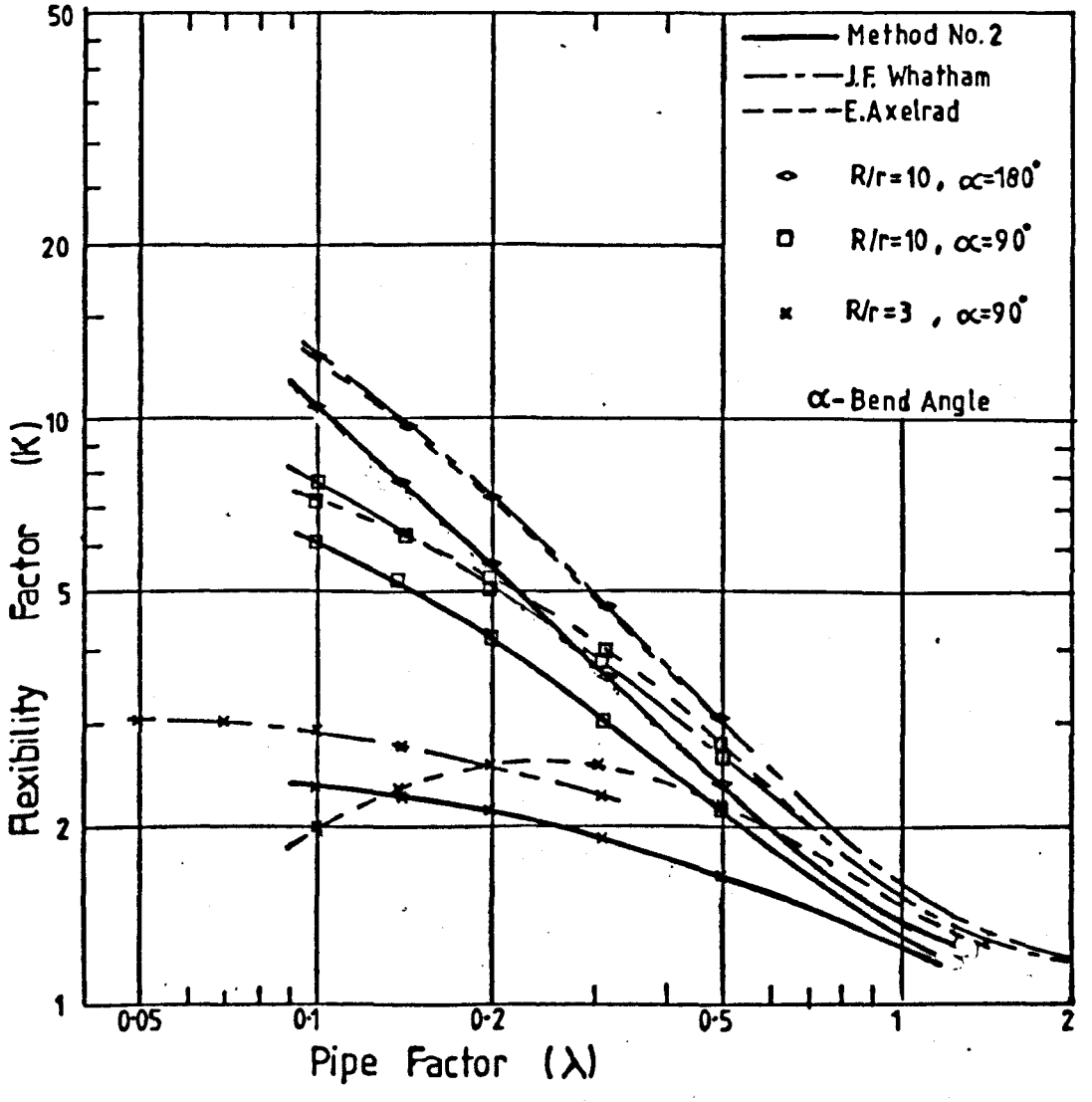

Comparison of Method 2 with Axelrad and Whatham.

Figure (3.9)

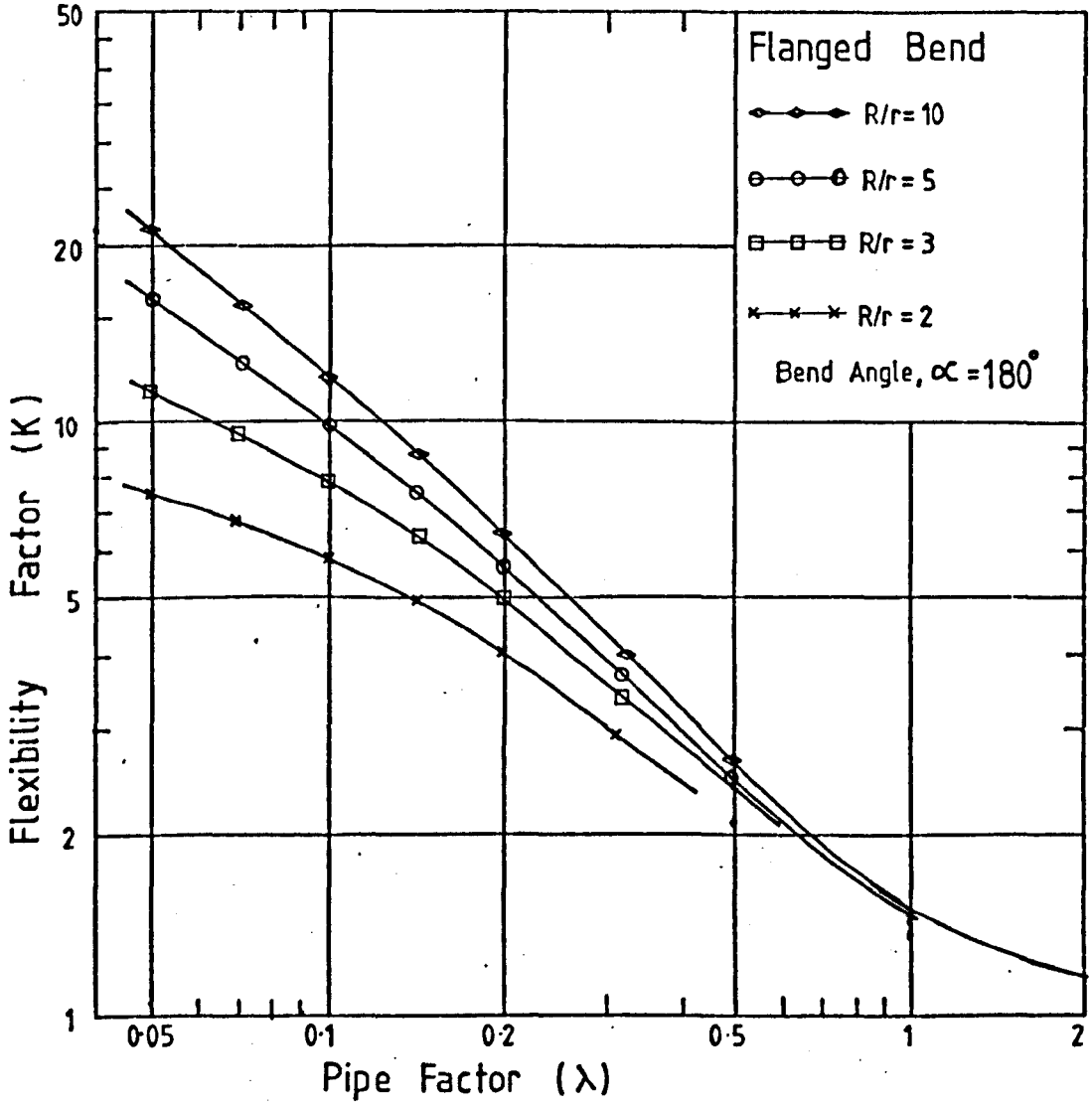

Theoretical Flexibility Factors

Figure (3·10)

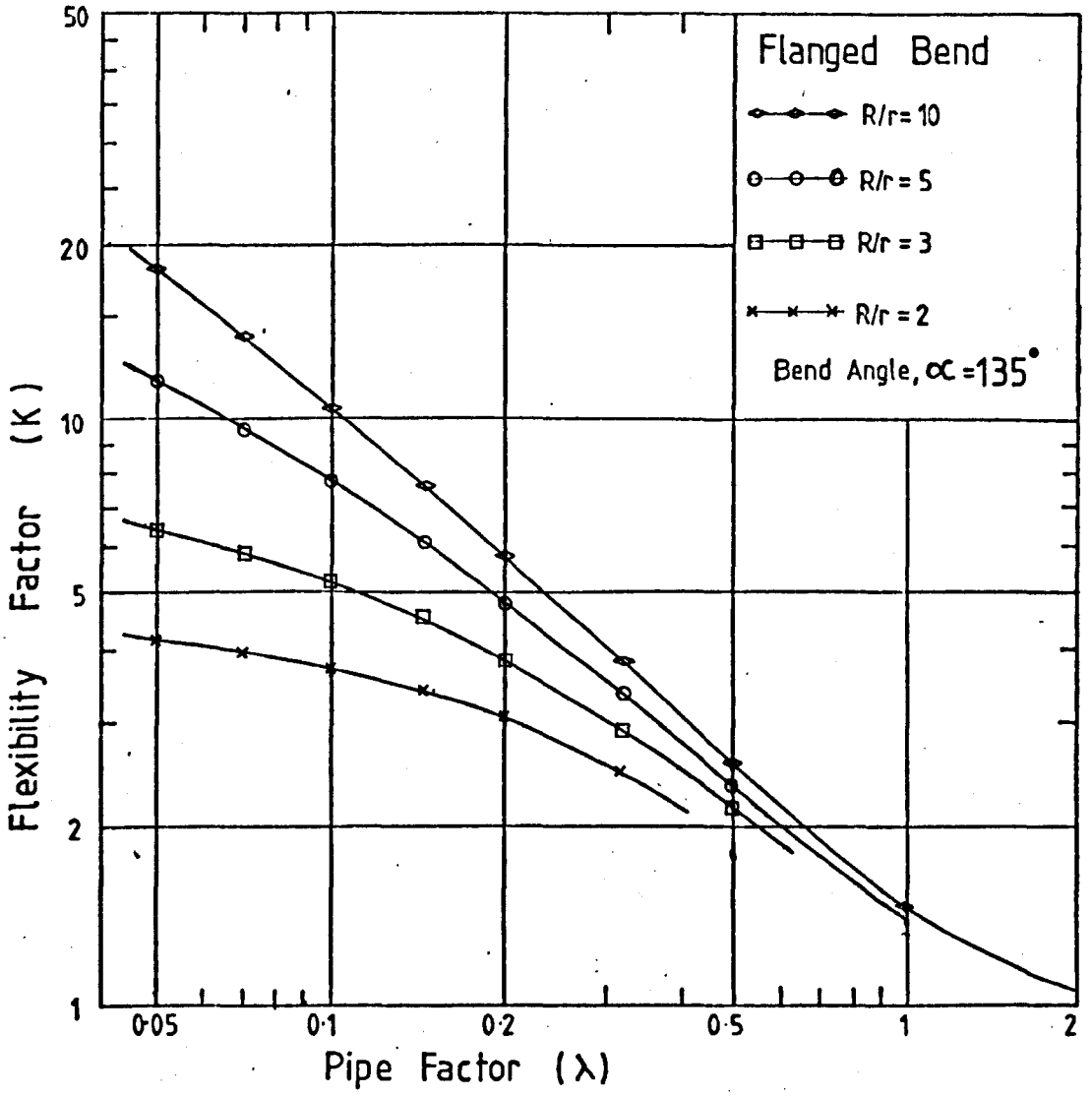

Theoretical Flexibility Factors

Figure (3·11)

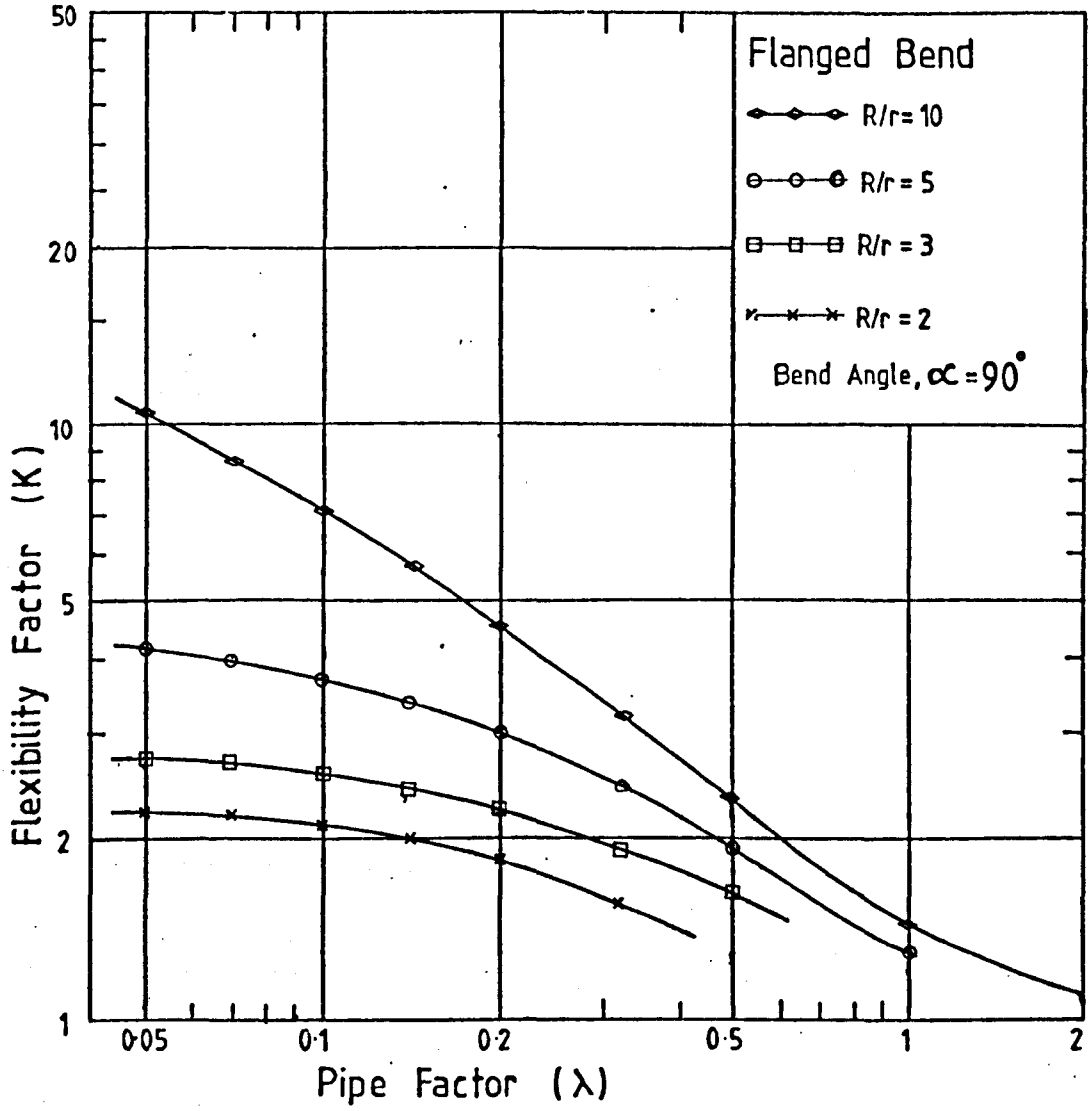

Theoretical Flexibility Factors

Figure (312)

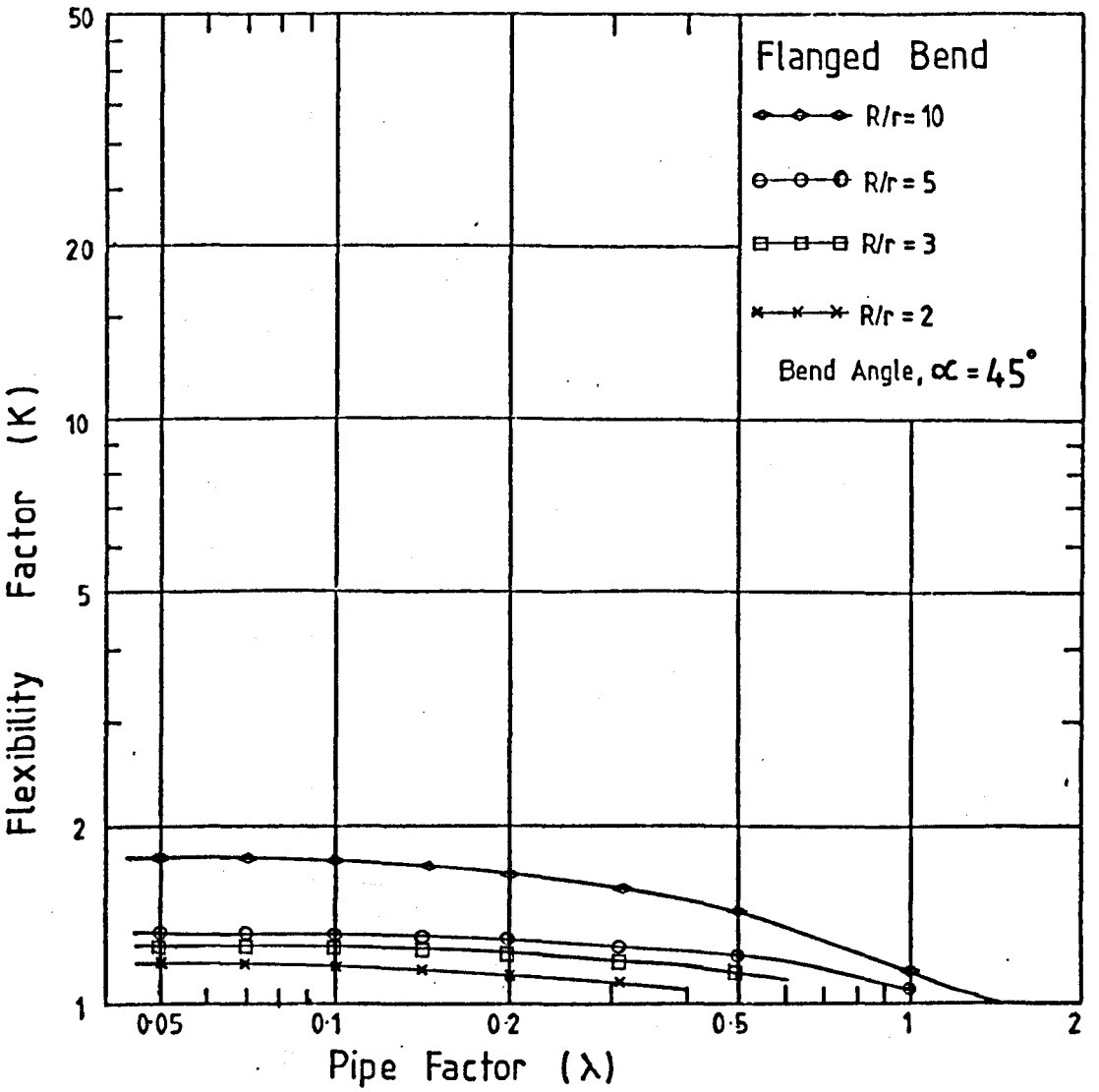

Theoretical Flexibility Factors

Figure (3·13)

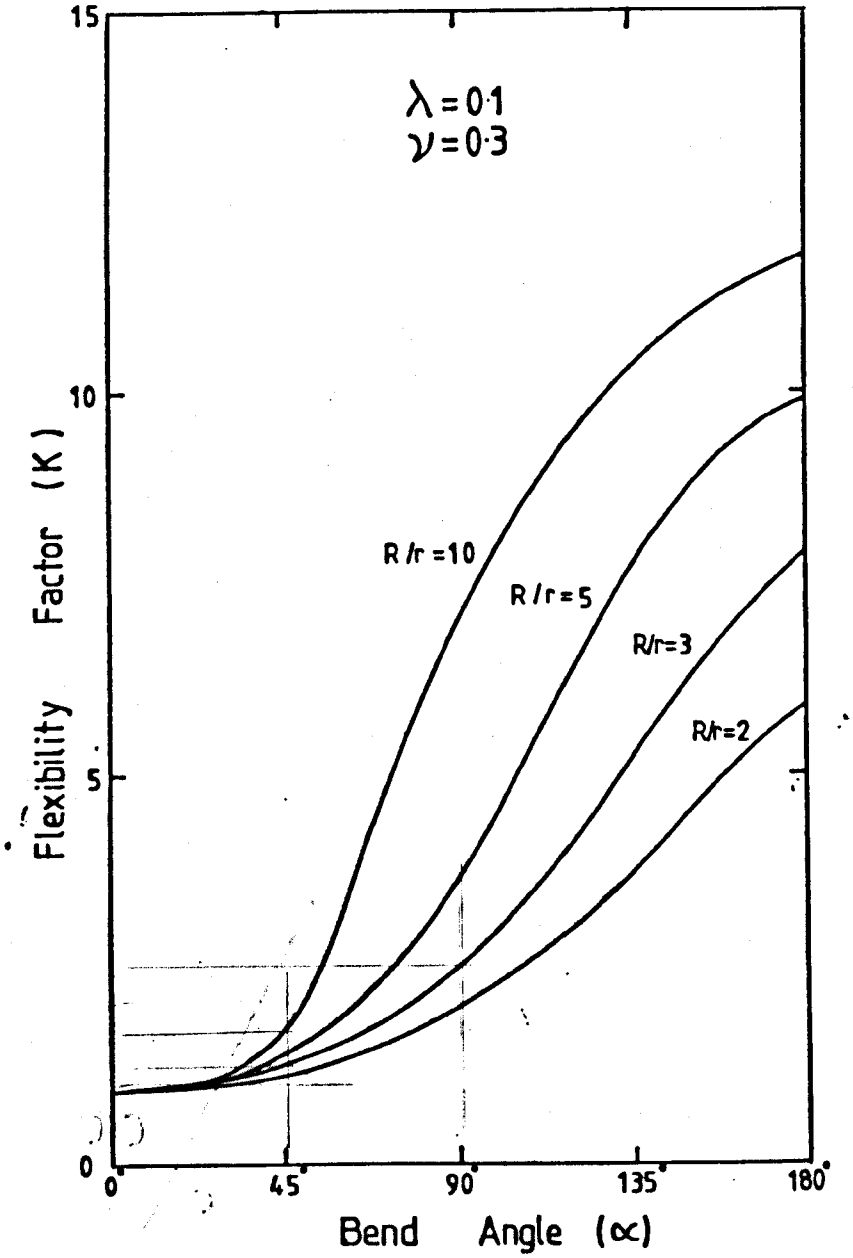

Typical Variation of Flexibility Factor Against Bend Angle

Figure (3·14)

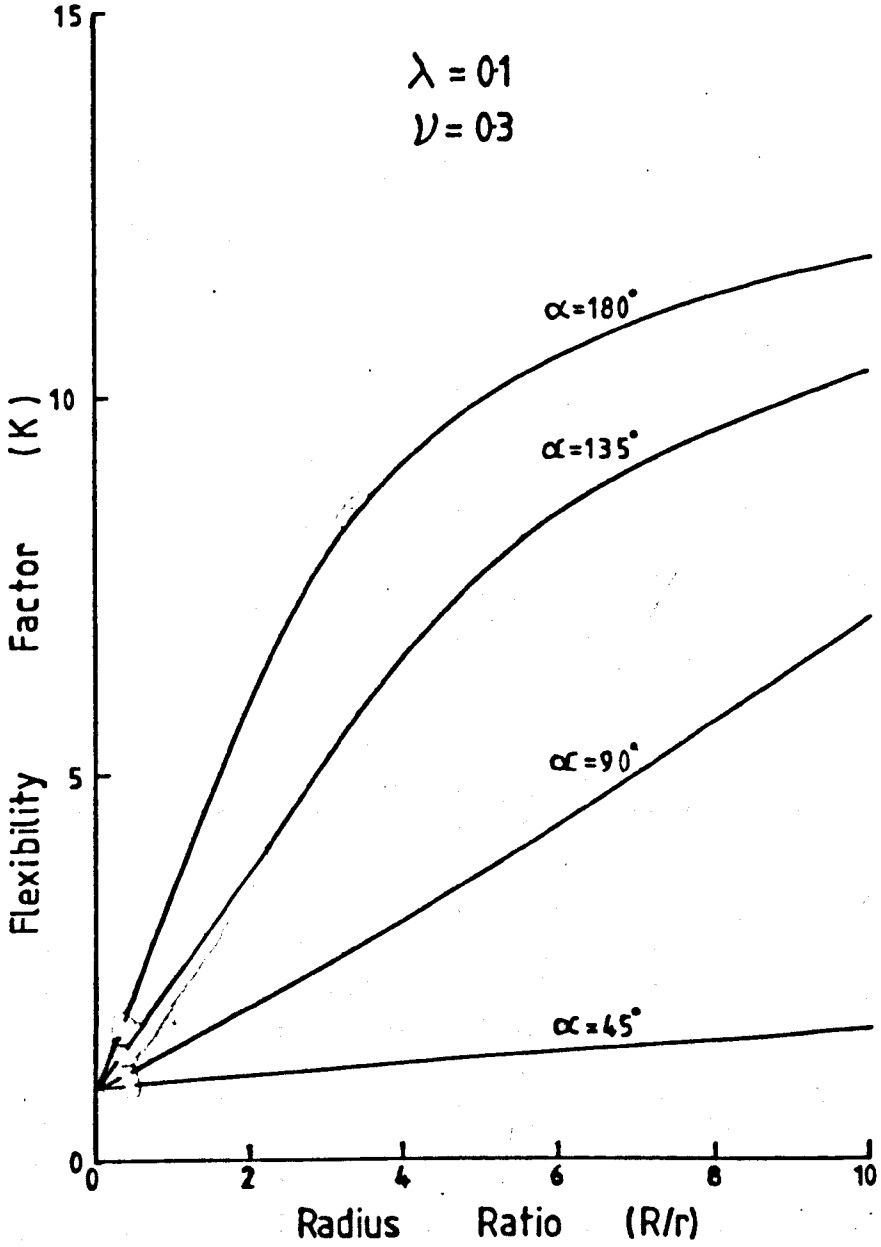

Typical Variation of Flexibility Factor Against Radius Ratio.

Figure (315)

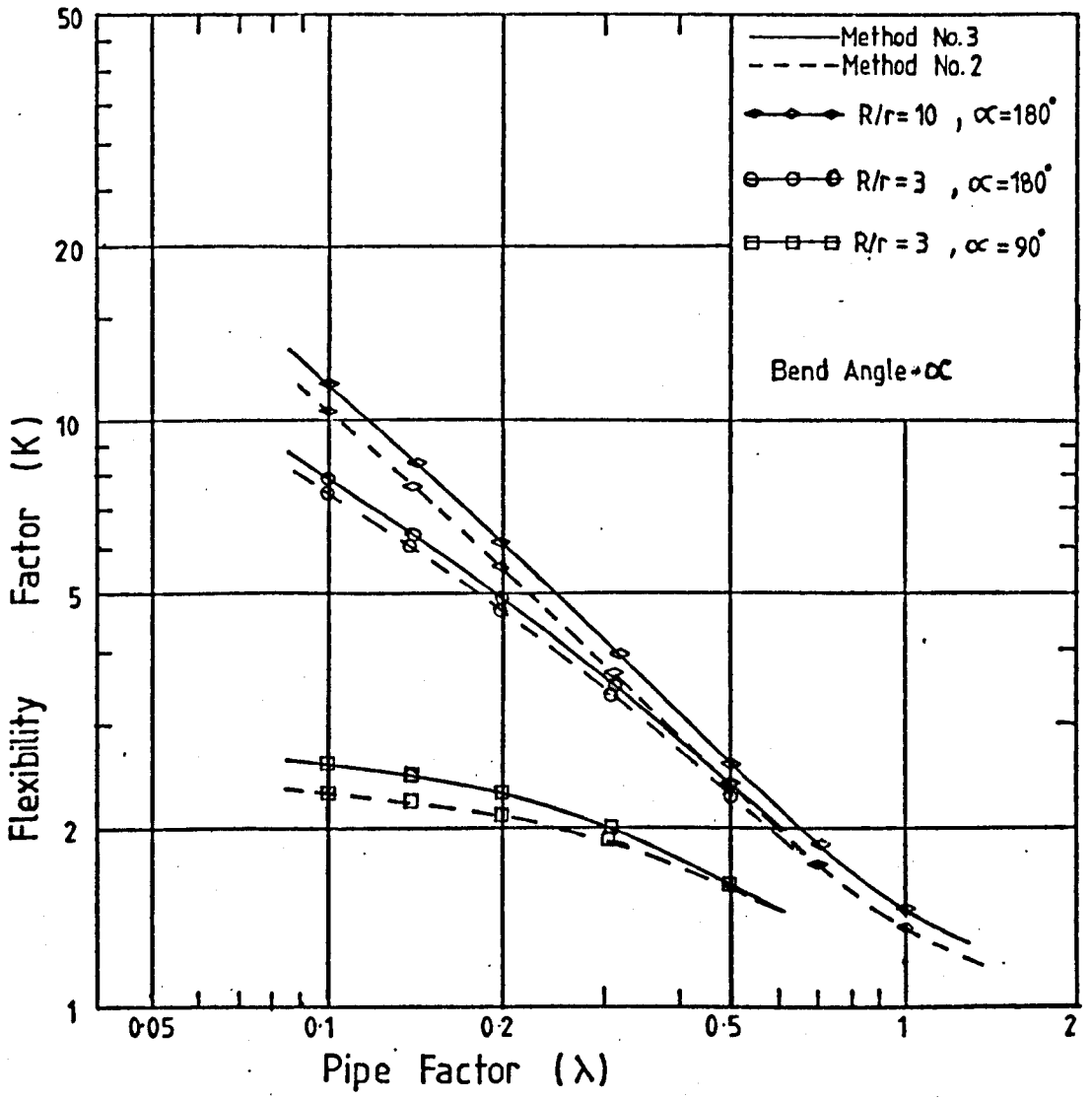

Comparison of Flexibilities from Methods 2 and 3.

Figure (3.16)

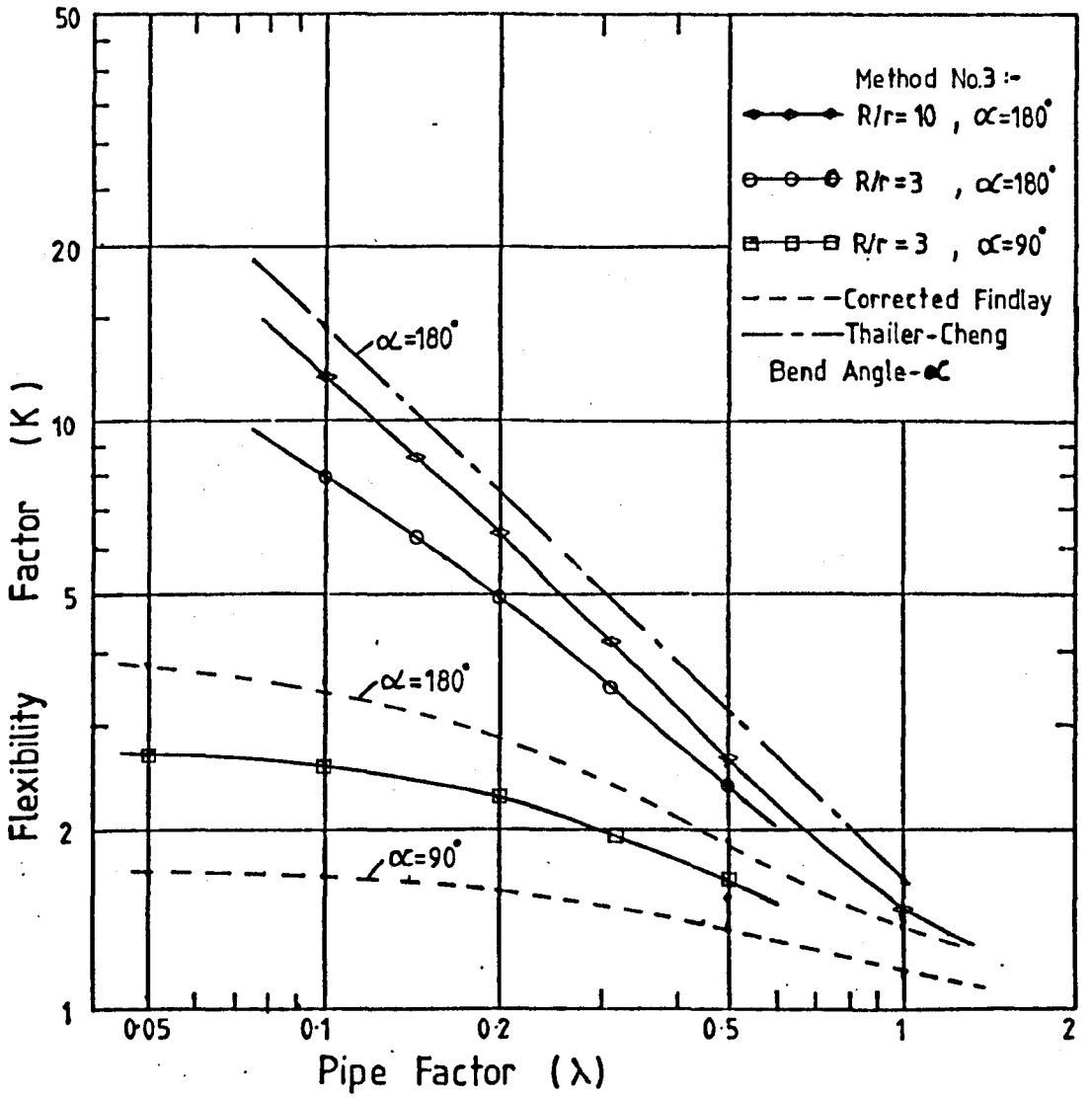

Comparison of Flexibility Factors from Findlay and Thailer-Cheng with Method No. 3

Figure (3.17)

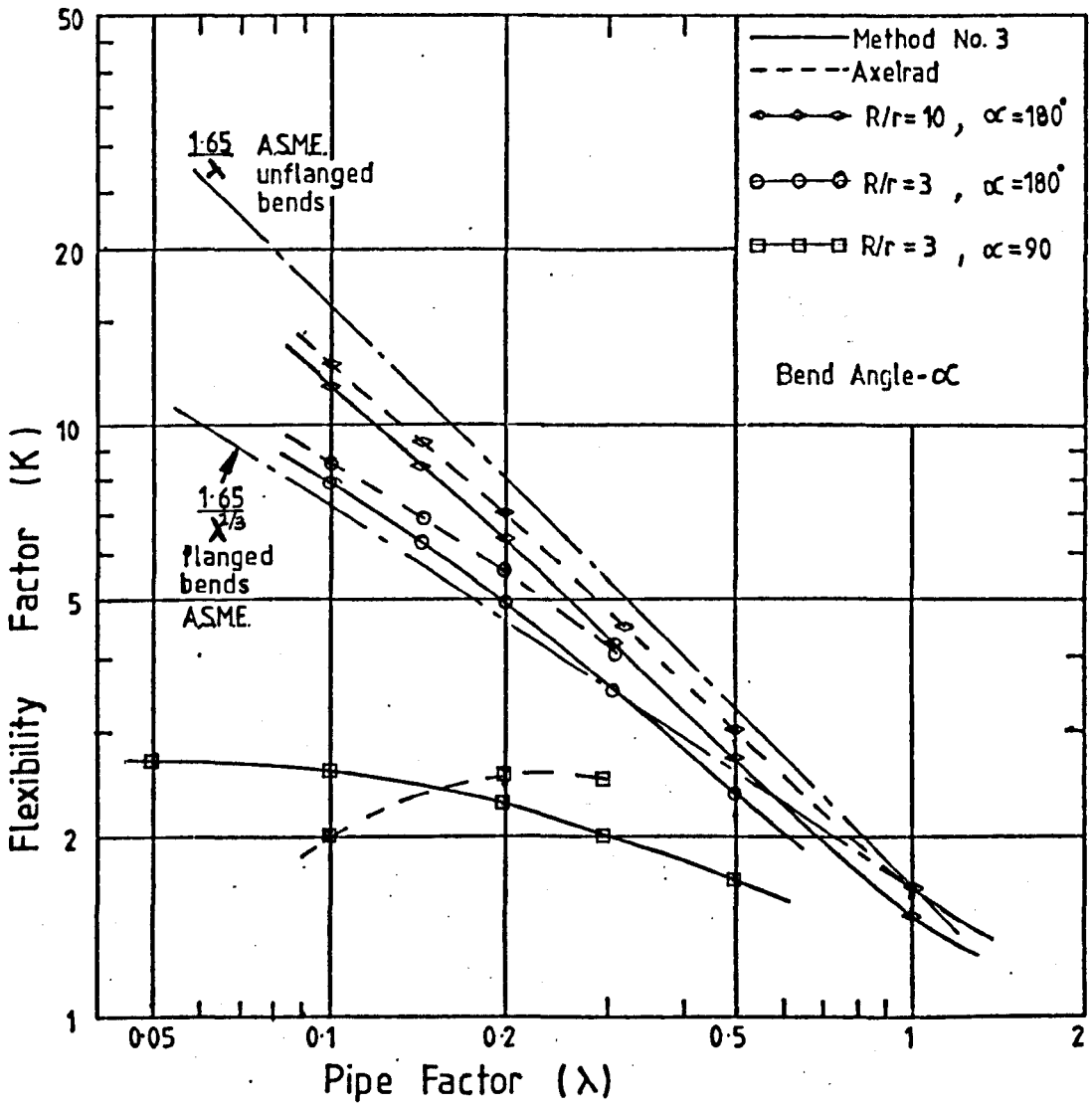

Comparison of Flexibility Factors from Axelrad and Method No. 3

Figure (3.18)

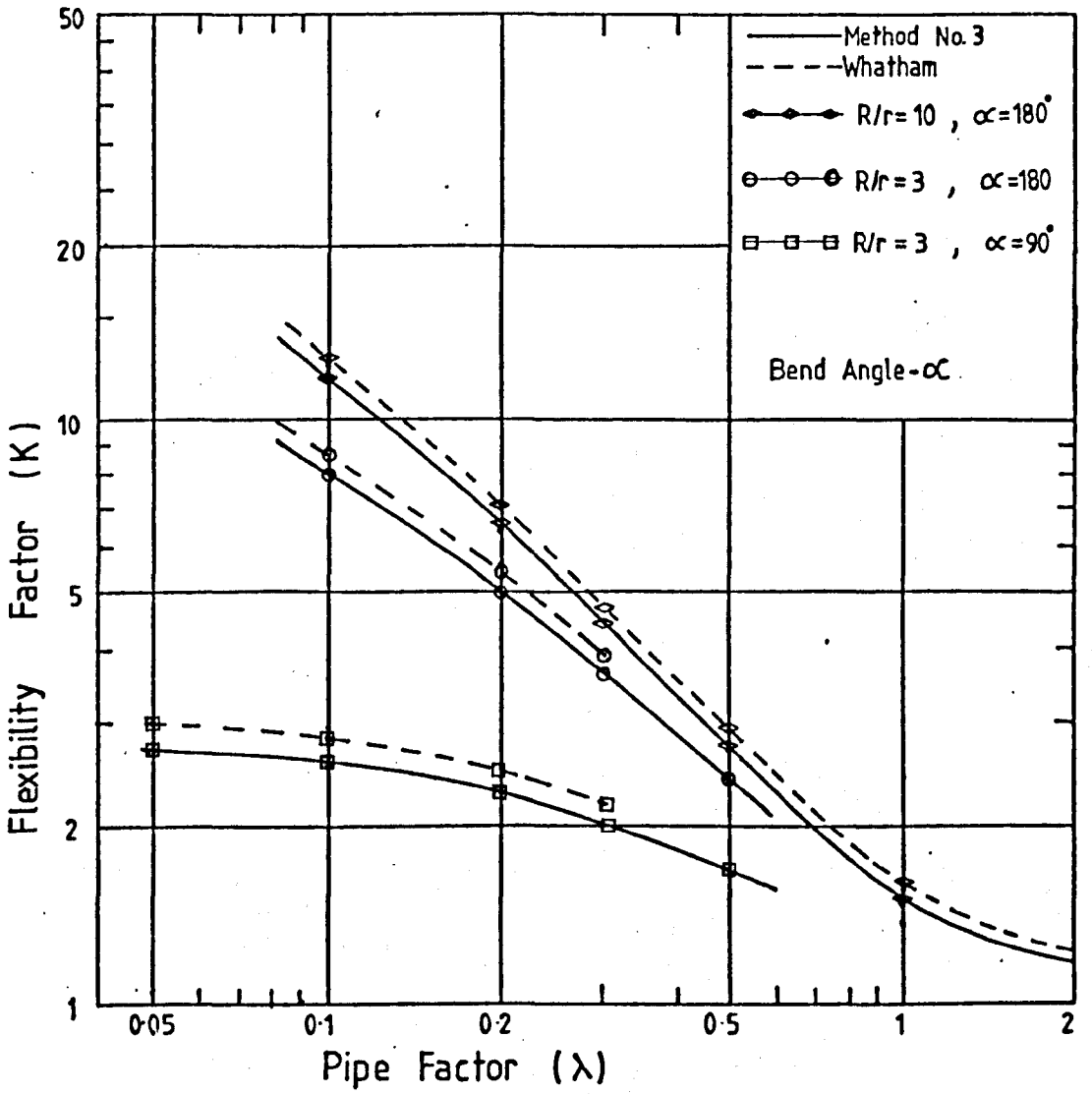

Comparison of Flexibility Factors from Whatham and Method No. 3.

Figure (3.19)

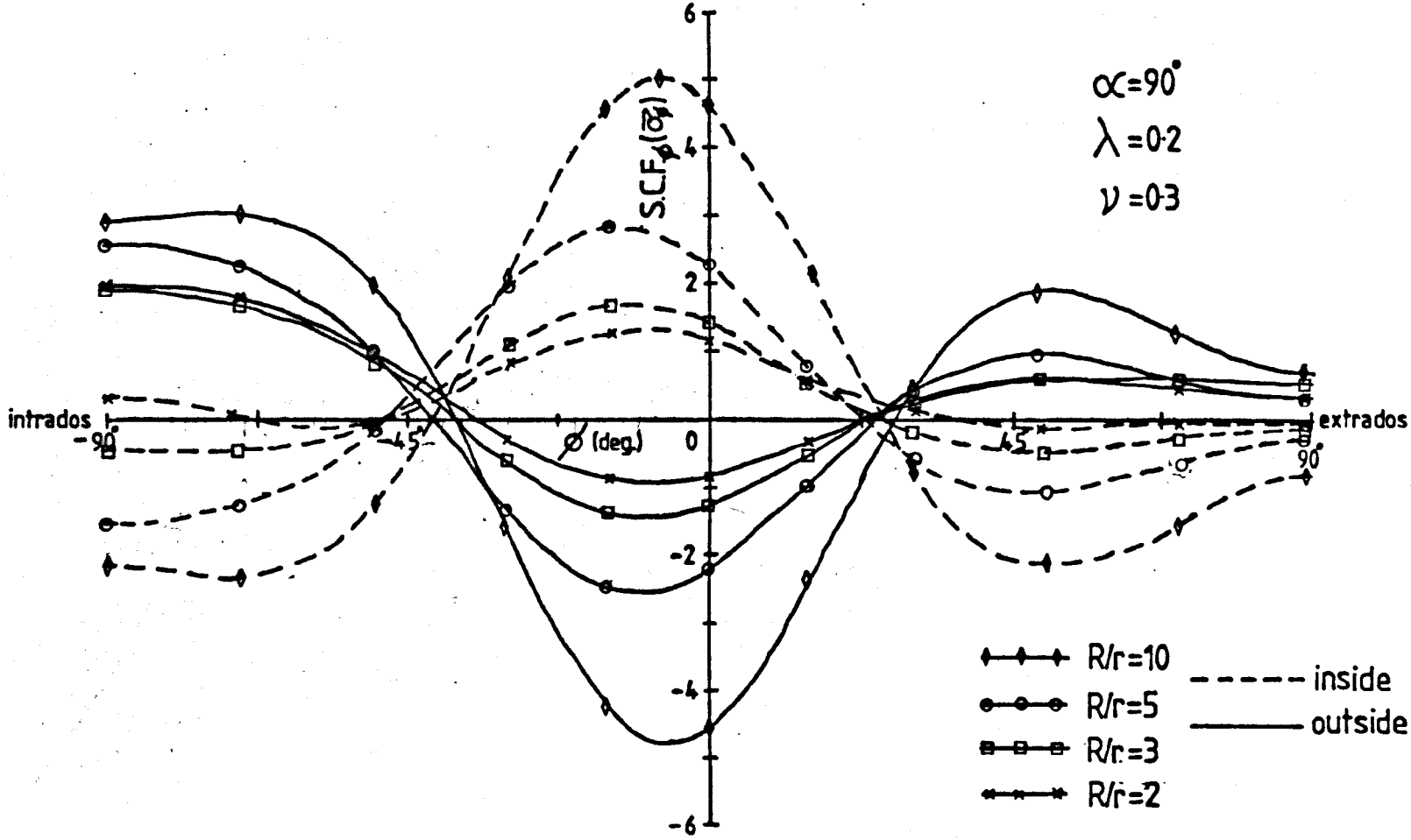

Typical Influence of the Radius Ratio on Meridional S.C.F. Distributions at $\theta=0^\circ$

Figure (3·20)

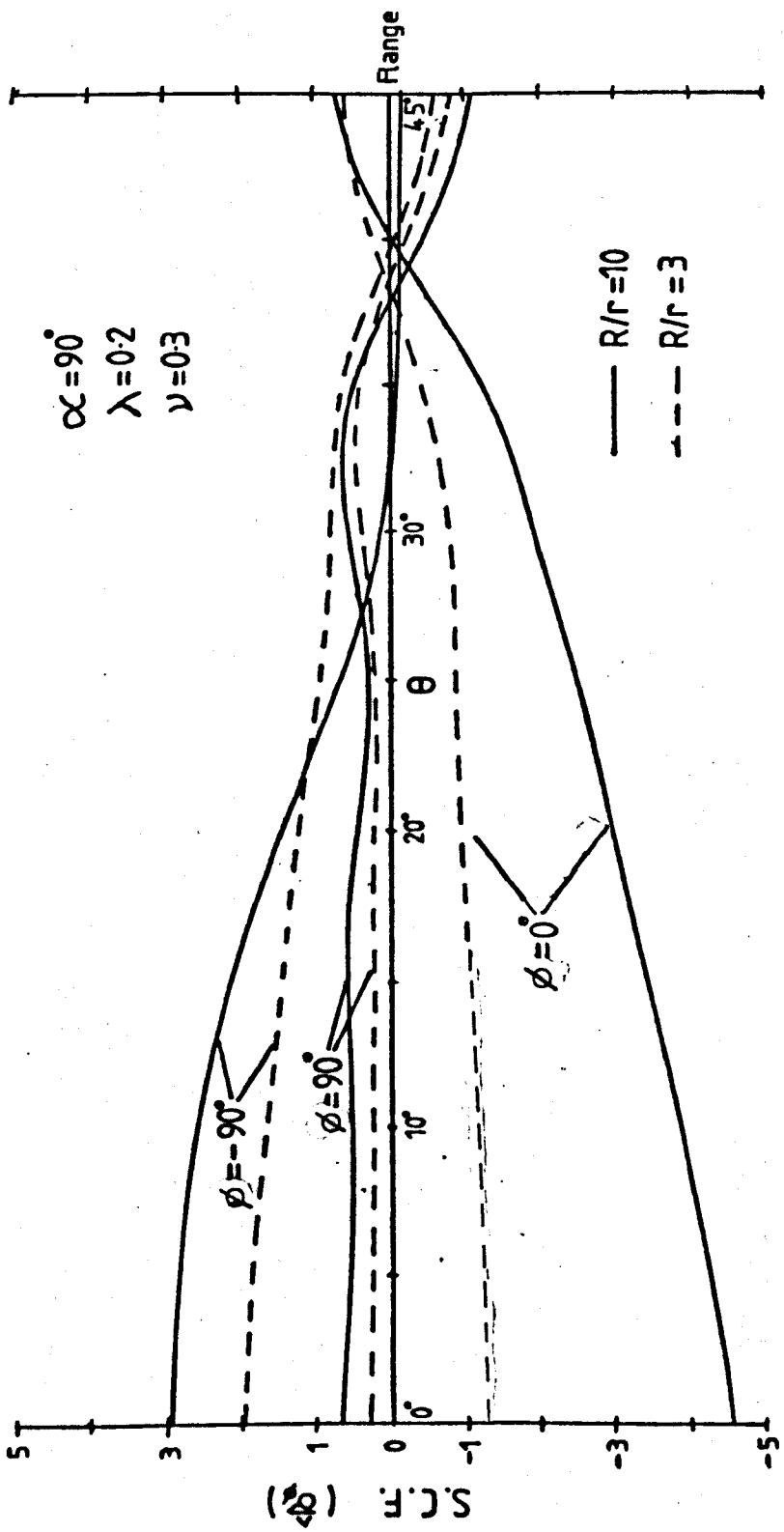

Meridional S.C.F. Distributions

Figure (3·21)

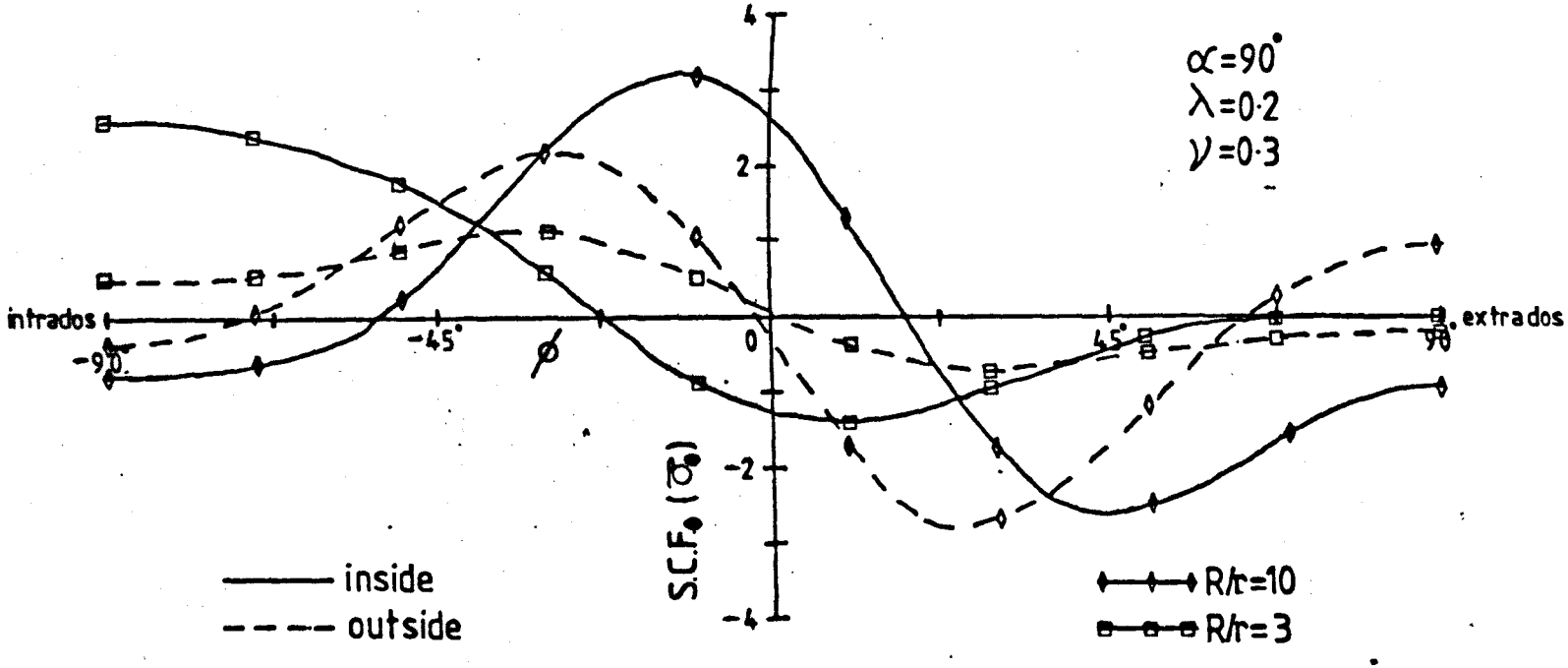

Typical Variation of Circumferential S.C.F.s. with Radius Ratio at θ=0°

figure (3.22)

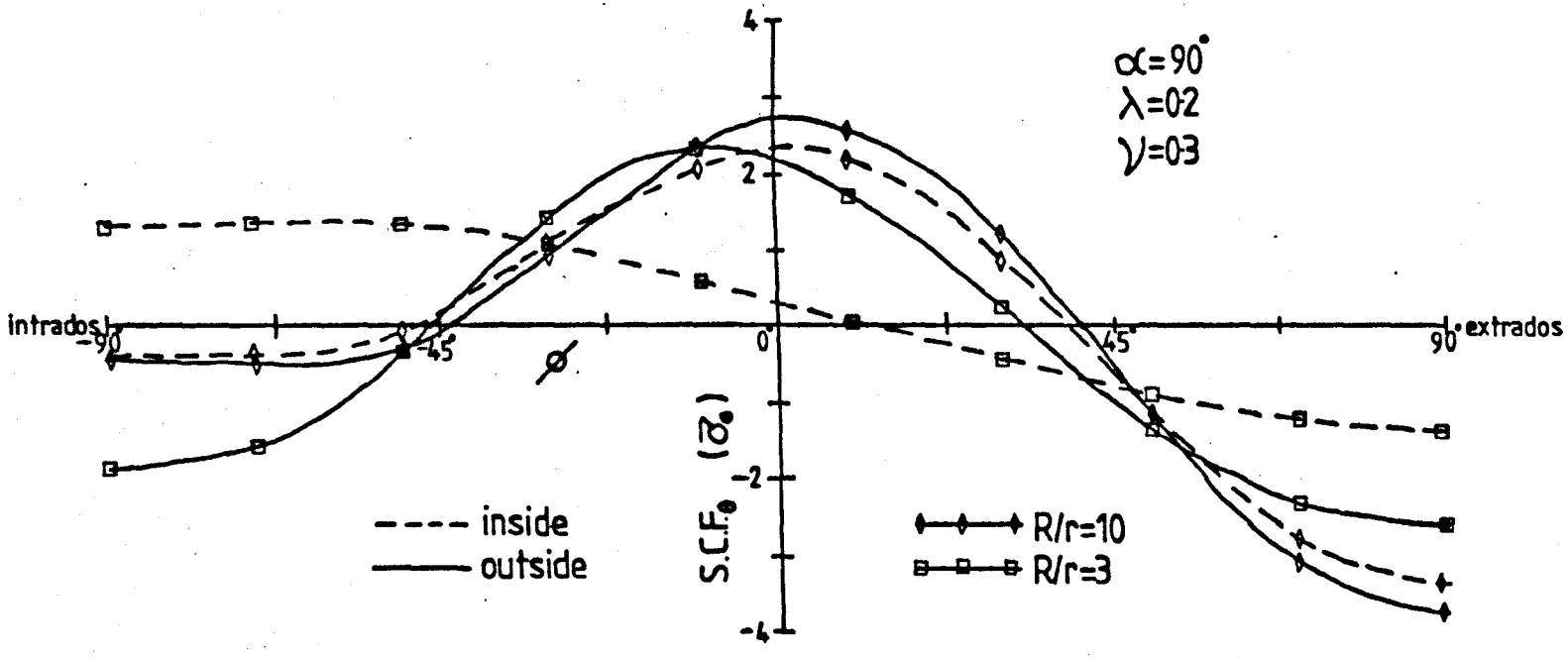

Typical Variation of Circumferential SCFs with Radius Ratio at $\theta=\alpha/2$

Figure (3·23)

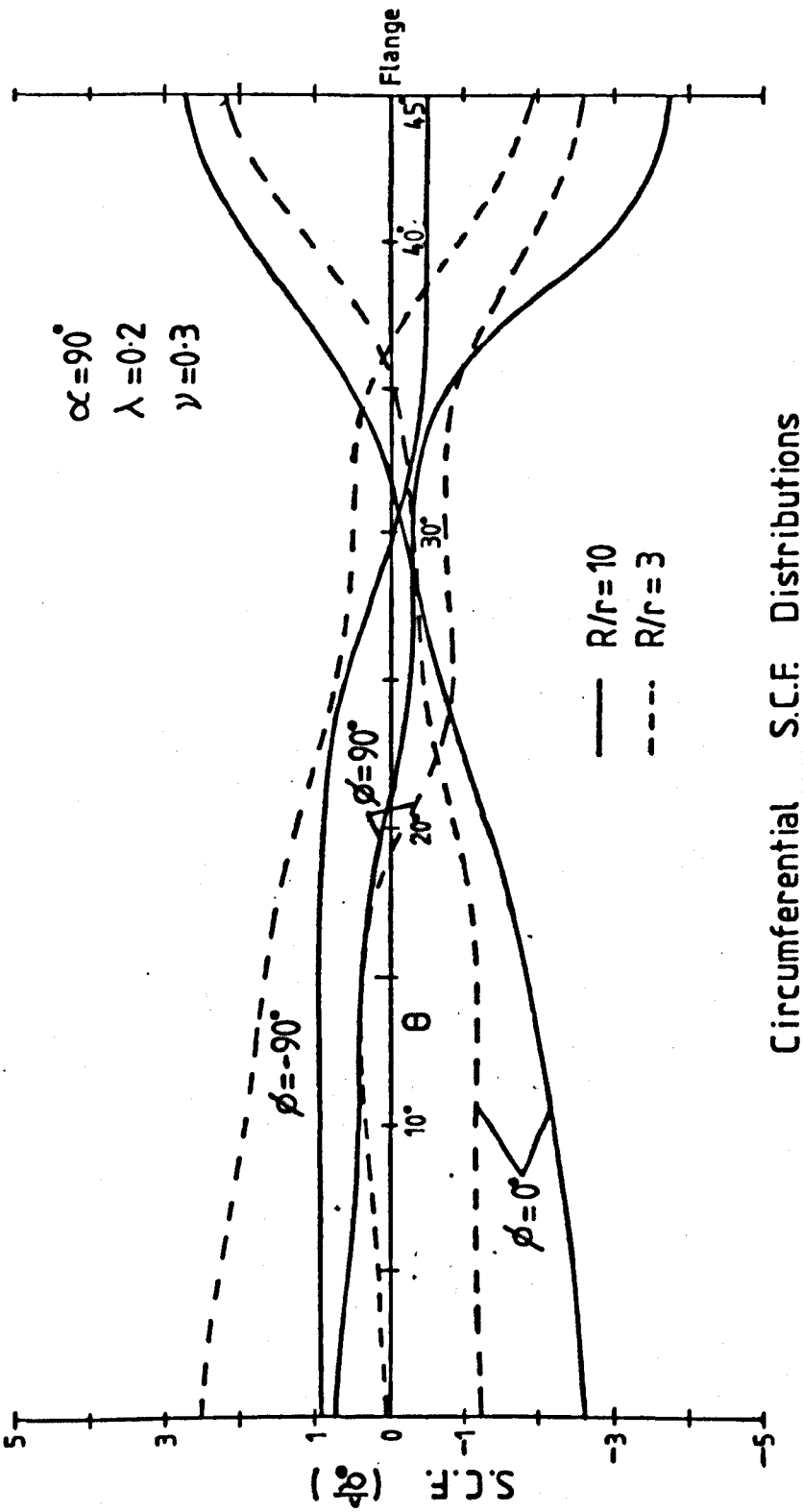
Flange
45°
40°
30°
20°
10°
θ
α=90°
λ=0·2
ν=0·3
R/r=10
R/r=3
ϕ=90°
ϕ=-90°
ϕ=0°
S.C.F. (σθ/σ)
5
3
1
0
-1
-3
-5
Circumferential S.C.F. Distributions

Figure (3·24)

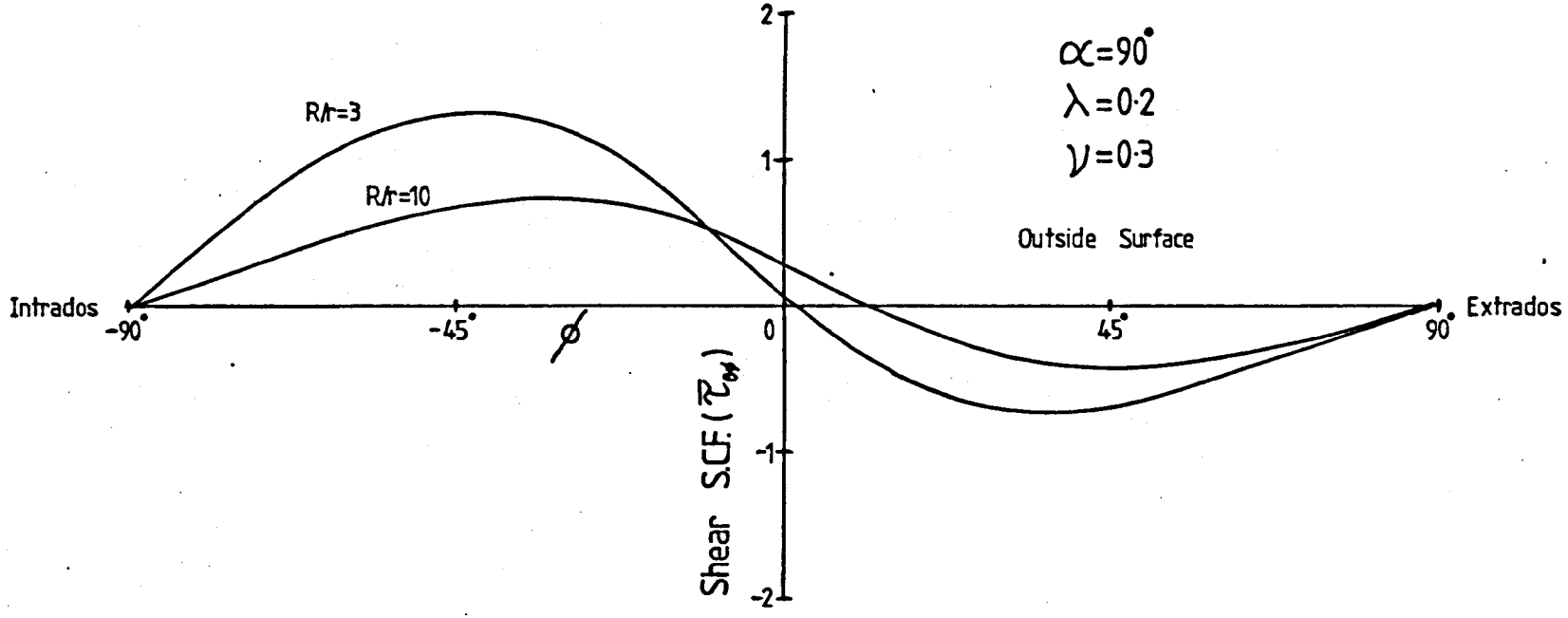

Typical Distributions of Shear S.C.Fs at $\theta = 35^{\circ}$

Figure (3.25)

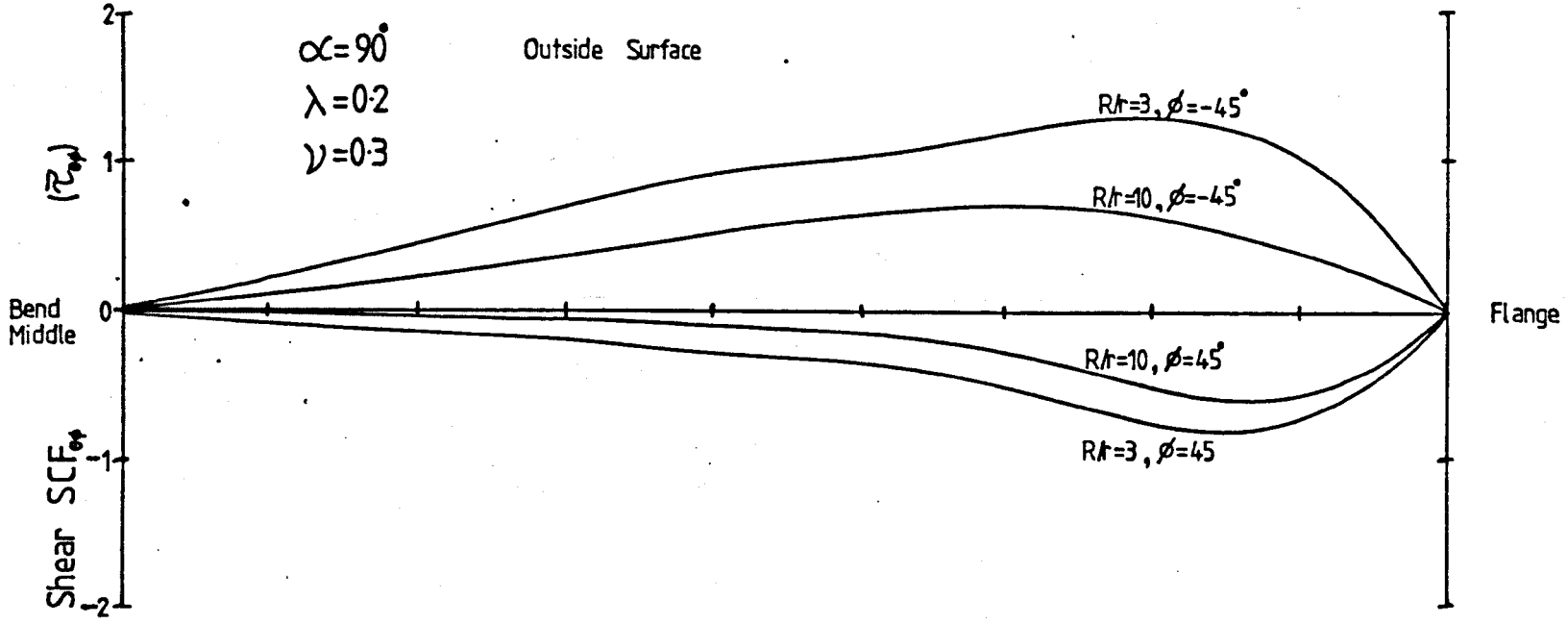

Typical Distributions of Shear S.C.F.s Along the Bend

Figure (3.26)

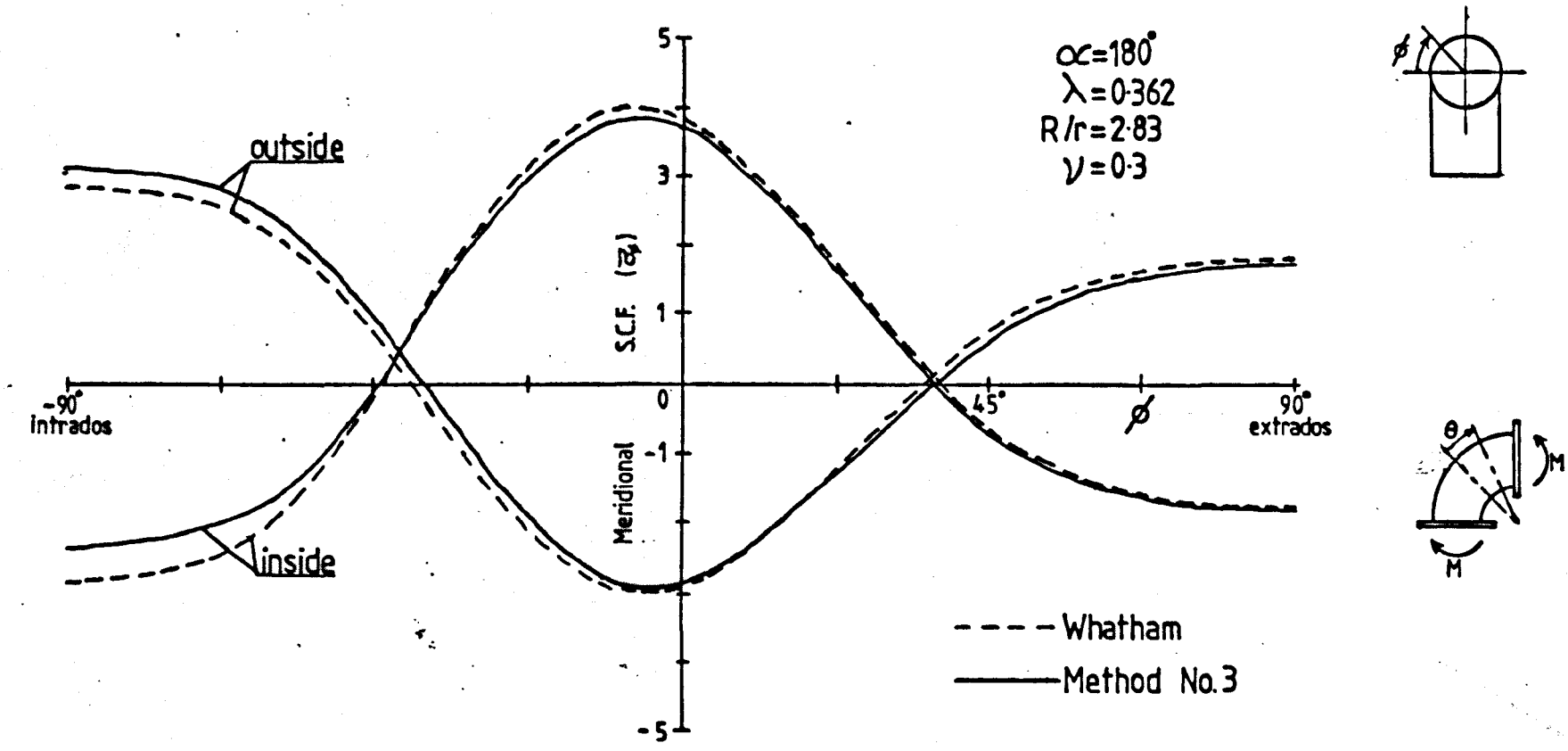

Comparison of Meridional S.C.F.s. at θ=0°

Figure (3·27)

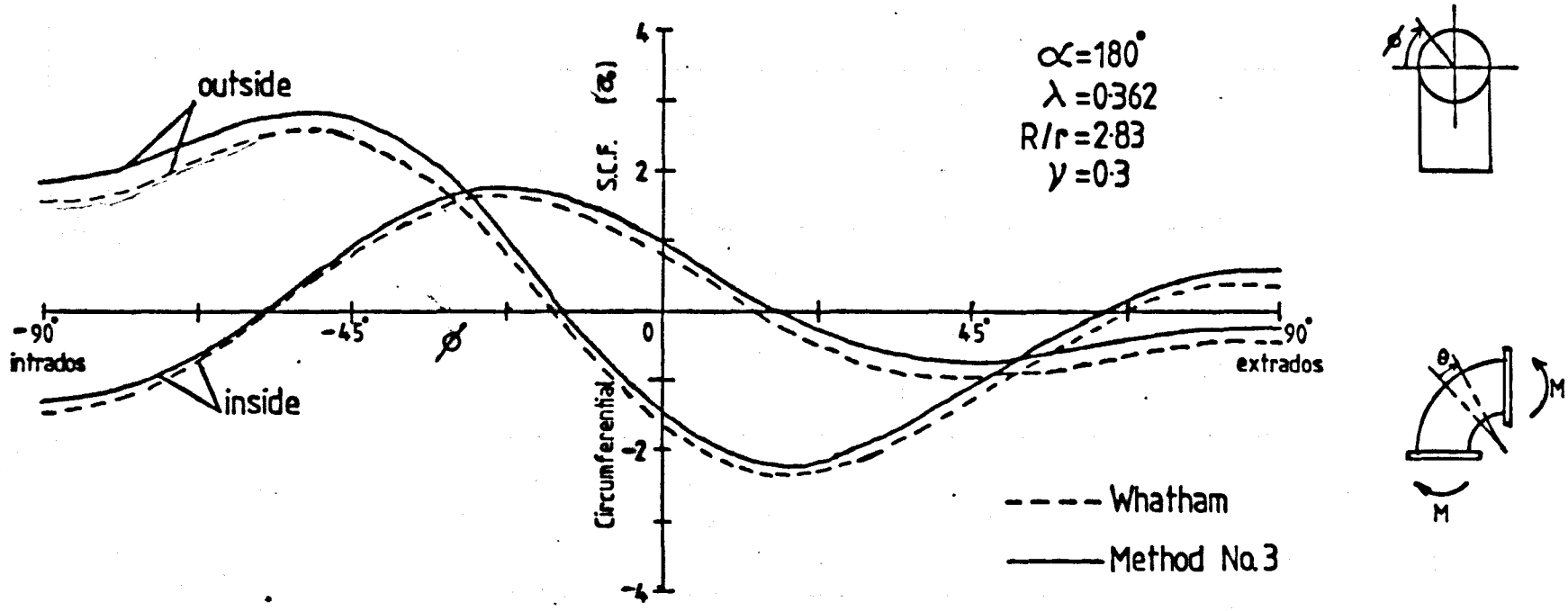

Comparison of Circumferential S C F at θ=0°

Figure (3.28)

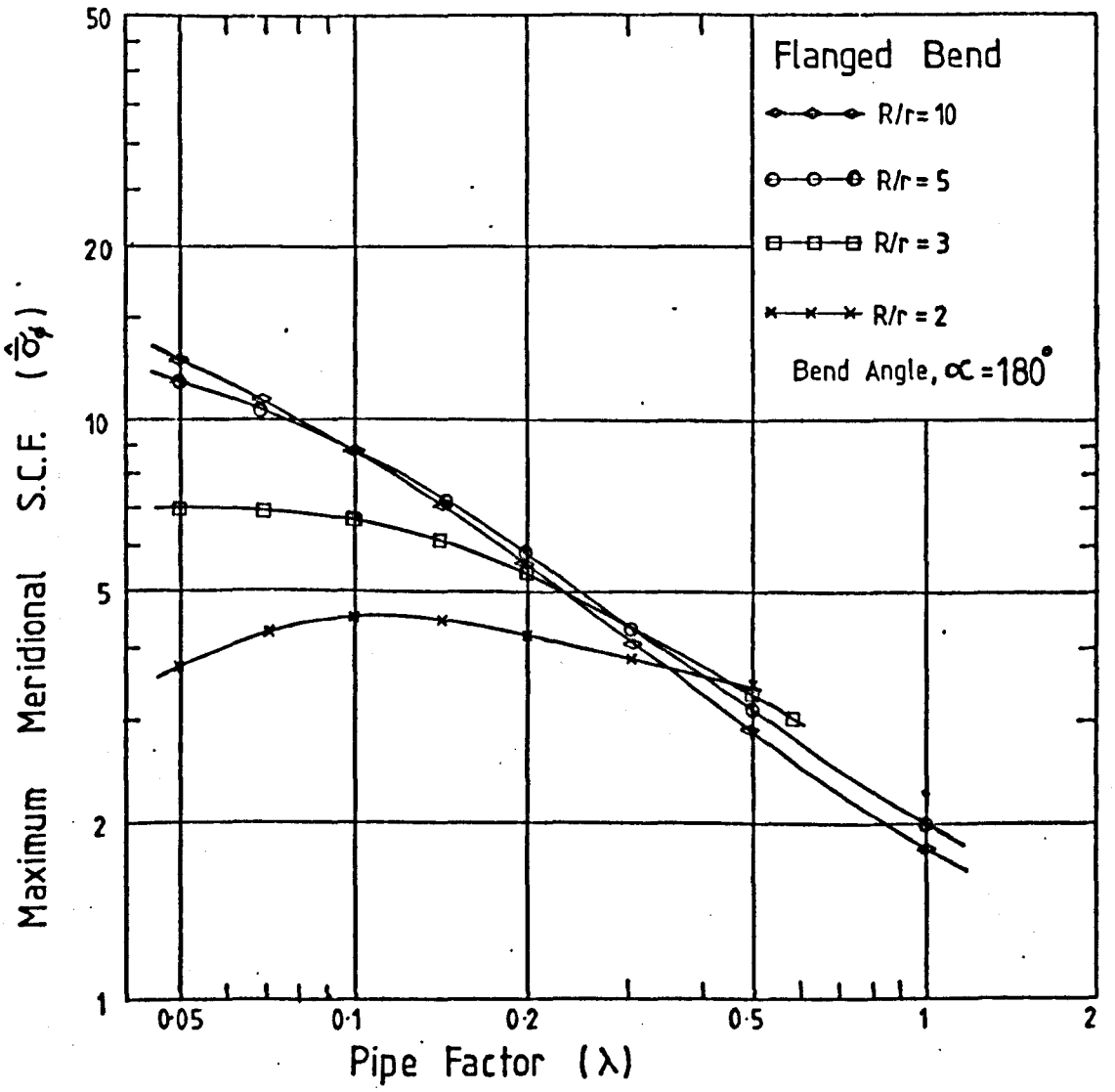

Maximum Meridional S.C.F.s

Figure (3·29)

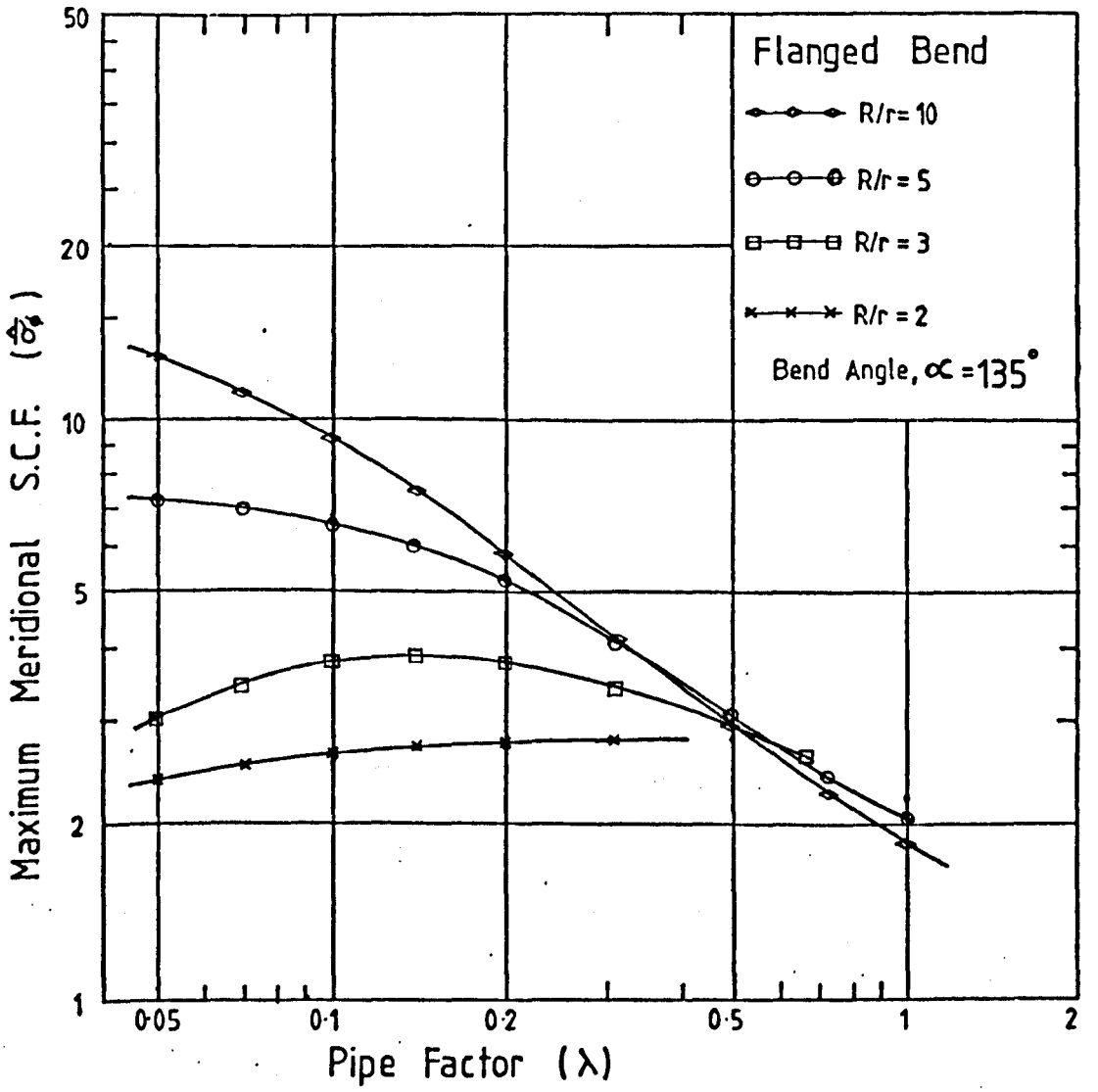

Maximum Meridional S.C.F.s

Figure (330)

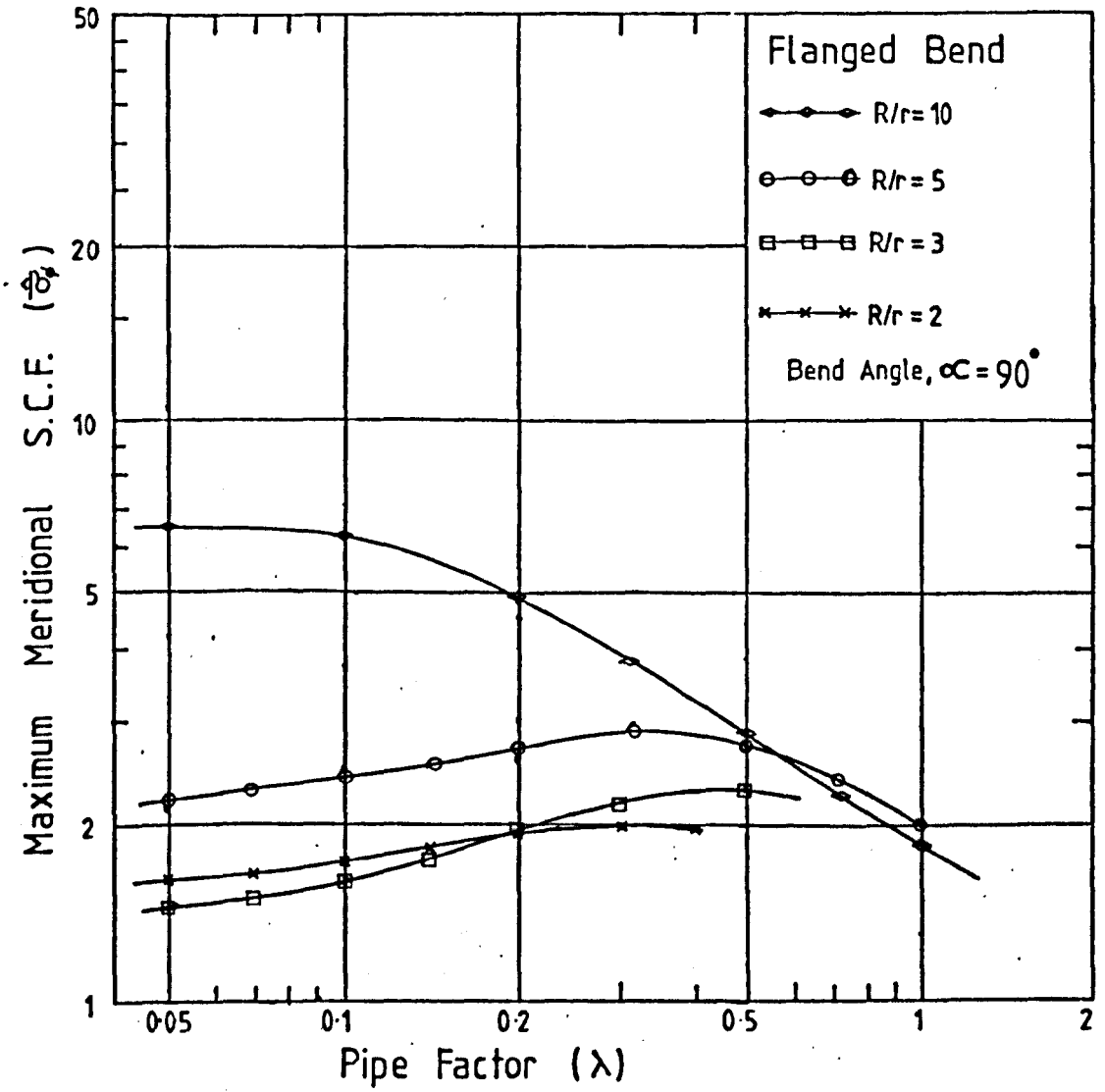

Maximum Meridional S.C.F.s

Figure (331)

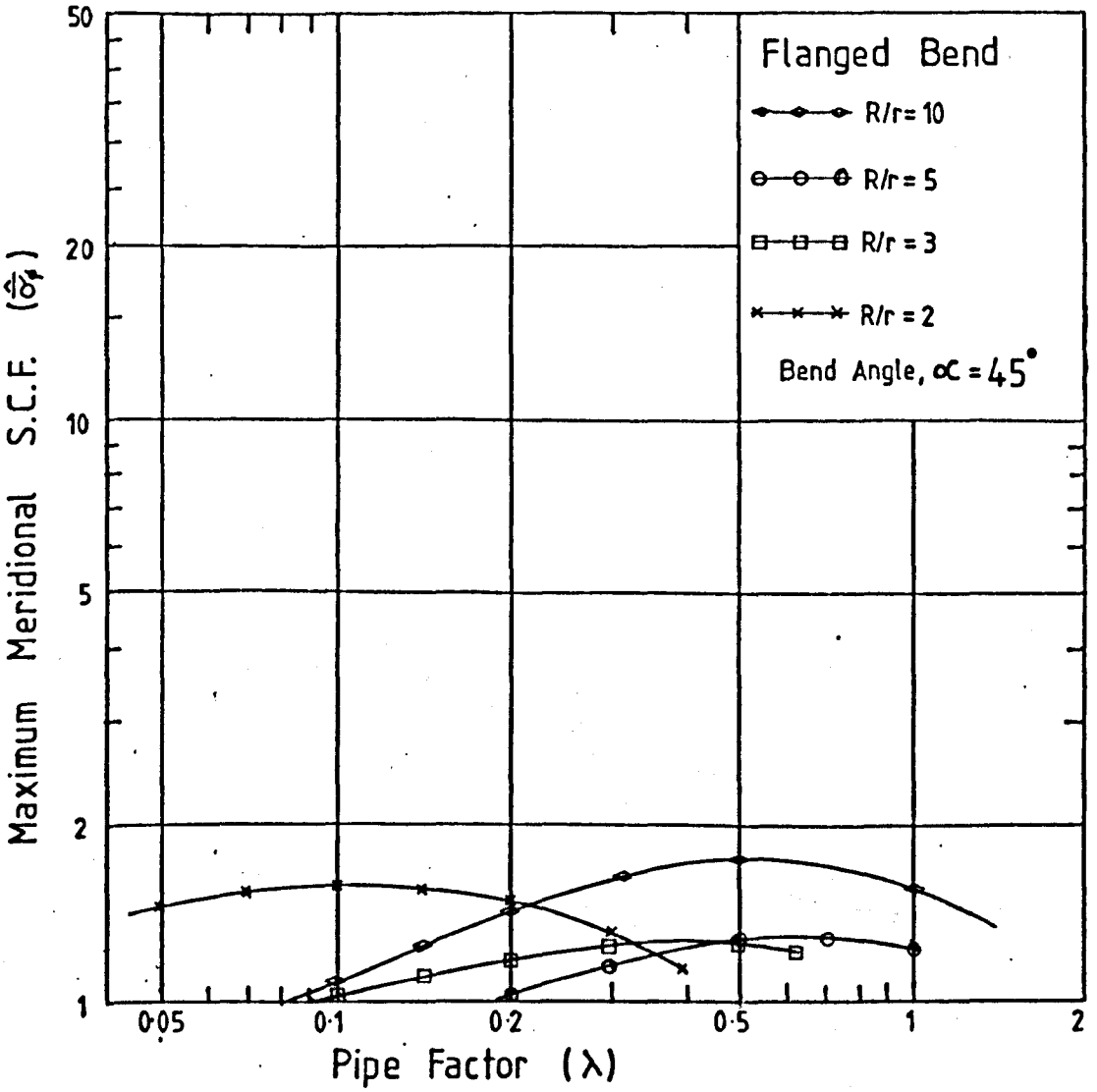

Maximum Meridional S.C.F.s

Figure (3·32)

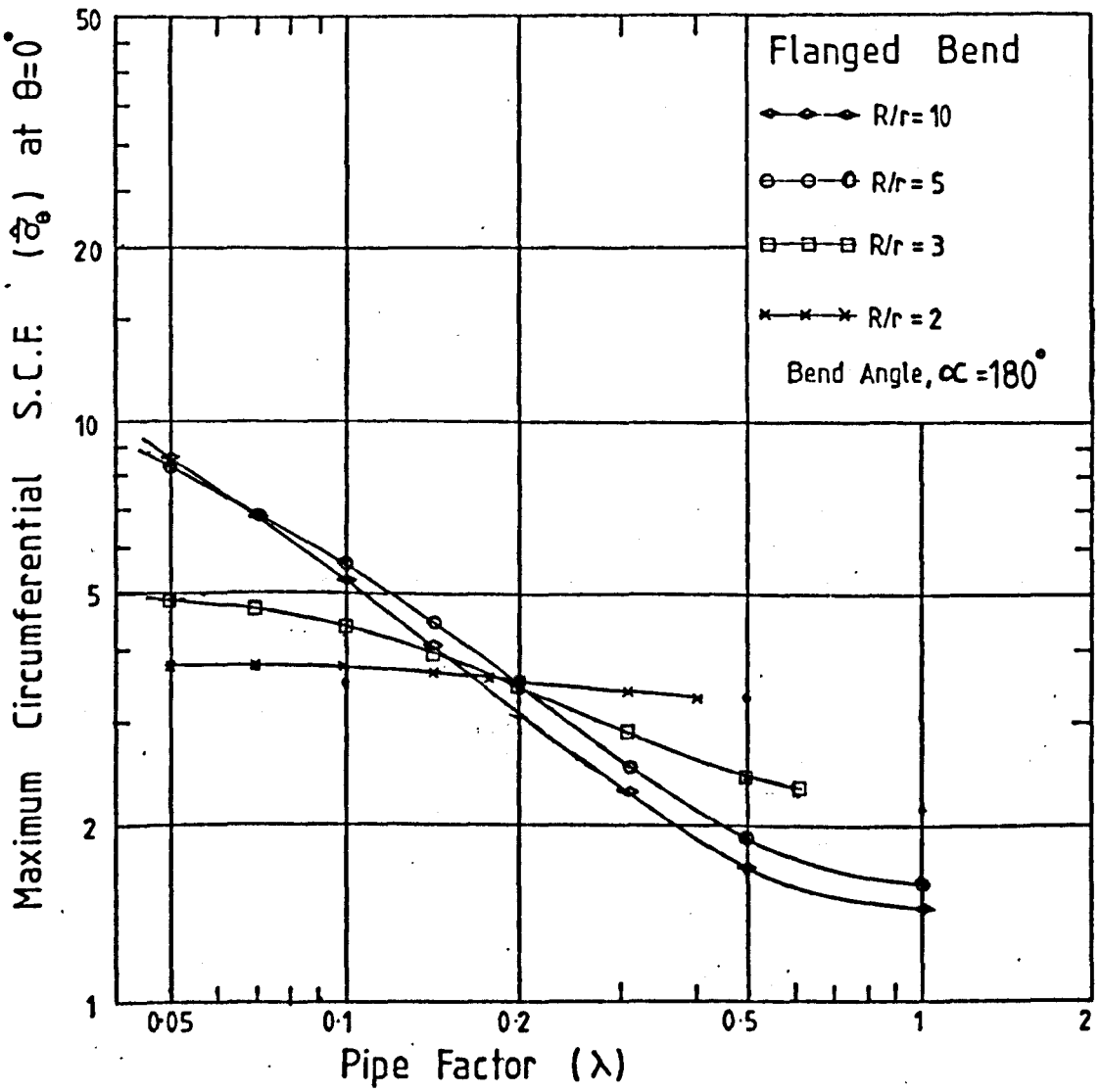

Maximum Circumferential S.C.F.s. at θ=0°

Figure (333)

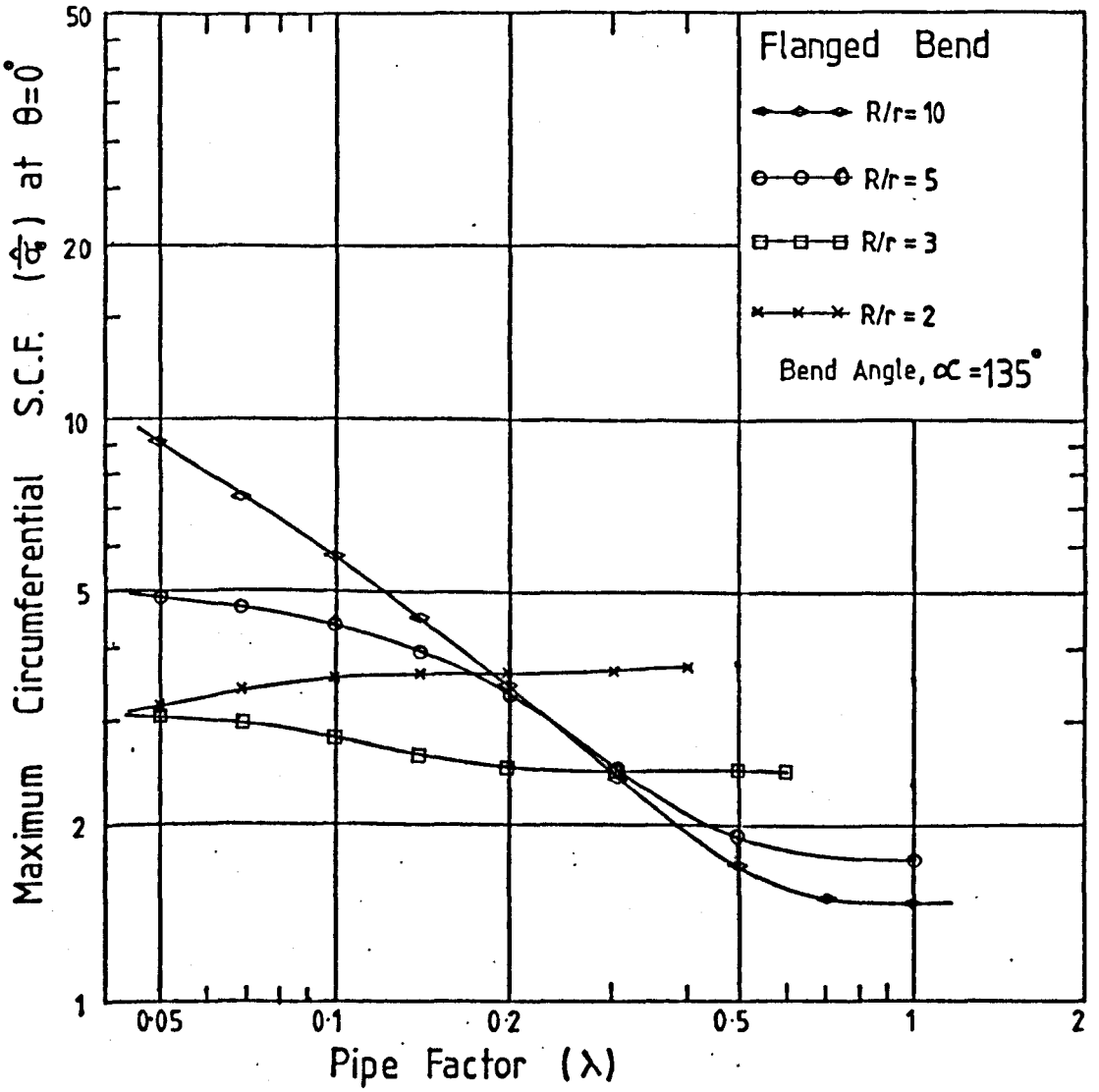

Maximum Circumferential S.C.F.s. at θ=0°

Figure (334)

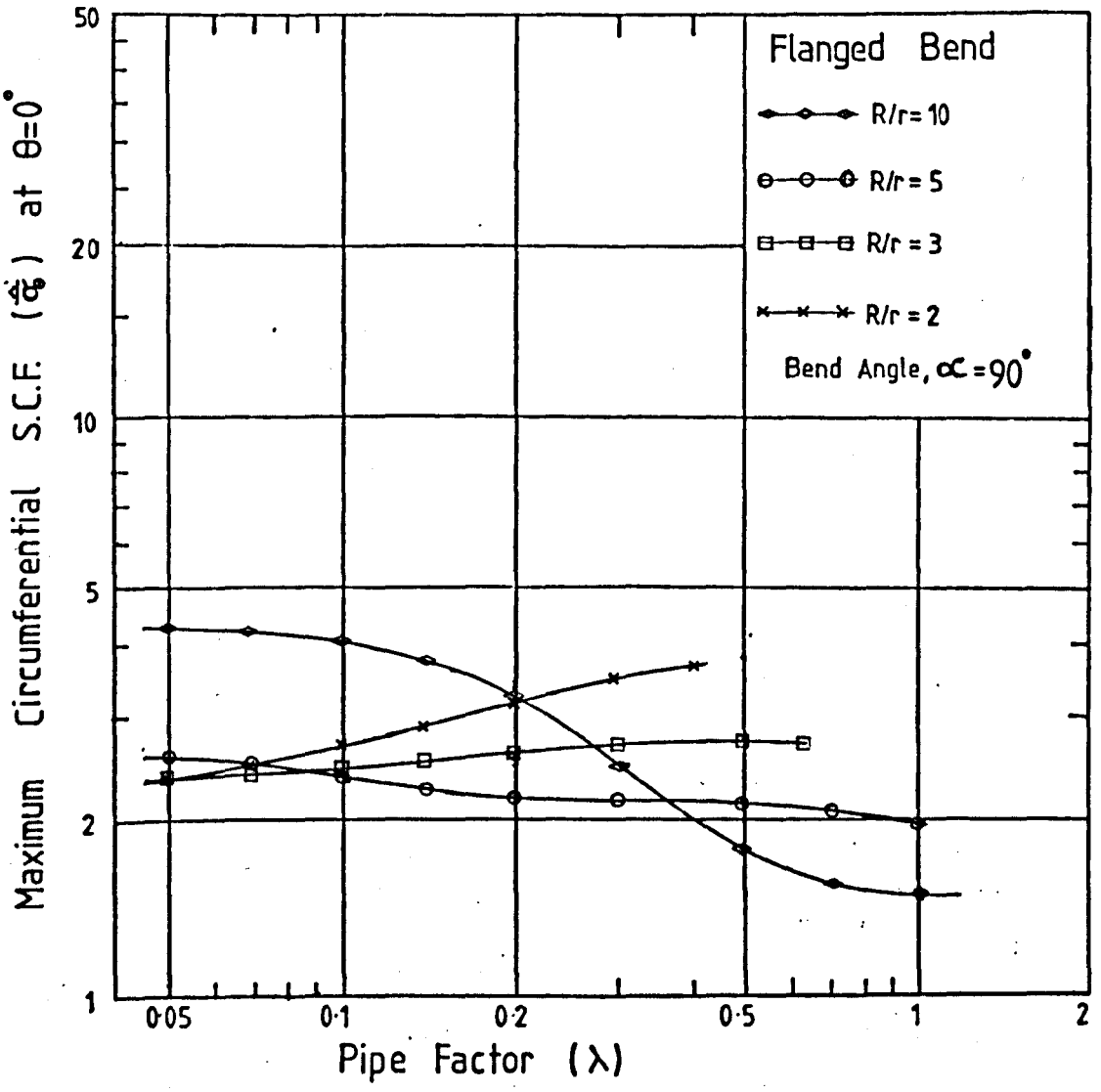

Maximum Circumferential S.C.F.s. at θ=0°

Figure (335)

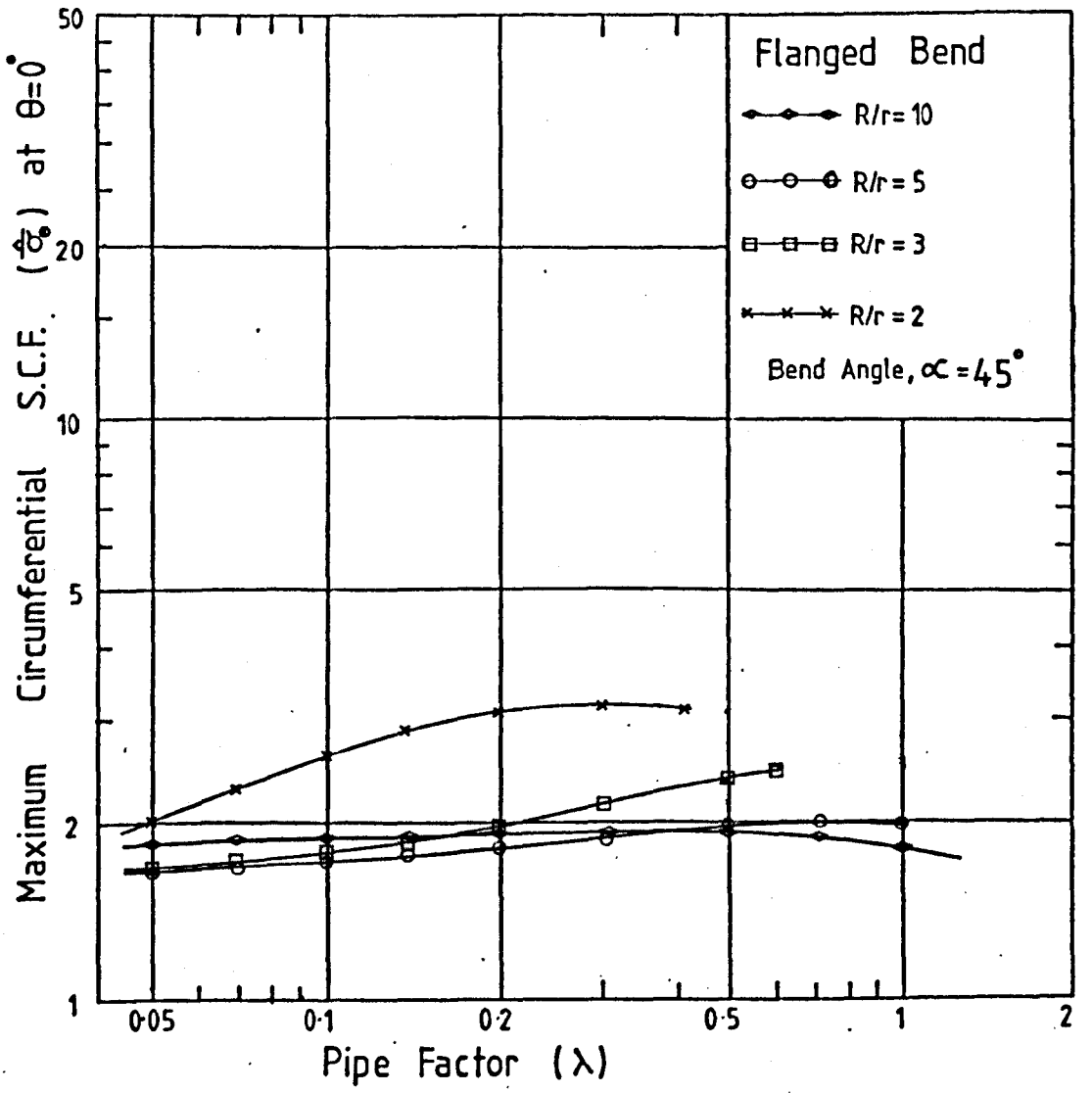

Maximum Circumferential S.C.F.s at $\theta=0^\circ$

Figure (3·36)

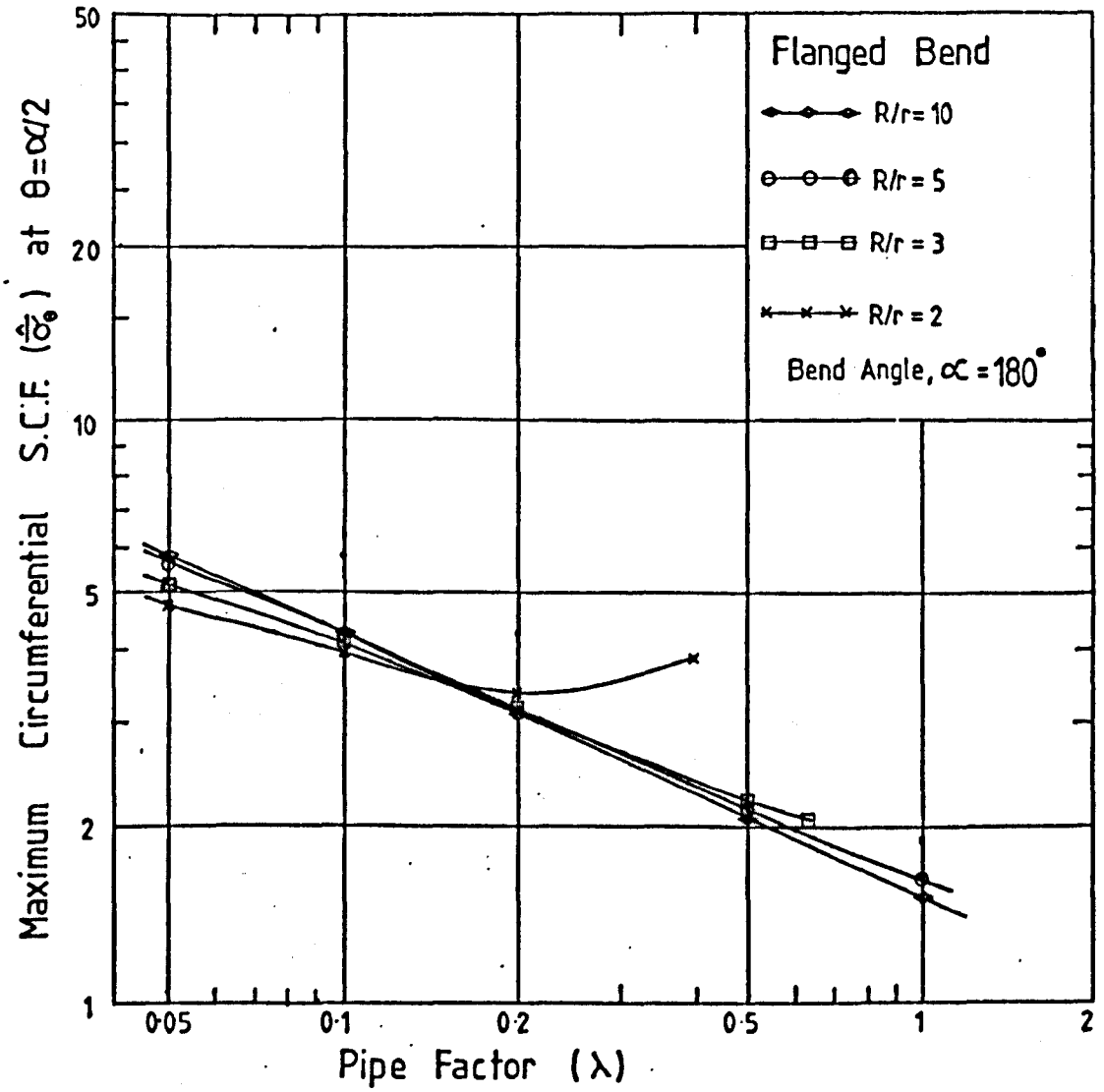

Maximum Circumferential S.C.F.s. at $\theta = \alpha/2$

Figure (3·37)

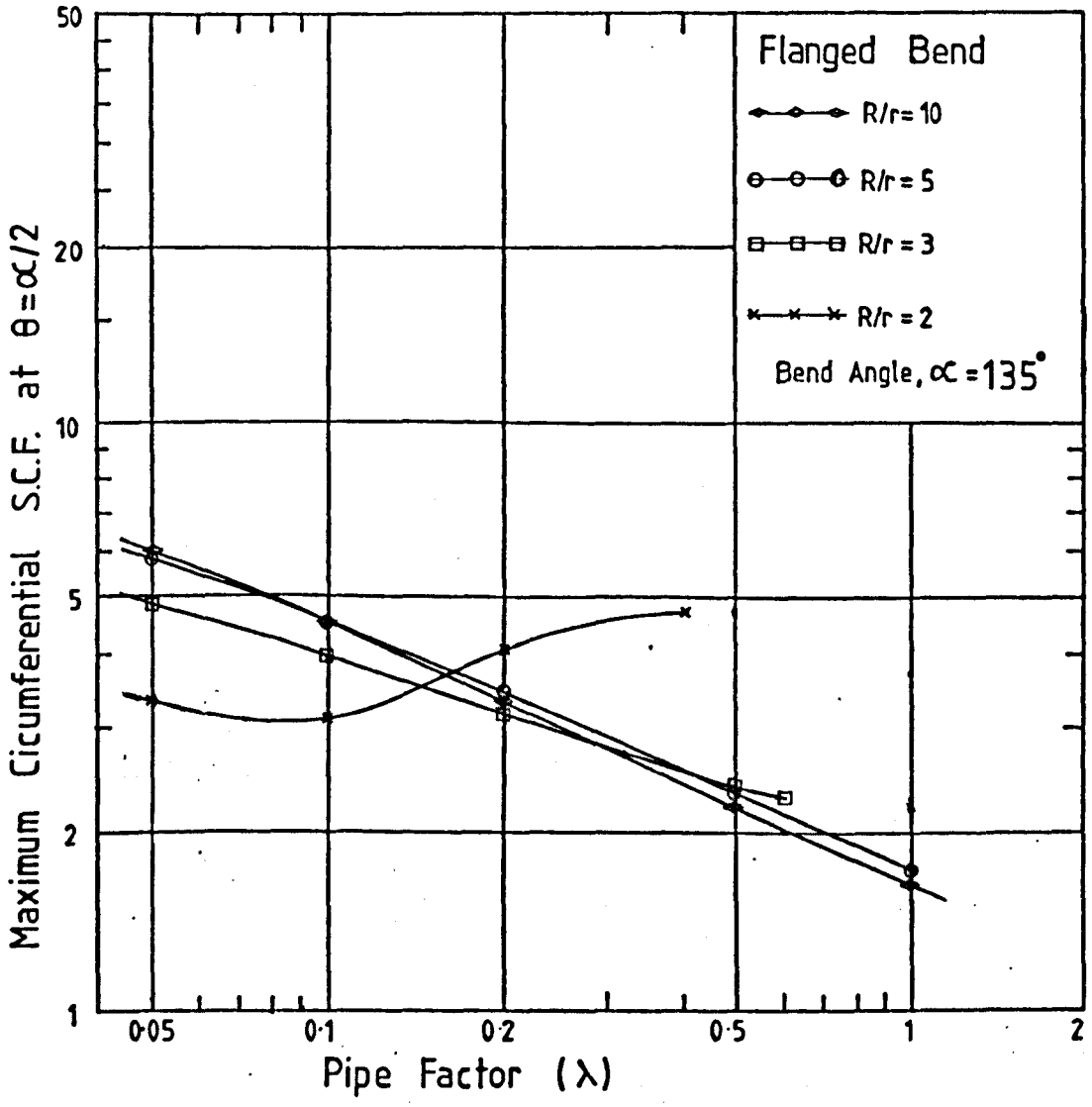

Maximum Circumferential SCFs at $\theta=\alpha/2$

Figure (338)

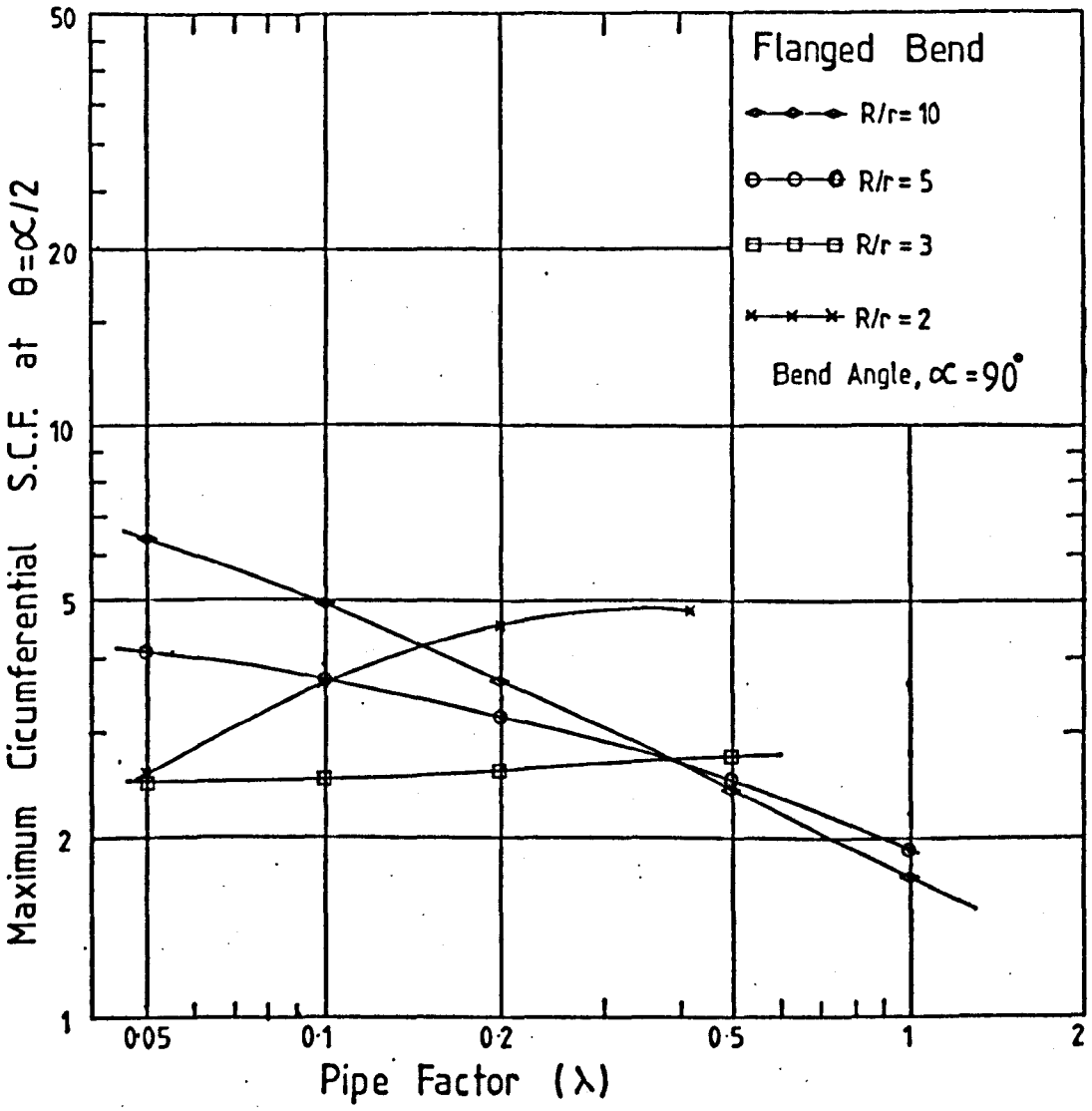

Maximum Circumferential SCFs at $\theta = \alpha/2$

Figure (3·39)

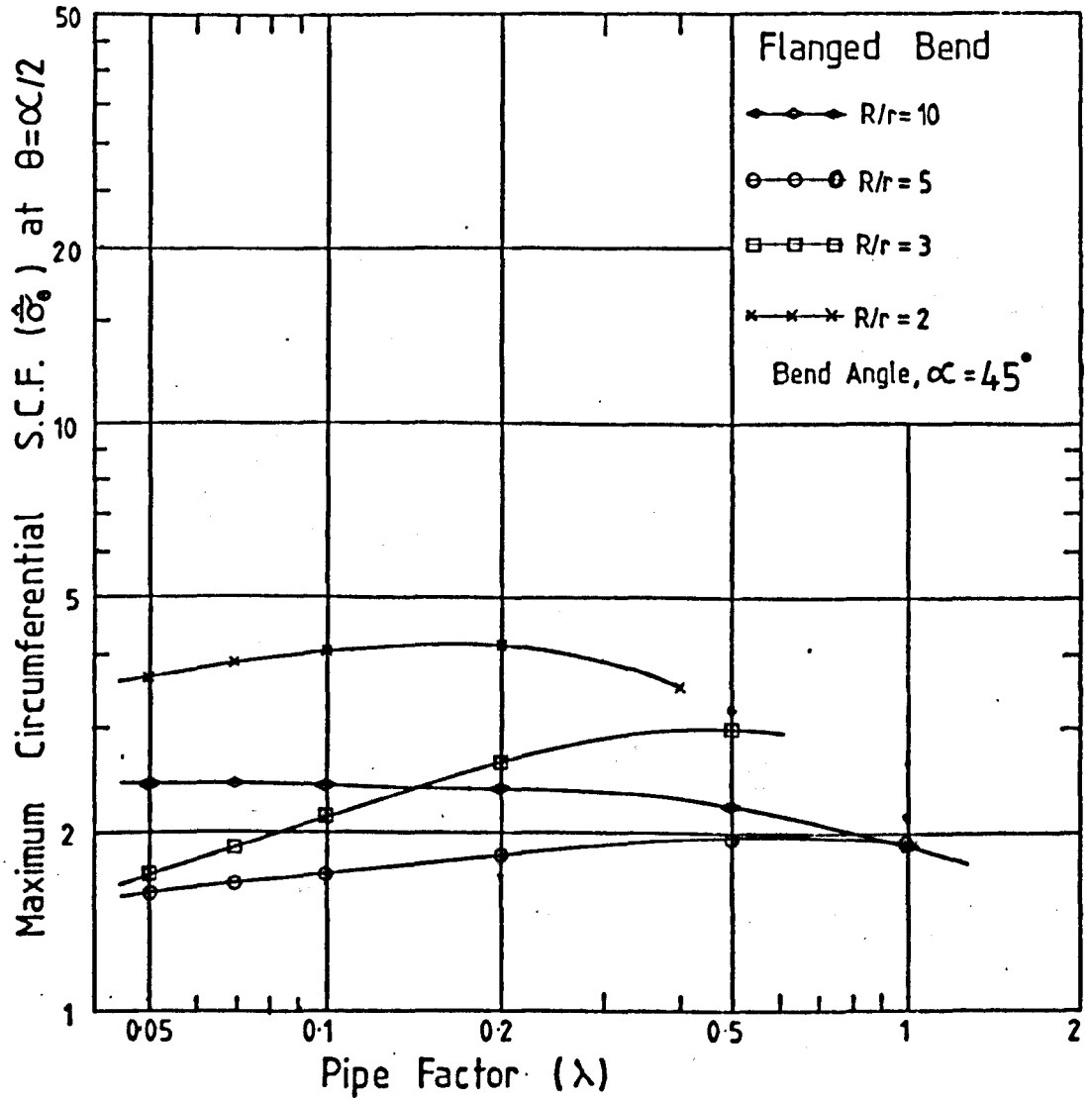

Maximum Circumferential S.C.F.s. at $\theta = \alpha/2$

Figure (340)

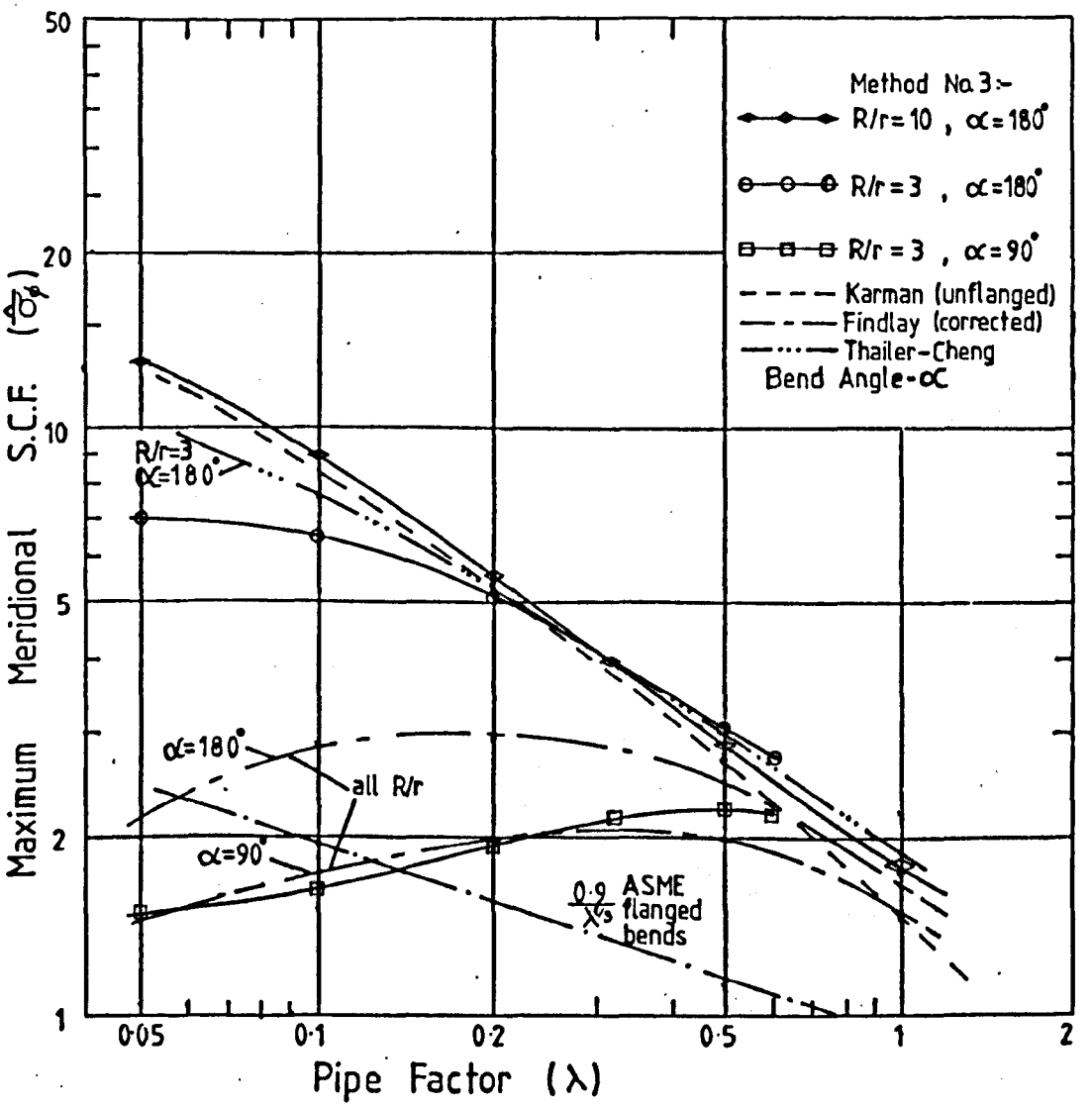

Theoretical Comparisons of Meridional S.C.Fs. with Method No. 3.

Figure (3.41)

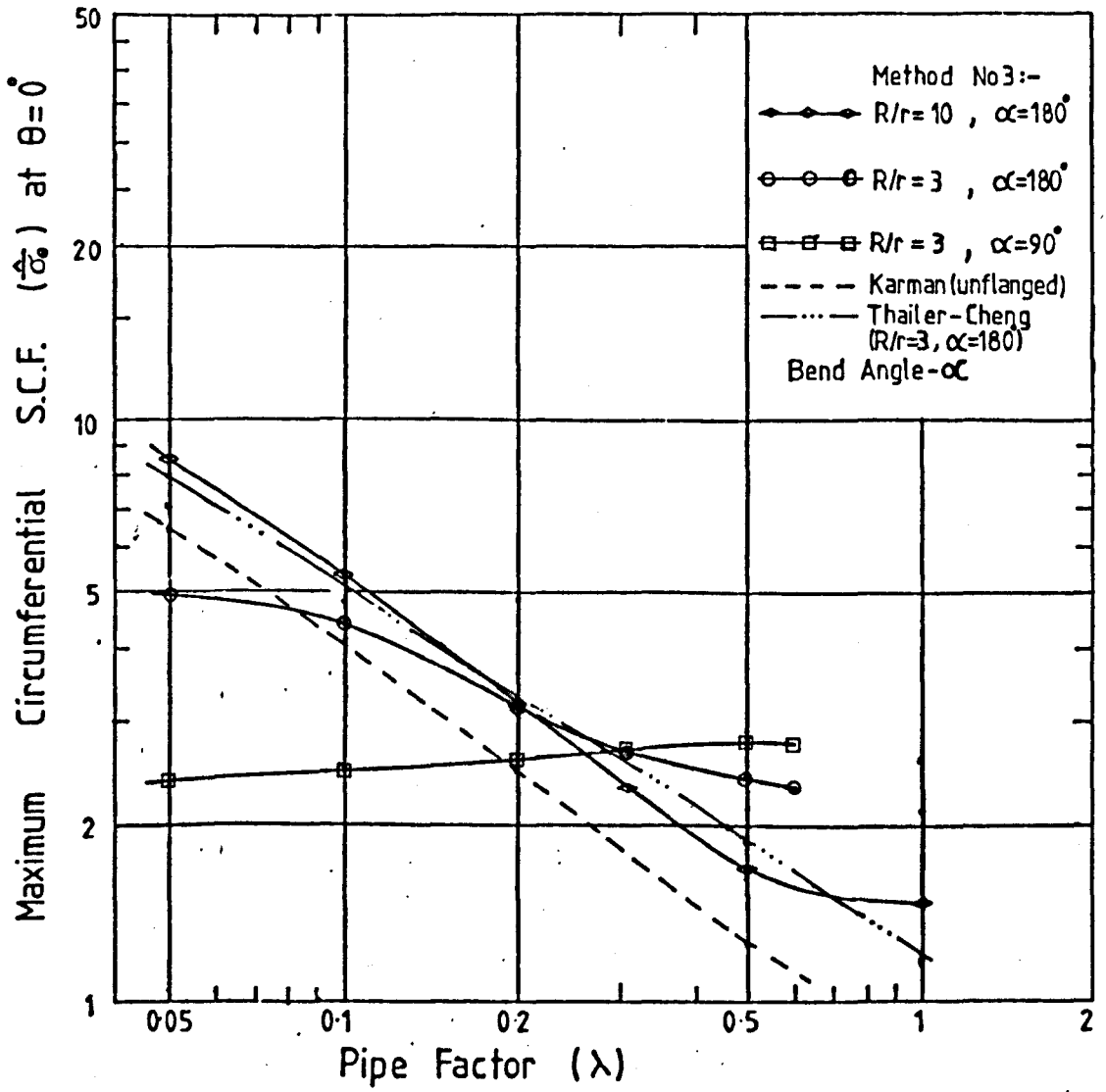

Comparison of Maximum Circumferential S.C.F.s. at $\theta=0^\circ$

Figure (342)

CHAPTER .4

EXPERIMENTS ON FLANGED BENDS AND COMPARISONS WITH THEORY

Abstract

A brief description is given of an experimental programme to determine the flexibility and stress characteristics of two smooth bends with flanged end constraints, loaded with in-plane bending.

Comparisons are made between the theory, method No. 3, and the experimental flexibility and stress factors presented by the present and previous authors.

CHAPTER (4)

EXPERIMENTS ON FLANGED BENDS AND COMPARISON WITH THEORY

(4.1) Present Experiments

- (a) Test Programme
- (b) Manufacturing Tolerances
- (c) Details of Test Rigs
- (d) Strain Gauging and Instrumentation
- (e) Evaluation of Stresses
- (f) Flexibility Measurement
- (g) Loading
- (h) Results

(4.2) Comparisons of Flexibility Factors from Theory and Experiment

(4.3) Maximum S.C.Fs.

(4.4) Stress Distributions

(4.1) Present Experiments

(4.1a) Test Programme

Two of the important functions of experiments, which are generally recognized, are firstly to confirm the theoretical approach and assumptions and secondly, where appropriate, to bridge the gap between theory and experiment. In the following sections, the theory developed in chapter (3), (method No. 3) will be compared with the present experimental work and also with relevant results from other sources.

It was the intention that the additional data provided herein should supplement available published results. Therefore, careful attention was given to the selection of the test configurations. First of all, forged bends were chosen because of their small manufacturing tolerances for out-of-roundness and thickness variations, secondly, the pipe diameters had to be sufficiently large to allow accurate positioning of strain gauges around the meridian and in addition reasonably low pipe factors (λ) and different bend angles were desirable to confirm theoretical convergence.

With this background, two carbon steel bends were selected for testing, the dimensions of which are tabulated below:-

Nominal Bend Dimensions

Bend No.	Outside Pipe Diameter	Bend Radius	Thickness	R/r	α	λ
1	6.625"	6"	0.28"	1.89	90°	0.17
2	6.625"	9"	0.28"	2.84	180°	0.25

Both bends were supplied by Munro and Miller [160]. The manufacturer advised that it was frequent industrial practice to specify "taper" or "weld-neck" flanges for direct connection to pipe bends. The theory presented earlier was for bends with rigid flanged terminations, more akin to the "slip-on" flange commonly used on straight pipes. It was therefore felt necessary to examine the influence of the two different types and each bend was supplied with one taper and one slip-on flange as shown in figures (4.1) and (4.2).

All welds were X-rayed and both assemblies were stress relieved.

(4.1b) Manufacturing Tolerances

There are a number of specifications available which stipulate the permissible manufacturing tolerances for smooth curved pipes. The above bends were supplied in accordance with British standard, BS 1640 [161] and American standard, ANSI B16.9 [162].

The external pipe diameters between $\phi = 0$ and $\phi = 180^\circ$ and between $\phi = -90^\circ$ and $\phi = +90^\circ$, at $\theta = 0$, were measured with a micrometer and found to be 6.625" and 6.617" respectively for bend No. 2. These are well within the permitted tolerance from the above codes of + 3/32" (0.0938") and -1/16 (0.0625") and give an ovality of better than 0.998.

Thicknesses were measured around a section at approximately $\theta = 40^\circ$ (close to the "slip-on" flange) for bend No. 2 and are given in the following table:-

ø	Thickness	ø	Thickness
0	.28	180	.285
45	.285	225	.28
90	.29	270	.28
135	.285	315	.28

These are within the limits of $\pm \frac{1}{16}$" ($\pm$ 0.0625") on wall thickness allowed by the above codes.

A similar dimensional survey was carried out on bend No. 1, which was also found to be within the above variations.

Accordingly, results presented herein will be based on the manufacturers nominal dimensions.

(4.1c) Details of Test Rigs

Bend No. 1

The test rig employed for bend No. 1 is shown in figures (4.3) and (4.4). The bend was bolted to a 1" thick plate connected to two parallel channel sections, which were bolted to the floor. A six foot long straight pipe with flanged ends was bolted to the free end of the bend. Loading was applied to the end of the tangent pipe via a wire rope by a hydraulic ram. The ram was activated by a conventional hand pressurized oil pump. The ram support was provided by a frame constructed from 2" angle iron. The load magnitude was measured by a previously calibrated load cell, incorporating strain gauges wired in a half bridge configuration, such that only axially applied loads were measured.

Ideally, to achieve a true comparison with theory, a uniform, in-plane bending moment should be applied to the bend. The system,

as/

as described above, is an experimental compromise involving a shear force and a small variation of the bending moment along the bend.

Bend No. 2

A diagram of the test rig for bend No. 2 is shown in figure (4.5). The loading system was virtually the same as the previous test. The supporting frame was considerably stiffer as it was intended for a more comprehensive set of tests involving various types of loading, not conducted by the present author.

(4.1d) Strain Gauging and Instrumentation

In both tests, electrical resistance strain gauges were employed for the measurement of surface strains. Details of the gauges were as follows:-

Type:	SHOWA N11 FA5/120/11
Gauge length:	5 mm
Nominal Resistance:	120 ohms
Gauge Factor:	2.10

The gauges were temperature compensated for mild steel. Attachment was made with Loctite LS 496 cement in accordance with manufacturers recommendations.

To obtain a reasonable experimental stress distribution from bend No. 1, it was decided to incorporate a total of 18 strain gauges on the outer surface of the bend. These were located in pairs, orientated along the principal bend axes, at the positions shown in figure (4.6).

A total of 24 strain gauges were employed on bend No. 2 at the positions indicated in figure (4.7).

An/

An "Elcomatic" automatic, digital, strain reading instrument was used to scan the gauges at each load step. The gauge readings in "ohm/ohm x 10^5" were printed out on a strip chart at the rate of one reading per second. Correct strain values were obtained by dividing the printout readings by the gauge factor x 10^5.

The gauges are wired to the internal quarter Wheatstone bridges of the Elcomatic unit using the standard three wire technique, minimising the effect of changes in gauge leads resistances [163], [164].

(4.1e) Evaluation of Stresses

The strains from each gauge were plotted against load to check linearity and correct operation. A typical example is given in figure (4.8). A line was fitted to the load-strain results for each gauge using a regression analysis on a computer [148]. For a plot of strain ϵ against load P at 'n' points, an equation can be fitted as follows,

$$\epsilon = a + bP \qquad \ldots (4.1)$$

where

$$b = \frac{\sum_{i=1}^{n} (P_i - \bar{P})(\epsilon_i - \bar{\epsilon})}{\sum_{i=1}^{n} (P_i - \bar{P})^2}$$

$$a = \left(\sum_{i=1}^{n} \epsilon_i - b \sum_{i=1}^{n} P_i\right)/n$$

$$\bar{P} = \sum_{i=1}^{n} P_i/n \qquad \bar{\epsilon} = \sum_{i=1}^{n} \epsilon_i/n \qquad \ldots (4.2)$$

The/

The strain at any load can be found from the slope, b.

The corresponding stresses for each gauge was obtained from the normal stress-strain relationships for a thin shell e.g.,

$$\sigma_1 = \frac{E}{(1-\nu^2)} [\epsilon_1 + \nu \epsilon_2]$$

... (4.3)

where the Young's Modulus, E, was taken as 29.9×10^6 lb/in^2 and poissons ratio, ν, as 0.3. The stress concentration factors (S.C.Fs.) were then found from,

$$\text{S.C.F.} = \sigma / \frac{Mr}{I}$$

... (4.4)

as previously defined. The bending moment, M, was taken as that at the centre section of each bend. For bend No. 1,

$$M = P(\ell + R \sin 45^\circ)$$

... (4.5)

where ℓ was the length of the loading arm pipe equal to 74" and R was the bend radius of 6". For bend No. 2,

$$M = P(\ell + R) \cos \xi - h \sin \xi$$

... (4.6)

where $\ell = 74"$, $R = 9"$, $h = 13\frac{3}{4}"$ and $\xi = 13.5^\circ$. ξ was the angle between the direction of the applied load and the vertical and h was the height of the point of application of the load from a line through the bend centre, $\theta = 0^\circ$.

(4.1f) Flexibility Measurement/

(4.1f) Flexibility Measurement

The flexibility of bend No. 2 was determined by measuring the rotation between the flanged ends of the bend. The rotations were measured using a telescope and mirror as shown in figure (4.9). Rotation of the mirror causes the cross-hair in the telescope to move along the scale positioned at the side of the telescope. The scale reading was taken at each load step. Figure (4.10) shows a typical plot of the applied load against the scale reading. Readings were taken with the mirror positioned on both flanges, from which the bend rotation, γ, was found from,

$$\gamma = \delta_L/2\ell_L - \delta_F/2\ell_F \qquad \ldots (4.7)$$

where δ_L was the change in the scale reading for the loaded flange, δ_F was the change at the fixed flange and ℓ_L and ℓ_F were the corresponding distances between the mirror and scale. The flexibility factor was then calculated from,

$$K = \gamma / \frac{MR\alpha}{EI} \qquad \ldots (4.8)$$

where M was taken as defined in equation (4.6).

The rotation between the ends of bend No. 1 was measured using a similar technique but was so small that it was swamped by the rotation of the base flange fixing and was close to the limit of the sensitivity of the measuring system. Although the flexibility factor will be given later, some doubt exists about its accuracy.

(4.1g) Loading/

(4.1g) Loading

The loading system for both bends was described in previous sections. During each test, the bends were loaded in ten increments and then unloaded in the same manner.

(4.1h) Results

The stress and strain factors determined for bends Nos. 1 and 2 are given in the tables Nos. 1 and 2 respectively. The flexibility factors for bends Nos. 1 and 2 were determined as 2.5 and 4.27 respectively.

Detailed comparisons of these results with the theory will be made in the following sections.

Table (4.1)

Experimental Results for Bend No. 1

Strain Gauge Number	Strain Factor		Stress Factor	
	$\bar{\epsilon}_\phi$	$\bar{\epsilon}_e$	$\bar{\sigma}_\phi$	$\bar{\sigma}_e$
0		2.16		2.71
1	1.03		1.84	
2		2.03		2.62
3	1.19		1.97	
4		1.53		1.87
5	0.57		1.13	
6		0.35		0.10
7	- 0.87		- 0.85	
8		- 1.06		- 1.46
9	- 0.92		- 1.36	
10		- 1.29		- 1.36
11	0.20		- 0.21	
12		- 0.75		- 0.60
13	0.69		0.51	
14		- 0.30		- 0.16
15	0.53		0.48	
16		- 0.18		- 0.07
17	0.39		0.37	

Table (4.2)

Experimental Results for Bend No. 2

Strain Gauge Number	Strain Factor		Stress Factor	
	$\overline{\epsilon}_\phi$	$\overline{\epsilon}_\theta$	$\overline{\sigma}_\phi$	$\overline{\sigma}_\theta$
0	1.24		1.37	
1		0.02		0.43
2	1.51		1.54	
3		- 0.36		0.10
4	1.51		1.15	
5		- 1.53		- 1.18
6	- 0.09		- 0.93	
7		- 2.52		- 2.79
8	- 2.89		- 3.48	
9		- 0.93		- 1.98
10	- 2.65		- 2.17	
11		2.26		1.61
12	0.72		1.68	
13		2.68		3.18
14	2.10		2.64	
15		0.99		1.78
16	1.83		2.13	
17		0.35		0.99
18	- 0.57		- 1.29	
19		- 2.01		- 2.40
20	0.90		1.41	
21		1.29		1.69
22	- 0.25		- 0.28	
23		- 0.02		- 0.10

(4.2) Comparisons of Flexibility Factors from Theory and Experiment

Comparisons of the flexibility factors from method No. 3, for bends with rigid flanges, with those obtained from the experiments of present and past authors are given in figures (4.11) and (4.12) for bend angles of 180° and 90° respectively. It can be seen, from a general point of view, that there exists a considerable spread of values and that each set of results seems to be somewhat dependent on their respective authors.

In references [89a] and [89b], and in the discussion to [28], Pardue and Vigness published the results of experiments conducted on nine bends with different pipe factors. Each bend was tested with subtended angles of 180° and 90° and had a nominal radius ratio of three. They also gave results for three 90° bends with nominal radius ratios of two. Tangent pipe and flange terminations were considered, the latter results being presented here. Their experiments indicated that different loadings, e.g. in-plane and out-of-plane bending, would give different flexibility factors for bends terminated by end constraints. As their intention was to derive some form of simple empirical relationship covering as wide a spectrum of bend parameters as possible, they averaged the flexibility factors from each component of loading and presented these instead of the separate factors. The values given in figures (4.11) and (4.12) therefore represent the average values from different loading, the vertical line through the average indicating the range of actual values they obtained. Pardue and Vigness gave very little detail about the flanges but in [89a] they state that they were cut from $\frac{1}{2}$" inch steel/

steel plate and soldered to the ends of the bends used previously for the bend-tangent experiments. The agreement between the flexibility factors of Pardue and Vigness and the present theory is reasonable for 180° bends, figure (4.11), but poor for 90° bends, figure (4.12). Comparison with these results can only really be made in a general sense since it is impossible to know where in their range of values the particular case of in-plane bending occurs. Further some doubt is introduced into their results by the relatively small thickness of their flanges which for certain geometries must have been little thicker than the bend wall.

The flexibility factors obtained by Vissat and Del Buono [90] for eight 180° degree bends of nominal R/r = 3 are given in figure (4.11). They adopted a different definition for their experimental flexibility factors to that used herein, i.e.

$$K = \frac{\delta}{\frac{2PR^2}{EI}\left[\frac{\pi R}{4} + a\right]}$$

where δ was the deflection measured between the ends of the tangent pipes. This gives a displacement flexibility factor for the whole system including the tangent pipe loading arms whereas the theoretical values from method No. 3 are rotational flexibility factors for the bend alone. One further curiousity of their results is that for certain geometries, bends with flanges had slightly higher flexibilities than those with tangent pipes. It can be seen in figure (4.11) that their results are generally slightly higher than the present theory.

In/

In support of his theory in [99], Findlay presented the results from tests conducted on three bends with rigid flanges. On two of his bends he used "adjustable" flanges. These were machined rings with 24 threaded holes around the circumference through which set studs were screwed to simulate actual flanges. The bends had tangent pipes welded to them, through which the load was applied. The flanges were supposed to permit an investigation of different bend angles, with the same bend system. Although these flanges may have sufficiently suppressed the radial and meridional tangential displacements, i.e. kept the pipe circular, in the present author's opinion it is unlikely that they would have adequately inhibited the mid-surface slope or the circumferential tangential displacement and cannot be considered as true rigid flanges. The flexibility factors from these are those for the 180° bends in figure (4.11) and the one with the lower pipe factor in figure (4.12). As expected, the results for the 180° bend angle agree more closely than the 90° bend angle. The third bend Findlay tested was a 90° bend with welded flanges. It can be seen that the flexibility factor from this bend agrees closely with the present theory.

Whatham [117] gave results from two 90° bends with radius ratios of 2.86 and 1.905. No details were given of the system used to test the bends. Figure (4.12) shows that his results agree closely with the present theory.

The flexibility factor for bend No. 1, shown in figure (4.12), can be seen to be higher than that predicted by the theory. However, as mentioned earlier, some doubt exists about its/

its accuracy. The experimental flexibility factor for bend No. 2, given in figure (4.11), shows good agreement with the theoretical value obtained from method No. 3.

(4.3) Maximum S.C.Fs.

Comparisons of the maximum meridional S.C.Fs. from method No. 3 and various experiments are given in figures (4.13) and (4.14) for 180° and 90° bends respectively. Maximum circumferential S.C.Fs. are given in figures (4.15) and (4.16) for the same bend angles.

In figures (4.13) and (4.15) it can be seen that relatively good agreement occurs between theory and experiment for 180° bends. Note that in (4.13) the maximum stresses on the outside surface of the bend are given since all of the authors, with the exception of Findlay, measured only outside surface stresses. Findlay's results as given are those from the outside surface. The true maximum for these bends would actually have been on the inside surface. The theoretical results in the other graphs are the true maxima which, as explained in chapter (3), occur on the outside surface.

Results for 90° bends in (4.14) and (4.16) show reasonable agreement, bearing in mind the comments made in section (4.2) with regard to Pardue and Vigness' and Findlay's experimental techniques. However, the S.C.Fs. from Pardue and Vigness were taken from [28] since these were given for in-plane bending alone.

(4.4) Stress Distributions

Stress distributions for flanged bends have only been published by two previous authors, Findlay [99] and Whatham [117].

Findlay/

Findlay published a detailed set of S.C.Fs for the meridional section at $\theta = 0^\circ$ for a 180° bend. His results are of particular interest since he examined stresses on both the inside and outside surfaces. His meridional and circumferential S.C.Fs. are given in figures (4.17) and (4.18). Comparison is also given with the theoretical results of Whatham. Close agreement occurs between theory and experiment at the position of maximum meridional stress but it is poorer towards the intrados and extrados. Experiment also shows a higher value for the maximum meridional stress on the inside surface. The relatively poor general agreement for this bend may be due to the adjustable flange used by Findlay, as described in section (4.2).

In [117] Whatham presented stress distributions for two 90° bends with $R/r = 2.86$ and 1.905. The meridional and circumferential S.C.Fs. for each bend are given in figures (4.19), (4.20), (4.21) and (4.22) together with Whatham's and present theories. The distributions demonstrate good general agreement. Figures (4.19) and (4.20) also contain Whatham's theoretical S.C.Fs. for unflanged bends, which illustrates the change incurred by flange constraints.

The S.C.Fs. from bends Nos. 1 and 2 at $\theta = 0$ are given in figures (4.23), (4.24), (4.25) and (4.26), again these show good agreement with the theory. Figure (4.27) shows a comparison of the theory with the S.C.Fs. from bend No. 2 at the rigid (slip-on) flange. It can be seen that the experimental flange stresses are slightly lower than the theory. As explained in chapter (3), this is to be expected because 'real' flanges are not completely rigid. From the strain factors given in table (4.2) for gauges 18, 20 and/

and 22 it should be noted that the meridional strain at the flange was not zero as the theory would predict. This may have been because the strain was measured adjacent to but not physically at the flange. Alternatively, it may have been because the flange did not remain circular. However, the experimental stress distribution at the bend centre is in fair agreement with the present theory, method No. 3, so that any inherent lack of rigidity in either the slip-on or the weld-neck flange does not appear to have influenced the peak stress unduly. This would appear to agree with the suggestion put forward in chapter (3) that the maximum stress at the bend centre would be less influenced by the flange dimensions than the stresses at the flange itself.

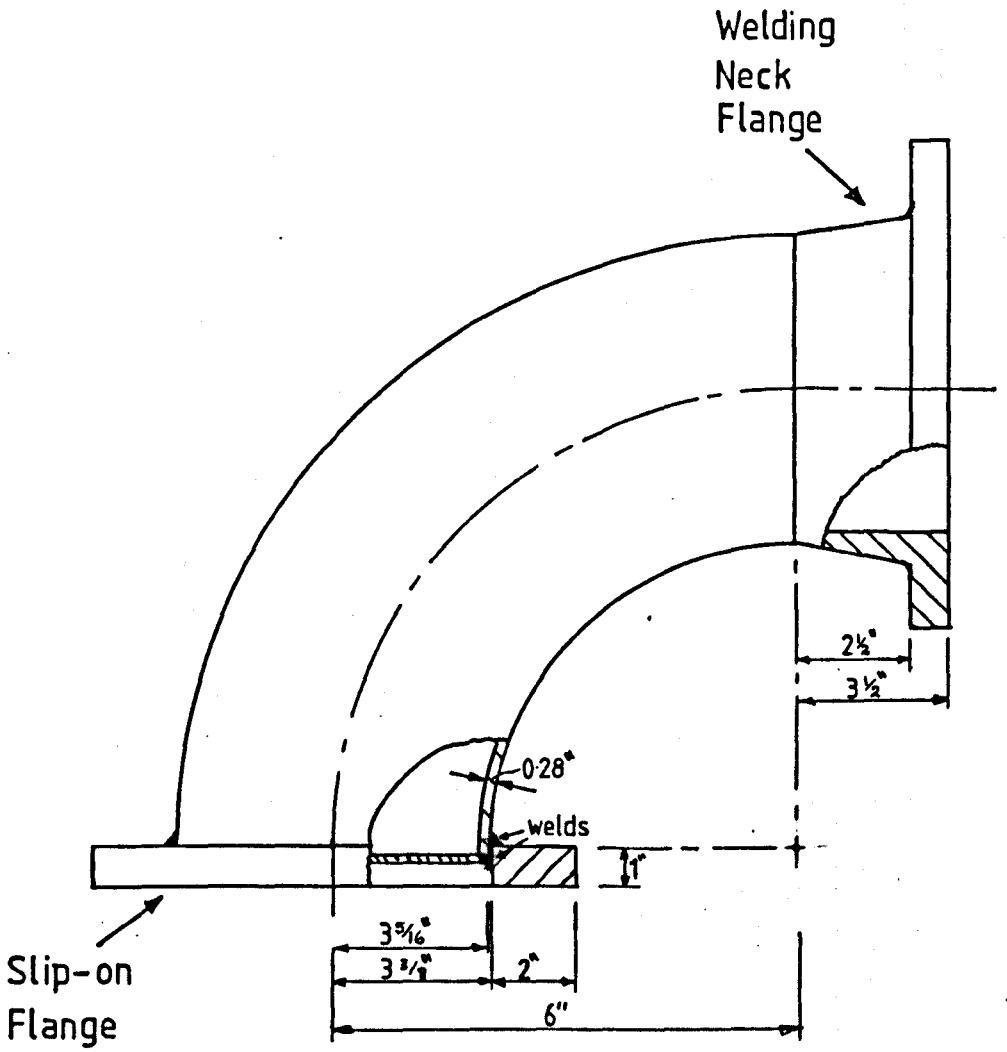

Bend No.1

Figure (4.1)

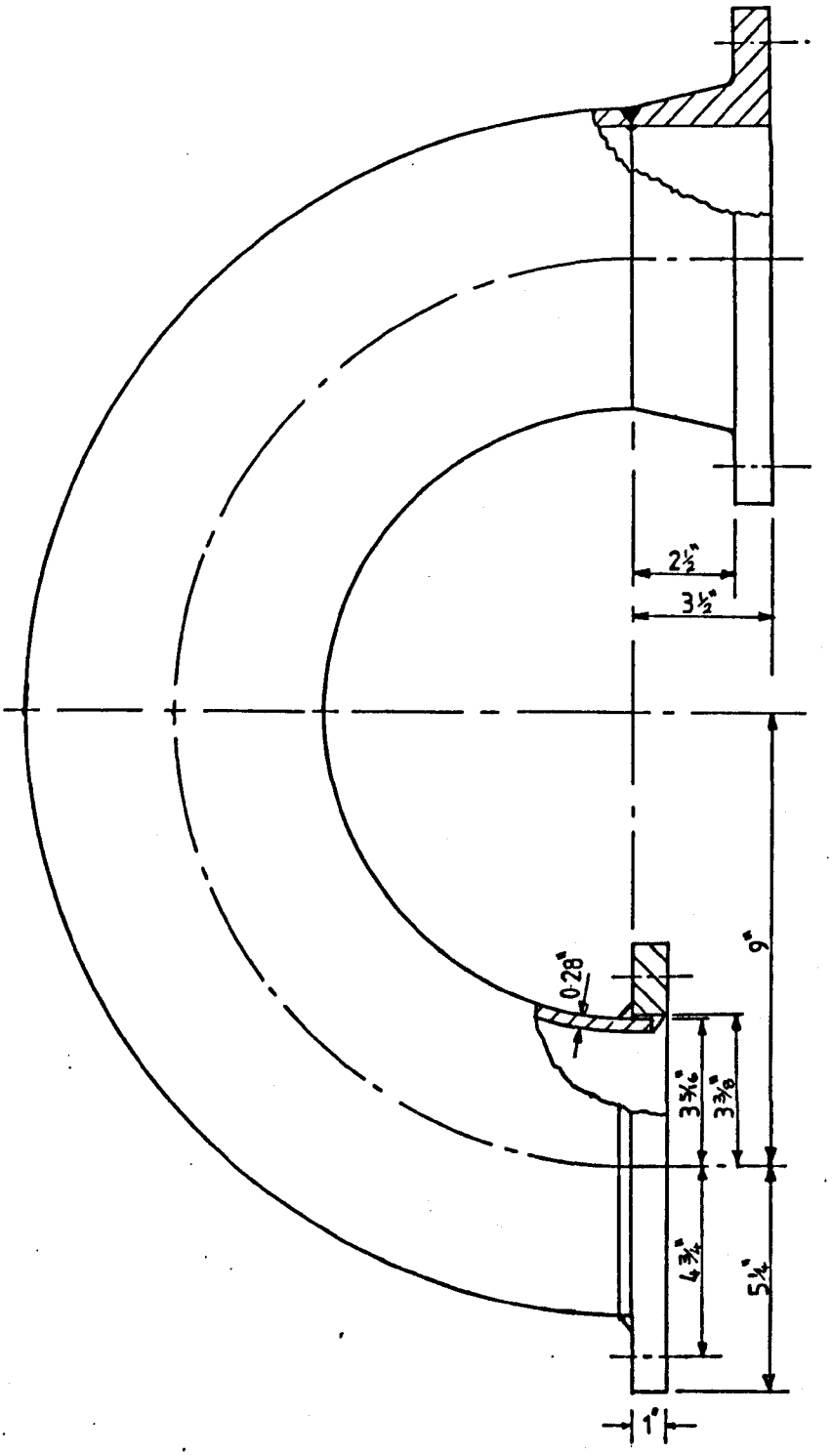

Bend No.2

Figure (4.2)

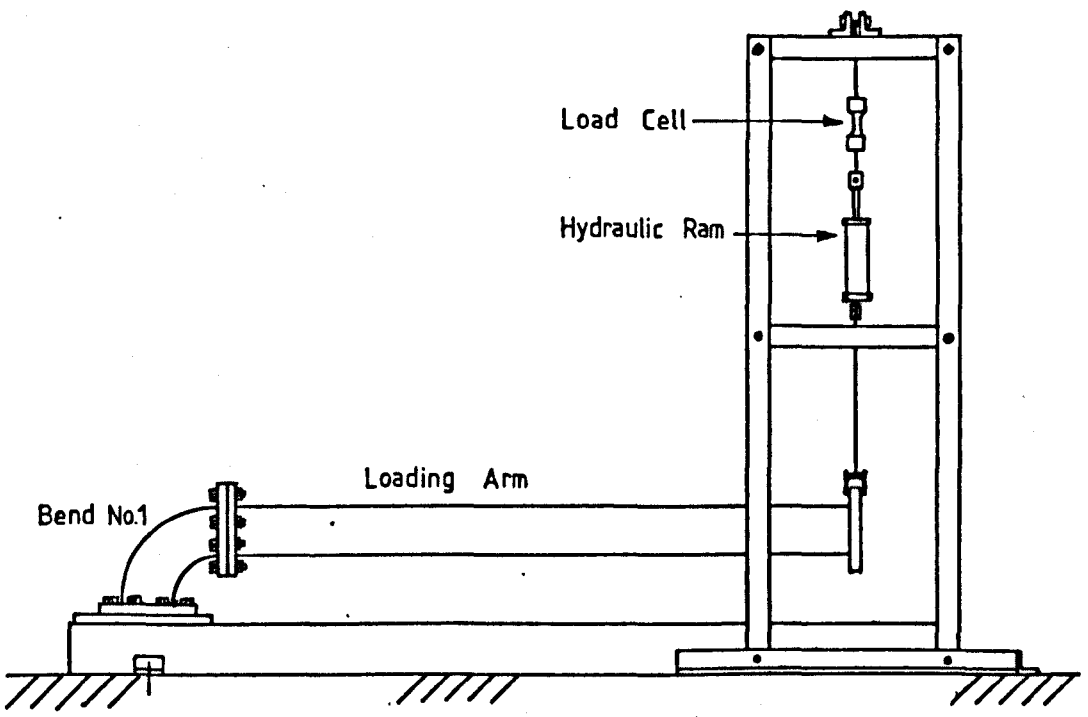

Loading Rig for Bend No.1

Figure (4.3)

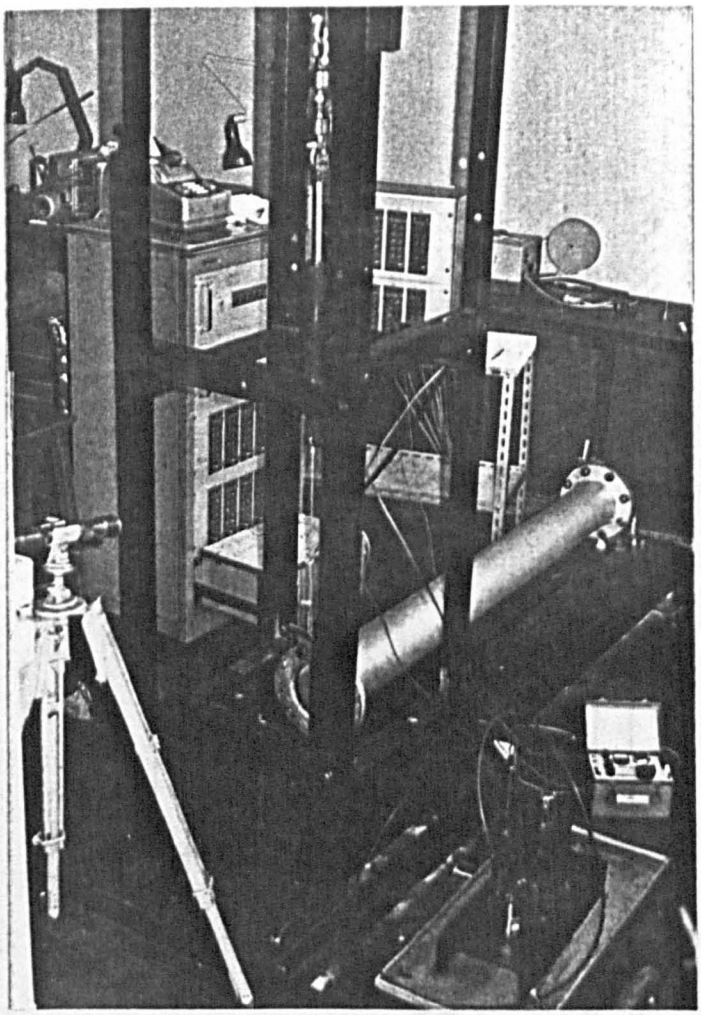

Bend No.1 Test Rig

Figure (4.4)

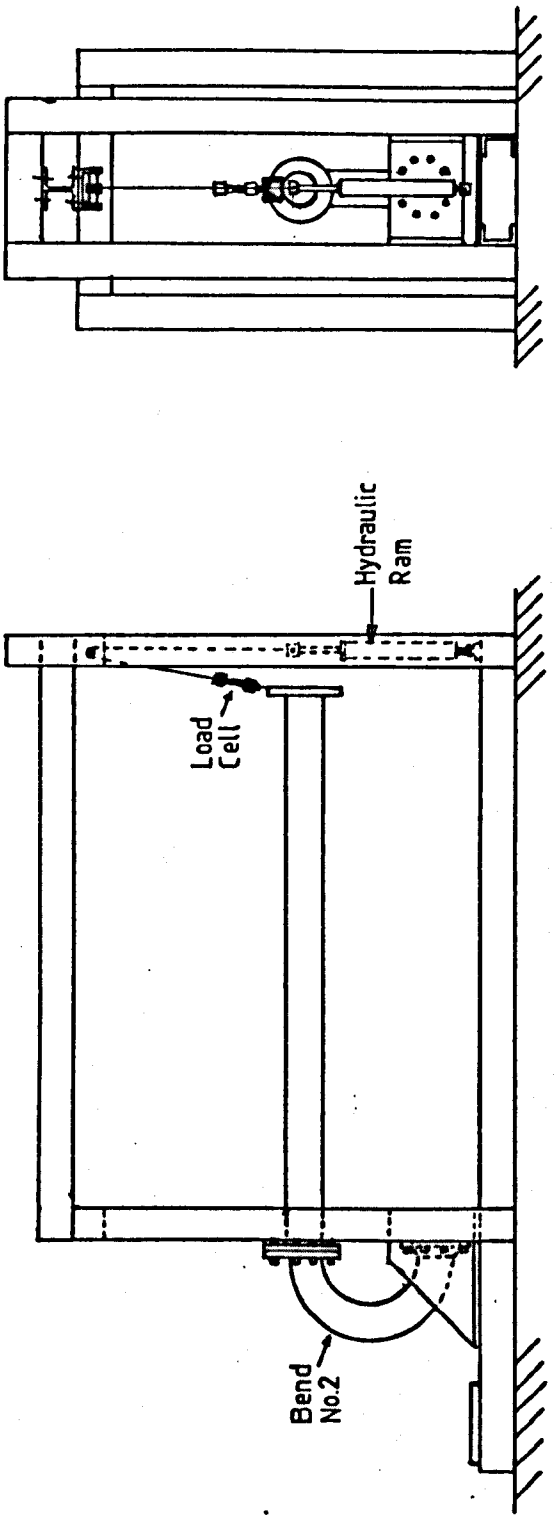

Test Rig for Bend No.2

Figure (4.5)

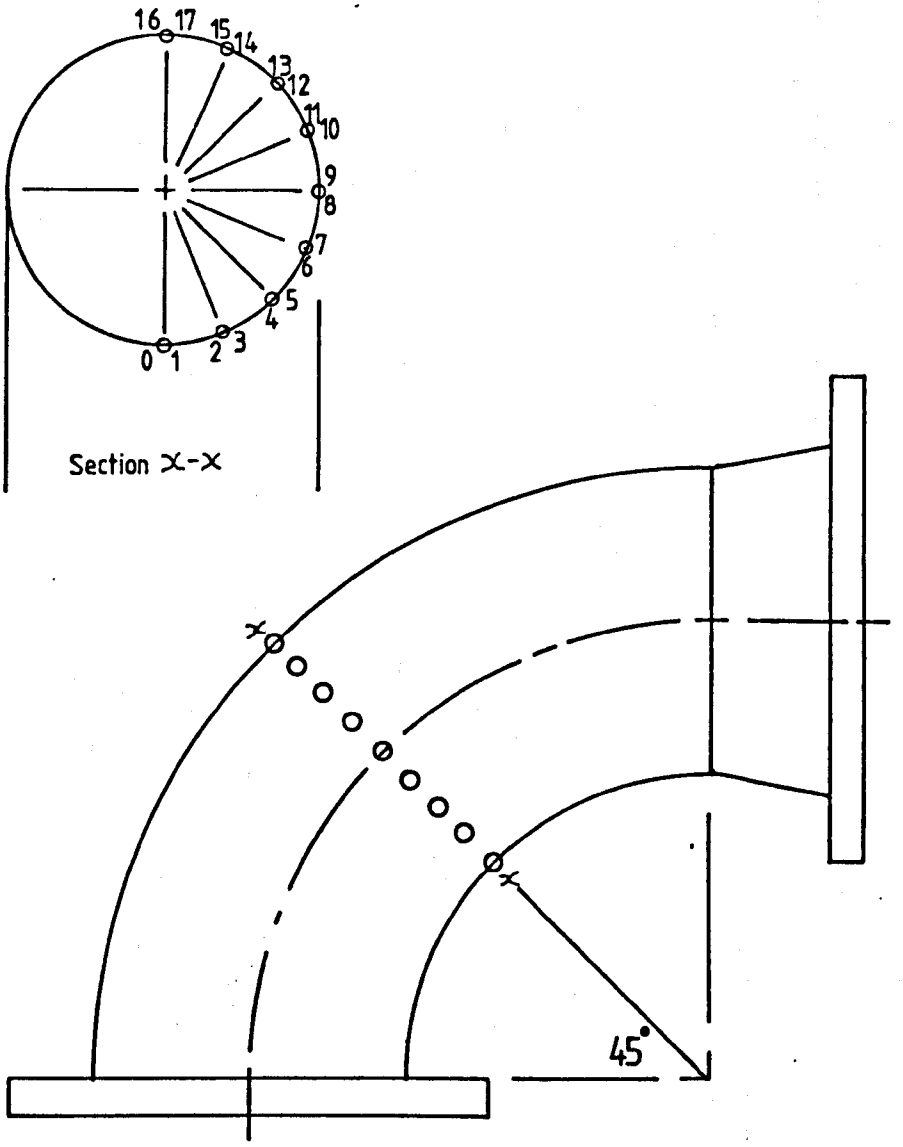

Strain Gauge Positions for Bend No.1

Figure (4.6)

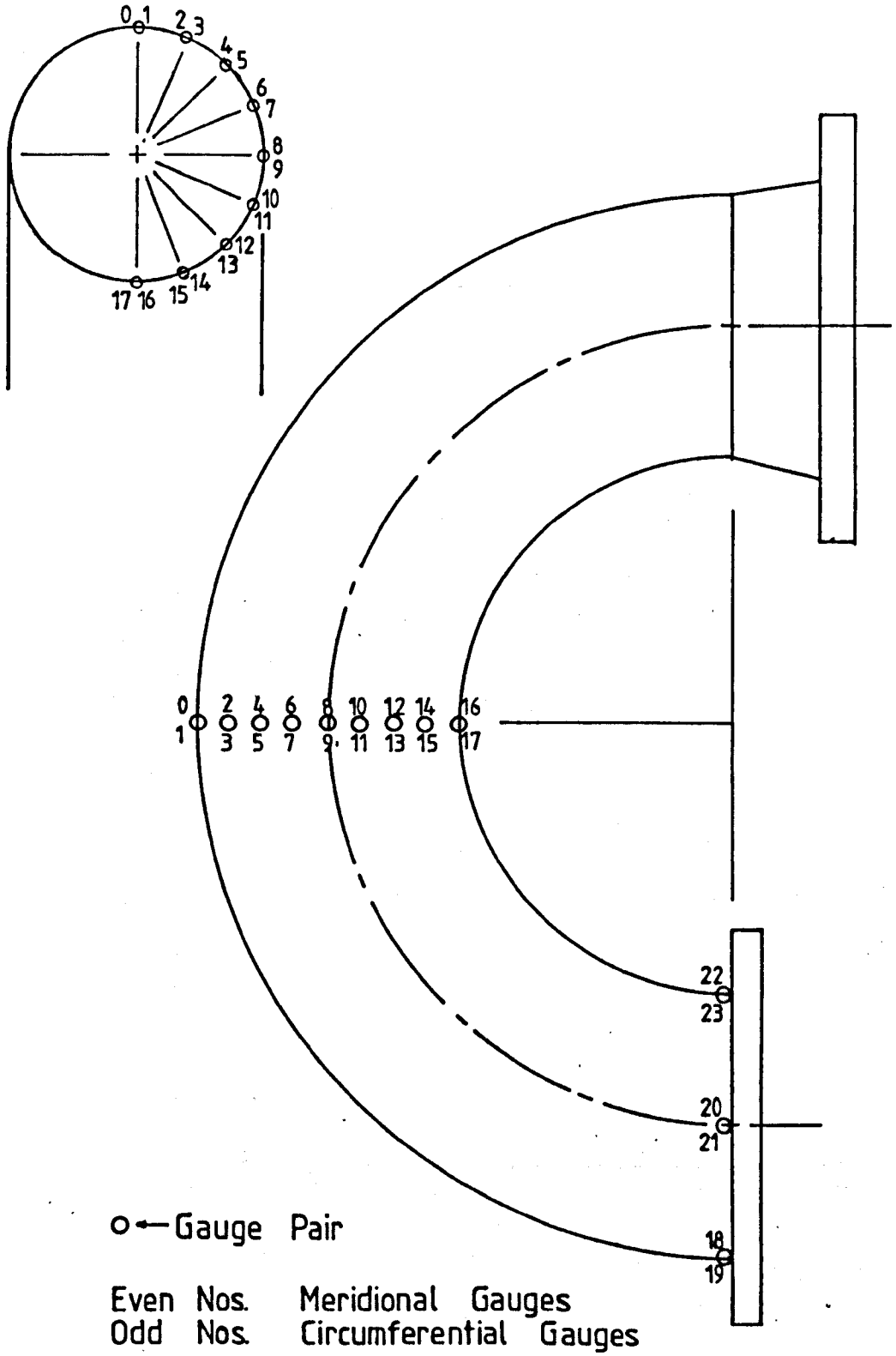

Strain Gauge Positions for Bend No. 2

Figure (4.7)

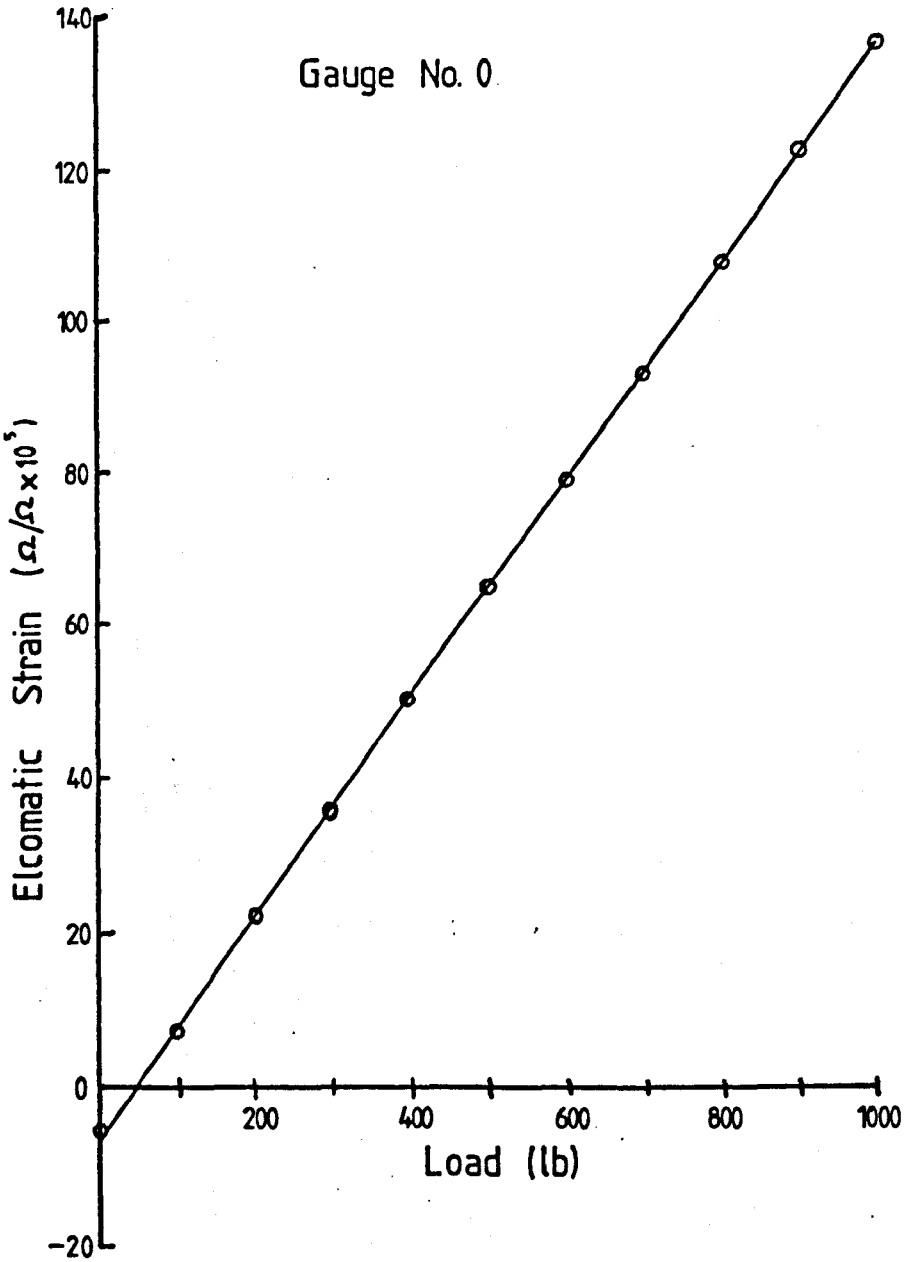

Typical Load/Strain Relationship for Bend No1

Figure (4.8)

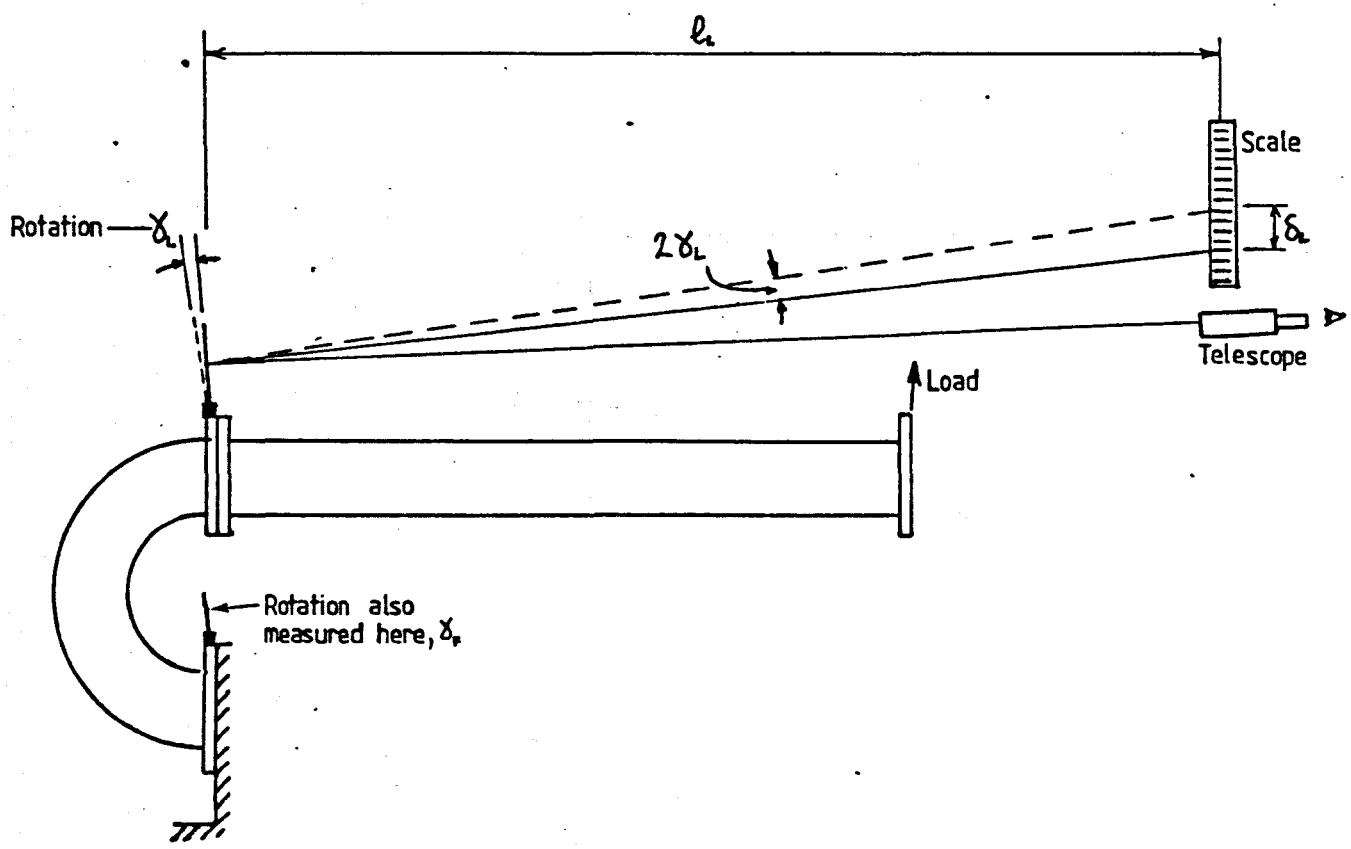

$$\gamma_L \doteq \frac{\delta_L}{2\ell_L}$$

Rotation Measurement

Figure (4.9)

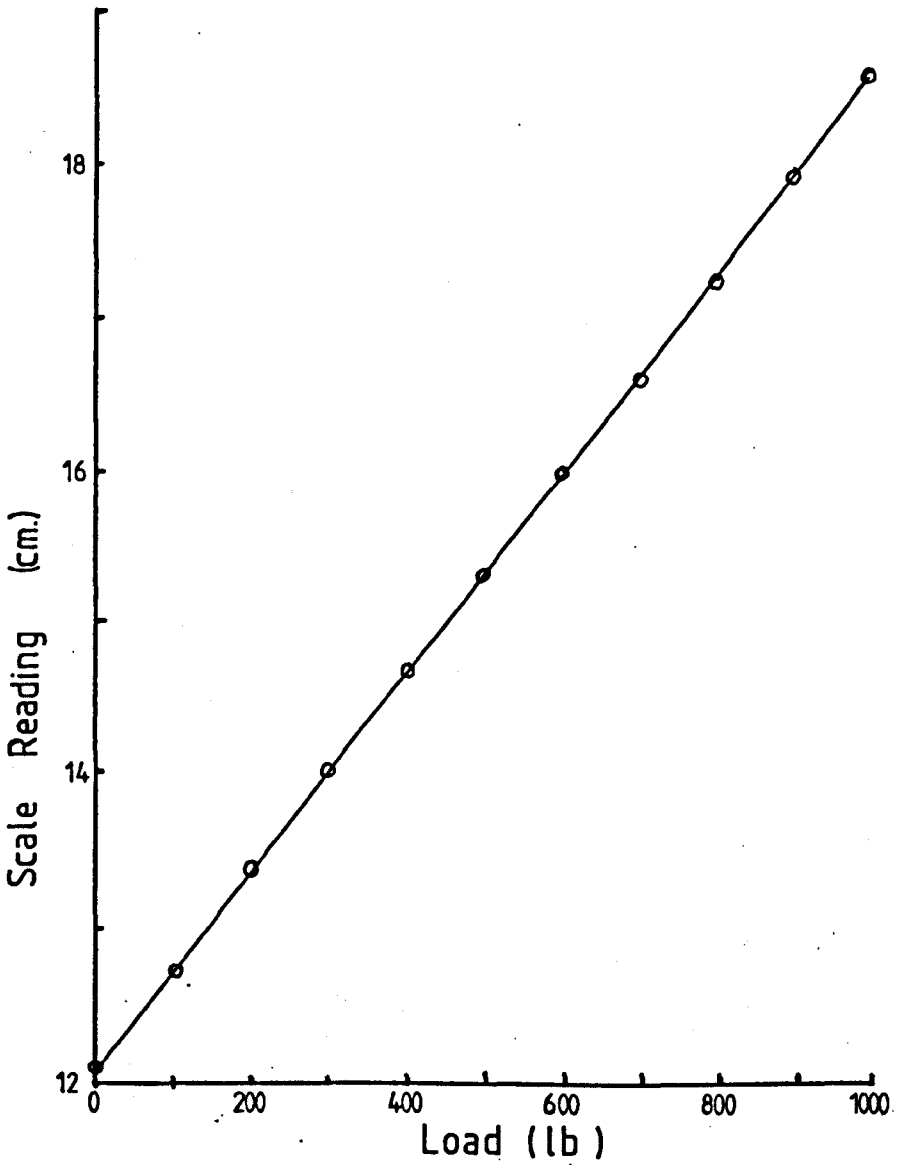

Typical Scale Readings from Rotation Measurements

Figure (4·10)

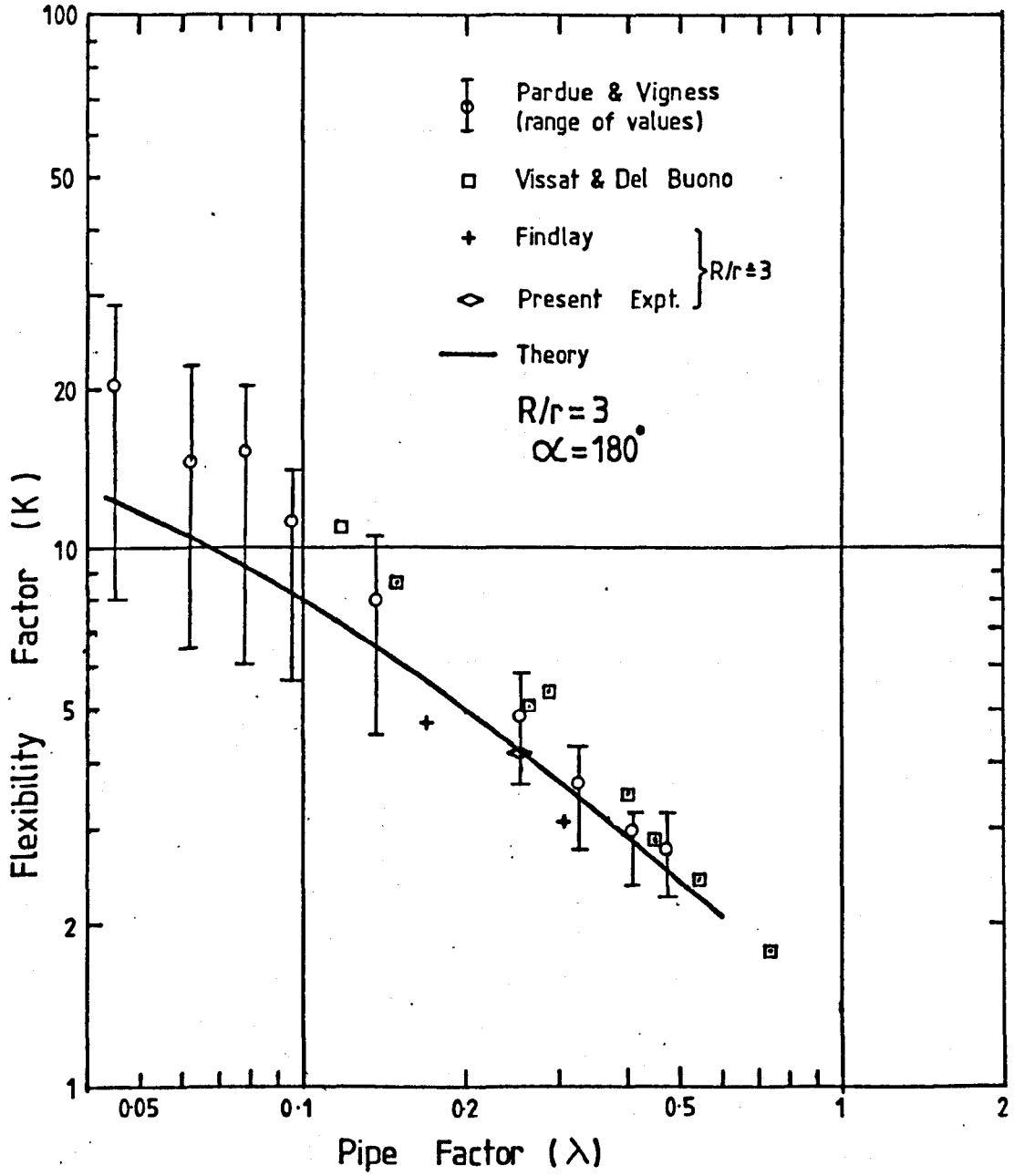

Comparison of Theory and Experiment for R/r=3, α=180°

Figure (4.11)

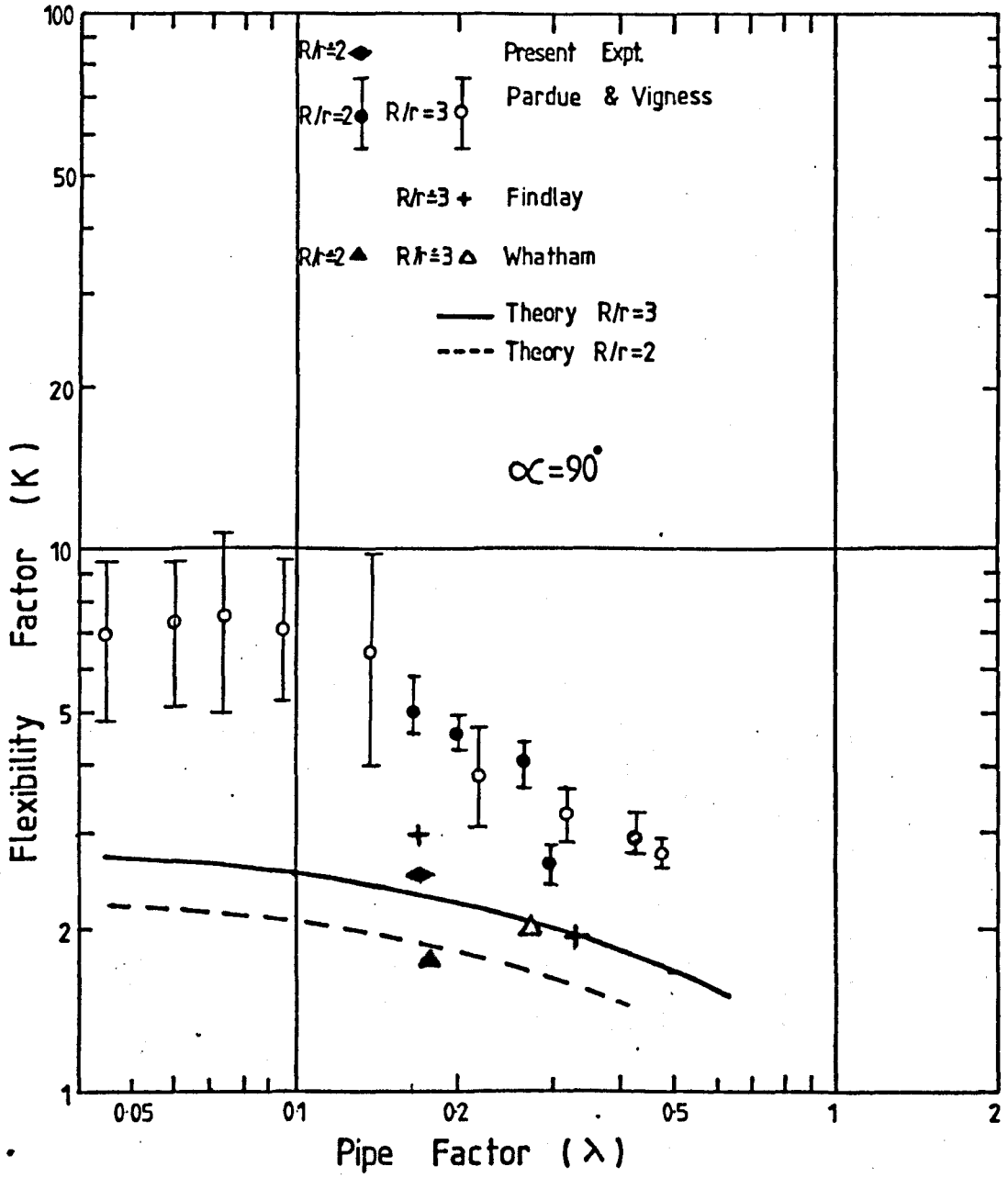

Flexibility Factors from Theory and Experiments for $\alpha = 90^{\circ}$

Figure (4.12)

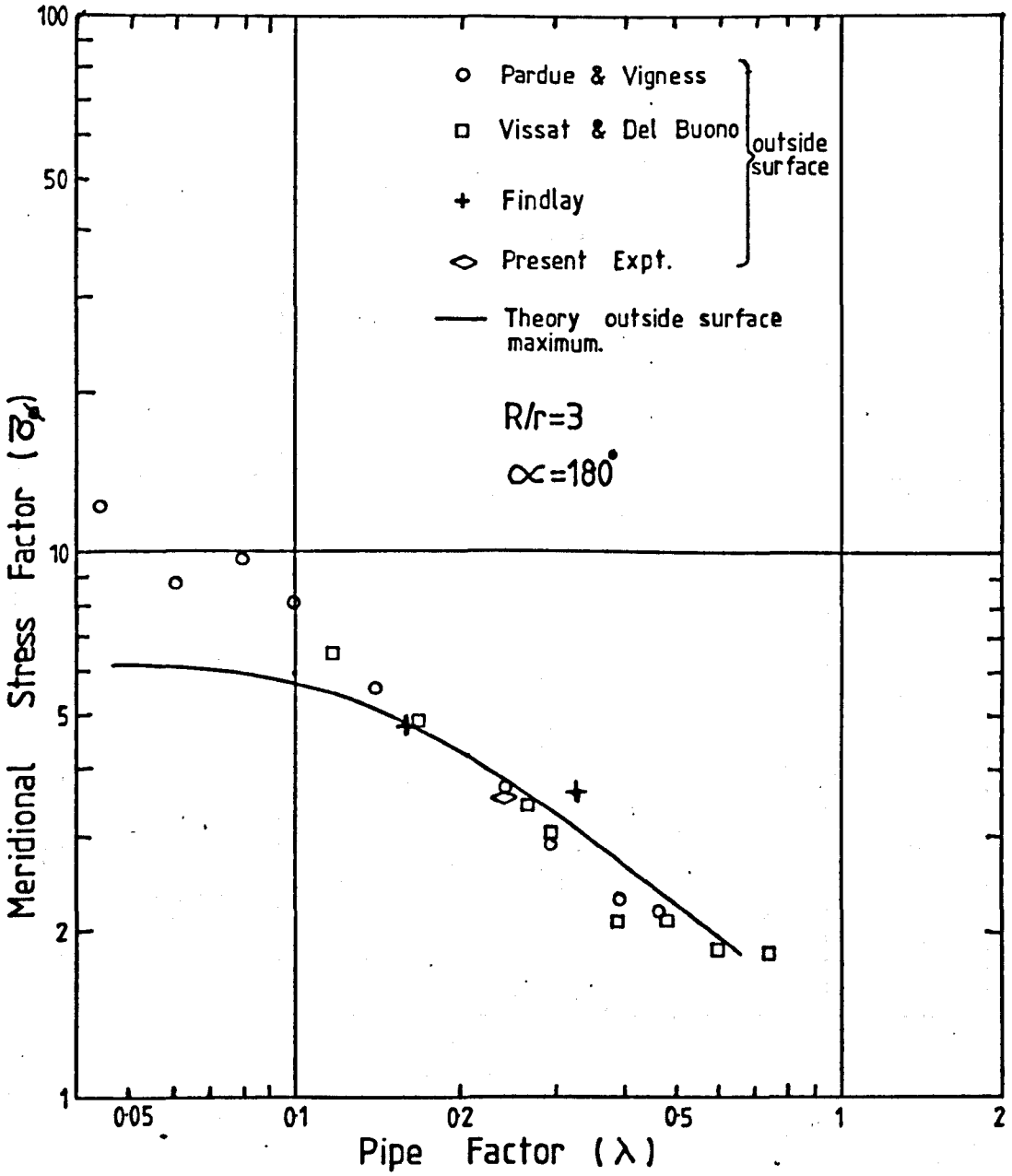

Meridional Stresses from Theory and Experiment for R/r=3 , α=180°

Figure (4.13)

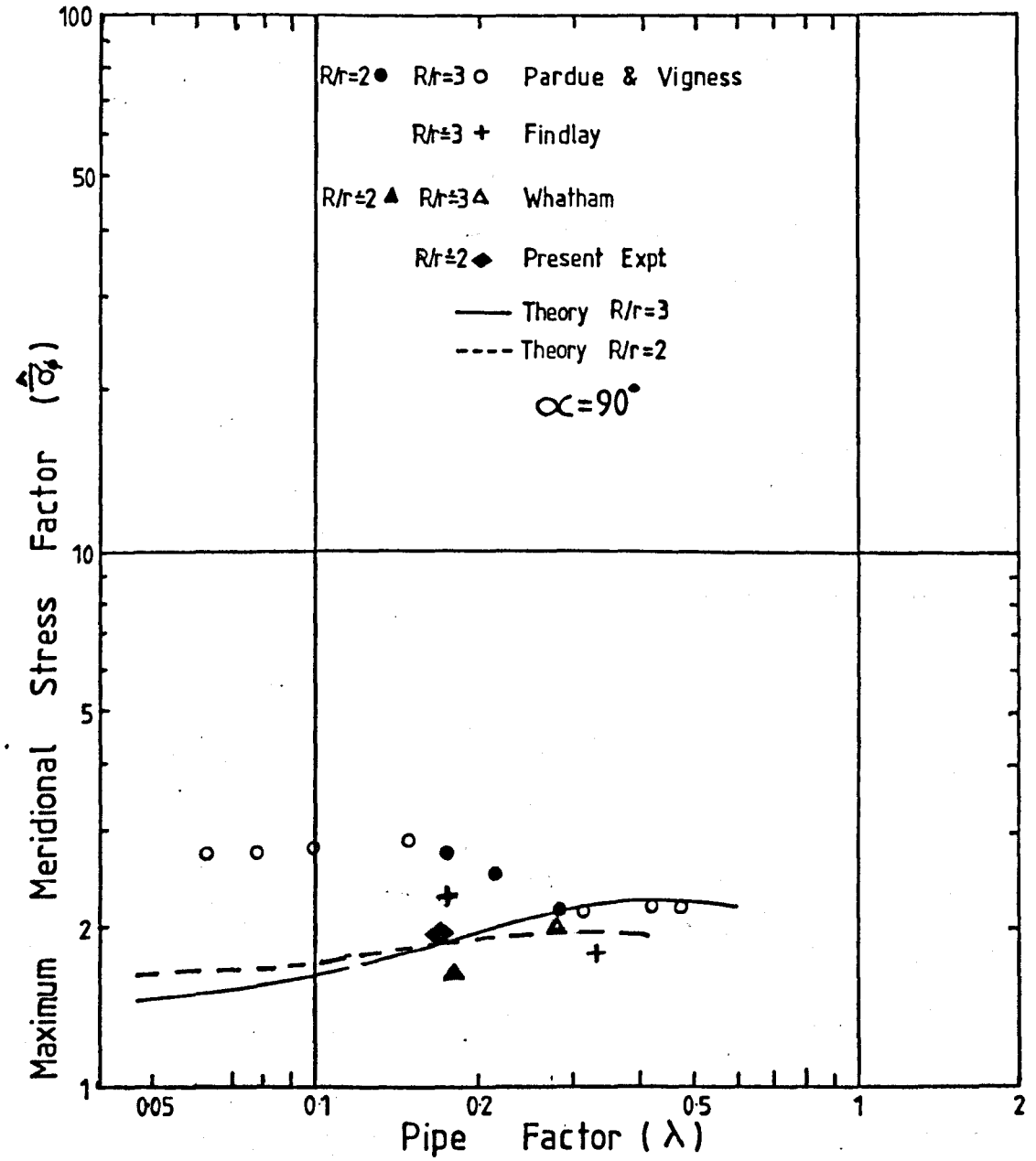

Meridional Stresses from Theory and Experiment for $\alpha=90^\circ$

Figure (4.14)

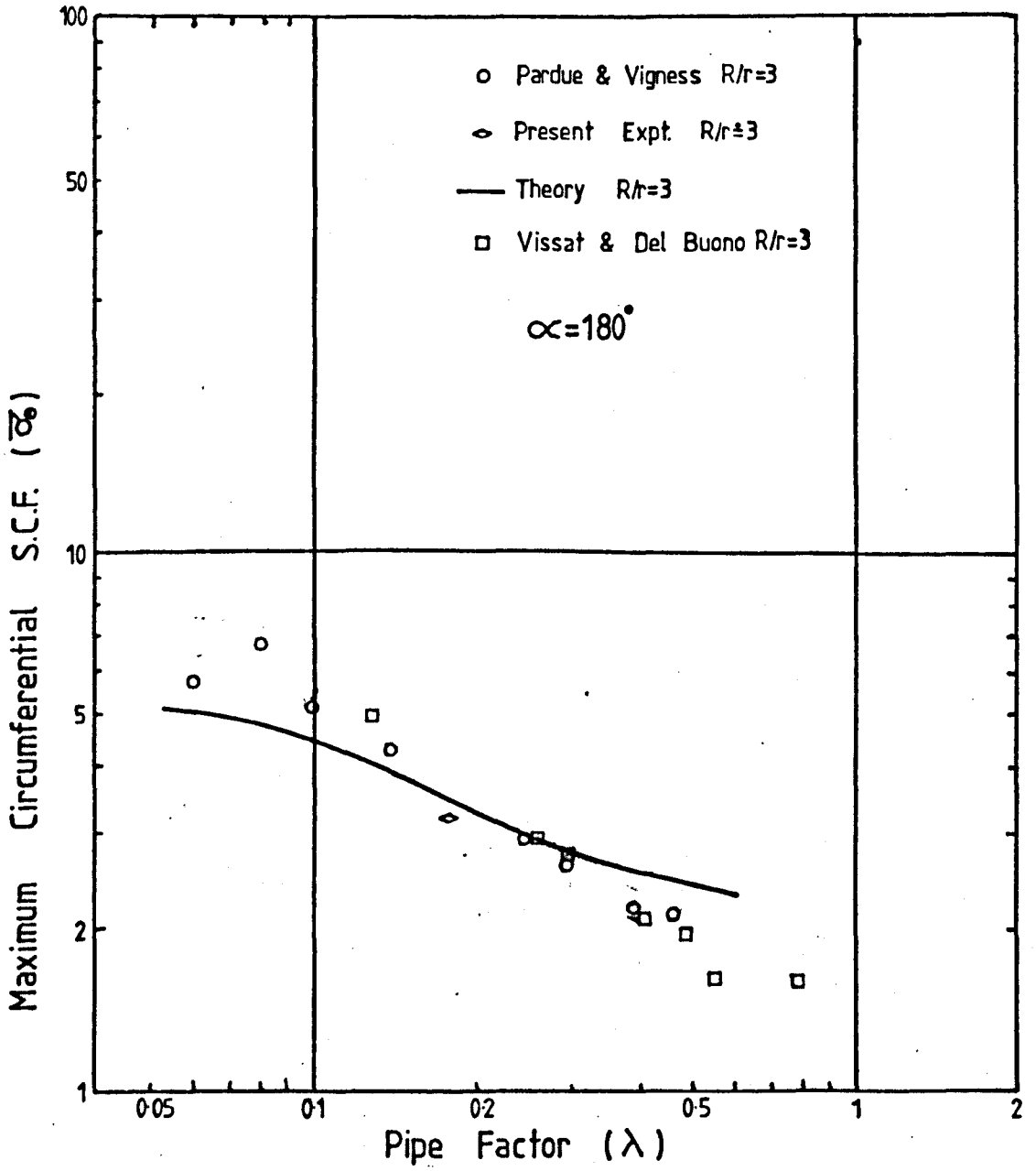

Circumferential S.C.F.s from Theory and Experiment for $\alpha=180^\circ$

Figure (4.15)

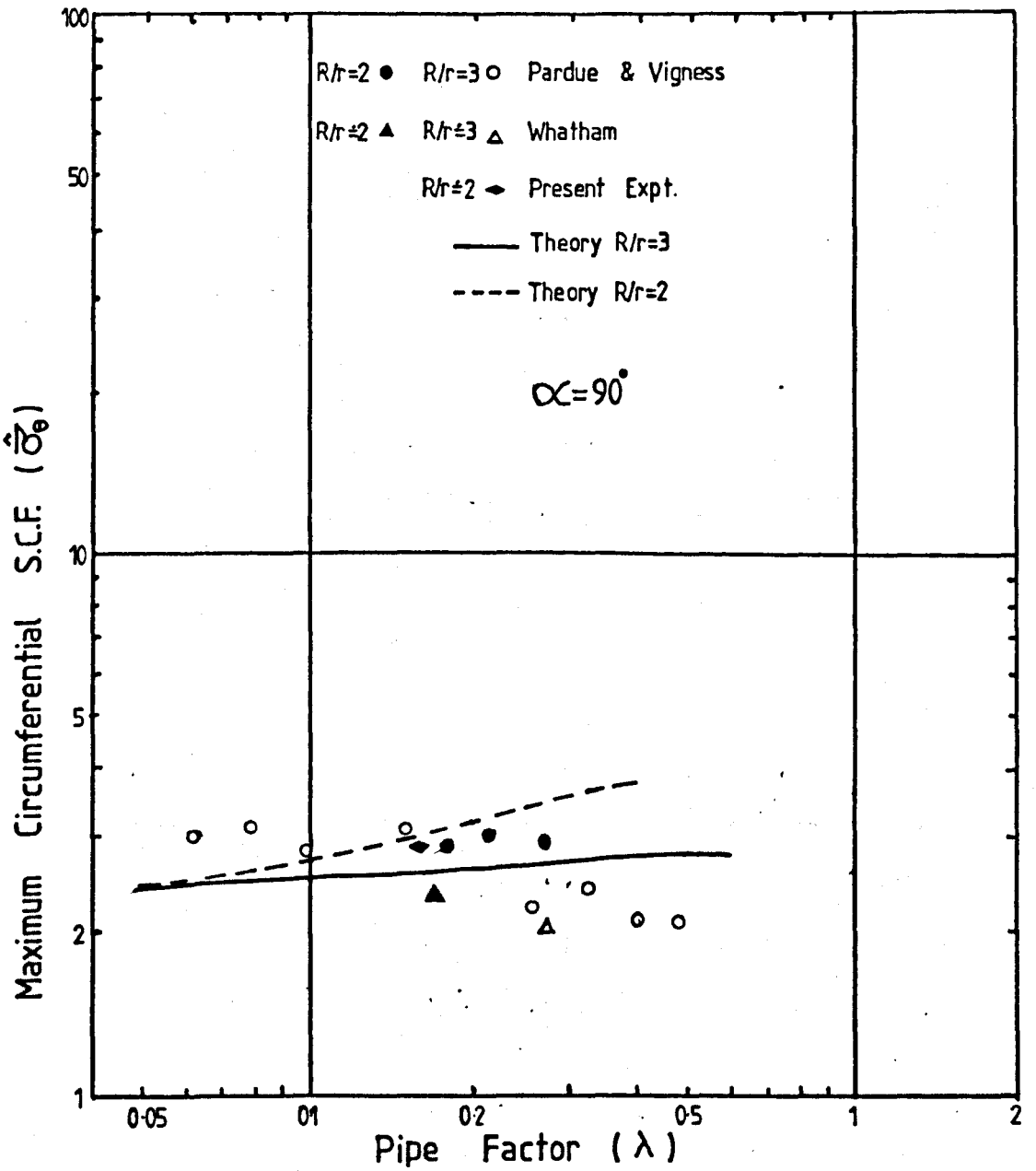

Circumferential S.C.Fs from Theory and Experiment for $\alpha=90^\circ$

Figure (4.16)

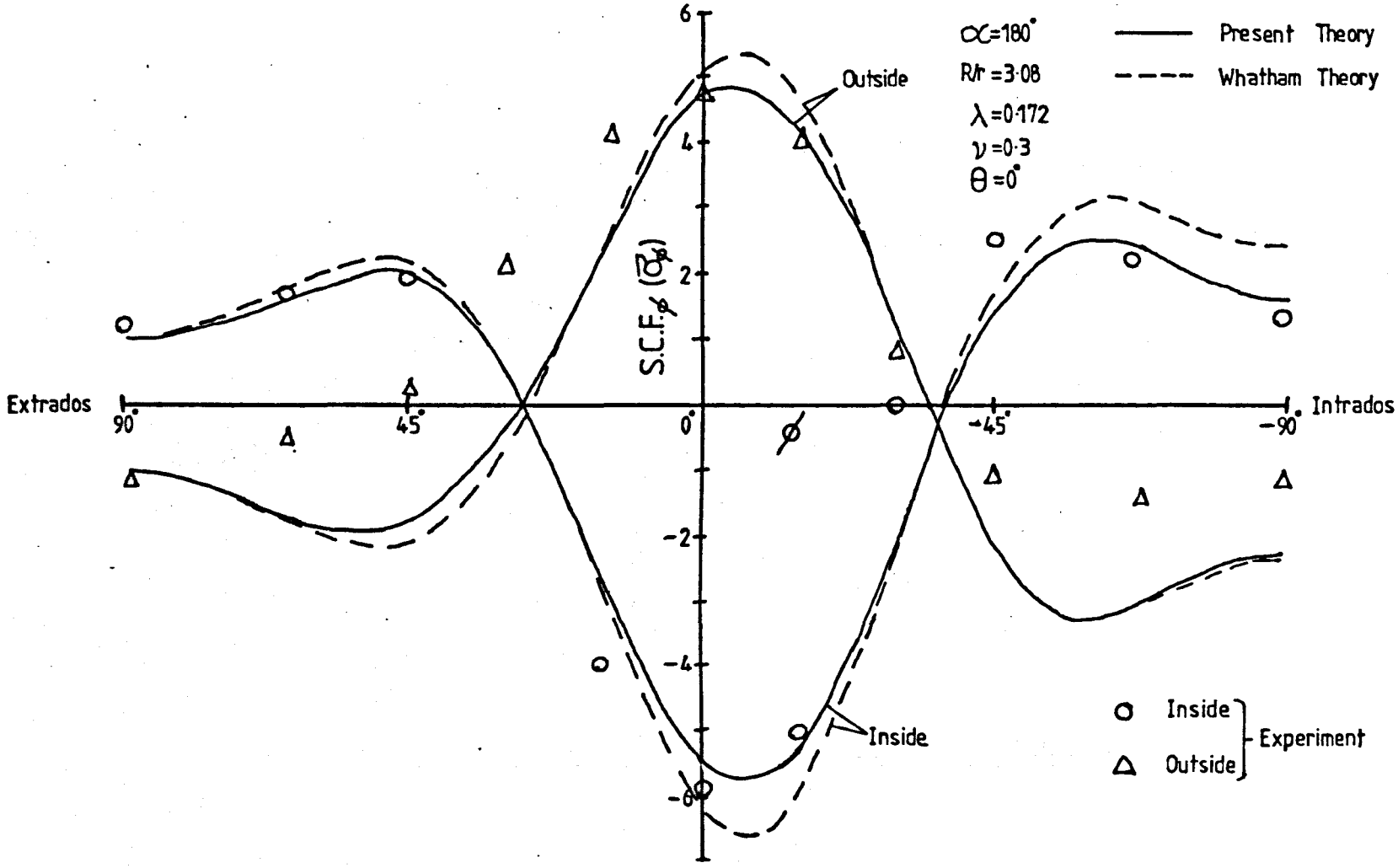

Findlay's Experimental Meridional S.C.F.s

Figure (4.17)

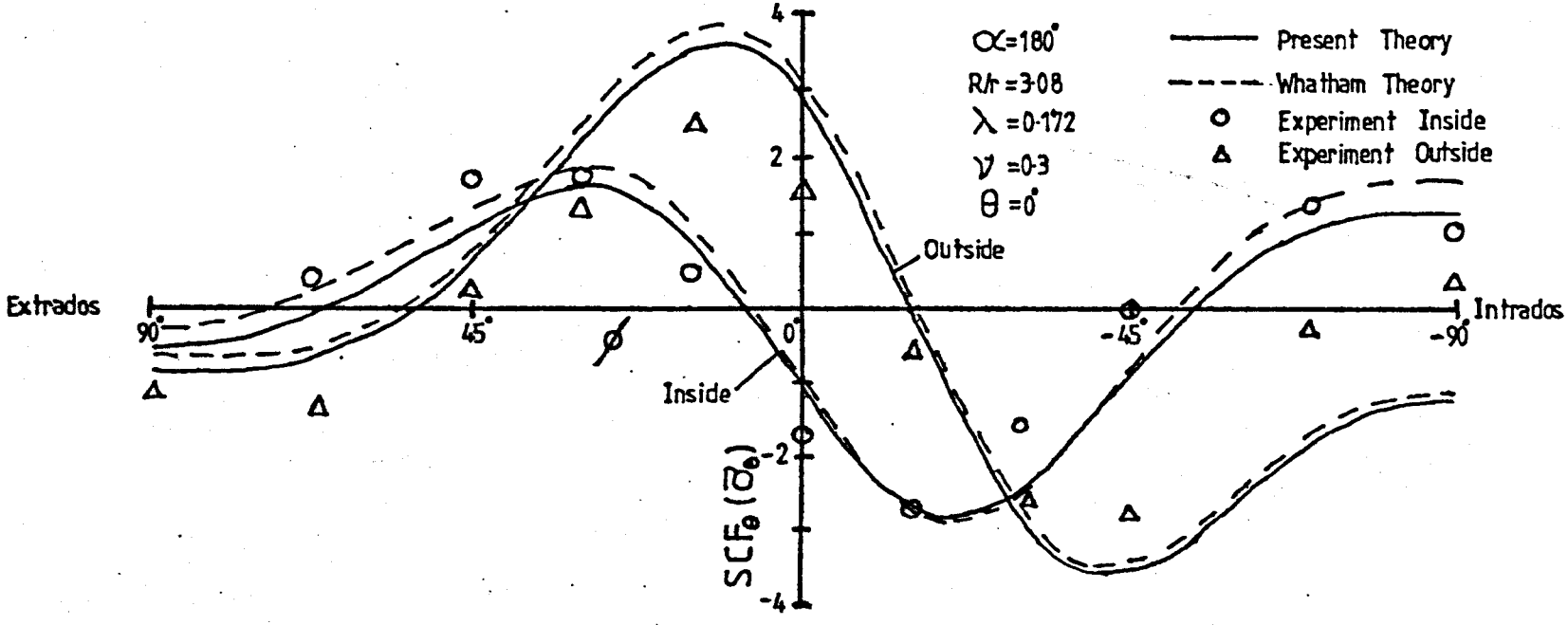

Findlay's Experimental Circumferential S.C.F.s

Figure (4.18)

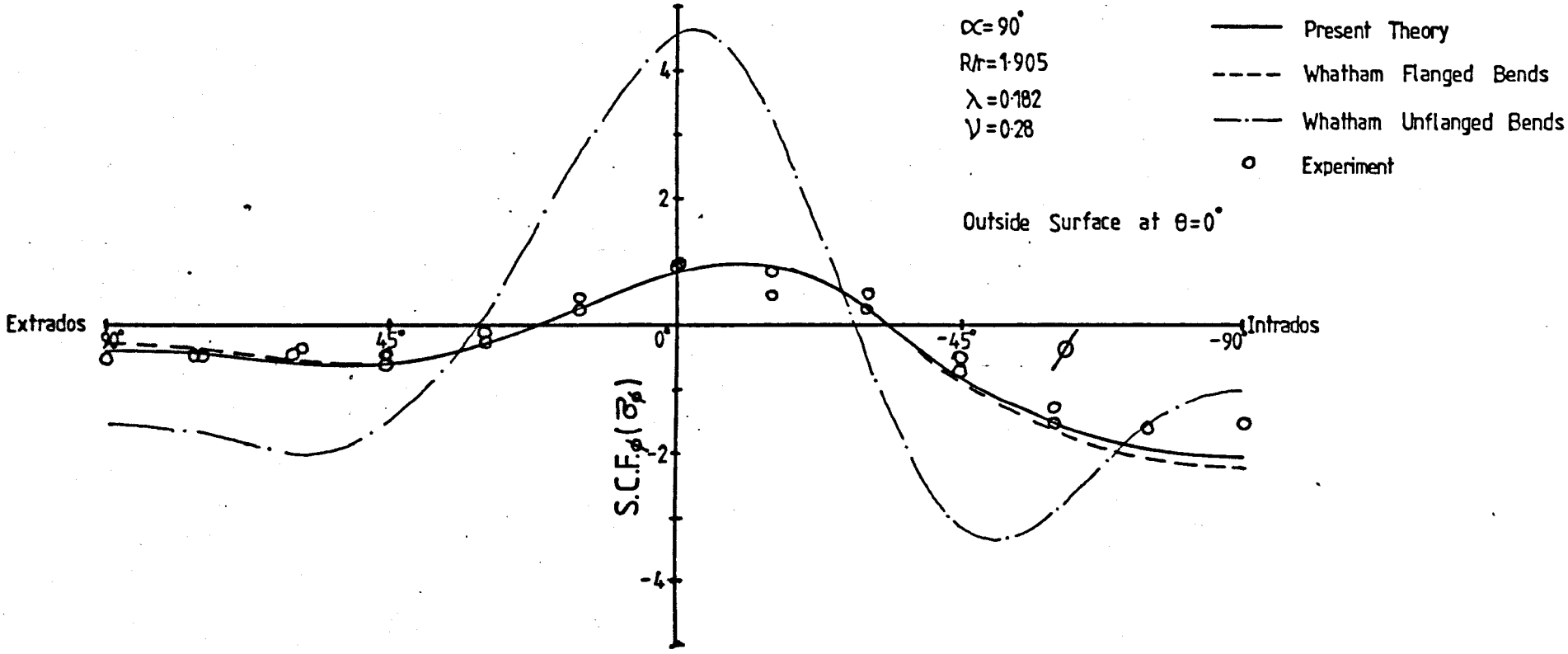

Whatham's Experimental Meridional S.C.F.s

Figure (4.19)

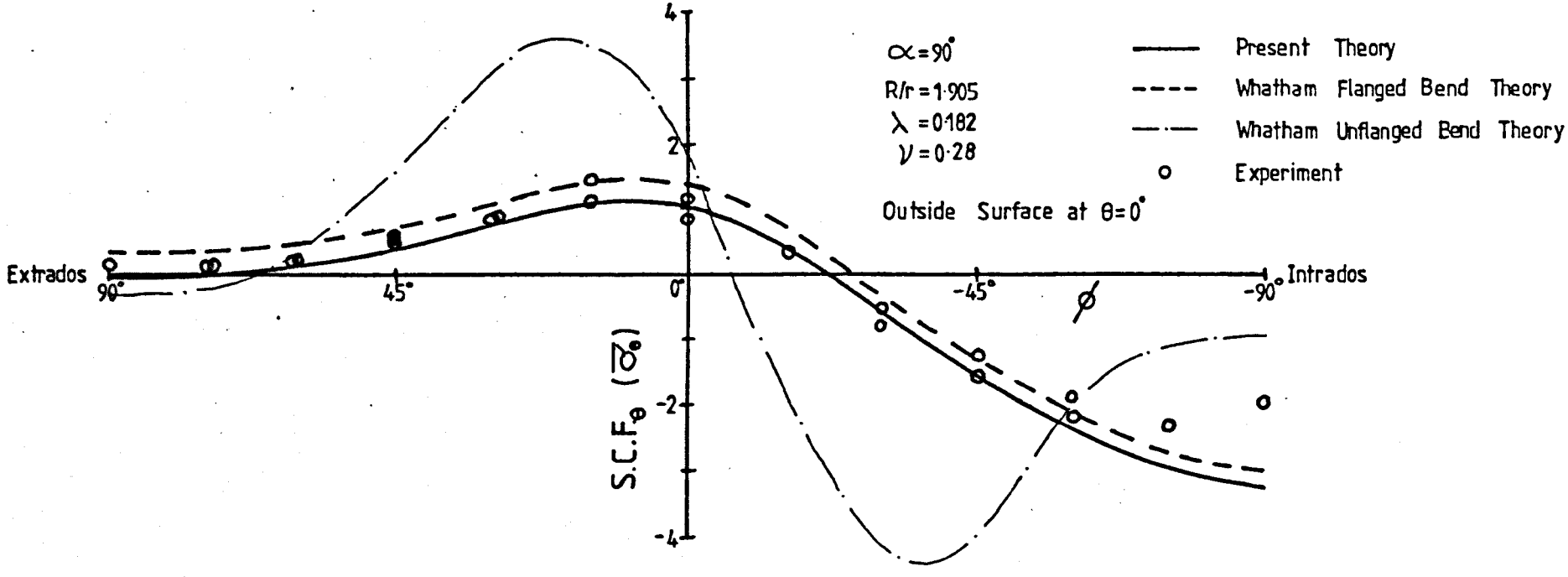

Whatham's Experimental Circumferential S.C.F.s

Figure (4.20)

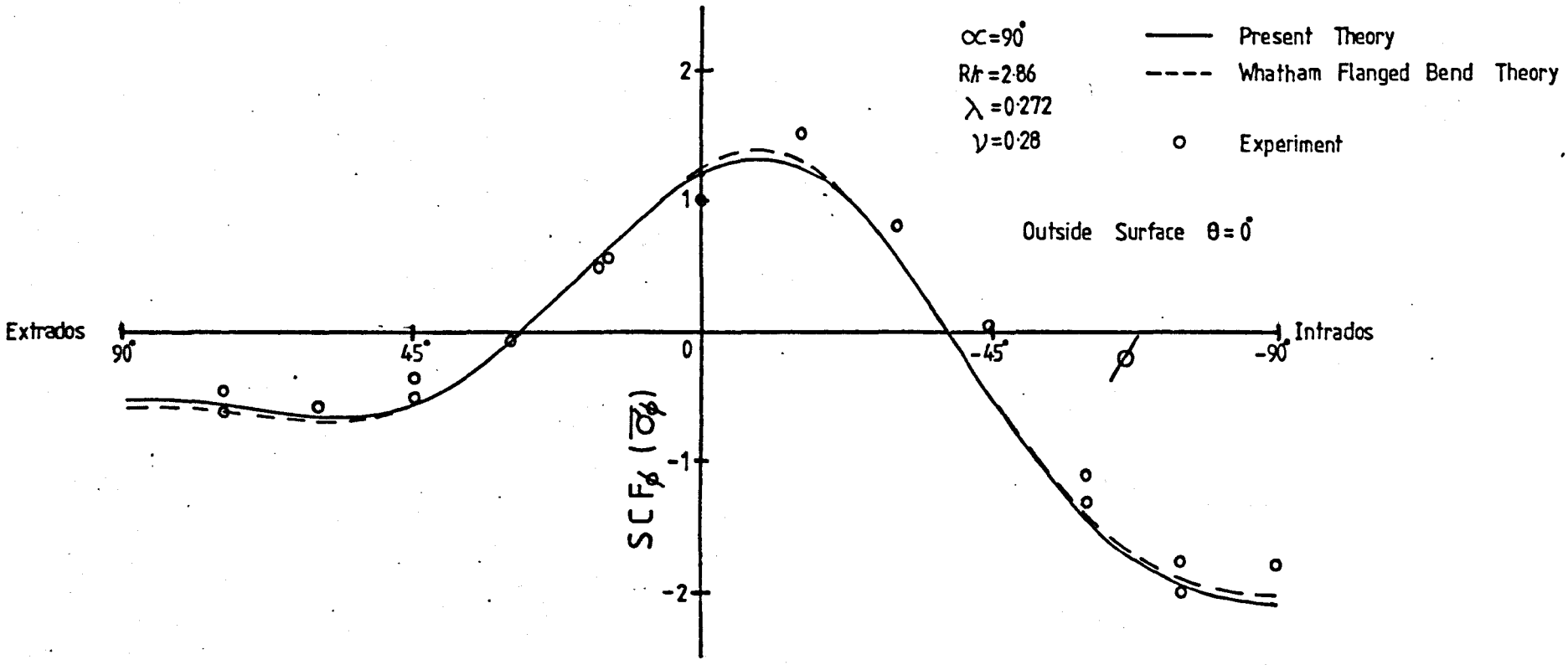

Whatham's Experimental Meridional S.C.F.s

Figure (4.21)

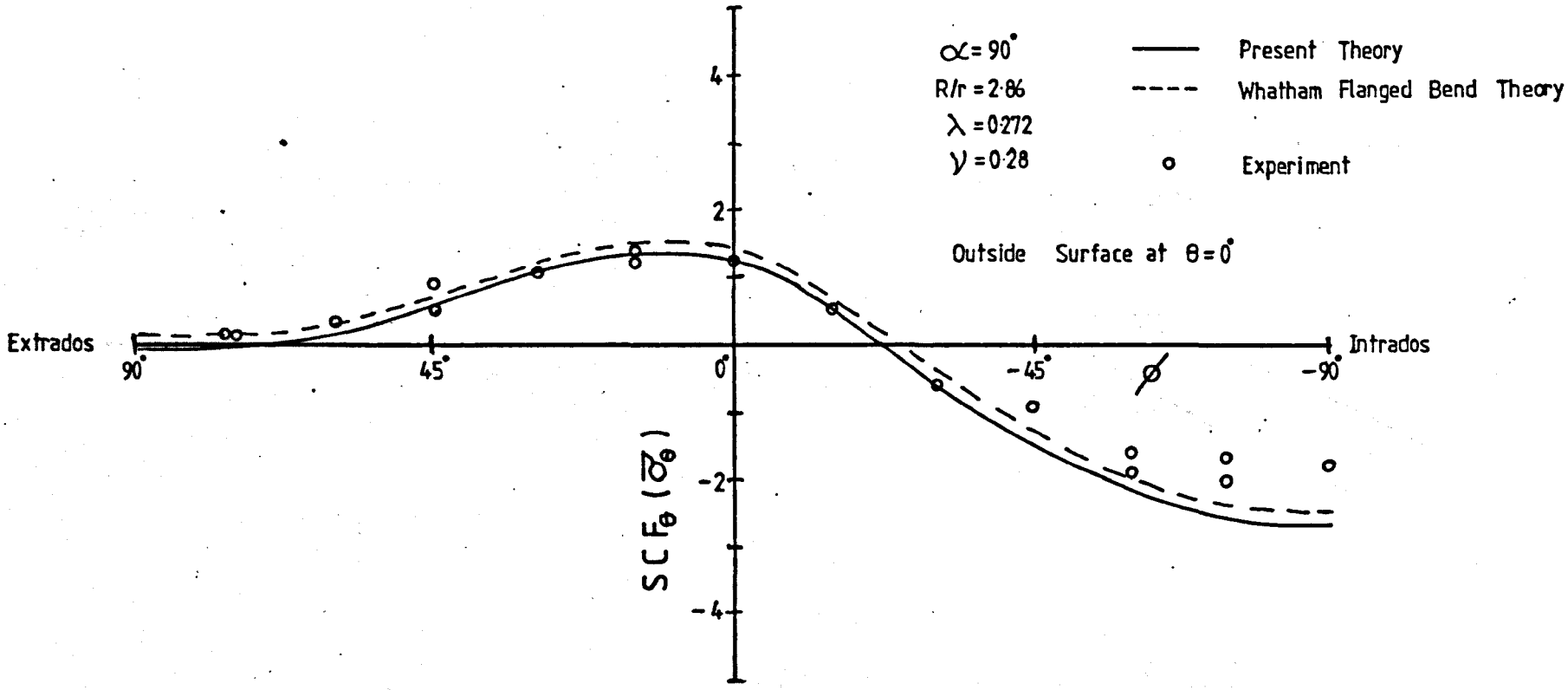

Whatham's Experimental Circumferential S.C.F.s

Figure (4.22)

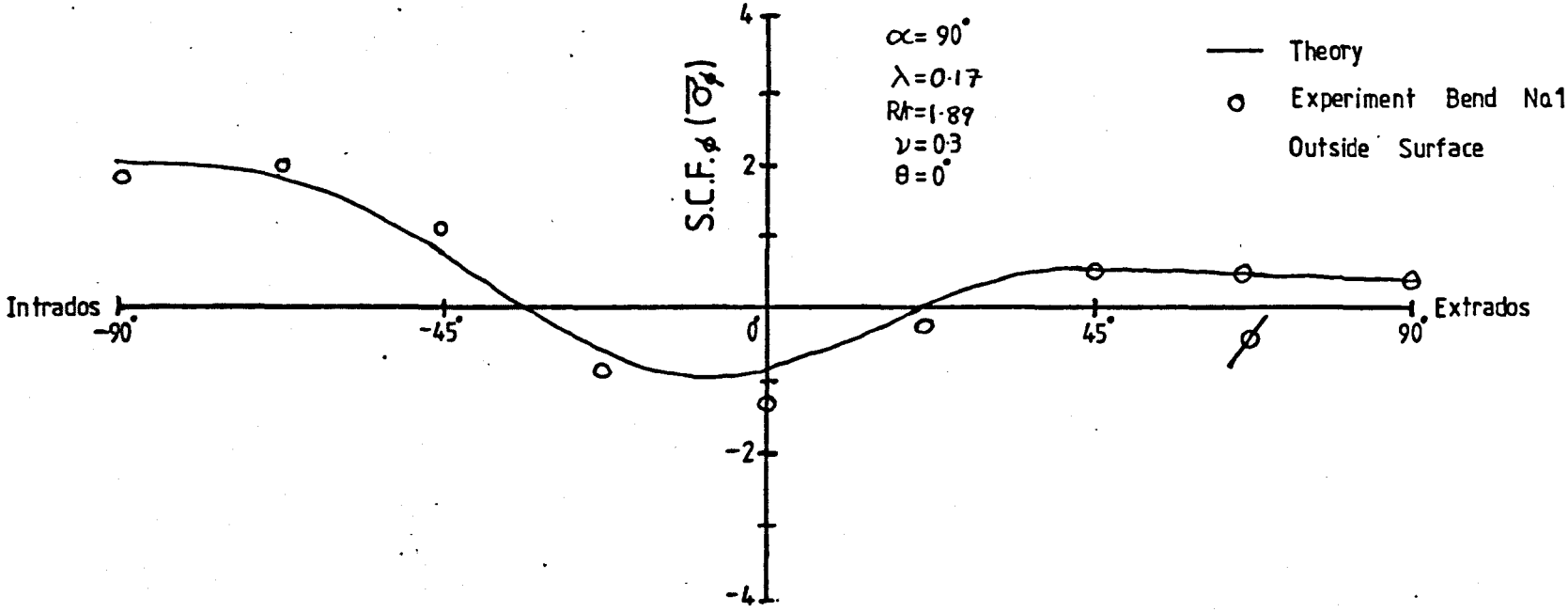

Experimental Meridional SCFs from Bend No.1 at $\theta = 0^\circ$

Figure (4.23)

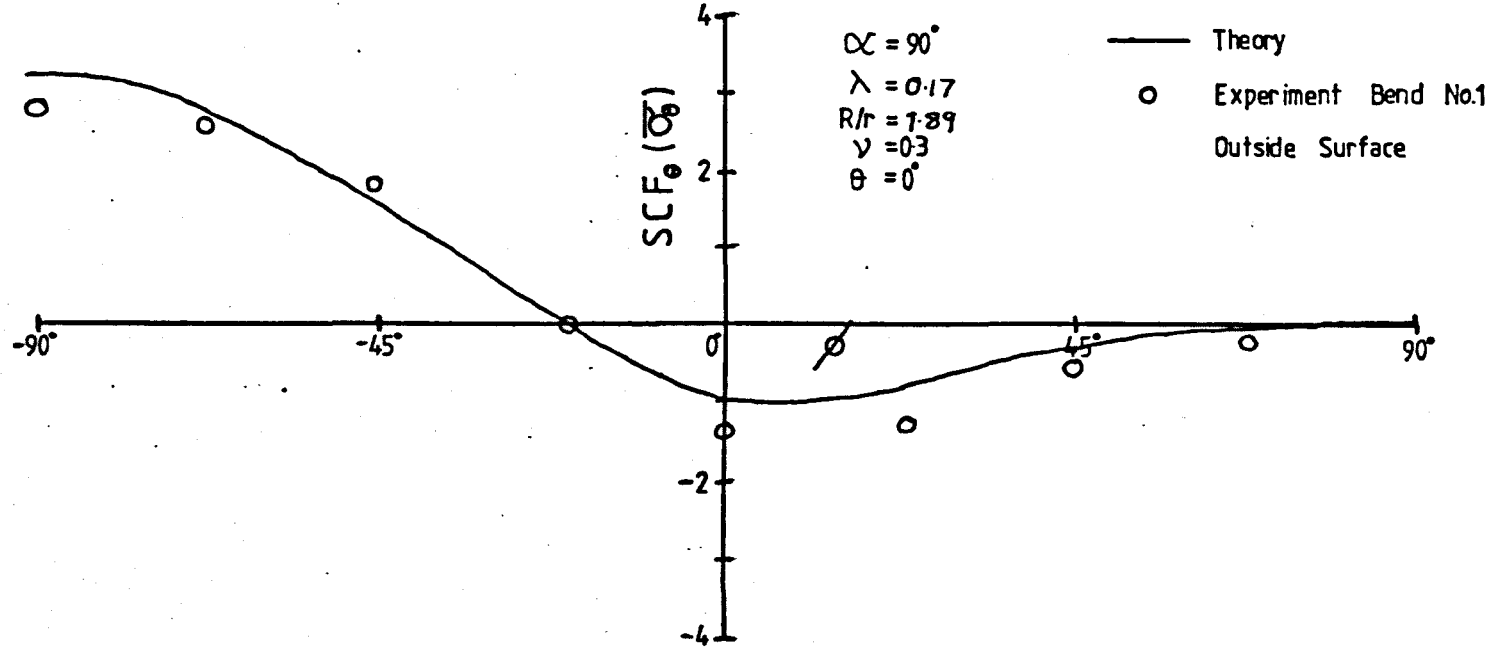

Experimental Circumferential S.C.Fs from Bend No.1 at $\theta = 0°$

Figure (4.24)

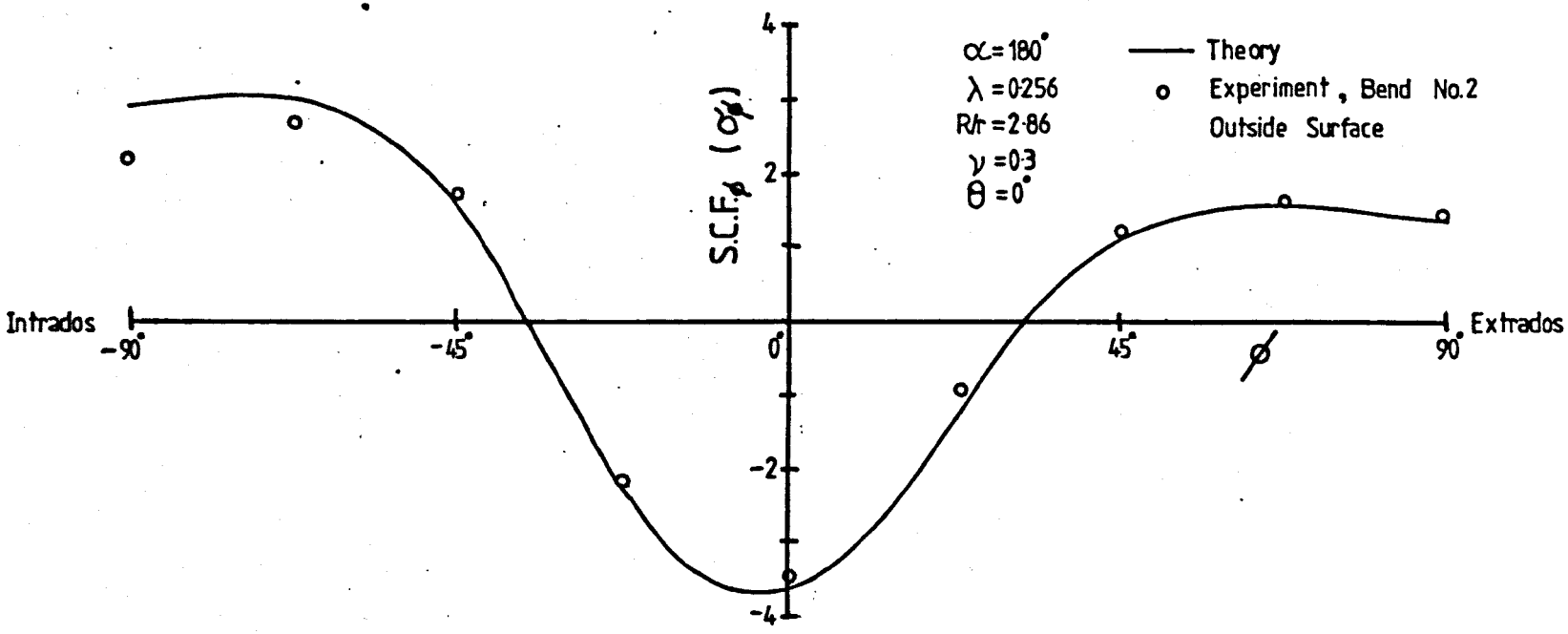

Experimental Meridional S.C.F.s from Bend No.2 at θ=0°

Figure (4.25)

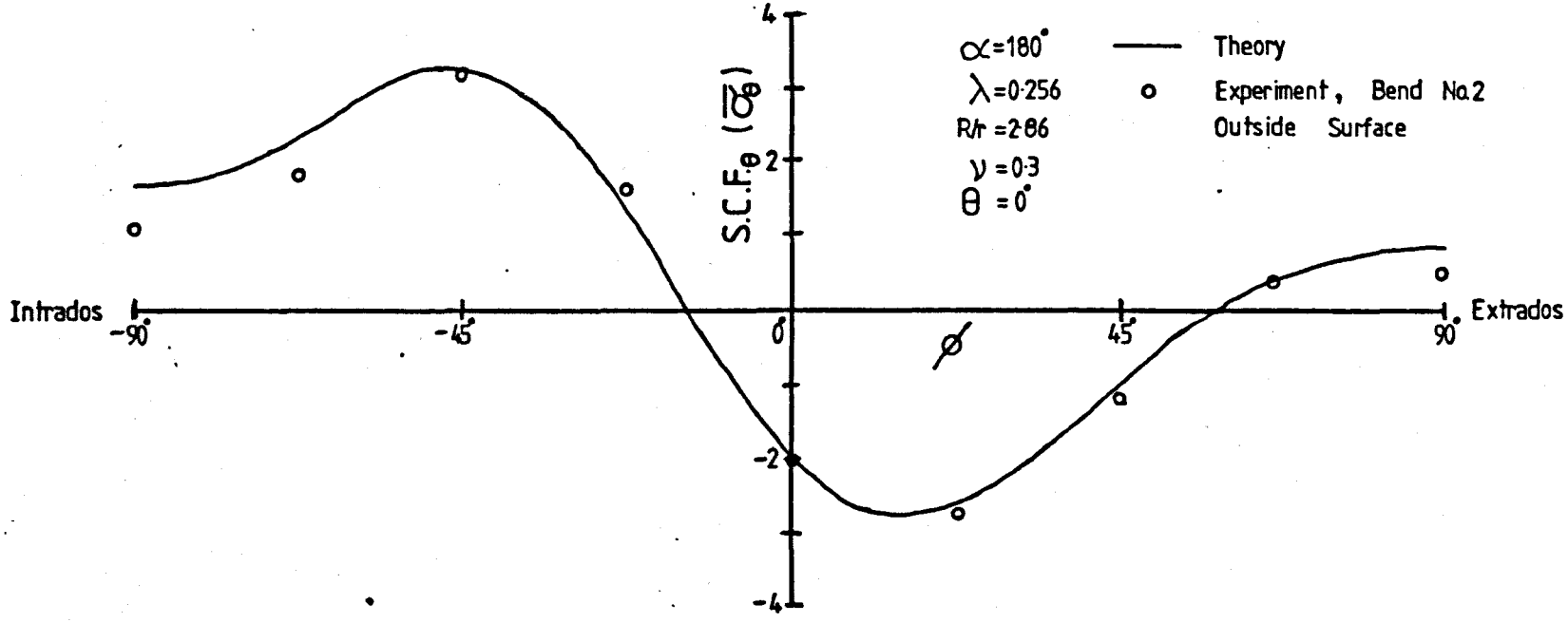

Experimental Circumferential S.C.F.s from Bend No.2 at $\theta = 0^\circ$

Figure (4.26)

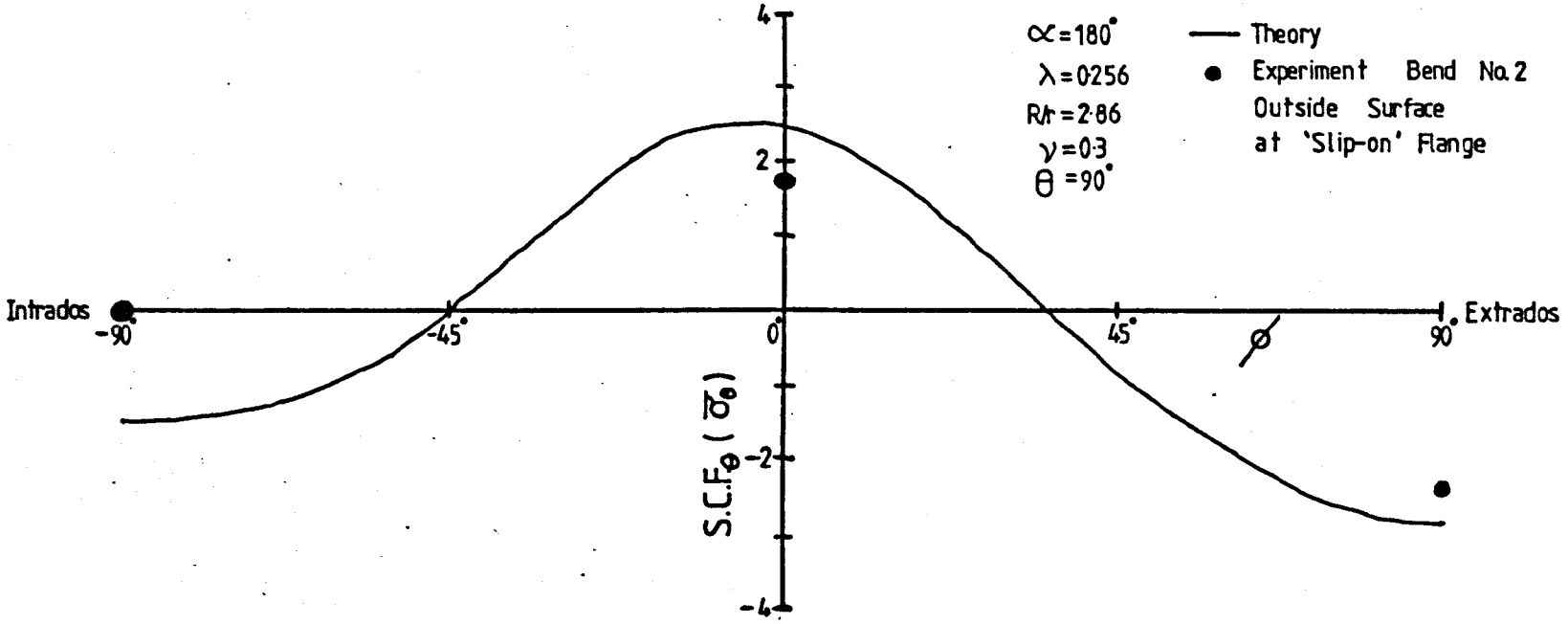

Experimental Circumferential S.C.F.s from Bend No. 2 at Slip-on Flange

Figure (4.27)

CHAPTER .5

THEORETICAL ANALYSIS OF A SMOOTH BEND WITH FLANGED TANGENT PIPES

Abstract

Theoretical solutions for the problem of a smooth pipe bend with connected tangent pipes, with flanged ends, under in-plane bending, are presented.

General displacements in the form of fourier series are suggested and these are used to derive the appropriate strains using the strain-displacement relations.

The first solution presented makes use of a simplified form of the displacements and strains. The total potential energy is formulated and integrated by hand, before being minimised to obtain a solution. Flexibility factors which are derived are discussed and compared with the results from other authors.

A numerical solution is then presented which uses the complete strains and displacements. Flexibility and stress concentration factors are presented for bends with long tangent pipes over a wide range of practical bend geometries. Approximate formulae for flexibility and maximum stresses are then given.

CHAPTER (5)

THEORETICAL ANALYSIS OF A SMOOTH BEND WITH FLANGED TANGENT PIPES UNDER IN-PLANE BENDING

(5.1) Introduction

(5.2) Displacements

- (a) Displacement Formulation
- (b) Rigid Section Displacements
- (c) Distortion Displacements

(5.3) Strains

(5.4) Solution Using Hand Integration

- (a) Method No. 4
- (b) Flexibility Factors from Method No. 4

(5.5) Method No. 5 : Numerical Solution

- (a) Formulation
- (b) Flexibility and Stress Concentration Factors

(5.6) Theoretical Results from Method No. 5

- (a) Integration convergence
- (b) Series convergence
- (c) Flexibility Factors from Method No. 5
- (d) Stress Concentration Factors from Method No. 5

(5.7) Conclusion

(5.1) Introduction

The effect of tangent pipes on the behaviour of smooth bends has been investigated experimentally by many authors over the last thirty years. Available evidence ([89]a and b , [90]) suggests that the effect of tangent pipes can be reasonably neglected providing the bend angle is greater than about 90°. However, because of experimental error, it is not uncommon to obtain a variation of up to 20% in the results from a series of tests, making the conclusion a little uncertain.

A number of finite element investigations (e.g. [97], [106], [115]) have been published using various different elements and programs. Many of these were restricted to a limited range of parameters which were of some particular interest to the author concerned. Perhaps the most noteworthy exception was that of Natarajan and Blomfield [97], who investigated several forms of end constraint, including tangent pipes, over a relatively wide range of parameters. They stated that tangents were significant even for 90° bends, where the flexibility and stresses could be about 15% lower than those of a 180° bend. Further, they concluded that the degree of significance was affected by the bend radius ratio. Their conclusions will be examined in more detail later.

A more analytic approach was adopted by Kalnins [93] to solve the problem. He used a combination of multisegment and finite difference techniques to solve the governing differential shell equations but only gave sample results. Wright et al. [108] attempted to use his computer program but found it gave seemingly anomalous results as was explained in section (1.3). More recently, Whatham and Thompson [119] presented an analysis for bends/

bends with flanged tangents similar to that used by Whatham [117] for flanged bends (see section (3.1)). They concluded that flanged tangents do not affect the flexibility or stresses in a bend if the tangents are more than one pipe circumference in length. Curiously, this was not entirely borne out by the results they presented which showed about a 10% lowering of the flexibility factors for 90° bends. Only 90° and 180° bends were examined and the results were presented in terms of the thickness ratio t/r. A few stress distributions were given but no graphs of peak stresses were presented.

The solution developed in this chapter is an extension of the work on flanged bends examined in chapter (3). The tangent pipes will be considered with flanged ends which makes the displacement boundary conditions simpler to specify. Flanged tangents are relatively common in practical pipelines, particularly on ships where ease of maintenance is of primal importance. Although flanged bends could be considered as a special case of a bend with zero length tangents, its formulation was presented separately because the tangent theory involves a new set of boundary conditions at the bend-tangent junction and uses slightly different assumptions. The work presented here will generally only contain details peculiar to the current problem, the general solution procedure being similar to that presented in chapter (3).

(5.2) Displacements

(5.2a) Displacement Formulation/

(5.2a) Displacement Formulation

As before, the displacements will be formulated in two components, rigid section displacements and distortion displacements, each of which is required to satisfy the boundary conditions. The definition of the components will be the same as that given in section (3.2a).

The displacements in the current problem are required to satisfy the conditions of symmetry and those of the rigid flange at the end of the tangent pipe as well as a new set of conditions, namely those of continuity between the bend and the tangent. For the latter requirement, displacements u, v, and ω and rotation β_θ (section (2.2)) on the bend must be equal to u, v, ω and β_x on the tangent, at the junction.

In the displacement derivations, use will be made of a non-dimensional co-ordinate along the length of the tangent pipes, defined as follows,

$$\theta = \frac{x}{R} \qquad \ldots (5.1)$$

where x is the length along the centreline of the bend-tangent assembly, measured from the bend centre ($\theta = 0$), and R is the radius of the bend. θ is the same co-ordinate as used for the bend where x is the arc length along the bend centreline from $\theta = 0$. Note that the overall length of the bend-tangent assembly centreline, with each tangent of length, ℓ, is,

$$L = 2\ell + R\alpha \qquad \ldots (5.2)$$

(5.2b)/

(5.2b) Rigid Section Displacements

The rigid section displacements for the bend are formulated in the manner explained in section (3.2b). The rigid section shell displacements u_R, v_R and ω_R can be found from the centreline displacements U_c and V_c using the following equations,

$$u_R = U_c + \gamma_c r \sin\phi \quad \text{where} \quad \gamma_c = \frac{1}{R}\left(U_c - \frac{\partial V_c}{\partial \theta}\right)$$

$$v_R = V_c \cos\phi \quad , \quad \omega_R = V_c \sin\phi$$

$$-\frac{\alpha}{2} \leq \theta \leq \frac{\alpha}{2} \qquad \ldots (5.3)$$

If the bend centreline displacements at the bend-tangent connection are U_c^b and V_c^b and the rotation γ_c^b, then the centreline displacements for the tangent are, (see fig. (5.1)),

$$U_c = U_c^b$$

$$V_c = V_c^b - \gamma_c R(\theta - \tfrac{\alpha}{2}) + V_c^T$$

$$\frac{\alpha}{2} \leq \theta \leq \frac{L}{2R} \qquad \ldots (5.4)$$

where V_c^T is the additional part of the rigid section displacements contributed by the tangent pipes. For (5.4) to be true, V_c^T and $(\partial V_c^T/\partial\theta)$ must be zero at $\theta = \alpha/2$. The corresponding rigid section shell displacements for the tangent pipes can be found from,

$$u_R = U_c^b + \gamma_c r \sin\phi \quad , \quad \gamma_c = \frac{-1}{R}\frac{\partial V_c}{\partial \theta}$$

$$v_R = V_c \cos\phi \quad , \quad \omega_R = V_c \sin\phi$$

$$\left(\frac{\alpha}{2} \leq \theta \leq L/2R\right) \qquad \ldots (5.5)$$

Note/

Note that χ_c is different for the bend and the tangent. The rigid section displacements as given by (5.3) and (5.5) satisfy the continuity conditions.

Note that in the derivation of the above relations, the assumption of small displacements was applied throughout.

U_c and V_c for the bend, $0 \leq \theta \leq \frac{\alpha}{2}$ (applying symmetry) will be taken with the same form as developed in section (3.2b), i.e.

$$V_c = -\sum_{j=1}^{n} D_j \sin^2\left(\frac{j\pi\theta}{2\alpha}\right)$$

$$U_c = \sum_{j=1}^{n} F_j \tfrac{1}{2}\left(\theta - \left(\frac{\alpha}{j\pi}\right)\sin\left(\frac{j\pi\theta}{\alpha}\right)\right) \qquad \ldots (5.6)$$

$$0 \leq \theta \leq \frac{\alpha}{2}$$

from these, U_c^b and V_c^b are

$$V_c^b = -\sum_{j=1}^{n} D_j \sin^2\left(\frac{j\pi}{4}\right)$$

$$U_c^b = \sum_{j=1}^{n} F_j \tfrac{1}{2}\left(\frac{\alpha}{2} - \left(\frac{\alpha}{j\pi}\right)\sin\left(\frac{j\pi}{2}\right)\right) \qquad \ldots (5.7)$$

V_c^T and $\frac{\partial V_c^T}{\partial \theta}$ are required to be zero at $\theta = \frac{\alpha}{2}$. These are satisfied by a polynomial series of the following form,

$$V_c^T = -\sum_{j=1}^{n} G_j \left(\theta - \tfrac{\alpha}{2}\right)^{j+1}$$

$$\ldots (5.8)$$

$$\frac{\alpha}{2} \leq \theta \leq \frac{L}{2R}$$

This form was found to be better than a trigonometric series for this particular displacement. The first term in series, j = 1, is the displacement form of an equivalent solid beam.

Substituting/

Substituting (5.6), (5.7) and (5.8) into (5.3) and (5.5) gives the rigid section shell displacements;

For the bend, $0 \leq \theta \leq \frac{\alpha}{2}$

$$u_R = \sum_{j=1}^{n} F_j \tfrac{1}{2}\left(\theta - \frac{\alpha}{j\pi}\sin\left(\frac{j\pi\theta}{\alpha}\right)\right)\left(1 + \frac{r}{R}\sin\phi\right)$$

$$+ \tfrac{1}{2}\sum_{j=1}^{n} D_j \left(\frac{j\pi}{\alpha}\right)\sin\left(\frac{j\pi\theta}{\alpha}\right)\frac{r}{R}\sin\phi$$

$$v_R = -\sum_{j=1}^{n} D_j \sin^2\left(\frac{j\pi\theta}{2\alpha}\right)\cos\phi$$

$$w_R = -\sum_{j=1}^{n} D_j \sin^2\left(\frac{j\pi\theta}{2\alpha}\right)\sin\phi$$

, $j = 1, 2, 3$ ---

For the tangent pipe, $\frac{\alpha}{2} \leq \theta \leq \frac{1}{2R}$

$$u_R = \sum_{j=1}^{n} F_j \tfrac{1}{2}\left(\frac{\alpha}{2} - \frac{\alpha}{j\pi}\sin\left(\frac{j\pi}{2}\right)\right)\left(1 + \frac{r}{R}\sin\phi\right) + \sum_{j=1}^{n} D_j \tfrac{1}{2}\left(\frac{j\pi}{\alpha}\right)\sin\left(\frac{j\pi}{\alpha}\right)\frac{r}{R}\sin\phi +$$

$$+ \sum_{j=1}^{n} G_j (j+1)\left(\theta - \tfrac{\alpha}{2}\right)^j \frac{r}{R}\sin\phi$$

$$v_R = \left[-\sum_{j=1}^{n} D_j \sin^2\left(\frac{j\pi}{4}\right) - \left(\sum_{j=1}^{n} F_j \tfrac{1}{2}\left(\frac{\alpha}{2} - \left(\frac{\alpha}{j\pi}\right)\sin\left(\frac{j\pi}{2}\right)\right) + \right.\right.$$

$$\left.\left. + \sum_{j=1}^{n} D_j \left(\frac{j\pi}{\alpha}\right)\tfrac{1}{2}\sin\left(\frac{j\pi}{2}\right)\right)\left(\theta - \tfrac{\alpha}{2}\right) - \sum_{j=1}^{n} G_j \left(\theta - \tfrac{\alpha}{2}\right)^{j+1}\right]\cos\phi$$

$$w_R = \left[-\sum_{j=1}^{n} D_j \sin^2\left(\frac{j\pi}{4}\right) - \left(\sum_{j=1}^{n} F_j \tfrac{1}{2}\left(\frac{\alpha}{2} - \left(\frac{\alpha}{j\pi}\right)\sin\left(\frac{j\pi}{2}\right)\right) + \right.\right.$$

$$\left.\left. + \sum_{j=1}^{n} D_j \left(\frac{j\pi}{\alpha}\right)\tfrac{1}{2}\sin\left(\frac{j\pi}{2}\right)\right)\left(\theta - \tfrac{\alpha}{2}\right) - \sum_{j=1}^{n} G_j \left(\theta - \tfrac{\alpha}{2}\right)^{j+1}\right]\sin\phi$$

, $j = 1, 2, 3$, ---

... (5.9)

(5.2c) Distortion Displacements

The meridional components of the distortion displacements will be taken with the same form as developed in sections (3.2d-f). Taking the circumferential displacements with the following form,

$$u(\theta) = \frac{r}{R}\sum_{m=1}^{\infty} A_m (m\eta)\sin(2m\eta\theta)$$

$$v(\theta) = \sum_{m=1}^{\infty} B_m\left(\psi_{om}\cos^2(m\eta\theta) - \psi_{em}\sin^2(m\eta\theta)\right)$$

$$\omega(\theta) = \sum_{m=1}^{\infty} C_m\left(\psi_{om}\cos^2(m\eta\theta) - \psi_{em}\sin^2(m\eta\theta)\right)$$

$$\eta = \frac{\pi R}{L} \quad , \quad 0 \le \theta \le L/2R \qquad \ldots (5.10)$$

for both the bend and the tangent pipe, would satisfy the three displacement continuity conditions, but violate the rotation continuity requirement, i.e.,

for the bend, $$\beta_\theta^b = \frac{1}{R'}\left(u_b \sin\phi - \frac{\partial \omega_b}{\partial \theta}\right)$$

$$= -\frac{1}{R}\frac{\partial \omega_b}{\partial \theta} + \frac{\sin\phi}{R'}\left(u_b + \frac{r}{R}\frac{\partial \omega_b}{\partial \theta}\right)$$

for the tangent, $$\beta_x^b = -\frac{\partial \omega_b}{\partial x} = \frac{-1}{R}\frac{\partial \omega}{\partial \theta}$$

$$\therefore \quad (\beta_\theta^b)_{\theta=\frac{\pi}{2}} \neq (\beta_x^b)_{\theta=\frac{\pi}{2}} \qquad \ldots (5.11)$$

The error in the slope condition from using continuous series displacements of the form in (5.10) is,

$$\left[\left(\beta_\theta^D\right)_{\theta=\frac{\alpha}{2}} - \left(\beta_x^D\right)_{\theta=\frac{\alpha}{2}}\right] = \frac{r \sin\phi}{R}\left[\frac{1}{R}\sum_{m=1}^{\infty}\left(A_m u(\phi) + C_m \omega(\phi)\right)(m\eta)\sin(m\eta\alpha)\right]$$

... (5.12)

which is of the order of $(\frac{r}{R}\sin\phi)$ x $(\beta_x^D)_{\theta=\frac{\alpha}{2}}$; it will be seen later that Cm $\omega(\phi)/n^2 \approx$ Am $u(\phi)$. Note also that $\beta_\theta^D = \beta_x^D$ at $\phi = 0$. It will be assumed herein that the above term, (5.12), can be neglected and equations (5.10) are sufficient.

The distortion displacements will be then taken as,

$$u_D = \frac{r}{R}\sum_{m=1}^{\infty}\sum_{n=2}^{\infty} A_{mn}\left(\psi_{en}\frac{1}{n^2}\cos n\phi + \psi_{on}\frac{1}{n^2}\sin n\phi\right)(m\eta)\sin(2m\eta\theta)$$

$$v_D = \sum_{m=1}^{\infty}\sum_{n=2}^{\infty} B_{mn}\left(-\psi_{en}\frac{1}{n}\sin n\phi + \psi_{on}\frac{1}{n}\cos n\phi\right)\left(\psi_{om}\cos^2(m\eta\theta) - \psi_{em}\sin^2(m\eta\theta)\right)$$

$$w_D = \sum_{m=1}^{\infty}\sum_{n=2}^{\infty} C_{mn}\left(\psi_{en}\cos n\phi + \psi_{on}\sin n\phi\right)\left(\psi_{om}\cos^2(m\eta\theta) - \psi_{em}\sin^2(m\eta\theta)\right)$$

$$+ \sum_{j=1}^{\infty} H_j\left(\psi_{oj}\cos^2(j\eta\theta) - \psi_{ej}\sin^2(j\eta\theta)\right)$$

... (5.13)

$$0 \le \theta \le \alpha/2R$$

The definition of ψ was given in equation (3.22). u_D, v_D and w_D as expressed in (5.13) satisfy the symmetry conditions, the flange conditions at the end of tangent and the continuity of u_D, v_D and w_D at the joint. Continuity of β_θ^D at the joint is only satisfied at $\phi = 0$.

Note that the rigid section displacements satisfied all of the boundary conditions exactly.

(5.3) Strains

The total displacements can be found by adding the rigid section and distortion displacements. The strains are obtained by substituting these into the strain-displacement equations for the bend (2.13) and the tangent pipe (2.20).

Bend: $0 \leq \theta \leq \alpha/2$

$$\epsilon_\phi = \frac{1}{r}\Big[\sum_m{}' \sum_n{}' (C_{mn} - B_{mn})(\psi_{en}\cos n\phi + \psi_{on}\sin n\phi)\times$$

$$\times(\psi_{om}\cos^2(m\eta\theta) - \psi_{em}\sin^2(m\eta\theta)) + \sum_j{}' H_j(\psi_{oj}\cos^2(j\eta\theta) - \psi_{ej}\sin^2(j\eta\theta))\Big]$$

$$\epsilon_\theta = \frac{1}{R'}\Big[\sum_j{}'\Big((F_j(1+\tfrac{r}{R}\sin\phi) - D_j)\sin^2\big(\tfrac{j\pi\theta}{2\alpha}\big) + D_j\tfrac{1}{2}\big(\tfrac{j\pi}{\alpha}\big)^2\cos\big(\tfrac{j\pi\theta}{\alpha}\big)\tfrac{r}{R}\sin\phi\Big)$$

$$+ \frac{2r}{R}\sum_m{}'\sum_n{}'\Big\{A_{mn}(\psi_{en}\cos n\phi + \psi_{on}\sin n\phi)\big(\tfrac{m\eta}{n}\big)^2\cos(2m\eta\theta)$$

$$+\Big(B_{mn}\big(-\psi_{en}\tfrac{1}{n}\sin n\phi + \psi_{on}\tfrac{1}{n}\cos n\phi\big)\cos\phi$$

$$+ C_{mn}(\psi_{en}\cos n\phi + \psi_{on}\sin n\phi)\sin\phi\Big)(\psi_{om}\cos^2(m\eta\theta) - \psi_{em}\sin^2(m\eta\theta))\Big\}$$

$$+ \sum_j{}' H_j(\psi_{oj}\cos^2(j\eta\theta) - \psi_{ej}\sin^2(j\eta\theta))\sin\phi\Big]$$

$$\gamma_{\theta\phi} = \frac{1}{R'}\Big[\sum_m{}'\sum_n{}'\Big\{(B_{mn} - A_{mn}\tfrac{R'}{R})(\psi_{en}\tfrac{1}{n}\sin n\phi - \psi_{on}\tfrac{1}{n}\cos n\phi)$$

$$- \tfrac{r}{R}A_{mn}(\psi_{en}\tfrac{1}{n^2}\cos n\phi + \psi_{on}\tfrac{1}{n^2}\sin n\phi)\cos\phi\Big\}(m\eta)\sin(2m\eta\theta)\Big]$$

$$K_\phi = \frac{1}{r^2}\Big[\sum_m{}'\sum_n{}'(n^2C_{mn} - B_{mn})(\psi_{en}\cos n\phi + \psi_{on}\sin n\phi)$$

$$\times(\psi_{om}\cos^2(m\eta\theta) - \psi_{em}\sin^2(m\eta\theta))\Big]$$

$$K_\theta = \frac{1}{R^{12}}\Big[\sum_j \Big(F_j \sin^2\Big(\frac{j\pi\theta}{\alpha}\Big) + D_j \tfrac{1}{2}\Big(\frac{j\pi}{\alpha}\Big)^2 \cos\Big(\frac{j\pi\theta}{\alpha}\Big)\Big)\Big(1+\frac{r}{R}\sin\phi\Big)\sin\phi$$

$$+\sum_m\sum_n\Big\{\frac{2r}{R}A_{mn}\Big(\psi_{en}\frac{1}{n^2}\cos n\phi + \psi_{on}\frac{1}{n^2}\sin n\phi\Big)\sin\phi$$

$$+2C_{mn}\Big(\psi_{en}\cos n\phi + \psi_{on}\sin n\phi\Big)\Big\}(m\eta)^2\cos(2m\eta\theta)$$

$$+\frac{R'}{r}\sum_m\sum_n\Big\{B_{mn}\Big(-\psi_{en}\frac{1}{n}\sin n\phi + \psi_{on}\frac{1}{n}\cos n\phi\Big)\cos\phi$$

$$+C_{mn}\Big(\psi_{en}\, n\sin n\phi - \psi_{on}\, n\cos n\phi\Big)\cos\phi\Big\}$$

$$\times\Big(\psi_{om}\cos^2(m\eta\theta) - \psi_{em}\sin^2(m\eta\theta)\Big)$$

$$+\sum_j H_j\, 2\Big(\frac{j\pi}{\alpha}\Big)^2\cos\Big(\frac{2j\pi\theta}{\alpha}\Big)\Big]$$

$$K_{\theta\phi} = \frac{1}{rR'}\Big[\sum_m\sum_n\Big\{A_{mn}\frac{r}{R}\Big(-\psi_{en}\frac{1}{n}\sin n\phi + \psi_{on}\frac{1}{n}\cos n\phi\Big)\sin\phi$$

$$-A_{mn}\frac{r^2}{RR'}\Big(\psi_{en}\frac{1}{n^2}\cos n\phi + \psi_{on}\frac{1}{n^2}\sin n\phi\Big)\cos\phi\sin\phi$$

$$+B_{mn}\Big(\psi_{en}\frac{1}{n}\sin n\phi - \psi_{on}\frac{1}{n}\cos n\phi\Big)$$

$$+C_{mn}\Big(-\psi_{en}\, n\sin n\phi + \psi_{on}\, n\cos n\phi\Big)$$

$$-C_{mn}\frac{r}{R'}\Big(\psi_{en}\cos n\phi + \psi_{on}\sin n\phi\Big)\cos\phi\Big\}(m\eta)\sin(2m\eta\theta)$$

$$-\frac{r}{R'}\sum_j H_j\cos\phi\Big(\frac{j\pi}{\alpha}\Big)\sin(2j\eta\theta)\Big] \qquad \text{(IV)}$$

... (5.14)

Tangent:/

Tangent: $\frac{\alpha}{2} \leq \theta \leq \frac{L}{2R}$

$$\epsilon_\phi = \frac{1}{r}\Big[\sum_m' \sum_n' (C_{mn} - B_{mn})\left(\psi_{en}\cos n\phi + \psi_{on}\sin n\phi\right)$$

$$\times \left(\psi_{om}\cos^2(m\eta\theta) - \psi_{em}\sin^2(m\eta\theta)\right)$$

$$+ \sum_j' H_j\left(\psi_{oj}\cos^2(j\eta\theta) - \psi_{ej}\sin^2(j\eta\theta)\right)\Big]$$

$$\epsilon_x = \frac{1}{R}\Big[\sum_j' G_j(j^2+j)\left(\theta - \tfrac{\alpha}{2}\right)^{j-1}\frac{r}{R}\sin\phi$$

$$+ \frac{2r}{R}\sum_m' \sum_n' A_{mn}\left(\psi_{en}\cos n\phi + \psi_{on}\sin n\phi\right)\left(\frac{m}{n}\right)^2\cos(2m\eta\theta)\Big]$$

$$\gamma_{x\phi} = \frac{1}{R}\Big[\sum_m' \sum_n' (B_{mn} - A_{mn})\left(\psi_{en}\cos n\phi - \psi_{on}\sin n\phi\right)\left(\frac{m\eta}{n}\right)\sin(2m\eta\theta)\Big]$$

$$K_\phi = \frac{1}{r^2}\Big[\sum_m' \sum_n' (n^2 C_{mn} - B_{mn})\left(\psi_{en}\cos n\phi + \psi_{on}\sin n\phi\right)$$

$$\times \left(\psi_{om}\cos^2(m\eta\theta) - \psi_{em}\sin^2(m\eta\theta)\right)\Big]$$

$$K_x = \frac{1}{R^2}\Big[\sum_j' G_j(j^2+j)\left(\theta - \tfrac{\alpha}{2}\right)^{j-1}\sin\phi$$

$$+ 2\sum_m' \sum_n' C_{mn}\left(\psi_{en}\cos n\phi + \psi_{on}\sin n\phi\right)(m\eta)^2\cos(2m\eta\theta)$$

$$+ 2\sum_j' H_j(j\eta)^2\cos(2j\eta\theta).\Big]$$

$$K_{x\phi} = \frac{1}{rR}\Big[\sum_m' \sum_n' \Big(B_{mn}\left(\psi_{en}\tfrac{1}{n}\sin n\phi - \psi_{on}\tfrac{1}{n}\cos n\phi\right)$$

$$+ C_{mn}\left(-\psi_{en}\, n\sin n\phi + \psi_{on}\, n\cos n\phi\right)\Big)(m\eta)\sin(2m\eta\theta)\Big]$$

... (5.15)

where $R' = R + r \sin \phi$, $\eta = \frac{\pi R}{L}$

and

$$W_j = \sum_{j=1}^{JT} \quad , j = 1, 2, 3, ---, JT$$

$$W_m = \sum_{m=1}^{MT} \quad , m = 1, 2, 3, ---, MT$$

$$W_c = \sum_{n=2}^{NT+1} \quad , n = 2, 3, 4, ---, NT+1$$

It should be noted that some of the above strains are slightly discontinuous at the bend-tangent boundary because of the assumption regarding slope continuity made earlier.

(5.4) Solution Using Hand Integration

(5.4a) Method No. 4

Before describing the more complex numerical procedure using the strains given by equations (5.14) and (5.15), it is worth examining a solution using hand integration and several of the assumptions explained in chapter (3).

For the bend the following assumptions are applied.

1. $\epsilon_\phi = 0$, or $U_b = -\int \omega_b \, d\phi$ (from (3.25)).

2. $\gamma_{\theta\phi} = 0$, or $U_D = \frac{r}{R} \iint \frac{\partial \omega_b}{\partial \theta} d\phi d\phi$ (from (3.39)).

3. $\frac{r}{R} \sin \phi \ll 1$

4. K_θ, K_ϕ neglected

5. $\epsilon_\theta^{\ell} = 0$ at $\phi = 0$, or $U_c = \int V_c d\theta$, (from (3.5)).

Assumptions 1., 2., and 4. are also applied to the tangent pipe but/

but 3. and 5. are not required. All of the shell displacements can be derived from V_c, V_c^T and ω_b which are taken as,

$$V_c = -\sum_{j=1}^{JT} D_j \sin^2\left(\frac{j\pi\theta}{2\alpha}\right) \qquad V_c^T = -\sum_{j=1}^{JT} G_j \left(\theta - \frac{\alpha}{2}\right)^{j+1}$$

$$\omega_b = \sum_{m=1}^{MT} \sum_{n=2,4}^{NT/2} C_{mn} \cos n\phi \left(\psi_{mo} \cos^2(m\eta\theta) - \psi_{me} \sin^2(m\eta\theta)\right) \qquad \ldots (5.16)$$

The simpler form of ω_b in (3.45) was tried but found to give poor convergence for longer tangent pipe lengths. The rigid section displacements, from (5.16), became the same as those in (5.9) with Fj replaced by Dj, and u_b and v_b become,

$$u_b = \frac{r}{R} \sum_{m=1}^{MT} \sum_{n=1}^{NT/2} C_{mn} \left(\frac{m\eta}{n^2}\right) \cos n\phi \sin(2m\eta\theta)$$

$$v_b = \sum_{m=1}^{MT} \sum_{n=1}^{NT} C_{mn} \frac{1}{n} \sin n\phi \left(\psi_{om} \cos^2(m\eta\theta) - \psi_{em} \sin^2(m\eta\theta)\right)$$

$$\ldots (5.17)$$

The displacements and assumptions give the strains as,

(Symmetric about $\theta = 0$)

Bend: $0 \le \theta \le \frac{\alpha}{2}$

$$\epsilon_\theta = \frac{1}{R}\left[\frac{r}{R} \sum_j D_j \frac{1}{2}\left(1 + \cos\left(\frac{j\pi\theta}{\alpha}\right)\left(\left(\frac{j\pi}{\alpha}\right)^2 - 1\right)\right) \sin\phi \right.$$

$$+ \sum_m \sum_n C_{mn} \left(\cos n\phi \sin\phi - \frac{1}{n} \sin n\phi \cos\phi\right)\left(\psi_{om} \cos^2(m\eta\theta) - \psi_{em} \sin^2(m\eta\theta)\right)$$

$$\left. + \frac{2r}{R} \sum_m \sum_n C_{mn} \left(\frac{m\eta}{n}\right)^2 \cos n\phi \cos(2m\eta\theta)\right]$$

$$K_\phi = \frac{1}{r^2}\left[\sum_m \sum_n C_{mn} (n^2 - 1) \cos n\phi \left(\psi_{om} \cos^2(m\eta\theta) - \psi_{em} \sin^2(m\eta\theta)\right)\right]$$

Tangent: $\frac{\alpha}{2} \leq \theta \leq L/2R$

$$\epsilon_x = \frac{1}{R}\left[\frac{r}{R}\sum_j' G_j (j^2+j)(\theta-\tfrac{\alpha}{2})^{j-1}\sin n\phi + \frac{2r}{R}\sum_m'\sum_n' C_{mn}\left(\frac{m\eta}{n}\right)^2 \cos n\phi \cos(2m\eta\theta)\right]$$

$$K_\phi = \frac{1}{r^2}\left[\sum_m'\sum_n' C_{mn}(n^2-1)\cos n\phi\left(\psi_{om}\cos^2(m\eta\theta) - \psi_{em}\sin^2(m\eta\theta)\right)\right]$$

where

$$\sum_m' = 1, 2, 3, \text{---}, MT \quad , \quad \sum_n' = 2, 4, 6, \text{---}, NTx2,$$
$$\sum_j' = 1, 2, 3, \text{---}, JT$$

... (5.18)

The total potential energy is found by substituting these into,

$$V = C\int_0^{2\pi}\int_0^{\frac{\alpha}{2}} \left[\epsilon_\theta^2 + \frac{t^2}{12}K_\phi^2\right] r R\, d\theta d\phi + C\int_0^{2\pi}\int_{\frac{\alpha}{2}}^{L/2R} \left[\epsilon_x^2 + \frac{t^2}{12}K_\phi^2\right] r R\, d\theta d\phi - M\gamma$$

where $C = \dfrac{Et}{(1-\nu^2)}$

... (5.19)

The rotation between the flanged ends of the tangent pipes, γ, is found from $2\gamma_c$ (Equation (5.5)) at $\theta = L/2R$ as,

$$\gamma = \frac{1}{R}\sum_j' D_j\left(\frac{\alpha}{2} + \sin\left(\frac{j\pi}{2}\right)\left(\frac{j\pi}{\alpha} - \frac{\alpha}{j\pi}\right)\right) + \frac{1}{R}\sum_j' G_j\, 2(j+1)\left(\ell/R\right)^j$$

... (5.20)

Substituting (5.18) and (5.20) into (5.19) and integrating gives,

$$\bar{V} = \sum_j' \sum_k' \bar{D}_j \bar{D}_k \Phi_1 + \sum_j' \sum_k' \bar{G}_j \bar{G}_k \Phi_{14} + \sum_j' \sum_m' \bar{C}_{m1} \bar{D}_j \Phi_{15} +$$

$$+ \sum_m' \sum_p' \sum_n' \left(\bar{C}_{mn} \bar{C}_{pn} \Phi_{16} + \bar{C}_{mn} \bar{C}_{p,n+2} \Phi_{17} \right) - \sum_j' \left(\bar{D}_j \Phi_5 + \bar{G}_j \Phi_{18} \right) \quad \ldots (5.21)$$

where $\bar{V} = V \Big/ \left(\frac{M \gamma_0}{2(1-\nu^2)} \right)$, $\gamma_0 = \frac{MR\alpha}{EI}$, $I = \pi r^3 t$

$$\bar{D}_j = \frac{D_j}{R\gamma_0} \quad , \quad \bar{G}_j = \frac{G_j}{R\gamma_0} \quad , \quad \bar{C}_{mn} = C_{mn} \left(\frac{\alpha}{r\gamma_0} \right)$$

j, k = 1, 2, 3, ----, JT

m, p = 1, 2, 3, ----, MT

n = 2, 4, 6, ----, NT×2

$$\Phi_{14} = 2\alpha \frac{(j^2+j)(k^2+k)}{(j+k-1)} (e/R)^{j+k-1}$$

$$\Phi_{15} = \frac{-3}{4} \left\{ \frac{\alpha}{2} (-1)^{m+1} + \frac{1}{2m\eta} \sin(m\eta\alpha) + (-1)^{m+1} \left(\frac{j\pi}{\alpha} - \frac{\alpha}{j\pi} \right) \sin\left(\frac{j\pi}{2} \right) \right.$$

$$\left. + \frac{1}{2} \left(\left(\frac{j\pi}{\alpha} \right)^2 - 1 \right) \left(\frac{\sin(m\eta\alpha + \frac{j\pi}{2})}{(x+y)} + \frac{\sin(m\eta\alpha - \frac{j\pi}{2})}{(x-y)} (1 - \delta_{x0}) + \frac{\alpha}{2} \delta_{x0} \right) \right\}$$

$$x = 2m\eta \qquad y = \frac{j\pi}{\alpha}$$

$$\Phi_{16} = \Phi_{19} \times \frac{(n^2+1)}{2n^2} + \left(1 + \frac{1}{2} \delta_{mp} (-1)^{m+p} \right) \frac{1}{R\alpha} \left(\frac{\lambda^2 (n^2-1)^2}{48} \right) + 2 \left(\frac{r}{R} \right)^2 \left(\frac{m\eta}{n!} \right)^4 \frac{L}{R\alpha} \delta_{mp}$$

$$\Phi_{17} = -\Phi_{19} \left(\frac{n^2 + 2n - 3}{2n(n+2)} \right)$$

$$\Phi_{18} = 4(J+1)(\ell/R)^3(1-\nu^2)$$

$$\Phi_{19} = \frac{1}{2\alpha}\left\{\frac{\alpha}{2}(-1)^{m+p} + \frac{1}{2m\eta}\sin(m\eta\alpha)(-1)^{p+1} + \frac{1}{2p\eta}\sin(p\eta\alpha)(-1)^{m+1}\right.$$

$$\left. + \frac{1}{2}\left(\frac{\sin(\eta\alpha(m+p))}{2\eta(m+p)} + \frac{\sin(\eta\alpha(m-p))}{2\eta(m-p)}(1-\delta_{mp}) + \frac{\alpha}{2}\delta_{mp}\right)\right\}$$

... (5.22)

Φ_1 and Φ_5 were given in equations (3.51). Details of the integrations are given in appendix (2).

The total potential energy is minimised by differentiating with respect to each of the displacement coefficients,

$$\frac{\partial \bar{V}}{\partial \bar{D}_j} = 2\sum_k' \bar{D}_k \Phi_1 + \sum_m' \bar{C}_{m,1}\Phi_{15} - \Phi_5 = 0$$

$$\frac{\partial \bar{V}}{\partial \bar{G}_j} = 2\sum_k' \bar{G}_k \Phi_{14} - \Phi_{18} = 0$$

$$\frac{\partial \bar{V}}{\partial \bar{C}_{mn}} = \sum_j' \bar{D}_j \Phi_{15} + 2\sum_p' \bar{C}_{pn}\Phi_{16} + \sum_p' \bar{C}_{p,n+2}\Phi_{17} + \sum_p' \bar{C}_{p,n-2}\Phi_{20}$$

... (5.23)

where

$$\Phi_{20} = -\Phi_{19}\left(\frac{n^2-2n-3}{2n(n-2)}\right) \qquad \text{... (5.24)}$$

This gives a set of linear simultaneous equations which can be solved as described in section (3.4a). The total number of equations to be solved is (JT x 2 + MT x NT).

The bend flexibility factors are obtained from the definition given in the introduction to chapter (1), and the end rotation/

rotation (5.20) i.e.

$$K = (\gamma - 2\gamma^T)/\gamma_o$$

$$= \sum_1^J \left[D_J \left(\frac{\alpha}{2} + \sin\left(\frac{J\pi}{2}\right)\left(\frac{J\pi}{\alpha} - \frac{\alpha}{J\pi}\right)\right) + \sum_1^J G_J\, 2(J+1)(\ell/R)^J \right] - (1-\nu^2)\frac{2\ell}{R\alpha}$$

... (5.25)

Note that simple beam theory would give γ^T as

$$\gamma^T = \frac{M\ell}{EI}$$

... (5.26)

but that a lower bound energy method such as that used herein would give,

$$\gamma^T = (1-\nu^2)\frac{M\ell}{EI}$$

... (5.27)

Although (5.26) is the more usually accepted form for γ^T, (5.27) is used in the equation for the flexibility factors (5.25) since this removes the tangent pipe end rotation which would be predicted by the present type of theory. γ_o is taken in its usual form (5.21).

(5.4b) Flexibility Factors from Method No. 4

The convergence problems for bends with end constraints was discussed earlier in section (3.4c). Similar principles will be applied in the examination of the convergence of the present method./

method.

Parameters selected for checking convergence were,

$\lambda = 0.1 \quad R/r = 10 \quad \ell/r = 10 \quad \alpha = 180^\circ \quad \nu = 0.3$

The following table gives some flexibility factors obtained using these parameters;

Table 5.1 - Flexibility Convergence

$\lambda = 0.1, R/r = 10, \ell/r = 10, \alpha = 180^\circ, \nu = 0.3$

JT	MT	NT	K
1	1	1	5.14
1	1	2	6.96
1	2	1	7.65
2	1	1	7.48
2	2	2	13.45
2	2	3	13.94
2	3	2	13.94
3	2	2	14.21
3	3	3	14.81
4	4	4	14.90
5	5	5	14.91

From table (5.1) it can be seen that the flexibility factor from the (3, 3, 3) system (JT, MT, NT) , using 15 coefficients, has converged to within 1% of the (5, 5, 5) system using 35 coefficients. The (3, 3, 3) system was deemed to be satisfactory and should be valid for $\lambda \geq 0.1$, $R/r \leq 10$, $\ell/r \leq 10$, $\alpha \leq 180^\circ$. This was confirmed for several other sets of parameters.

For the current problem, flexibility factors are dependent on the pipe factor, λ, radius ratio, R/r, length/radius ratio, ℓ/r, and bend angle, α. Figure (5.2) shows the variation of the flexibility/

flexibility factor with tangent pipe length for $\alpha = 180^\circ$, $\lambda = 0.1$, and R/r = 10, 3, and 2. It can be seen that the flexibility factor increases rapidly with increasing length, until the tangent length is approximately $(2\pi r)$, the tube circumference, when it approaches a virtually constant value which is dependent on the radius ratio. Since the tangent pipes have flanged ends, $\ell/r = 0$ corresponds to a flanged bend. Note that because the displacements used here are different from Methods Nos. 1 and 2, the values at $\ell/r = 0$ are slightly different, but they are still lower than flexibilities from method No. 3. Because of the number of parameters involved in the current problem, it would be difficult to present flexibilit for various different tangent pipe lengths. Therefore, the remainder of the results presented in this section will be for $\ell/r = 10$, which figure (5.2) shows to be a reasonable approximation to an infinite tangent pipe length. These results are suitable for bend lengths greater than, $2\pi r$, with less than about 2% error from length variation.

Typical results from method No. 4 with (3, 3, 3) are given in figures (5.3), (5.4), (5.5) and (5.6) for bend angles of 180°, 90°, 45° and 20° respectively. Each figure contains curves for radius ratios (R/r) of 10, 3, and 2. Figure (5.3) shows a small variation with the radius ratio for 180° bends, but this increases with the lower bend angles. For R/r = 10, $\alpha = 180^\circ$ the flexibility factor is about 7% lower than that predicted by the axisymmetric type Karman [2] analysis, with the $(1 - \nu^2)$ term included [4], for bends without end constraints. For R/r = 2, $\alpha = 20^\circ$ it is only about one third of the corresponding Karman values. Thus the flexibility factors are significantly affected by tangent pipe end constraints/

constraints for lower bend angles and radius ratios.

Comparisons of published theoretical and finite element work with method No. 4 are given in figures (5.7) and (5.8). The present results are generally lower than the others which is perhaps to be expected from a lower bound energy type analysis. The factors from Rodabaugh et al [110], Ohtsubo and Watanabe [115] and Whatham and Thompson [119] appear to show reasonable agreement with each other, however a general conclusion cannot be drawn because of the restricted set of parameters they examined. Natarajan and Blomfield's [97] results are approximately 8% lower than these results which may be due to the $(1 - \nu^2)$ being included in their finite element, but not in the work of the others. Further evidence of this is provided by the comparisons given by each, of their methods without tangent pipes, with the Clark and Reissner [26] asymptotic formula, equation (1.15). The latter formula is included in figures (5.7) and (5.8).

Method No. 4 gives flexibility factors which are about 12% lower than those of Natarajan and Blomfield. This suggests that some improvements may be necessary to the present method. Method No. 5, to be presented in section (5.5) removes many of the assumptions included in method No. 4.

(5.5) Method No. 5: Numerical Solution

(5.5a) Formulation

This method is basically an extension of method No. 3 to include tangent pipes. As the numerical procedure is almost identical only the changes will be described in detail along with the/

the formulation of the total potential energy (T.P.E.) from the displacements, (5.9) and (5.13), and strains, (5.14) and (5.15), developed earlier.

The complete total potential energy expression for the bend-tangent assembly is,

$$V = 2C \int_{-\frac{\pi}{2}}^{\frac{\pi}{2}} \int_{0}^{\alpha/2} \left[(\epsilon_\phi + \epsilon_\theta)^2 - 2(1-\nu)(\epsilon_\theta \epsilon_\phi - \tfrac{1}{4}\gamma_{\theta\phi}^2) \right] r R' \, d\theta \, d\phi$$

$$+ 2D \int_{-\frac{\pi}{2}}^{\frac{\pi}{2}} \int_{0}^{\alpha/2} \left[(K_\phi + K_\theta)^2 - 2(1-\nu)(K_\theta K_\phi - K_{\theta\phi}^2) \right] r R' \, d\theta \, d\phi$$

$$+ 2C \int_{-\frac{\pi}{2}}^{\frac{\pi}{2}} \int_{0}^{L/2R} \left[(\epsilon_\phi + \epsilon_x)^2 - 2(1-\nu)(\epsilon_x \epsilon_\phi - \tfrac{1}{4}\gamma_{x\phi}^2) \right] r R \, d\theta \, d\phi$$

$$+ 2D \int_{-\frac{\pi}{2}}^{\frac{\pi}{2}} \int_{0}^{L/2R} \left[(K_\phi + K_x)^2 - 2(1-\nu)(K_x K_\phi - K_{x\phi}^2) \right] r R \, d\theta \, d\phi$$

$$- M\gamma$$

where $C = \frac{Et}{(1-\nu^2)}$, $D = \frac{Et^3}{12(1-\nu^2)}$, $R' = R + r \sin\phi$

... (5.28)

Note that the assemblies symmetries have been used in (5.28).

The rotation between the ends of the tangent pipes, γ , is found from $2\gamma_c$ (equation (5.5)) at $\theta = L/2R$, as,

$$\gamma = \frac{1}{R} \sum_{j=1}^{j\pi} \left[F_j \left(\frac{\alpha}{2} - \frac{\alpha}{j\pi} \sin\left(\frac{j\pi}{2}\right) \right) + D_j \left(\frac{j\pi}{\alpha} \right) \sin\left(\frac{j\pi}{2}\right) + G_j \, 2(j+1)\left(\ell/R\right)^j \right]$$

... (5.29)

The strains and curvatures in equations (5.14) and (5.15) can/

can be substituted into (5.28) to give the complete T.P.E. function. This is then non-dimensionalised using,

$$\bar{V} = V \Big/ \left(\frac{2M\gamma_0}{(1-\nu^2)\pi\alpha}\right)$$

... (5.30)

Using this the T.P.E. function (5.28) can be written as, (see section (3.5f)

$$\bar{V} = \bar{\Phi} - (1-\nu^2)\frac{\pi\alpha}{2}\frac{\gamma}{\gamma_0}$$

where for this case,

$$\bar{\Phi} = \int_{-\frac{\pi}{2}}^{\frac{\pi}{2}}\int_{0}^{\frac{\alpha}{2}}\Big[(\bar{\epsilon}_\phi+\bar{\epsilon}_\theta)^2 - 2(1-\nu)\left(\bar{\epsilon}_\theta\bar{\epsilon}_\phi - \tfrac{1}{4}\bar{\gamma}^2_{\theta\phi}\right) + \frac{\lambda^2}{12}\left\{(\bar{K}_\phi+\bar{K}_\theta)^2 - 2(1-\nu)\left(\bar{K}_\theta\bar{K}_\phi - \bar{K}^2_{\theta\phi}\right)\right\}\Big] Z\, d\theta d\phi$$

$$+ \int_{-\frac{\pi}{2}}^{\frac{\pi}{2}}\int_{\frac{\alpha}{2}}^{\gamma_2 R}\Big[(\bar{\epsilon}_\phi+\bar{\epsilon}_x)^2 - 2(1-\nu)\left(\epsilon_x\epsilon_\phi - \tfrac{1}{4}\bar{\gamma}^2_{x\phi}\right) + \frac{\lambda^2}{12}\left\{(\bar{K}_\phi+\bar{K}_x)^2 - 2(1-\nu)\left(\bar{K}_x\bar{K}_\phi - \bar{K}^2_{x\phi}\right)\right\}\Big] Z\, d\theta d\phi$$

$$Z = 1 + \frac{r}{R}\sin\phi \qquad \text{... (5.31)}$$

The non-dimensionalised strains, $\bar{\epsilon}$, and curvatures $\bar{K}$, are,

$$\bar{\epsilon} = \epsilon\frac{R\alpha}{r\gamma_0} \quad , \quad \bar{K} = K\frac{r\alpha}{R\gamma_0}$$

... (5.32)

The/

The displacement coefficients are non-dimensionalised using,

$$\bar{A}_{mn} = A_{mn}\left(\frac{\alpha}{r\gamma_0}\right) \quad , \quad \bar{B}_{mn} = B_{mn}\left(\frac{\alpha}{r\gamma_0}\right) \quad , \quad \bar{C}_{mn} = C_{mn}\left(\frac{\alpha}{r\gamma_0}\right)$$

$$\bar{D}_j = \frac{D_j}{R\gamma_0} \quad , \quad \bar{F}_j = \frac{F_j}{R\gamma_0} \quad , \quad \bar{G}_j = \frac{G_j}{R\gamma_0} \quad , \quad \bar{H}_j = \frac{H_j}{R\gamma_0}$$

... (5.33)

Appendix (4) contains the strains from (5.14) and (5.15) in a form which makes programming for a computer relatively straightforward. A listing of the computer program is given in Appendix (5).

(5.5b) Flexibility and Stress Concentration Factors

The flexibility factors can be determined from the end rotation (5.29) and the definition given in section (1.1), as

$$K = (\gamma - 2\gamma^T)/\gamma_0$$

$$= \sum_{j=1}^{m}\left[\bar{F}_j\left(\frac{\alpha}{2}-\left(\frac{\alpha}{j\pi}\right)\sin\left(\frac{j\pi}{2}\right)\right)+\bar{D}_j\left(\frac{j\pi}{\alpha}\right)\sin\left(\frac{j\pi}{2}\right)+\bar{G}_j\,2(j+1)(\ell/R)^j\right]-(1-\nu^2)\frac{2\ell}{R\alpha}$$

where $\gamma^T = (1-\nu^2)\frac{M\ell}{EI}$, $\gamma_0 = \frac{MR\alpha}{EI}$ ... (5.34)

γ^T is the end rotation of one of the tangent pipes loaded on its own, as would be predicted by an energy analysis of the type used herein. This causes the additional flexibility of the assembly, created by the bend and the tangents to be included in the bend flexibility factor so that flexibility factors will not be required for the tangent pipes in the analysis of piping systems.

Stress/

Stress concentration factors (S.C.Fs.) can be determined as described in section (3.5i).

(5.6) Theoretical Results from Method No. 5

(5.6a) Integration Convergence

In the flanged bend problem, the T.P.E. was integrated numerically in the θ and ϕ dimensions using an extension of Simpson's one third rule (3.5d). The number of integration points found to be necessary for convergence of the flexibility factors was $P_\theta = 9$ and $P_\phi = 17$. In the current problem, the T.P.E. function also has to be integrated along the tangent pipe. The number of points found necessary for this using $\lambda = 0.07$, $R/r = 10$, $\ell/r = 10$, $\alpha = 180^\circ$ and $\nu = 0.3$ was $P_x = 9$. $P_\theta = 9$, $P_x = 9$ and $P_\phi = 17$ was used for the results given herein unless otherwise stated.

(5.6b) Series Convergence

Series convergence was examined for $\lambda = 0.07$, $R/r = 10$, $\ell/r = 10$, $\alpha = 180^\circ$ and $\nu = 0.3$ using the principles discussed in section (3.4c). As with the flanged bend, section (3.6c), JT = 5, MT = 5 and NT = 6 was found to give satisfactory convergence. This requires the use of 110 displacement coefficients.

(5.6c) Flexibility Factors from Method No. 5

Typical variations of flexibility factor with tangent pipe length are shown in figure (5.9). It can be seen that the flexibility/

flexibility of a bend tends to a constant value as the tangent pipe length increases. As with method No. 4, section (5.4b), $\ell/r = 10$ is a reasonable approximation to an infinite tangent pipe length and the results obtained from this value can be used for $\ell/r > 2\pi$ with less than 2% error from length variation.

Flexibility factors for bends with connected flanged tangents of length greater that $2\pi r$ are given in figures (5.10), (5.11), (5.12) and (5.13) for 180°, 90°, 45° and 20° bends respectively. Each figure has curves for bend radius ratios (R/r) of 10, 3, and 2. The results were all obtained using $\ell/r = 10$. The figures show that bends with shorter angles and smaller radius ratios have the lowest flexibilities. It can be seen that tangent/bend assemblies have a relatively small variation of flexibility with radius ratio, much less than flanged bends. The difference between the flexibilities of bends with R/r = 3 and 2 is less than 6% for bend angles, α, greater than 90°, although this increases to 13% for 45° bends. The reduction with bend angle is much greater, e.g. about 25% between 180° and 45° for R/r = 3.

The variation of flexibility with pipe factor is approximately linear on the log-log plots for all bend angles and radius ratios, over reasonably wide practical ranges of pipe factor. Use was made of this in deriving the approximate formulae given in figure (5.14). The formulae,

$$K = \mu_k \frac{F}{\lambda} \cdot$$

where

R/r	10	3	2
F	1.54	1.50	1.46

... (5.35)

employs/

employs a correction factor μ_k , given in figure (5.14), which is dependent on the bend angle and the radius ratio. These formulae have an accuracy better than 5% for flexibilities greater than 2. Generally, they should not be used for $K < 2$.

Comparisons with published theoretical and finite element work, and method No. 4, are given in figures (5.15) and (5.16). The present method agrees relatively closely with the finite element work of Natarajan and Blomfield. This latter work forms the basis of the results given by the Engineering Sciences Data Unit (E.S.D.U.) [129] and it was from this that the results were generally taken. It can be seen that method No. 4 predicts flexibility factors which are about 12% lower than method No. 5. This improves at higher λ. The flexibility factors given by Rodabaugh et al [110], Ohtsubo and Watanabe [115] and Whatham and Thompson [119] show reasonable agreement with each other and are about 8% higher than those from the present method. As suggested in section (5.4b), this may be due to the familiar $(1 - \nu^2)$ term which plagued the earlier analyses of bends without end constraints. Also given in figures (5.15) and (5.16) are the flexibility factors recommended by A.S.M.E. [133] and most other codes (see section (1.4)). Clearly this can be seriously in error for smaller angle bends of short radius.

(5.6d) Stress Concentration Factors from Method No. 5

Stress Distributions

Some typical distributions for meridional and circumferential stresses are given in figures (5.17) and (5.18) respectively, for $\alpha = 90^\circ$, $\lambda = 0.1$, $\ell/r = 10$ and $\nu = 0.3$. Both figures contain graphs/

graphs for R/r = 10 and 2.

From figure (5.17) it can be seen that the peak meridional stress occurs on the inside surface, close to $\phi = 0$. Note that it is removed toward the intrados by about 2° for R/r = 10 and 6° for R/r = 2, i.e. it moves away from $\phi = 0$ as R/r reduces. The maximum stress is shown to decrease as R/r reduces but this is not always true for other bend geometries, as will be seen later. Also, for bends with flexibility factors less than about three, the maximum meridional stress usually occurs on the outside surface at the intrados. The peak stress is always at the centre of the bend, $\theta = 0$.

Figure (5.18) shows that the position of the maximum circumferential stress is dependent on the bend geometry. For R/r = 10 it is on the inside surface at about $\phi = -15^\circ$ and for R/r = 2 it is on the outside surface at about $\phi = -32^\circ$. For bends with higher flexibility factors, $\hat{\sigma}_\theta$ usually occurs on the outside surface, and between $\phi = 0$ and the extrados. For bends with lower flexibilities, $K < 2$, the maximum often occurs on the outside surface at the intrados.

Maximum Meridional S.C.Fs.

Maximum meridional S.C.Fs. are given in figures (5.19), (5.20), (5.21) and (5.22) for bend angles of 180°, 90°, 45° and 20° respectively, each figure containing curves for R/r = 10, 3, and 2. All results were obtained at $\theta = 0$, with $\ell/r = 10$.

Figure (5.19) shows that stresses reduce with R/r for $\alpha = 180^\circ$ but for lower bend angles, figures (5.20), (5.21) and (5.22), the reverse is more often true. The change in the shape of/

of the curves, for lower bend angles at higher values of the pipe factor, λ , usually corresponds to the change in the position of the peak meridional stress as explained earlier.

Maximum Circumferential S.C.Fs.

Maximum circumferential S.C.Fs. are given in figures (5.23), (5.24), (5.25) and (5.26) for the same geometries as before.

The complex shapes of these curves are related to the changing positions of the maximum stress as previously discussed. At lower pipe factors the maximum circumferential stress increases with radius ratio, but it decreases with radius ratio at higher factors.

Overall Maximum S.C.Fs.

The highest stress for bends with flanged tangents, with $\ell/r \geqslant 2\pi$, usually is the peak meridional stress ($\hat{\sigma}_\phi$). For low bend angles and radius ratios, e.g. $\theta = 20^\circ$ and $R/r = 2$, the maximum can however be the peak circumferential stress ($\hat{\sigma}_\theta$).

An approximate formula for the maximum meridional S.C.F. is given in figure (5.27), as

$$\hat{\sigma} = \mu \frac{2.27}{\lambda^{0.6}} \qquad \ldots (5.36)$$

This formula, using the correction factor, μ, given in figure (5.27) has an accuracy of better than 5% for stress factors greater than about 2.5. It should only be used for R/r between 2 and 3 and bend angles greater than about 20°.

Comparisons of Theoretical Peak S.C.Fs./

Comparisons of Theoretical Peak S.C.Fs.

Publications on end effects tend to only present a set of values for flexibility factors. Figure (5.28) gives a comparison of method No. 5 with most of the available stress data.

It can be seen that Natarajan and Blomfield's [97] stresses are about 10% higher than those from method no. 5, whereas those of Ohtsubo and Watanabe [115] are almost coincident with the present values. This is in contrast to the comparison obtained for flexibility factors. The results from Rodabaugh et al [110] give rough agreement with [97]. Also given in figure (5.28) are the results from the Clark and Reissner [26] asymptotic formula,

$$\hat{\sigma}_{\phi} = \frac{1.95}{\lambda^{2/3}} \qquad \ldots (5.37)$$

It can be seen that for the particular geometries considered, this overestimates the meridional stresses.

(5.7) Conclusion

A numeric, theoretical solution technique, method No. 5, has been presented which provides results for smooth pipe bends with connected flanged tangent pipes. The derived flexibility and stress concentration factors compare favourably with published theoretical data. Approximate formulae were developed which give the flexibility and stress factors over a wide range of practical geometries, to within 5% of those from Method No. 5.

A simpler technique, method no. 4, was examined and was shown to give bend flexibility factors which were less than 12% lower than those from method No. 5, for pipe factors greater than 0.1.

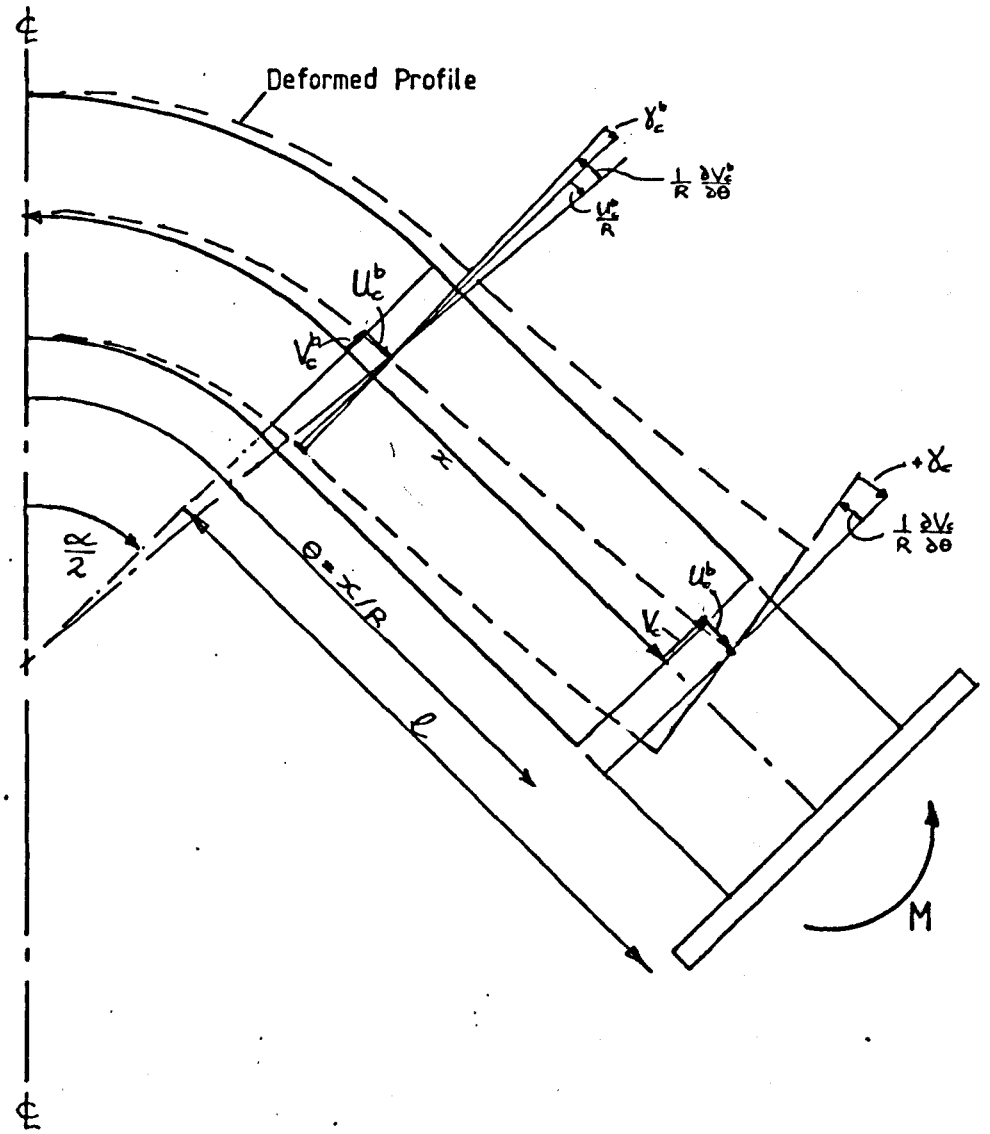

Rigid Section Displacements

Figure (5.1)

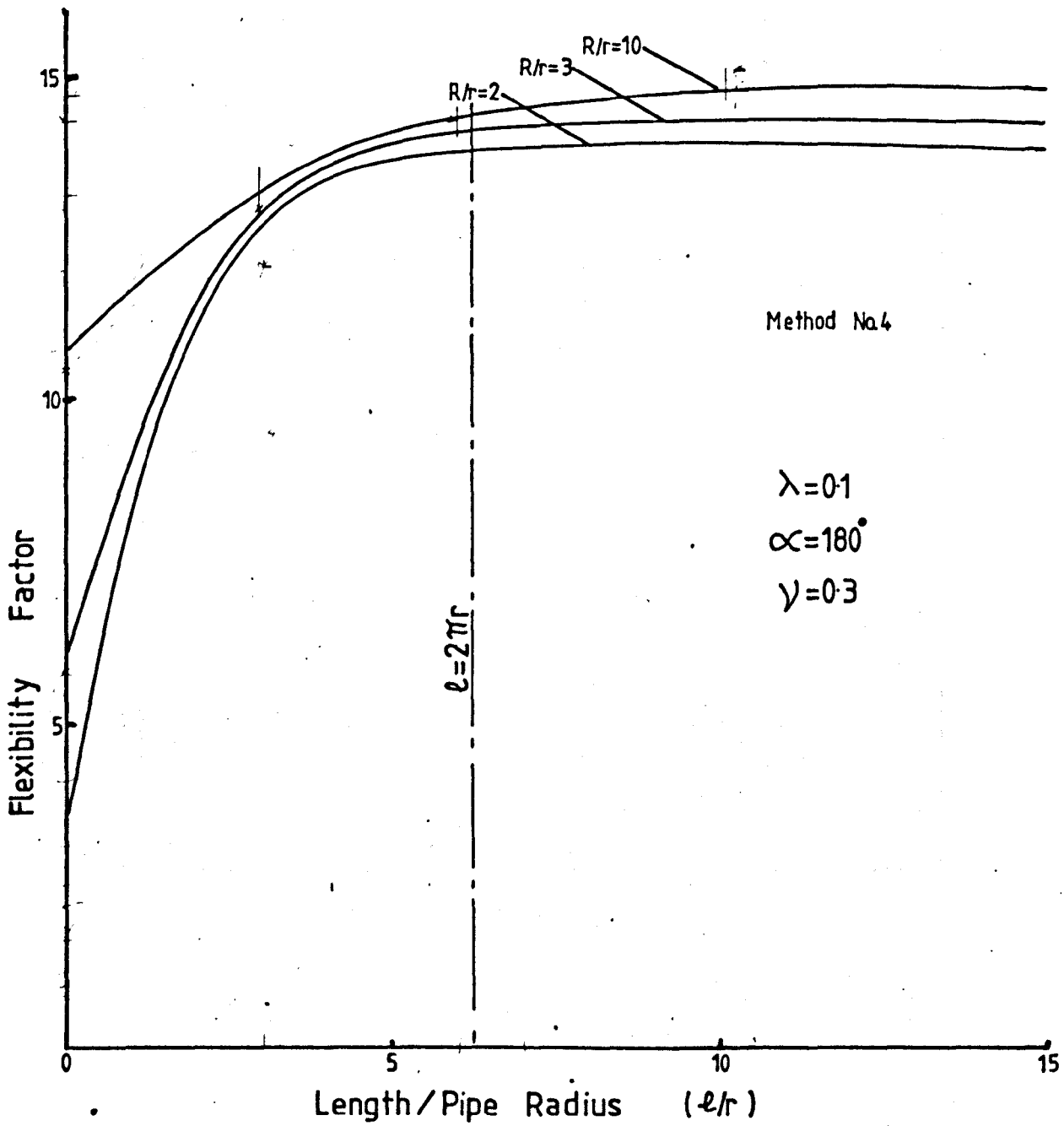

Variation of Flexibility with Tangent Pipe Length

Figure (5·2)

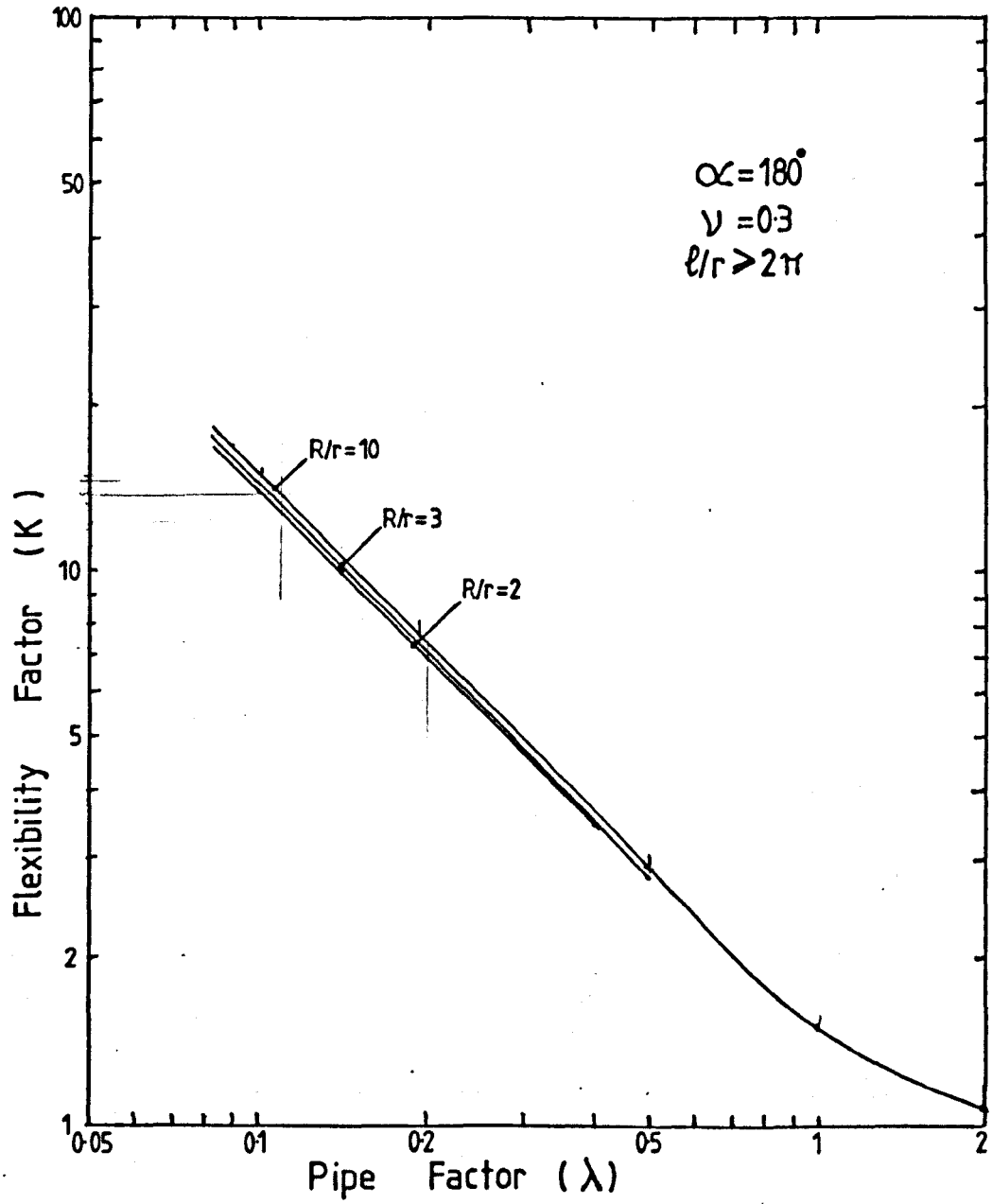

Flexibility Factors from Method No.4

Figure (5.3)

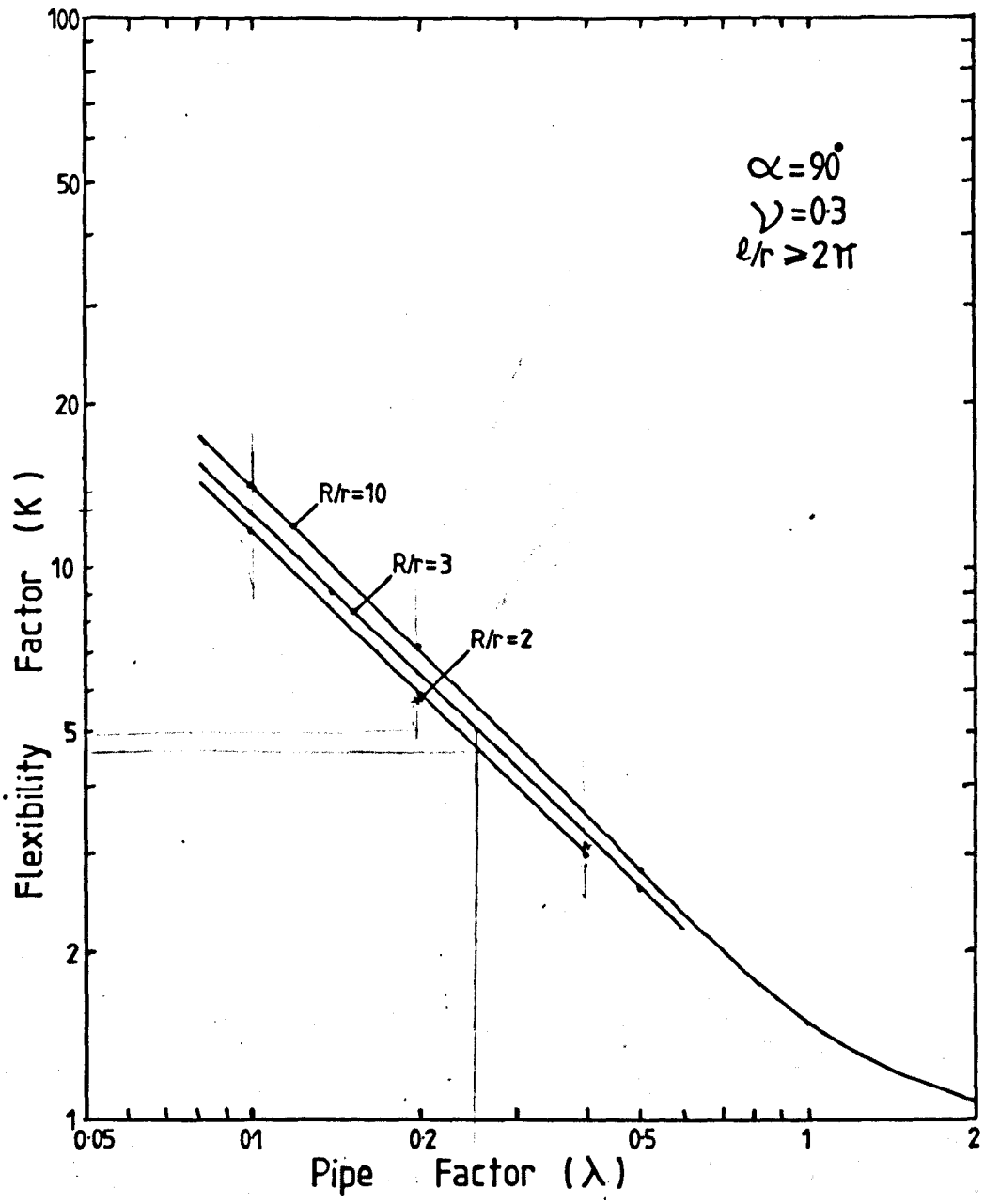

Flexibility Factors from Method No.4

Figure (5.4)

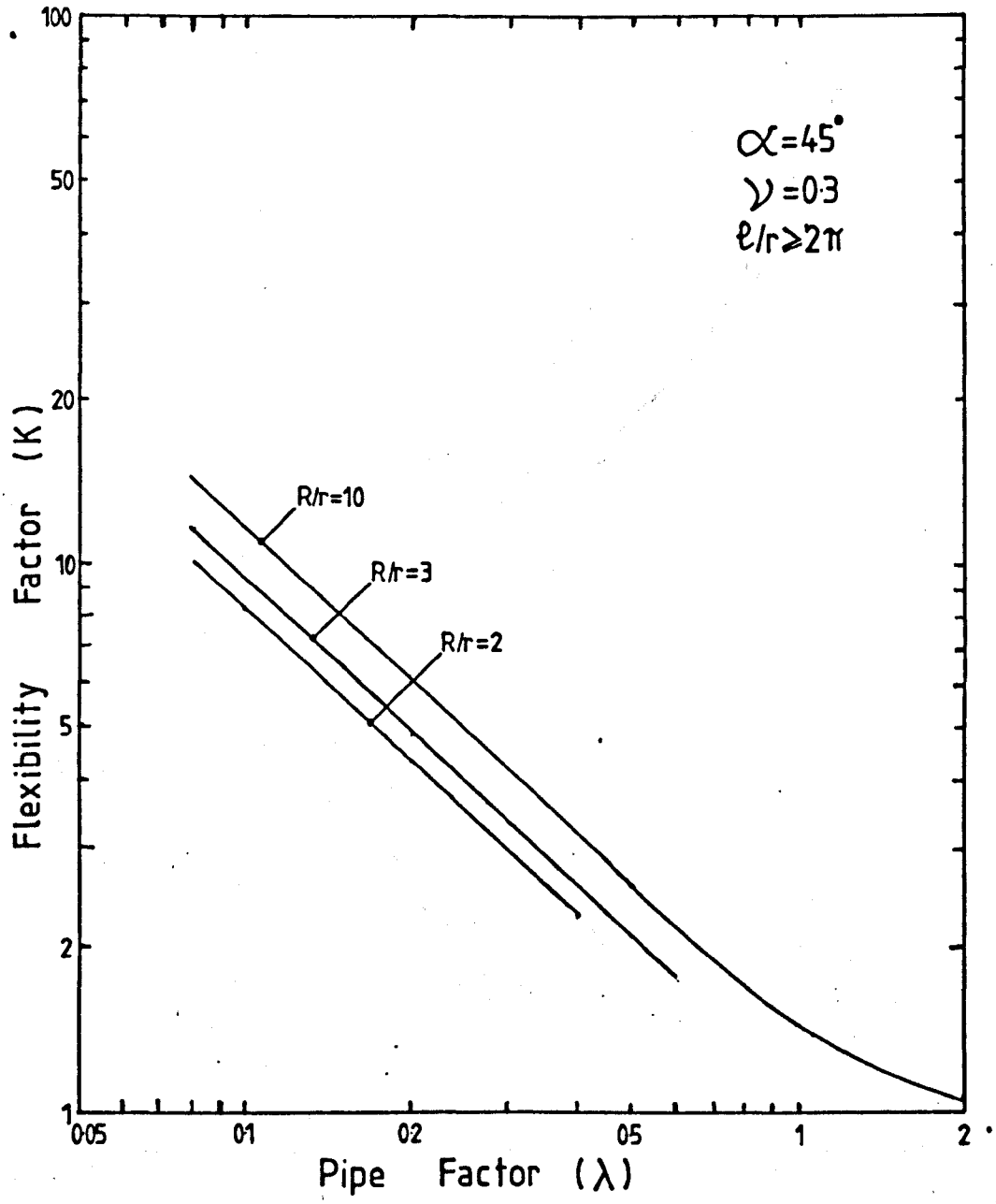

Flexibility Factors from Method No.4

Figure (5.5)

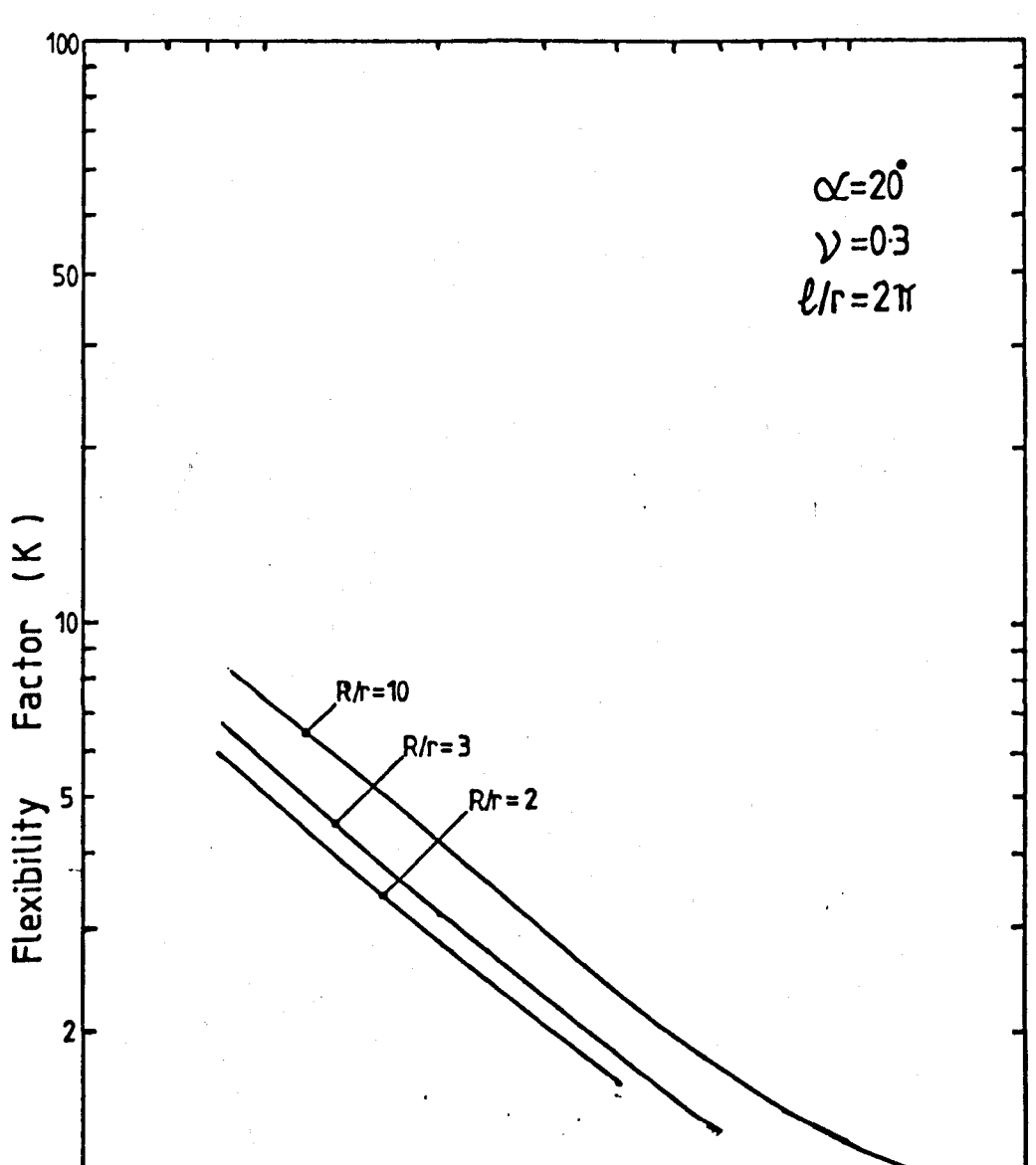

Flexibility Factors from Method No.4

Figure (5.6)

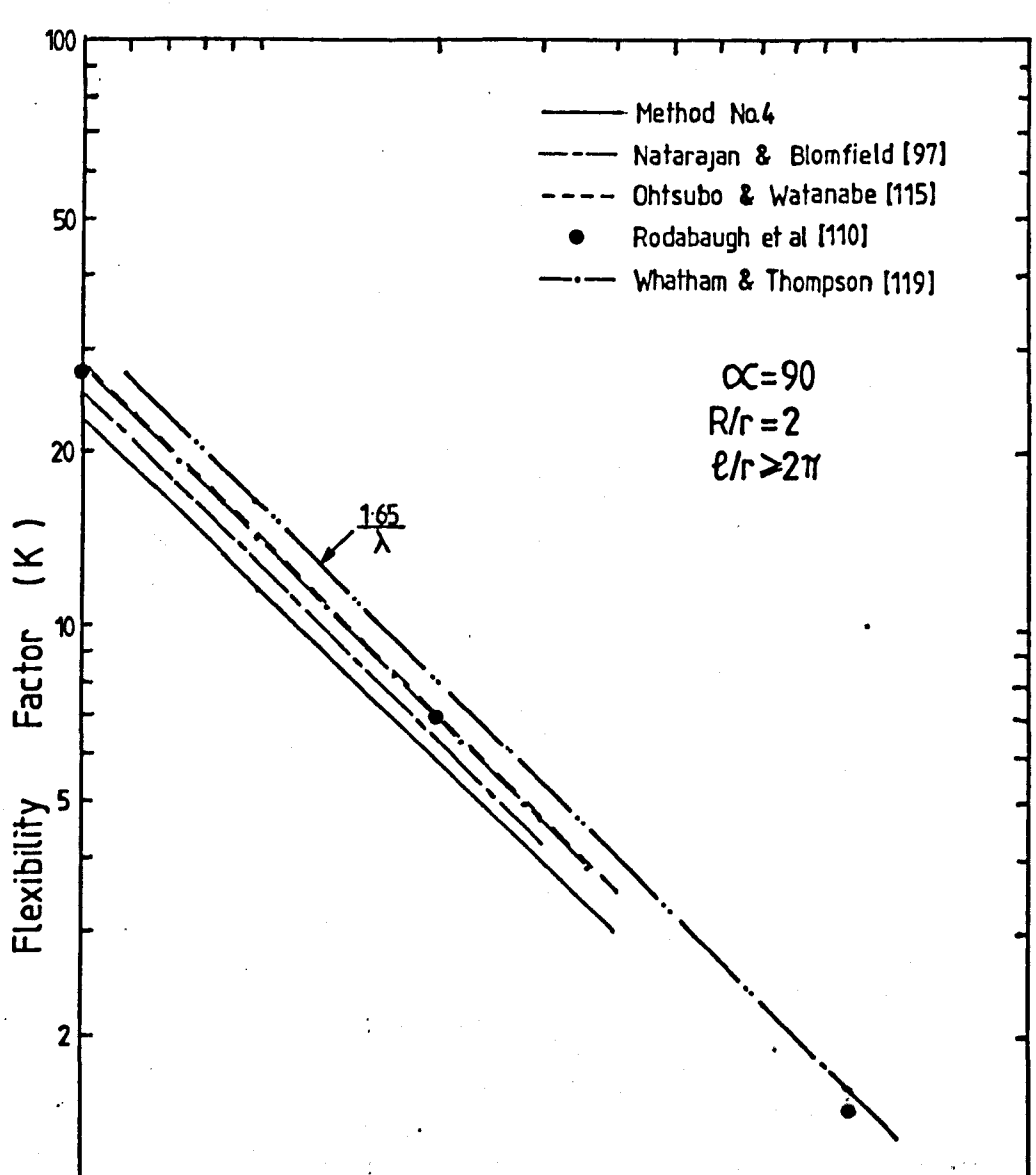

Comparison of Flexibility Factors

Figure (5.7)

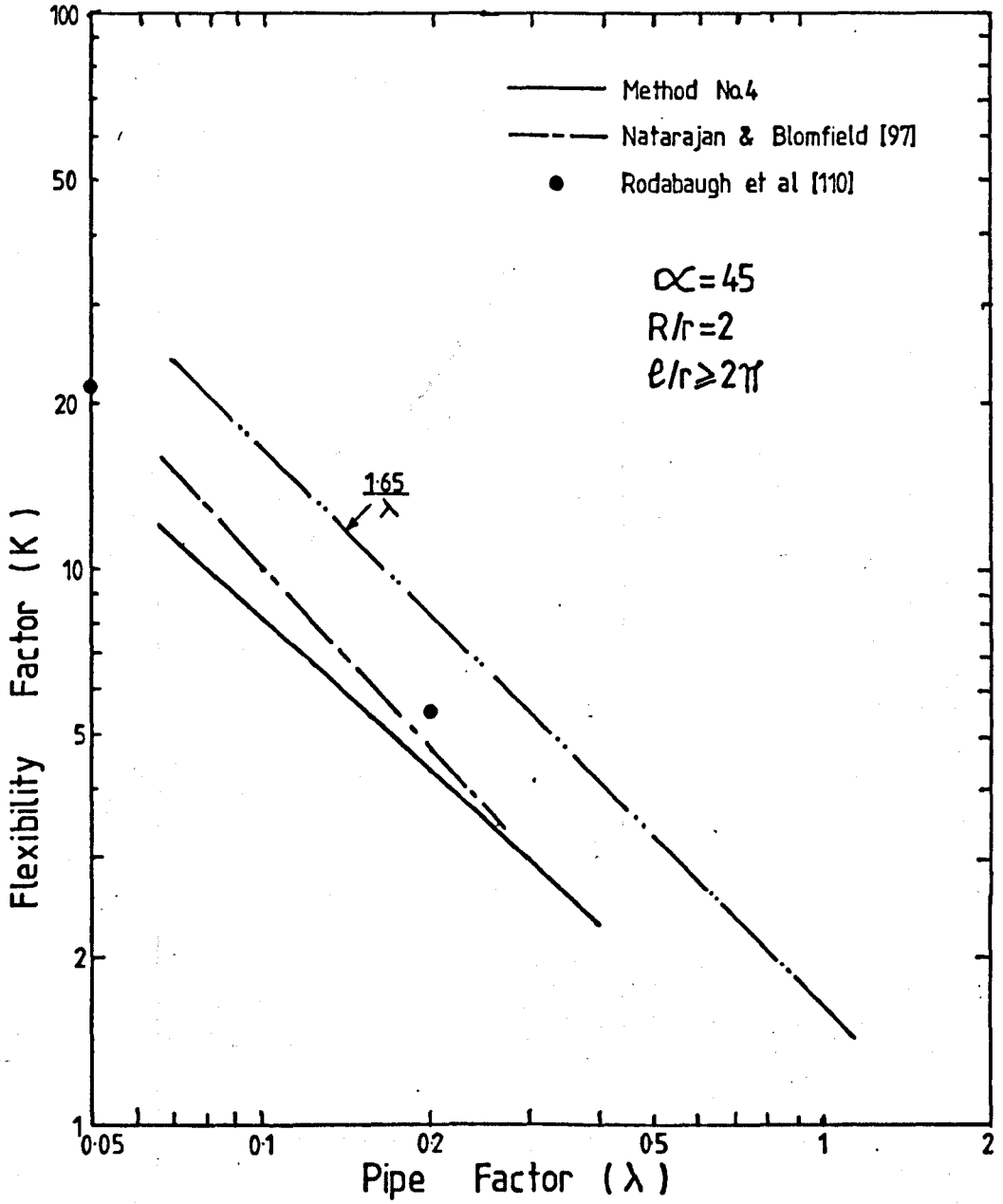

Comparison of Flexibility Factors

Figure (5.8)

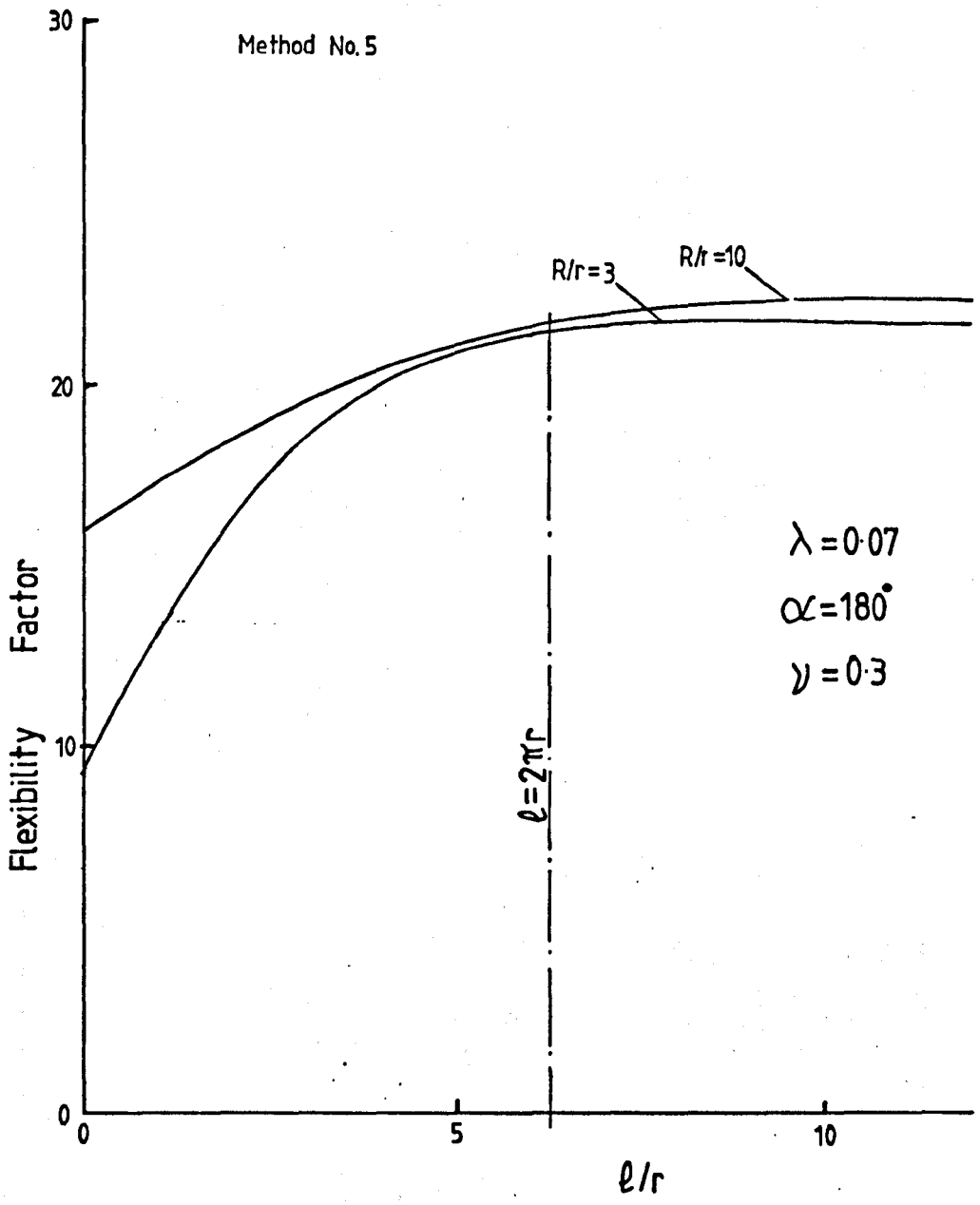

Variation of Flexibility with Tangent Pipe Length

Figure (5.9)

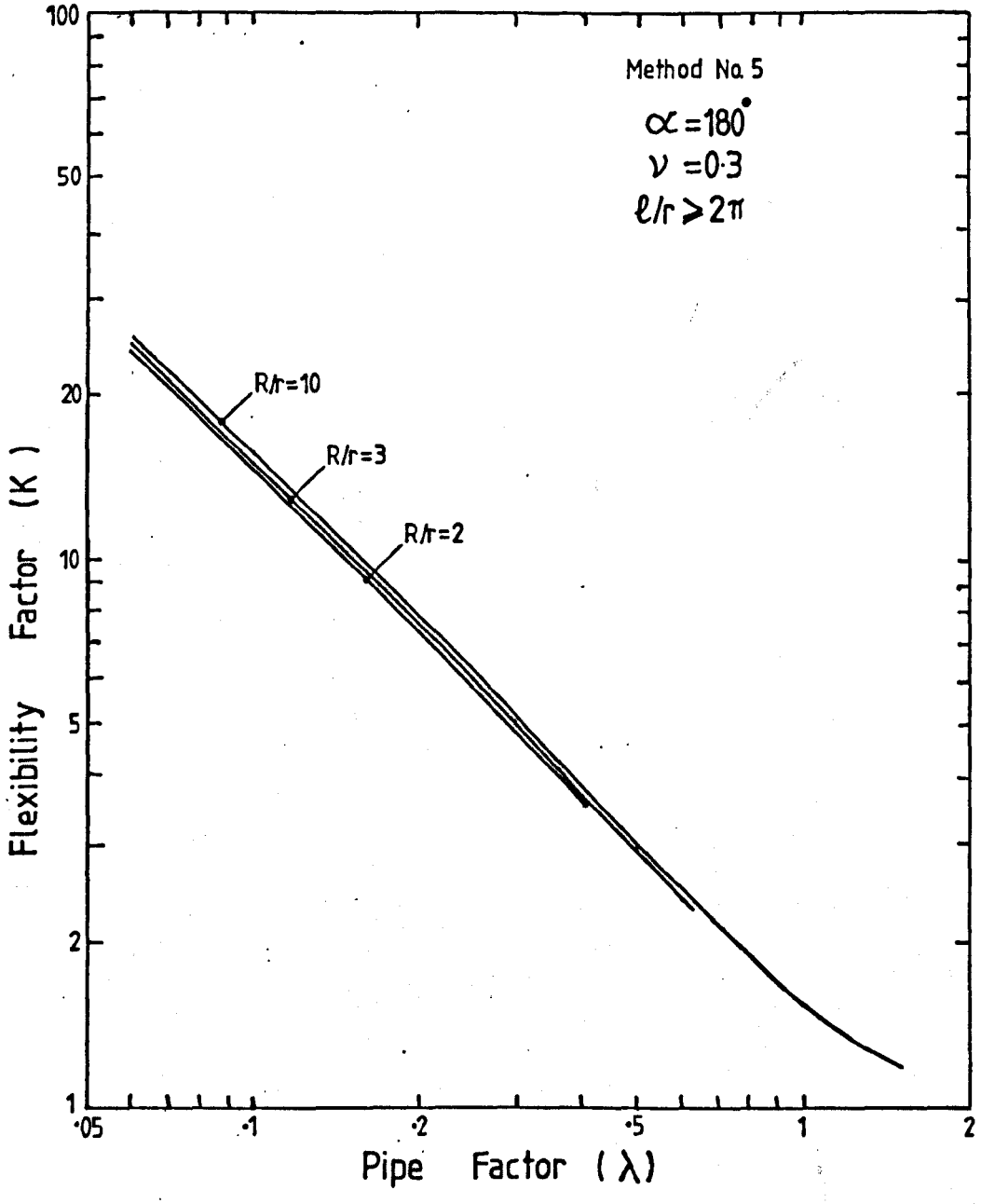

Flexibility Factors
for $\alpha=180^{\circ}$

Figure (5.10)

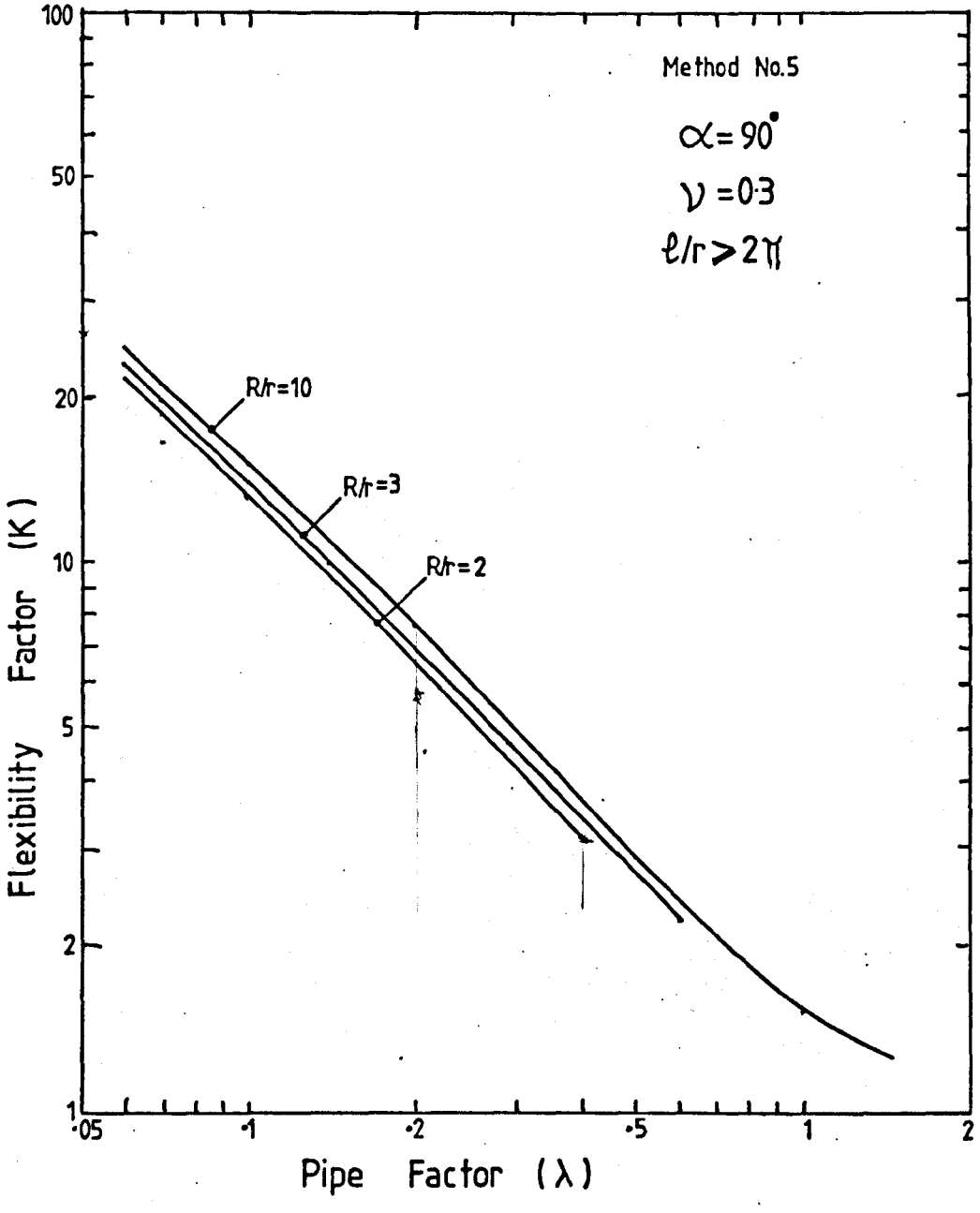

Flexibility Factors for $\alpha=90^{\circ}$

Figure (5.11)

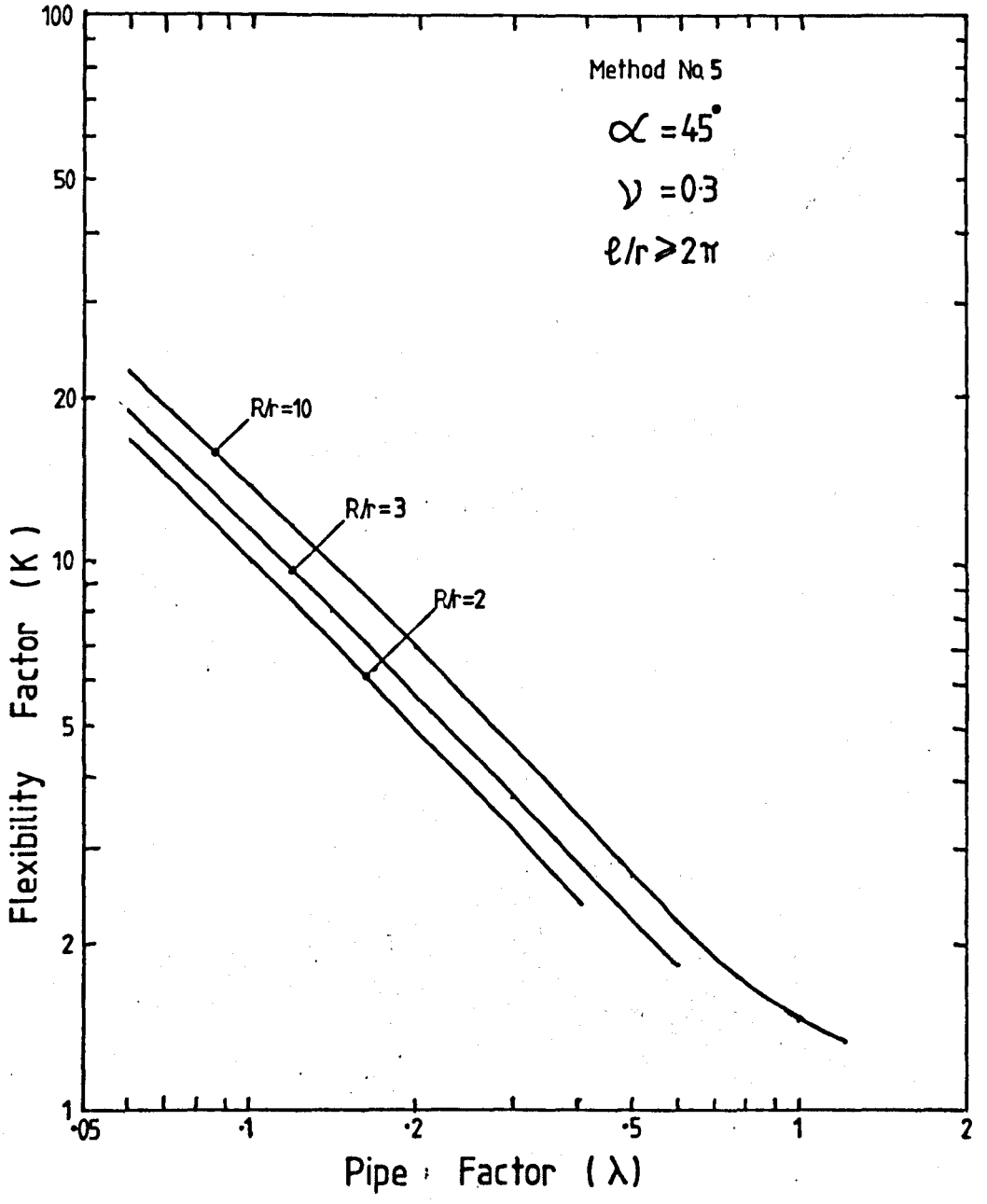

Flexibility Factors for $\alpha=45^{\circ}$

Figure (5.12)

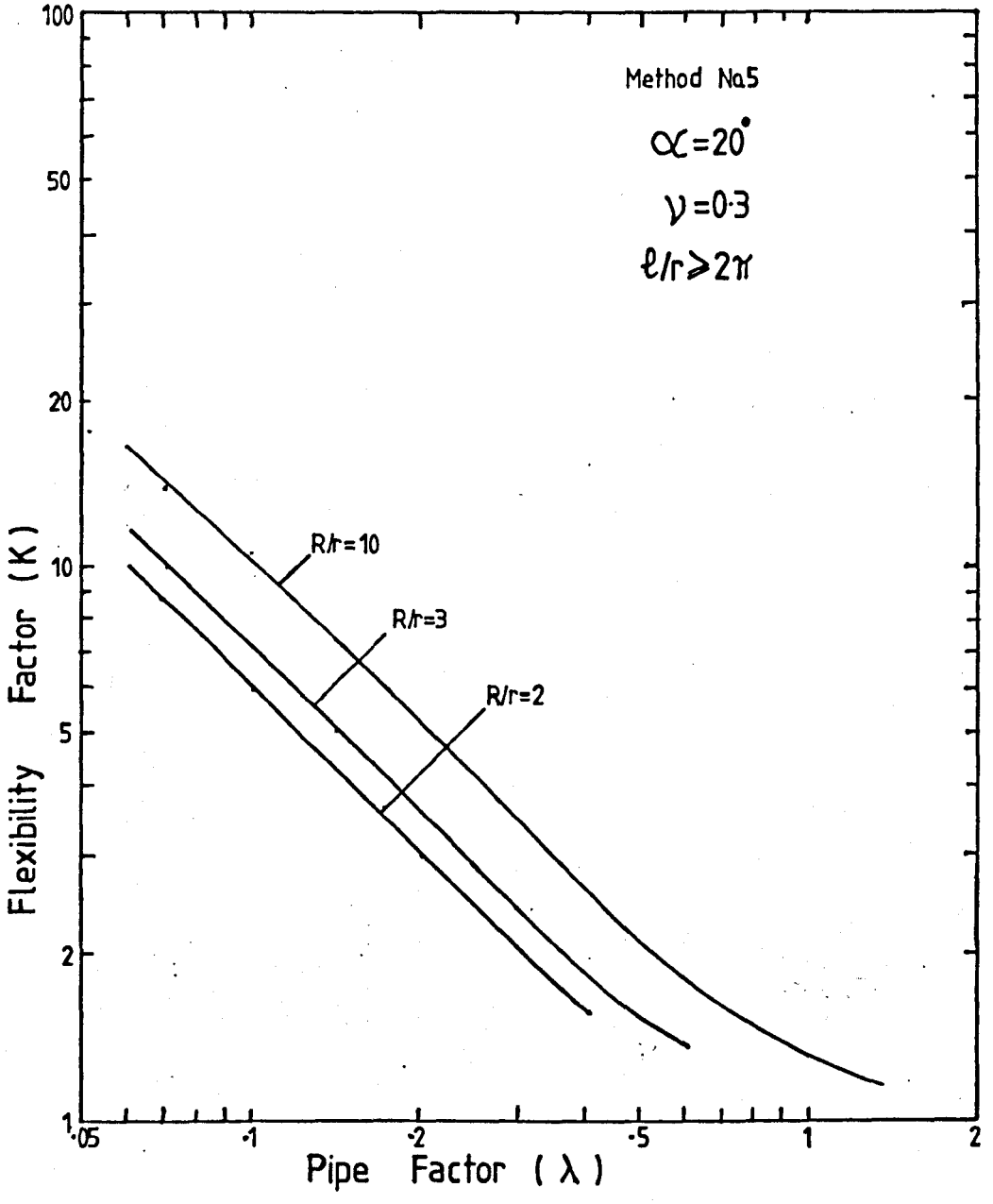

Flexibility Factors for $\alpha=20^{\circ}$

Figure (5.13)

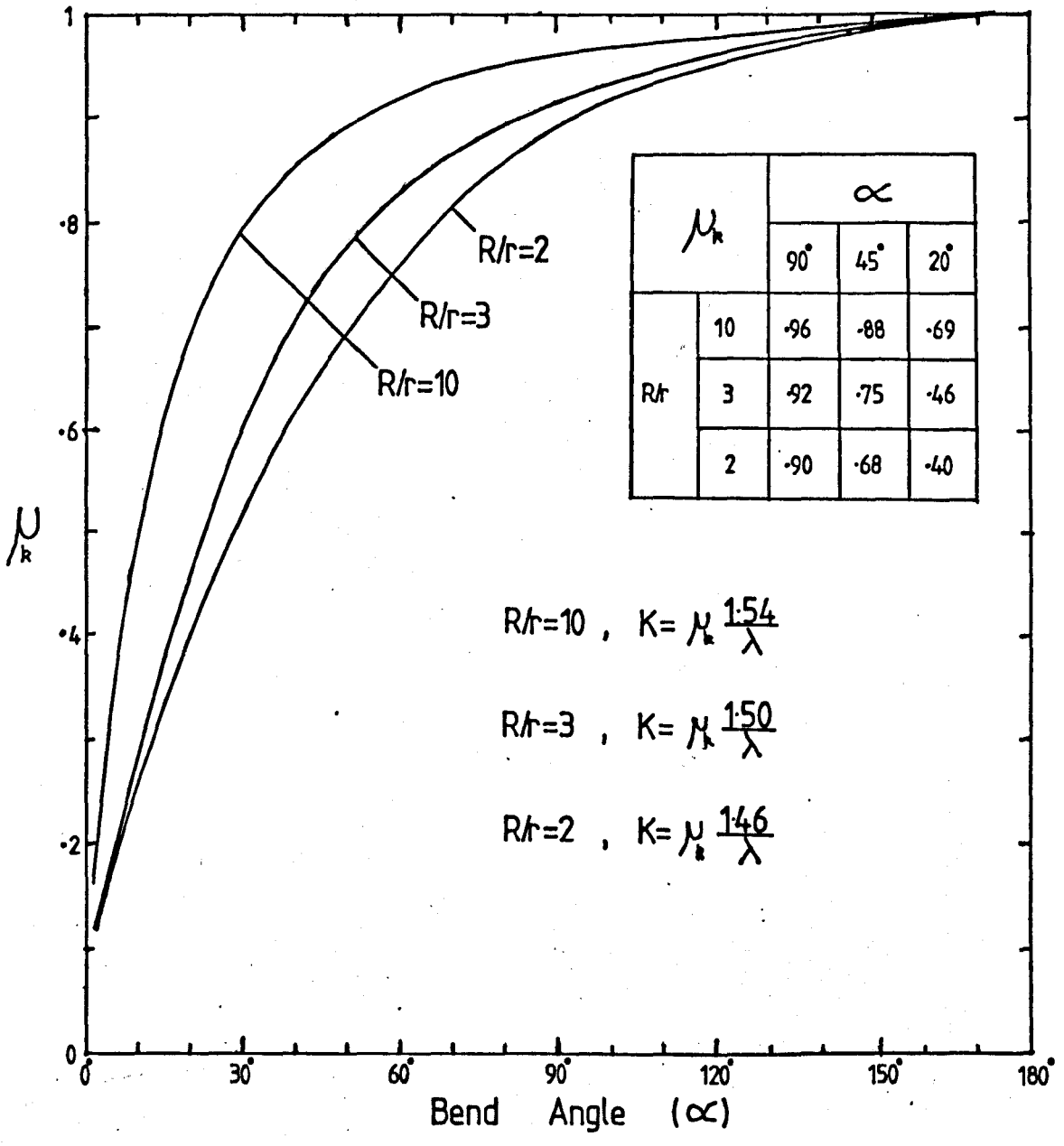

μ_k		∝		
		90°	45°	20°
R/r	10	·96	·88	·69
	3	·92	·75	·46
	2	·90	·68	·40

Approximate Formulae for Flexibility Factors

Figure (5.14)

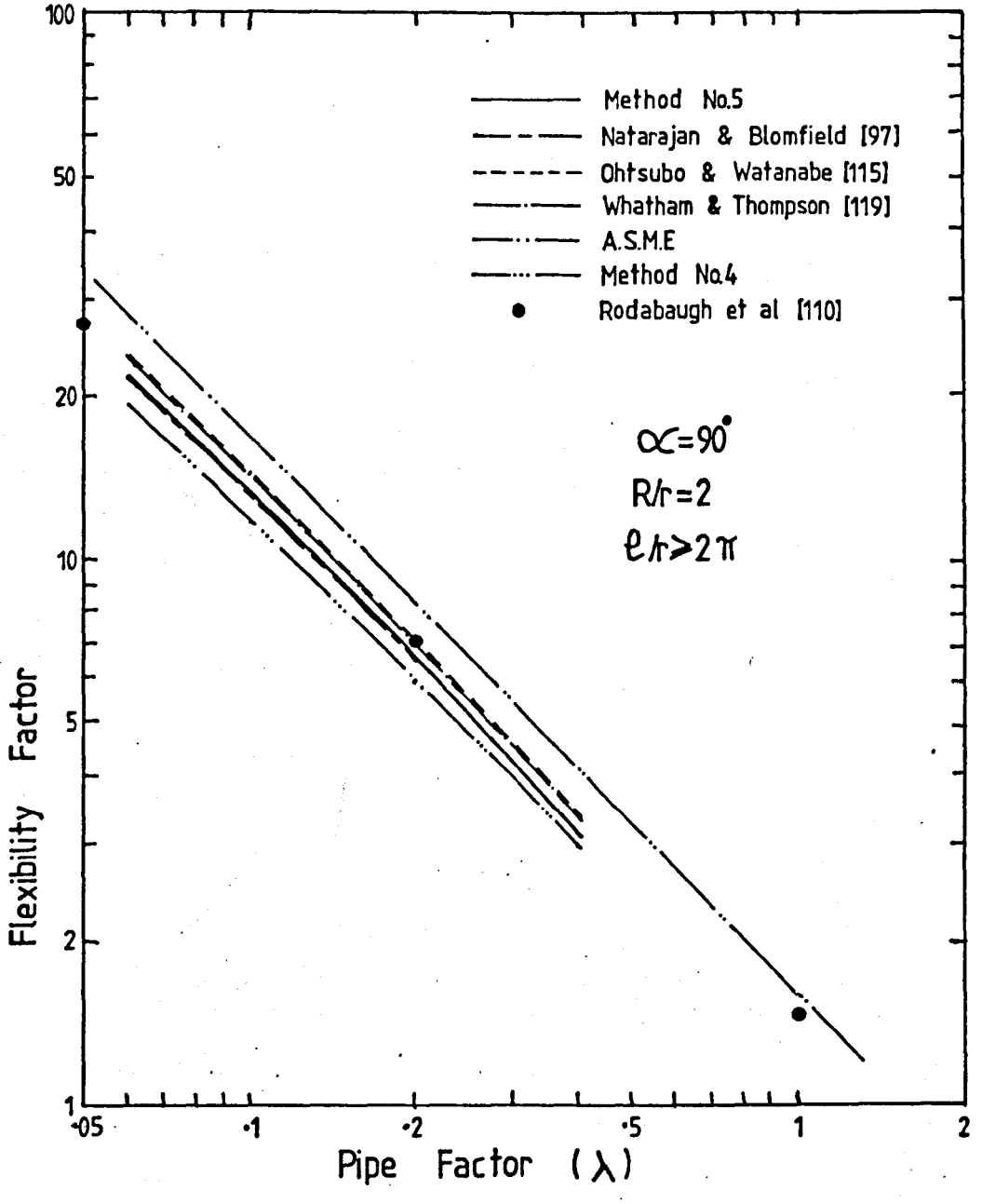

Comparison of Flexibility Factors

Figure (5.15)

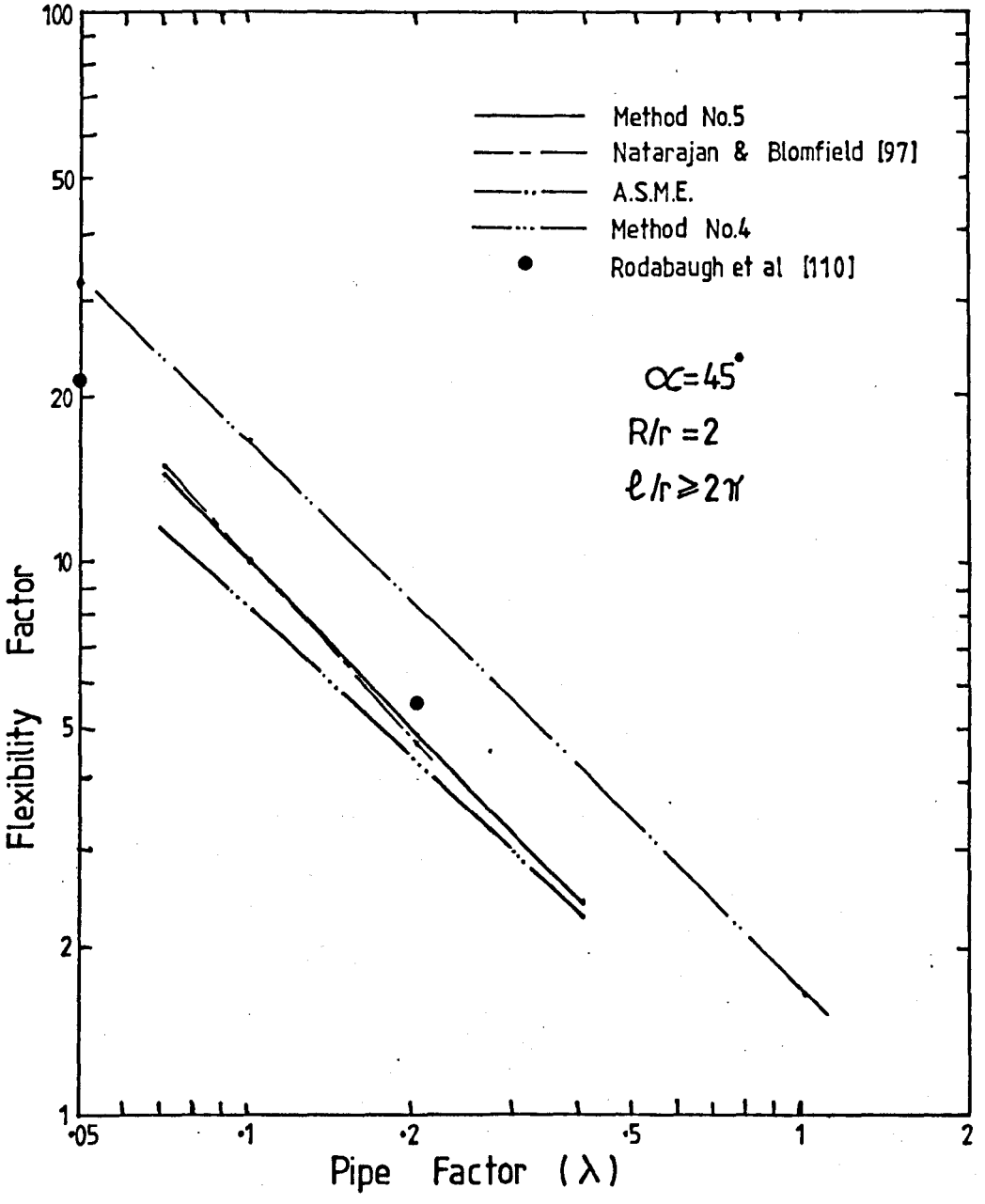

Comparison of Flexibility Factors

Figure (5.16)

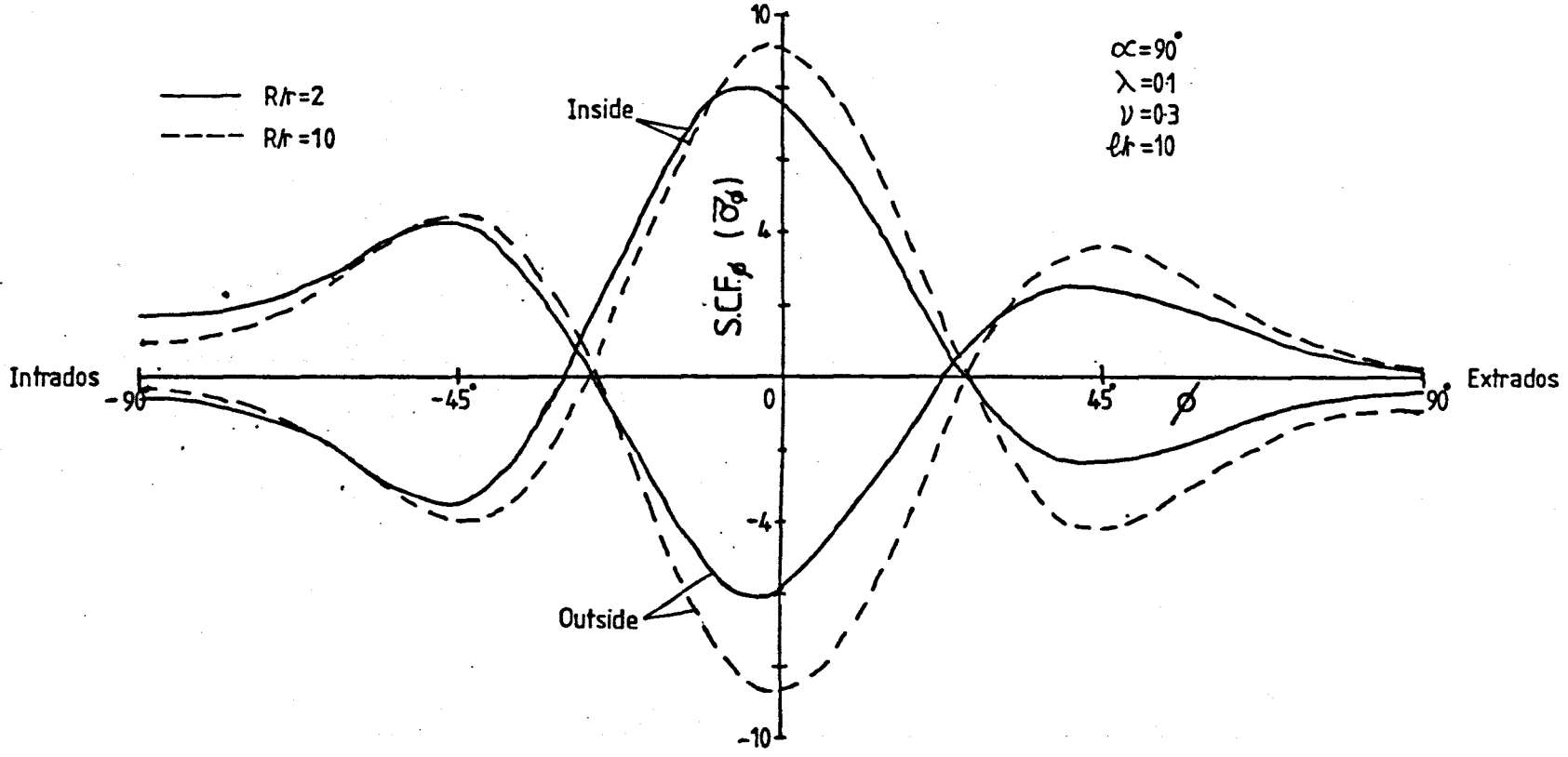

Typical Meridional Stress Distributions at $\theta = 0^{\circ}$

Figure (5.17)

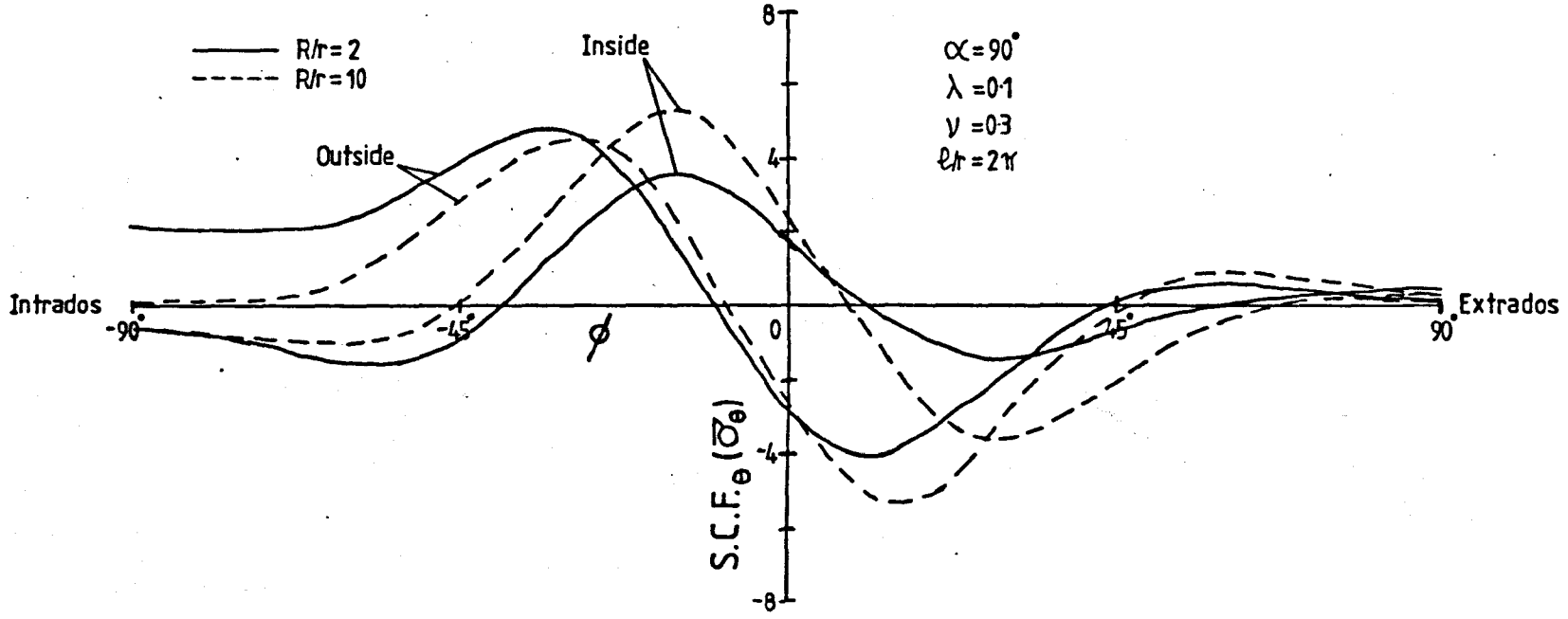

Typical Circumferential Stress Distributions at $\theta = 0^\circ$

Figure (5.18)

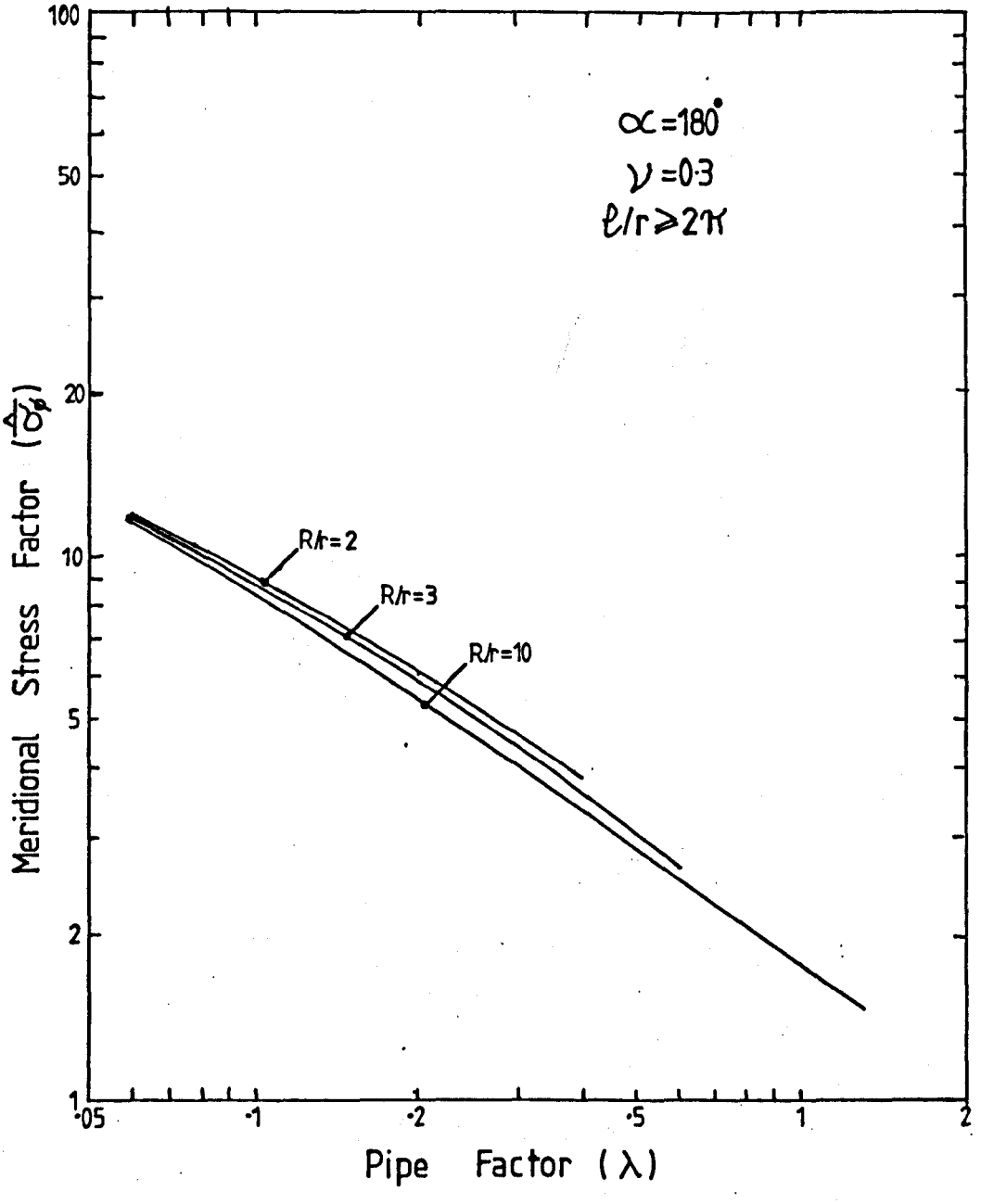

Meridional Stress Factors for $\alpha = 180^\circ$

Figure (5.19)

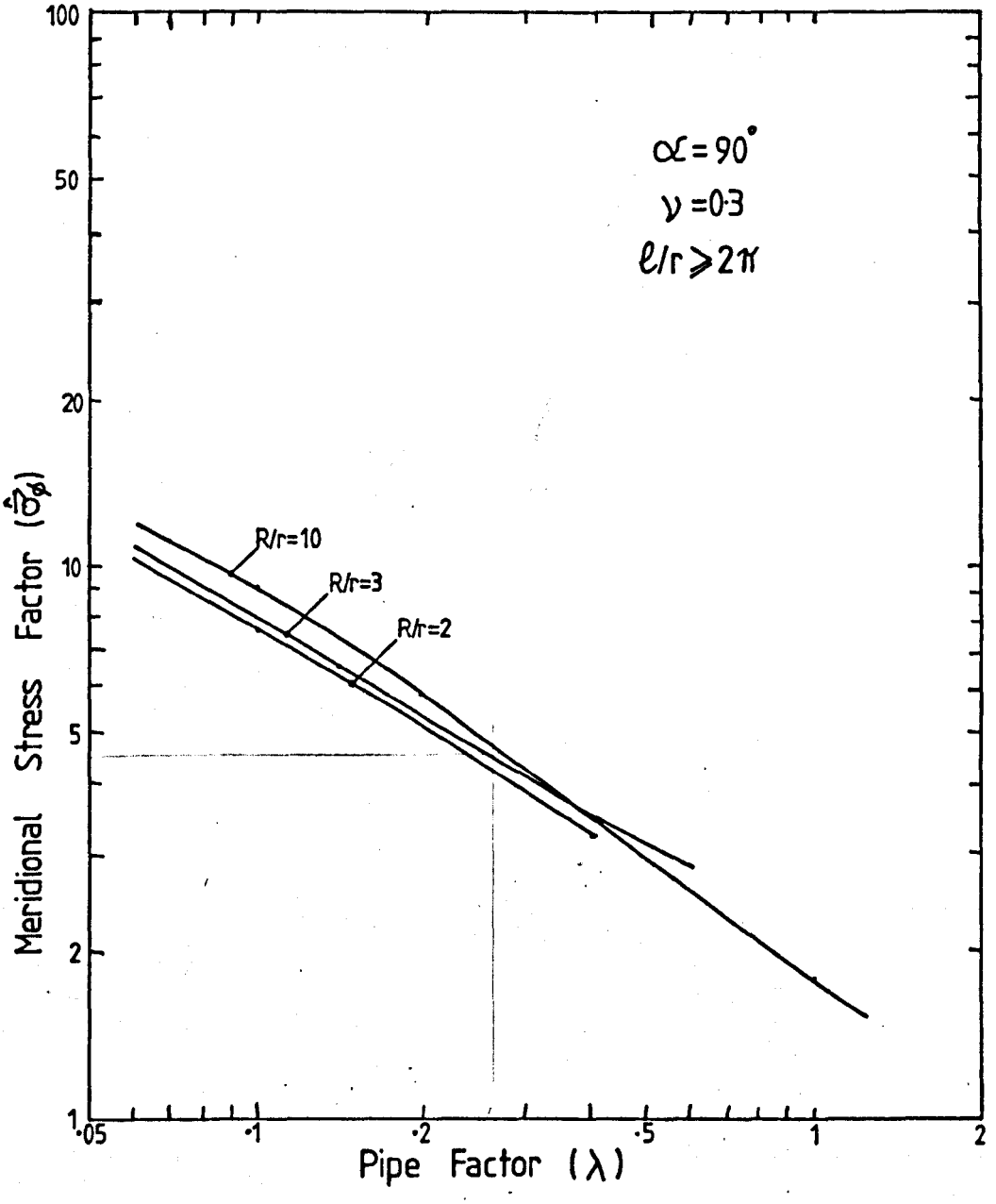

Meridional Stress Factors for $\alpha = 90^\circ$

Figure (5.20)

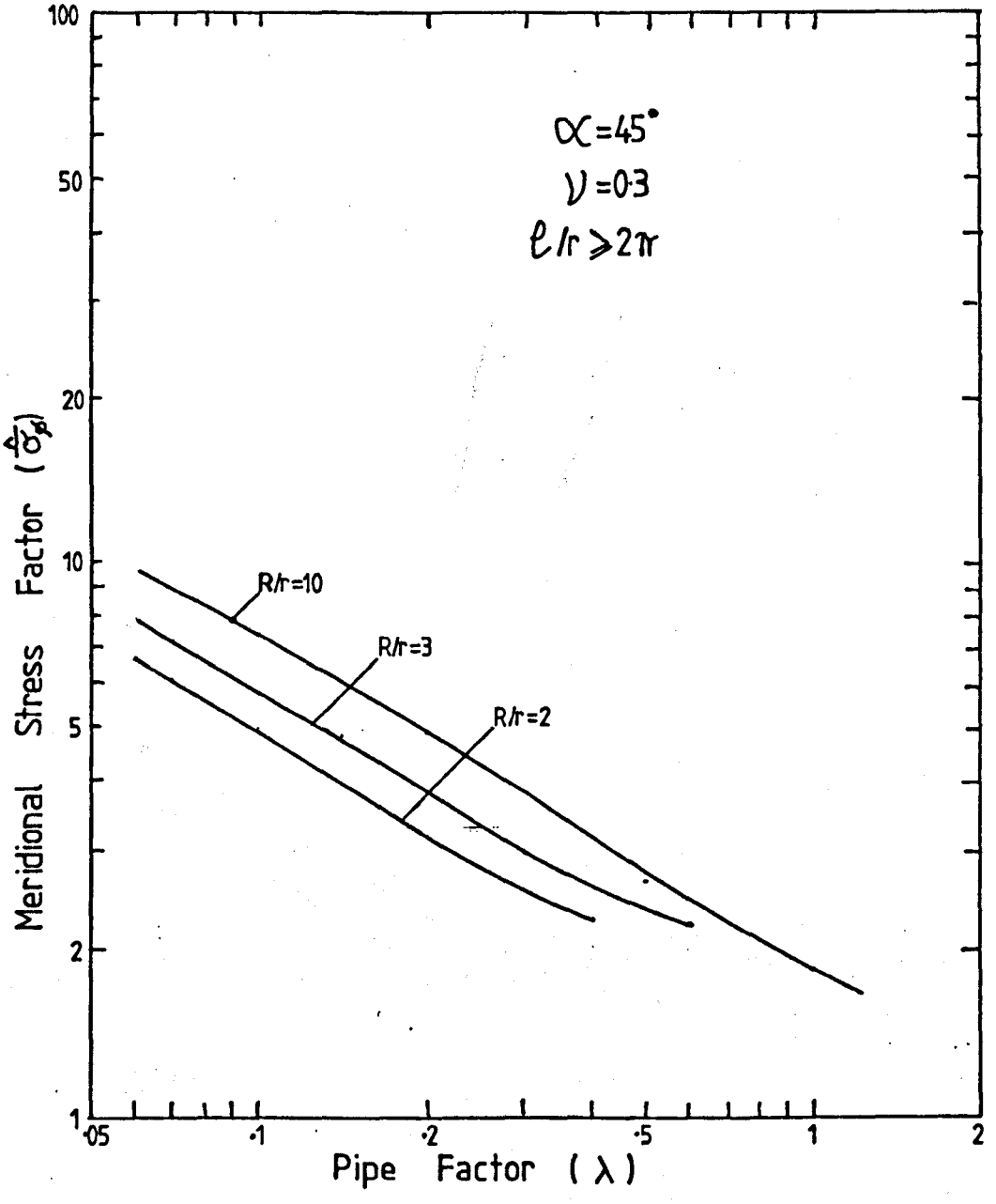

Meridional Stress Factors for $\alpha = 45^\circ$

Figure (5.21)

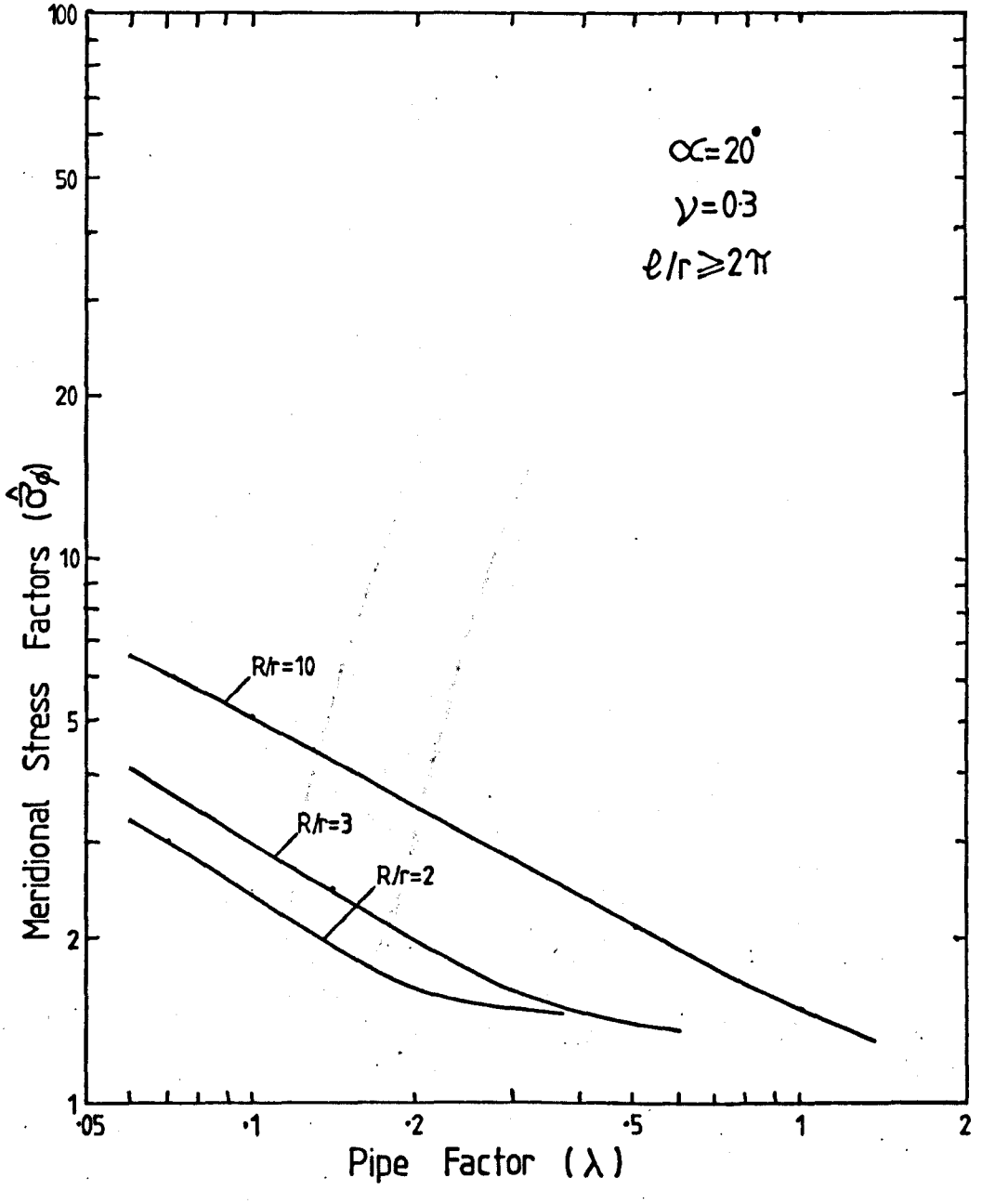

Meridional Stress Factors for $\alpha=20^\circ$

Figure (5.22)

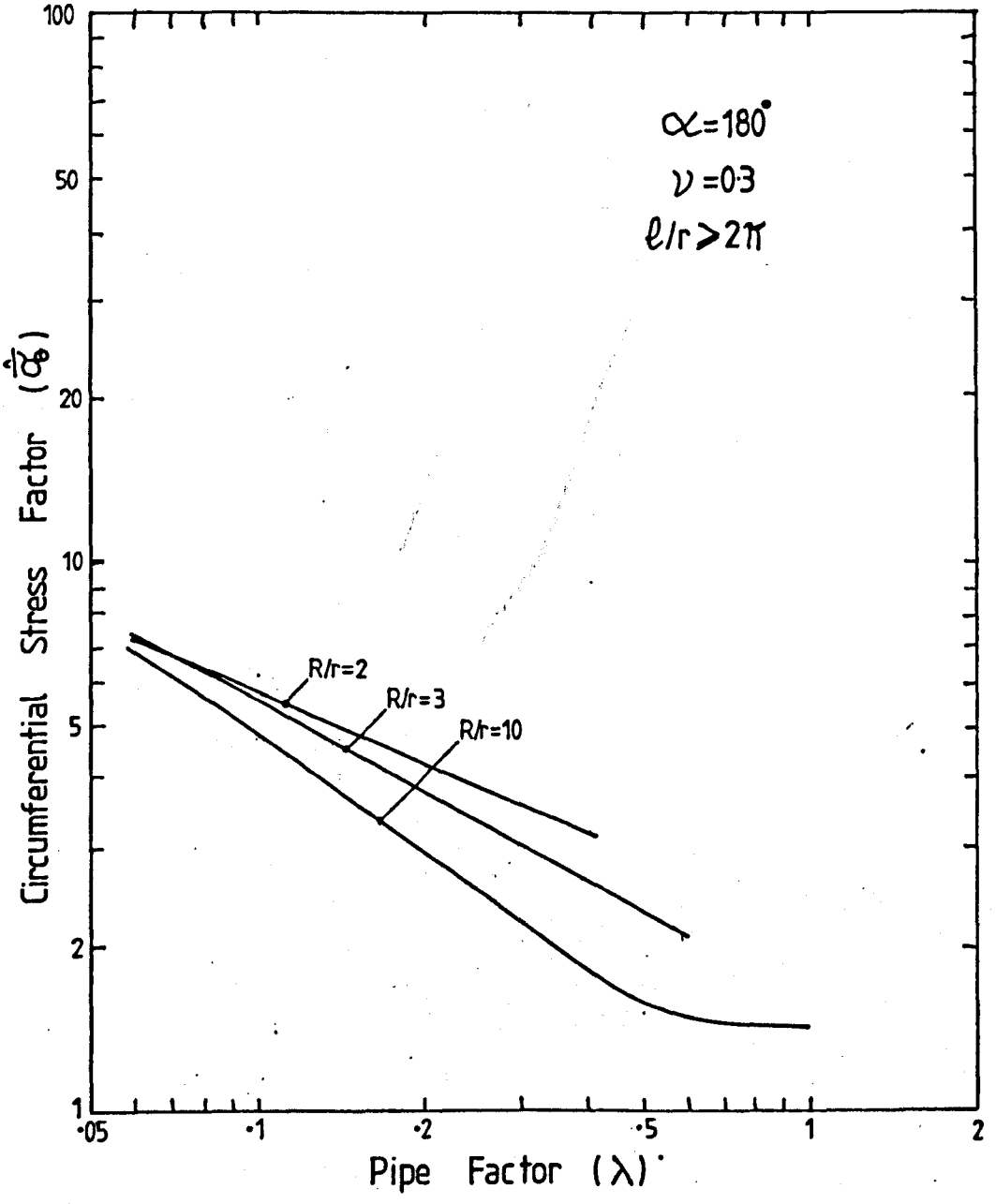

Circumferential Stress Factors for $\alpha=180^\circ$

Figure (5.23)

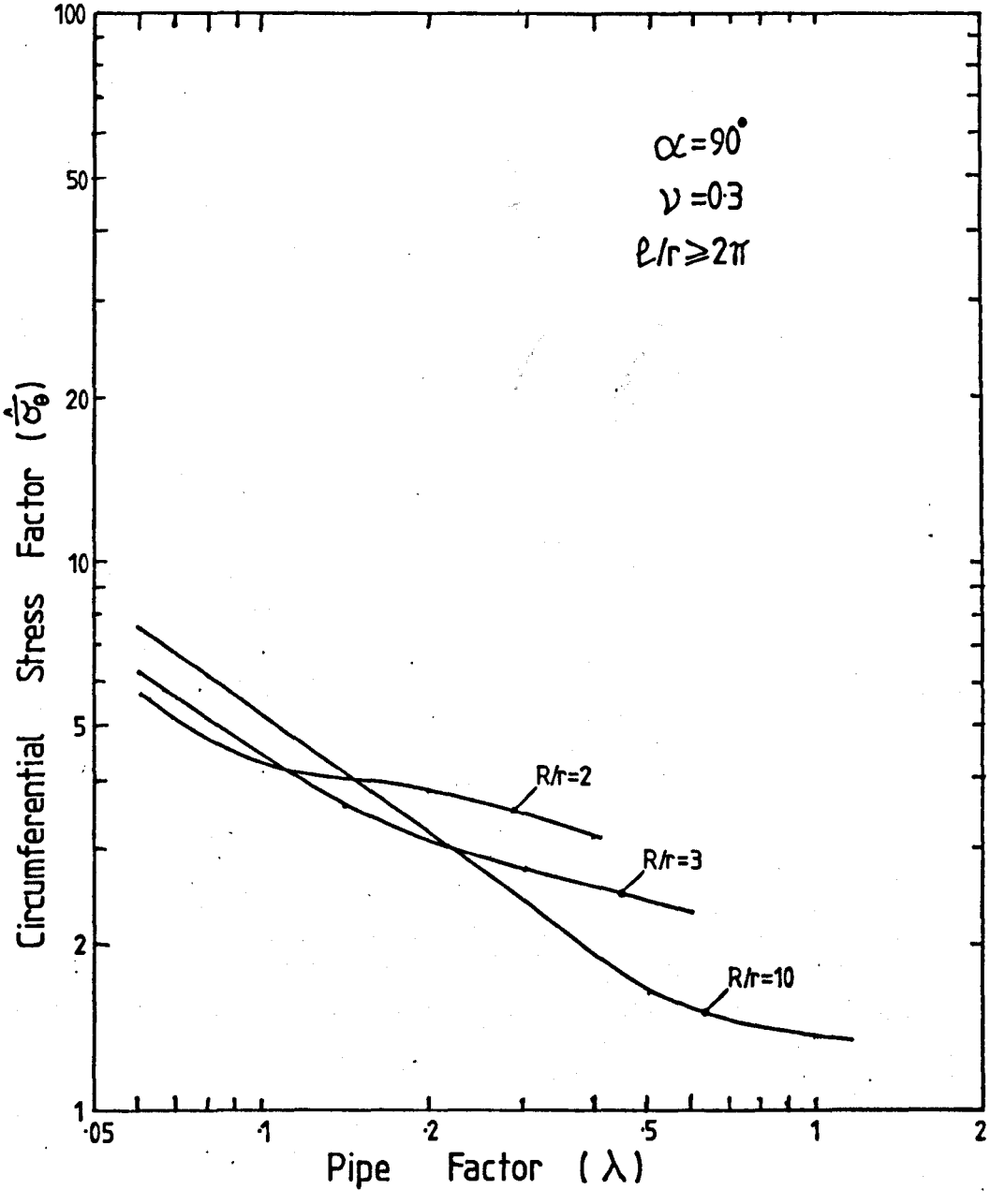

Circumferential Stress Factors for $\alpha=90^\circ$

Figure (5.24)

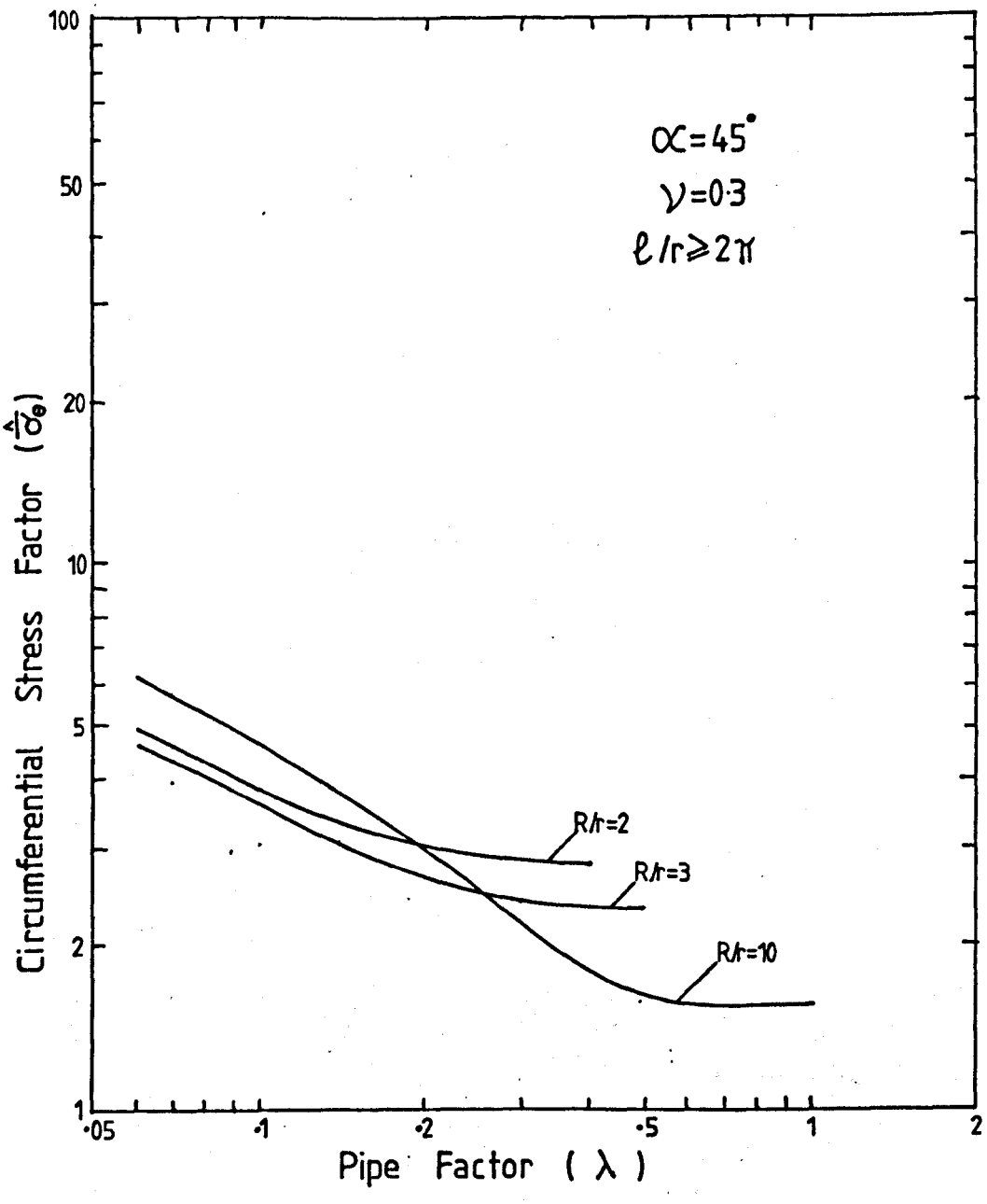

Circumferential Stress Factors for $\alpha=45^\circ$

Figure (5.25)

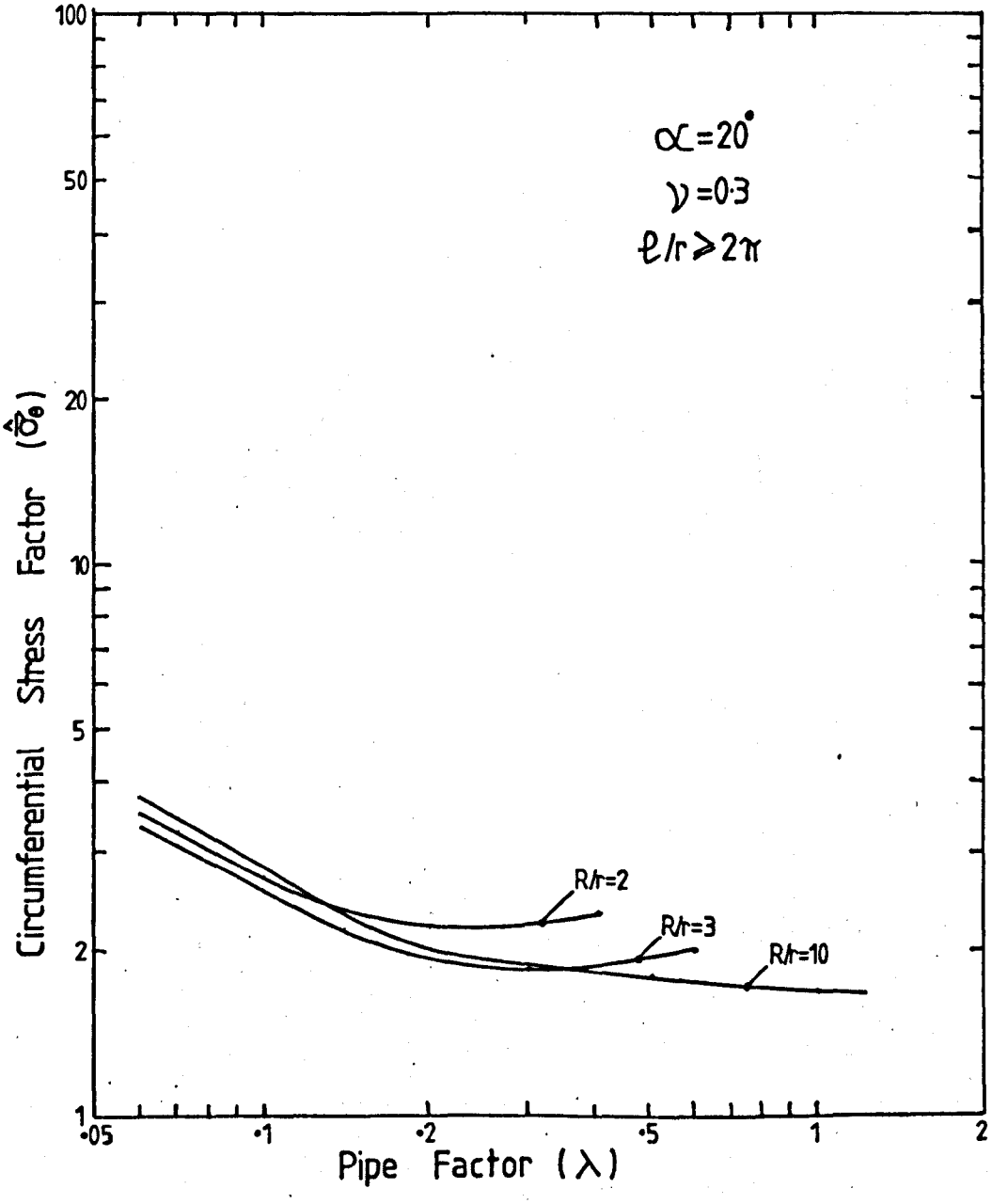

Circumferential Stress Factors for $\alpha = 20^\circ$

Figure (5.26)

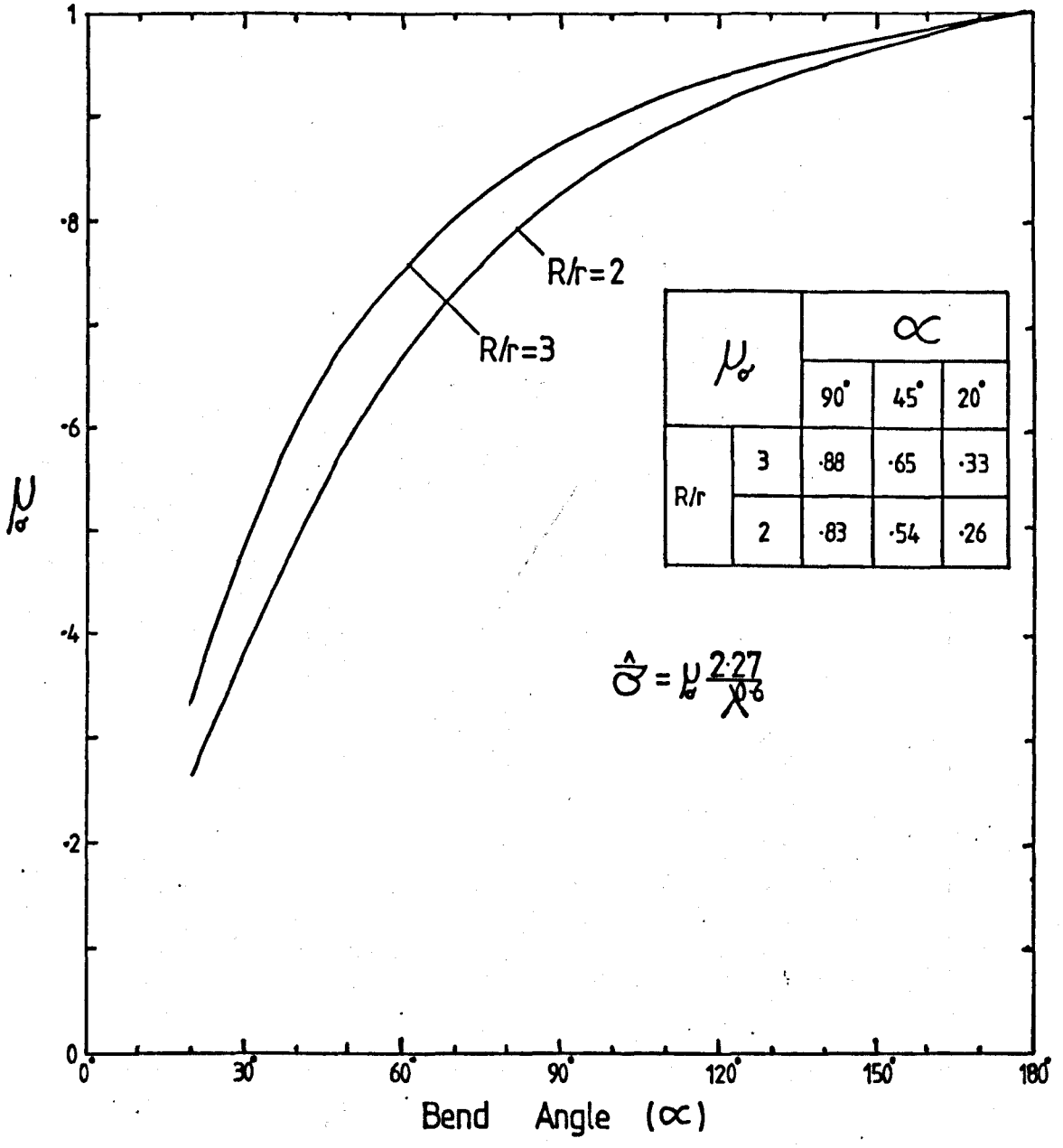

μ_σ		∝		
		90°	45°	20°
R/r	3	·88	·65	·33
	2	·83	·54	·26

Approximate Formula for Maximum Stress

Figure (5.27)

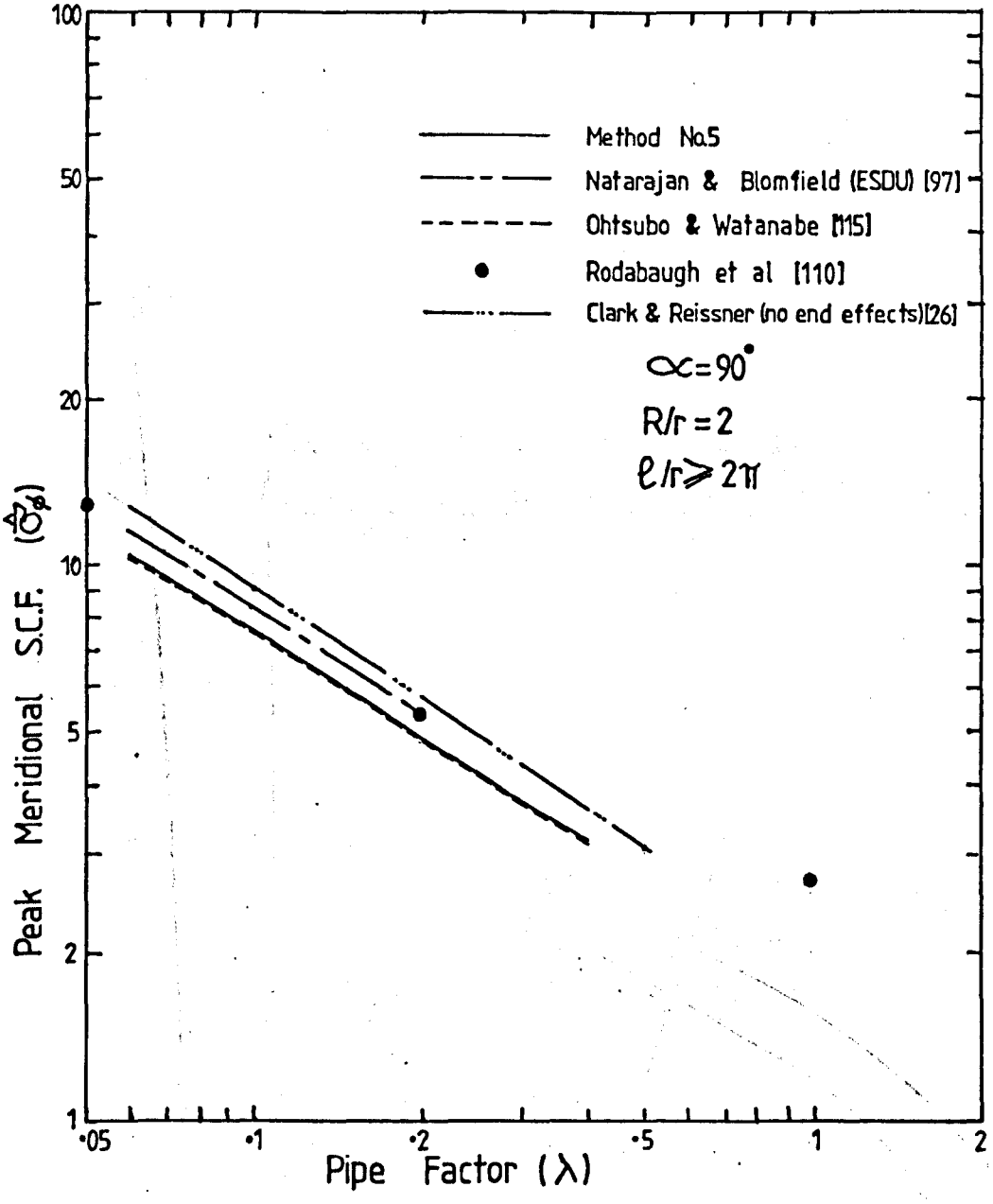

Comparison of Peak Meridional S.C.F.s

Figure (5.28)

CHAPTER .6

EXPERIMENTS ON BENDS WITH TANGENTS AND COMPARISONS WITH THEORY

Abstract

Details are given of in-plane bending tests performed on two 90° bend-tangent assemblies.

The theory developed in chapter (5), method No. 5, is compared against the experimental flexibility and maximum stress factors obtained by present and past authors. Further, detailed comparisons are made between theoretical and experimental stress distributions for the bend-tangent assemblies.

CHAPTER (6)

EXPERIMENTS ON BENDS WITH TANGENTS AND COMPARISON WITH THEORY

(6.1) Test Programme

(6.2) Comparison of Flexibility Factors from Theory and Experiment

(6.3) Maximum S.C.Fs.

(6.4) Experimental Stress Distributions

(6.1) Test Programme

Two bends were selected for testing with subtended angles of 90°. This angle was chosen for two reasons, firstly because it is probably the most commonly used in practice and secondly, the theory suggested that it would demonstrate the effect of the tangent pipes.. The dimensions of the bendsare given in the following table:-

Bend No.	Outside Pipe Diameter	R	r	t	R/r	ℓ/r	λ	α
3	6.625"	9"	3.25	0.135"	2.77	7.4	0.11	90°
4	6.625"	9"	3.17"	0.28"	2.84	7.57	0.25	90°

The dimensions were checked and found to conform to BS 1640 [161]. The bends were part of a more extensive experimental programme being carried out at the University of Strathclyde. Both stainless steel bends, $E = 28.2 \times 10^6$ lb/in^2 and $\nu = 0.28$, were supplied by Munro and Miller [160]. Flanges were welded to the end of the tangent pipes.

The test procedure was almost identical to that given in chapter (4) and in the following only a brief description for each bend will be given.

A total of 134 strain gauges were employed on bend No. 3 at the positions shown in figures (6.1), (6.2) and (6.3). At $\theta = 0°$, 'strip' gauges were employed around the position where the maximum stress was expected. Each strip had five 2mm gauges which, were orientated along the meridian. Details of these gauges were as follows,

Type:	SHOWA R51 - FA 2
Gauge length:	2mm
Nominal Resistance:	120
Gauge Factor:	2.1

Ordinary 5mm gauges were used opposite each second gauge on the strip, orientated along the circumferential direction. All of the strain gauges were temperature compensated for stainless steel. Bend No. 3 was tested on the rig shown earlier in figure (4.5).

Bend No. 4 used 18 strain gauges at the positions given in figure (6.4) and was tested in the rig shown earlier in figure (4.3).

Readings were taken from the strain gauges at each of the ten load increments. The best straight line was fitted to the data and the stress factors were calculated as described in chapter (4). These are given in tables (6.1) and (6.2) for bends Nos. 3 and 4 respectively.

Table (6.1)

Stress Factors for Bend No. 3

Gauge No.	Stress Factor	Gauge No.	Stress Factor	Gauge No.	Stress Factor	Gauge No.	Stress Factor	Gauge No.	Stress Factor
0	- 2.20	30	0.34	60	0.10	90	0.37	120	- 5.29
1	- 1.67	31	1.57	61	1.86	91	1.32	121	- 5.62
2	0.29	32	- 0.23	62	- 2.62	92	- 0.72	122	- 5.80
3	0.08	33	1.51	63	0.93	93	2.45	123	- 6.05
4	1.58	34	- 2.08	64	- 2.93	94	- 3.65	124	- 5.94
5	1.20	35	- 0.42	65	- 5.31	95	- 0.27	125	- 5.97
6	- 1.71	36	- 1.71	66	3.66	96	2.62	126	- 5.75
7	- 0.48	37	- 3.89	67	- 0.38	97	- 2.94	127	- 6.37
8	0.31	38	5.31	68	1.91	98	4.00	128	- 5.50
9	- 0.08	39	0.34	69	2.96	99	3.51	129	- 3.68
10	0.93	40	2.02	70	0.81	100	1.24	130	- 3.10
11	0.03	41	1.84	71	1.47	101	2.46	131	- 2.16
12	- 1.50	42	1.23	72	4.6	102	0.54	132	- 1.12
13	0.50	43	2.05	73	- 5.32	103	1.37	133	- 0.10
14	0.27	44	0.33	74	0.24	104	-		
15	- 0.45	45	1.17	75	0.62	105	- 5.51		
16	0.82	46	0.03	76	0.24	106	-		
17	0.23	47	1.74	77	1.90	107	- 6.01		
18	- 0.70	48	- 1.98	78	- 2.62	108	-		
19	1.61	49	0.76	79	1.30	109	- 5.78		
20	0.25	50	- 2.15	80	- 3.22	110	- 6.18		
21	- 1.11	51	- 4.40	81	- 5.52	111	- 5.92		
22	0.88	52	2.89	82	4.17	112	- 5.82		
23	0.67	53	- 0.70	83	0.02	113	- 5.47		
24	- 0.05	54	1.89	84	1.82	114	- 3.87		
25	1.82	55	2.66	85	3.10	115	- 3.35		
26	- 0.16	56	- 3.71	86	0.59	116	- 2.17		
27	- 1.85	57	0.21	87	1.28	117	- 1.23		
28	0.73	58	0.21	88	0.17	118	- 0.12		
29	0.86	59	0.75	89	0.60	119			

Table (6.2)

Stress Factors for Bend No. 4

Gauge No.	Stress Factor	Gauge No.	Stress Factor
0	- 0.34	9	3.33
1	1.26	10	- 1.53
2	0.09	11	1.62
3	- 1.29	12	- 2.91
4	- 0.36	13	- 1.56
5	- 1.37	14	- 1.78
6	2.67	15	- 2.52
7	- 1.23	16	- 1.22
8	1.66	17	- 2.32

(6.2) Comparison of Flexibility Factors from Theory and Experiment

Comparison of the flexibility factors from method No. 5, for bend/tangent assemblies ($\ell/r \geq 2\pi$), with those obtained from the experiments of past and present authors is given in figures (6.5) and (6.6), for bend angles of 180° and 90° respectively.

As explained in section (4.2), the flexibility factors published by Pardue and Vigness [89] are an average of factors for several different types of loading. Their average values are given in figures (6.5) and (6.6) with a vertical line through the averages indicating the range of actual values. Although it is impossible to know which part of the ranges apply to in-plane bending, their flexibility factors show reasonable agreement with the present theory.

In/

In [28], Gross and Ford published an experimental investigation of flexibility short radius bends. Although not intended as such, their results are applicable to the study of bends with connected tangents. Gross and Ford's flexibility factors, shown in figure (6.6), are slightly higher than the present theory predicts. However, their flexibility factors were based on displacement measurements and are not strictly comparable to the rotation flexibilities given by the present theory.

Vissat and Del Buono gave flexibility factors for a series of 180° bends in [90], which are shown in figure (6.5). As before, these were derived using a different flexibility factor definition from the current one. However, their results compare favourably with the theory.

Imamasa and Uragami [106] obtained experimental flexibility factors for bends with connected tangent pipes, which are shown in figure (6.6). It can be seen that their results show good comparison to the predictions of the theory.

(6.3) Maximum S.C.Fs.

Comparisons of maximum meridional S.C.Fs. from theory and experiment on the outside surface are given in figures (6.7) and (6.8) for 180° and 90° bends respectively. The various results on both figures show good comparisons, particularly for the 90° bend angle. For the 180° bend angle the experimental meridional S.C.Fs. are slightly lower at the higher pipe factors. This may be because the experimental S.C.Fs. were measured at $\phi = 0$, whereas for higher pipe factors, the position of the maximum tends to be slightly/

slightly nearer the intrados.

The corresponding maximum circumferential S.C.Fs. are given in figures (6.9) and (6.10). It can be seen that although the overall comparison is favourable, the theoretical results from method No. 5 show slightly better correlation with the peak circumferential stresses from the present experimental programme and with those from Imamasa and Uragami [106] and Gross and Ford [28] than with those from Pardue and Vigness [89].

(6.4) Experimental Stress Distributions

Figure (6.11) shows the experimental distribution of meridional S.C.Fs. from bend No. 3 along the pipe centreline, $\phi = 0$, together with the corresponding theoretical distribution from method No. 5. The experimental stresses are generally slightly lower than the theory but show reasonable agreement.

Figures (6.12), (6.13) and (6.14) illustrate the distribution of meridional S.C.Fs. at $\theta = 0^{\circ}$, $\theta = 22.5^{\circ}$ and $\theta = 45^{\circ}$ respectively, for bend No. 3. Each figure shows good agreement between theory and experiment. In figure (6.14), the stresses from the theory on the bend and tangent sides of the connection at $\theta = 45^{\circ}$ are given. As indicated in chapter (5), a slight discontinuity occurs in the stresses at the junction due to the displacement slope continuity problem discussed in section (5.2). However, both stresses are reasonably close and show general agreement with the experimental values. The circumferential S.C.Fs. from bend No. 3 are shown in figure (6.15), again showing reasonable agreement.

The/

The meridional and circumferential stress distributions for bend No. 4 are given in figures (6.16) and (6.17), respectively. Both figures show a good comparison between theory and experiment.

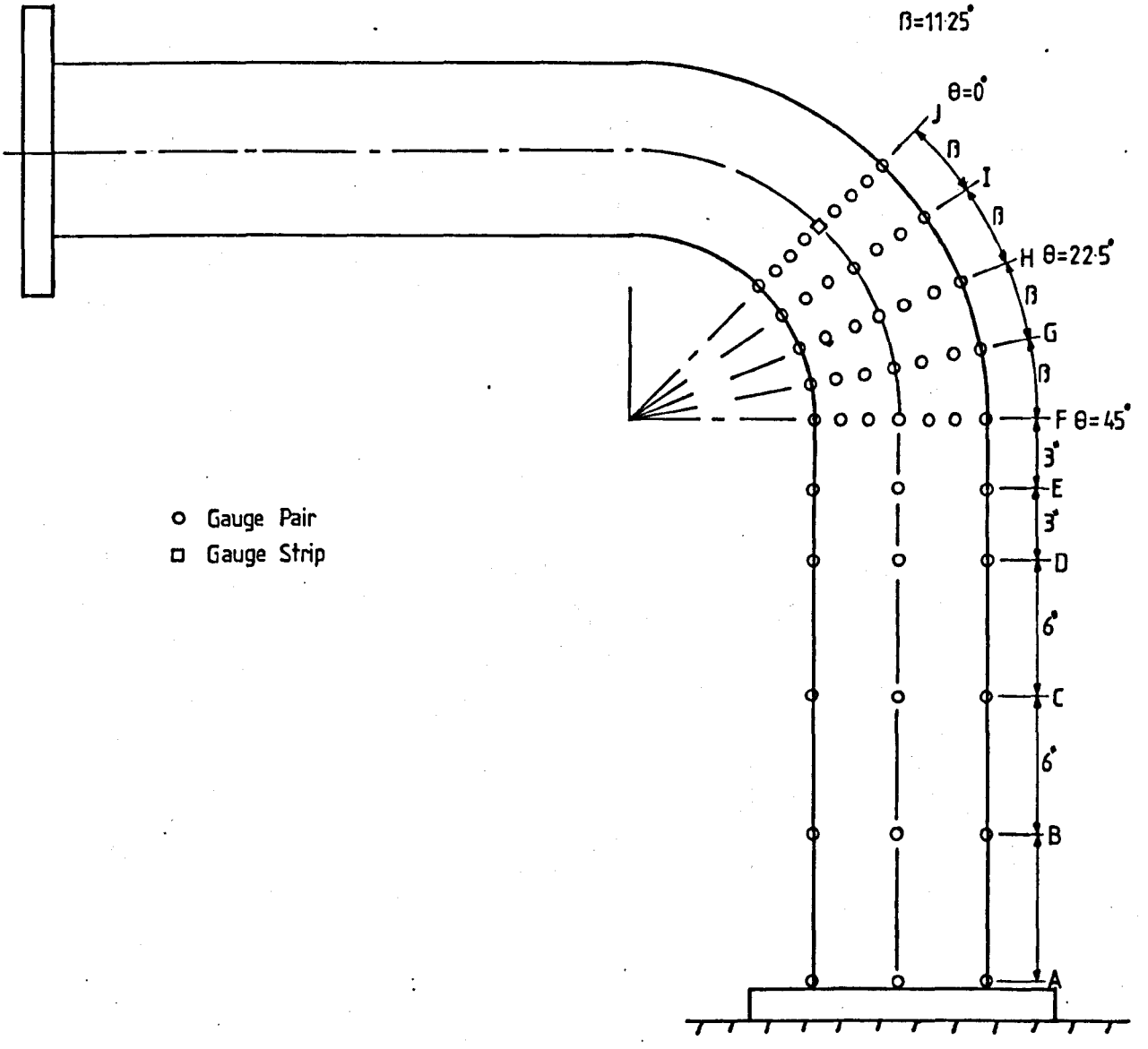

Strain Gauge Layout for Bend No.3

Figure (6.1)

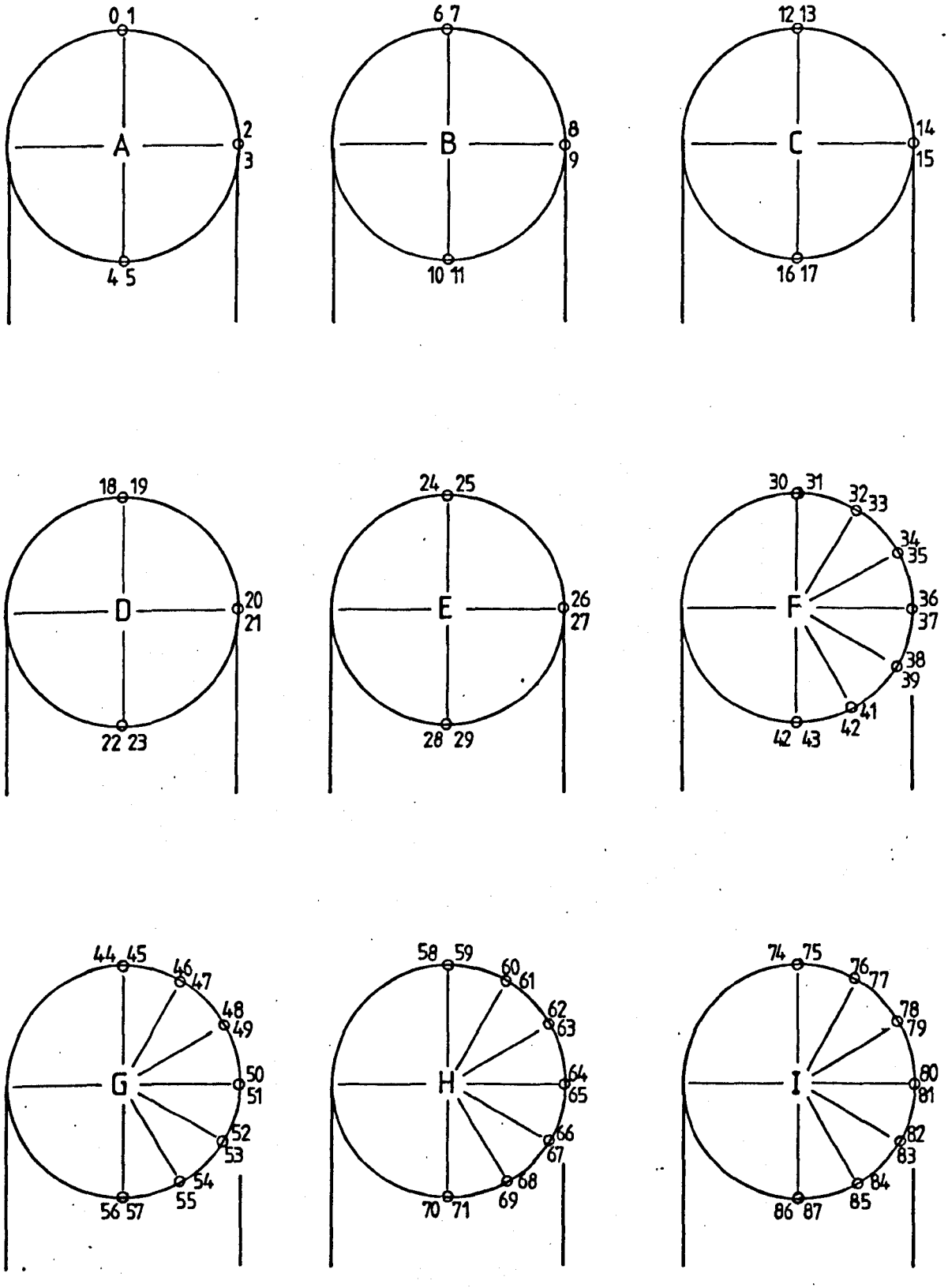

Even Nos. — Circumferential (θ)

Odd Nos. — Meridional (ϕ)

Bend No 3

Strain Gauge Layout — Sections

Figure (6.2)

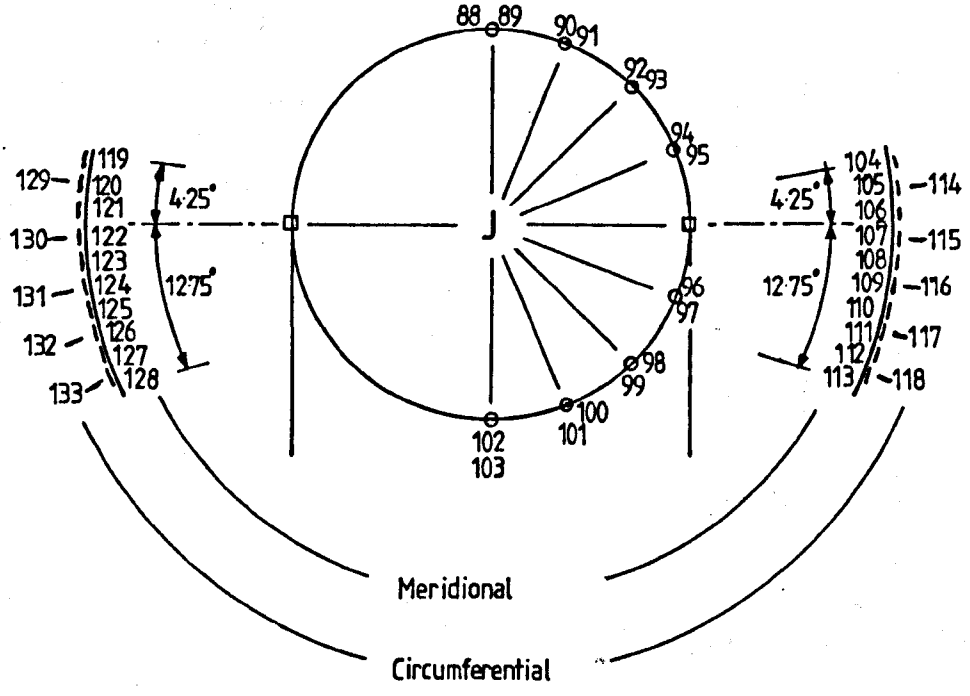

Bend No. 3

Strain Gauge Layout for Section J

Figure (6.3)

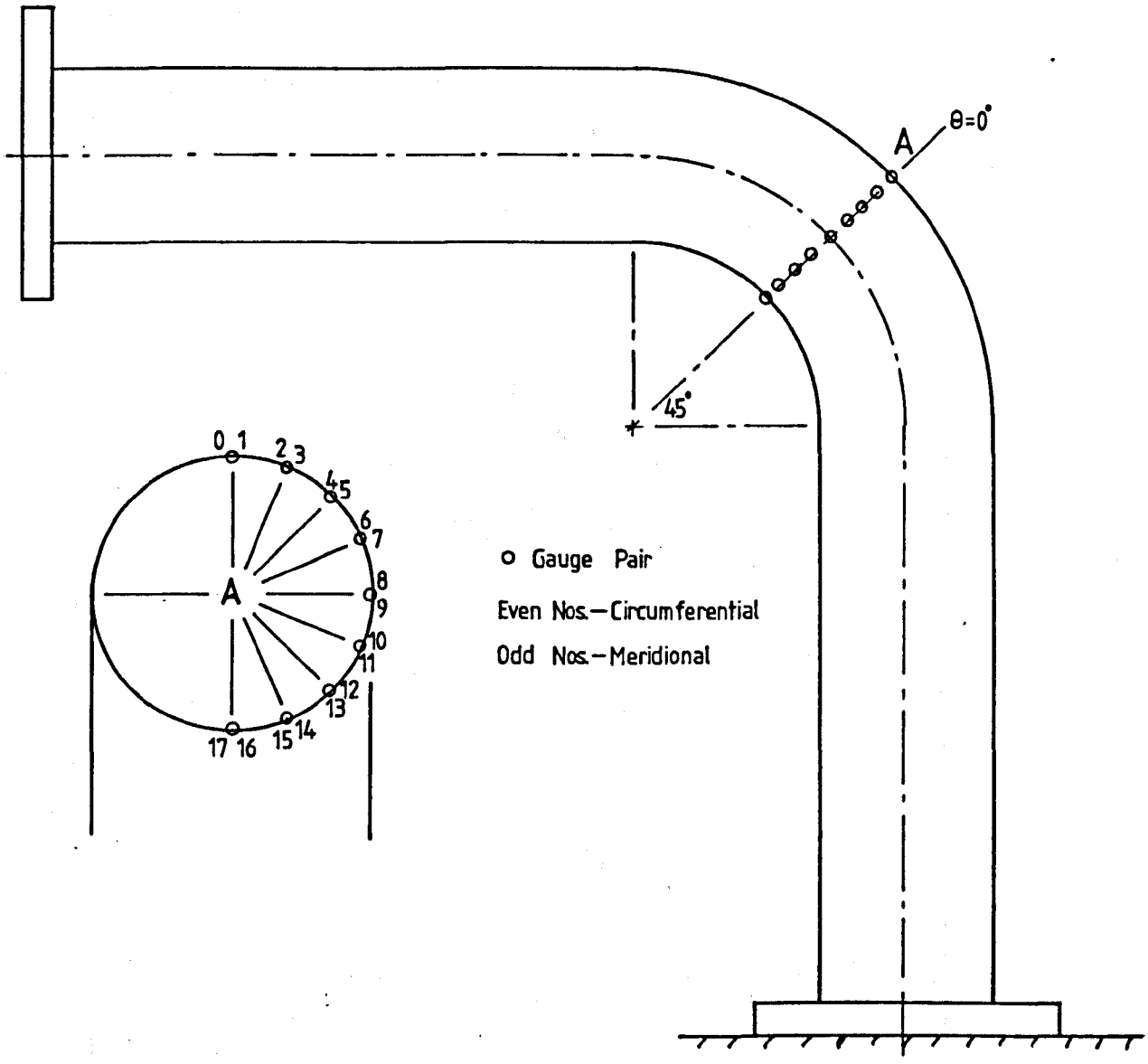

Strain Gauge Positions for Bend No.4

Figure (6.4)

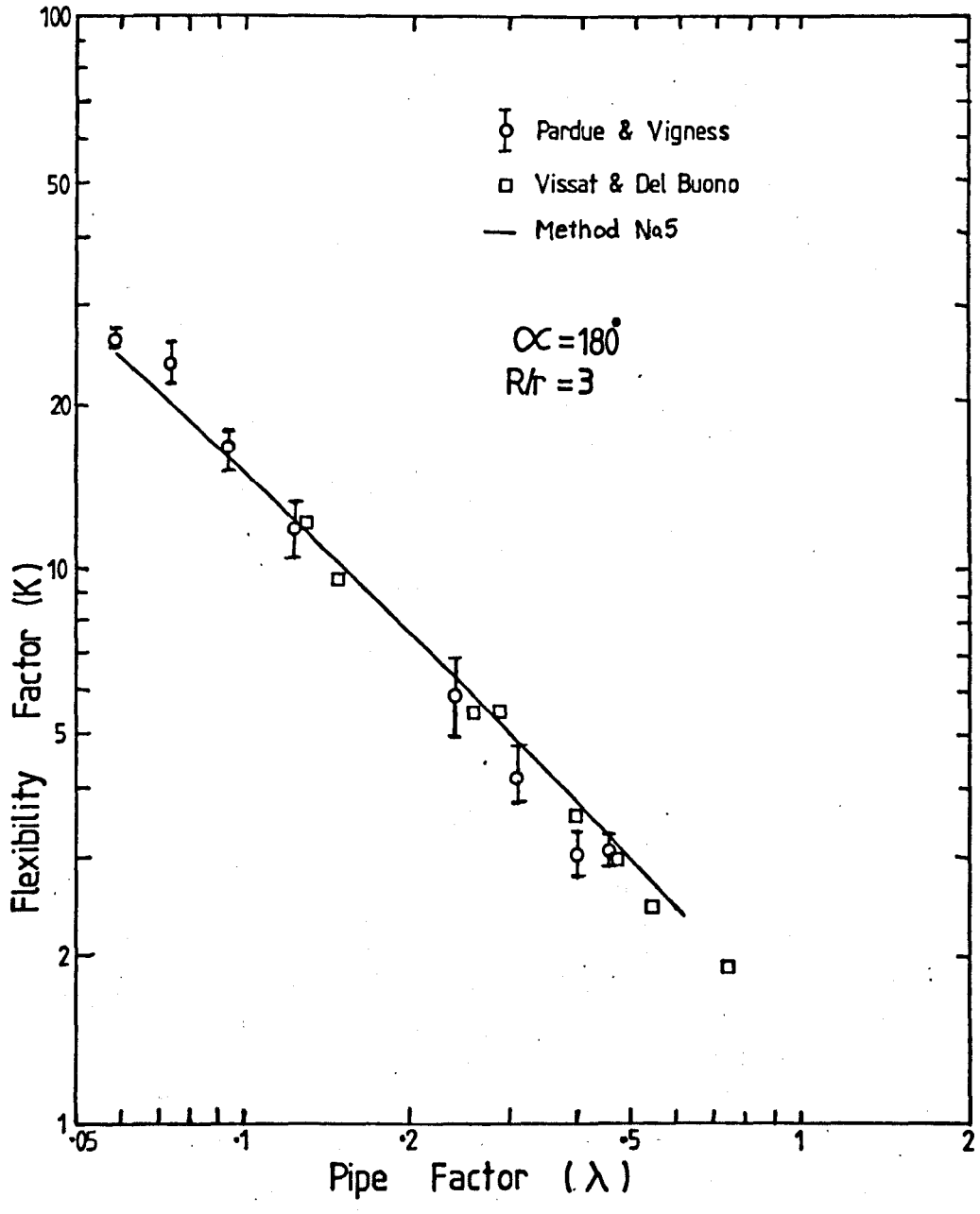

Flexibility Factors from Theory and Experiment

Figure (6.5)

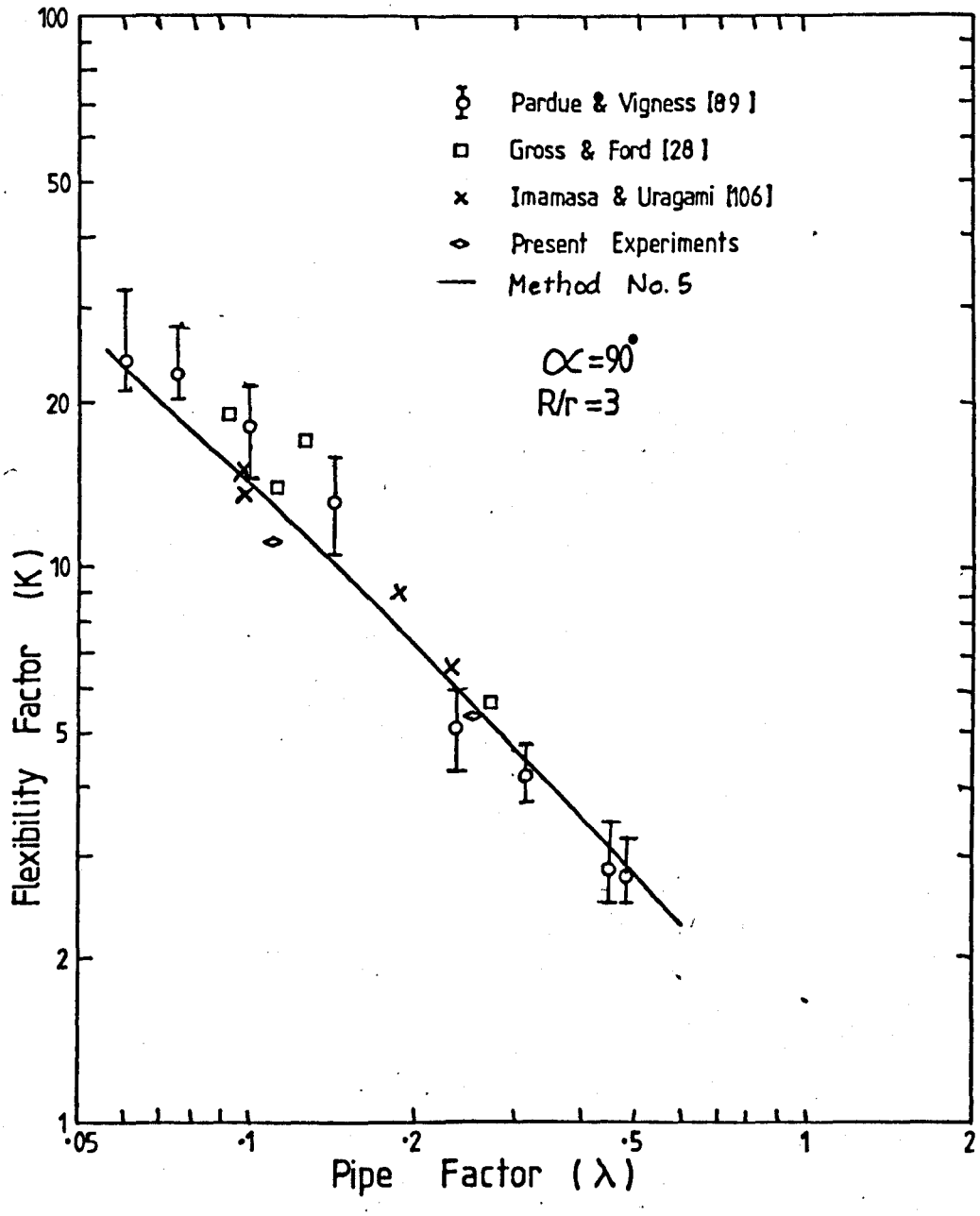

Flexibility Factors from Theory and Experiment

Figure (6.6)

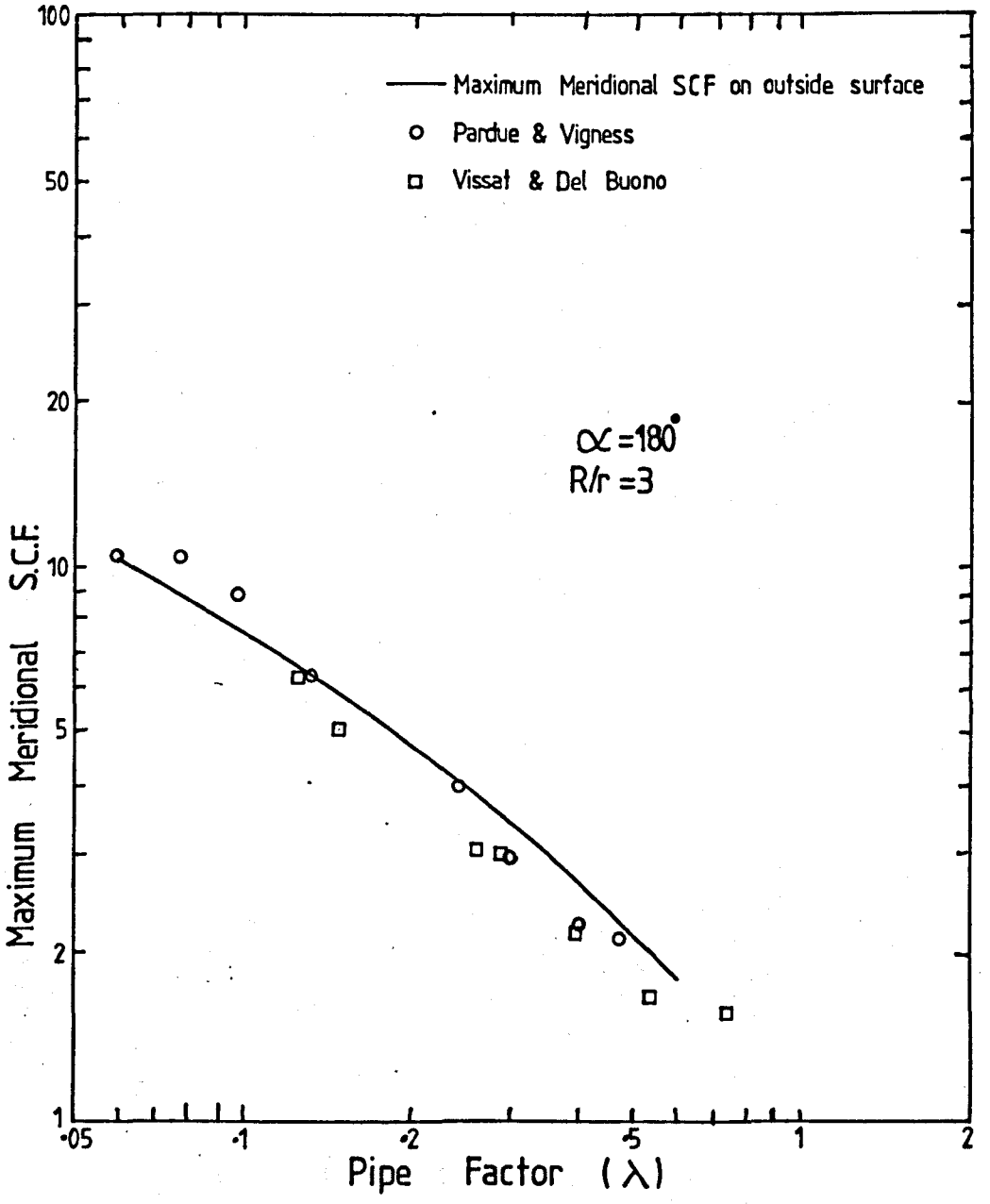

Meridional S.C.Fs from Theory and Experiment

Figure (6.7)

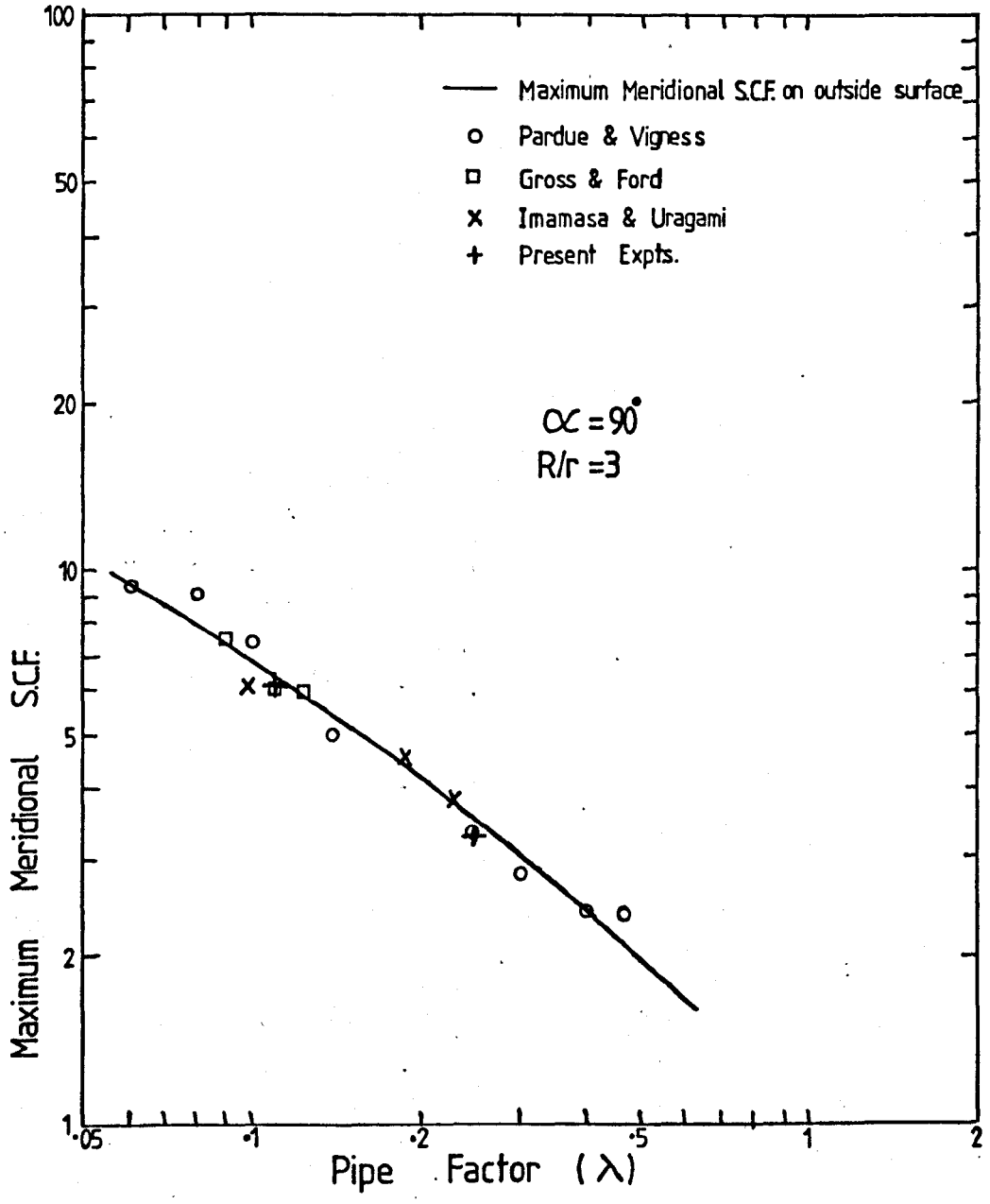

Meridional SCFs from Theory and Experiment

Figure (6.8)

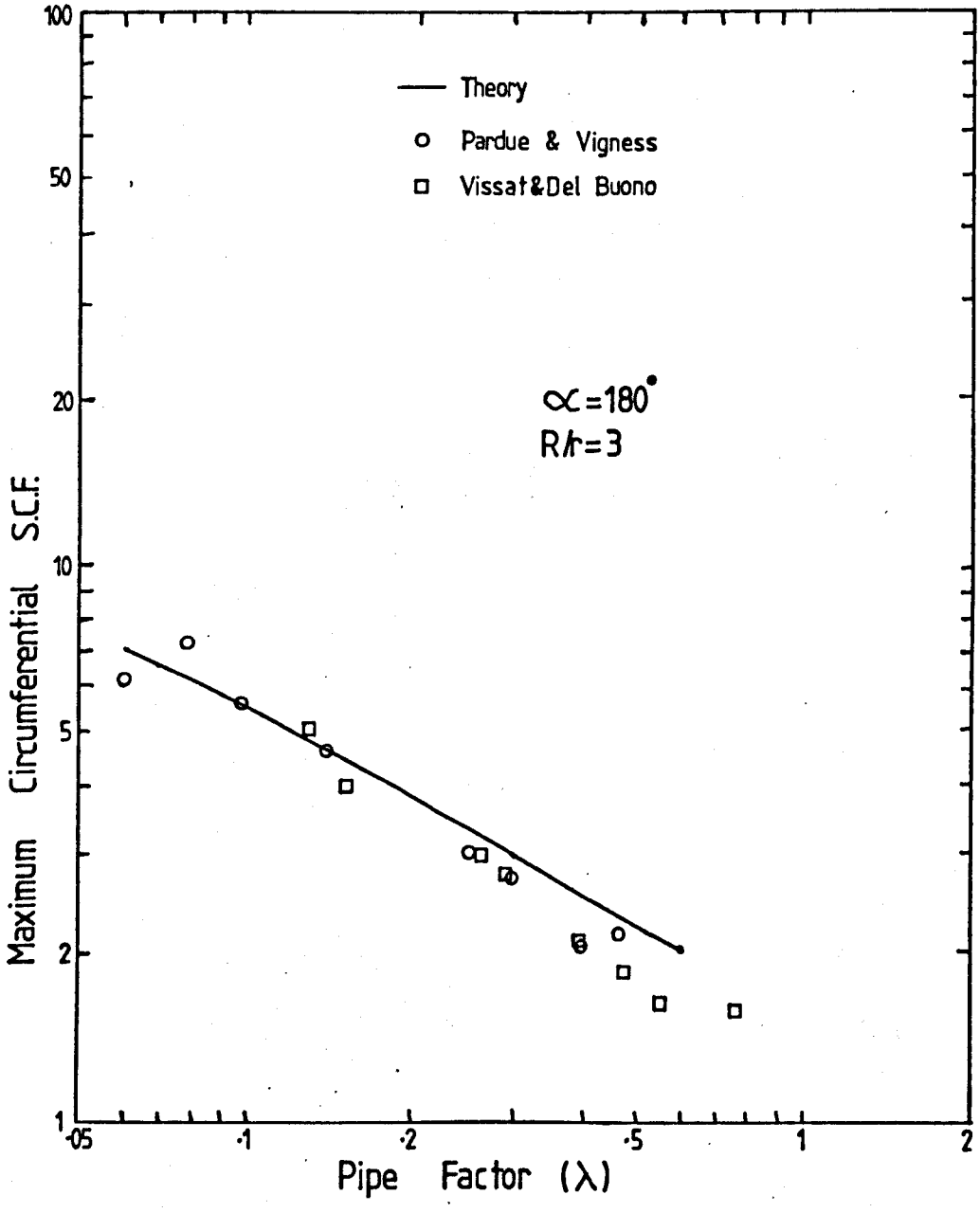

Circumferential SCFs from Theory and Experiment

Figure (6.9)

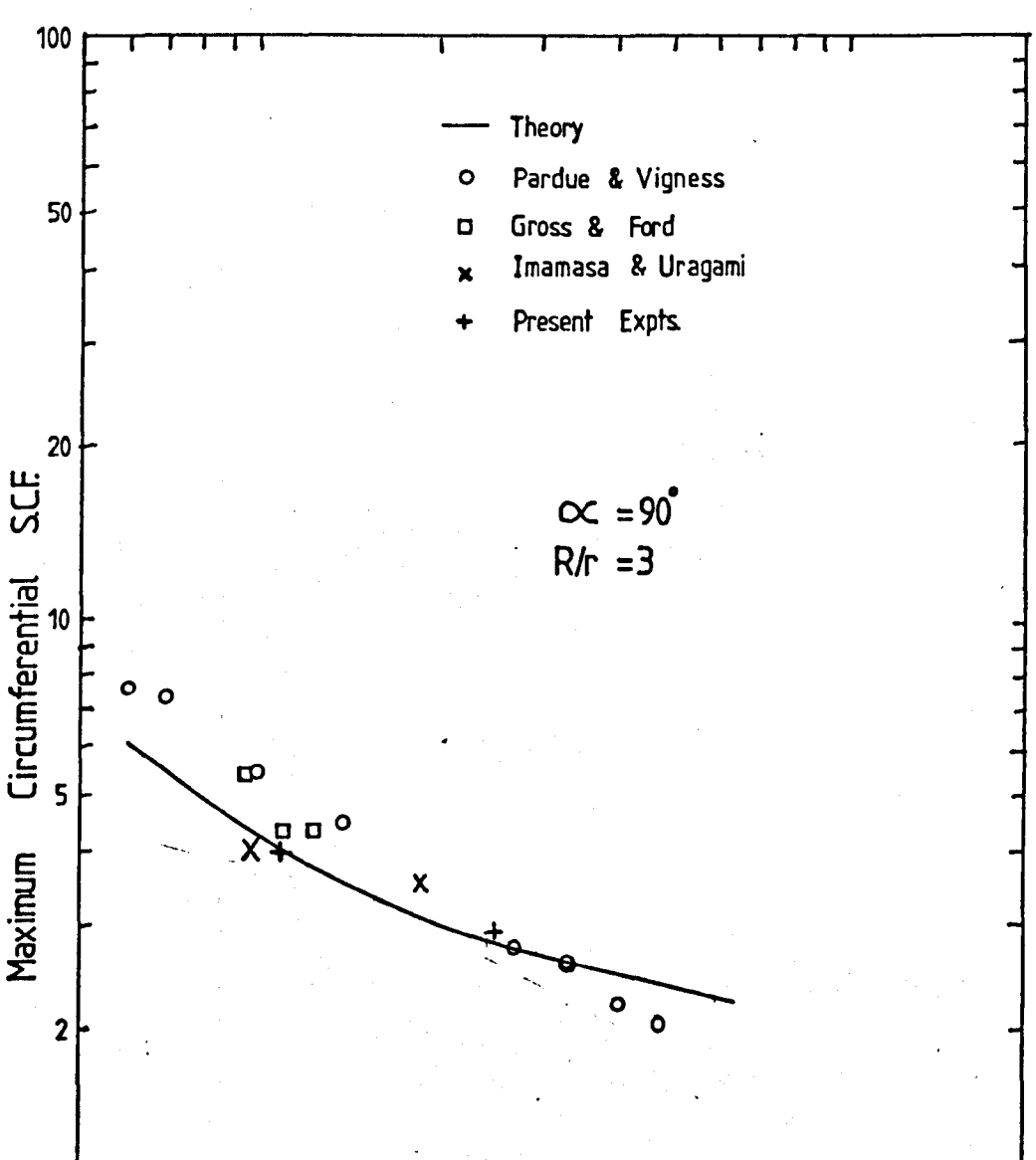

Circumferential SCFs from Theory and Experiment

Figure (6.10)

PAGE NUMBERING AS ORIGINAL

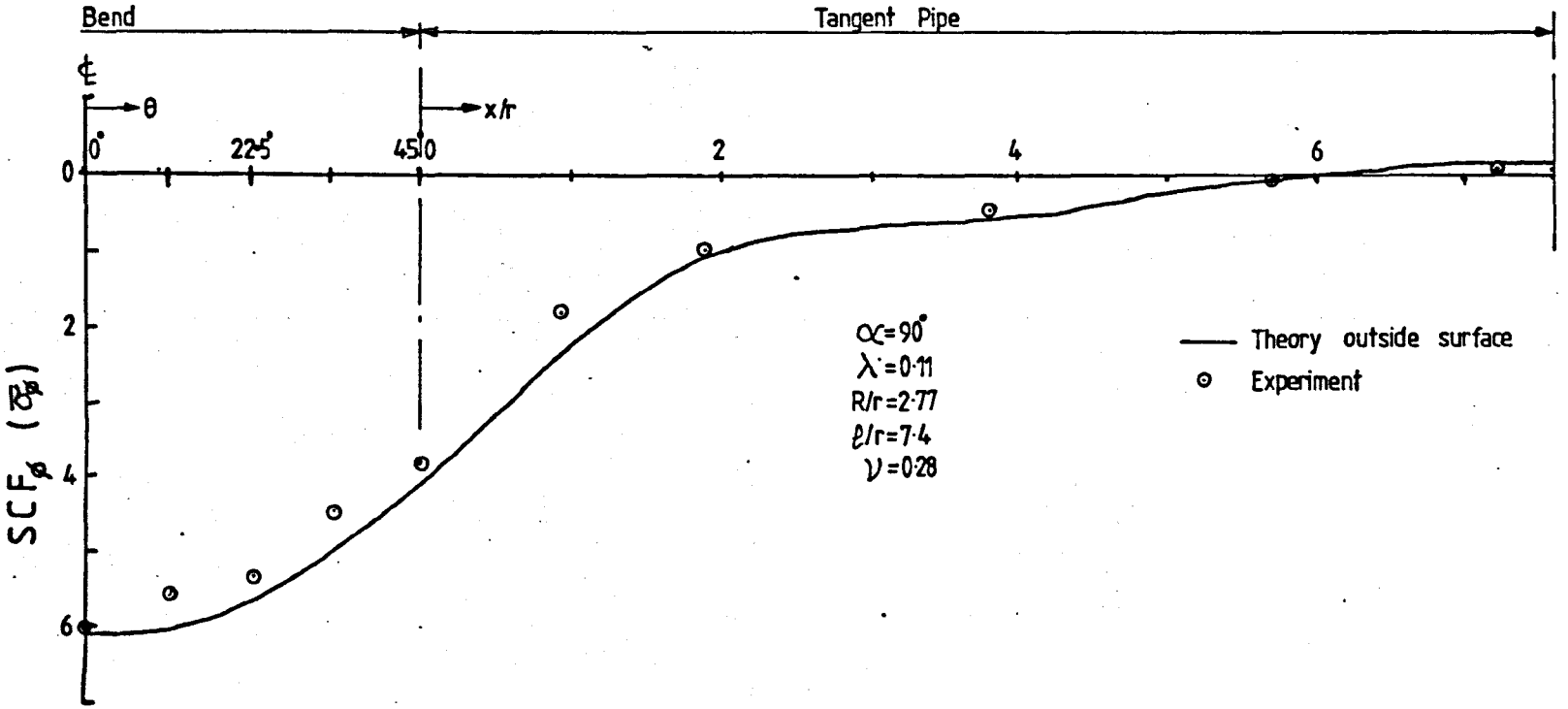

Experimental Meridional SCFs from Bend No.3 at $\phi=0^\circ$

Figure (6·11)

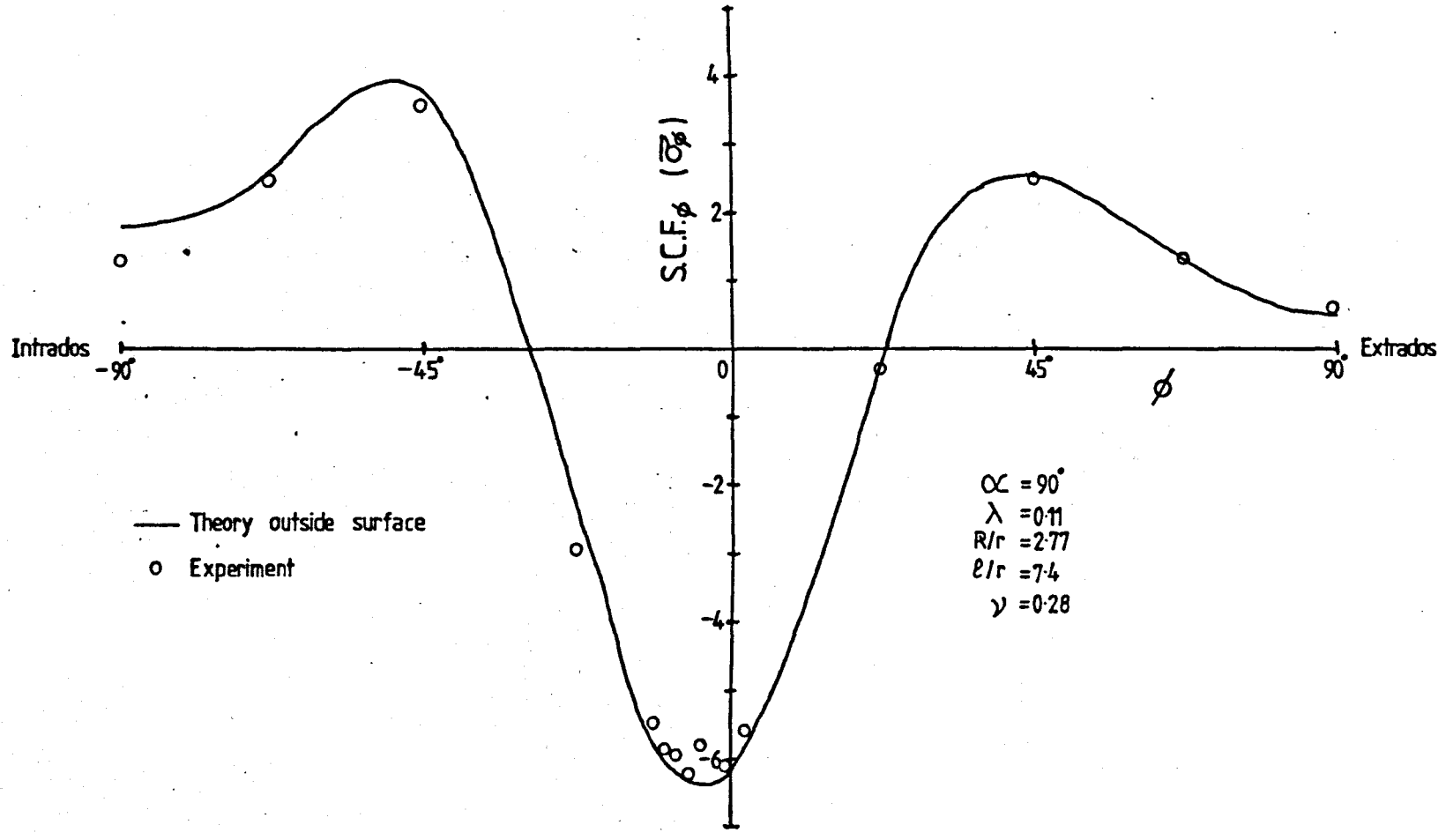

Experimental Meridional S.C.F.s from Bend No.3 at θ=0°

Figure (6.12)

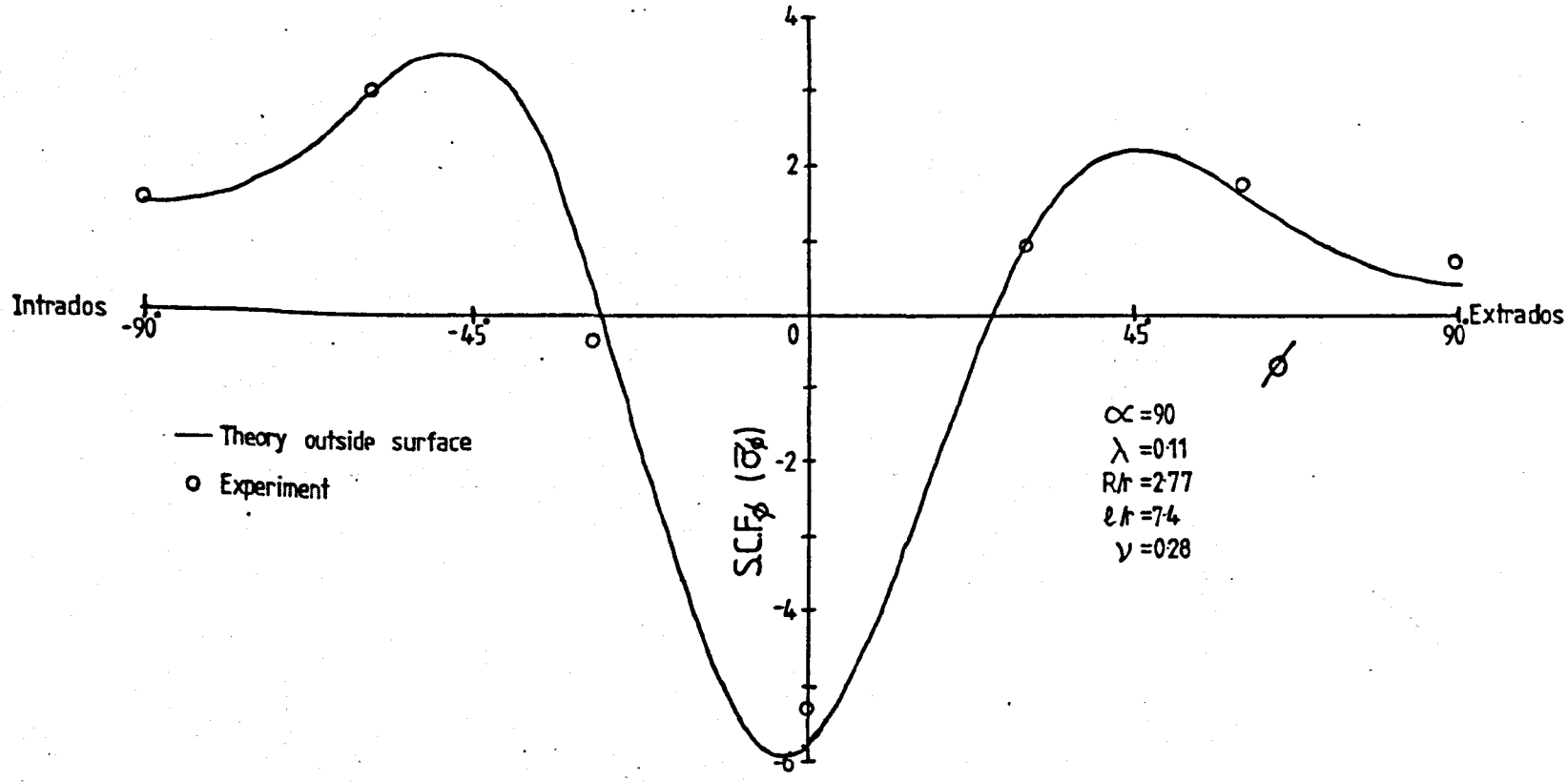

Experimental Meridional S.C.F.s from Bend No. 3 at $\theta = 22.5^\circ$

Figure (6.13)

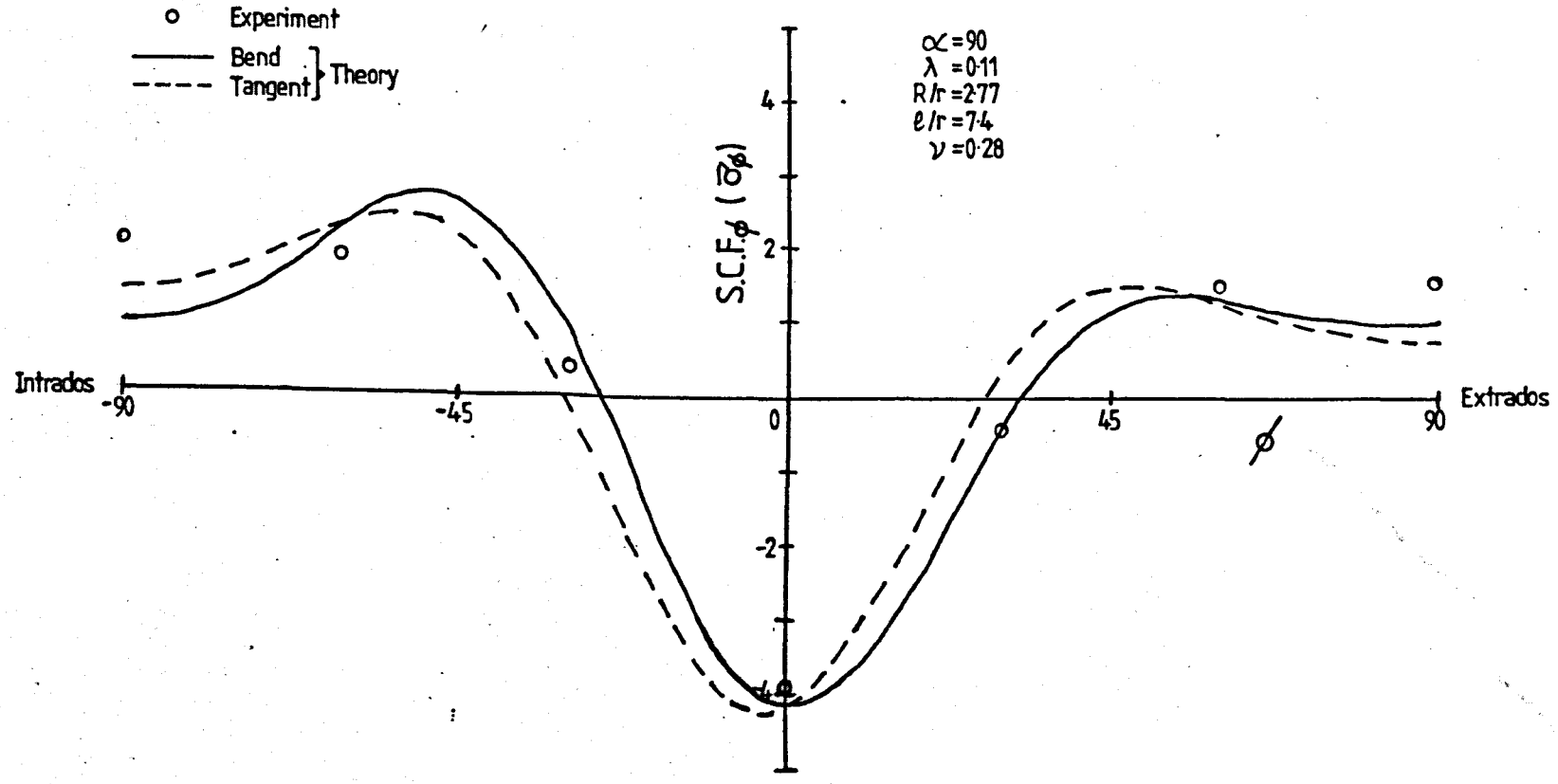

Experimental Meridional SCFs from Bend No.3 at θ=45°

Figure (6.14)

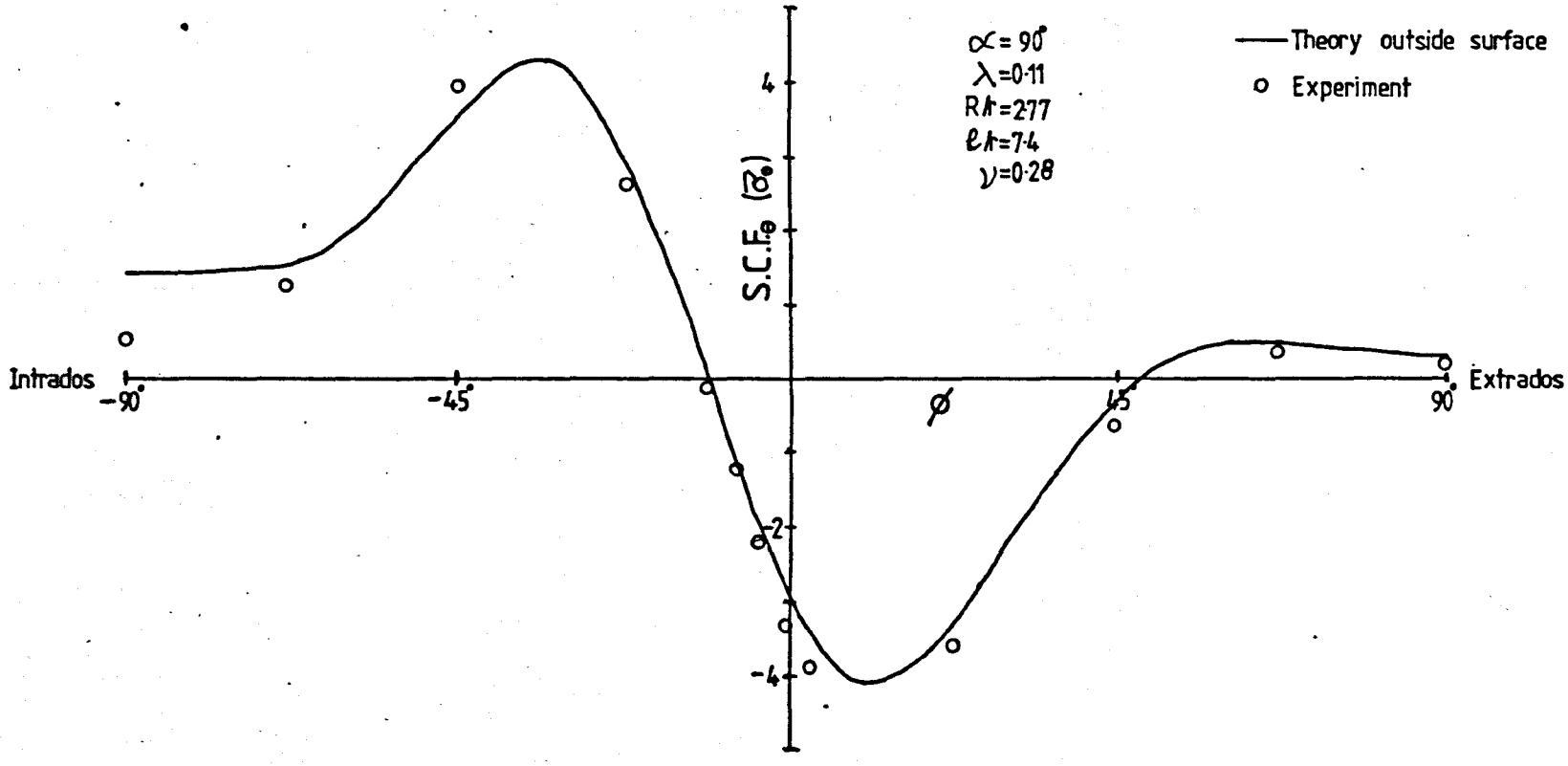

Experimental Circumferential SCFs from Bend No.3 at $\theta = 0^{\circ}$

Figure (6.15)

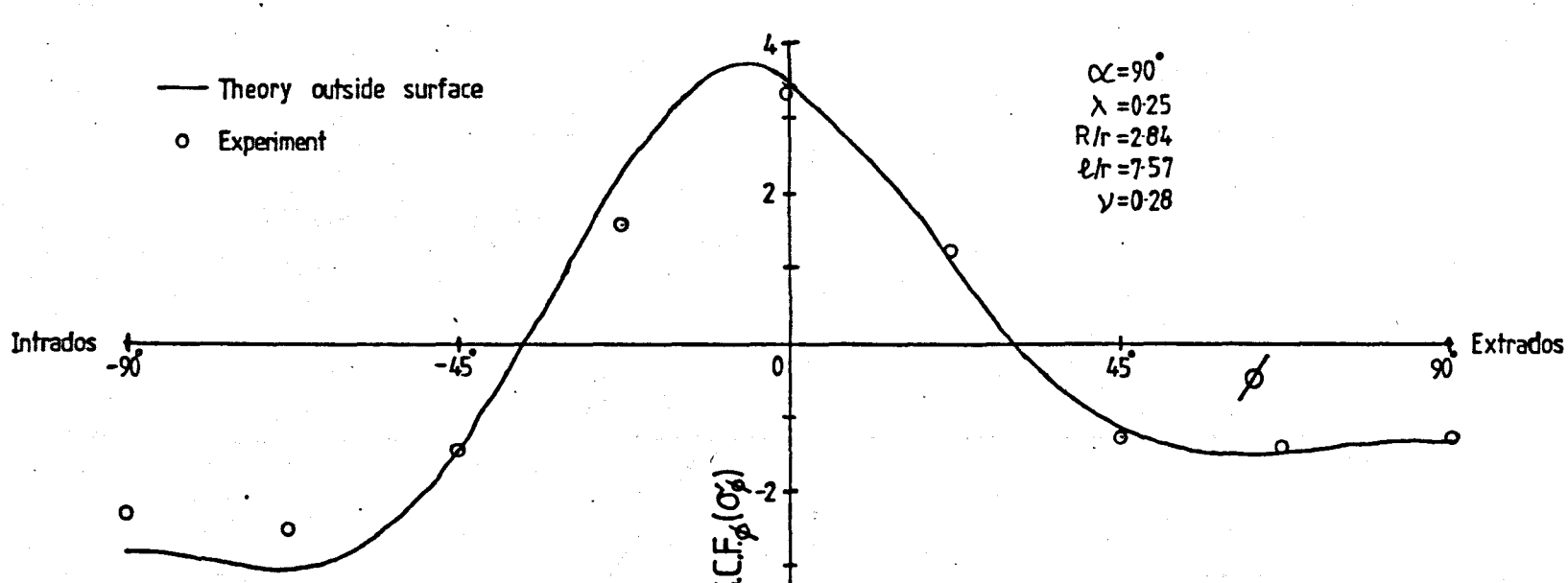

Experimental Meridional SCFs from Bend No.4 at θ=0°

Figure. (6.16)

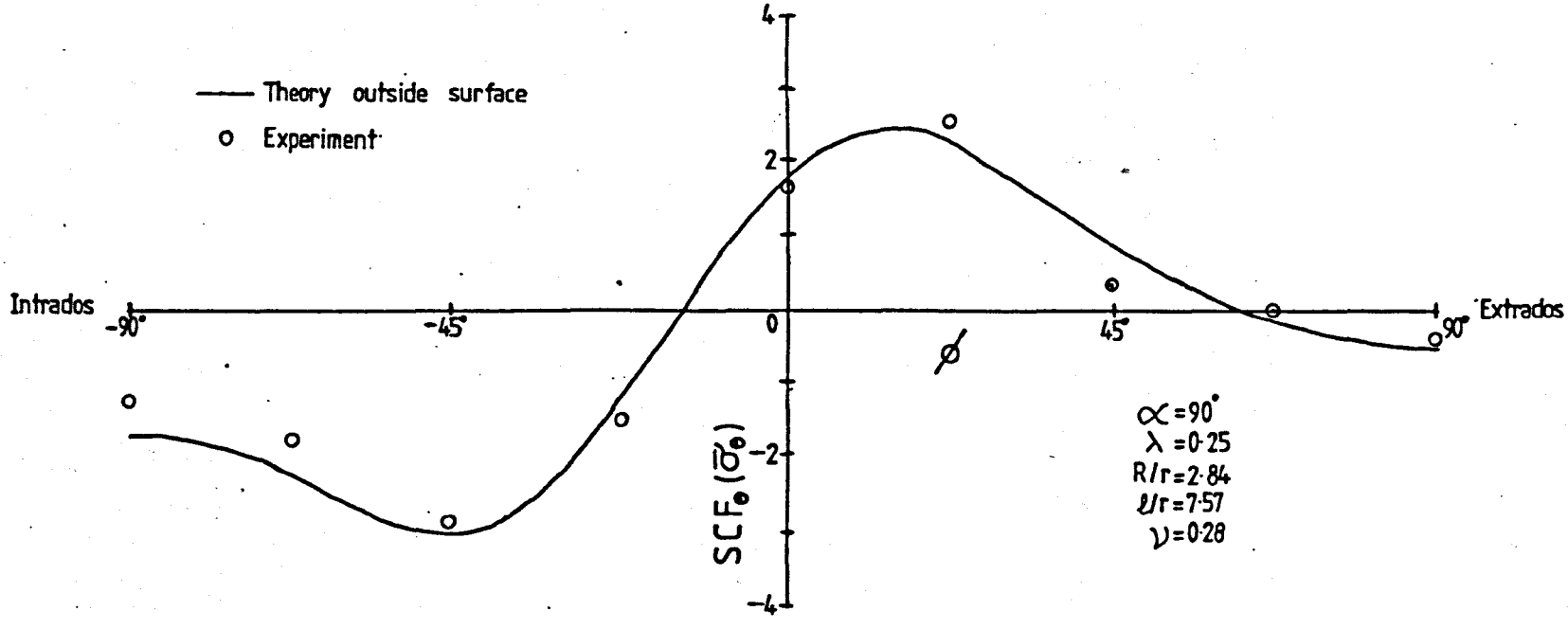

Experimental Circumferential SCFs from Bend No4 at $\theta = 0°$

Figure (6.17)

CHAPTER .7

COMBINED BENDING AND PRESSURE FOR FLANGED BENDS AND OTHER POSSIBLE EXTENSIONS TO THE THEORY

Abstract

Some possible extensions of the methods given in chapters (3) and (5) are discussed. Method No. 2 is extended to deal with combined bending and internal pressure for flanged bends and some typical flexibility factors are given. An explanation is presented of how to extend methods Nos. 3 and 5 to include pressure. Other possible components of loading are then discussed along with their corresponding displacement boundary conditions. Two alternative types of end constraints are briefly reviewed and finally a possible extension of the theory to isothermal stationary creep is examined.

CHAPTER (7)

COMBINED BENDING AND PRESSURE FOR FLANGED BENDS AND OTHER POSSIBLE EXTENSIONS TO THE THEORY

(7.1) Introduction

(7.2) Combined Bending and Internal Pressure

(7.3) Other Possible Loadings

(7.4) Other Types of End Constraint

(7.5) Creep

(7.1) Introduction

Results were presented earlier for two of the more important smooth pipe bend problems, namely the influence of flange and tangent pipe end constraints on bends under in-plane bending. The solution technique used in methods nos. 3 and 5 could be extended to examine other aspects of pipe bend behaviour. To have attempted to present these herein would, because of space and time limitations, have restricted the detailed examination of the major problems in chapters (3) and (5).

In the following sections a brief review will be given of possible ways to extend the numerical solution procedure to investigate other material, geometry and loading problems. A slightly more detailed investigation, with a few typical results, will be given for the problem of a smooth bend with flanges under combined bending and internal pressure. This problem is of particular interest since no published results exist for it. For tangent pipes, flexibilities for the more practical bend angles 90° and 180° are close to the results for bends without end constraints and therefore the results of Dodge and Moore [40] for combined bending and pressure should be a useful first approximation.

(7.2) Combined Bending and Internal Pressure

The analysis of smooth bends, without end constraints, under combined bending and pressure has been extensively reported in the literature. See in particular references [14, 29, 30, 31, 40, 42] discussed in section (1.2). The works of Kafka and Dunn [29], Rodabaugh and George [31] and Dodge and Moore [40]are of special interest/

interest in the present context since they employed lower bound type energy analyses and their works were more advanced than [14]. The conclusion from all of these investigations was that the second order pressure effect could significantly reduce the flexibility of bends, particularly for bends with low pipe factors (λ). None of the publications on end effects is known to include combined bending and pressure.

The membrane stresses arising from internal pressure, P, in a toroid are well established and can easily be derived from equilibrium considerations as,

$$\sigma_\phi = \frac{Pr}{2t}\,\frac{\left(2+\frac{r}{R}\sin\phi\right)}{\left(1+\frac{r}{R}\sin\phi\right)}$$

$$\sigma_\theta = \frac{Pr}{2t} \qquad \ldots (7.1)$$

However, these equations are not completely satisfactory in that, when the displacements are evaluated via the stress-strain relations, they give rise to singularities in displacements. Improved solutions are available, e.g. Reissner [165], but these are only minor modifications of (7.1). The above equations are suitable for most purposes. The corresponding strains can be derived from (7.1), using the normal stress-strain relations for a linear elastic material as,

$$\epsilon_\theta = \frac{Pr}{2Et}\left(\frac{2+\frac{r}{R}\sin\phi}{1+\frac{r}{R}\sin\phi} - \nu\right)$$

$$\epsilon_\phi = \frac{Pr}{2Et}\left(1 - \nu\,\frac{2+\frac{r}{R}\sin\phi}{1+\frac{r}{R}\sin\phi}\right) \qquad \ldots (7.2)$$

For/

For combined bending and pressure the problem is more complicated. For a linear elastic analysis, strains due to pressure are not included in the energy expression but the T.P.E. is modified by an extra term involving the potential of the pressure due to the change in area of the cross-section caused by the distortion displacements. To a first order, the change in area is zero but to a second order it can be found as (see Appendix (6)),

$$\Delta A = \frac{1}{2}\int_0^{2\pi}\left[2\omega r + \omega^2 + v^2 + \omega\frac{\partial v}{\partial \phi} - v\frac{\partial \omega}{\partial \phi}\right] d\phi \qquad \ldots (7.3)$$

Since the pressure strains are not included in the T.P.E. but are superimposed after a solution has been obtained, then the cross-section must be assumed to be inextensible for terms involving the pressure. Imposing second order inextensibility on (7.3) (see Appendix (6)) gives,

$$\Delta A = -\frac{1}{2}\int_0^{\pi}\left[\left(\frac{\partial \omega}{\partial \phi}\right)^2 + \left(\frac{\partial v}{\partial \phi}\right)^2 + \left(\frac{\partial v}{\partial \phi}\right)(2r+\omega) - v\frac{\partial \omega}{\partial \phi}\right] d\phi \qquad \ldots (7.4)$$

For a bend with no end effects the series displacements of the form in equations (3.12) were substituted into (7.4) and the expression integrated. However, when end effects are included, the displacements also vary in the circumferential direction, i.e. the change in cross sectional area varies along the bend, and the expression (7.4) has to be integrated with respect to θ to give the change in volume for the bend. The pressure potential term is then given by,

$$p\tfrac{1}{2}\int_0^{\pi}\int_0^{\alpha}\left[\left(\frac{\partial w}{\partial \phi}\right)^2+\left(\frac{\partial v}{\partial \phi}\right)^2+\left(\frac{\partial v}{\partial \phi}\right)(2r+w)-v\frac{\partial w}{\partial \phi}\right]d\phi R'd\theta \qquad \ldots (7.5)$$

It is relatively straightforward to substitute the distortion displacements into (7.5) and obtain the necessary modification to the T.P.E. but it should be appreciated that a solution will involve some five parameters for flanged bends and six for tangent-bend assemblies, making a comprehensive survey difficult. As an example of the influence of pressure, consider first the problem of the flanged bend using method No. 2. This method was the best of the simpler solutions of the flanged bend problem and avoids the complexity of method No. 3. Substituting the distortion part of the displacements given in (3.55), into (7.5), gives,

$$\frac{pR\pi\alpha}{4}\sum_m'\sum_p\sum_n C_{mn}C_{pn}(n^2-1)(1+\tfrac{1}{2}\delta_{mp}) \qquad \ldots (7.6)$$

which can be non-dimensionalised using (3.58), i.e. dividing by $(M\,\chi_0/2(1-\nu^2))$, to give,

$$\frac{1}{2}\$\sum_1'\sum_1'\sum \bar{C}_{mn}\bar{C}_{pn}(n^2-1)(1+\tfrac{1}{2}\delta_{mp})(1-\nu^2) \qquad \ldots (7.7)$$

where $\$=\dfrac{pR^2}{Ert}$

This term is added to the existing T.P.E. expression in (3.50), which is then minimised in the usual manner. Some typical results are shown in figures (7.1) and (7.2). It can be seen that pressure has more influence when the flexibility factor without pressure is higher.

One/

One could also extend the analysis to the most general case considered herein, namely method No. 5 for tangent pipes. The extension will be outlined but not evaluated. The additional energy term for method No. 5 could be determined in a similar manner using the displacements given in equations (5.13). Equation (7.5) can be non-dimensionalised using (5.30) to give the pressure potential as,

$$(1-\nu^2)\,\$\left[\int_{-\frac{\pi}{2}}^{\frac{\pi}{2}}\int_{0}^{\frac{\alpha}{2}} \Phi_p\, Z\, d\phi\, d\theta + \int_{-\frac{\pi}{2}}^{\frac{\pi}{2}}\int_{\frac{\alpha}{2}}^{\frac{\alpha}{2}+\frac{L}{R}} \Phi_p\, d\phi\, d\theta\right] \qquad \ldots (7.8)$$

where

$$\Phi_p = \left[\left(\frac{\partial\bar{\omega}}{\partial\phi}\right)^2 + \left(\frac{\partial\bar{v}}{\partial\phi}\right)^2 + \frac{\partial\bar{v}}{\partial\phi}\bar{\omega} - \bar{v}\frac{\partial\bar{\omega}}{\partial\phi}\right]$$

$$Z = 1 + \frac{r}{R}\sin\phi \quad , \quad \$ = \frac{pR^2}{Ert} \quad , \quad \bar{v} = v\frac{\alpha}{r\gamma_0} \quad , \quad \bar{\omega} = \omega\frac{\alpha}{r\gamma_0}$$

Note that the second term in (7.8) involves the integration of the change in area along the tangent pipe. The $2r\left(\frac{\partial v}{\partial\phi}\right)$ term in equation (7.5) is not included in (7.8) since it can be shown to integrate to a zero value. The integrations in (7.8) could be performed numerically in the same way as the strain energy. (See section (3.5d)). Method No. 3 for flanged bends could be considered as a special case of method No. 5 with zero length tangents.

Once a solution has been obtained using equations (7.8) and (5.31) the flexibility factors are obtained in the usual way. The stresses could be obtained by adding the stresses due to bending, equation (3.86) using the new coefficients and the stresses due to/

to pressure, (7.1).

In [81] Boyle and Spence pointed out that the above type of solution is not entirely correct. By performing a nonlinear analysis of a bend without end effects they showed that the flexibility factor was dependent on a further parameter, the ratio of bending moment to pressure. They concluded that the above type of analysis is adequate for relatively lower pressures.

(7.3) Other Possible Loadings

The six basic external components of pipe bend loading are in-plane and out-of-plane bending, torque, in-plane and out-of-plane shear loading and axial loading. These are illustrated in figure (7.3). In-plane bending has been extensively examined herein using a prescribed displacement type energy technique. Most of the boundary conditions for this case were determined from the two symmetries of the problem i.e. through $\phi = -90^{\circ}$ and $\phi = +90^{\circ}$ and through $\theta = 0^{\circ}$. These symmetries also allowed a reduction in the computer solution time by a factor of four because of the smaller integration requirements. The other forms of loading are slightly more difficult.

One further asset of the in-plane bending moment is that the applied and reaction loads are identical for all subtended bend angles. For the other types of loading these must differ for the maintenance of external equilibrium, with the exception of a few special cases.

When extending the present techniques to other loadings each of these points would have to be considered. For any particular case it should be relatively straightforward to specify the/

the necessary boundary conditions. The in-plane shear and axial loads could make use of the same rigid section displacements as described in sections (3.2b) and (5.2b), however the other loads would require something different, but perhaps developed along similar lines. The distortion displacements for in-plane loading could use the same meridional functions, i.e. $u(\phi)$, $v(\phi)$ and $\omega(\phi)$, but would require new circumferential series which satisfied the new boundary conditions. These could be determined using fourier series in a similar manner to the in-plane bending case using the methods in section (3.2d-f). Out-of-plane bending and shear loading, and torque would require complete fourier series, involving all even and odd terms in the meridional functions, for a solution of the type given herein.

Of all of the components of loading considered above, perhaps the second most important, after in-plane bending, is out-of-plane bending. However, it is probably the most difficult loading to obtain a solution for.

(7.4) Other Types of End Constraint

The end constraints previously considered are perhaps the most common type of bend connections but two other possible forms are 'S' bends and bends with one flange and one tangent pipe as shown in figure (7.4). For in-plane bending, these could be examined using the methods developed herein relatively easily.

A bend with one flange and one tangent could make use of the rigid section displacements in section (5.2b) and the meridional component of the distortion series but would require different circumferential series satisfying the new boundary conditions./

conditions. Since the bend behaviour would be non-symmetric the whole circumferential length of the assembly would have to be examined. The simplest boundary conditions could be achieved by fully fixing the free end of the bend, i.e. putting u, v, w and β_θ equal to zero, and treating the tangent pipe as explained in chapter (5).

The 'S' bend is a more difficult problem since one part of the bend is being 'opened' and the other 'closed'. At the connection between the parts, the distortion displacements from each side will almost cancel each other but not quite. The circumferential components of the distortion series would have to satisfy the continuity requirements at the two bend-tangent connections and at the bend-bend connection.

Both of these problems were considered by Natarajan and Blomfield [97] using finite element analysis. They only examined a limited range of parameters, but their results suggest that the flexibility of a bend with one flange and one tangent cannot be approximated by taking an average of the flexibility factors for the bends with two flanges and two tangents, as may at first be intuitively imagined.

(7.5) Creep

In recent years, considerable attention has been given to the problem of creep in pipework components, particularly smooth bends. The techniques described herein for examining smooth bends with end effects could be modified to deal with isothermal stationary creep conditions following the method given by Spence [70].

A/

A Norton [67] stationary creep law could be used, i.e.

$$(\dot{\epsilon}/\dot{\epsilon}_o) = (\sigma/\sigma_o)^n \qquad \ldots (7.9)$$

together with the approximate strain energy rate equation given by Mackenzie [166],

$$U = \frac{n}{n+1}\frac{\sigma_o t}{\epsilon_o^{1/n}}\left(\frac{4}{3}\right)^{\frac{n+1}{2n}}\int\int\left[(\dot{\epsilon}_\phi+\dot{\epsilon}_\theta)^2-(\dot{\epsilon}_\theta\dot{\epsilon}_\phi-\tfrac{1}{4}\dot{\gamma}_{\theta\phi}^2)+A\frac{t^2}{4}\left((\dot{\kappa}_\phi+\dot{\kappa}_\theta)^2-(\dot{\kappa}_\theta\dot{\kappa}_\phi-\dot{\kappa}_{\theta\phi}^2)\right)\right]^{\frac{n+1}{2n}} r R' d\theta d\phi \qquad \ldots (7.10)$$

where $\dot{\epsilon}$ and $\dot{\kappa}$ are the strain and curvature rates.
The displacement rates could be used with a similar form to the displacements in chapters (3) and (5), and the same thin shell strain-displacement (rate) relationships to derive the strain rates. These could be substituted into (7.10) which would then be minimised to obtain the displacement rate coefficients. Because the energy is no longer a quadratic function the minimisation procedure developed in section (3.5c) cannot be used. A direct numerical minimisation technique would have to be employed and this would involve a considerable increase in the solution time. Experiments of this type of procedure with the earlier problems suggests that the necessary time for a fully converged solution may exceed the reliability limits of the currently available mainframe computers. For a first approximation, some of the simplifications used in methods Nos. 1. 2 and 4 could be employed.

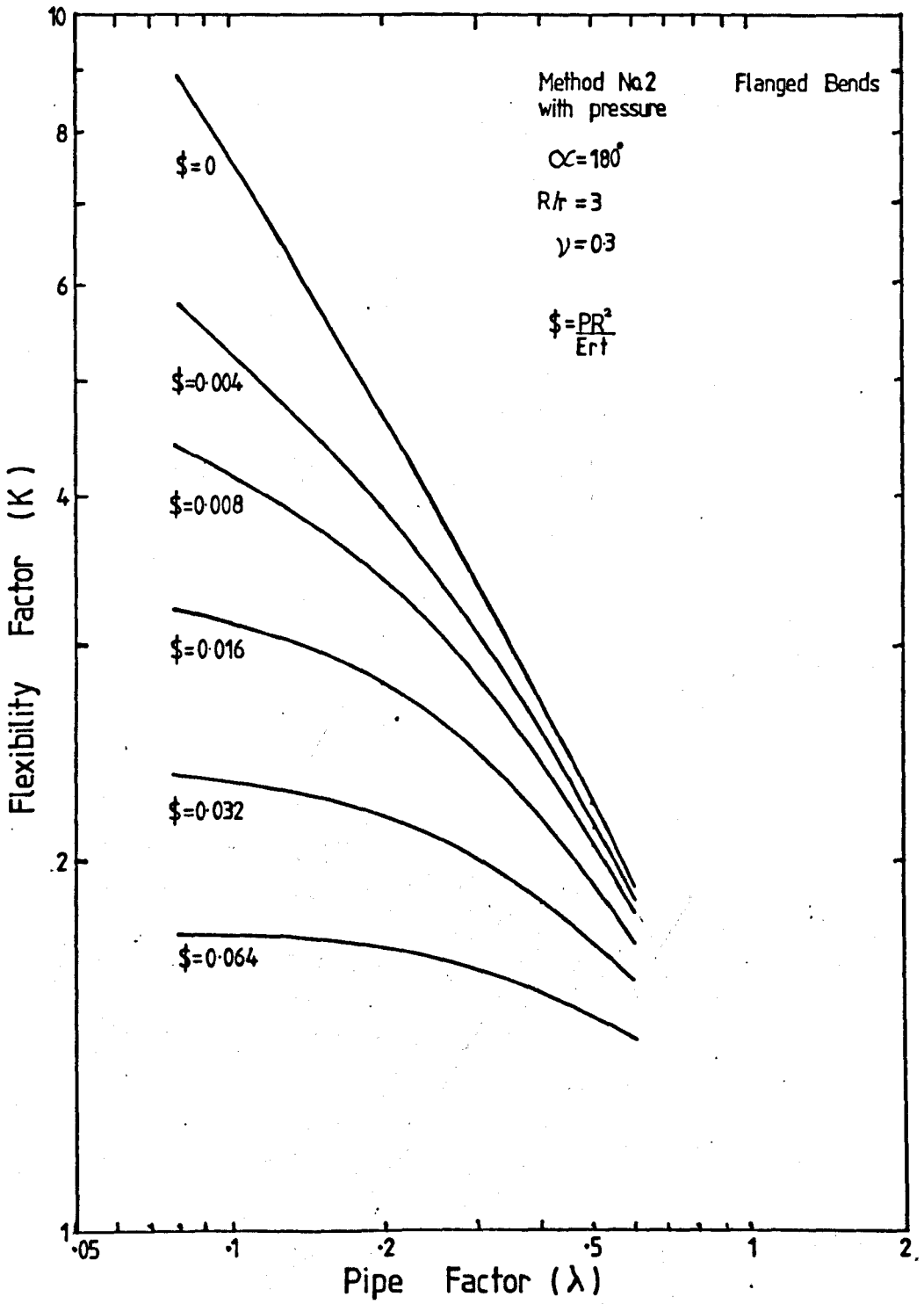

Typical Flexibility Factors for Combined Bending and Pressure

Figure (7.1)

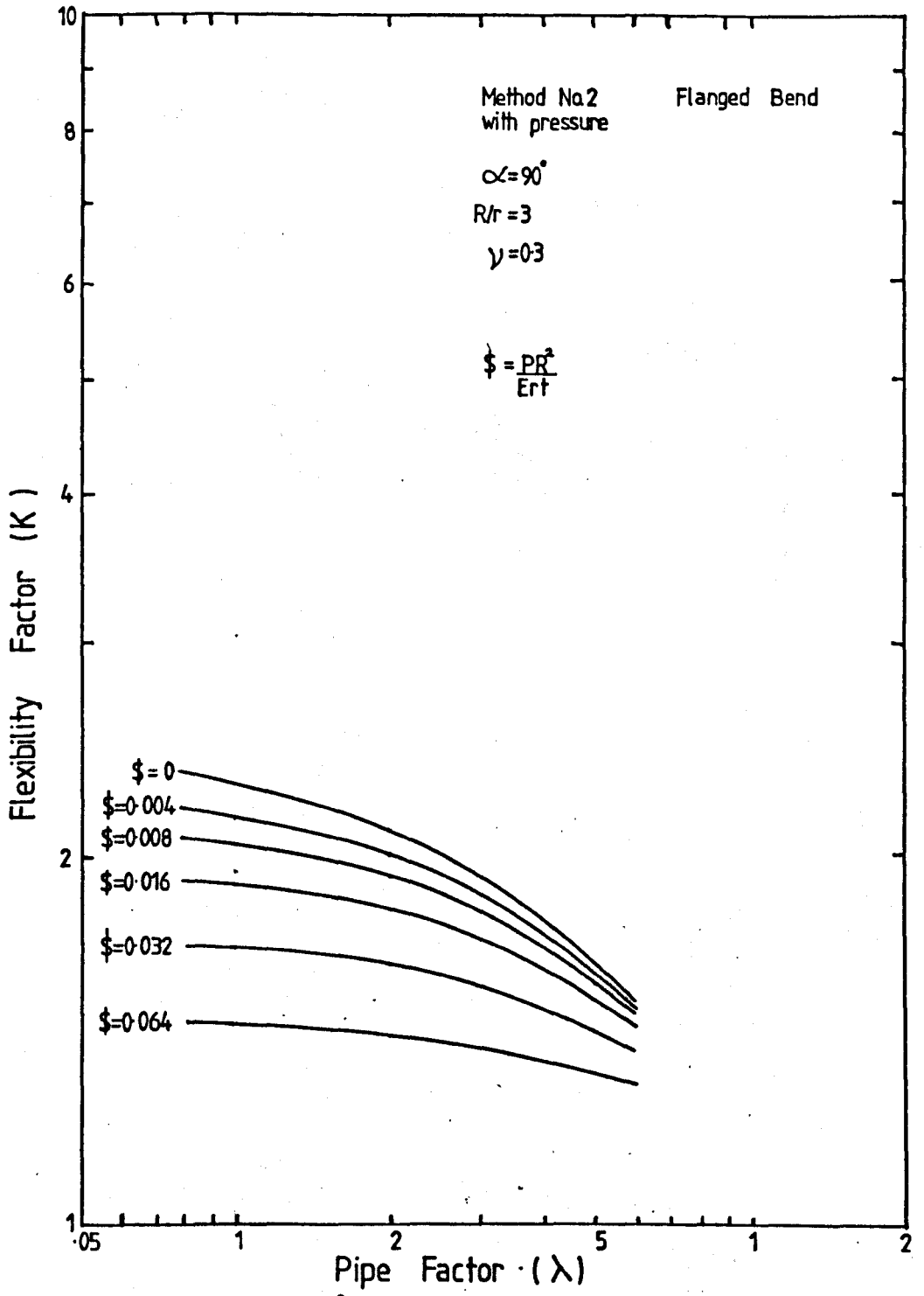

Typical Flexibility Factors for Combined Bending and Pressure

Figure (7.2)

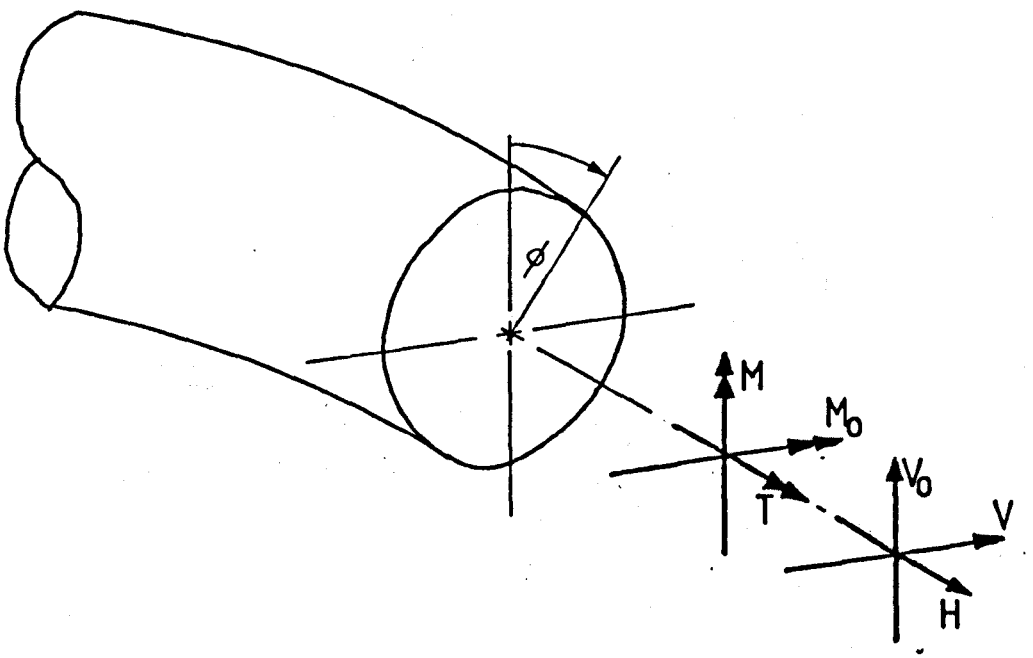

M In-plane Bending

M_o Out-of-plane Bending

T Torque

V In-plane Shear

V_o Out-of-plane Shear

H Axial Load

Basic Components of Loading

Figure (7.3)

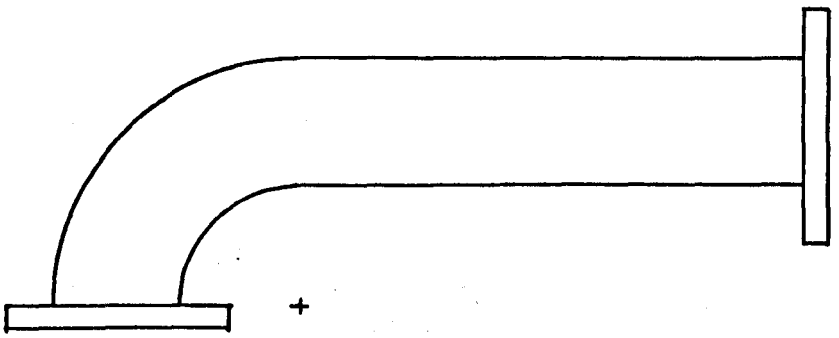

Bend with one flange & one tangent pipe

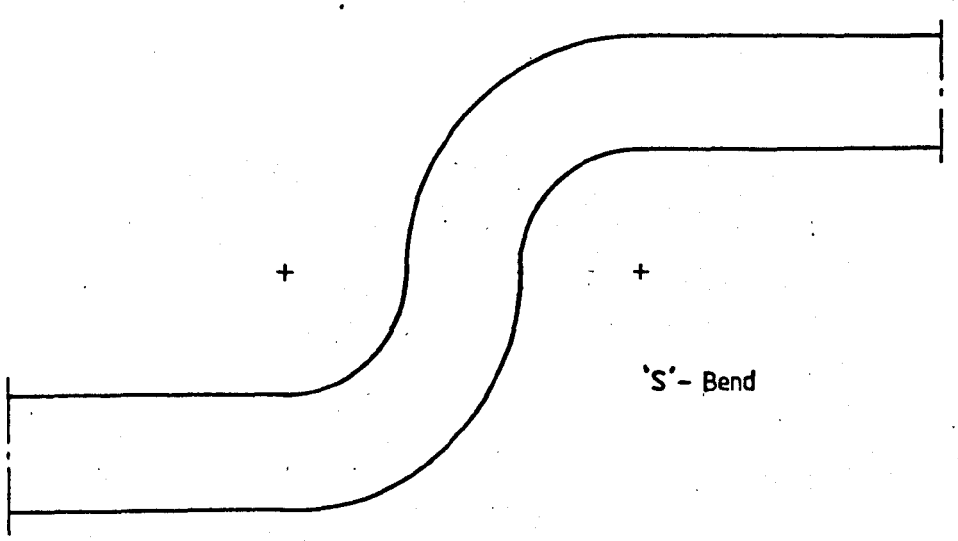

Alternative End Constraints

Figure (7.4)

GENERAL CONCLUSIONS

GENERAL CONCLUSIONS

A variety of theoretical solutions describing the behaviour of smooth pipe bends, with flange or tangent pipe end constraints, under in-plane bending, have been developed.

Flanged Bends

Three different solutions to the flanged bend problem have been presented, namely methods nos. 1, 2, and 3. They differ from each other mainly by the number of assumptions involved, method No. 1 using the most assumptions and method No. 3 using the least. When compared for various geometries method No. 1 was shown to yield substantially lower bend flexibility factors than either method No. 2 or 3. The difference was up to 50% for low radius ratios, $R/r \leq 3$, and bend angles, $\alpha \leq 90^{\circ}$. This was principally due to the assumption of zero shear strain and the assumed insignificance of the odd meridional fourier terms in the radial distortion displacement. Method No. 2, which removed these assumptions, gave flexibility factors which were less than 12% lower than those from method No. 3 for $\lambda \geq 0.1$. This latter difference was mainly caused by the importance of the terms in the circumferential distortion series which method No. 2 ignored. Method No. 3, which involved a complex numerical solution procedure, removed most of the assumptions of the other methods and gave the highest (and hence best) flexibility factors.

Method No. 3 demonstrated that the incorporation of rigid flanges on the ends of a bend can cause a significant reduction in its flexibility, the flexibility reducing with bend angle and radius/

radius ratio and increasing as the pipe factor reduces. The location and magnitude of the maximum stress on a flanged bend was shown to be dependent on the bend angle, radius ratio and pipe factor but without any simple trends. The maximum stress may occur at the centre of the bend ($\theta = 0$) or at the flange, on the inside or the outside surface and may be in the direction of either of the principal axes. The maximum stress at the flange can be significantly affected by the flange rigidity but the bend centre stresses are less influenced.

Method No. 3 was compared with results from the previously published flanged bend theories of Thailer-Cheng [95], Findlay [99], Axelrad [104] and Whatham [117]. Examination of the works of Thailer-Cheng and Findlay revealed that both contained assumptions which the present work has shown to be largely invalid. Comparison with the flexibility factors of Axelrad showed fair agreement with method No. 3 but the agreement was better for higher flexibilities, which was consistent with his assumptions. Comparison with Whatham's results showed a good general agreement, his flexibility factors being up to 10% higher.

The theoretical results from method No. 3 compared favourably with the tests conducted during the present programme of work. Method No. 3 also yielded reasonable agreement with much of the published applicable experimental evidence, particularly with that obtained in the last ten years. It is perhaps unfortunate that the most comprehensive set of experimental data on flanged bends dates back to Pardue and Vigness [89] in 1952 and the actual details of their tests are not completely clear. There/

There is a real need for a systematic experimental survey covering lower pipe factors ($\lambda < 0.1$) and lower bend angles ($\alpha < 90^{\circ}$).

Bend-Tangent Assemblies

Two different theoretical solutions have been developed for the problem of a smooth pipe bend with connected flanged tangent pipes, methods Nos. 4 and 5, again differing by their inherent assumptions. Method No. 4 involved a number of assumptions which previously were commonly used and substantiated in the theories which ignored end constraints. However, method No. 4 was shown to give flexibility factors which were up to 12% lower than those from method No. 5. The latter method involved a complex numerical solution which allowed the removal of most of the previous assumptions. In method No. 5 one particular assumption remained, involving the continuity of the shell surface slope across the connection between the tangent pipe and the bend. The slope given by the assumed displacements was continuous at $\phi = 0$ but was violated elsewhere to a degree dependent on radius ratio.

The flexibility of bends with connected tangent pipes was shown to be appreciably lower than that predicted by any theory ignoring end constraints, particularly for bend angles less than 90°. The bend flexibility was shown to reduce with tangent pipe length, ℓ, for ℓ less than one pipe circumference, $2\pi r$. Flexibility also reduced with bend angle and radius ratio and increased as the pipe factor reduced. For bend angles greater than about 20° the maximum stress on the bend usually occured at the bend centre ($\theta = 0$) on the inside surface in the meridional direction.

Method/

Method No. 5 gave good agreement when compared with published finite element and theoretical results for bends with connected tangent pipes. As with the results for bends without end constraints, these results show some deviation depending on the solution procedure which was adopted, e.g. depending on whether or not the $(1 - \nu^2)$ term was involved.

The theoretical results from method No. 5 compared favourably with published experimental data and gave good agreement with the tests performed during the present work. Comparison of the experimental stress distributions and the published theoretical work confirms that the assumption involving the slope continuity did not unduly affect the overall behaviour, except locally at the junction.

Design Codes

Comparison of the results presented herein for bends with end constraints with the current recommendations in most of the present design codes would suggest that the codes need some modification. Simple formulae have been suggested which could relatively easily be adopted into these codes to describe the behaviour of bends with connected long tangent pipes. For bends with flanged ends, simple general formulae are not possible but a graphical presentation of the results could be used.

BIBLIOGRAPHY

1. BANTLIN, A. "Formanderung und Beanspruchung Febernder Ausfleichrochen". Zeits V.D.I. Vol. 2, pp. 43 - 49, 1910.

2. KARMAN, Von T. "Uber die Formanderung Dunnwandiger Röhre insb esonders federnder Ausgleichrohre". Zeits V.D.I. Vol. 55, pp. 1889 - 1895, 1911.

3. MARBEC, M. "Flexibilité des tubes". Bull. Assoc. Techn. Maritime Aeronaut. Vol. 22, pp. 441 - 475, 1911.

4. SPENCE, J. "On the Bounding of Pipe Bend Flexibility Factors". Nuc. Eng. and Design, Vol. 12, No. 1, pp. 39 - 47, 1970.

5. LORENZ, H. "Die Biegung Krummer Röhre". Physik. Zeits Vol. 13, pp. 768 - 774, 1912.

6. TIMOSHENKO, S. "Bending Stresses in Curved Tubes of Rectangular Cross-sections". Trans. A.S.M.E., Vol. 45, pp. 135 - 140, 1923.

7. HOVGAARD, W. "The Elastic Deformation of Pipe Bends". J. of Math. & Phys. of M.I.T., Vol. VI, No. 2, pp. 69 - 118, 1926.

8. HOVGAARD, W. "Deformation of Plane Pipes". J. of Math, & Phys. of M.I.T., Vol. VII, pp. 198 - 238, 1928.

9. WAHL, A. M. "Stresses & Reactions in Expansion Pipe Bends". Trans. A.S.M.E., Vol. 50, pp. 241 - 262, 1928.

10. MARKL, A. R. C. "Piping Flexibility Analysis". Trans. A.S.M.E., Vol. 77, pp. 419 - 441, 1955.

11. JENKS, H. E. "Design of Steam Piping to Care for Expansion". Trans. A.S.M.E., Vol. 51, pp. 443 - 444, 1929.

12. THULOUP, M. A. "Essai sur la Fatigue des Tuyaux Minces à Fibre moyenne plane au gauche". Bull. Assoc. Techn. Maritime Aeronaut, Vol. 32, p643, 1928.

13. THULOUP, M. A. "Sur la Deformation et les Tensions Internes des Tuyaux à ligne moyenne plane". ibid, Vol. 36, 1932.

14. THULOUP, M. A. "Remarques sur le calcul des Tuyaux Minces sous Pression". ibid, Vol. 41, 1937.

15. TUEDA, M. "Mathematical Theories of Bourdon Pressure Tubes and Bending of Curved Pipes". Mem. Coll. Eng., Kyoto Imperial Univ., First Rep., Vol. 8, p. 102, 1934. Second Rep., Vol. 9, p. 132, 1936.

16. KARL, H. "Biegung gekrümmter, dunnwandiger Rohre". Zeits Angew. Math, Mech., Vol. 23, pp. 331 - 345, 1943.

17. VIGNESS, I. "Elastic Properties of Curved Tubes". Trans. A.S.M.E., Vol. 65, pp. 105 - 120, 1943.

18. BESKIN, L. "Bending of Curved Thin Tubes". Trans. A.S.M.E., Vol. 67, p. A - 1, 1945.

19. BARTHELEMY, J. "Étude de la Déformation et des Tensions Internes des Tuyaux a Ligne Moyenne Plane, sans Pression Interne". Bull. Assoc. Techn. Maritime Aeronaut, Vol. 45, p. 139, 1946.

20. BARTHELEMY, J. "Étude de la Deformation et des Tensions Internes des Tuyaux à Ligne Moyenne Plane soumis à des Efforts Extérieurs et à une Pression Interne". ibid, Vol. 46, p. 411, 1947.

21. DE LEIRIS, H.
BARTHELEMY, J. "Determination des Deformations et des Tensions dans un Tuyau à Section Ovale". ibid, Vol. 47, p. 147, 1948.

22. DE LEIRIS, H.
BARTHELEMY, J. "Deformations et Tensions dans les Tuyaux à Ligne Moyenne Plane". French paper, Source uncertain, p. 308 - 321, c. 1950.

23. HUBER, M. T. "The Bending of the Curved Tube of Elliptic Section". Proc. 7th International Congress for Applied Mechs., Vol. 1, p. 322, 1949.

24. HUBER, M. T. Polish Publication "Archiwum Mechaniki Stosowanej". Vol. 1, No. 2, 1949.

25. REISSNER, E. "On Bending of Curved Thin-Walled Tubes". Proc. Natl. Acad. Sci. U.S., Vol. 35, pp. 204 - 208, 1949.

26. CLARK, R. A.
REISSNER, E. "Bending of Curved Tubes". Advances in Applied Mechs., Vol. II, 1951.

27. GROSS, N. "Experiments in Short-Radius Pipe Bends". Proc. I. Mech. E., (B). Vol. 1B, p. 465, 1952 - 1953.

28. GROSS, N.
FORD, H.
"The Flexibility of Short-Radius Pipe Bends". Proc. I. Mech. E., (B). Vol. 1B, p. 480, 1952 - 1953.

29. KAFKA, P. G.
DUNN, M. B.
"Stiffness of Curved Circular Tubes with Internal Pressure". Trans. A.S.M.E., J. of Applied Mechs., Vol. 78, p. 247, 1956.

30. CRANDALL, S. H.
DAHL, N. C.
"The influence of Pressure on the Bending of curved Tubes". Proc. 9th International Congress of Applied Mechs. pp. 101 - 111, 1956.

31. RODABAUGH, E. C.
GEORGE, H. H.
"Effect of Internal Pressure on Flexibility and Stress-Intensification Factors of Curved Pipe or Welding Elbows". Trans. A.S.M.E., Vol. 79, pp. 939 - 948, 1957.

32. TURNER, C. E.
FORD, H.
"Examination of the Theories for Calculating the Stresses in Pipe Bends Subjected to In-Plane Bending". Proc. I. Mech. E., Vol. 171, p. 513, 1957.

33. FINDLAY, G. E.
SPENCE, J.
"In-plane Bending of a Large 90° Smooth Bend". J. of Strain Analysis, Vol. 1, No. 4, p. 290, 1966.

34. JONES, N.
"On the Design of Pipe Bends". Nuc. Eng. & Design, Vol. 4, pp. 399 - 405, 1966.

35. JONES, N.
"In-Plane Bending of a Short-Radius Curved Pipe Bend". Trans. A.S.M.E., J. of Eng. for Industry, Vol. 89, ser. B, p. 271, 1967.

36. CHENG, D. H.
THAILER, H. J.
"In-Plane Bending of Curved Circular Tubes". Trans. A.S.M.E., J. Eng. for Industry, Vol. 90, Ser. B, No. 4, p. 666, 1968.

37. CHENG, D. H.
THAILER, H. J.
"On the Bending of Curved Circular Tubes". ibid, Vol. 92, Ser. B, No. 1, pp. 62 - 66, 1970.

38. FINDLAY, G. E.
SPENCE, J.
"Bending of Pipe Bends with Elliptic Cross-section". Weld. Res. Counc. Bull., No. 164, 1971.

39. SPENCE, J.
FINDLAY, G. E.
"The Effect of Thickness Variations on the Behaviour of Smooth Curved Pipes Under External Bending". A.S.M.E./ C.S.M.E. Press. Ves. and Piping Conf., Montreal, June 1978, A.S.M.E. paper No. 78-PVP-93.

40. DODGE, W. G.
MOORE, S. E.
"Stress Indices and Flexibility Factors for Moment Loadings on Elbows and Curved Pipes". Welding Res. Counc. Bull., No. 179, 1972.

41. DODGE, W. G.
MOORE, S. E.
"ELBOW: A Fortran Program for the Calculation of Stresses, Stress Indices and Flexibility Factors for Elbows and Curved Pipes". Oak Ridge Nat. Lab. Rep., No. ORNL-TM-4098.

42. BLOMFIELD, J. A.
TURNER, C. E.
"Theory of Thin Elastic Shells applied to Pipe Bends Subjected to Bending and Internal Pressure". Jrnl. of Strain Analysis, pp. 285 - 293, Vol. 7, No. 4, 1972.

43. KITCHING
BOND, M. P.
"Out of Circularity Effects in a Pipe Subjected to Pressure and Bending Loads". Jrnl. of Strain Analysis, Vol. 7, No. 4, 1972.

44. THOMPSON, J. J.
"Shell Theory Analysis of Pure In-Plane Bending of a Pipe Bend". Proc. 3rd Int. Conf. Struct. Mech. in Reactor Tech., London, 1975.

45. MARCAL, P. V.
"Elastic Plastic Behaviour of Pipe Bends with In-plane Bending". Jrnl. of Strain Analysis, Vol. 2, No. 1, pp. 84 - 90, 1967.

46. BOLT, S. E.
GREENSTREET, W. L.
"Experimental Determination of Plastic Collapse Loads for Pipe Elbows". Pressure Vessels and Piping Conf., San Francisco, 1971.

47. SPENCE, J.
FINDLAY, G. E.
"Limit Loads for Pipe Bends Under In-Plane Bending". 2nd Int. Conf. Press. Ves. Tech., San Antonio, Texas, Vol. 1, pp. 393 - 399, 1973.

48. CALLADINE, C. R.
"Limit Analysis of Curved Tubes". Jrnl. of Mech. Eng. Sc., Vol. 16, No. 2, pp. 85 - 87, 1974.

49. MELLOW, R. H.
GRIFFIN, D. S.
"Plastic Collapse Loads for Pipe Elbows Using Inelastic Analysis". Trans. A.S.M.E., Jrnl. Press. Ves. Tech., Vol. 96, p. 177, 1974.

50. SPENCE, J.
FINDLAY, G. E.
"Limit Moments for Non-Circular Cross-Sections (Elliptical) Pipe Bends". 4th SMIRT, San Francisco, 1977.

51. PAN, Y.
YETTER, R.
"Inelastic Analysis of Pipelines in the FFTF CLS Module". A.S.M.E. Conf. Press. Ves. and Piping Analysis and Computers, Miami, pp. 59 - 75, 1974.

52. 'MARC'
"MARC - CDC Non-Linear Finite Element Analysis Program" - MARC Analysis Corp. and CDC Minneapolis, 1974.

53. LARSON, L. D.
STOKEY, W. F.
FRANZEN, W. E.
"An Approximate model for an elastic plastic pipe element under combined loading". Trans. A.S.M.E., Ser. J., Jrnl. Press. Ves. Tech. 97, pp. 22 - 28, 1975.

54. LAZZERI, L.
"An Elastoplastic Elbow Element, Theory and Applications". 5th Int. Conf. on Struc. Mech. in Reactor Tech., Berlin, 1979.

55. LAZZERI, L.
"A Model for a Strain Hardening Pipe Element". A.S.M.E. paper no. 77-PVP-47.

56. DENNISON, R. L.
"The strength and Flexibility of Corrugated and Creased Bend Piping". Jrnl. of Am. Soc. Naval Eng., Vol. 47, pp. 343 - 432, 1935.

57. ROSSHEIM, R. B.
MARKL, A. R. C.
"The Significance of and Suggested Limits for the Stresses in Pipe Lines Due to the Combined Effects of Pressure and Expansion". Trans. A.S.M.E., Vol. 62, pp. 443 - 464, 1940.

58. MARKL, A. R. C. "Fatigue Tests of Welding Elbows and Comparable Double-Mitre Bends". Trans. A.S.M.E., Vol. 69, pp. 869 - 879, 1947.

59. MARKL, A. R. C. "Fatigue Tests of Piping Components". Trans. A.S.M.E., Vol. 74, p. 287, 1952.

60. LANE, P. H. R. "Fatigue Tests on Seamless Mild Steel Pipe Bends". B.W.R.A. (Confidential Report) No. 16/41/56, 1956.

61. BLOMFIELD, J. A.
JACKSON, P. B. M. "Fatigue Tests on Some Cupro-Nickel Pipe Bends and a Comparison of some Failure Prediction Methods". 1st Int. Conf. on Press. Ves. Tech., Delft, p. 11 - 95, pp. 1221 - 1231, 1969.

62. BLOMFIELD, J. A. "The Elastic Plastic Behaviour of Pipe Bends Subjected to Cyclic Loading". Ph.D. Thesis, Uni. of London, 1970.

63. DOYEN, J. J.
MARINI, J. "Propogation of Inadequate Joint Penetration Defects of Welded Elbows". 4th Int. Conf. Struct. Mech. in Reactor Tech., San Francisco, 1977.

64. JAMES, L. A. "Estimation of Crack Extension in a Piping Elbow Using Fracture Mechanics Techniques". Jrnl. of Press. Ves. Tech., p. 273, Nov. 1974.

65. KACHANOV, L. M. "O Plastichenshom Izgibe Krivgich Funkostennyich Trub". Igv. Akad. Wauk S.S.R. OTD, Vol. 5, p. 42, 1957.

66. SPENCE, J.
MACKENZIE, A. C.
"Stationary Creep Deformation of a Smooth Pipe Bend Under In-Plane Bending Moments". Int. Jnrl. Mech. Sc., Vol. 11, pp. 387 - 394, 1969.

67. NORTON, F. H.
"The Creep of Steel at High Temperature". McGraw-Hill, London, 1929.

68. SPENCE, J.
"Creep Behaviour of Smooth Curved Pipes under bending". 1st Int. Conf. on Press. Ves. Tech. Delft, pp. 309 - 315, 1969.

69. SPENCE, J.
"An Upper Bound Analysis for the Deformation of Smooth Pipe Bends in Creep". 2nd Int. Union of Theo. and Applied Mech. sym on Creep in Structures, Gottenburg, 1970.

70. SPENCE, J.
"Creep of Pipe Bends". Doctoral Dissertation, Univ. of Strathclyde, 1971.

71. SPENCE, J.
"An Analysis for Pipework Systems Under Creep Conditions". Proc. 1st Int. Conf. Struct Mech. Reactor Tech. 1971.

72. SPENCE, J.
"Creep Analysis of Smooth Curved Pipes Under In-Plane Bending". Jrnl. of Mech. Eng. Sc., Vol. 15, No. 4, pp. 252 - 265, 1973.

73a SPENCE, J.
"Stationary Creep Stresses for Elliptical Cross-Section Pipe Bends Subject to In-Plane Bending". A.S.M.E., Jrnl. of Press. Ves. Tech., Vol. 96, pp. 162 - 171, 1974.

73b SPENCE, J. "A Note on the Gross Correction for Noncircular Inelastic Pipe Bends Under In-Plane Bending". A.S.M.E., Jrnl. of Press. Ves. Tech., Vol. 101, pp. 102 - 104, 1979.

74. SPENCE, J. "The Creep deformation of Elliptical Cross-Section Pipe Bends Under In-Plane Bending". Int. Conf. Creep and Fatigue, A.S.M.E./I. Mech. E., Philadelphia, 1974.

75. SPENCE, J. "The Creep Behaviour of Short Radius Pipe Bends". 3rd Int. Conf. Struct. Mech. Reactor Tech., London, 1975.

76. WORKMAN, G. H.
RODABAUGH, E. C. "Strain Concentration in an Elbow in a Piping System Under High Temperature Relaxation Conditions". A.S.M.E., 2nd Int. Conf. Press. Ves. Tech., San Antonio, Texas, 1973.

77. WORKMAN, G. H.
RODABAUGH, E. C. "Simplified Second Stage Creep/ Relaxation Analysis of Moderately Complex Spatially Three Dimensional Piping Systems". Jrnl. of Press. Ves. Tech., Trans. A.S.M.E., Vol. 94, pp. 184 - 192, 1974.

78. HIBBITT, H. D.
SORENSON, E. P.
MARCAL, P. V. "The Elastic-Plastic and Creep Analysis of Pipelines by Finite Elements". 2nd Int. Conf. Press. Ves. Tech., San Antonio, Texas, 1973.

79. MELLOW, R. M.
SCHELLER, J. D. "Simplified Inelastic (Plastic and Creep) Analysis of Pipe Elbows Subjected to In-Plane and Out-of-Plane Bending". A.S.M.E., 2nd Nat. Cong. on Press. Ves. and Piping, San Francisco, 1975.

80. BOYLE, J. T. "Rational Creep Mechanics". Doctoral Dissertation, Univ. of Strathclyde, 1975.

81. BOYLE, J. T.
SPENCE, J. "The Nonlinear Analysis of Pressurized Curved Pipes". 3rd Int. Conf. Press. Ves. Tech., Tokyo, pp. 121 - 131, 1977.

82. BOYLE, J. T.
SPENCE, J. "An Analysis of Out-of-Plane Bending of Curved Pipes in Creep". Proc. I.W.G.F.R. Conf. Fast Breeder Reactors, Pittsburgh, 1976.

83. BOYLE, J. T.
SPENCE, J. "The Flexibility of Curved Pipes in Creep". Trans. A.S.M.E., Jrnl. Press. Ves. Tech., Vol. 99, pp. 844 - 853, 1977.

84. BOYLE, J. T.
SPENCE, J. "The Analysis of Piping Systems for Creep". 4th Struct. Mech. in Reactor Tech. Conf., San Francisco, 1977.

85. GRIFFITH, W. I.
RODABAUGH, E. C. "Tests at Room Temperature and 1100° F on a 4 inch Sch. 10 Elbow-Pipe Assembly Subjected to In-Plane Moment Loading". Press. Ves. and Piping: Verification and Qualification of Inelastic Analysis Computer Programs, A.S.M.E., pp. 59 - 78, 1975.

86. IMAZU, A.
MIURA, R.
NAKUMARA, K.
NAGATA, T.
OKABOYASHI, K. "Elevated Temperature Elastic-Plastic Creep Test of an Elbow Subjected to In-Plane Moment Loading". Press. Ves. and Piping Conf., A.S.M.E., Mexico, 1976.

87. IMAZU, A.
NAKAMURA, K.
"Simplified Creep Buckling Analysis of Elbows Under In-Plane Bending". 5th Struct. Mech. in Reactor Tech., Berlin, 1979.

88. SPENCE, J.
BOYLE, J. T.
"Benchmark Assessment of a Routine Procedure for the Inelastic Analysis of Piping Systems by Simplified Methods". Press. Ves. and Piping Conf., Montreal, 1978. (A.S.M.E. spec. pub. No. PVP-PB-029)

89a PARDUE, T. E.
VIGNESS, I.
"Properties of Thin Walled Curved Tubes of Short Bend Radius". Trans. A.S.M.E., Vol. 73, pp. 77 - 84, 1951.

89b PARDUE, T. E.
VIGNESS, I.
"Characteristics of Pipe Bends under Applied Moments". Naval Research Laboratory, Rep. No. 111292, Dec. 1953.

90. VISSAT, P. L.
DEL BUONO, A. J.
"In-Plane Bending Properties of Welding Elbows". Trans. A.S.M.E., Vol. 77, p. 161, 1955.

91. SMITH, R. T.
FORD, H.
"Experiments on Pipelines and Pipe Bends Subjected to Three-Dimensional Loading". Jrnl. Mech. Eng. Sc., Vol. 9, No. 2, p. 124, 1967.

92. KALNINS, A.
"Analysis of Shells of Revolution Subjected to Symmetrical and Non-symmetrical Loads". Jrnl. App. Mech., Vol. 31, pp. 467 - 476, 1964.

93. KALNINS, A.
"Analysis of Curved Thin Walled Shells of Revolution". A.I.A.A. Jrnl., Vol. 6, No. 4, pp. 584 - 588, 1968.

94. KALNINS, A. "Stress Analysis of Curved Tubes". 1st Int. Conf. on Press. Ves. Tech., Delft, The Netherlands, p. 223, 1969.

95. THAILER, H. J.
CHENG, D. H. "In-Plane Bending of a U - Shaped Circular Tube With End Constraints". Jrnl. Eng. for Industry, Vol. 92, No. 4, pp. 792 - 796, 1970.

96. NATARAJAN, R. "Finite Element Stress Analysis of Pipe Bends Using Doubly Curved Shell Elements". Doctoral Dissertation, Univ. of London, 1971.

97. BLOMFIELD, J. A.
NATARAJAN, R. "Piping Analysis - The Need to Establish Correct Flexibility Factors for Bends". Conf. on "The Use of Computers in Pressure Vessel Design", Inst. of Mech. Eng., 1971.

98. NATARAJAN, R.
BLOMFIELD, J. A. "Stress Analysis of Curved Pipes with End Constraints". Computers and Structures, Vol. 5, pp. 187 - 196, 1975.

99. FINDLAY, G. E. "A Study of Smooth Pipe Bends Under In-Plane Bending with Reference to End Constraints". Doctoral Dissertation, Univ. of London, 1973.

100. FINDLAY, G. E.
SPENCE, J. "The Effects of Flanges on Smooth Pipe Bends in Piping Systems". 2nd Int. Conf. Struct. Mech. in Reactor Tech., Berlin, 1973.

101. FINDLAY, G. E.
SPENCE, J. "Flexibility of Smooth Circular Curved Tubes with Flanged End Constraints". Int. Jrnl. of Press. Ves. and Piping, 1979.

102. FINDLAY, G. E.
SPENCE, J.
"Stress Analysis of Smooth Curved Tubes with Flanged End Constraints". Int. Jrnl. of Press. Ves. and Piping, 1979.

103. AKSEL'RAD, E. L.
KVASNIKOV, B. N.
"Semi-zero-moment Theory of Curvilinear Bar-Shells". Izv. AN SSSR., Mekhanika Tverdogo Tela, Vol. 9, No. 2, pp. 139 - 147, 1974.
Translation: Mech. of Solids, pp. 125 - 133, 1974.

104. AXELRAD, E.
"Flexible Shell Theory and Buckling of Toroidal Shells and Tubes". Ingenieur Archiv, pp. 95 - 104, 1978.

105. AXELRAD, E.
Private Communication, 1978.

106. IMAMASA, J.
URAGAMI, K.
"Experimental Study of Flexibility Factors and Stresses of Welding Elbows with End Effects". 2nd Int. conf. Press. Ves. Conf., San Antonio, pp. 417 - 426, 1973.

107. ARAI, K.
"Finite Element Method With Consideration to the Continuity of Normal Slope". Mitsubishi Technical Bulletin, No. 79, 1972.

108. WRIGHT, W. B.
RODABAUGH, E. C.
THAILER, H. J.
"Influence of End Effects on Stresses and Flexibility of a Piping Elbow with In-Plane Moment". Conf. Press. Ves. and Piping, Analysis and Computers, Miami, 1974.

109. SOBEL, L. H.
"In-Plane Bending of Elbows". Computers and Structures, Vol. 7, pp. 701 - 715, 1977.

110. RODABAUGH, E. C.
MOORE, S. E.
ISKANDER, S. K.
"End Effects on Elbows Subjected to Moment Loading". ORNL/sub/2913-0, 1977.

111. EPACA
"Theory and Users Manual for EPACA, General Purpose Finite Element Analysis Program for Three-Dimensional Thick Shell Structures". Argonne Code Centre, Argonne Nat. Lab., Argonne. Also: Nuc. Eng. and Design, 28, pp. 414 - 445, 1974.

112. KANO, T.
IWATA, K.
ASAKURA, J.
TAKEDA, H.
"Stress Distributions of an Elbow with Straight Pipes". 4th Int. Conf. Struct. Mech. Reactor Tech., San Francisco, 1977.

113. DE SALVO, G. J.
SWANSON, J. A.
"ANSYS User's Manual". 1972.

114. ASKA
"ASKA part 1 - Linear Static Analysis Users Reference Manual". ISD-Rep. No. 73, Univ. of Stuttgart, 1971.

115. OHTSUBO, H.
WATANABE, O.
"Flexibility and Stress Factors of Pipe Bends - An Analysis by the Finite Ring Method". Trans. A.S.M.E., Jrnl. of Press. Ves. Tech., 1977.

116. OHTSUBO, H.
WATANABE, O.
"Stress Analysis of Pipe Bends by Ring Elements". Trans. A.S.M.E., Jrnl. of Press. Ves. Tech., 1978.

117. WHATHAM, J. F.
"In-Plane Bending of Flanged Pipe Elbows". Metal Struct. Conf., Inst. of Eng., Perth, Australia, 1978.

118. NOVOZHILOV, V. V. "Thin Shell Theory". Wolters-Noordhoff, Groningen, The Netherlands, 1970.

119. WHATHAM, J. F.
THOMPSON, J. J. "The Bending and Pressurizing of Pipe Bends with Flanged Tangents". Nuc. Eng. and Des., pp. 17 - 28, 1979.

120. KANO, T.
IWATO, K.
et al. "Detailed Analysis of Three Elbow Pipe Assemblies". 5th Conf. Struct. Mech. in Reactor Tech., Berlin, 1979.

121. FINAS "Development for FBR. Inelastic Structural Analysis System FINAS (II)". SJ 240 78-01, Power Reactors and Nuclear Fuel Dev. Corp., 1978.

122. TAKEDA, H.
ASAI, S.
IWATA, K. "A New Finite Element for Structural Analysis of Piping Systems". 5th Int. Conf. Struct. Mech. in Reactor Tech., Berlin, 1979.

123. BATHE, K. J.
ALMEIDA, C. A. "A Simple and Effective Pipe Elbow Element- Linear Analysis". Jrnl. of App. Mech., Vol. 47, 1980.

124. KWEE, H. K. "Stress Distributions and Flexibility of the Suction Bend of the Primary Sodium/Pump LMFBR - SNR 300". 5th Int. Conf. Struct. Mech. Reactor Tech., Berlin, 1979.

125. BROUARD, D.
TREMBLAIS, A.
VRILLON, B. "In-Plane and Out of Plane Bending Tests on Carbon Steel Pipe Bends". 5th Int. Conf. Struct. Mech. Reactor Tech., Berlin, 1979.

126. BRITISH STANDARD "BS 806: Ferrous Pipes and Piping Installations for and in Connection with Land Boilers". 1975.

127. BRITISH STANDARD "BS 3351: Piping Systems for Petroleum Refineries and Petrochemical plant". 1971.

128. HOVGAARD, W. "Stresses in Three Dimensional Pipe Bends". Trans. A.S.M.E., Vol. 57, p. 413, 1935.

129. E.S.D.U. "Flexibilities of and Stresses in Thin Pipe Bends Under In-Plane Bending: Influence of Bend Angle and Tangent Pipe Ends". Eng. Sci. Data Unit, 1975.

130. A.S.A. "A.S.A. B. 31.3 - 1966: Petroleum Refinery Piping".

131. U.S.A.S. "U.S.A.S. B31.10: Power Piping".

132. U.S.A.S. "U.S.A.S. B31.7: Nuclear Power Piping".

133. A.S.M.E. "A.S.M.E. Boiler and Pressure Vessel Codes: Section III, Nuclear Power Plant Components". 1974.

134. FLUGGE, W. "Stresses in Shells". Springer-Verlag, 1973.

135. LOVE, A. E. H. "The Mathematical Theory of Elasticity". Dover Publications, N.Y., 1944.

136. REISSNER, E. "A New Derivation of the Equations for the Deformation of Elastic Shells". Am. Jrnl. Math., Vol. LXIII, No. 1, pp. 177 - 184, 1941.

137. SANDERS, J. L. "Nonlinear Theories for Thin Shells". Quarterly of App. Math., Vol. XXI, No. 1, pp. 21 - 36, 1963.

138. KOITER, W. T. "On the Nonlinear Theory of Thin Elastic Shells". Proc. Kon. Akad. Weben, Vol. 69, pp. 1 - 54, 1966.

139. NOVOZHILOV, V. V. "Thin Shell Theory". (Trans. ed. P. G. Lowe), P. Noordhoff Ltd., Netherlands, 1964.

140. KRAUS, H. "Thin Elastic Shells". John Wiley & Sons, 1967.

141. DYM, C. L. "Introduction to the Theory of Shells". Peragamon Press, 1974.

142. SANDERS, J. L. "An Improved First Approximation Theory for Thin Shells". N.A.S.A., Rep. 24, June, 1959.

143. KOITER, W. T. "The Theory of Thin Elastic Shells". Int. Union of Theo. and App. Mechs. Proc. Sym., Delft, 1959. (North Holland Pub. Co.)

144. GOLDENVEIZER, A. L. "Theory of Elastic Thin Shells". Trans. E. Herrmann, New York, 1961.

145. DONNELL, L. "A Discussion of Thin Shell Theory". Proc. Fifth Cong. App. Mech., 1939.

146. MUSHTARI, K . M. "Certain Generalizations of the Theory of Thin Shells". Izv. fiz. Mat. Ob-va Pri Kaz. Un-te., XI, 1938.

147. VLASOV, V. Z. "On the Theory of Elastic Shells". D.A.N., S.S.S.R., Vol. 68, 1949.

148. GERALD, C. F. "Applied Numerical Analysis". Addison - Wesley Pub. Co., 1973.

149. FOX, L.
MAYERS, D. F. "Computing Methods For Scientists And Engineers". Clarendon Press, Oxford, 1968.

150. TIMOSHENKO, S. P.
GOODIER, J. N. "Theory of Elasticity". 3rd ed., McGraw-Hill Kogakusha Ltd., 1970.

151. SYMONDS, P. S. Appendix to [89]

152. KREYSZIG, E. "Advanced Engineering Mathematics". 3rd ed., J. Wiley & Sons, 1972.

153. ALCOCK, D. "Illustrating BASIC". Cambridge Univ. Press, 1979.

154. NELDER, J. A.
MEAD, R. "A Simplex Method for Function Minimization". Comp. J., Vol. 7, pp. 308 - 313, 1965.

155. HOOKE, R.
JEEVES, T. A. "Direct Search Solution of Numerical and Statistical Problems". J. Assoc. Comp. Mach., Vol. 8, No. 2, pp. 212 - 229, 1961.

156. TIERNAY, J. A. "Calculas and Analytic Geometry". Allyn and Bacon, 1969.

157. MEYER, C. "Solution of Linear Equations - State of the Art". Proc. A.S.C.E., Jrnl. Struct. Div., Vol. 99, No. 5T7, 1973.

158. CALDERBANK, V. J. "A Course on Programming in FORTRAN IV". Chapman and Hall Ltd., 1974.

159. WHATHAM, J. F. — Private Communication, 1979.

160. MUNRO MILLER — "Carbon Steel Forged Butt-Welding Pipe Fittings". Munro & Miller, Sighthill, Edinburgh.

161. BRITISH STANDARD — "BS 1640: Part, Steel Butt Welding Pipe Fittings for the Petroleum Industry". 1967.

162. ANSI — "ANSI B16.9 - W58: Wrought Steel Butt Welding Fittings".

163. HOLMAN, J. P. — "Experimental Methods for Engineers". 3rd ed. McGraw-Hill Book Co., 1978.

164. POTMA, T. — "Strain Gauges - Theory and Application". Philips Paperbacks, 1967.

165. REISSNER, E. — "On Stresses and Deformations in Toroidal Shells of Circular Cross-Section which are acted upon by uniform normal pressure". Quart. App. Mechs., Vol. 21, No. 3, p. 177, 1963.

166. MACKENZIE, A. C. — "On the Equations for Steady State Creep of Thin Shells". J. Mech. Eng. Sci., Vol. 7, No. 1, p. 114, 1965. (Research Notes).

APPENDIX (1)

GOVERNING DIFFERENTIAL DISPLACEMENT EQUATIONS

APPENDIX (1)

(a) Governing Differential Displacement Equations for a Toroidal Shell

The governing differential displacement equations for a toroidal shell were obtained by substituting the strain-displacement equations (2.13) into the constitutive relations (2.14) and then substituting the results into the equilibrium equations (2.15). These are given by;

$$a_1\frac{\partial^2 u}{\partial\theta\partial\phi}+b_1\frac{\partial u}{\partial\theta}+c_1\frac{\partial^2 v}{\partial\phi^2}+d_1\frac{\partial v}{\partial\phi}+e_1 v+f_1\frac{\partial^2 v}{\partial\theta^2}+g_1\frac{\partial^3 w}{\partial\phi^3}+h_1\frac{\partial^2 w}{\partial\phi^2}$$

$$+i_1\frac{\partial w}{\partial\phi}+j_1 w+k_1\frac{\partial^2 w}{\partial\theta^2}+\ell_1\frac{\partial^3 w}{\partial\theta^2\partial\phi}=-\frac{rR'}{C}q_\phi \qquad (1)$$

where

$$a_1=\frac{1+\nu}{2}+(2-\nu)\frac{T}{\rho}\sin\phi\ ,\quad b_1=-\frac{(3-\nu)}{2\rho}\cos\phi+\left(\frac{\nu T}{\rho}-(3-\nu)\frac{T}{\rho^2}\sin\phi\right)\cos\phi$$

$$c_1=\rho(1+T)\ ,\quad d_1=(1+T)\cos\phi\ ,\quad e_1=-(1+T)\left(\nu\sin\phi+\cos^2\phi/\rho^2\right)$$

$$f_1=(1-\nu)\left(\tfrac{1}{2}+2T\right)/\rho\ ,\quad g_1=-\rho T\ ,\quad h_1=-T\cos\phi$$

$$i_1=\rho+\nu(1+T)\sin\phi+\frac{T}{\rho^2}\cos^2\phi\ ,\quad j_1=\cos\phi\left(1-\tfrac{1}{\rho}\sin\phi\right)$$

$$k_1=(3-\nu)\frac{T}{\rho^2}\cos\phi\ ,\quad \ell_1=-(2-\nu)\frac{T}{\rho}\ .$$

$$a_2\frac{\partial^2 u}{\partial\theta^2}+b_2\frac{\partial^2 u}{\partial\phi^2}+c_2\frac{\partial u}{\partial\phi}+d_2 u+e_4\frac{\partial^2 v}{\partial\theta\partial\phi}+f_2\frac{\partial v}{\partial\theta}+g_2\frac{\partial^3 w}{\partial\theta^3}$$

$$+h_2\frac{\partial w}{\partial\theta}+i_2\frac{\partial^2 w}{\partial\theta\partial\phi}+j_2\frac{\partial^3 w}{\partial\theta\partial\phi^2}=-\frac{rR'}{C}q_\theta \qquad (2)$$

where,

$$a_2 = \frac{1}{\rho}\left(1 + \frac{t}{\rho^2}\sin^2\phi\right) \quad , \quad b_2 = (1-\nu)\left(\frac{\rho}{2} + \frac{2T}{\rho}\sin^2\phi\right)$$

$$c_2 = (1-\nu)\left(\frac{1}{2} + \frac{T}{\rho}\left(4 - \frac{2}{\rho}\sin\phi\right)\sin\phi\right)\cos\phi$$

$$d_2 = (1-\nu)\left(\frac{1}{2}\left(\sin\phi - \frac{1}{\rho}\cos^2\phi\right) - \frac{2T}{\rho^2}\left(\sin\phi\left(\cos^2\phi\left(1 - \frac{\sin\phi}{\rho}\right) + \cos 2\phi\right)\right)\right)$$

$$e_2 = \frac{1+\nu}{2} + (2-\nu)\frac{T}{\rho}\sin\phi \quad , \quad f_2 = \left(\left(\frac{3-\nu}{2} + \left(2(1-\nu) + \frac{\sin\phi}{\rho}\right)T\right)\frac{\cos\phi}{\rho}\right.$$

$$g_2 = -\frac{T}{\rho^3}\sin\phi \quad , \quad h_2 = \nu + \frac{\sin\phi}{\rho} - 2(1-\nu)\frac{T}{\rho^2}\left(\sin^2\phi - \cos^2\phi\left(1 - \frac{\sin\phi}{\rho}\right)\right)$$

$$i_2 = \left((1-2\nu)\frac{\sin\phi}{\rho} - 2(1-\nu)\frac{T}{\rho}\sin\phi\right. \quad , \quad j_2 = -2(1-\nu)\frac{T}{\rho}\sin\phi$$

$$a_3\frac{\partial^3 u}{\partial\theta\partial\phi^2} + b_3\frac{\partial^2 u}{\partial\theta\partial\phi} + c_3\frac{\partial^3 u}{\partial\theta^3} + d_3\frac{\partial u}{\partial\theta} + e_3\frac{\partial^3 v}{\partial\phi^3} + f_3\frac{\partial^2 v}{\partial\phi^2} + g_3\frac{\partial v}{\partial\phi}$$

$$+ h_3 v + i_3\frac{\partial^2 v}{\partial\theta^2} + j_3\frac{\partial^3 v}{\partial\theta^2\partial\phi} + k_3\frac{\partial^4 w}{\partial\phi^4} + l_3\frac{\partial^3 w}{\partial\phi^3} + m_3\frac{\partial^2 w}{\partial\phi^2} + n_3\frac{\partial w}{\partial\phi}$$

$$+ o_3 w + p_3\frac{\partial^2 w}{\partial\theta^2} + q_3\frac{\partial^4 w}{\partial\theta^4} + r_3\frac{\partial^3 w}{\partial\phi\partial\theta^2} + s_3\frac{\partial^4 w}{\partial\phi^2\partial\theta^2} = \frac{rR'}{C}q_n \qquad (3)$$

where,

$$a_3 = (2-\nu)\frac{T}{\rho}\sin\phi \quad , \quad b_3 = \left(2 - 3\frac{\sin\phi}{\rho}\right)\frac{T\cos\phi}{\rho} \quad , \quad c_3 = \frac{T}{\rho^3}\sin\phi$$

$$d_3 = -\nu - \frac{\sin\phi}{\rho} + \left(-\nu\sin\phi - (3-\nu)\frac{\cos 2\phi}{\rho} - \nu\frac{\cos^2\phi}{\rho} + \frac{4}{\rho^2}\sin\phi\cos^2\phi\right)\frac{T}{\rho}$$

$$e_3 = \rho T \quad , \quad f_3 = 2T\cos\phi \quad , \quad g_3 = -\rho - \nu\sin\phi - \left((1+\nu)\sin\phi + \cos^2\phi\right)T$$

$$h_3 = -\left(\nu + \frac{\sin\phi}{\rho}\right)\cos\phi - \left(\nu\cos\phi - \frac{\sin 2\phi}{\rho} - \frac{\cos^2\phi}{\rho^2}\right)T$$

$$i_3 = \frac{T}{\rho^2}\cos\phi \quad , \quad j_3 = (2-\nu)\frac{T}{\rho} \quad , \quad k_3 = -\rho T \quad , \quad l_3 = -2T\cos\phi$$

$$p_3 = -((3-\nu)\sin\phi + 4\frac{\cos^2\phi}{\rho})\frac{T}{\rho^2} \quad , \quad q_3 = \frac{-T}{\rho^3}$$

$$r_3 = \frac{2T}{\rho^2}\cos\phi \quad , \quad s_3 = -\frac{2T}{\rho}$$

also

$$T = \frac{t^2}{12r^2} \quad , C = \frac{Et}{(1-\nu^2)} \quad , \rho = \frac{R'}{r} = \frac{R}{r}\left(1 + \frac{r}{R}\sin\phi\right)$$

(b) Governing Differential Displacement Equations for a cylinder

Substituting equations (2.20) into (2.21) and substituting the result into (2.22) gives,

$$a_4\frac{\partial u}{\partial\phi\partial y} + b_4\frac{\partial^2 v}{\partial\phi^2} + c_4\frac{\partial^2 v}{\partial y^2} + d_4\frac{\partial^3\omega}{\partial\phi^3} + e_4\frac{\partial\omega}{\partial\phi} + f_4\frac{\partial^3\omega}{\partial\phi\partial y^2} = -\frac{rl}{C}q_\phi \qquad (4)$$

where

$$a_4 = \frac{(1+\nu)}{2} \quad , \quad b_4 = \frac{(1+T)}{L} \quad , \quad c_4 = (1-\nu)\left(\tfrac{1}{2}+2T\right)L$$

$$d_4 = \frac{-T}{L} \quad , \quad e_4 = \frac{1}{L} \quad , \quad f_4 = -(2-\nu)TL$$

$$a_5\frac{\partial^2 u}{\partial\phi^2} + b_5\frac{\partial^2 u}{\partial y^2} + c_5\frac{\partial^2 v}{\partial\phi\partial y} + d_5\frac{\partial\omega}{\partial y} = -\frac{rl}{C}q_x \qquad (5)$$

where

$$a_5 = \frac{(1-\nu)}{2L} \quad , \quad b_5 = L \quad , \quad c_5 = \frac{(1+\nu)}{2} \quad , \quad d_5 = \nu$$

$$a_6\frac{\partial u}{\partial y} + b_6\frac{\partial^3 v}{\partial\phi^3} + c_6\frac{\partial v}{\partial\phi} + d_6\frac{\partial^3 v}{\partial\phi\partial y^2} + e_6\frac{\partial^4\omega}{\partial\phi^4} + f_6\frac{\partial^4\omega}{\partial\phi^2\partial y^2}$$

$$+ g_6\frac{\partial^4\omega}{\partial y^4} + h_6\omega = -\frac{rl}{C}q_n \qquad (6)$$

where

$$a_6 = -\nu \quad , \quad b_6 = \frac{T}{L} \quad , \quad c_6 = \frac{-1}{L} \quad , \quad d_6 = (2-\nu)TL$$

$$e_6 = \frac{-T}{L} \quad , \quad f_6 = -2TL \, , \quad g_6 = -TL^3 \quad , \quad h_6 = \frac{-1}{L}$$

also,

$$T = \frac{t^2}{12\,r^2} \qquad L = \frac{r}{\ell}$$

$$c = \frac{E\,t}{(1-\nu)} \qquad y = \frac{x}{\ell}$$

APPENDIX (2)

INTEGRATION DETAILS

APPENDIX (2)

Integration Details, Method No. 1

$$\bar{V}(\epsilon_\theta) = \frac{2}{\alpha}\int_0^{2\pi}\int_0^{\pi}\Big[\alpha\sum_j \bar{D}_j\Big(1+\cos\Big(\frac{j\pi\theta}{\alpha}\Big)\Big(\Big(\frac{j\pi}{\alpha}\Big)^2-1\Big)\Big)\sin\phi$$
$$+\sum_m\sum_n \bar{C}_{mn}\cos^2\Big(\frac{m\pi\theta}{\alpha}\Big)\Big(\cos n\phi\sin\phi-\frac{1}{2n}\sin n\phi\cos\phi\Big)$$
$$+\frac{2r}{R}\sum_m\sum_n \bar{C}_{mn}\Big(\frac{m\pi}{n\alpha}\Big)^2\cos n\phi\cos\Big(\frac{2m\pi\theta}{\alpha}\Big)\Big]^2 d\theta d\phi$$

$$= \Big[\sum_j\sum_k \bar{D}_j\bar{D}_k\frac{\alpha}{2}\Big\{\frac{\alpha}{2}+\Big(\frac{j\pi}{\alpha}-\frac{\alpha}{j\pi}\Big)\sin\Big(\frac{j\pi}{2}\Big)+\Big(\frac{k\pi}{\alpha}-\frac{\alpha}{k\pi}\Big)\sin\Big(\frac{k\pi}{2}\Big)$$
$$+\frac{1}{2}\Big(\Big(\frac{j\pi}{\alpha}\Big)^2-1\Big)\Big(\Big(\frac{k\pi}{\alpha}\Big)^2-1\Big)\Big(\frac{\sin\big(\frac{\pi}{2}(j+k)\big)}{\frac{\pi}{\alpha}(j+k)}+\frac{\sin\big(\frac{\pi}{2}(j-k)\big)}{\frac{\pi}{\alpha}(j-k)}(1-\delta_{jk})+\frac{\alpha}{2}\delta_{jk}\Big)\Big\}$$
$$-\sum_m\sum_j \bar{C}_{mj}\bar{D}_j\frac{3}{2}\Big\{\frac{\alpha}{4}+\frac{1}{2}\Big(\frac{j\pi}{\alpha}-\frac{\alpha}{j\pi}\Big)\sin\Big(\frac{j\pi}{2}\Big)$$
$$+\frac{1}{4}\Big(\Big(\frac{j\pi}{\alpha}\Big)^2-1\Big)\Big(\frac{\sin\big(\frac{\pi}{2}(2m+j)\big)}{\frac{\pi}{\alpha}(2m+j)}+\frac{\sin\big(\frac{\pi}{2}(2m-j)\big)}{\frac{\pi}{\alpha}(2m-j)}(1-\delta_{j(2m)})+\frac{\alpha}{2}\delta_{j(2m)}\Big)\Big\}$$
$$+\sum_m\sum_p\sum_n\Big\{\Big(1+\frac{1}{2}\delta_{mp}\Big)\Big(\bar{C}_{pn}\bar{C}_{mn}\frac{(n^2+1)}{8n^2}-\bar{C}_{mn}\bar{C}_{p,n+2}\frac{n^2+2n-3}{8n(n+2)}\Big)\Big\}$$
$$+\sum_m\sum_n\Big\{\bar{C}_{mn}^2\,2\Big(\frac{r}{R}\Big)^2\Big(\frac{m\pi}{n\alpha}\Big)^4\Big\}\Big]$$

$$\bar{V}(\kappa\phi) = \frac{2}{\alpha}\int_0^{\pi}\int_0^{\pi}\frac{\lambda^2}{12}\Big[\sum_m\sum_n \bar{C}_{mn}(n^2-1)\cos n\phi\cos^2\Big(\frac{m\pi\theta}{\alpha}\Big)\Big]^2 d\theta d\phi$$

$$= \Big[\sum_m\sum_p\sum_n \bar{C}_{mn}\bar{C}_{pn}\Big(1+\frac{1}{2}\delta_{mp}\Big)\frac{\lambda^2}{48}(n^2-1)^2\Big]$$

Method No. 2

$$\bar{V}(\epsilon_\theta) = \frac{2}{\alpha}\int_0^{\pi}\int_0^{\pi}\Big[\alpha\sum_j \bar{D}_j\Big(1+\cos\Big(\frac{j\pi\theta}{\alpha}\Big)\Big(\Big(\frac{j\pi}{\alpha}\Big)^2-1\Big)\Big)\sin\phi$$
$$+\sum_m\sum_n\frac{2r}{R}\bar{A}_{mn}\Big(\psi_{en}\cos n\phi+\psi_{on}\sin n\phi\Big)\Big(\frac{m\pi}{n\alpha}\Big)^2\cos\Big(\frac{2m\pi\theta}{\alpha}\Big)$$
$$+\sum_m\sum_n \bar{C}_{mn}\Big(\psi_{en}\Big(\cos n\phi\sin\phi-\frac{1}{n}\sin n\phi\cos\phi\Big)$$
$$+\psi_{on}\Big(\sin n\phi\sin\phi+\frac{1}{n}\cos n\phi\cos\phi\Big)\Big)\cos^2\Big(\frac{m\pi\theta}{\alpha}\Big)\Big]^2 d\theta d\phi$$

$$= \Big[\sum_j' \sum_k' D_j D_k \frac{\alpha}{2} \Big\{ \frac{\alpha}{2} + \Big(\frac{j\pi}{\alpha} - \frac{\alpha}{j\pi}\Big) \sin\Big(\frac{j\pi}{2}\Big) + \Big(\frac{k\pi}{\alpha} - \frac{\alpha}{k\pi}\Big) \sin\Big(\frac{k\pi}{2}\Big)$$
$$+ \frac{1}{2}\Big(\Big(\frac{j\pi}{\alpha}\Big)^2 - 1\Big)\Big(\Big(\frac{k\pi}{\alpha}\Big)^2 - 1\Big)\Big(\frac{\sin\left(\frac{\pi}{2}(j+k)\right)}{\frac{\pi}{\alpha}(j+k)} + \frac{\sin\left(\frac{\pi}{2}(j-k)\right)}{\frac{\pi}{\alpha}(j-k)}(1-\delta_{jk}) + \frac{\alpha}{2}\delta_{jk} \Big) \Big\}$$
$$- \sum_m' \sum_j' \bar{C}_{m1} \bar{D}_j \frac{3}{2} \Big\{ \frac{\alpha}{4} + \frac{1}{2}\Big(\frac{j\pi}{\alpha} - \frac{\alpha}{j\pi}\Big) \sin\Big(\frac{j\pi}{2}\Big)$$
$$+ \frac{1}{4}\Big(\Big(\frac{j\pi}{\alpha}\Big)^2 - 1\Big)\Big(\frac{\sin\left(\frac{\pi}{2}(2m+j)\right)}{\frac{\pi}{\alpha}(2m+j)} + \frac{\sin\left(\frac{\pi}{2}(2m-j)\right)}{\frac{\pi}{\alpha}(2m-j)}(1-\delta_{j(2m)}) + \frac{\alpha}{2}\delta_{j(2m)} \Big) \Big\}$$
$$+ \sum_m' \sum_p \sum_n' \Big\{ \Big(1 + \frac{1}{2}\delta_{mp}\Big)\Big(\bar{C}_{pn} \bar{C}_{mn} \frac{n^2+1}{8n^2} - C_{mn} C_{pn+2} \frac{n^2+2n-3}{8n(n+2)} \Big) \Big\}$$
$$+ \sum_m' \sum_n' \bar{C}_{mn} \frac{r}{2R} \Big(\frac{m\pi}{n\alpha}\Big)^2 \Big\{ A_{mn+1} \frac{n(n-1)}{(n+1)^2}(-1)^n - A_{mn-1} \frac{n(n+1)}{(n-1)^2}(-1)^n \Big\}$$
$$+ \sum_m \sum_n \bar{A}_{mn}^2 \Big\{ 2\Big(\frac{r}{R}\Big)^2 \Big(\frac{m\pi}{n\alpha}\Big)^4 \Big\} \Big] .$$

$$\bar{V}(\bar{\gamma}_{\theta\phi}) = \frac{(1-\nu)}{2} \frac{2}{\alpha} \int_0^{\pi} \int_0^{\alpha} \Big[\sum_m' \sum_n' \left(\bar{C}_{mn} - \bar{A}_{mn}\right)\left(\psi_{en} \sin n\phi - \psi_{on} \cos n\phi\right)$$
$$\times \Big(\frac{m\pi}{\alpha}\Big) \sin\Big(\frac{2m\pi\theta}{\alpha}\Big) \Big]^2 d\theta\, d\phi$$

$$= \Big[\frac{(1-\nu)}{4} \sum_m' \sum_n' \left(\bar{C}_{mn} - A_{mn}\right)^2 \Big(\frac{m\pi}{n\alpha}\Big)^2 \Big]$$

$$\bar{V}(K_\phi) = \frac{2}{\alpha} \int_0^{\pi} \int_0^{\alpha} \frac{\lambda^2}{12} \Big[\sum_m' \sum_n' \bar{C}_{mn}(n^2-1)\left(\psi_{en} \cos n\phi + \psi_{on} \sin n\phi\right)$$
$$\times \cos^2\Big(\frac{m\pi\theta}{\alpha}\Big) \Big]^2 d\theta\, d\phi$$

$$= \Big[\sum_m' \sum_p' \sum_n' \bar{C}_{mn} \bar{C}_{pn} \Big(1 + \frac{1}{2}\delta_{mp}\Big) \frac{\lambda^2}{48} (n^2-1)^2 \Big]$$

Method No. 4

$$\bar{V}(\epsilon_\theta) = \frac{2}{\alpha}\int_0^{\pi}\int_0^{\frac{\alpha}{2}} \Big[\alpha \sum_j' D_j \tfrac{1}{2}\Big(1+\cos\Big(\tfrac{j\pi\theta}{\alpha}\Big)\Big(\Big(\tfrac{j\pi}{\alpha}\Big)^2-1\Big)\Big)\sin\phi$$
$$+\sum_m'\sum_n' C_{mn}\Big(\cos n\phi\sin\phi-\frac{1}{2n}\sin n\phi\cos\phi\Big)\Big(\psi_{om}\cos^2(m\eta\theta)-\psi_{em}\sin^2(m\eta\theta)\Big)$$
$$+\frac{2r}{R}\sum_m'\sum_n' C_{mn}\Big(\frac{m\eta}{n}\Big)^2\cos n\phi\cos(2m\eta\theta)\Big]^2 d\theta d\phi$$

$$= \Big[\sum_j'\sum_k' D_j D_k \frac{\alpha}{2}\Big\{\frac{\alpha}{2}+\Big(\frac{j\pi}{\alpha}-\frac{\alpha}{j\pi}\Big)\sin\Big(\frac{j\pi}{2}\Big)+\Big(\frac{k\pi}{\alpha}-\frac{\alpha}{k\pi}\Big)\sin\Big(\frac{k\pi}{2}\Big)$$
$$+\frac{1}{2}\Big(\Big(\frac{j\pi}{\alpha}\Big)^2-1\Big)\Big(\Big(\frac{k\pi}{\alpha}\Big)^2-1\Big)\Big(\frac{\sin\left(\frac{\pi}{2}(j+k)\right)}{\frac{\pi}{2}(j+k)}+\frac{\sin\left(\frac{\pi}{2}(j-k)\right)}{\frac{\pi}{2}(j-k)}(1-\delta_{jk})+\frac{\alpha}{2}\delta_{jk}\Big)\Big\}$$
$$-\sum_m'\sum_n' \bar{C}_{m1} D_j \frac{3}{4}\Big\{\frac{\alpha}{2}(-1)^{m+1}+\frac{1}{2m\eta}\sin(m\eta\alpha)+(-1)^{m+1}\Big(\frac{j\pi}{\alpha}-\frac{\alpha}{j\pi}\Big)\sin\Big(\frac{j\pi}{2}\Big)$$
$$+\frac{1}{2}\Big(\Big(\frac{j\pi}{\alpha}\Big)^2-1\Big)\Big(\frac{\sin\left(m\eta\alpha+\frac{j\pi}{2}\right)}{(x+y)}+\frac{\sin\left(m\eta\alpha-\frac{j\pi}{2}\right)}{(x-y)}(1-\delta_{xy})+\frac{\alpha}{2}\delta_{xy}\Big)\Big\}$$
$$+\sum_m'\sum_p'\sum_n' \frac{1}{2\alpha}\Big\{\Big(\frac{\alpha}{2}(-1)^{m+p}+\frac{1}{2m\eta}\sin(m\eta\alpha)(-1)^{p+1}+\frac{1}{2p\eta}\sin(p\eta\alpha)(-1)^{m+1}$$
$$+\frac{1}{2}\Big(\frac{\sin(\eta\alpha(m+p))}{2\eta(m+p)}+\frac{\sin(\eta\alpha(m-p))}{2\eta(m-p)}(1-\delta_{mp})+\frac{\alpha}{2}\delta_{mp}\Big)\Big)$$
$$\times\Big(\bar{C}_{mn}\bar{C}_{pn}\frac{n^2+1}{2n^2}-\bar{C}_{mn}C_{pn+1}\frac{n^2+2n-3}{2n(n+2)}\Big)\Big\}$$
$$+\sum_m'\sum_p'\sum_n' \bar{C}_{mn}\bar{C}_{pn}\Big\{\frac{2}{\alpha}\Big(\frac{r}{R}\Big)^2\Big(\frac{m\eta}{n}\Big)^4\Big(\frac{1}{2}\Big(\frac{\sin(\eta\alpha(m+p))}{2\eta(m+p)}+\frac{\sin(\eta\alpha(m-p))}{2\eta(m-p)}(1-\delta_{mp})+\frac{\alpha}{2}\delta_{mp}\Big)\Big)\Big\}\Big]$$

$$V(\epsilon_\alpha) = \frac{2}{\alpha}\int_0^{2\pi}\int_{\frac{\pi}{2}}^{\frac{3\pi}{2}} \Big[\alpha\sum_j' G_j(j^2+j)\Big(\theta-\frac{\alpha}{2}\Big)^{j-1}\sin\phi$$
$$+\frac{2r}{R}\sum_m'\sum_n' C_{mn}\Big(\frac{m\eta}{n}\Big)^2\cos n\phi\cos(2m\eta\theta)\Big]^2 d\theta d\phi$$

$$= \Big[\sum_j'\sum_k' D_j D_k 2\alpha\frac{(j^2+j)(k^2+k)}{(j+k-1)}(\ell/R)^{j+k-1}$$
$$+\sum_m'\sum_p'\sum_n' \bar{C}_{mn}\bar{C}_{pn}\Big\{\frac{2}{\alpha}\Big(\frac{r}{R}\Big)^2\Big(\frac{m\eta}{n}\Big)^4\Big(\frac{L}{R\alpha}\delta_{mp}$$
$$-\frac{1}{2}\Big(\frac{\sin(\eta\alpha(m+p))}{2\eta(m+p)}+\frac{\sin(\eta\alpha(m-p))}{2\eta(m-p)}(1-\delta_{mp})+\frac{\alpha}{2}\delta_{mp}\Big)\Big)\Big\}\Big]$$

$$\overline{V}(\kappa_\phi) = \frac{2}{\alpha}\int_0^{2\pi}\int_0^{\frac{1}{2R}} \frac{\lambda^2}{12}\left[\sum_m\sum_n C_{mn}(n^2-1)\cos n\phi\left(\psi_{om}\cos^2(m\eta\theta) - \psi_{em}\sin^2(m\eta\theta)\right)\right]^2 d\theta d\phi$$

$$= \sum_m\sum_p\sum_n \overline{C}_{mn}\overline{C}_{pn}\left\{\left(1+\tfrac{1}{2}\delta_{mp}(-1)^{m+p}\right)\frac{L}{R\alpha}\,\frac{\lambda^2(n^2-1)^2}{48}\right\}$$

$$x = 2m\eta \qquad y = \frac{4\pi}{\alpha}$$

APPENDIX (3)

SOLUTION OF LINEAR SIMULTANEOUS EQUATIONS

GAUSS ALGORITHM

APPENDIX (3)

Solution of Linear Simultaneous Equations - Gauss Algorithm

Consider the system of equations,

$$\begin{aligned} a_{11}x_1 + a_{12}x_2 + \cdots + a_{1n}x_n &= b_1 \\ a_{21}x_1 + a_{22}x_2 + \cdots + a_{2n}x_n &= b_2 \\ \vdots \qquad\quad \vdots \qquad\quad \vdots \qquad\quad \vdots \\ a_{n1}x_1 + a_{n2}x_2 + \cdots + a_{nn}x_n &= b_n \end{aligned} \qquad (1)$$

These can be written in matrix form as follows,

$$\begin{bmatrix} a_{11} & a_{12} & \cdots & a_{1n} \\ a_{21} & a_{22} & & a_{2n} \\ \vdots & \vdots & & \vdots \\ a_{n1} & a_{n2} & \cdots & a_{nn} \end{bmatrix} \begin{Bmatrix} x_1 \\ x_2 \\ \vdots \\ x_n \end{Bmatrix} = \begin{Bmatrix} b_1 \\ b_2 \\ \vdots \\ b_n \end{Bmatrix} \qquad (2)$$

or $$[A]\{x\} = \{b\}$$

where $[A]$ is the coefficient matrix, $\{x\}$ is the unknown solution vector and $\{b\}$ is the known right hand side vector. To eliminate unknown x_i, it is necessary to first modify the coefficient matrix and right hand vector, by forward substitution, as follows;

for i = 1, 2, 3, —— n - 1

$$a_{jk} = a_{jk} - \frac{a_{ji}\, a_{ik}}{a_{ii}} \quad , \quad j, k = i + 1, \text{——}, n \qquad (3)$$

$$b_j = b_j - \frac{a_{ji}\, b_i}{a_{ii}} \quad , \quad j = i + 1 \text{——}, n \qquad (4)$$

where a_{ij} is the element in the i^{th} row and j^{th} column of the coefficient/

coefficient matrix and b_i the i^{th} element of the right hand side vector. When i = n, the n^{th} equation is solved for the x_n unknown,

$$x_n = b_n / a_{nn} \tag{5}$$

Other unknowns, x_i, are found by back substitution using,

$$x_i = \left(b_i - \sum_{j=i+1}^{n} a_{ij} x_j\right)/a_{ii} \quad , \; i = n-1, n-2, \ldots, 1 \tag{6}$$

If the coefficient matrix is symmetric, i.e. $a_{ij} = a_{ji}$, then only the elements of the upper triangle need to be operated on during the forward substitution using, instead of equation (3),

$$a_{jk} = a_{jk} - \frac{a_{ij} a_{ik}}{a_{ii}} \quad , \qquad \begin{aligned} k &= j, j+1, \text{---}, n \\ j &= i+1, i+2, \text{---}, n \end{aligned} \tag{7}$$

This requires slightly more than half of the original operations. Note that a_{ji} in equation (3) has become a_{ij} in (7).

APPENDIX (4)

STRAINS FOR COMPUTER SOLUTION

APPENDIX (4)

Strains for Computer Solution

The strains for the flange and tangent pipe problems will be given together by making use of the η parameter,

$$\eta = \frac{R\pi}{L} = \frac{R\pi}{(2\ell + R\alpha)} \tag{1}$$

which for a zero length tangent, i.e. $\ell = 0$, becomes,

$$\eta = \frac{\pi}{\alpha} \tag{2}$$

Therefore, the strains given for the bend become those for a flanged bend when $\ell = 0$.

The strains given in equations (5.14) for the bend and (5.15) for the tangent pipes, using the non-dimensionalisation given in equations (5.32) and (5.33), are

For the bend: $0 \leq \theta \leq \frac{\alpha}{2}$

$$\bar{\epsilon}_\phi = \left[\sum_m \sum_n (C_{mn} - B_{mn}) C_1 \times S_1 + \sum_j H_j \times S_1\right] \frac{R}{r}$$

$$\bar{\epsilon}_\theta = \left[\sum_j \left((F_j - D_j) \times S_4 \times \frac{R}{r} + (F_j \times S_4 + D_j \times S_5 + H_j \times S_1) \sin\phi\right)\right.$$
$$\left. + \sum_m \sum_n \left(A_{mn} \times C_2 \times S_3 + (B_{mn} \times C_3 + C_{mn} \times C_4) \times S_1\right)\right] \frac{1}{Z}$$

$$\bar{\gamma}_{\theta\phi} = \left[\sum_m \sum_n (A_{mn} \times C_5 + B_{mn} \times C_6) \times S_2\right] \frac{1}{Z}$$

$$\bar{K}_\phi = \left[\sum_m \sum_n (C_{mn} \times C_7 - B_{mn} \times C_1) \times S_1\right]$$

$$\bar{K}_\theta = \left[\sum_j \left((F_j \times S_4 + D_j \times S_5) \times \frac{R}{r} \times Z \times \sin\phi + H_j \times S_3\right)\right.$$
$$\left. + \sum_m \sum_n \left((A_{mn} \times C_8 + C_{mn} \times C_1) \times S_3 + (B_{mn} \times C_9 + C_{mn} \times C_{10}) \times S_1\right)\right] \left(\frac{r}{RZ}\right)^2$$

$$\bar{K}_{\theta\phi} = \left[\sum_m \sum_n \left(A_{mn} \times C_{11} + B_{mn} \times C_6 + C_{mn} \times C_{12}\right) \times S_2 - \sum_j H_j \times S_2 \times \cos\phi \times \left(\frac{r}{Rz}\right)\right] \left(\frac{r}{Rz}\right)$$

For the tangent Pipe: $\frac{\alpha}{2} \leq \theta \leq L/2R$

$$\bar{\epsilon}_\phi = \left[\sum_m \sum_n \left(C_{mn} - B_{mn}\right) \times C_1 \times S_1 + \sum_j H_j \times S_1\right] \times \frac{R}{r}$$

$$\bar{\epsilon}_x = \left[\sum_j G_j \times S_6 \times \sin\phi + \sum_m \sum_n A_{mn} \times C_2 \times S_3\right]$$

$$\bar{\gamma}_{x\phi} = \left[\sum_m \sum_n \left(B_{mn} - A_{mn}\right) \times C_6 \times S_2\right]$$

$$K_\phi = \left[\sum_m \sum_n \left(C_{mn} \times C_7 - B_{mn} \times C_1\right) \times S_1\right]$$

$$K_x = \left[\sum_j \left(G_j \times S_6 \times \frac{R}{r} \times \sin\phi + H_j \times S_3\right) + \sum_m \sum_n C_{mn} \times C_1 \times S_3\right] \left(\frac{r}{R}\right)^2$$

$$K_{x\phi} = \left[\sum_m \sum_n \left(B_{mn} \times C_6 + C_{mn} \times C_{13}\right) \times S_2\right] \left(\frac{r}{R}\right)$$

where,

$$S_1 = \psi_{mo} \cos^2(m\eta\theta) - \psi_{me} \sin^2(m\eta\theta)$$

$$S_2 = (m\eta) \sin(2m\eta\theta)$$

$$S_3 = 2(m\eta)^2 \cos(2m\eta\theta)$$

$$S_4 = \alpha \times \sin^2\left(\frac{\lambda\pi\theta}{2\alpha}\right)$$

$$S_5 = \frac{1}{2}\left(\frac{\lambda\pi}{\alpha}\right)^2 \cos\left(\frac{\lambda\pi\theta}{\alpha}\right)$$

$$S_6 = \frac{\alpha}{2}\delta_{j1} + (1 - \delta_{j1})\alpha(j^2 + j)\left(\theta - \frac{\alpha}{2}\right)^{j-1}$$

$$C_0 = \sin\phi$$

$$C_1 = \psi_{ne} \cos n\phi + \psi_{no} \sin n\phi$$

$$C_2 = \left(\psi_{ne} \cos n\phi + \psi_{no} \sin n\phi\right) \frac{r}{Rn^2}$$

$$C_3 = \left(-\psi_{ne} \sin n\phi + \psi_{no} \cos n\phi\right) \cos\phi / n$$

$$C_4 = \left(\psi_{ne}\cos n\phi + \psi_{no}\sin n\phi\right)\sin\phi$$

$$C_5 = \left(-\psi_{ne}\sin n\phi + \psi_{no}\cos n\phi\right)\frac{z}{n} - \left(\psi_{ne}\cos n\phi + \psi_{no}\sin n\phi\right)\frac{r}{R}\frac{1}{n^2}$$

$$C_6 = \left(\psi_{ne}\sin n\phi - \psi_{no}\cos n\phi\right)\frac{1}{n}$$

$$C_7 = \left(\psi_{ne}\cos n\phi + \psi_{no}\sin n\phi\right)n^2$$

$$C_8 = \left(\psi_{ne}\cos n\phi + \psi_{no}\sin n\phi\right)\frac{r}{R}\frac{\sin\phi}{n^2}$$

$$C_9 = \left(-\psi_{ne}\sin n\phi + \psi_{no}\cos n\phi\right)\frac{R}{r}\frac{z}{n}$$

$$C_{10} = \left(\psi_{ne}\sin n\phi - \psi_{no}\cos n\phi\right)\frac{R}{r}zn$$

$$C_{11} = \left(-\psi_{ne}\sin n\phi + \psi_{no}\cos n\phi\right)\frac{r}{R}\frac{1}{n} - \left(\psi_{ne}\cos n\phi + \psi_{no}\sin n\phi\right)\frac{\cos\phi\sin\phi}{z^2n^2}\left(\frac{r}{R}\right)^2$$

$$C_{12} = \left(-\psi_{ne}\sin n\phi + \psi_{no}\cos n\phi\right)n - \left(\psi_{ne}\cos n\phi + \psi_{no}\sin n\phi\right)\frac{\cos\phi}{z}\left(\frac{r}{R}\right)$$

$$C_{13} = \left(-\psi_{ne}\sin n\phi + \psi_{no}\cos n\phi\right)n$$

APPENDIX (5)

COMPUTER PROGRAM FOR METHODS NOS. 3 AND 5

```
C
C
C     LOWER BOUND ENERGY ANALYSIS OF
C     PIPE BENDS WITH RIGID FLANGES
C     AND TANGENT PIPES
C
C
C
C
C
C
C
C     BY G. THOMSON
C     DEPT. OF MECHANICS OF MATERIALS.
C
      IMPLICIT REAL*8 (A-H,O-Z)
      REAL*8 LAM(10)
      REAL*8 AS(5,25),AC(5,25)
      REAL*8 UC(5,25),US(5,25),VQ(5,25),CY(25)
      REAL*8 DE(120)
      REAL*8 C(5,8)
      REAL*8 A(120,120),B(120),D(120)
      REAL*8 LAMDA,MU,KY
      REAL*8 KXY
      REAL*8 BS(5,8)
      REAL*8 CC(5,25),SS(5,25)
      REAL*8 LA,MG,CM(5,25),CE(5,25),SE(5,25)
      REAL*8 VC(5,25),VV(5),WE(25),WY(25),SY(25),Z(25)
      REAL*8 C1(8,25),C2(8,25),C3(8,25),C4(8,25),C5(8,25)
      REAL*8 VS(5,25),VY(5),KX
      REAL*8 C6(8,25),C7(8,25),C8(8,25),C9(8,25)
      REAL*8 C10(8,25),C11(8,25),C12(8,25)
      REAL*8 WET(25),VT(5),LR,C13(8,25)
      INTEGER E,Y,T4
      INTEGER P,H,V,TP
      INTEGER RP,CP
      COMMON/BLK1/CM,CE,SE,VC,VV,SY,Z,C1,C2,C3,C4,C5,LA,MG,C13
      COMMON/BLK2/JT,MT,NT,NE,NY,HE,HY,WE,WY,RR,AS,AC,T4,NET,WET,HET
      COMMON/BLK3/VS,VY,C6,C7,C8,C9,C10,C11,C12,CC,SS,UC,US,VQ,CY,SM
C
C
C
C     READ IN PIPE PARAMETERS.
C
C     PIDAL- PI/BEND ANGLE  I.E.  FOR 90 DEGREE BEND, PIDAL=2.
C     LAN  - NUMBER OF DIFFERENT LAMDA'S TO BE EXAMINED
C     RR   - BEND RADIUS/PIPE RADIUS
C     LR   - TANGENT PIPE LENGTH/PIPE RADIUS
C     MU   - POISSONS RATIO FOR PIPE MATERIAL
C     LAM  - LAMDA'S TO BE EXAMINED
C     JT   - NUMBER OF TERMS IN RIGID DISPLACEMENT SERIES
C     MT   - NUMBER OF TERMS IN DISTORTION SERIES, IN THETA DIRECTION
C     NT   - NUMBER OF TERMS IN DISTORTION SERIES IN PHI DIRECTION
C     SM   - DIRECTION OF MOMENT ( +1 FOR OPENING,-1 FOR CLOSING)
C     NE   - NUMBER OF INTEGRATION POINTS ON BEND IN THETA DIRECTION
C     NET  - NUMBER OF INTEGRATION POINTS ON TANGENT IN THETA DIRECTION
C     NY   - NUMBER OF INTEGRATION POINTS IN THE PHI DIRECTION
C
```

```
C
C     LAMDA=THICKNESS*BEND RADIUS/(PIPE RADIUS)**2
C
C
C     THE PIPE RADIUS IS THE RADIUS OF THE TUBE BORE + HALF
C     OF THE THICKNESS OF THE TUBE SECTION.
C     THE BEND RADIUS IS THE RADIUS OF THE BEND ARC AT THE
C     CENTRELINE (NEUTRAL AXIS)
C
C     SPECIFYING A ZERO LENGTH TANGENT  GIVES THE RESULTS FOR A PIPE
C     BEND WITH FLANGES.
C
C
C
C
      READ (1,*)PIDAL,LAN,RR,LR,MU
      READ (1,*)(LAM(I),I=1,LAN)
      READ (1,*)JT,MT,NT
      READ (1,*)SM
      READ (1,*)NE,NET,NY
      DO 999 ILA=1,LAN
      LAMDA=LAM(ILA)
C
C     SET ARRAY AND SERIES PARAMETERS
C
C
      NN=NT+1
      NO=JT*4+MT*NT*3
      PI=3.14159265360
      PD=PIDAL
      ALPHA=PI/PIDAL
      IA=120
      DO 3 J=1,NO
      B(J)=0.0
      DO 3 K=1,NO
3     A(J,K)=0.0
C
C
C     THESE FORMATS ARE OUT OF POSITION BUT ARE USED LATER.
12    FORMAT (///'    C - SERIES CONSTANTS  '///)
13    FORMAT (1X,' M/N ',5X,10(I2,8X)//)
15    FORMAT (1X,I4,3X,10(2X,F8.4)/)
24    FORMAT (///'    A - SERIES CONSTANTS   '///)
16    FORMAT (///////' BEND ANGLE = ',F8.4//
     1' PIPE FACTOR, LAMDA = ',F8.4//
     1' RADIUS RATIO = ',F8.4//' POISSONS RATIO = ',F8.4//////)
18    FORMAT (///' FLEXIBILITY FACTOR = ',F8.4//////)
C
C
C
      AL=ALPHA
C     T4 IS SET TO 3 FOR FLANGED BENDS AND 4 FOR TANGENTS
      T4=4
      IF (LR.EQ.0.0)T4=3
      RL=RR/(LR*2+RR*AL)
C
```

```
C     SET INTEGRATION PARAMETERS.
C
      E3=0.5/RL
      E2=AL*0.5
      E1=0.0
      Y2=PI*0.5
      Y1=-Y2
      HET=(E3-E2)/(NET-1)
      HE=(E2-E1)/(NE-1)
      HY=(Y2-Y1)/(NY-1)
      LA=LAMDA**2/12.0
      MG=(1.0-MU)*2.0
C
C     SET-UP TRIGONOMETRIC ARRAYS FOR FUNCTION SUBROUTINE
C
C     EACH FUNCTION IS CALCULATED AT EACH INTEGRATION POINT
C     THUS ELIMIMINATING THE TIME CONSUMING FUNCTION
C     EVALUATIONS DURING THE T.P.E SUBROUTINE(FUNCT).
C
C
      MJ=MT
      IF (JT.GT.MT)MJ=JT
C
C     CIRCUMFERENTIAL FUNCTIONS
C
C     PIPE BEND
C
      DO 800 E=1,NE
      EE=(E-1)*HE+E1
      WE(E)=3.0+(-1.0)**E
      IF (E.EQ.1.0R.E.EQ.NE)WE(E)=1.0
      DO 801 M=1,MJ
      SE(M,E)=SIN(M*PI*RL*EE*2.0)*M*PI*RL
      CE(M,E)=COS(M*PI*RL*EE*2.0)*(M*PI*RL)**2*2.0
      IF ((-1)**M.GT.0)GOTO 803
      CM(M,E)=COS(M*PI*RL*EE)**2
      GOTO 801
803   CM(M,E)=-SIN(M*PI*RL*EE)**2
801   CONTINUE
      DO 800 J=1,JT
      VS(J,E)=SIN(J*PD*EE*0.5)**2*AL*SM
      VC(J,E)=0.5*(J*PD)**2*COS(J*PD*EE)*AL*SM
800   CONTINUE
C
C     END ROTATIONS
C
      DO 810 J=1,JT
      VV(J)=AL/2.0-SIN(J*PI/2.0)/(J*PD)
      VY(J)=J*PD*SIN(J*PI/2.0)
      VT(J)=2.0*(J+1)*(LR/RR)**J
810   CONTINUE
      IF (T4.EQ.3)GO TO 852
C
```

```
C       TANGENT PIPE
C
        NEET=NE+NET
        NE1=NE+1
        DO 850 E=NE1,NEET
        EE=(E-NE-1)*HET+E2
        WET(E)=3.0+(-1.0)**(E-NE)
        IF (E.EQ.NE1.OR.E.EQ.NEET)WET(E)=1.0
        DO 851 M=1,MJ
        SE(M,E)=SIN(M*PI*RL*EE*2.0)*M*PI*RL
        CE(M,E)=COS(M*PI*RL*EE*2.0)*(M*PI*RL)**2*2.0
        IF ((-1)**M.LT.0)CM(M,E)=COS(M*PI*RL*EE)**2
        IF ((-1)**M.GT.0)CM(M,E)=-SIN(M*PI*RL*EE)**2
851     CONTINUE
        DO 850 J=1,JT
        VQ(J,E)=AL*2.0*SM
        IF (J.GT.1)VQ(J,E)=J*(J+1)*(EE-AL/2.0)**(J-1)*AL*SM
850     CONTINUE
852     CONTINUE
C
        NN=NT+1
C
C
C       MERIDIONAL FUNCTIONS
C
        DO 820 Y=1,NY
        YY=(Y-1)*HY+Y1
        WY(Y)=3.0+(-1.0)**Y
        IF (Y.EQ.1.0R.Y.EQ.NY)WY(Y)=1.0
        SY(Y)=SIN(YY)
        CY(Y)=COS(YY)
        Z(Y)=1.0+SY(Y)/RR
        DO 820 N=2,NN
        SY2=SIN(N*YY)
        CY2=COS(N*YY)
        NP=N-1
        IF ((-1)**N.LT.0)GO TO 821
C
C        N - EVEN
C
        C1(NP,Y)=CY2
        C2(NP,Y)=CY2/(RR*N**2)
        C3(NP,Y)=-SY2*CY(Y)/N
        C4(NP,Y)=CY2*SY(Y)
        C5(NP,Y)=-Z(Y)*SY2/N-CY2*CY(Y)/(N**2*RR)
        C6(NP,Y)=SY2/N
        C7(NP,Y)=N**2*CY2
        C8(NP,Y)=CY2*SY(Y)/(N**2*RR)
        C9(NP,Y)=-Z(Y)*RR*SY2*CY(Y)/N
        C10(NP,Y)=Z(Y)*RR*SY2*CY(Y)*N
        C11(NP,Y)=-SY2*SY(Y)/(N*RR)-CY2*CY(Y)*SY(Y)/(Z(Y)*(RR*N)**2)
        C12(NP,Y)=-N*SY2-CY2*CY(Y)/(Z(Y)*RR)
        C13(NP,Y)=-SY2*N
        GO TO 820
C
```

```
C      N - ODD
C
821    C1(NP,Y)=SY2
       C2(NP,Y)=SY2/(RR*N**2)
       C3(NP,Y)=CY2*CY(Y)/N
       C4(NP,Y)=SY2*SY(Y)
       C5(NP,Y)=Z(Y)*CY2/N-SY2*CY(Y)/(RR*N**2)
       C6(NP,Y)=-CY2/N
       C7(NP,Y)=N**2*SY2
       C8(NP,Y)=SY2*SY(Y)/(RR*N**2)
       C9(NP,Y)=Z(Y)*RR*CY2*CY(Y)/N
       C10(NP,Y)=-Z(Y)*RR*CY2*CY(Y)*N
       C11(NP,Y)=CY2*SY(Y)/(N*RR)-SY2*CY(Y)*SY(Y)/(Z(Y)*(RR*N)**2)
       C12(NP,Y)=N*CY2-SY2*CY(Y)/(Z(Y)*RR)
       C13(NP,Y)=CY2*N
820    CONTINUE
C
C
C      MATRIX ORDER
C
       NO=JT*T4+MT*NT*3
C
C
C
C      THE FOLLOWING SECTION CONTAINS THE MINIMISATION
C      PROCEDURE. THE PRESENT SECTION ONLY CONSIDERS
C      THE QUADRATIC PART OF THE ENERGY FUNCTION. TO
C      COPE WITH LINEAR AND CONSTANT TERMS IT WOULD
C      HAVE TO BE MODIFIED AS SUGGESTED IN SECTION(3.5)
C      OF MY PHD. THESIS. THE PRESENT SECTION IS ADEQUATE
C      FOR PRESENT REQUIREMENTS.
C
C
C      INITIALISE ARRAYS
C
       DO 100 RP=1,NO
       D(RP)=0.0
100    B(RP)=0.0
       NOM1=NO-1
C
C      CALCULATE LEADING DIAGONAL TERMS FOR MATRIX.
C
       DO 101 RP=1,NO
       D(RP)=1.0
       CALL FUNCT(NO,D,F,RP,RP)
       DE(RP)=F
       A(RP,RP)=F*2.0
101    D(RP)=0.0
C
C      CALCULATE OFF DIAGONAL TERMS FOR MATRIX.
C      LOWER TRIANGLE FOUND FROM SYMMETRY.
C
       DO 102 RP=1,NOM1
       IRP=RP+1
       D(RP)=1.0
       DO 103 CP=IRP,NO
       D(CP)=1.0
       CALL FUNCT(NO,D,F,CP,RP)
       A(RP,CP)=F-DE(RP)-DE(CP)
       A(CP,RP)=A(RP,CP)
103    D(CP)=0.0
102    D(RP)=0.0
```

```
C
C       SET UP RIGHT HAND SIDE VECTOR.
C
C
        DO 104 J=1,JT
        B(J)=VY(J)*(1.0-MU**2)*PI*AL/2.0
        IF (T4.EQ.4) B(J+JT*3)=VT(J)*(1.0-MU**2)*PI*AL/2.0
104     B(J+JT)=VV(J)*(1.0-MU**2)*PI*AL/2.0
C
C       SOLVE MATRIX
C
        CALL SOLVE(NO,IA,A,B,D)
C
C
C
        DO 400 M=1,MT
        DO 400 N=1,NT
        MP=JT*T4+M+MT*(N-1)
        C(M,N)=D(MP)
        BS(M,N)=D(MP+MT*NT*2)
400     A(M,N)=D(MP+MT*NT)
C
        WRITE (2,995)
995     FORMAT (////////////
       1'*************************************************************'
       2/'*************************************************************'
       3///'          STRUCTURAL ANALYSIS OF A SMOOTH PIPE BEND'
       4//'                WITH FLANGED TANGENT PIPES.'
       5///'*************************************************************'
       6/'*************************************************************'//)
        WRITE (2,993)
993     FORMAT (//' D-SERIES ** V & W RIGID SECTION DISPLACEMENTS'
       1/' F-SERIES ** U - CENTRELINE RIGID SECTION DISPLACEMENTS'
       3/' H-SERIES ** W - CONSTANT RADIAL EXPANSION DISPLACEMENTS'//)
        WRITE (2,980)JT,MT,NT,NO
980     FORMAT (///' NUMBER OF TERMS IN RIGID SERIES, JT = ',I6
       1/' NUMBER OF TERMS IN DISTORTION SERIES, MT = ',I6
       1,5X,' NT = ',I6
       2/' TOTAL NUMBER OF COEFFICIENTS, NO = ',I6///)
        WRITE (2,640)
640     FORMAT (////'   D - SERIES        F - SERIES        H - SERIES'
       1//)
C
C       CALCULATION OF FLEXIBILITY FACTOR
C
        FLEX=0.0
        DO 750 J=1,JT
        FLEX=FLEX+D(J)*VY(J)+D(J+JT)*VV(J)
        IF (T4.EQ.4) FLEX=FLEX+D(J+JT*3)*VT(J)
750     WRITE (2,751) D(J), D(J+JT), D(J+JT*2)
751     FORMAT (1X,F10.4,7X,F10.4,7X,F10.4)
        IF (T4.NE.4)GO TO 755
        WRITE (2,752)
752     FORMAT (///'   G - SERIES'///)
        DO 753 J=1,JT
753     WRITE (2,754) D(J+JT*3)
754     FORMAT (1X,F10.4)
755     CONTINUE
```

```
      WRITE (2,992)
  992 FORMAT (//' U - DISTORTION DISPLACEMENT'/)
      WRITE (2,24)
      WRITE (2,13)(N,N=2,NN)
      DO 652 M=1,MT
  652 WRITE (2,15)M,(A(M,N),N=1,NT)
      WRITE (2,991)
  991 FORMAT (//' V - DISTORTION DISPLACEMENT'/)
      WRITE (2,653)
  653 FORMAT (///'    B - SERIES CONSTANTS  '///)
      WRITE (2,13)(N,N=2,NN)
      DO 654 M=1,MT
  654 WRITE (2,15)M,(BS(M,N),N=1,NT)
      WRITE (2,990)
  990 FORMAT (//' W - DISTORTION DISPLACEMENT'/)
      WRITE (2,12)
      WRITE (2,13)(N,N=2,NN)
      DO 655 M=1,MT
  655 WRITE (2,15)M,(C(M,N),N=1,NT)
      WRITE (2,998)NE,NET,NY
  998 FORMAT (//' NUMBER OF INTEGRATION POINTS.'/
     1' CIRCUMFERENTIAL POINTS, BEND,  NE = ',I5,
     1'    TANGENT,  NET = ',I5/
     2' MERIDIONAL POINTS,       NY = ',I5//)
      IF (SM.EQ.1)WRITE (2,997)
      IF (SM.EQ.-1)WRITE (2,996)
  997 FORMAT (//' IN-PLANE BENDING, CLOSING MOMENT.'//)
  996 FORMAT (//' IN-PLANE BENDING, OPENING MOMENT.'//)
      WRITE (2,16)ALPHA,LAMDA,RR,MU
      WRITE (2,660)LR
  660 FORMAT (//' TANGENT PIPE LENGTH/BORE RATIO = ',F8.4//////)
C
C     CORRECT FLEXIBILITY FACTOR FOR TANGENT
C     PIPE FLEXIBILITY.
C
      FLEX=FLEX-2.0*(1-MU**2)*LR/(AL*RR)
      WRITE (2,18)FLEX
      WRITE (2,994)
  994 FORMAT (///' STRESS AND STRAIN FACTORS.'/
     1/' THE MERIDIONAL ANGLE AROUND THE BORE IS PHI.'/
     2' THE CIRCUMFERENTIAL ANGLE IS THETA.'///)
C
C     CALCULATION OF STRESS FACTORS AND PRINTING OUT.
C
C
      NE1=NE+1
      NEET=NE+NET
      IF (T4.EQ.3)NEET=NE
      DO 401 E=1,NEET
      S=1.0
      IF (E.GE.NE1)S=0.0
      IF (E.EQ.NE1)WRITE(2,3010)
 3010 FORMAT (//////' ***   TANGENT PIPE   ***'//////)
      EE=(E-1)*HE*180/PI
      IF (E.EQ.NE1)EE=EE-HE*180/PI
      WRITE (2,450)EE
  450 FORMAT (//////'  THETA  =  ',F6.2//)
```

```
      WRITE (2,451)
451   FORMAT (1X,' STRAINS',44X,'STRESSES'//'  MERID.',4X,
     1'CIRCUMFERENTIAL',6X,'MERIDIONAL'
     1,10X,'CIRCUMFERENTIAL',6X,'MERIDIONAL',10X,'SHEAR STRESSES'//
     2'  ANGLE',3X,'INSIDE',5X,'OUTSIDE',3X,'INSIDE',4X,'OUTSIDE',4X,
     3'INSIDE',5X,'OUTSIDE',3X,'INSIDE',4X,'OUTSIDE',3X,'INSIDE',
     44X,'OUTSIDE'//)
      V1=0.0
      V2=0.0
      V5=0.0
      V6=0.0
      DO 402 J=1,JT
      IF (E.GE.NE1)GO TO 3000
      V1=V1+(D(J+JT)-D(J))*VS(J,E)*RR
      V2=V2+D(J+JT)*VS(J,E)+D(J)*VC(J,E)
      GO TO 3001
3000  V2=V2+D(J+JT*3)*VQ(J,E)
3001  V5=V5+D(J+JT*2)*CM(J,E)
402   V6=V6+D(J+JT*2)*CE(J,E)
      DO 401 Y=1,NY
      ZY=Z(Y)
      IF (E.GE.NE1)ZY=1.0
      F1=V5
      F2=V1+(V2+V5)*SY(Y)
      IF (E.GE.NE1) F2=V2*SY(Y)
      F3=0.0
      F4=0.0
      F5=V2*RR*SY(Y)*ZY+V6
      F6=0.0
      DO 403 N=1,NT
      DO 403 M=1,MT
      F1=F1+(C(M,N)*CM(M,E)-BS(M,N)*CM(M,E))*C1(N,Y)
      F2=F2+(BS(M,N)*C3(N,Y)+C(M,N)*C4(N,Y))*S*CM(M,E)
     1+A(M,N)*C2(N,Y)*CE(M,E)
      F3=F3+(A(M,N)*(C5(N,Y)*S-(1.0-S)*C6(N,Y))+BS(M,N)*C6(N,Y))
     1*SE(M,E)
      F4=F4+(C(M,N)*C7(N,Y)-BS(M,N)*C1(N,Y))*CM(M,E)
      F5=F5+A(M,N)*C8(N,Y)*CE(M,E)*S+C(M,N)*C1(N,Y)*CE(M,E)
     1+(BS(M,N)*C9(N,Y)+C(M,N)*C10(N,Y))*CM(M,E)*S
      F6=F6+(A(M,N)*C11(N,Y)+C(M,N)*C12(N,Y)+BS(M,N)*C6(N,Y))
     1*SE(M,E)*S
      F6=F6+(BS(M,N)*C6(N,Y)+C(M,N)*C13(N,Y))*SE(M,E)*(1.0-S)
403   CONTINUE
      EY=F1*RR
      EX=F2/ZY
      EXY=F3/ZY
      KY=LAMDA*F4/2.0
      KX=LAMDA*F5/(2.0*(RR*ZY)**2)
      KXY=LAMDA*F6/(2.0*RR*ZY)
      EXI=EX-KX
      EXO=EX+KX
      EYI=EY-KY
      EYO=EY+KY
      MG=1.0/(1.0-MU**2)
      SXI=(EXI+MU*EYI)*MG
      SXO=(EXO+MU*EYO)*MG
      SYI=(EYI+MU*EXI)*MG
      SYO=(EYO+MU*EXO)*MG
```

```
      SXYI=(EXY/2-KXY)/(1.0+MU)
      SXYO=(EXY/2+KXY)/(1.0+MU)
      YY=(Y-1)*HY*180.0/PI-90.0
      WRITE (2,404)YY,EXI,EXO,EYI,EYO,SXI,SXO,SYI,SYO,SXYI,SXYO
404   FORMAT (1X,F7.2,3X,10(F7.3,3X))
401   CONTINUE
999   CONTINUE
      STOP
      END
      SUBROUTINE FUNCT(NO,D,F,CP,RP)
      IMPLICIT REAL*8 (A-H,O-Z)
C
C
C     CALCULATION OF STRAIN ENERGY PART OF TOTAL POTENTIAL
C     ENERGY FOR BOTH FLANGED BENDS AND BEND/TANGENT ASSEMBLIES.
C
C
      REAL*8 AC(5,25),AS(5,25)
      REAL*8 UC(5,25),US(5,25),VQ(5,25),CY(25)
      REAL*8 D(120),F
      REAL*8 CC(5,25),SS(5,25)
      REAL*8 MG,LA,CM(5,25),CE(5,25),SE(5,25),VC(5,25),VV(5)
      REAL*8 SY(25),Z(25),C1(8,25),C2(8,25),C3(8,25),C4(8,25),C5(8,25)
      REAL*8 A(5,8),C(5,8),WE(25),WY(25),WET(25),C13(8,25)
      REAL*8 B(5,8),VS(5,25),VY(5)
      REAL*8 C6(8,25),C7(8,25),C8(8,25),C9(8,25)
      REAL*8 C10(8,25),C11(8,25),C12(8,25)
      INTEGER CP,RP
      INTEGER E,Y,T4
      COMMON/BLK1/CM,CE,SE,VC,VV,SY,Z,C1,C2,C3,C4,C5,LA,MG,C13
      COMMON/BLK2/JT,MT,NT,NE,NY,HE,HY,WE,WY,RR,AS,AC,T4,NET,WET,HET
      COMMON/BLK3/VS,VY,C6,C7,C8,C9,C10,C11,C12,CC,SS,UC,US,VQ,CY,SM
      DO 1 M=1,MT
      DO 1 N=1,NT
      MJ=JT*T4+M+MT*(N-1)
      C(M,N)=D(MJ)
      B(M,N)=D(MJ+MT*NT*2)
1     A(M,N)=D(MJ+MT*NT)
      MNT=MT*NT
      F=0.0
      DO 2 E=1,NE
      V1=0.0
      V2=0.0
      V5=0.0
      V6=0.0
      V7=0.0
      J1=0
      DO 3 K=1,2
      J=CP
      IF (K.EQ.2)J=RP
      IF (J.GT.JT*3)GOTO 3
      IF (J.GT.JT)J=J-JT
      IF (J.GT.JT)J=J-JT
      IF (J.EQ.J1)GO TO 3
      J1=J
```

```
      V1=V1+(D(J+JT)-D(J))*VS(J,E)*RR
      V2=V2+D(J+JT)*VS(J,E)+D(J)*VC(J,E)
      V5=V5+D(J+JT*2)*CM(J,E)
      V6=V6+D(J+JT*2)*CE(J,E)
      V7=V7+D(J+JT*2)*SE(J,E)
3     CONTINUE
      DO 2 Y=1,NY
      F1=V5
      F2=V1+(V2+V5)*SY(Y)
      F3=0.0
      F4=0.0
      F5=V2*RR*SY(Y)*Z(Y)+V6
      F6=(-V7)*CY(Y)/(Z(Y)*RR)
      MN1=0
      DO 4 K=1,2
      MN=CP
      IF (K.EQ.2)MN=RP
      IF (MN.LE.JT*T4)GOTO 4
      MN=MN-JT*T4
      IF (MN.GT.MNT)MN=MN-MNT
      IF (MN.GT.MNT)MN=MN-MNT
      IF (MN.EQ.MN1)GOTO 4
      MN1=MN
      N=(MN-1)/MT+1
      M=MN-MT*(N-1)
      SEE=SE(M,E)
      CEE=CE(M,E)
      CME=CM(M,E)
      AMN=A(M,N)
      BMN=B(M,N)
      CMN=C(M,N)
      C1Y=C1(N,Y)
      C6Y=C6(N,Y)
      F1=F1+(CMN-BMN)*C1Y*CME
      F2=F2+(BMN*C3(N,Y)+CMN*C4(N,Y))*CME+AMN*C2(N,Y)*CEE
      F3=F3+(AMN*C5(N,Y)+BMN*C6Y)*SEE
      F4=F4+(CMN*C7(N,Y)-BMN*C1Y)*CME
      F5=F5+(AMN*C8(N,Y)+CMN*C1Y)*CEE
     1+(BMN*C9(N,Y)+CMN*C10(N,Y))*CME
      F6=F6+(AMN*C11(N,Y)+CMN*C12(N,Y)+BMN*C6Y)*SEE
4      CONTINUE
2     F=F+((F1*RR+F2/Z(Y))**2*Z(Y)
     1-(F1*F2*RR-F3**2*0.25/Z(Y))*MG
     2+LA*((F4+F5/(RR*Z(Y))**2)**2*Z(Y)
     3-(F4*F5-F6**2)*MG/(Z(Y)*RR**2)))
     4*WE(E)*WY(Y)*HE*HY/9.0
      IF (T4.EQ.3)GO TO 8
      NEET=NE+NET
      NE1=NE+1
      DO 5 E=NE1,NEET
      V2=0.0
      V5=0.0
      V6=0.0
      J1=0
```

```
      DO  6 K=1,2
      J=CP
      IF (K.EQ.2)J=RP
      IF (J.GT.JT*4.OR.J.LE.JT*2)GO  TO  6
      J=J-JT*2
      IF (J.GT.JT)J=J-JT
      IF (J.EQ.J1)GO  TO  6
      J1=J
      V2=V2+D(J+JT*3)*VQ(J,E)
      V5=V5+D(J+JT*2)*CM(J,E)
      V6=V6+D(J+JT*2)*CE(J,E)
    6 CONTINUE
      DO  5 Y=1,NY
      F1=V5
      F2=V2*SY(Y)
      F3=0.0
      F4=0.0
      F5=V2*RR*SY(Y)+V6
      F6=0.0
      MN1=0
      DO  7 K=1,2
      MN=CP
      IF (K.EQ.2)MN=RP
      IF (MN.LE.JT*4)GO  TO  7
      MN=MN-JT*4
      IF (MN.GT.MNT)MN=MN-MNT
      IF (MN.GT.MNT)MN=MN-MNT
      IF (MN.EQ.MN1)GO  TO  7
      MN1=MN
      N=(MN-1)/MT+1
      M=MN-MT*(N-1)
      AMN=A(M,N)
      BMN=B(M,N)
      CMN=C(M,N)
      F1=F1+(CMN-BMN)*C1(N,Y)*CM(M,E)
      F2=F2+AMN*CE(M,E)*C2(N,Y)
      F3=F3+(BMN-AMN)*SE(M,E)*C6(N,Y)
      F4=F4+(CMN*C7(N,Y)-BMN*C1(N,Y))*CM(M,E)
      F5=F5+CMN*C1(N,Y)*CE(M,E)
      F6=F6+(BMN*C6(N,Y)+CMN*C13(N,Y))*SE(M,E)
    7 CONTINUE
    5 F=F+((F1*RR+F2)**2-(F1*F2*RR-F3**2*0.25)*MG
     1+LA*((F4+F5/RR**2)**2-(F4*F5-F6**2)*MG/RR**2)
     2)*WET(E)*WY(Y)*HET*HY/9.0
    8 CONTINUE
      RETURN
      END
```

APPENDIX (6)

SECOND ORDER CHANGE IN CROSS-SECTIONAL AREA DUE TO BENDING

APPENDIX (6)

(a) Second Order Change in Cross-Sectional Area Due to Bending

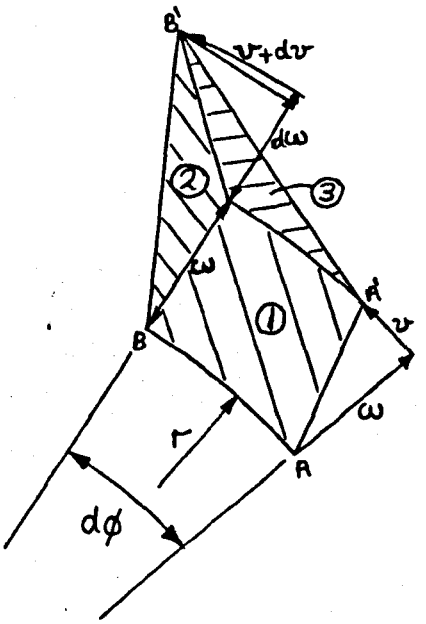

Following Kafka and Dunn [29], the area covered by displacement of a segment AB of the meridian to some position A′ B′, from the above diagram is,

$$\delta A = ① + ② + ③ \tag{1}$$

where

$$① = \tfrac{1}{2}\left(r\,d\phi + (r+\omega)d\phi - v\right)\omega$$
$$② = \tfrac{1}{2}\,\omega\,(v + dv)$$
$$③ = \tfrac{1}{2}\left((r+\omega)d\phi - v\right)\left(d\omega - (v+dv)d\phi\right) \tag{2}$$

Neglecting terms of greater than second order, the change in area of the segment can be found as,

$$\delta A = \tfrac{1}{2}\left(2\omega r + \omega^2 + v^2 + \omega\frac{dv}{d\phi} - v\frac{d\omega}{d\phi}\right) \tag{3}$$

The total change in area of the cross-section can be found by integrating (3) around the meridian, i.e.,

$$\Delta A = \frac{1}{2}\int_0^{2\pi}\left(2\omega r + \omega^2 + v^2 + \omega\frac{dv}{d\phi} - v\frac{d\omega}{d\phi}\right)d\phi \qquad (4)$$

(b) Second Order Meridian Inextensibility

The equation governing the second order inextensibility of the meridian can be determined by putting $(AB)^2 = (A'B')^2$, where,

$$(AB)^2 = (r\,d\phi)^2$$
$$(A'B')^2 = \left((r+\omega)d\phi + (v+dv) - v\right)^2 + \left(d\omega - (v-dv)d\phi\right) \qquad (5)$$

Putting $(AB)^2 = (A'B')^2$ and neglecting terms of higher than second order gives,

$$\left(v - \frac{d\omega}{d\phi}\right)^2 + \left(\omega + \frac{dv}{d\phi}\right) + 2r\left(\omega + \frac{dv}{d\phi}\right) = 0 \qquad (6)$$

Substituting (6) into (4) gives the change in cross-sectional area as,

$$\Delta A = -\frac{1}{2}\int_0^{2\pi}\left(\left(\frac{d\omega}{d\phi}\right)^2 + \left(\frac{dv}{d\phi}\right)^2 + \left(\frac{dv}{d\phi}\right)(2r+\omega) - v\left(\frac{d\omega}{d\phi}\right)\right)d\phi \qquad (7)$$

ACKNOWLEDGEMENTS

All of the work presented was carried out in the Department of Mechanics of Materials of the University of Strathclyde. The author wishes to record his thanks to:

Professor J. M. Harvey, A.R.C.S.T., B.Sc., M.S., Ph.D., C.Eng. F.I.Mech.E., head of the department, for the use of the department's facilities,

Science Research Council and Ferranti Ltd., who provided financial support for the project,

Mr. K. Rae, B.Sc., M.Sc., and Mr. A. Lambie, for their assistance during various parts of the experimental programme,

Dr. J. T. Boyle, B.Sc., Ph.D., A.F.I.M.A., for his advice on various aspects of the theory,

University of Strathclyde Computing Department for the use of their facilities,

Mrs. P. R. Heneghan for carefully typing the thesis.

Finally, the writer wishes to thank Professor J. Spence, A.R.C.S.T., B.Sc., M.Sc., Ph.D., D.Sc., C.Eng. F.I.Mech.E., who supervised the project, for his advice and assistance throughout.